MICROBIAL RESPONSE TO A RAPIDLY CHANGING MARINE ENVIRONMENT: GLOBAL WARMING AND OCEAN ACIDIFICATION

EDITED BY: Mi Sun Yun, Jun Sun, Connie Lovejoy and Sang Heon Lee

PUBLISHED IN: Frontiers in Microbiology

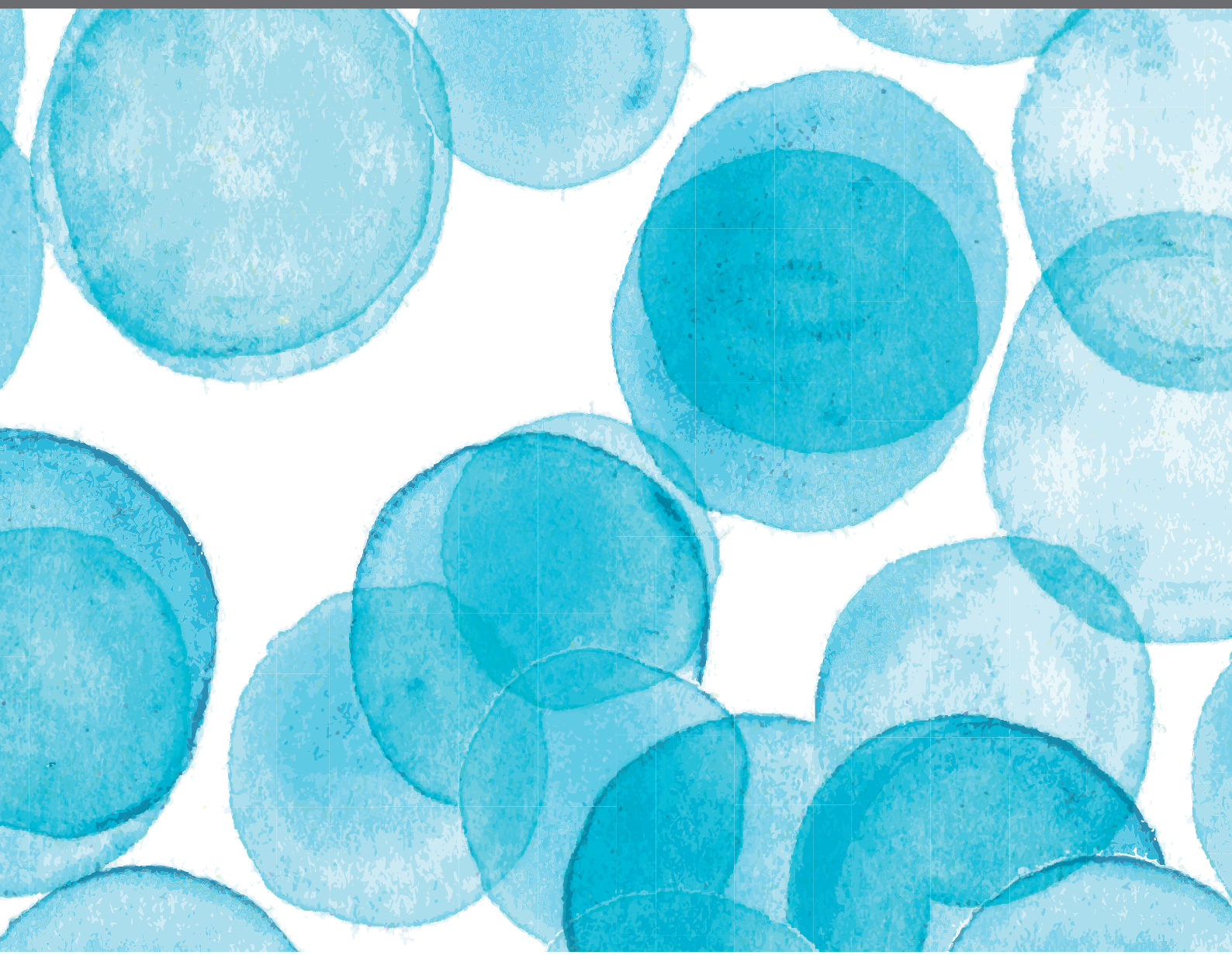

frontiers Research Topics

frontiers

ISSN 1664-8714
ISBN 978-2-88971-365-3
DOI 10.3389/978-2-88971-365-3

About Frontiers

Frontiers is more than just an open-access publisher of scholarly articles: it is a pioneering approach to the world of academia, radically improving the way scholarly research is managed. The grand vision of Frontiers is a world where all people have an equal opportunity to seek, share and generate knowledge. Frontiers provides immediate and permanent online open access to all its publications, but this alone is not enough to realize our grand goals.

Frontiers Journal Series

The Frontiers Journal Series is a multi-tier and interdisciplinary set of open-access, online journals, promising a paradigm shift from the current review, selection and dissemination processes in academic publishing. All Frontiers journals are driven by researchers for researchers; therefore, they constitute a service to the scholarly community. At the same time, the Frontiers Journal Series operates on a revolutionary invention, the tiered publishing system, initially addressing specific communities of scholars, and gradually climbing up to broader public understanding, thus serving the interests of the lay society, too.

Dedication to Quality

Each Frontiers article is a landmark of the highest quality, thanks to genuinely collaborative interactions between authors and review editors, who include some of the world's best academicians. Research must be certified by peers before entering a stream of knowledge that may eventually reach the public - and shape society; therefore, Frontiers only applies the most rigorous and unbiased reviews.
Frontiers revolutionizes research publishing by freely delivering the most outstanding research, evaluated with no bias from both the academic and social point of view. By applying the most advanced information technologies, Frontiers is catapulting scholarly publishing into a new generation.

What are Frontiers Research Topics?

Frontiers Research Topics are very popular trademarks of the Frontiers Journals Series: they are collections of at least ten articles, all centered on a particular subject. With their unique mix of varied contributions from Original Research to Review Articles, Frontiers Research Topics unify the most influential researchers, the latest key findings and historical advances in a hot research area! Find out more on how to host your own Frontiers Research Topic or contribute to one as an author by contacting the Frontiers Editorial Office: frontiersin.org/about/contact

MICROBIAL RESPONSE TO A RAPIDLY CHANGING MARINE ENVIRONMENT: GLOBAL WARMING AND OCEAN ACIDIFICATION

Topic Editors:
Mi Sun Yun, Tianjin University of Science and Technology, China
Jun Sun, China University of Geosciences, China
Connie Lovejoy, Laval University, Canada
Sang Heon Lee, Pusan National University, South Korea

Citation: Yun, M. S., Sun, J., Lovejoy, C., Lee, S. H., eds. (2021). Microbial Response to a Rapidly Changing Marine Environment: Global Warming and Ocean Acidification. Lausanne: Frontiers Media SA. doi: 10.3389/978-2-88971-365-3

Table of Contents

frontiers in Microbiology

EDITORIAL
published: 09 August 2021
doi: 10.3389/fmicb.2021.731732

Editorial: Microbial Response to a Rapidly Changing Marine Environment: Global Warming and Ocean Acidification

Mi Sun Yun[1]*, *Jun Sun*[1,2], *Connie Lovejoy*[3] and *Sang Heon Lee*[4]

[1] College of Marine and Environmental Sciences, Tianjin University of Science and Technology, Tianjin, China, [2] College of Marine Science and Technology, China University of Geosciences Wuhan, Wuhan, China, [3] Département de Biologie, Université Laval, Quebec, QC, Canada, [4] Department of Oceanography, Pusan National University, Busan, South Korea

Keywords: microbial community, marine environment, ecosystem, warming, ocean acidification

Editorial on the Research Topic

Microbial Response to a Rapidly Changing Marine Environment: Global Warming and Ocean Acidification

OPEN ACCESS

Edited by:
Tony Gutierrez,
Heriot-Watt University,
United Kingdom

Reviewed by:
Jennifer Pratscher,
The Lyell Centre, United Kingdom

***Correspondence:**
Mi Sun Yun
misunyun@pusan.ac.kr

Specialty section:
This article was submitted to Aquatic Microbiology, a section of the journal Frontiers in Microbiology

Received: *28 June 2021*
Accepted: *15 July 2021*
Published: *09 August 2021*

Citation:
Yun MS, Sun J, Lovejoy C and Lee SH (2021) Editorial: Microbial Response to a Rapidly Changing Marine Environment: Global Warming and Ocean Acidification. Front. Microbiol. 12:731732. doi: 10.3389/fmicb.2021.731732

The World Ocean is undergoing rapid and substantial changes, particularly, in terms of warming and acidification. Global sea surface temperatures have risen by 0.7°C in recent years (2005–2014) relative to pre-industrial times (1870–1899) (Gattuso et al., 2015). The ocean pH is decreasing in response to the increasing anthropogenic CO_2 emissions (Ocean Acidification; OA). This clear trend of ocean warming and acidification was documented in the fifth Assessment Report (AR5) by Intergovernmental Panel on Climate Change (IPCC). The warming of the surface ocean could increase stratification, suppress transport of nutrients into the upper photic zone and alter hydrographic properties or patterns of ocean circulation. The effects of OA include the changes of seawater carbonate chemistry such as an increase in partial pressure of seawater CO_2 (pCO_2) concentration and a decrease in calcium carbonate ($CaCO_3$) saturation state (Royal Society, 2005; IPCC, 2014). Consequently, the warming and acidification will have substantial impacts on the growth and survival of marine organisms (e.g., Brander, 2010; Doney et al., 2012; Hollowed et al., 2013). In particular, microbes, as a vital component of the marine ecosystem that includes microalga (phytoplankton), protists, fungi, viruses, and the two main groups of prokaryotes (Bacteria and Archaea), are vulnerable to these environmental changes. Since these microscopic organisms drive major biogeochemical cycles and support higher food webs globally, physiological, and ecological alterations in microbial communities caused by marine environmental changes can herald changes not only in pathways of energy transfer through the food web but also in global biogeochemical cycles. Considering the microbial communities' pivotal roles in the marine ecosystem and biogeochemical cycles, it is important to understand recent changes in microbial communities and how future changes might arise under the ongoing environmental forcing of the warming and acidifying oceans.

The goal of this Research Topic was to collect studies on present and future possible changes in microbial communities with respect to environmental change and their consequences within various oceans. The topic contains 10 diverse scientific contributions on many fundamental questions related to microbial communities in oceanic environments, and report on physiological and ecological responses of microbial communities to environmental changes. The studies from a range of geographic regions were collected, from more coastal systems to open oceans, and include Tera Nova Bay in Antarctica, Mediterranean waters, the East/Japan Sea, the

South China Sea, the Western Pacific Ocean, the South Pacific Ocean, and the Ross Sea of the Southern Ocean. In the context of taxonomic diversity, heterotrophic bacteria, viruses, microalga, and other prokaryotes were included in this Research Topic.

Out of the 10 works published, seven of them are focused on the phytoplankton communities, or single species of microalgae, or environmental drivers. Kim et al. describe the seasonal variability in the macromolecular composition of the sea surface in front of the Korean station in Terra Nova Bay, Ross Sea, Antarctica. They show changes in organic matter composition mainly derived by changes in phytoplankton metabolism between the productive and the non-productive season. Their study helps us to understand the effect of future climate change on the composition of organic matter derived from phytoplankton in the polar oceans. Biochemical compositions such as macromolecular and amino acids of phytoplankton in the Ross Sea, Antarctica was investigated by Jo et al.. They found distinct differences in the biochemical composition between two major bloom-forming phytoplankton groups (diatoms and *Phaeocystis antarctica*). They discuss how these different compositions may highlight the different strategies of these two phytoplankton communities to cope with ongoing environmental changes in the Antarctic Ocean. Kang et al. demonstrate the differences in carbon uptake rates and intracellular biochemical compositions between two different size fractions of phytoplankton to understand the ecological roles of the small phytoplankton in terms of food quantity and quality in the East/Japan Sea where the water temperature has rapidly increased. Their findings show that the increase of small phytoplankton under the warming ocean conditions could negatively affect the primary productivity and caloric content, with further consequences on the marine food webs. The photosynthetic responses to oceanic physio-chemical conditions and phytoplankton communities in the oligotrophic Western Pacific Ocean were presented by Wei et al.. Their study found that the important biotic variables influencing Fv/Fm are diatoms, Prochlorococcus, and picoeukaryotes, whilst the maximum of primary production is closely related to cyanobacteria, dinoflagellates, and *Synechococcus*. The detailed investigation of a chromophytic phytoplankton community using high-throughput sequencing of rbcL genes in the Western Pacific Ocean was presented by Pujari et al.. The authors found that the diversity of RuBisCO encoding rbcL gene varies with depth and across latitudes in the Western Pacific Ocean. The variation observed in chromophytic phytoplankton suggests the strong influence of environmental variables on biological production induced by oceanographic features. Thangaraj et al. investigated comprehensive proteomic profiling of diatom *Skeletonema dohrnii* with a change of temperature and silicate deprivation based on the iTRAQ proteomic approach, to understand the effect of the temperature and nutrient on the physiology of marine diatoms growth and photosynthesis. Their study shows that the proteome analysis for environmental stress-response of diatoms could extend our understanding for the potential impacts of climate change on the physiological adjustment to the metabolic process of phytoplankton. Sow et al. present a clear and concise description of the biogeography of *Phaeocystis* along a transect from the ice edge to the equator in the South Pacific Ocean, by way of high-throughput 18S rRNA gene sequencing. Their study shows that *Phaeocystis* could be occasionally highly abundant and diverse in the South Pacific Ocean, whereas the oceanic fronts could be the driving force for the distribution and structure of *Phaeocystis* assemblages in the ocean. Their work greatly expands our knowledge about the biodiversity patterns and abundances of *Phaeocystis* as a globally important nano-eukaryote.

Three of the 10 published works have focused on the response of viruses, prokaryotes or microbial communities to environmental stress. The response of viruses to two anthropogenic stressors (OA and eutrophication) was presented by Malits et al.. Their study demonstrates that the effect of OA on viral dynamics and viral-mediated mortality varies depending on the nutrient regime of the studied systems. It helps us to understand how viral-mediated mortality of microbes (VMMM) can be modified with environmental forcing. Another work looks into the contribution of grazers and viruses in controlling ecologically distinct prokaryotic sub-groups (i.e., high nucleic acid (HNA) and low nucleic acid (LNA) cells) along a cross-shore nutrient gradient in the northern South China Sea (Hu et al.). Their study shows how the nutrient regime influences the fate of ecologically relevant prokaryotic groups in the actual context of global warming and the anticipated oligotrophication of the future ocean. Sörenson et al. address the resilience of a marine microbial community, cultivated in an outdoor photobioreactor, when exposed to a naturally occurring seasonal stress. Differential gene expression analyses suggest that community function at warm temperatures is based on concomitant utilization of inorganic and organic carbon assigned to autotrophs and heterotrophs, while at colder temperatures, the uptake of organic carbon was performed primarily by autotrophs. Overall, the microbial community maintains a similar level of diversity and function within and across autotrophic and heterotrophic levels, confirming the cross-scale resilience theory.

The topics of the papers published in this Research Topic range from viruses, prokaryotes to phytoplankton and cover microbial communities from the various oceans. The studies confirm that the changes already occurring in ocean environments affect the metabolism and physiology of microbial communities, and further suggest that future changes will impact the physiological and ecological function or strategy of the microbial community in the marine ecosystem. Since most of these studies focus on the response of a single taxonomic population of microbes to environmental changes, our special issue highlights the need for studies to understand how ecological interactions occurring within and among the microbial community in the changing ocean will affect ecosystem structure and function. Finally, we hope that the group of papers that we have drawn together here will be a valuable addition to the accumulating observational evidence of how microbial communities are responding to the climate-related changes and consequently useful for evaluating and predicting the ongoing and future responses of marine ecosystems associated with the global climate change.

AUTHOR CONTRIBUTIONS

MSY wrote the text with input from CL. All other authors commented on and approved the text.

FUNDING

JS was financially supported by the National Key Research and Development Project of China (2019YFC1407805) and the Changjiang Scholar Program of Chinese Ministry of Education (T2014253). CL was supported by the Natural Science and Engineering Council (NSERC) Canada. Support for SL was provided by the project entitled Long-term change of structure and function in marine ecosystems of Korea funded by the Ministry of Oceans and Fisheries, South Korea.

ACKNOWLEDGMENTS

We thank all the contributing authors and reviewers to this Research Topic. Also, we would like to thank the editorial staff at Frontiers in Microbiology and in aquatic microbiology for their initial invitation and professional support throughout.

REFERENCES

Brander, K. (2010). Impacts of climate change on fisheries. *J. Mar. Syst.* 79, 389–402. doi: 10.1016/j.jmarsys.2008.12.015

Doney, S. C., Ruckelshaus, M., Duffy, J. E., Barry, J. P., Chan, F., English, C. A., et al. (2012). Climate change impacts on marine ecosystems. *Ann. Rev. Mar. Sci.* 4, 11–37. doi: 10.1146/annurev-marine-041911-111611

Gattuso, J.-P., Magnan, A., Billé, R., Cheung, W. W. L., Howes, E. L., Joos, F., et al. (2015). Contrasting futures for ocean and society from different anthropogenic CO2 emissions scenarios. *Science* 349:aac4722. doi: 10.1126/science.aac4722

Hollowed, A. B., Barange, M., Beamish, R. J., Brander, K., Cochrane, K., Drinkwater, K., et al. (2013). Projected impacts of climate change on marine fish and fisheries. *ICES J. Mar. Sci.* 70, 1023–1037. doi: 10.1093/icesjms/fst081

IPCC (2014). "Climate change 2014: synthesis report," in *Contribution of Working Groups I, II and III to the Fifth Assessment Report of the Intergovernmental Panel on Climate Change, Core Writing Team*, eds R. K. Pachauri and L. A. Meyer (Geneva: IPCC).

Royal Society (2005). *Ocean Acidification Due to Increasing Atmospheric Carbon Dioxide*. London: The Royal Society.

Conflict of Interest: The authors declare that the research was conducted in the absence of any commercial or financial relationships that could be construed as a potential conflict of interest.

Publisher's Note: All claims expressed in this article are solely those of the authors and do not necessarily represent those of their affiliated organizations, or those of the publisher, the editors and the reviewers. Any product that may be evaluated in this article, or claim that may be made by its manufacturer, is not guaranteed or endorsed by the publisher.

frontiers in Microbiology

ORIGINAL RESEARCH
published: 04 August 2020
doi: 10.3389/fmicb.2020.01774

Physiological and Ecological Responses of Photosynthetic Processes to Oceanic Properties and Phytoplankton Communities in the Oligotrophic Western Pacific Ocean

*Yuqiu Wei[1], Zhuo Chen[2,3], Congcong Guo[1], Qi Zhong[1], Chao Wu[2,3] and Jun Sun[2,3]**

[1] Institute of Marine Science and Technology, Shandong University, Qingdao, China, [2] Research Centre for Indian Ocean Ecosystem, Tianjin University of Science and Technology, Tianjin, China, [3] Tianjin Key Laboratory of Marine Resources and Chemistry, Tianjin University of Science and Technology, Tianjin, China

Understanding the dynamics of primary productivity in a rapidly changing marine environment requires mechanistic insight into the photosynthetic processes (light absorption characteristics and electron transport) in response to the variability of environmental conditions and algal species. Here, we examined the photosynthetic performance and related physiological and ecological responses to oceanic properties [temperature, salinity, light, size-fractionated chlorophyll *a* (Chl *a*) and nutrients] and phytoplankton communities in the oligotrophic Western Pacific Ocean (WPO). Our results revealed high variability in the maximum (F_v/F_m; 0.08–0.26) and effective (F_q'/F_m'; 0.02–0.22) photochemical efficiency, the efficiency of charge separation (F_q'/F_v'; 0.19–1.06), the photosynthetic electron transfer rates (ETR_{RCII}; 0.02–5.89 mol e^- mol $RCII^{-1}$ s^{-1}) and the maximum of primary production [PP_{max}; 0.04–8.59 mg C (mg chl *a*)$^{-1}$ h^{-1}]. All these photosynthetic characteristics showed a depth-specific dependency based on respective nonlinear regression models. On physiological scales, variability in light absorption parameters F_v/F_m and F_q'/F_m' notably correlated with light availability and size-fractionated Chl *a*, while both ETR_{RCII} and PP_{max} were correlated to temperature, light, and ambient nutrient concentration. Since the presence of nonphotochemical quenching (NPQ_{NSV}; 2.33–12.31) and increasing reductant are used for functions other than carbon fixation, we observed nonparallel changes in the ETR_{RCII} and F_v/F_m, F_q'/F_m', F_q'/F_v'. In addition, we found that the important biotic variables influencing F_v/F_m were diatoms (cells $>$ 2 μm), picosized *Prochlorococcus*, and eukaryotes, but the PP_{max} was closely related to large cyanobacteria (cells $>$ 2 μm), dinoflagellates, and picosized *Synechococcus*. The implication is that, on ecological scales, an interaction among temperature, light, and nutrient availability may be key in driving the dynamics of primary productivity in the WPO, while large cyanobacteria, dinoflagellates, and picosized *Synechococcus* may have a high contribution to the primary production. Overall, the photosynthetic processes are interactively affected by complex abiotic and biotic variables in marine ecosystems, rather than by a single variable.

Keywords: phytoplankton, photosynthesis, primary production, oceanic properties, Western Pacific Ocean

OPEN ACCESS

Edited by:
Nona Sheila Romualdo Agawin, University of the Balearic Islands, Spain

Reviewed by:
Yonghong Bi, Institute of Hydrobiology (CAS), China
Weimin Ma, Shanghai Normal University, China

****Correspondence:***
Jun Sun
phytoplankton@163.com

Specialty section:
This article was submitted to Aquatic Microbiology, a section of the journal Frontiers in Microbiology

Received: *09 May 2020*
Accepted: *06 July 2020*
Published: *04 August 2020*

Citation:
Wei Y, Chen Z, Guo C, Zhong Q, Wu C and Sun J (2020) Physiological and Ecological Responses of Photosynthetic Processes to Oceanic Properties and Phytoplankton Communities in the Oligotrophic Western Pacific Ocean. Front. Microbiol. 11:1774. doi: 10.3389/fmicb.2020.01774

INTRODUCTION

Current trends of change in oligotrophic marine ecosystems with ongoing climate change include warming, acidification, oligotrophication, and the increases in water column stratification and light penetration (Gao et al., 2019). All of these anticipated changes will inevitably interact to affect the photosynthetic performance of phytoplankton and hence marine primary productivity (Gao et al., 2012; Hoppe et al., 2015; Schuback et al., 2017; Hughes et al., 2018). On physiological scales, these effects can be observed as rapid metabolic adjustments (seconds to hours), while they are manifested as phytoplankton species succession on ecological scales (days to months) (Schuback and Tortell, 2019). To adapt to the changing marine environment, phytoplankton have evolved extreme photophysiological plasticity, ultimately leading to different physiological and ecological responses of photosynthetic processes to environmental variability (Moore et al., 2006; Claquin et al., 2008; Wei et al., 2019b). Accurately evaluating the photosynthetic processes in marine phytoplankton and their capacity to respond to environmental changes is, therefore, relevant to help predict ongoing climate impacts on the dynamics of marine primary productivity.

The photosynthetic processes comprise a series of diverse physiological and biochemical reactions, leading from light absorption via electron transport to carbon fixation (Schuback and Tortell, 2019). In recent years, fast repetition rate fluorometry (FRRF) has been advocated as major means of rapidly estimating the variability of light absorption characteristics and electron transport at unprecedented spatial and temporal resolution (Moore et al., 2003; Smyth et al., 2004; Oxborough et al., 2012; Aardema et al., 2018). Importantly, measurements of these photosynthetic processes can be linked synchronously to measurements of physical and/or chemical variables at the time of sampling (Lawrenz et al., 2013). Although not measuring CO_2-fixation directly, these FRRF measurements can provide photosynthetic electron transfer rates (ETR_{RCII}) of photosystem II (PSII). Thereafter, the ecologically relevant rates of carbon fixation can be converted by FRRF-derived ETR_{RCII} through a conversion factor, i.e., the effective electron requirement for carbon fixation (Melrose et al., 2006; Zhu et al., 2016; Schuback et al., 2017; Morelle and Claquin, 2018). Additionally, the applicability of FRRF-based measurements to estimate marine primary production, alone or in combination with other techniques, are potentially limited since the light absorption characteristics and electron transport vary significantly in response to environmental constraints or combinations thereof and changes in species taxonomy and physiology (Lawrenz et al., 2013; Jin et al., 2016; Schuback et al., 2017; Xie et al., 2018; Wei et al., 2019b; Zhu et al., 2019). As such, more recent studies have sought to better characterize the extent and nature of variation between these photosynthetic processes and environmental/biological variables (Moore et al., 2003; Suggett et al., 2009; Schuback et al., 2017, etc.). If possible, *in situ* measurements of FRRF-derived primary productivity in marine ecosystems can be achieved at the photophysiological level.

Yet to our knowledge, there is no direct experimental investigation in evaluating the variability of photosynthetic processes and in quantifying the primary productivity based on FRRF measurements in the Western Pacific Ocean (WPO) (Richardson et al., 2016). Our goal here is to determine the variability of light absorption characteristics and electron transport [mainly including photosynthetic quantum efficiency (F_v/F_m, F_q'/F_m', and F_q'/F_v'), functional absorption cross-section (σ_{PSII}), nonphotochemical quenching (NPQ), ETR_{RCII}], FRRF-derived primary production, and associated oceanic properties [temperature, salinity, light, size-fractionated chlorophyll *a* (Chl *a*), and nutrients] and phytoplankton communities (micro/nano- and picosized classes). With these data, we can test the hypothesis that photosynthetic performance and primary productivity of phytoplankton vary widely across environmental conditions and algal species in the WPO. We can also infer (1) how the photosynthetic processes respond to specific environmental variable and species composition on physiological scales and (2) what is the key in driving the dynamics of WPO primary productivity on ecological scales. Such physiological and ecological insights will be vital roles in improving the parameterization of photosynthetic performance in marine primary production estimates.

MATERIALS AND METHODS

Studied Stations and Sampling

Our experiments were conducted aboard the R/V *Kexue* during a fall cruise (3–28 October 2018) in the WPO (**Figure 1**). Samples were collected from four to five depths at a total of eight stations; detailed information of stations and sampling are given in **Table 1**.

Seawater samples were collected using 12-L Niskin bottles on a rosette equipped with a Sea-Bird Conductivity, Temperature and Depth (CTD) sensor (SBE 19 Plus). Water temperature and salinity were recorded with a CTD system *in situ* at the same time. Seawater samples for FRRF measurements (5–7 ml) were acclimated in low light irradiance for 20 min to allow the oxidation of electron transport chain (ETC) and NPQ relaxation, and then analyzed in shipboard laboratory (Smyth et al., 2004; Suggett et al., 2009). *In situ* light intensity was measured in parallel using an underwater photosynthetically active radiation (PAR, 400–700 nm, μmol quanta m^{-2} s^{-1}) sensor (RBR, XRX-620). Samples (1,000 ml) for micro-/nanophytoplankton (cell sizes $>$ 2 μm) analysis were fixed on board with 2% buffered formalin and stored in darkness. Seawater samples (∼2 ml) for picophytoplankton analysis ($<$2 μm) were incubated in the dark without treatment for 10–15 min at room temperature to avoid loss of resolution and changes in cell counting due to fixation (1% final concentration of paraformaldehyde) or freezing, and then quickly stored at −80°C liquid nitrogen (Jiao et al., 2005; Wei et al., 2019a). Seawater samples for size-fractionated Chl *a* (1,000 ml) were filtered serially through 2 μm × 47 mm nylon membrane and 0.2 μm × 47 mm polycarbonate membrane filters under low vacuum pressure ($<$0.04 MPa), therewith immediately freeze trapped in liquid nitrogen for further analysis. Filtered

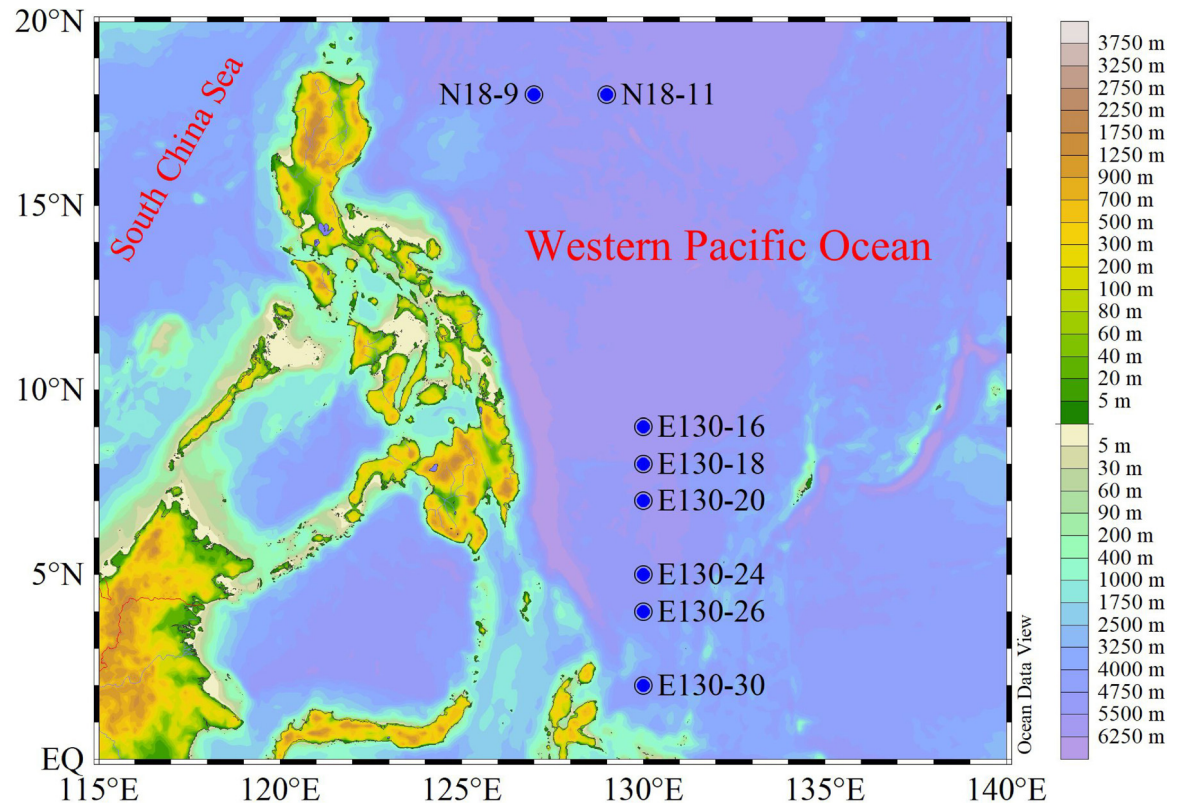

FIGURE 1 | Study area and sampling stations for the Western Pacific Ocean (WPO) cruise during fall. N18-9 and N18-11 denote the northern stations, while E130-16, E130-18, E130-20, E130-24, E130-26, and E130-30 represent the southern stations.

TABLE 1 | Information of stations and sampling depths for biological and environmental parameters during the Western Pacific Ocean (WPO) cruise.

Station	Latitude (°E)	Longitude (°N)	Sampling depths (m)	
			Photosynthetic properties and light irradiance in the upper Z_{eu}	Temperature, salinity, nutrients, size-fractionated Chl *a*, and phytoplankton
N18-9	127	18	5, 25, 45, 100	5, 25, 45, 100, 150
N18-11	129	18	5, 25, 45, 100	5, 25, 45, 100, 150
E130-16	130	9	5, 25, 50, 104	5, 25, 50, 104, 150
E130-18	130	8	5, 25, 50, 90	5, 25, 50, 90, 150
E130-20	130	7	5, 25, 50, 100	5, 25, 50, 85, 150
E130-24	130	5	5, 25, 60, 100	5, 25, 60, 100, 150
E130-26	130	4	5, 25, 50, 75	5, 25, 50, 75, 150
E130-30	130	2	5, 25, 50, 78	5, 25, 50, 78, 150

samples (0.45 μm, cellulose acetate membrane) for nutrient analysis were frozen at −20°C until processing.

Z_{eu}, the euphotic zone depth, defined here as depth with 1% of surface PAR.

Biological Sample Analysis

All FRRF measurements for PSII photosynthetic properties were conducted on an *in situ* FastOcean sensor with Act2 system (Chelsea Technologies Group, Ltd.). We applied a single-turnover (ST) protocol consisting of 100 flashlets (Fet, a single 1 μs excitation pulse from LEDs) with 2.0 μs Fet pitch to obtain saturation and relaxation sequences. Subsequently, we measured these ST-Fet sequences continuously (2.0-μs interval) throughout the light curve and programmed the length of each light step to make all derived parameters to reach steady state. Blue LED (450 nm) can excite Chl *a* pigments, covering the light absorption spectrum of most photosynthetic algae such as diatoms and dinoflagellates, etc. In mixed phytoplankton communities of the WPO, cyanobacteria mainly use various phycobilin pigments in phycobilisomes to absorb light, instead of Chl *a* (McConnell et al., 2002). However, the phycobilin pigments were excited at longer wavelengths ranging from green

and orange/red light. We thus provided the excitation power by LEDs (E_{LED}) at three wavelengths centered on 450, 530, and 624 nm to cover the broad range of absorption spectrum to improve the light absorption and generate a saturating pulse, i.e., enough light absorbed to close all PSII reaction centers (RCII). The $R\sigma_{PSII}$ values (probability of an RCII being closed during the first Fet saturation phase) reported by Act2 system provided a useful indication of E_{LED} optimization. Ideally, the dark-adapted values of $R\sigma_{PSII}$ should fall between 0.05 and 0.07 with any of the LED combinations used. During the cruise, the usable range extended to between 0.03 and 0.08, approximately. At steady state, fluorescence-light response curves were retrieved subsequently by exposing each sample sequentially to 8–12 actinic background irradiances spanning from 0 to 1,000 μmol quanta m^{-2} s^{-1}. In addition, the retention time of initial light condition was twice as long as the dark adaptation and subsequent light steps.

Micro-/nanophytoplankton samples were concentrated with 100 ml settlement columns for 24–48 h according to the Utermöhl method (Sun and Liu, 2003; Wei et al., 2017). The taxonomy and abundance of micro-/nanophytoplankton were identified and counted, respectively, under an inverted microscope (Motic BA300) at 200 (or 400) × magnification. According to different fluorescence signals and light-scattering characteristics, picophytoplankton including *Synechococcus* (Syn), *Prochlorococcus* (Pro), and picoeukaryotes (PEuks) were classified and quantified by flow cytometry (BD Accuri C6), respectively, following the standard methods detailed in Jiao et al. (2005) and Wei et al. (2019a). Meanwhile, 2-μm fluorescent beads (Polysciences) were added to 1 ml replicated samples just before analysis as the instrument internal standard.

Nutrients containing ammonium, phosphate, nitrate, nitrite, and silicate were measured by Technicon AA3 Auto-Analyzer (Bran+Luebbe). Dissolved inorganic nitrogen (DIN; the sum of the concentrations of ammonium, nitrite, and nitrate) was analyzed using the method of copper–cadmium column reduction. Dissolved inorganic phosphorus (DIP) and silicate (DSi) were measured using molybdenum blue reagents and standard molybdic acids, respectively (Karl and Tien, 1992; Brzezinski and Nelson, 1995). Furthermore, we imposed a minimum nutrient concentration of 0.01 μmol L^{-1} to avoid issues with detection limits. Size-fractionated Chl *a* filters were extracted in 5 ml 90% acetone (4°C for 24 h). After removal of the filters, Chl *a* concentrations were performed on a CE Turner Designs Fluorometer following the acidification method of Welschmeyer (1994).

FRRF-Derived Photophysiological Parameters

FRRF-derived photophysiological parameters corresponding to each actinic light level were derived by an iterative nonlinear fitting procedure and recorded from the average of all acquisitions. According to the classical biophysical model of Kolber et al. (1998), the minimum and maximum fluorescence (F) yields for dark-regulated state (F_o and F_m) and for light-regulated state (F' and F_m') were measured, respectively. The functional absorption cross-section of PSII (σ_{PSII} in darkness or σ_{PSII}' under ambient light, Å $RCII^{-1}$) can be determined by parameterizing the fluorescence–light response curve of F yields from F_o (F') to F_m (F_m'). In this way, the maximum [F_v/F_m = (F_m - F_o)/F_m] and effective [F_q'/F_m' = (F_m' - F')/F_m'] photochemical efficiency of PSII under dark-adapted and light-regulated states were calculated, respectively, as per Oxborough et al. (2000).

The PSII operating efficiency (F_q'/F_v') quantified the fraction of functional RCII and accounted for the extent of photochemical quenching/(energy conversion) by PSII (i.e., the efficiency of charge separation in RCII) (Suggett et al., 2003; Melrose et al., 2006). NPQ at given light level was derived from normalized Stern–Volmer quenching coefficient, defined as NPQ_{NSV} [NPQ_{NSV} = F_o'/F_v', where F_o' represented the minimum F yield in the presence of NPQ_{NSV}, was estimated as F_o' = $F_o/(F_v/F_m + F_o/F_m')$] (Müller et al., 2001; Moore et al., 2003; Xie et al., 2018; Wei et al., 2019b).

$$F_q' \Big/ F_v' = \left(F_m' - F'\right) \Big/ \left(F_m' - F_o'\right) \quad (1)$$

Our FRRF measurement protocol allowed for reliable estimation of σ_{PSII}' in the existence of NPQ_{NSV}. The instantaneous RCII normalized ETR_{RCII} (mol e^- mol $RCII^{-1}$ s^{-1}) for each light level was calculated as the product of PAR (E, μmol quanta m^{-2} s^{-1}), σ_{PSII}' at E, F_q'/F_v' and the constant value (6.022×10^{-3}) for converting μmol quanta to quanta and Å^2 (10^{-20} m^2) to m^2 according to biophysical sigma-based algorithm (Suggett et al., 2003; Schuback et al., 2015; Xie et al., 2018):

$$ETR_{RCII} = E \times \sigma'_{PSII} \times \frac{F_q'}{F_v'} \times 6.022 \times 10^{-3} \quad (2)$$

In this study, the ^{14}C-measured data were not collected as part of the experiments included here because the abiotic and/or biotic variables would be lost using a region-specific conversion factor, especially to monitor the physiological responses to environmental changes on primary productivity. However, we measured the charge separation rate per unit volume in PSII [JV_{PSII}, electrons (PSII m^{-3}) s^{-1}], which generally correlates well with photosynthetic O_2 evolution (Oxborough et al., 2012) and can roughly provide an estimate of theoretical maximum of primary production {PP_{max} [mg C (mg chl *a*)$^{-1}$ h^{-1}]} (Wei et al., 2019b).

$$PPmax = k \times JV_{PSII} = k \times \sigma_{PSII} \times [RCII] \times (1 - C) \times E_{LED} \quad (3)$$

$$[RCII] = \frac{K_R}{E_{LED}} \times \frac{F_O}{\sigma_{PSII}} \quad (4)$$

where [RCII] is the concentration of PSII reaction centers with units of mol RCII m^{-3}; (1-C) is the fraction of RCII in the open state, denoted here as q^p [q^p = (F'-F_o')/(F_m'-F_o')]; E_{LED} is the intensity of the fluorometer (photons m^{-2} s^{-1}); and K_R is a specific constant (photons m^{-3} s^{-1}). The specific constant *k* includes the following conversions: 3,600 s h^{-1}, 0.25 C quanta^{-1}, 12 g C mol^{-1}, and 200–950 mol Chl *a* mol $RCII^{-1}$ (Smyth et al., 2004; Suggett et al., 2009; Oxborough et al., 2012).

Statistical Analyses

Average data are given values ± SD (standard deviation). Spearman correlation analyses (r) were used to examine the significant relationship among abiotic and/or biotic parameters (SPSS, V 25). Analysis results were subsequently visualized based on "pheatmap" package in R software (V 3.6.1). The nonlinear regression models (NRMs; Origin V 8.5) and t-test (Prism) could provide the curve fit of depth-specific photosynthetic parameters (Lawrenz et al., 2013; Richardson et al., 2016). Statistical significance level was set to 0.05. Abundance of phytoplankton communities was $\log_{10}$-transformed to improve the normality. Unless otherwise stated, photosynthetic parameters, phytoplankton abundance, and Chl *a* concentration used for presenting the spatial variation are expressed as depth-weighted averages (as calculated by dividing the trapezoidal integration of measured values for each variable by the maximum sampling depth). The depth-weighted average equation was calculated as (Wei et al., 2019b):

$$A = \left[\sum_{n}^{n+1} \frac{(A_i + A_{i+1})}{2} \times (D_{i+1} - D_i)\right] / (D_{\mathrm{MSL}} - D_{\mathrm{S}}) \quad (5)$$

where A_{i} is the photosynthetic parameter or phytoplankton abundance (cells L^{-1}) at sampling layer i; n is the number of sampling layers, and D_{i} is the depth at sampling layer i (m); and D_{MSL} and D_{S} are the depths of maximum sampling layer (m) and the surface sampling depth (5 m), respectively.

RESULTS

Temperature, Salinity, Light Intensity, and Nutrients

Within the upper 50 m, water temperature generally ranged from 26.7 to 29.8°C, except at stations N18-9 and N18-11 where water temperature were relatively lower (approximately 24.9–26.5°C) (**Figure 2**). However, the salinity observed in the upper 50 m at stations N18-9 and N18-11 (34.5–34.7) were much higher than other sampling stations (<34.4). These results suggest that the contrasting differences of temperature and salinity at stations N18-9 and N18-11 relative to other stations may be potentially affected by the Kuroshio current. Apart from the northern stations N18-9 and N18-11, water temperature rapidly decreased to nearly 11.4–19.9°C from 25 to 150 m across other sampling stations. In particular, the average temperature at stations E130-18 and E130-20 were obviously lower within the upper 150 m (**Table 2**). Analysis of the satellite altimetry[1] revealed that a cold eddy was present at stations E130-18 and E130-20. Surface light intensity ranged from 56 to 993 μmol quanta m^{-2} s^{-1} but decreased drastically to 0 μmol quanta m^{-2} s^{-1} at 100–125 m.

As expected, nutrients were consistently low within the upper 50 m in the WPO (**Figures 2D–F**). DIN concentration in the upper 50 m ranged from 0.24 to 2.15 μmol L^{-1}, with an average of 0.89 ± 0.45 μmol L^{-1}. DIP was near the limiting concentration (<0.1 μmol L^{-1}) or undetectable within the upper 50 m, averaging 0.06 ± 0.03 μmol L^{-1}. DSi was also considerably low, ranging from 0.25 to 1.21 μmol L^{-1} (averaging 0.68 ± 0.21 μmol L^{-1}) in the upper 50 m. Due to the influence of cold eddy, average DIN, DIP, and DSi concentrations at stations E130-18 and E130-20 were all relatively higher than other sampling stations (**Table 2**). In contrast to these eddy-sampled stations, average nutrient concentrations at stations N18-9 and N18-11 were obviously lower as a consequence of the Kuroshio influence.

[1]http://icdc.cen.uni-hamburg.de/1/daten/ocean/ssh-aviso/

Variability in Abundances of Micro-/Nano- and Picophytoplankton and Size-Fractionated Chl *a*

Depth-weighted average abundance of the total micro-/nanophytoplankton varied from 0.02 × 10^4 to 5.32 × 10^4 cells L^{-1} and averaged at 1.90 ± 0.71 × 10^4 cells L^{-1} (**Figure 3A**). The average composition (in terms of abundance) of the micro-/nanophytoplankton community was 70 ± 30% cyanobacteria, 22 ± 12% diatoms, 7 ± 3% dinoflagellates, and 1 ± 1% chrysophyte. Cyanobacteria (mainly containing *R. intracellularis*, *T. thiebautii*, *T. hildebrandtii*, *T. erythraeum*) were the numerically dominant component of the micro-/nanophytoplankton in the WPO. Obvious spatial variations in depth-weighted average abundances of micro-/nano-sized diatoms, dinoflagellates, and cyanobacteria were observed from northern stations to southern stations, with an increase in cyanobacteria, but a decrease in diatoms and dinoflagellates. Species in chrysophyte were recorded more sparsely among all sampling stations, only including *D. fibula*.

Depth-weighted average abundance of the total picophytoplankton was generally between 0.65 × 10^7 and 3.41 × 10^7 cells L^{-1} in the WPO, with lower abundance found at stations E130-18 and E130-20 (**Figure 3B**). Apparently, picophytoplankton abundance was nearly three to five orders of magnitude more abundant than micro/nanophytoplankton, indicating that picophytoplankton contributed a large proportion of the phytoplankton communities. This could be further confirmed by the significant fraction of picosized Chl *a* to the total, averaging 75 ± 7% and ranging from 62 to 84% (**Figure 3C**). At all stations, Pro (average 1.71 ± 1.04 × 10^7 cells L^{-1}) was typically more abundant than Syn (average 2.69 ± 1.73 × 10^6 cells L^{-1}) and PEuks (average 7.95 ± 2.88 × 10^5 cells L^{-1}). The relative proportions of Pro and Syn to total picophytoplankton abundance averaged 80 ± 12% and 15 ± 9%, respectively, suggesting that the picophytoplankton fraction was primarily characterized by a high abundance of picocyanobacteria (i.e., Pro and Syn).

Depth-weighted average concentration of the total Chl *a* was considerably low in the WPO, averaging 0.43 ± 0.11 μg L^{-1} (range, 0.19–0.55 μg L^{-1}, **Figure 3C**). The Chl *a* concentration in micro-/nanosized fraction (referred to as "micro/nano-Chl *a*") ranged from 0.05 to 0.21 μg L^{-1} (average, 0.11 ± 0.05 μg L^{-1}), and the average contribution of micro-/nano-Chl *a* to the total was 25 ± 7% (range, 16–38%). Picosized Chl *a* (referred to as "pico-Chl *a*") was typically between 0.14 and 0.41 μg L^{-1}, with an average of 0.32 ± 0.09 μg L^{-1}. Pico-Chl *a* was two- to

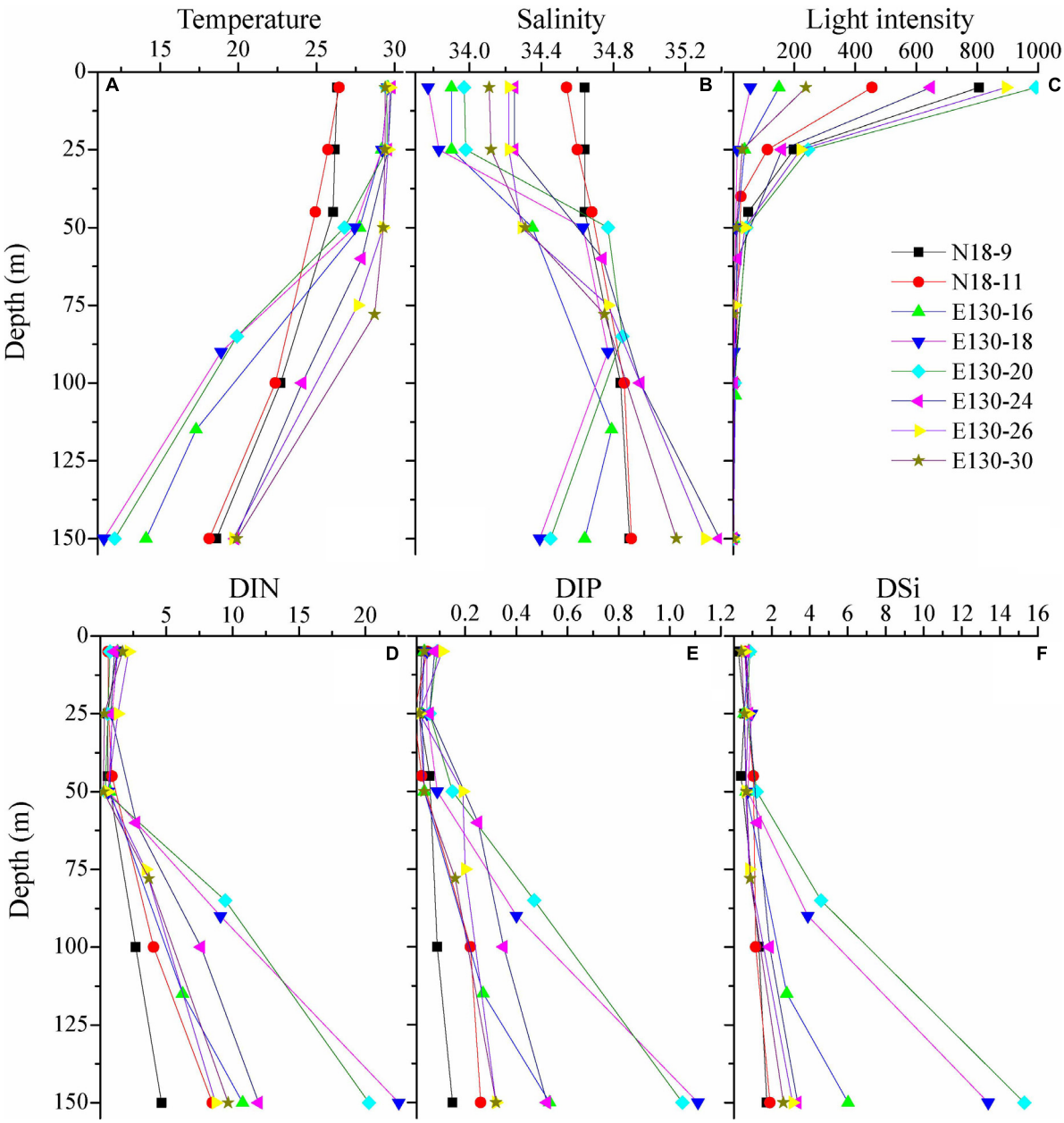

FIGURE 2 | Vertical profiles for **(A)** temperature (°C), **(B)** salinity, **(C)** light intensity (μmol quanta m^{-2} s^{-1}), and concentrations (μmol L^{-1}) of **(D)** dissolved inorganic nitrogen (DIN), **(E)** dissolved inorganic phosphorus (DIP), and **(F)** dissolved inorganic silicate (DSi). Symbols and colors represent different sampling stations as shown in **(C)**.

fourfold greater than micro-/nano-Chl *a* among stations, thus contributing a significant proportion of the total (∼75%).

FRRF-Derived Photophysiological Characteristics

NRM analysis revealed that FRRF-derived photophysiological parameters and primary production (JV_{PSII}-based PP_{max}) varied dramatically with depth in the upper Z_{eu} zone (0.1% surface light level; **Figure 4**). F_v/F_m was generally between 0.08 and 0.26 (average 0.16 ± 0.05, unitless), with a subsurface maximum of the curve fit found between 50 and 75 m depth (**Figure 4A**). Overall, F_v/F_m was low throughout the Z_{eu} and among stations. The curve fit for depth dependency of F_q'/F_m' (range, 0.02–0.22 and average 0.12 ± 0.05, unitless) analogously followed the fitting trend observed for F_v/F_m (**Figure 4B**); this is partly because there was a huge auto-correlation between these two parameters (r = 0.85, p < 0.01; **Figure 5A**). F_q'/F_v' showed a different depth-dependence pattern in vertical profile, averaging 0.74 ± 0.21 (range, 0.19–1.06, unitless; **Figure 4C**).

TABLE 2 | Mean values (±SD) of temperature (°C), salinity, and nutrient concentrations (μmol L^{-1}) at different sampling stations.

Stations/factors	Temperature	Salinity	DIN	DIP	DSi
N18-9	23.9 ± 3.4	34.7 ± 0.1	1.95 ± 0.73	0.07 ± 0.05	0.85 ± 0.64
N18-11	23.5 ± 3.4	34.7 ± 0.2	2.93 ± 1.42	0.11 ± 0.09	1.09 ± 0.51
E130-16	23.5 ± 7.3	34.3 ± 0.4	3.99 ± 1.44	0.18 ± 0.13	2.16 ± 1.35
E130-18	23.3 ± 7.9	34.3 ± 0.5	6.89 ± 2.42	0.34 ± 0.17	3.92 ± 2.45
E130-20	23.5 ± 7.5	34.4 ± 0.4	6.29 ± 2.71	0.36 ± 0.14	4.53 ± 2.23
E130-24	26.2 ± 4.3	34.7 ± 0.5	4.84 ± 1.82	0.25 ± 0.19	1.59 ± 1.11
E130-26	27.2 ± 4.3	34.6 ± 0.5	3.25 ± 1.23	0.16 ± 0.11	1.18 ± 0.07
E130-30	27.3 ± 4.2	34.5 ± 0.5	3.12 ± 1.91	0.11 ± 0.06	1.02 ± 0.91

DIN, dissolved inorganic nitrogen; DIP, dissolved inorganic phosphorus; DSi, dissolved inorganic silicate.

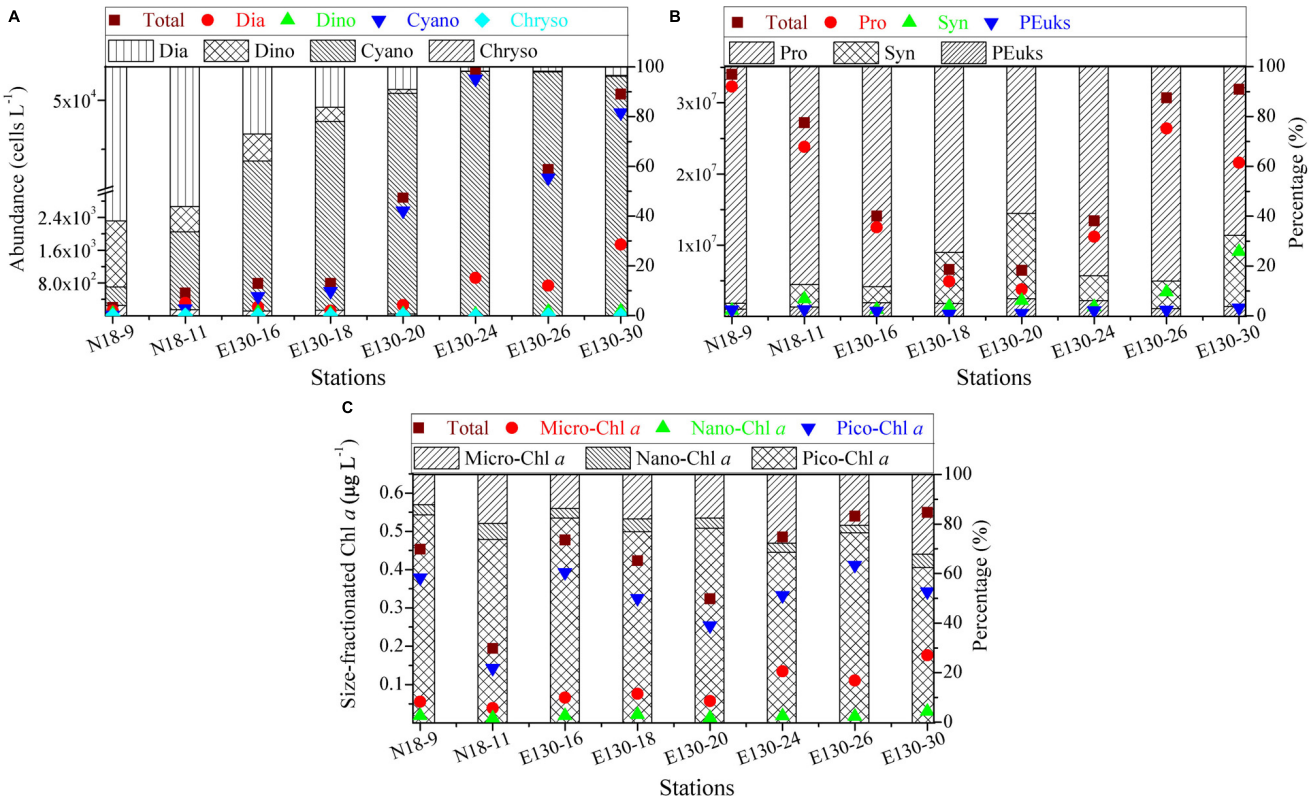

FIGURE 3 | Spatial variations in abundances (cells L^{-1}) of **(A)** micro-/nanophytoplankton and **(B)** picophytoplankton, and in concentrations (μg L^{-1}) of **(C)** size-fractionated Chl *a* along with the relative proportions of their respective components among sampling stations. Symbols and colors represent the depth-weighted averages of phytoplankton abundance and size-fractionated Chl *a* concentration, corresponding to the *y* axis on the left. Note the scale break in **(A)** and logarithmic scale in **(B)**. Different shades denote the fraction of total abundance or total Chl *a* concentration, respectively. Dia, diatoms, Dino, dinoflagellates, Cyano, cyanobacteria, Chryso, chrysophyte; Syn, *Synechococcus*, Pro, *Prochlorococcus*, PEuks, picoeukaryotes; micro-, nano-, and pico-Chl *a* represent micro-, nano-, and picosized phytoplankton Chl *a*, respectively.

The fitted profile for F_q'/F_v' had yet lower surface values and a shallower subsurface maximum estimating ~0.81 at 25 m (Model C, **Table 3**). The variation in F_q'/F_v' across all sampling stations was correlated to the variation in F_q'/F_m'(r = 0.59, p < 0.01; Eq. 1). NPQ_{NSV} was typically between 2.33 and 12.31 and averaged 5.95 ± 2.51 (unitless), and a trend of decreased NPQ_{NSV} with depth was observed in vertical curve fit (**Figure 4D**). Because of the endogenous changes in metabolic energy allocation, NPQ_{NSV} showed negative correlations with F_v/F_m (r = -0.97, p < 0.01; **Figure 5A**) and F_q'/F_m' (r = -0.87, p < 0.01). Compared to other depth-dependence profiles, σ_{PSII} was less variable (**Figure 4E**), ranging from 2.16 to 3.36 Å $RCII^{-1}$ with an average value of 2.76 ± 0.29 Å $RCII^{-1}$. There was no meaningful correlation between σ_{PSII} and other photophysiological parameters (p > 0.05). At all stations, ETR_{RCII} ranged from 0.02 to 5.89 mol e^- mol $RCII^{-1}$ s^{-1} (average, 1.33 ± 1.06 mol e^- mol $RCII^{-1}$ s^{-1}) within the upper Z_{eu} (**Figure 4F**). The curve-fitting ETR_{RCII} was generally

higher in the surface (~3.44 mol e^- mol $RCII^{-1}$ s^{-1}, Model F; **Table 3**), with a rapid decline at depths deeper than 15–25 m. A positive correlation was observed between ETR_{RCII} and JV_{PSII} ($r = 0.98$, $p < 0.01$; **Figure 5B**), suggesting that the overall JV_{PSII} variation was potentially driven by the ETR_{RCII}. Similarly, JV_{PSII} was maximum at the surface [0.16 electrons (PSII m^{-3}) s^{-1}] and declined with depth to a minimum value of 0.008 electrons (PSII m^{-3}) s^{-1} at 100 m (**Figure 4G**). The curve fit for depth dependency of JV_{PSII} showed a consistent trend with JV_{PSII}-based PP_{max} (**Figure 4H**, Eq. 3). Within the upper Z_{eu}, JV_{PSII}-based PP_{max} ranged from 0.04 to 8.59 mg C (mg chl a)$^{-1}$ h^{-1}, with an average value of 1.92 ± 1.41 mg C (mg chl a)$^{-1}$ h^{-1}. Both ETR_{RCII} and JV_{PSII}-based PP_{max} were negatively correlated with the alteration of photochemical efficiency (F_v/F_m, F_q'/F_m', F_q'/F_v'; $p < 0.05$), but positively correlated with NPQ_{NSV} ($p < 0.01$; **Figure 5**).

The curve fit in **Figures 4A–H** are results produced by models A–H, respectively.

Depth-weighted average values of FRRF-derived photophysiological parameters and JV_{PSII}-based PP_{max} were markedly different across all sampling stations (**Figure 6**). The depth-weighted average F_v/F_m (unitless) was higher at station E130-30 (0.22), but lower at stations N18-9 and E130-16, 26 (0.11–0.15). However, the spatial variability for depth-weighted average F_v/F_m and F_q'/F_m' were broadly similar ($r = 0.85$, $p < 0.01$). The depth-weighted average NPQ_{NSV} (unitless) was approximately twofold higher at stations N18-9 and E130-16, 26 (6.05–7.31) than at station E130-30 (3.58). At the eddy-sampled station E130-18, F_q'/F_v' was relatively higher, with the depth-weighted average of 0.91 (unitless), whereas σ_{PSII}, ETR_{RCII}, JV_{PSII}, and JV_{PSII}-based PP_{max} were lower than other stations. Among all stations, the spatial variations in depth-weighted averages of ETR_{RCII} and JV_{PSII} (JV_{PSII}-based PP_{max}) showed greater similarity ($r = 0.91$, $p < 0.01$): their values were much higher at stations N18-9 and E130-20.

DISCUSSION

Physiological and Ecological Responses of Photosynthetic Processes to Oceanic Properties

While our dataset is too small to draw general conclusions, our experimental results allow us to gain some physiological and ecological insights into how the dominant environmental constraints and algal species regulate the light absorption characteristics and electron transport and what is the key in driving the dynamics of WPO primary productivity. Light absorption parameters F_v/F_m and F_q'/F_m' showed positive correlations with size-fractionated Chl a ($p < 0.01$; **Figure 7**), suggesting that the light absorption characteristics in photosynthetic process are potentially controlled by the variability in phytoplankton communities (Suggett et al., 2009; Schuback et al., 2017; Zhu et al., 2019; Wei et al., 2019b). Certainly, this result appears to be exemplified to differing degrees by the significant relationships between F_v/F_m and large diatoms (cells > 2 μm), picosized Pro and PEuks (see **Figure 8A** below). With average DIN/DIP ratio notably less than the 16:1 Redfield ratio (**Figure 2** and **Table 2**), the growth of WPO phytoplankton communities are significantly limited by nutrient availability (Saito et al., 2002). As a physiological consequence of nutrient limitation (Oxborough et al., 2012; Jin et al., 2016; Zhu et al., 2016), F_v/F_m and F_q'/F_m' were considerably low throughout the Z_{eu} and among stations (**Figures 4**, **6**). From a photophysiological point of view, the photochemical efficiency in natural phytoplankton assemblages is indirectly affected by the nutrient level (Moore et al., 2006; Rabouille and Claquin, 2016; Schuback et al., 2016). Therefore, the variation in magnitude of F_v/F_m and F_q'/F_m' can be used as a predictor for nutrient use efficiency of marine ecosystems across considerable environmental gradients. However, only nutrient availability is inadequate to explain and predict the magnitude and variability of these derived light absorption parameters (Claquin et al., 2008; Lawrenz et al., 2013). Typically, variability in irradiance level was another primary driver of variability in F_v/F_m, F_q'/F_m', and F_q'/F_v' in the WPO ($p < 0.05$; **Figure 7**). The depth-specific fitting values of these light absorption characteristics we observed were higher at the subsurface (**Figure 4**), and one important explanation for this is that the interactive effects of light and nutrient levels lead to an increase in these light absorption parameters (Moore et al., 2006; Suggett et al., 2009; Zhu et al., 2019). In contrast, the strong effects of excess irradiance pressure and limitation by nutrients in the surface inhibited the F_v/F_m, F_q'/F_m', and F_q'/F_v' (**Figure 4**; Schuback et al., 2017; Wei et al., 2019b). Consistent with previous observations (Melrose et al., 2006; Claquin et al., 2008; Jin et al., 2016; Xie et al., 2018, etc.), variability in temperature exerted an evident influence on F_v/F_m and σ_{PSII} ($p < 0.05$; **Figure 7**). The fact that F_v/F_m and σ_{PSII} varied as a function of temperature does not necessarily imply a direct temperature effect on F_v/F_m and σ_{PSII}, as temperature can affect other photosynthetic complexes (Richardson et al., 2016). For instance, moderate heat stress is critical for the activity of RuBisCo enzyme in photosynthetic process (Jensen, 2000). Overall, on ecological scales, water temperature, light, and nutrient availability are important environmental variables in regulating the light absorption process.

NPQ_{NSV} was negatively correlated with the light absorption parameters F_v/F_m and F_q'/F_m' ($p < 0.01$; **Figure 5**), indicating that the photochemical efficiency in electron transport process may be limited by the expression of NPQ_{NSV} (alleviating excess energy pressure and minimizing the potential for photooxidative damage) (Müller et al., 2001; Schuback et al., 2016; Zhu et al., 2016). Indeed, we observed that NPQ_{NSV} was significantly correlated with PAR ($p < 0.05$; **Figure 7**), further demonstrating the strong effect of irradiance levels on the photosynthetic processes. As expected, we simulated a higher NPQ_{NSV} for surface phytoplankton assemblages (**Figure 4**), reflecting photophysiological adaptation to optimize photosynthesis under high irradiance level (Müller et al., 2001; Gao et al., 2012; Aardema et al., 2018). Nonparallel changes in the ETR_{RCII} and F_v/F_m, F_q'/F_m', and F_q'/F_v' ($p < 0.05$; **Figure 5**) imply a decoupling of light absorption at the level of RCII and electron transport in ETC, since the presence of NPQ_{NSV} and

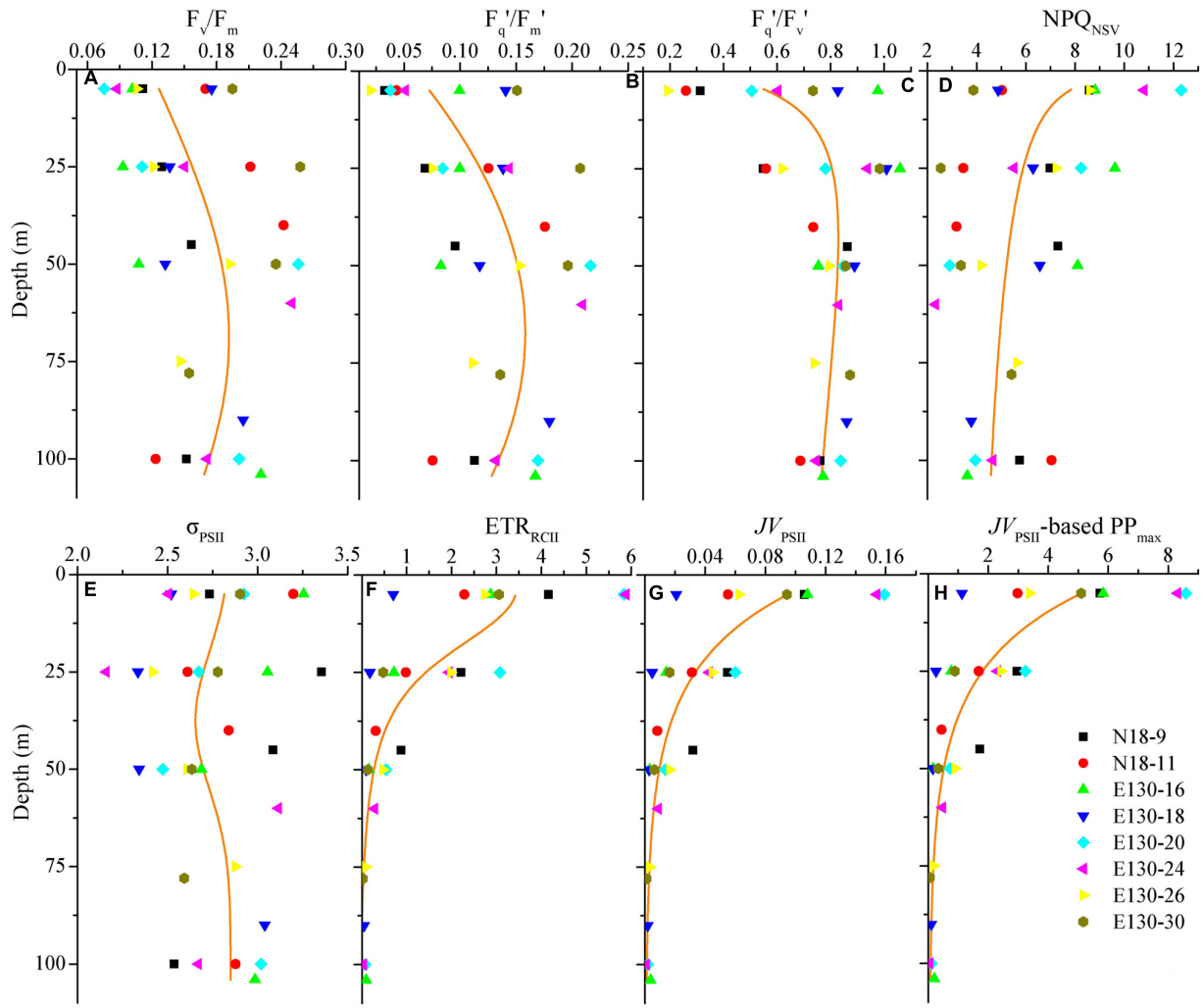

FIGURE 4 | Vertical profiles for photosynthetic parameters of **(A)** F_v/F_m, **(B)** F_q'/F_m', **(C)** F_q'/F_v', **(D)** NPQ_{NSV}, **(E)** σ_{PSII} (Å $RCII^{-1}$), **(F)** ETR_{RCII} (mol e^- mol $RCII^{-1}$ s^{-1}), **(G)** JV_{PSII} [electrons (PSII m^{-3}) s^{-1}], and **(H)** JV_{PSII}-based PP_{max} [mg C (mg chl *a*)$^{-1}$ h^{-1}]. Symbols and colors represent different sampling stations as shown in **(H)**. Solid lines denote the curve fit for the depth dependence of photosynthetic parameters and PP_{max}. Note that these curve fit are inferred from all data points of photosynthetic parameters and PP_{max} against depth according to the NRM models shown in **Table 3**.

TABLE 3 | The nonlinear regression model (NRM) models for the curve fit of photosynthetic parameters and PP_{max} vs. depth (*d*) along with the NRM-fitting variance (R^2) and two-tailed *t*-test (*p*).

NRM models	Parametric formulas	R^2	*p*
Model A	$\ln[(F_v/F_m) - 0.01] = -1.7 - (d - 69)^2/9{,}112$	0.31	$p < 0.0001$
Model B	$F_q'/F_m' = 256{,}240/[(d - 67)^2 + 106{,}227] - 2.25$	0.49	$p < 0.0001$
Model C	$\ln[(F_q'/F_v') - 0.31] = 4.64 - \ln(d) - [\ln(d/904.99)]^2/6.08$	0.42	$p < 0.0001$
Model D	$NPQ_{NSV} = 10.47d^{-0.17}$	0.34	$p < 0.0001$
Model E	$\ln(2.85-\sigma_{PSII}) = -1.66 - (d - 37)^2/614.6$	0.26	$p < 0.0001$
Model F	$ETR_{RCII} = 3.5/(1 + d^{2.75}/4{,}935) - 0.0037$	0.75	$p < 0.0001$
Model G	$JV_{PSII} = 42.07/[(d+ 3.37)^2 + 361.5] - 0.0025$	0.74	$p < 0.0001$
Model H	JV_{PSII}-based $PP_{max} = 2{,}270.69/[(d+ 3.37)^2 + 361.5] - 0.132$	0.74	$p < 0.0001$

increasing reductant are used for functions other than carbon fixation (Behrenfeld et al., 2002; Richardson et al., 2016). Due to excess irradiance energy in the surface water, the processes regulating electron transport and preventing overreduction in ETC are closely associated with the expression of NPQ_{NSV} (Smyth et al., 2004; Hughes et al., 2018). It is apparent that

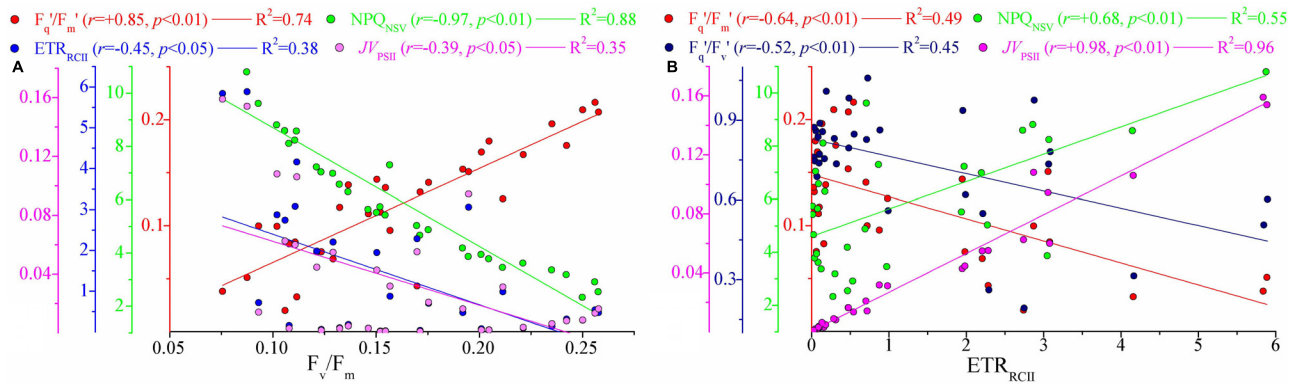

FIGURE 5 | Significant relationships among photophysiological parameters. **(A)** F_v/F_m vs. F_q'/F_m', NPQ_{NSV}, ETR_{RCII} (mol e^- mol $RCII^{-1}$ s^{-1}), and JV_{PSII} [electrons (PSII m^{-3}) s^{-1}]; **(B)** ETR_{RCII} (mol e^- mol $RCII^{-1}$ s^{-1}) *vs.* F_q'/F_m', NPQ_{NSV}, F_q'/F_v', and JV_{PSII} [electrons (PSII m^{-3}) s^{-1}]. Lines represent the least square regression, which is statistically significant for both cases (Spearman correlation coefficient *r*-, *p*-value, and regression variance R^2). Symbol color indicates different photosynthetic parameter. The colored *y*-axes correspond to the variability in magnitude of respective photosynthetic parameters. Note difference in *y*-axis scale.

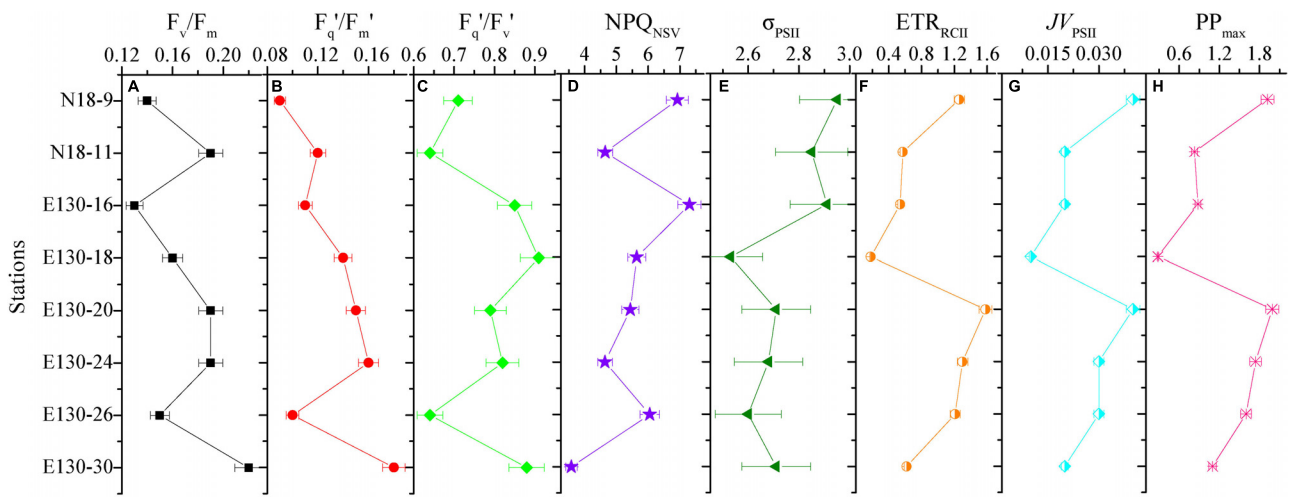

FIGURE 6 | Variability in the depth-weighted averages of fast repetition rate fluorometry (FRRF)-derived photophysiological properties and primary production for each station. **(A)** F_v/F_m, **(B)** F_q'/F_m', **(C)** F_q'/F_v', **(D)** NPQ_{NSV}, **(E)** σ_{PSII} (Å $RCII^{-1}$), **(F)** ETR_{RCII} (mol e^- mol $RCII^{-1}$ s^{-1}), **(G)** JV_{PSII} [electrons (PSII m^{-3}) s^{-1}], and **(H)** JV_{PSII}-based PP_{max} [mg C (mg chl *a*)$^{-1}$ h^{-1}]. The error presented with each depth-weighted average is the 95% confidence interval. Note difference in *x*-axis scale.

the NPQ_{NSV} process can effectively achieve energy-allocation balance, providing mechanistic insight into the decoupling of photosynthetic electron transport and carbon fixation and even the NPQ_{NSV}-based primary production (Schuback et al., 2015, 2016; Wei et al., 2019b). Thus, ETR_{RCII} and JV_{PSII}-based PP_{max} were closely correlated to NPQ_{NSV} ($p < 0.01$; **Figure 5**). In other words, changes in ETR_{RCII} and JV_{PSII}-based PP_{max} can be attributed to the NPQ_{NSV} process. Both ETR_{RCII} and JV_{PSII}-based PP_{max} showed significant temperature and light-dependent responses in natural phytoplankton assemblages ($p < 0.01$; **Figure 7**), suggesting that temperature and light are determinants in regulating the dynamics of ETR_{RCII} and PP_{max}. Based on this, we can thus conclude that the fitting trends of decreased ETR_{RCII} and PP_{max} with depth were controlled by temperature and light (**Figure 4**). Phytoplankton are acclimated to the high and variable light conditions of the surface layer to alleviate excess energy pressure through faster reoxidation of Q_A^- and a larger PQ pool (Schuback et al., 2017), resulting in the higher ETR_{RCII} we observed. On the other hand, photoacclimation to lower irradiance stimulates an increase in Chl *a* per cell near the subsurface, which, in turn, decreases the Chl *a*-normalized PP_{max} (Behrenfeld et al., 2002; Moore et al., 2006). Nutrients also had a potential effect on the variations in ETR_{RCII} and PP_{max} ($p < 0.05$; **Figure 7**), but negatively. This result is in good agreement with previous findings of Richardson et al. (2016) who found both the maximum rate of photosynthesis and the slope of the photosynthesis *vs.* light curve are negatively correlated with ambient nutrient concentration, thus indicating a possible influence of an interaction among light, temperature, and nutrient availability on ETR_{RCII} and PP_{max}.

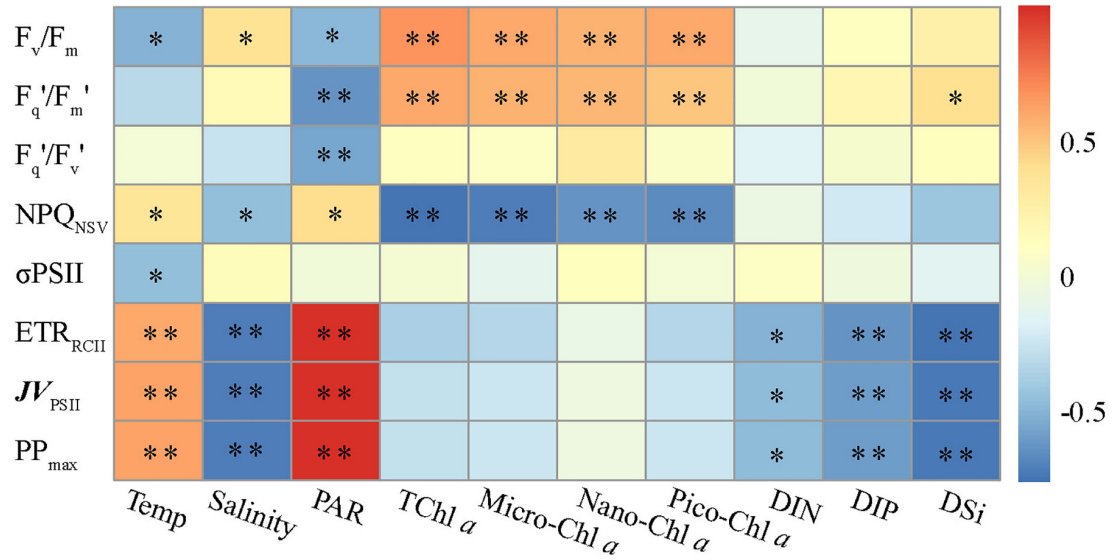

FIGURE 7 | Relationships between photosynthetic parameters and various environmental factors. Spearman correlation coefficients (*r*) ranged from negative to positive and are indicated by color intensity changing from dark blue to red, respectively. $^{**}p < 0.01$; $^{*}p < 0.05$ (two-tailed). Temp is temperature, TChl *a* is total Chl *a*. Micro-, nano-, and pico-Chl *a* represent micro-, nano-, and picosized phytoplankton Chl *a*, respectively. DIN, dissolved inorganic nitrogen; DIP, dissolved inorganic phosphorus; DSi, dissolved inorganic silicate.

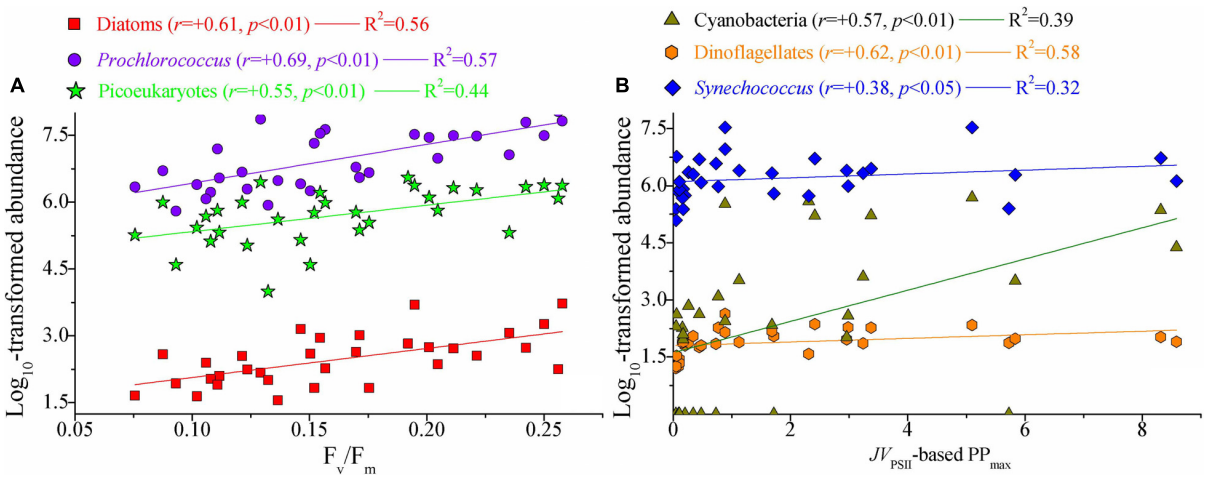

FIGURE 8 | Significant relationships between photosynthetic parameters and natural phytoplankton communities. **(A)** F_v/F_m *vs*. large diatoms, picosized Pro, and PEuks; **(B)** JV_{PSII}-based PP_{max} [mg C (mg chl *a*)$^{-1}$ h^{-1}] vs. cyanobacteria, dinoflagellates, and Syn. Lines represent the least square regression, which is statistically significant for both cases (Spearman correlation coefficient *r*-, *p*-value, and regression variance R^2). Symbols and colors represent different phytoplankton populations. Phytoplankton abundance (cells L^{-1}) data were log transformed prior to analysis. Note the difference in *x*-axis scale.

Collectively, these tight endogenous and exogenous regulations of the photosynthetic processes upstream from carbon fixation allow phytoplankton assemblages to balance light absorption with electron flow, electron transport, and carbon fixation (Müller et al., 2001; Murata et al., 2007; Schuback et al., 2017).

Photosynthetic Processes in Relation to Natural Phytoplankton Communities

Marine primary production estimates are highly dependent on assumptions regarding the photosynthetic potential of the resident phytoplankton communities (Richardson et al., 2016). Little is known, however, about the physiological and ecological responses of photosynthetic processes to natural phytoplankton populations. Such physiological and ecological effects of the photosynthetic response in relation to natural phytoplankton communities are clearly evident in our dataset (**Figure 8**). Light absorption parameter F_v/F_m was clearly correlated with large diatoms (cells > 2 μm), Pro and PEuks ($p < 0.01$). In marine ecosystems, F_v/F_m is known to vary systematically among taxonomic groups, but the highest recorded F_v/F_m

values (∼0.65–0.70) are measured for large diatoms (Suggett et al., 2003). The light harvesting antennas of diatoms are known as Chl *a*/*c* and fucoxanthin (Fx) binding proteins, or FCPs, and enable diatoms to efficiently adapt to rapidly changing light intensity. Recently, Pi et al. (2019) reported the structure of PSII-Fx Chl *a*/*c* binding protein supercomplex (PSII-FCPII) from the diatom *Chaetoceros gracilis*, and revealed that the distinct pigment-protein network of the PSII-FCPII supercomplex contributes to efficient light energy harvesting in the diatoms. In the present study, therefore, variation in F_v/F_m was closely associated with the large diatoms. There are two NPQ mechanisms in the diatoms, one associated with antenna units attached to PSII and the other associated with antenna units that detach from PSII (Miloslavina et al., 2009). In particular, the bindings of Chl *c* and Fx further enhance the capabilities of these NPQ mechanisms to dissipate excess energy when necessary (Wang et al., 2019), potentially resulting in the decoupling between large diatoms and JV_{PSII}-based PP_{max} on physiological and ecological scales. However, none of these NPQ mechanisms would be expected to affect the maximum photochemical efficiency (F_v/F_m) of photosynthesis in diatoms (Torres et al., 2014). Picocyanobacteria Pro is also characterized by relatively high values of F_v/F_m (0.55–0.65) (Bruyant et al., 2005). Values of F_v/F_m for picosized PEuks (e.g., *Aureococcus anophagefferens*) are typically between 0.3 and 0.4 (Suggett et al., 2009). Although F_v/F_m values in excess of 0.60 to 0.65 have been measured for some specific species of large cyanobacteria (i.e., *Cyanotheca* and *Anabaena*), values can be as low as 0.1–0.4 for most micro-/nanosized cyanobacteria (Berman-Frank et al., 2003). Phycobiliprotein (PBP) plays an exceptional role in light harvesting in cyanobacteria, but PBPs harvest light in the region of 490–650 nm where the Chl and carotenoids have poor light absorption properties (Campbell et al., 1998). On the other hand, the relatively low F_v/F_m values in large cyanobacteria may be attributed to the substantial phycocyanin concentrations, from which the fluorescence emission band overlaps with that from Chl *a* and, hence, leading to lower values for F_v/F_m (McConnell et al., 2002). However, picocyanobacteria Syn with low concentrations of phycocyanin still has relatively low values of F_v/F_m (Suggett et al., 2009). Overall, these significant correlations between F_v/F_m and algal species may be driven by photoacclimation or a number of evolutionary selection pressure related to the light absorption and energy transfer. The functional and structural advantages in the photosystems of the dominant algal species provide another possible rationale for the intimate correlations between F_v/F_m and algal species (Moore et al., 2003, 2006). Thus, it is not surprising that F_v/F_m correlated with large diatoms and Pro given they were the dominant components of micro-/nano- and picosized phytoplankton communities, respectively (**Figure 3**). As with F_v/F_m, F_q'/F_m' showed significant relations with large diatoms, picosized Pro, and PEuks ($p < 0.01$). The implication is that large diatoms, picosized Pro, and PEuks are the keys in driving the light absorption process.

JV_{PSII}-based PP_{max} was markedly associated with micro-/nanosized cyanobacteria and dinoflagellates, and picocyanobacteria Syn ($p < 0.05$). We suggest that these algal species may contribute significantly to the WPO primary production on ecological scales. Recently, the orange carotenoid protein (OCP), a carotenoid binding protein, has been found to exist quite widely in marine cyanobacteria, which has an advantage in coping with the excess excitation energy over other algae (Bailey and Grossman, 2008; Sedoud et al., 2014). We thus speculate that the presence of OCP may effectively regulate energy dissipation downstream of light absorption and improve the photosynthetic efficiency through more robust excitation energy transfer. In addition, NPQ_{NSV} in cyanobacteria is triggered by strong blue light, with almost no induction at wavelengths above 520 nm, the utilization of harvested light energy in cyanobacteria becomes more efficient (Bailey and Grossman, 2008). The significant relationship we found between JV_{PSII}-based PP_{max} and dinoflagellates and Syn agrees well with previous findings of Richardson et al. (2016) who found the dinoflagellates and Syn associated with a higher PP_{max} (the maximum rate of photosynthesis) than large diatoms. Differently, our earlier work in the Bay of Bengal has suggested that the variability in large diatoms and cyanobacteria appeared to be the major drivers of variability in gross primary production (Wei et al., 2019b). Given the wide diversity of the phytoplankton communities in marine ecosystems, therefore, we cannot use the region-specific relationships we find here as being universal for the global ocean. Richardson et al. (2016) proposed an explanation for the relatively large contribution of dinoflagellates to PP_{max} that a small number of dinoflagellates with large biovolume can provide the dominant biovolume in the phytoplankton communities, resulting in a greater increase in light absorption capability and energy transfer efficiency. This involves changes in many relevant biochemical or physiological processes such as package effect, area of photosynthetic membrane space available, cellular resources required for the production of RCII, and membrane intrinsic antennae (Suggett et al., 2009). Another possibility, to some extent, is that some dinoflagellates under natural environments may have more efficient photosynthesis than other algal species. As discussed above, large diatoms and picocyanobacteria Pro showed a relatively high F_v/F_m but were not associated with PP_{max}. This fits well with the fact that F_v/F_m was negatively correlated with JV_{PSII}-based PP_{max} (r = -0.39, $p < 0.05$), since the presence of NPQ_{NSV} process and additional reductant are used for functions. Additionally, this negative correlation may arguably be the results of photoacclimation and the influences of temperature and nutrient concentration. That photosynthetic parameters are closely related to different taxonomic groups provides some implications for improving the parameterization of the factors influencing photosynthetic potential, although not universal for the global ocean under all conditions. It is well known that the physical processes in the ocean play important roles in affecting primary production (Falkowski et al., 1991; Furuya et al., 1998). In the present study, however, we did not find any evidence that the Kuroshio and cold eddy have specific or one-way effects on the photosynthetic performance in the WPO. This is arguably because the photosynthetic processes are interactively influenced by complex abiotic and biotic variables in marine ecosystems, rather than by a single variable.

DATA AVAILABILITY STATEMENT

All datasets presented in this study are included in the article/supplementary material.

AUTHOR CONTRIBUTIONS

JS and YW designed the experiment. YW and QZ collected the samples. YW, ZC, CG, and QZ performed the sample analysis. YW wrote the manuscript, with contribution from all authors. All authors read and approved the final manuscript.

FUNDING

This research was financially supported by the National Key Research and Development Project of China (2019YFC1407805), the National Natural Science Foundation of China (41876134, 41676112, and 41276124), the Key Project of Natural Science Foundation for Tianjin (17JCZDJC40000), the University Innovation Team Training Program for Tianjin (TD12-5003), the Tianjin 131 Innovation Team Program (20180314), and the Changjiang Scholars Program of Chinese Ministry of Education (T2014253) to JS.

REFERENCES

Aardema, H. M., Rijkeboer, M., Lefebvre, A., Veen, A., and Kromkamp, J. C. (2018). High resolution in situ measurements of phytoplankton photosynthesis and abundance in the Dutch North Sea. *Ocean Sci. Discuss.* 1–37.

Bailey, S., and Grossman, A. R. (2008). Photoprotection in cyanobacteria: regulation of light harvesting†. *Photochem. Photobiol.* 84, 1410–1420. doi: 10.1111/j.1751-1097.2008.00453.x

Behrenfeld, M. J., Maranon, E., Siegel, D., and Hooker, S. B. (2002). Photoacclimation and nutrient-based model of light-saturated photosynthesis for quantifying oceanic primary production. *Mar. Ecol. Prog. Ser.* 228, 103–117. doi: 10.3354/meps228103

Berman-Frank, I., Lundgren, P., and Falkowski, P. (2003). Nitrogen fixation and photosynthetic oxygen evolution in cyanobacteria. *Res. Microbiol.* 154, 157–164. doi: 10.1016/s0923-2508(03)00029-9

Bruyant, F., Babin, M., Genty, B., Prasil, O., Behrenfeld, M. J., and Claustre, H. (2005). Diel variations in the photosynthetic parameters of *Prochlorococcus* strain pcc 9511: combined effects of light and cell cycle. *Limnol. Oceanogr.* 50, 850–863. doi: 10.4319/lo.2005.50.3.0850

Brzezinski, M. A., and Nelson, D. M. (1995). The annual silica cycle in the sargasso sea near bermuda. *Deep Sea Res. Part I Oceanogr. Res. Pap.* 42, 1215–1237. doi: 10.1016/0967-0637(95)93592-3

Campbell, D., Hurry, V., Clarke, A. K., Gustafsson, P., and Oquist, G. (1998). Chlorophyll fluorescence analysis of cyanobacterial photosynthesis and acclimation. *Microbiol. Mol. Biol. Rev.* 62, 667–683. doi: 10.1128/mmbr.62.3.667-683.1998

Claquin, P., Probert, I., Lefebvre, S., and Veron, B. (2008). Effects of temperature on photosynthetic parameters and TEP production in eight species of marine microalgae. *Aquat. Microb. Ecol.* 51, 1–11. doi: 10.3354/ame01187

Falkowski, P. G., Ziemann, D., Kolber, Z., and Bienfang, P. K. (1991). Role of eddy pumping in enhancing primary production in the ocean. *Nature* 352, 55–58. doi: 10.1038/352055a0

Furuya, K., Hasegawa, O., Yoshikawa, T., and Taguchi, S. (1998). Photosynthesis-irradiance relationship of phytoplankton and primary production in the vicinity of kuroshio warm core ring in spring. *J. Oceanogr.* 54, 545–552. doi: 10.1007/bf02742456

Gao, K., Beardall, J., Häder, D. P., Hall-Spencer, J. M., Gao, G., and Hutchins, D. A. (2019). Effects of ocean acidification on marine photosynthetic organisms under the concurrent influences of warming, UV radiation and deoxygenation. *Front. Mar. Sci.* 6:322. doi: 10.3389/fmars.2019.00322

Gao, K., Xu, J., Gao, G., Li, Y., Hutchins, D. A., Huang, B., et al. (2012). Rising CO2 and increased light exposure synergistically reduce marine primary productivity. *Nat. Clim. Change* 2, 519–523. doi: 10.1038/nclimate1507

Hoppe, C. J., Holtz, L. M., Trimborn, S., and Rost, B. (2015). Ocean acidification decreases the light-use efficiency in an A ntarctic diatom under dynamic but not constant light. *New Phytol.* 207, 159–171. doi: 10.1111/nph.13334

Hughes, D. J., Varkey, D., Doblin, M. A., Ingleton, T., Mcinnes, A., Ralph, P. J., et al. (2018). Impact of nitrogen availability upon the electron requirement for carbon fixation in Australian coastal phytoplankton communities. *Limnol. Oceanogr.* 63, 1891–1910. doi: 10.1002/lno.10814

Jensen, R. G. (2000). Activation of Rubisco regulates photosynthesis at high temperature and CO2. *Proc. Natl. Acad. Sci. U.S.A.* 97, 12937–12938. doi: 10.1073/pnas.97.24.12937

Jiao, N., Yang, Y., Hong, N., Ma, Y., Harada, S., Koshikawa, H., et al. (2005). Dynamics of autotrophic picoplankton and heterotrophic bacteria in the east china sea. *Cont. Shelf Res.* 25, 1265–1279. doi: 10.1016/j.csr.2005.01.002

Jin, P., Gao, G., Liu, X., Li, F., Tong, S., Ding, J., et al. (2016). Contrasting photophysiological characteristics of phytoplankton assemblages in the Northern South China Sea. *PLoS One* 11:e0153555. doi: 10.1371/journal.pone.0153555

Karl, D. M., and Tien, G. (1992). MAGIC: a sensitive and precise method for measuring dissolved phosphorus in aquatic environments. *Limnol. Oceanogr.* 37, 105–116. doi: 10.4319/lo.1992.37.1.0105

Kolber, Z. S., Prášil, O., and Falkowski, P. G. (1998). Measurements of variable chlorophyll fluorescence using fast repetition rate techniques: defining methodology and experimental protocols. *Biochim. Biophys. Acta Bioenerget.* 1367, 88–106. doi: 10.1016/s0005-2728(98)00135-2

Lawrenz, E., Silsbe, G., Capuzzo, E., Ylöstalo, P., Forster, R. M., Simis, S. G., et al. (2013). Predicting the electron requirement for carbon fixation in seas and oceans. *PLoS One* 8:e58137. doi: 10.1371/journal.pone.0058137

McConnell, M. D., Koop, R., Vasil'ev, S., and Bruce, D. (2002). Regulation of the distribution of chlorophyll and phycobilin-absorbed excitation energy in cyanobacteria. A structure-based model for the light state transition. *Plant Physiol.* 130, 1201–1212. doi: 10.1104/pp.009845

Melrose, D. C., Oviatt, C. A., O'Reilly, J. E., and Berman, M. S. (2006). Comparisons of fast repetition rate fluorescence estimated primary production and 14C uptake by phytoplankton. *Mar. Ecol. Prog. Ser.* 311, 37–46. doi: 10.3354/meps311037

Miloslavina, Y., Grouneva, I., Lambrev, P. H., Lepetit, B., Goss, R., Wilhelm, C., et al. (2009). Ultrafast fluorescence study on the location and mechanism of non-photochemical quenching in diatoms. *Biochim. Biophys. Acta Bioenerget.* 1787, 1189–1197. doi: 10.1016/j.bbabio.2009.05.012

Moore, C. M., Suggett, D., Holligan, P. M., Sharples, J., Abraham, E. R., Lucas, M. I., et al. (2003). Physical controls on phytoplankton physiology and production at a shelf sea front: a fast repetition-rate fluorometer based field study. *Mar. Ecol. Prog. Ser.* 259, 29–45. doi: 10.3354/meps259029

Moore, C. M., Suggett, D. J., Hickman, A. E., Kim, Y. N., Tweddle, J. F., Sharples, J., et al. (2006). Phytoplankton photoacclimation and photoadaptation in response to environmental gradients in a shelf sea. *Limnol. Oceanogr.* 51, 936–949. doi: 10.4319/lo.2006.51.2.0936

Morelle, J., and Claquin, P. (2018). Electron requirements for carbon incorporation along a diel light cycle in three marine diatom species. *Photosynth. Res.* 137, 201–214. doi: 10.1007/s11120-018-0491-2

Müller, P., Li, X. P., and Niyogi, K. K. (2001). Non-photochemical quenching. A response to excess light energy. *Plant Physiol.* 125, 1558–1566. doi: 10.1104/pp.125.4.1558

Murata, N., Takahashi, S., Nishiyama, Y., and Allakhverdiev, S. I. (2007). Photoinhibition of photosystem II under environmental stress. *Biochim. Biophys. Acta* 1767, 414–421. doi: 10.1016/j.bbabio.2006.11.019

Oxborough, K., Hanlon, A. R. M., Underwood, G. J. C., and Baker, N. R. (2000). In vivo estimation of the photosystem II photochemical efficiency of individual

microphytobenthic cells using high-resolution imaging of chlorophyll a fluorescence. *Limnol. Oceanogr.* 45, 1420–1425. doi: 10.4319/lo.2000.45.6.1420

Oxborough, K., Moore, C. M., Suggett, D. J., Lawson, T., Chan, H. G., and Geider, R. J. (2012). Direct estimation of functional PSII reaction center concentration and PSII electron flux on a volume basis: a new approach to the analysis of Fast Repetition Rate fluorometry (FRRf) data. *Limnol. Oceanogr. Methods* 10, 142–154. doi: 10.4319/lom.2012.10.142

Pi, X., Zhao, S., Wang, W., Liu, D., Xu, C., Han, G., et al. (2019). The pigment-protein network of a diatom photosystem II-light-harvesting antenna supercomplex. *Science* 365:eaax4406. doi: 10.1126/science.aax4406

Rabouille, S., and Claquin, P. (2016). Photosystem-II shutdown evolved with N itrogen fixation in the unicellular diazotroph C rocosphaera watsonii. *Environ. Microbiol.* 18, 477–485. doi: 10.1111/1462-2920.13157

Richardson, K., Bendtsen, J., Kragh, T., and Mousing, E. A. (2016). Constraining the distribution of photosynthetic parameters in the Global Ocean. *Front. Mar. Sci.* 3:269. doi: 10.3389/fmars.2016.00269

Saito, H., Tsuda, A., and Kasai, H. (2002). Nutrient and plankton dynamics in the Oyashio region of the western subarctic Pacific Ocean. *Deep Sea Res. Part IITop. Stud. Oceanogr.* 49, 5463–5486. doi: 10.1016/s0967-0645(02)00204-7

Schuback, N., Flecken, M., Maldonado, M. T., and Tortell, P. D. (2016). Diurnal variation in the coupling of photosynthetic electron transport and carbon fixation in iron-limited phytoplankton in the NE subarctic Pacific. *Biogeosciences* 13, 16803–16845. doi: 10.5194/bgd-12-16803-2015

Schuback, N., Hoppe, C. J., Tremblay, J. É, Maldonado, M. T., and Tortell, P. D. (2017). Primary productivity and the coupling of photosynthetic electron transport and carbon fixation in the Arctic Ocean. *Limnol. Oceanogr.* 62, 898–921. doi: 10.1002/lno.10475

Schuback, N., Schallenberg, C., Duckham, C., Maldonado, M. T., and Tortell, P. D. (2015). Interacting effects of light and iron availability on the coupling of photosynthetic electron transport and CO2-assimilation in marine phytoplankton. *PLoS One* 10:e0133235. doi: 10.1371/journal.pone.0133235

Schuback, N., and Tortell, P. D. (2019). Diurnal regulation of photosynthetic light absorption, electron transport and carbon fixation in two contrasting oceanic environments. *Biogeosciences* 16, 1381–1399. doi: 10.5194/bg-16-1381-2019

Sedoud, A., Lopezigual, R., Rehman, A. U., Wilson, A., Perreau, F., Boulay, C., et al. (2014). The cyanobacterial photoactive orange carotenoid protein is an excellent singlet oxygen quencher. *Plant Cell* 26, 1781–1791. doi: 10.1105/tpc.114.123802

Smyth, T. J., Pemberton, K. L., Aiken, J., and Geider, R. J. (2004). A methodology to determine primary production and phytoplankton photosynthetic parameters from fast repetition rate fluorometry. *J. Plankton Res.* 26, 1337–1350. doi: 10.1093/plankt/fbh124

Suggett, D. J., Moore, C. M., Hickman, A. E., and Geider, R. J. (2009). Interpretation of fast repetition rate (FRR) fluorescence: signatures of phytoplankton community structure versus physiological state. *Mar. Ecol. Prog. Ser.* 376, 1–19. doi: 10.3354/meps07830

Suggett, D. J., Oxborough, K., Baker, N. R., MacIntyre, H. L., Kana, T. M., and Geider, R. J. (2003). Fast repetition rate and pulse amplitude modulation chlorophyll a fluorescence measurements for assessment of photosynthetic electron transport in marine phytoplankton. *Eur. J. Phycol.* 38, 371–384. doi: 10.1080/09670260310001612655

Sun, J., and Liu, D. (2003). Geometric models for calculating cell biovolume and surface area for phytoplankton. *J. Plankton Res.* 25, 1331–1346. doi: 10.1093/plankt/fbg096

Torres, M. A., Ritchie, R. J., Lilley, R., Grillet, C., and Larkum, A. (2014). Measurement of photosynthesis and photosynthetic efficiency in two diatoms. *N. Z. J. Bot.* 52, 6–27. doi: 10.1080/0028825x.2013.831917

Wang, W., Yu, L., Xu, C., Tomizaki, T., Zhao, S., Umena, Y., et al. (2019). Structural basis for blue-green light harvesting and energy dissipation in diatoms. *Science* 363:eaav0365. doi: 10.1126/science.aav0365

Wei, Y., Liu, H., Zhang, X., Xue, B., Munir, S., and Sun, J. (2017). Physicochemical conditions in affecting the distribution of spring phytoplankton community. *Chin. J. Oceanol. Limnol.* 35, 1342–1361. doi: 10.1007/s00343-017-6190-6

Wei, Y., Sun, J., Zhang, X., Wang, J., and Huang, K. (2019a). Picophytoplankton size and biomass around equatorial eastern Indian Ocean. *MicrobiologyOpen* 8:e00629. doi: 10.1002/mbo3.629

Wei, Y., Zhao, X., and Sun, J. (2019b). Fast repetition rate fluorometry (FRRF) derived phytoplankton primary productivity in the Bay of Bengal. *Front. Microbiol.* 10:1164. doi: 10.3389/fmicb.2019.01164

Welschmeyer, N. A. (1994). Fluorometric analysis of chlorophyll a in the presence of chlorophyll b and pheopigments. *Limnol. Oceanogr.* 39, 1985–1992. doi: 10.4319/lo.1994.39.8.1985

Xie, Y., Laws, E. A., Yang, L., and Huang, B. (2018). Diel patterns of variable fluorescence and carbon fixation of picocyanobacteria *Prochlorococcus*-dominated phytoplankton in the South China Sea basin. *Front. Microbiol.* 9:1589. doi: 10.3389/fmicb.2018.01589

Zhu, Y., Ishizaka, J., Tripathy, S. C., Wang, S., Mino, Y., Matsuno, T., et al. (2016). Variation of the photosynthetic electron transfer rate and electron requirement for daily net carbon fixation in Ariake Bay. Japan. *J. Oceanogr.* 72, 761–776. doi: 10.1007/s10872-016-0370-4

Zhu, Y., Suggett, D., Liu, C., He, J., Lin, L., Le, F., et al. (2019). Primary productivity dynamics in the summer Arctic Ocean confirms broad regulation of the electron requirement for carbon fixation by light-phytoplankton community interaction. *Front. Mar. Sci.* 6:275. doi: 10.3389/fmars.2019.00275

Conflict of Interest: The authors declare that the research was conducted in the absence of any commercial or financial relationships that could be construed as a potential conflict of interest.

frontiers in Microbiology

ORIGINAL RESEARCH
published: 15 December 2020
doi: 10.3389/fmicb.2020.612053

Elevated Contribution of Low Nucleic Acid Prokaryotes and Viral Lysis to the Prokaryotic Community Along the Nutrient Gradient From an Estuary to Open Ocean Transect

Chen Hu[1,2], Xiaowei Chen[1,2], Liuqian Yu[3], Dapeng Xu[1,2] and Nianzhi Jiao[1,2]**

[1] State Key Laboratory of Marine Environmental Science, College of Ocean and Earth Sciences, Institute of Marine Microbes and Ecospheres, Xiamen University, Xiamen, China, [2] Fujian Key Laboratory of Marine Carbon Sequestration, Xiamen University, Xiamen, China, [3] Department of Ocean Science, The Hong Kong University of Science and Technology, Hong Kong, China

OPEN ACCESS

Edited by:
Jun Sun, Tianjin University of Science and Technology, China

Reviewed by:
Gwo-Ching Gong, National Taiwan Ocean University, Taiwan
Anne-Claire Baudoux, Centre National de la Recherche Scientifique (CNRS), France

***Correspondence:**
Dapeng Xu
dapengxu@xmu.edu.cn
Nianzhi Jiao
jiao@xmu.edu.cn

Specialty section:
This article was submitted to Aquatic Microbiology, a section of the journal Frontiers in Microbiology

Received: *30 September 2020*
Accepted: *20 November 2020*
Published: *15 December 2020*

Citation:
Hu C, Chen X, Yu L, Xu D and Jiao N (2020) Elevated Contribution of Low Nucleic Acid Prokaryotes and Viral Lysis to the Prokaryotic Community Along the Nutrient Gradient From an Estuary to Open Ocean Transect. Front. Microbiol. 11:612053. doi: 10.3389/fmicb.2020.612053

Prokaryotes represent the largest living biomass reservoir in aquatic environments and play a crucial role in the global ocean. However, the factors that shape the abundance and potential growth rate of the ecologically distinct prokaryotic subgroups [i.e., high nucleic acid (HNA) and low nucleic acid (LNA) cells] along varying trophic conditions in the ocean remain poorly understood. This study conducted a series of modified dilution experiments to investigate how the abundance and potential growth rate of HNA and LNA prokaryotes and their regulating factors (i.e., protozoan grazing and viral lysis) change along a cross-shore nutrient gradient in the northern South China Sea. The results showed that the abundance of both HNA and LNA cells was significantly positively correlated with the abundance of heterotrophic nanoflagellates and viruses, whereas only HNA abundance exhibited a significant positive correlation with nutrient level. With a decreasing nutrient concentration, the potential growth rate of the HNA subgroup declined significantly, while that of the LNA subgroup was significantly enhanced, leading to an elevated relative potential growth rate of the LNA to HNA subgroup under decreasing nutrient levels. Furthermore, our data revealed different regulatory roles of protozoan grazing and viral lysis on the HNA and LNA subgroups, with HNA suffering higher mortality pressure from grazing than from lysis in contrast to LNA, which experienced equivalent pressures. As the nutrient levels declined, the relative contribution of lysis to the mortality of the HNA subgroup increased significantly, in contrast to the insignificant change in that of the LNA subgroup. Our results indicated the elevated role of LNA cells in the prokaryotic community and the enhanced viral lysis pressure on the total prokaryotes under oligotrophic conditions. This implies a weakened efficiency of carbon cycling within the microbial loop and enhanced viral lysis to shunt more carbon and energy flow in the future ocean, in which oligotrophication will be strengthened due to global warming.

Keywords: HNA and LNA prokaryotes, protozoan grazing, viral lysis, nutrient gradient, northern South China Sea

INTRODUCTION

Representing the largest living biomass reservoir (Suttle, 2007) and critical components of the microbial loop (Azam et al., 1983) in aquatic environments, prokaryotes play a crucial role in biogeochemical cycling in the global ocean. Consequently, even subtle changes in prokaryotic abundance and metabolic activity in response to varying environmental conditions would be amplified to substantially affect the structure and function of the marine ecosystem (Edwards and Richardson, 2004; Morán et al., 2010). Comprehensive knowledge of how the abundance and metabolic activity of prokaryotes and their regulating factors react to changes in the marine environment, such as the strengthened ocean oligotrophication due to the global warming-enhanced stratification (Agusti et al., 2017), is thus of critical importance.

The flow cytometry technique has revealed that prokaryotes cluster into high nucleic acid (HNA) cells and low nucleic acid (LNA) cells, and the two subgroups may be physiologically and ecologically distinct (Li et al., 1995; Gasol et al., 1999; Bouvier et al., 2007). Initially, the HNA cells were proposed to be the more dynamic and actively growing fraction of the prokaryotic community (Lebaron et al., 2001; Servais et al., 2003), while the LNA cells were considered to be the potentially dormant or dead cells (Jellett et al., 1996; Gasol et al., 1999). Such a view was later challenged when the LNA cells were found to exhibit substantial heterotrophic activity, comparable to that of the HNA cells (Zubkov et al., 2001; Longnecker et al., 2005; Scharek and Latasa, 2007; Huete-Stauffer and Morán, 2012). Indeed, the LNA cells, such as SAR11 bacteria, have small, streamlined genomes, and limited genetic repertoires and thereby a lower metabolic rate, weakened capability to utilize dissolved organic carbon (DOC), and narrower breadth of potential ecological niches (Giovannoni et al., 2005; Giovannoni, 2017). However, the compact genomes that LNA cells possess reduce their metabolic burden of replication under low resource availability, enabling them to gain a competitive advantage over HNA cells when or where nutrients are limited (Servais et al., 2003; Longnecker et al., 2005, 2006; Mojica et al., 2019). A natural hypothesis follows that the relative potential growth rate of LNA cells over HNA cells may increase as the aquatic environment becomes more oligotrophic. This hypothesis and the underlying roles of the potentially different regulating factors of the HNA and LNA subgroups, as of now, have not been investigated.

It is widely recognized that prokaryotic abundance and potential growth rate are dynamically controlled by both bottom-up (i.e., resource availability such as the inorganic nutrients) (Church, 2008) and top-down (i.e., mortality mediated by protozoan grazing and viral lysis) (Sanders et al., 1992; Thingstad and Lignell, 1997) factors. Among the top-down regulators, protozoa are the dominating grazers of prokaryotes and can transfer as much as 100% of the prokaryotic production to higher trophic levels in the ocean (Vazquez-Dominguez et al., 2006; Pearce et al., 2010), whereas viral lysis can contribute to 10–50% of daily prokaryotic mortality (Weinbauer et al., 2002) and is found to have a comparable contribution as that of protozoan grazing in particular situations (Fuhrman and Noble, 1995). In contrast to protozoan grazing, the viral lysis of prokaryotes causes the release of cellular material that is rich in organic matter into the surrounding environment for easy uptake by prokaryotes and thus redirects carbon and energy fluxes from higher trophic levels toward heterotrophic microbial processing (termed as "viral shunt") (Suttle, 2005).

Previous studies demonstrated that the relative importance of protozoan grazing and viral lysis on prokaryotes varies by trophic status (Bettarel et al., 2004; Danovaro et al., 2008; Tsai et al., 2013b) and water depth (Nagata et al., 2010; Tsai et al., 2016; Lara et al., 2017). Furthermore, the relative contribution of the two top-down factors may be affected by the physiological state of different prokaryotic subgroups, which in turn shapes the community composition of prokaryotic assemblages (del Giorgio and Gasol, 2008). Several studies have observed that more active prokaryotic subgroups such as the HNA cells are preferentially grazed by protozoa (i.e., so-called selective grazing) (Gonzalez et al., 1990; del Giorgio et al., 1996; Sintes and del Giorgio, 2014; Baltar et al., 2016), whereas less active subgroups such as the LNA cells prevent heavy grazing because of their intrinsic low metabolic rates and small size, and thereby can achieve persistence and dominance under situations of strong grazing pressure (Segovia et al., 2018). Likewise, viruses are also recognized to exert disproportionately larger impacts on the dominant and fast-growing prokaryotic subgroup, following the "kill the winner" hypothesis, because viral replication largely relies on a host's metabolic machinery and energy supply (Fuhrma and Suttle, 1993; Weinbauer, 2004; Chen et al., 2019a). However, strong top-down impact of viruses on SAR11 cells, the typical LNA prokaryotic subgroup, has been observed in an oligotrophic ocean (Zhao et al., 2013). This suggests that viruses can significantly impact LNA cells in contrast to protozoan grazing that is generally reported to place greater pressure on HNA over LNA cells. Such distinct regulating impacts by grazing and lysis on prokaryotic subgroups of different physiological states may contribute to the hypothesis mentioned above, namely, the elevated role of LNA cells in the prokaryotic community under more oligotrophic conditions. This, to the best of our knowledge, has not been explored yet.

This study aims to investigate how the abundance and potential growth rate of two distinct prokaryotic subgroups (i.e., HNA and LNA) and their regulating factors, including protozoan grazing and viral lysis, change under different trophic conditions in the natural environment. A series of modified dilution experiments were conducted along a transect spanning the nutrient-rich coastal zone to an area of nutrient-depleted open ocean in the northern South China Sea (SCS) in November 2016. Being the largest marginal sea in the northern Pacific, the SCS is an ideal testbed because it harbors both a river-dominated shelf region (i.e., the northern shelf is affected by large freshwater and terrestrial inputs from the Pearl River) and a vast area of an oligotrophic deep basin, facilitating the investigation of the differing regulatory impacts of protozoan grazing and viral

lysis on the HNA and LNA subgroups under various nutrient conditions in the ocean.

MATERIALS AND METHODS

Study Sites and Sampling

Six sampling sites along a transect spanning the shelf water neighboring the Pearl River Estuary (PRE) to the deep basin of the northern SCS (**Figure 1**) were visited during a research cruise in November 2016. Water temperature and salinity were derived from a probe mounted on the CTD rosette (SBE9/11 plus, Sea-Bird Electronics Inc., United States) (**Supplementary Table 1**), and water samples were collected using 10-L Niskin bottles. The concentrations of nitrate (NO_3^-), nitrite (NO_2^-), silicate (SiO_3^{2-}), and phosphate (PO_4^{3-}) in the samples were determined by using an Auto Analysis III, AA3 instrument (Bran-Luebbe, Germany) in the main lab. Hereinafter, the sum of the nitrate and nitrite concentrations is referred to as the dissolved inorganic nitrogen (DIN). Samples for biological analysis, including prokaryotic and viral abundance, were prefiltered through 20-μm mesh filters to remove large particles and zooplankton.

Abundance of Prokaryotes and Virus-Like Particles

Samples for determining abundance of prokaryotes and virus-like particles (VLP) were prepared via the following steps: 2-mL samples were fixed with glutaraldehyde at a final concentration of 0.5%, held at room temperature for 15 min in the dark, shock-frozen in liquid nitrogen, and stored at −80°C until analysis. Prokaryotic abundance was determined using flow cytometry (BD Accuri C6, United States) with a laser emitting light at 488 nm. Prior to analysis, the samples were thawed to room temperature, and 990-μL subsamples were stained

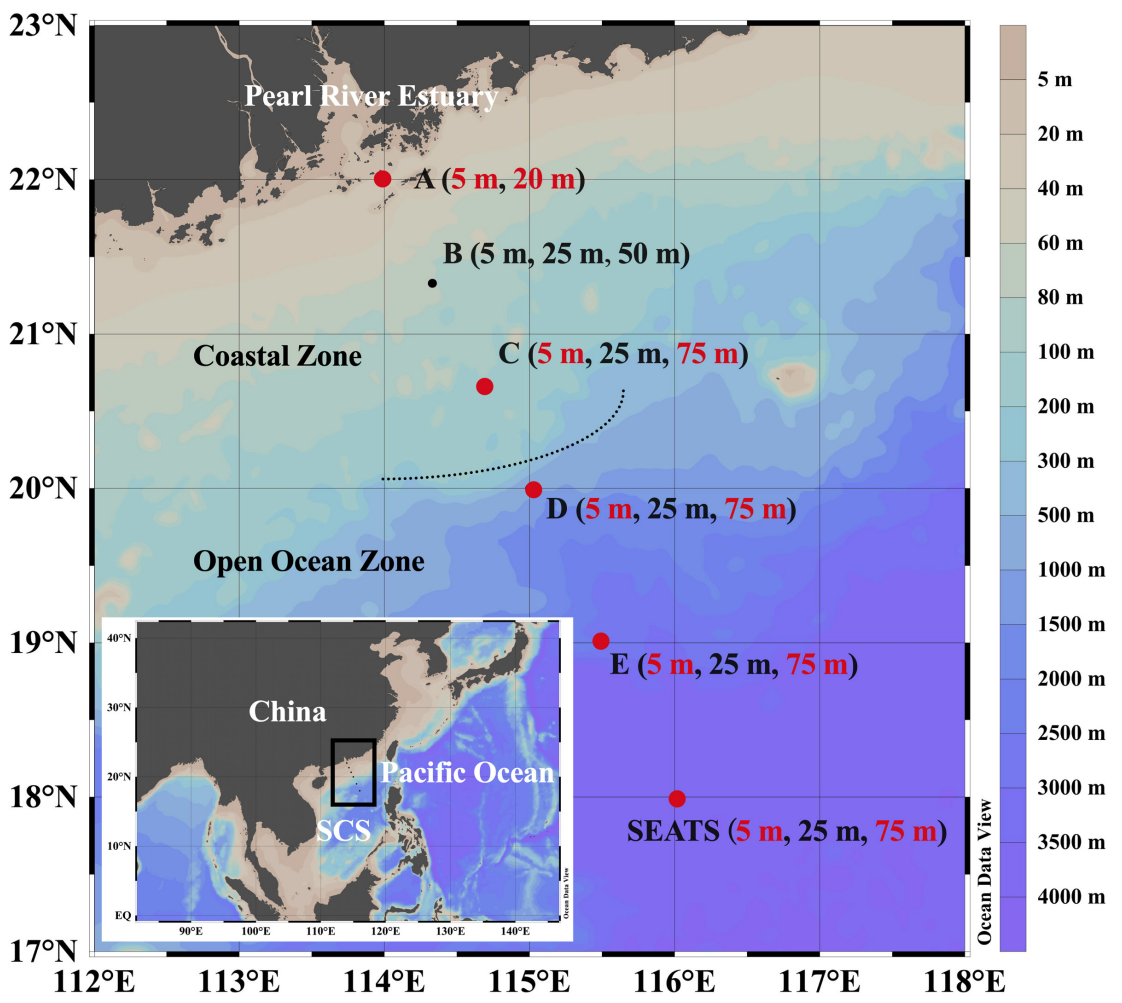

FIGURE 1 | Geographic locations of the sampling stations in the northern South China Sea (SCS). Dots denote the sampling stations, and depths listed in the bracket denote the sampling depths of chemical variables and prokaryotic parameters of each station. Dots and texts in red indicate the stations and corresponding surface and subsurface depths where dilution experiments were conducted and heterotrophic nanoflagellate samples were collected. The map was generated using Ocean Data View software (Schlitzer, 2020).

in the dark with SYBR green I solution (Molecular Probes, United States) and then held at room temperature for 15 min (Gasol and del Giorgio, 2000). Prokaryotes were enumerated on flow cytometry by their signature in a plot of side scatter (SSC) versus green fluorescence (**Supplementary Figure 1A**). VLP abundance was determined using flow cytometry (Epics Altra II, Beckman Coulter, United States) after staining with SYBR green I (Molecular Probe, United States) based on an established protocol (Brussaard, 2004; **Supplementary Figure 1B**). Fluorescent beads with a diameter of 1 μm (Molecular Probes Inc., United States) were added as an internal standard to both the prokaryotic and VLP samples.

The high and low nucleic acid content (HNA and LNA) prokaryotic subgroups were discriminated based on their respective signature in the cytogram plot of SSC versus green fluorescence (Gasol et al., 1999). All flow cytometric data analysis was performed with the FlowJo vX.0.7 software (Tree Star, United States).

Nanoflagellate Abundance

Heterotrophic nanoflagellate (HNF) abundance was measured by the following steps: 50-mL subsamples were fixed with glutaraldehyde at a final concentration of 1%, filtered through 0.45-μm polycarbonate black filters, and stained with DAPI (4,6-diamidino 2-phenylindole) at a final concentration of 10 μg mL^{-1} (Sherr et al., 1993; Yang et al., 2020). HNFs on the filters were counted along several transects using epifluorescence microscopy (Olympus BX51, Olympus America Inc., Center Valley, PA, United States) at ×1000 magnification. At least 50–100 HNF cells were counted in at least 25 fields per filter.

Dilution Experimental Setup

A modified parallel dilution technique was utilized to estimate prokaryotic mortality mediated by protozoan grazing and viral lysis following Evans et al. (2003). Dilution experiments were carried out at the surface (5 m) and subsurface (20 m for the shallowest station A and 75 m for the remaining stations) layers of five stations (station A, C, D, E, and SEATS), as highlighted in **Figure 1**.

Briefly, seawater was first passed through a 20-μm mesh and then filtered through a tangential flow filtration system with a 0.2-μm and 30-kDa pore size polyvinylidene difluoride cartridges (Labscale, Millipore, United States) to generate the grazer-free and virus-free diluents, respectively (**Supplementary Figure 2**). The polycarbonate bottles used in the experiments were acid-cleaned with 10% HCl and rigorously rinsed with Milli-Q water. The diluents were added to 250-mL polycarbonate bottles in the correct proportions to generate a parallel t_0 dilution series (20, 40, 60, and 100% of whole seawater). From each of these t_0 bottles, triplicate 50-mL polycarbonate bottles were rinsed twice with diluents and then gently filled with diluents by siphoning to minimize physical damage to the grazers, viruses, and prokaryotes. Immediately after completing the above preparation steps, the 50-ml polycarbonate bottles (21 bottles in total for each experiment) were incubated in an on-deck incubator for 24 h with *in situ* light simulated by covering with a neutral density plastic sheet and under the same temperature as the seawater at the time they were sampled by running seawater at that temperature. Triplicate 2-mL samples were collected at the start and the end of incubation to measure the prokaryotic abundance.

Interpretation of Dilution Experiments Results

The net growth rate of the prokaryotes (k, d^{-1}) was calculated for each sample based on the prokaryotic abundance at the start and the end of the incubation experiment (N_{t_0} and N_t), assuming exponential growth (Landry and Hassett, 1982):

$$k = \ln\left(\frac{N_t}{N_{t_0}}\right)/(t - t_0)$$

The slope of the regression of the net growth rate versus the dilution factor for the grazer-free dilution series is interpreted as the protozoan grazing-mediated prokaryotic mortality (PMM), whereas the slope of the regression for the virus-free dilution series reflects the combined impact of protozoan grazing and viral lysis. Therefore, the viral lysis-mediated prokaryotic mortality (VMM) can be obtained from the difference between the slopes of the regression lines from the two-dilution series (**Supplementary Figure 3**). Potential prokaryotic growth (PPG) was determined as the y-intercept value of the regression line obtained from the virus-free dilution series. PPG, PMM, and VMM rates were calculated separately for the HNA and LNA subgroups.

Statistical Analysis

GraphPad Prism 7 (GraphPad, United States) software was used to perform all statistical analyses. Briefly, a least-square regression analysis was conducted to analyze the relationship between the net growth rate and fractions of the grazer-free and virus-free dilution series. The PMM and VMM rates were analyzed using an *F*-test to assess whether a significant difference between the two sources of mortality existed, and a *P*-value less than 0.05 was considered significant. Shapiro–Wilk *W* tests were used to examine the data normality before analysis, and logarithm transformation was performed if necessary. Significant differences between samples were determined using paired *t*-tests. The relationships between the prokaryotic parameters and abiotic or biotic variables were examined using Spearman's rank correlation analysis with a significance level (α) of 0.05.

RESULTS

Physical and Chemical Characteristics

The temperature of the upper 70 m water generally increased from nearshore station A to offshore station SEATS (**Figure 2A** and **Supplementary Table 1**). Vertically, the temperatures at shallower stations A and B were almost homogeneous throughout the entire water column, while the other offshore stations exhibited a mixed layer of approximately 60∼70 m thick lying above the colder deep waters (**Figure 2A**). The salinity of the upper 70 m water showed a pronounced gradient that was impacted by the fresh river plume, with station A affected by the plume possessing the lowest salinity and the remaining stations

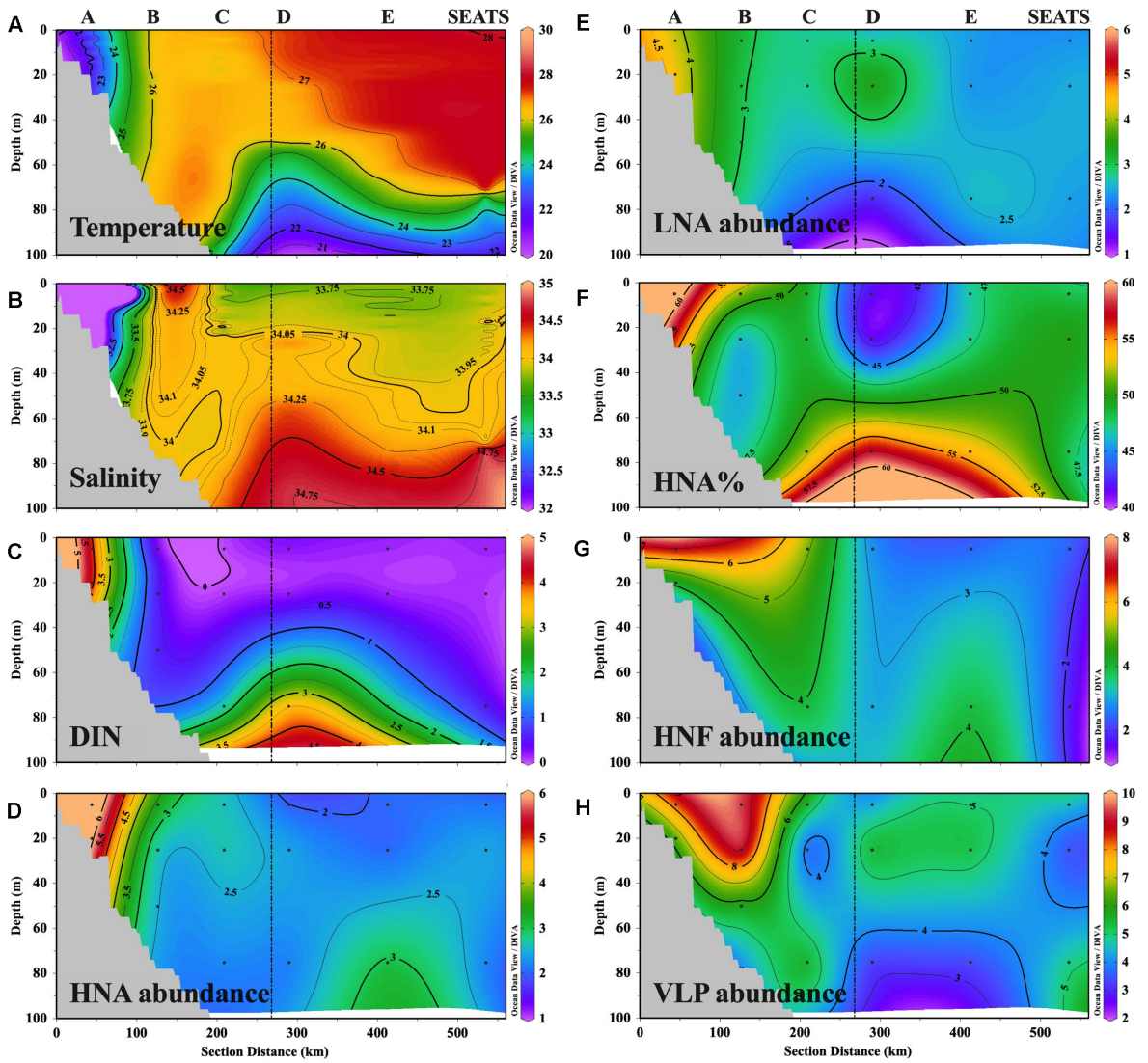

FIGURE 2 | Transect distributions of **(A)** temperature (°C), **(B)** salinity, **(C)** DIN concentration (μmol L^{-1}), **(D,E)** abundance (10^5 cells ml^{-1}) of HNA cells and LNA cells, **(F)** ratio of HNA cell abundance in total prokaryotic abundance (HNA%), **(G)** abundance (10^2 cells ml^{-1}) of heterotrophic nanoflagellate (HNF), and **(H)** abundance (10^6 cells ml^{-1}) of virus-like particles (VLP). The figure was plotted with Ocean Data View software (Schlitzer, 2020).

with minor plume influence having a higher salinity (**Figure 2B**). Similar to temperature, the vertical distribution of the salinity at stations A and B was more homogeneous than that of the other offshore stations, where the salinity generally increased with depth (**Figure 2B**).

The spatial distribution of DIN along the transect largely mirrored that of the physical variables, with higher and vertically more mixed concentrations at the station affected by the nutrient-rich river plume (i.e., A has the highest surface DIN, with mean ± standard deviation of 4.15 ± 0.06 μmol L^{-1}), whereas distinctly lower surface (0.11–0.35 μmol L^{-1}) but higher subsurface concentrations (0.55–3.96 μmol L^{-1}) were observed at the other offshore stations that were minimally affected by the plume (**Figure 2C**). The distribution pattern of silicate was similar to that of DIN while phosphate concentrations did not show a clear spatial distribution pattern (**Supplementary Figure 4**).

Microbial Abundance

Similar to the physical and chemical characteristics of the sample locations, the spatial distribution of HNA abundance also showed an environmental gradient along the transect that was shaped by river inputs. Namely, HNA abundance was distinctly higher at station A and lower at the offshore stations, except for a relatively high subsurface value at 75 m depth at E (**Figure 2D**). The environmental gradient of the distribution of LNA abundance was weak, with the peak at station A (**Figure 2E**). The percentage of HNA abundance in total prokaryotic abundance (HNA%) was higher at A (60 ± 2%) and the subsurface layer of the offshore stations C (52%), D (58%), and E (54%) where the

DIN concentration was higher (**Figure 2F**). The distribution pattern of the HNF (**Figure 2G**) and VLP abundance (**Figure 2H**) largely mirrored that of HNA and LNA abundance, with the values generally decreasing offshore from A toward SEATS (**Supplementary Table 1**).

Potential Prokaryotic Growth Rate

The potential growth rate of the HNA group (PPG-H) at the surface generally decreased offshore (**Figure 3A**), while no apparent along-transect trend was found for subsurface PPG-H (**Figure 3B**). The subsurface average (2.30 ± 0.38 d^{-1}) was significantly higher than the surface average (1.59 ± 0.68 d^{-1}) (paired *t*-test, $P < 0.05$), where the maximum subsurface PPG-H (at A) was nearly fourfold greater than the minimum surface PPG-H (at SEATS).

The potential growth rate of the LNA subgroup (PPG-L) at the surface generally increased offshore from A to E but slightly declined to SEATS (**Figure 3C**), while PPG-L in the subsurface water persistently increased from A to SEATS (**Figure 3D**). The surface average of PPG-L (0.72 ± 0.12 d^{-1}) was significantly (paired *t*-test, $P < 0.05$) higher than the subsurface average (0.55 ± 0.17 d^{-1}).

The ratio of potential growth rates of HNA to LNA (PPG-H/PPG-L) reflects the relative activity of the HNA cells to the LNA cells. The maximum ratio was recorded at the subsurface layer of A (8.54), and the minimum was at the surface layer of SEATS (0.87) (**Supplementary Table 2**). Linear regression analysis of all surface and subsurface measurements further showed that the ratio of PPG-H/PPG-L was positively related to the DIN concentration ($R^2 = 0.65$, $P < 0.005$) (**Figure 4A**).

Prokaryotic Grazing-Mediated and Lysis-Mediated Mortality Rate

Protozoan grazing-mediated mortality of the HNA subgroup (PMM-H) was higher at nearshore station A than at the offshore stations and was significantly higher in the subsurface than surface layers (paired *t*-test, $P < 0.05$) (**Figure 3A**). No clear spatial trend was found for viral lysis-mediated mortality of the HNA subgroup (VMM-H) except that the subsurface values were generally higher than the surface values (**Figure 3B**). Linear regression analysis of all surface and subsurface measurements further showed that PMM-H was positively related to the DIN concentration ($R^2 = 0.46$, $P < 0.05$) while there is no significant correlation between VMM-H and DIN (**Figure 4B**).

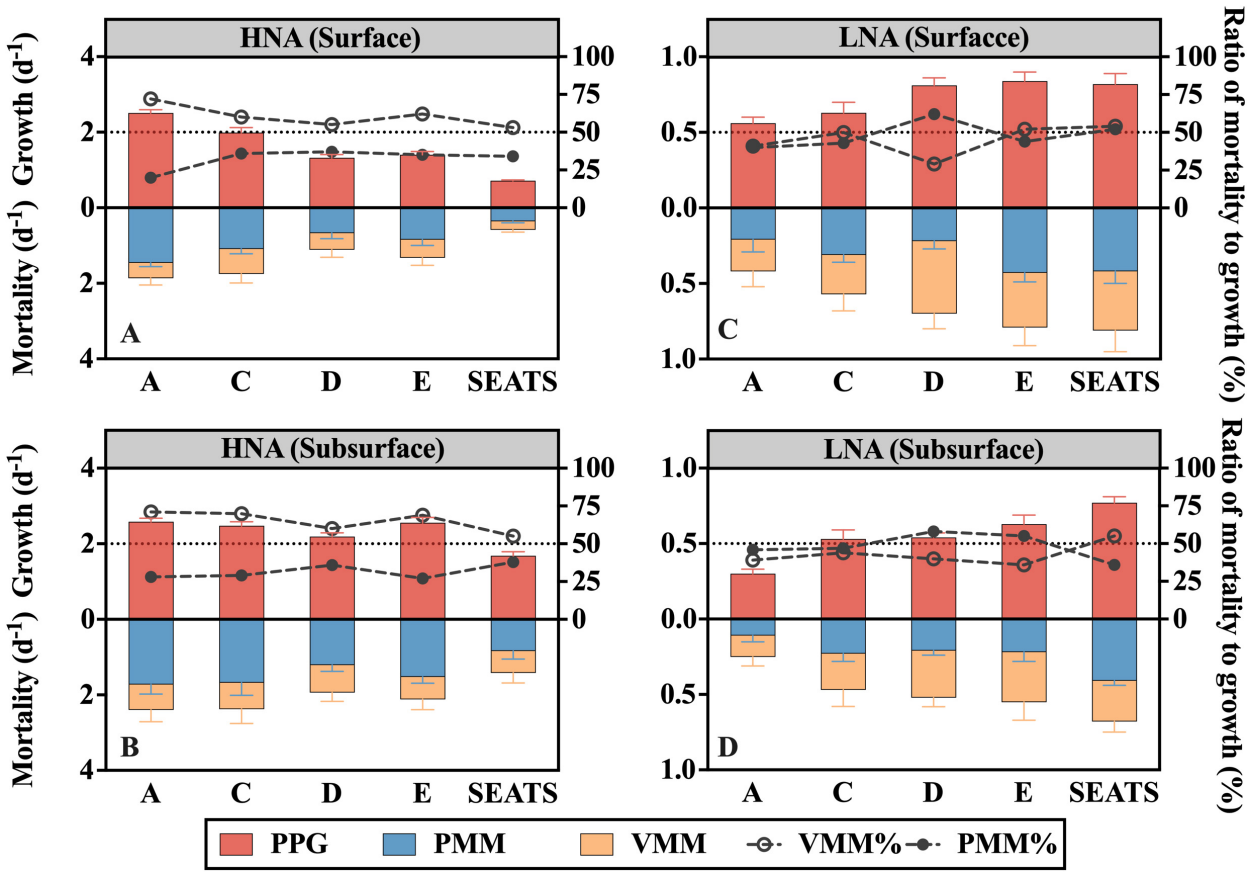

FIGURE 3 | Potential prokaryotic growth rate (PPG), mortality rate mediated by protozoan grazing (PMM) and viral lysis (VMM), and ratios of PMM (PMM%, filled dots) or VMM (VMM%, empty dots) to PPG for the **(A,B)** HNA subgroup and **(C,D)** LNA subgroup at stations along the transect at the surface and subsurface layers. The horizontal dashed line denotes the ratio of 50%.

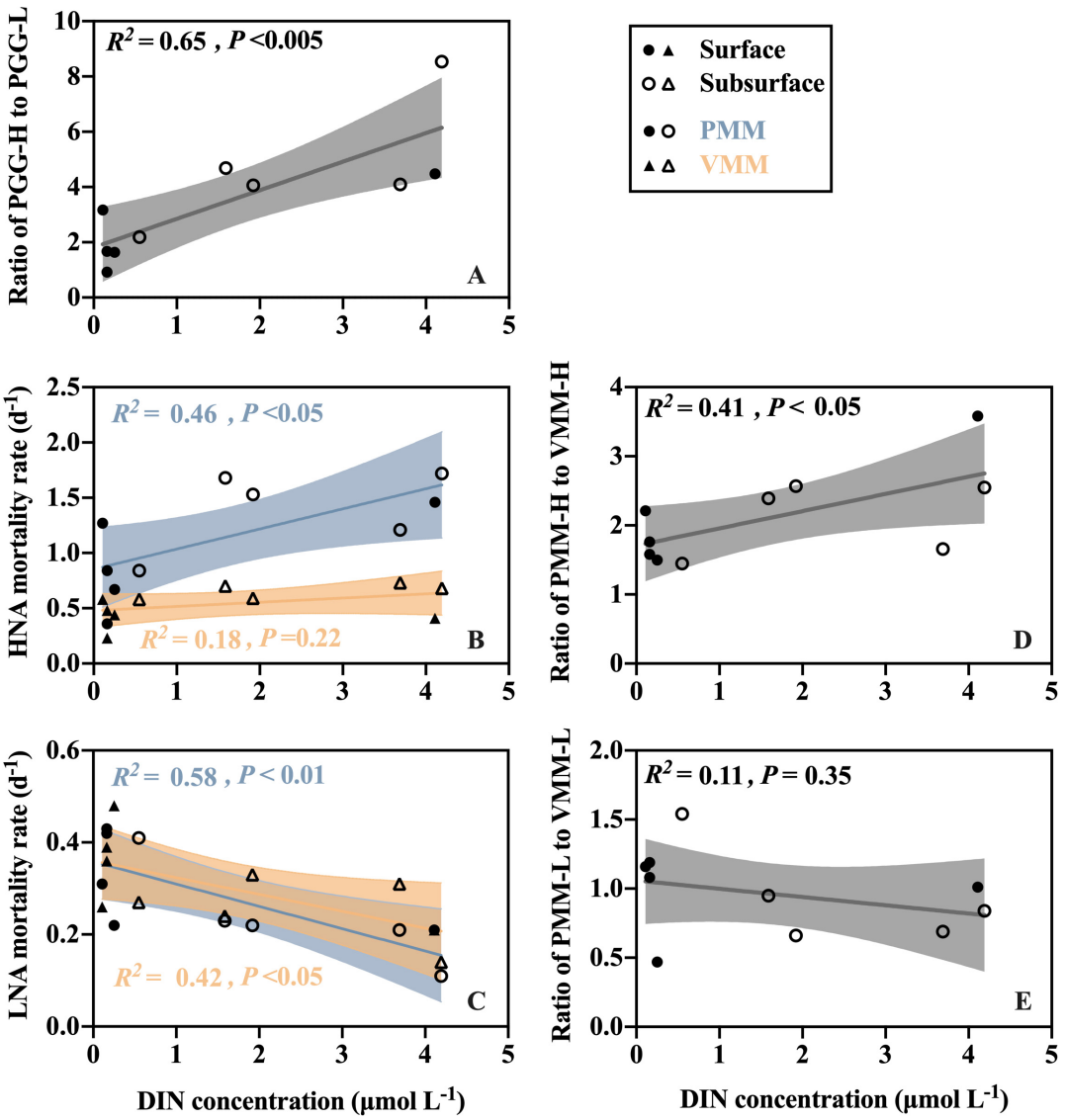

FIGURE 4 | Linear correlations between DIN concentration and **(A)** the ratio of HNA prokaryotic potential growth rate (PPG-H) to LNA prokaryotic potential growth rate (PPG-L), **(B,C)** the protozoan grazing-mediated mortality rate (PMM) and viral lysis-mediated mortality rate (VMM) for the **(B)** HNA and **(C)** LNA subgroups, and **(D,E)** the ratio of protozoan grazing-mediated mortality (PMM) to viral lysis-mediated mortality (VMM) for the **(D)** HNA and **(E)** LNA subgroups.

The sum of PMM-H and VMM-H accounted for approximately 87∼96% and 93∼99% of the HNA prokaryotic production in the surface and subsurface layers, respectively. Specifically, protozoan grazing consumed more than 50% of the HNA prokaryotic production in both the surface and subsurface layers of all stations (**Figures 3A,B**).

The ratio of PMM-H to VMM-H (PMM-H/VMM-H) represents the relative contribution of protozoan grazing over viral lysis to the mortality of the HNA subgroup, where a ratio value higher than 1 indicates greater contribution by grazing than lysis and vice versa. The ratio of PMM-H/VMM-H was distinctly higher than 1 for all surface and subsurface samples (**Figure 5**). At the surface, the ratio was remarkably higher at nearshore station A (3.58) than at the offshore stations (average was 1.63 ± 0.11) (**Figure 5A**), while no clear spatial trend was found for the ratio values at subsurface (range from 1.45 to 2.57) (**Figure 5B**). After clumping all surface and subsurface measurements, linear regression analysis showed that the PMM-H/VMM-H ratio was positively related to the DIN concentration ($R^2 = 0.41$, $P < 0.05$) (**Figure 4D**).

The protozoan grazing-mediated mortality of the LNA subgroup (PMM-L) did not show a clear trend along the transect, although a significant difference was found between layers (paired t-test, $P < 0.05$), with the surface value of each station generally higher than its subsurface counterpart (**Figures 3C,D**). The distribution pattern of viral lysis-mediated mortality of the LNA group (VMM-L) in the surface waters was similar to VMM-H, increasing offshore (**Figure 3C**), whereas

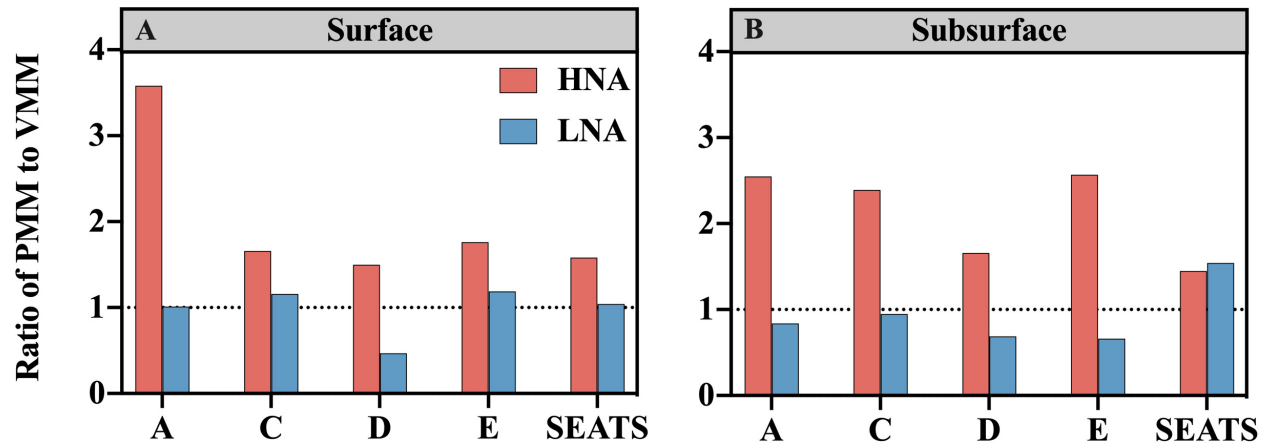

FIGURE 5 | Ratios of protozoan grazing-mediated mortality (PMM) to viral lysis-mediated mortality (VMM) for the HNA subgroup (red bars) and LNA subgroup (blue bars) at stations along the transect at the **(A)** surface and **(B)** subsurface layers. The horizontal dashed line denotes the ratio of 1.

no clear spatial trend was found for the subsurface VMM-L (**Figure 3D**). Based on the linear regression analysis of all surface and subsurface measurements, both PMM-L and VMM-L were negatively related to the DIN concentration ($R^2 = 0.58$, $P < 0.01$ and $R^2 = 0.42$, $P < 0.05$) (**Figure 4C**). The sum of PMM-L and VMM-L accounted for approximately 81∼105% and 85∼97% of the LNA prokaryotic production at surface and subsurface layers, respectively. Specifically, protozoan grazing consumed less than 50% of the LNA prokaryotic production at the majority of the stations (**Figures 3C,D**).

No clear spatial trend was found for the ratio of protozoan grazing to viral lysis of the LNA subgroup (PMM-L/VMM-L) in the surface (**Figure 5A**) or subsurface waters (**Figure 5B**). The PMM-L/VMM-L averaging over the entire transect (0.96 ± 0.31) was very close to 1, which was much lower than the transect average of PMM-H/VMM-H (2.07 ± 0.06). In contrast to the HNA subgroup, no significant linear correlation was found between PMM-L/VMM-L ratio and DIN concentration (**Figure 4E**).

Abiotic and Biotic Drivers of Prokaryote Abundance and Potential Growth Rate

Spearman's rank correlation analysis was used to reveal the potential drivers of prokaryote abundance and potential growth rate (**Figure 6**). HNA abundance was strongly, positively related to silicate concentration ($r = 0.44$, $P < 0.05$), HNF abundance ($r = 0.77$, $P < 0.01$), VLP abundance ($r = 0.46$, $P < 0.05$), and protozoan grazing on the HNA subgroup ($r = 0.73$, $P < 0.05$) and was negatively related to temperature ($r = -0.53$, $P < 0.05$). Conversely, LNA abundance was not related to any nutrient but was strongly, positively related to HNF abundance ($r = 0.58$, $P < 0.05$) and VLP abundance ($r = 0.63$, $P < 0.01$). HNA% exhibited similar correlation analysis results as the HNA abundance except that HNA% was also significantly positively related to DIN ($r = 0.51$, $P < 0.05$) but not VLP abundance, despite the positive correlation between the abundance of VLP and each subgroup.

The potential growth rate of the HNA group was positively related to DIN and silicate concentrations ($r = 0.80$ and 0.82, $P < 0.01$), HNF abundance ($r = 0.71$, $P < 0.05$), and protozoan grazing and viral lysis of the HNA subgroup ($r = 0.94$, $P < 0.001$ and $r = 0.58$, $P < 0.05$). Specifically, the correlation between PPG-H and grazing was more significant than that between PPG-H and lysis. In contrast to PPG-H, PPG-L showed negative correlations with DIN and silicate concentrations ($r = -0.72$, $P < 0.05$ and $r = -0.83$, $P < 0.01$) and had comparable significant, positive correlations with protozoan grazing and viral lysis on the LNA subgroup ($r = 0.78$ and $r = 0.83$, $P < 0.01$).

DISCUSSION

The cross-shore transect in the northern SCS possessed a clear nutrient gradient, which provides an ideal testbed to investigate how the abundance and potential growth rate of HNA and LNA prokaryotes and their regulating factors (i.e., protozoan grazing and viral lysis) respond to various nutrient conditions. The transect survey was carried out in the early winter season when the relatively strong northeast wind prevailed, and the Pearl River discharge was less than the annual mean, resulting in a narrower offshore plume extension (Yin et al., 2001). This fact was reflected by the pronounced environmental gradient shown in the upper water along the surveyed transect, which transited from the colder, fresher, and nutrient-rich water at nearshore station A to the warmer, saltier, and nutrient-poor water at offshore SEATS. Vertically, while the shallower stations A and B (<75 m) were well mixed, the other deeper stations offshore exhibited a distinct vertical gradient with nutrient-depleted surface water lying on the nutrient-replete subsurface water (>70 m).

Differential Responses of HNA and LNA Prokaryotes to Varying Trophic Status

The abundance of the HNA and LNA subgroups responded differently to the abiotic and biotic variables. Specifically,

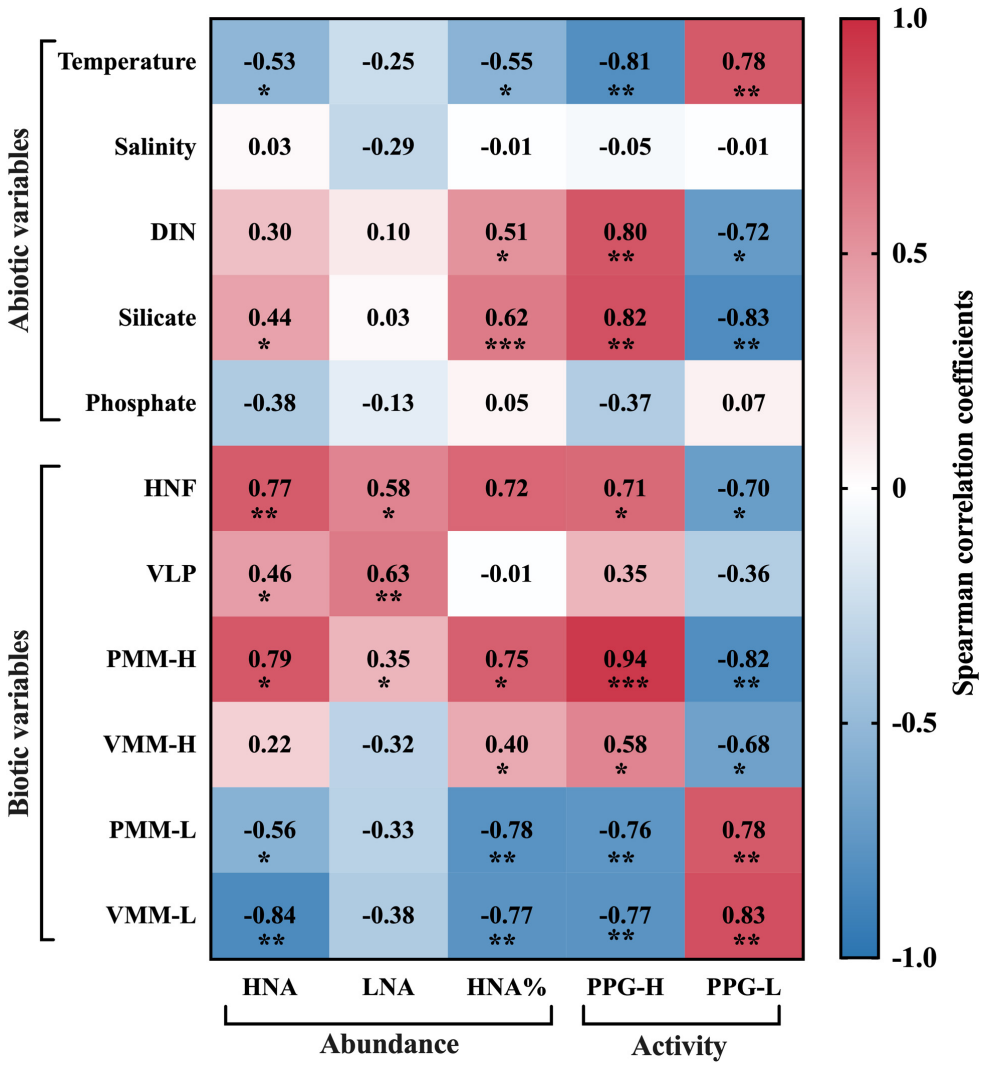

FIGURE 6 | Spearman's rank correlation coefficients between prokaryotic parameters and abiotic and biotic variables, where * denotes that the correlation is significant at the $P < 0.05$ level, ** at the $P < 0.01$ level, and *** at the $P < 0.001$ level.

the spatial distribution of HNA abundance exhibited an environmental gradient along the transect that was similar to the physical and chemical characteristics, i.e., decreasing from coastal to open ocean, and was generally higher at the subsurface than the surface waters of the open ocean. In contrast, the spatial distribution of LNA abundance showed a weaker gradient along the transect. The different responses of the abundance of the two subgroups to environmental factors were further reflected by the fact that HNA abundance was significantly correlated with both silicate concentration and temperature, while LNA abundance was not related to any abiotic factor. It follows that the HNA subgroup is more responsive to environmental variations than the LNA subgroup. A similar phenomenon was observed in the Atlantic Ocean where HNA abundance changed more than twofold between seasons, acting similar to an r-strategist or opportunist, while the LNA subgroup demonstrated more equilibrium dynamics over the same period, likely following the k-strategy (Mojica et al., 2019). This tendency can be attributed to the higher genome complexity of HNA than LNA cells, which enables the HNA subgroup to have a higher capacity for exploiting pulses of nutrients (Azam, 1998) as well as the ability to occupy a greater variety of ecological niches (Philippot et al., 2010; Schattenhofer et al., 2011). Indeed, the HNA subgroup consists of more versatile and faster-growing cells and possesses larger genomes, while the LNA subgroup is commonly dominated by oligotrophs, which have smaller, less flexible genomes (Zubkov et al., 2001; Longnecker et al., 2005; Mary et al., 2006; Schattenhofer et al., 2011). The compact genomes that LNA cells possess place them at a competitive disadvantage against HNA cells in nutrient-rich conditions, but their reduced metabolic burden of replication gains them a competitive advantage over HNA cells in an oligotrophic environment or during periods of limited resource availability (Mojica et al., 2019). This perspective is well supported by our

data, which showed that the relative contribution of HNA to total prokaryotic abundance, HNA%, significantly decreased with decreasing DIN and silicate concentration.

Similar to HNA abundance, the spatial distribution of HNA prokaryotic potential growth rate (PPG-H) showed a clear environmental gradient, largely mirroring the distribution pattern of DIN and silicate concentration, i.e., declining offshore, and was significantly higher at the nutrient-rich subsurface of the open ocean than the nutrient-poor surface of the open ocean. The spatial distribution of LNA prokaryotic potential growth rate (PPG-L) showed the opposite pattern to PPG-H and nutrient distributions, which generally increased from coastal to open ocean and was higher at the surface than subsurface waters of the open ocean. This reverse response of HNA and LNA cells to nutrient levels is also reflected by the significant positive correlations between PPG-H and DIN and silicate concentration in contrast to the significant negative correlations between the PPG-L and DIN and silicate concentration. As a result, a significant positive linear relation was found between the PPG-H/PPG-L ratio and DIN concentration, suggesting that the relative activity of the HNA cells decreased while that of the LNA cells increased under oligotrophication. This finding is consistent with other studies that found that open ocean oligotrophic communities, compared to coastal or shelf communities, have a higher proportion of heterotrophic activity ascribed to the LNA subgroup (Servais et al., 2003; Longnecker et al., 2005, 2006). The contrasting response of HNA and LNA potential growth rate across nutrient gradients is also attributable to the higher genome complexity of the HNA than LNA cells, which allows HNA to gain a competitive advantage in situations of abundant resources while placing LNA cells at an advantageous state in the resource-limited environment, as discussed above (Zubkov et al., 2001; Schattenhofer et al., 2011).

The increasing fraction of LNA abundance in total prokaryotic abundance (indicated by declining HNA%) and increasing relative activity of LNA cells (indicated by declining PPG-H/PPG-L ratio) with decreasing nutrients revealed in our data may suggest a reduced capacity of the total prokaryotic community to degrade and utilize DOC under the more oligotrophic conditions. This is associated with that LNA cells, compared to the HNA cells, have lower metabolic rate and weaker capability to degrade and utilize DOC due to their small streamlined genomes, limited genetic repertoires, and simpler extracellular hydrolase system (Giovannoni et al., 2005; Giovannoni, 2017). A similar point of view has been raised by Zubkov et al. (2004) who hypothesized that LNA cells only consume the labile fraction of organic nutrients, while HNA cells also feed on more refractory sources.

Elevated Contribution of Viral Lysis With Declining Nutrient

Protozoan grazing and viral lysis are well recognized as the major agents of the top-down control of prokaryotes (Thingstad and Lignell, 1997). Previous studies across different aquatic environments (Calbet et al., 2001; Weinbauer, 2004; Corte et al., 2012; Tsai et al., 2013a; Baltar et al., 2016; Wigington et al., 2016; Chen et al., 2019b; Li et al., 2019; Wei et al., 2019) have indicated significant positive correlations between prokaryote abundance with HNF and/or VLP abundance. Our data further revealed that the close correlation with HNF and VLP abundance also existed in each prokaryotic subgroup, the HNA and LNA. The tight coupling between prokaryotic subgroups and their respective top-down control factors is additionally supported by the high percentages of protozoan grazing and viral lysis in accounting for HNA prokaryotic production (87–99%) and LNA prokaryotic production (81–105%).

Importantly, our results indicated the contrasting regulating impacts of protozoan grazing and viral lysis on the abundance and potential growth rates of the HNA and LNA subgroups. The protozoan grazing profoundly impacted HNA abundance but not the LNA abundance, as suggested by the correlation analysis. On the contrary, VLP abundance was found to be significantly, positively correlated with both HNA and LNA abundance and the correlation between VLP abundance and LNA subgroup was stronger and more significant than that of HNA. The contrasting regulatory role of protozoan grazing and viral lysis on the HNA and LNA subgroups is also reflected in the prokaryotic potential growth rates. The HNA subgroup exhibited a stronger and more significant correlation with protozoan grazing than viral lysis, whereas the correlations between the LNA subgroup and grazing and lysis were more or less equivalent. In other words, the HNA cells were subjected to greater top-down control from grazing than lysis, while the LNA cells experienced equivalent pressures from the two regulators. This is well evidenced by the higher grazing to virus lysis ratio for HNA (ranging from 1.45 to 3.58) than for the LNA subgroup (0.47 to 1.54). We attribute the greater protozoan grazing pressure on the HNA than LNA cells to the selective grazing strategy of protozoa. Namely, the protozoa preferentially graze HNA cells that belong to the actively growing portion of the prokaryotic assemblage (del Giorgio et al., 1996; Baltar et al., 2016), whereas the less active prokaryote subgroup, such as the LNA cells, are less heavily grazed due to their intrinsically low metabolic rates and small size (Segovia et al., 2018). On the contrary, viral lysis may have weaker preference to different prokaryotic subgroups than grazing does, as evidenced by the lower VMM-H/VMM-L ratio than PMM-H/PMM-L ratio (**Supplementary Table 2**). Previously, high abundance of viruses to infect SAR11 population, the typical LNA prokaryotic subgroup, has been observed widespread in the oligotrophic ocean (Zhao et al., 2013), suggesting that viral lysis can profoundly impact LNA prokaryotic subgroup. That discovery has stimulated a hot debate on whether the abundant viruses infecting SAR11 cells is contradictory with the "Kill the Winner" theory (Giovannoni et al., 2013; Våge et al., 2013). For example, Våge et al. (2013) suggested that the high abundance of SAR11 cells and their phage could co-exist when strains of all species are dispersed over the entire growth-rate axis; under such scenario, most of the viruses would lysis the fastest growing strains (i.e., the "winner strains") to keep them at low abundance while allowing the slow-growing strains to dominate consequently, which is consistent with the "Kill the Winner" theory. More future works are still needed

to unveil the mechanism of viruses infecting the less active but abundant prokaryotic subgroup. Nevertheless, the more comparable regulatory impact of grazing and lysis on LNA cells as revealed in our data is due to a combination of the weaker preference of viral lysis on HNA over LNA cells and the relatively lower protozoan grazing pressure on LNA cells.

Another interesting finding is that the relative role of protozoan grazing to viral lysis (indicated by the ratio of grazing to lysis) in regard to the HNA and LNA subgroups responded differently to varying nutrient levels. Specifically, the relative importance of grazing on the HNA subgroup declined with decreasing nutrient concentration, which may be explained by the reduced food quality or availability under lower nutrients, because food quality (e.g., cell size, cell surface properties) and availability are known to influence protozoan grazers and grazing rates (Monger and Landry, 1991; Christaki et al., 1998; Monger et al., 1999). The declining food availability is supported by our data that abundance of picoeukaryote, one of the primary producers supplying fresh DOC, significantly decreased with decreasing DIN concentration (R^2 = 0.32, P < 0.05; **Supplementary Figure 5**). On the contrary, both grazing and lysis on the LNA subgroup significantly increased with declining nutrient concentration because the LNA subgroup gains a more competitive advantage as the nutrients become limited in the environment. This identical direction of change in grazing and lysis on LNA cells with varying nutrient levels largely explains why there was no significant change in the ratio of grazing to lysis on the LNA subgroup along the varying trophic conditions. Nevertheless, given the relatively lower impact ratio of grazing to lysis on LNA compared to the HNA subgroup, an increase in the LNA contribution to the prokaryotic community together with an increase in impact ratio of grazing to lysis on HNA

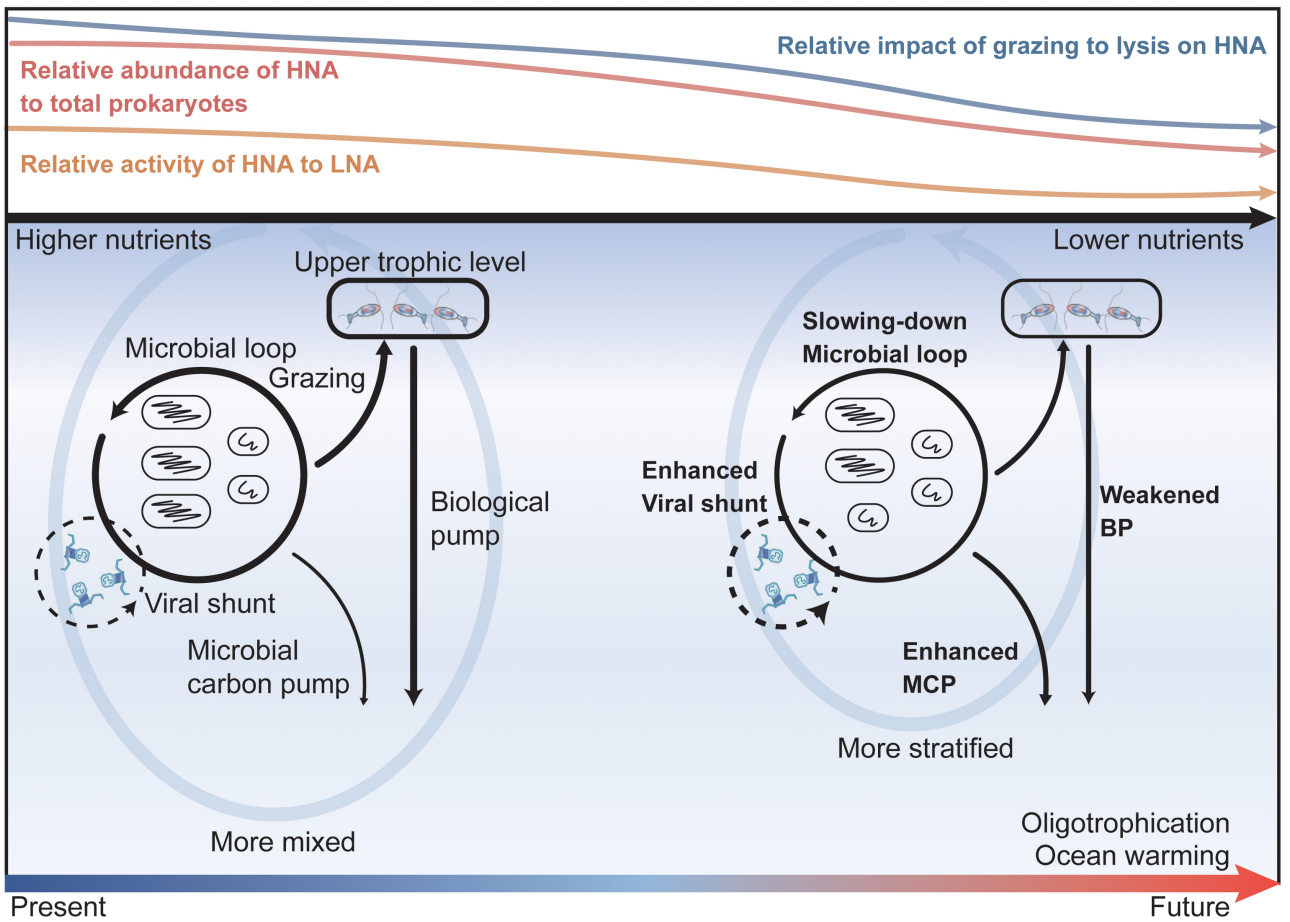

FIGURE 7 | A summary schematic and implications for future ocean oligotrophication scenarios. The colored curves on the top sketch the responses of prokaryotic abundance, activity (indicated by prokaryotic potential growth rate), and regulating top-down impacts to the declining nutrient levels revealed in our study. Namely, as the nutrient level decreases, the relative contribution of HNA abundance to the total prokaryotes (red curve), the relative activity of the HNA cells to LNA cells (orange curve), and the relative impact of grazing to lysis on the HNA cells (blue curve) all decrease. The lower column of the figure depicts the potential changes (denoted by the width of the black arrows), implied from our study, in the efficiency of the microbial loop, viral shunt, biological pump (BP), and microbial carbon pump (MCP) under future ocean warming and oligotrophication. Driven by global warming, the future ocean will be warmer, more stratified, and have a weaker vertical nutrient supply and an enhanced oligotrophication in the upper ocean. Under the strengthened ocean oligotrophication state, the efficiency of the microbial loop will be retarded, and viral shunt will be enhanced while the carbon and energy directed to the upper trophic level will be reduced, which will consequently enhance the efficiency of the microbial carbon pump while weakening the efficiency of the biological pump in carbon sequestration.

subgroup with decreasing nutrient levels, as our data revealed, imply that the relative impact of grazing on the mortality of the total prokaryotic community will decrease while that of viral lysis will increase under more oligotrophic conditions.

Implications for Carbon Cycling and Sequestration in Future Ocean

Our data revealed that as the nutrient concentrations declined, the proportion of LNA abundance to total prokaryotes, the relative prokaryotic potential growth rate of the LNA to HNA cells, and the relative impact of viral lysis to protozoan grazing on total prokaryotes all increased. Such responses of prokaryotic abundance and potential growth rate and their top-down regulating factors to the decreasing nutrient levels have important implications for carbon cycling and sequestration in the future ocean (**Figure 7**). The anticipated ocean warming under global climate change is expected to enhance oligotrophication of the upper ocean as a consequence of the reduced diffusive vertical nutrient supply driven by the strengthening stratification (Hoegh-Guldberg and Bruno, 2010; Agusti et al., 2017). Under this increased oligotrophication, the ocean is expected to embrace a future of retarding carbon cycling in the microbial loop (due to the elevated role of the LNA subgroup in regard to the total prokaryotic community) and enhanced viral shunt to retain the carbon and energy flow within the microbial loop (due to the higher relative contribution of viral lysis to the mortality of the total prokaryotes). While these changes will weaken the efficiency of the biological pump following the reduced energy and carbon fluxes directing to the upper trophic levels, they will also promote the accumulation of refractory DOC, according to the theory of the microbial carbon pump (MCP) (Jiao et al., 2010, 2014, 2018), and thus enhance carbon sequestration in the ocean. This, in turn, will stimulate negative feedback to the global warming associated with the accelerated release of anthropogenic CO_2.

CONCLUSION

This study revealed that the potential growth rate of the HNA and LNA subgroups responded reversely along the nutrient gradient. Namely, as the nutrient concentrations decreased, the HNA potential growth rate significantly decreased, while that of the LNA markedly increased, thus yielding an increasing relative potential growth rate of the LNA subgroup with declining nutrient levels. Furthermore, there existed contrasting regulatory impacts of protozoan grazing and viral lysis on the HNA and LNA subgroups, where the HNA subgroup experienced higher pressure from grazing than lysis while the LNA subgroup was subjected to an equivalent impact from grazing and lysis. The relative role of lysis to grazing on the HNA subgroup increased with decreasing nutrients. Taken together, our results revealed an elevated contribution of LNA cells to the prokaryotic community and a relatively greater virus-mediated mortality pressure on total prokaryotes under more oligotrophic conditions. This implies a weakened efficiency of carbon cycling within the microbial loop and enhanced viral lysis to shunt more carbon and energy flow in the anticipated future ocean oligotrophication driven by global warming.

DATA AVAILABILITY STATEMENT

The raw data supporting the conclusions of this article will be made available by the authors, without undue reservation.

AUTHOR CONTRIBUTIONS

CH designed and performed the experiments under the supervision of DX and NJ. CH carried out the formal analysis with assistance and inputs from XC and LY. CH wrote the manuscript with contributions from all co-authors. All authors contributed to the article and approved the submitted version.

FUNDING

This work was funded by the National Key Research and Development Program of China (2016YFA0601400) and the National Natural Science Foundation of China (Nos. 91751207, 41876142, and 41861144018).

ACKNOWLEDGMENTS

We thank the captains and crews of the R/V ShiYan III for their excellent support during the cruise. We also thank Jia Sun for providing the nutrient and CTD data and Ruanhong Cai for constructive comments on the earlier version of the manuscript.

SUPPLEMENTARY MATERIAL

The Supplementary Material for this article can be found online at: https://www.frontiersin.org/articles/10.3389/fmicb.2020.612053/full#supplementary-material

REFERENCES

Agusti, S., Martinez-Ayala, J., Regaudie-de-Gioux, A., and Duarte, C. M. (2017). Oligotrophication and metabolic slowing-down of a NW mediterranean coastal ecosystem. *Front. Mar. Sci.* 4:432. doi: 10.3389/fmars.2017.00432

Azam, F. (1998). Oceanography: microbial control of oceanic carbon flux: the plot thickens. *Science* 280, 694–696. doi: 10.1126/science.280.5364.694

Azam, F., Fenchel, T., Field, J. G., Gray, J. S., Meyer-Reil, L. A., and Thingstad, F. (1983). The ecological role of water-column microbes in the Sea. *Mar. Ecol. Prog. Ser.* 10, 257–263. doi: 10.3354/meps010257

Baltar, F., Palovaara, J., Unrein, F., Catala, P., Hornák, K., Šimek, K., et al. (2016). Marine bacterial community structure resilience to changes in protist predation under phytoplankton bloom conditions. *ISME J.* 10, 568–581. doi: 10.1038/ismej.2015.135

Bettarel, Y., Sime-Ngando, T., Amblard, C., and Dolan, J. (2004). Viral activity in two contrasting lake ecosystems. *Appl. Environ. Microb.* 70, 2941–2951. doi: 10.1128/aem.70.5.2941-2951.2004

Bouvier, T., del Giorgio, P. A., and Gasol, J. M. (2007). A comparative study of the cytometric characteristics of high and low nucleic-acid bacterioplankton cells from different aquatic ecosystems. *Environ. Microbiol.* 9, 2050–2066. doi: 10.1111/j.1462-2920.2007.01321.x

Brussaard, C. P. D. (2004). Optimization of procedures for counting viruses by flow cytometry. *Appl. Environ. Microb.* 70, 1506–1513. doi: 10.1128/aem.70.3.1506-1513.2004

Calbet, A., Landry, M. R., and Nunnery, S. (2001). Bacteria-flagellate interactions in the microbial food web of the oligotrophic subtropical North Pacific. *Aquat. Microb. Ecol.* 23, 283–292. doi: 10.3354/ame023283

Chen, X., Ma, R., Yang, Y., Jiao, N., and Zhang, R. (2019a). Viral regulation on bacterial community impacted by lysis-lysogeny switch: a microcosm experiment in eutrophic coastal waters. *Front. Microbiol.* 10:1763. doi: 10.3389/fmicb.2019.01763

Chen, X., Wei, W., Wang, J., Li, H., Sun, J., Ma, R., et al. (2019b). Tide driven microbial dynamics through virus-host interactions in the estuarine ecosystem. *Water Res.* 160, 118–129. doi: 10.1016/j.watres.2019.05.051

Christaki, U., Dolan, J. R., Pelegri, S., and Rassoulzadegan, F. (1998). Consumption of picoplankton-size particles by marine ciliates: effects of physiological state of the ciliate and particle quality. *Limnol. Oceanogr.* 43, 458–464. doi: 10.4319/lo.1998.43.3.0458

Church, M. J. (2008). "Resource control of bacterial dynamics in the sea," in *Microbial Ecology of the Oceans*, ed. D. L. Kirchman (Manoa: University of Hawaii), 335–382. doi: 10.1002/9780470281840.ch10

Corte, D. D., Sintes, E., Yokokawa, T., Reinthaler, T., and Herndl, G. J. (2012). Links between viruses and prokaryotes throughout the water column along a North Atlantic latitudinal transect. *ISME J.* 6, 1566–1577. doi: 10.1038/ismej.2011.214

Danovaro, R., Dell'Anno, A., Corinaldesi, C., Magagnini, M., Noble, R., Tamburini, C., et al. (2008). Major viral impact on the functioning of benthic deep-sea ecosystems. *Nature* 454, 1084–1087. doi: 10.1038/nature07268

del Giorgio, P. A., and Gasol, J. M. (2008). Physiological structure and single-cell activity in marine bacterioplankton. *Microb. Ecol. Ocean.* 2, 243–285. doi: 10.1002/9780470281840.ch8

del Giorgio, P. A., Gasol, J. M., Vaqué, D., Mura, P., Agustí, S., and Duarte, C. M. (1996). Bacterioplankton community structure: protists control net production and the proportion of active bacteria in a coastal marine community. *Limnol. Oceanogr.* 41, 1169–1179. doi: 10.4319/lo.1996.41.6.1169

Edwards, M., and Richardson, A. J. (2004). Impact of climate change on marine pelagic phenology and trophic mismatch. *Nature* 430, 881–884. doi: 10.1038/nature02808

Evans, C., Archer, S. D., Jacquet, S., and Wilson, W. H. (2003). Direct estimates of the contribution of viral lysis and microzooplankton grazing to the decline of a Micromonas spp. population. *Aquat. Microb. Ecol.* 30, 207–219. doi: 10.3354/ame030207

Fuhrma, J. A., and Suttle, C. A. (1993). Viruses in marine planktonic systems. *Oceanography* 6, 50–62. doi: 10.2307/43924641

Fuhrman, J. A., and Noble, R. T. (1995). Viruses and protists cause similar bacterial mortality in coastal seawater. *Limnol. Oceanogr.* 40, 1236–1242. doi: 10.4319/lo.1995.40.7.1236

Gasol, J. M., and del Giorgio, P. A. (2000). Using flow cytometry for counting natural planktonic bacteria and understanding the structure of planktonic bacterial communities. *Sci. Mar.* 64, 197–224. doi: 10.3989/scimar.2000.64n2197

Gasol, J. M., Zweifel, U. L., Peters, F., Fuhrman, J. A., and Hagström, A. (1999). Significance of size and nucleic acid content heterogeneity as measured by flow cytometry in natural planktonic bacteria. *Appl. Environ. Microb.* 65, 4475–4483. doi: 10.1128/aem.65.10.4475-4483.1999

Giovannoni, S., Temperton, B., and Zhao, Y. (2013). Giovannoni et al. reply. *Nature* 499, E4–E5. doi: 10.1038/nature12388

Giovannoni, S. J. (2017). SAR11 bacteria: the most abundant plankton in the oceans. *Annu. Rev. Mar. Sci.* 9, 231–255. doi: 10.1146/annurev-marine-010814-015934

Giovannoni, S. J., Tripp, H. J., Givan, S., Podar, M., Vergin, K. L., Baptista, D., et al. (2005). Genome streamlining in a cosmopolitan oceanic bacterium. *Science* 309, 1242–1245. doi: 10.1126/science.1114057

Gonzalez, J. M., Sherr, E. B., and Sherr, B. F. (1990). Size-selective grazing on bacteria by natural assemblages of estuarine flagellates and ciliates. *Appl. Environ. Microb.* 56, 583–589. doi: 10.1128/aem.56.3.583-589.1990

Hoegh-Guldberg, O., and Bruno, J. F. (2010). The impact of climate change on the world's marine ecosystems. *Science* 328, 1523–1528. doi: 10.1126/science.1189930

Huete-Stauffer, T. M., and Morán, X. (2012). Dynamics of heterotrophic bacteria in temperate coastal waters: similar net growth but different controls in low and high nucleic acid cells. *Aquat. Microb. Ecol.* 67, 211–223. doi: 10.3354/ame01590

Jellett, J. F., Li, W. K. W., Dickie, P. M., Boraie, A., and Kepkay, P. E. (1996). Metabolic activity of bacterioplankton communities assessed by flow cytometry and single carbon substrate utilization. *Mar. Ecol. Prog. Ser.* 136, 213–225. doi: 10.3354/meps136213

Jiao, N., Cai, R., Zheng, Q., Tang, K., Liu, J., Jiao, F., et al. (2018). Unveiling the enigma of refractory carbon in the ocean. *Natl. Sci. Rev.* 5, 459–463. doi: 10.1093/nsr/nwy020

Jiao, N., Herndl, G. J., Hansell, D. A., Benner, R., Kattner, G., Wilhelm, S. W., et al. (2010). Microbial production of recalcitrant dissolved organic matter: long-term carbon storage in the global ocean. *Nat. Rev. Microbiol.* 8, 593–599. doi: 10.1038/nrmicro2386

Jiao, N., Robinson, C., Azam, F., Thomas, H., Baltar, F., Dang, H., et al. (2014). Mechanisms of microbial carbon sequestration in the ocean – future research directions. *Biogeosciences* 11, 5285–5306. doi: 10.5194/bg-11-5285-2014

Landry, M. R., and Hassett, R. P. (1982). Estimating the grazing impact of marine micro-zooplankton. *Mar. Biol.* 67, 283–288. doi: 10.1007/bf00397668

Lara, E., Vaqué, D., Sà, E. L., Boras, J. A., Gomes, A., Borrull, E., et al. (2017). Unveiling the role and life strategies of viruses from the surface to the dark ocean. *Sci. Adv.* 3, e1602565. doi: 10.1126/sciadv.1602565

Lebaron, P., Servais, P., Agogue, H., Courties, C., and Joux, F. (2001). Does the high nucleic acid content of individual bacterial cells allow us to discriminate between active cells and inactive cells in aquatic systems? *Appl. Environ. Microb.* 67, 1775–1782. doi: 10.1128/aem.67.4.1775-1782.2001

Li, W. K. W., Jellett, J. F., and Dickie, P. M. (1995). DNA distributions in planktonic bacteria stained with TOTO or TO-PRO. *Limnol. Oceanogr.* 40, 1485–1495. doi: 10.4319/lo.1995.40.8.1485

Li, X., Xu, J., Shi, Z., Xu, D., Li, R., Li, Q., et al. (2019). Regulation of protist grazing on bacterioplankton by hydrological conditions in coastal waters. *Estuar. Coast Shelf. Sci.* 218, 1–8. doi: 10.1016/j.ecss.2018.11.013

Longnecker, K., Sherr, B. F., and Sherr, E. B. (2005). Activity and phylogenetic diversity of bacterial cells with high and low nucleic acid content and electron transport system activity in an upwelling ecosystem. *Appl. Environ. Microb.* 71, 7737–7749. doi: 10.1128/aem.71.12.7737-7749.2005

Longnecker, K., Sherr, B. F., and Sherr, E. B. (2006). Variation in cell-specific rates of leucine and thymidine incorporation by marine bacteria with high and with low nucleic acid content off the Oregon coast. *Aquat. Microb. Ecol.* 43, 113–125. doi: 10.3354/ame043113

Mary, I., Heywood, J., Fuchs, B., Amann, R., Tarran, G., Burkill, P., et al. (2006). SAR11 dominance among metabolically active low nucleic acid bacterioplankton in surface waters along an Atlantic meridional transect. *Aquat. Microb. Ecol.* 45, 107–113. doi: 10.3354/ame045107

Mojica, K. D. A., Carlson, C. A., and Behrenfeld, M. J. (2019). Regulation of low and high nucleic acid fluorescent heterotrophic prokaryote subpopulations and links to viral-induced mortality within natural prokaryote-virus communities. *Microbial. Ecol.* 67, 5210–5218. doi: 10.1007/s00248-019-01393-9

Monger, B., and Landry, M. (1991). Prey-size dependency of grazing by free-living marine flagellates. *Mar. Ecol. Prog. Ser.* 74, 239–248. doi: 10.3354/meps074239

Monger, B. C., Landry, M. R., and Brown, S. L. (1999). Feeding selection of heterotrophic marine nanoflagellates based on the surface hydrophobicity of their picoplankton prey. *Limnol. Oceanogr.* 44, 1917–1927. doi: 10.4319/lo.1999.44.8.1917

Morán, X. A. G., Lopez-Urrutia, A., Calvo-Díaz, A., and Li, W. K. W. (2010). Increasing importance of small phytoplankton in a warmer ocean. *Global Change Biol.* 16, 1137–1144. doi: 10.1111/j.1365-2486.2009.01960.x

Nagata, T., Tamburini, C., Arístegui, J., Baltar, F., Bochdansky, A. B., Fonda-Umani, S., et al. (2010). Emerging concepts on microbial processes in the bathypelagic ocean – ecology, biogeochemistry, and genomics. *Deep Sea Res. Part II Top. Stud. Oceanogr.* 57, 1519–1536. doi: 10.1016/j.dsr2.2010.02.019

Pearce, I., Davidson, A. T., Thomson, P. G., Wright, S., and van den Enden, R. (2010). Marine microbial ecology off East Antarctica (30 - 80°E): rates of bacterial and phytoplankton growth and grazing by heterotrophic protists. *Deep Sea Res. Part II Top. Stud. Oceanogr.* 57, 849–862. doi: 10.1016/j.dsr2.2008.04.039

Philippot, L., Andersson, S. G. E., Battin, T. J., Prosser, J. I., Schimel, J. P., Whitman, W. B., et al. (2010). The ecological coherence of high bacterial taxonomic ranks. *Nat. Rev. Microbiol.* 8, 523–529. doi: 10.1038/nrmicro2367

Sanders, R. W., Caron, D. A., and Berninger, U. G. (1992). Relationships between bacteria and heterotrophic nanoplankton in marine and fresh waters: an inter-ecosystem comparison. *Mar. Ecol. Prog. Ser.* 86, 1–14. doi: 10.3354/meps086001

Scharek, R., and Latasa, M. (2007). Growth, grazing and carbon flux of high and low nucleic acid bacteria differ in surface and deep chlorophyll maximum layers in the NW Mediterranean Sea. *Aquat. Microb. Ecol.* 46, 153–161. doi: 10.3354/ame046153

Schattenhofer, M., Wulf, J., Kostadinov, I., Glöckner, F. O., Zubkov, M. V., and Fuchs, B. M. (2011). Phylogenetic characterisation of picoplanktonic populations with high and low nucleic acid content in the North Atlantic Ocean. *Syst. Appl. Microbiol.* 34, 470–475. doi: 10.1016/j.syapm.2011.01.008

Schlitzer, R. (2020). *Ocean Data View*. Available online at: odv.awi.de

Segovia, B. T., Meira, B. R., Lansac-Toha, F. M., Amadeo, F. E., Unrein, F., Velho, L. F. M., et al. (2018). Growth and cytometric diversity of bacterial assemblages under different top–down control regimes by using a size-fractionation approach. *J. Plankton Res.* 40, 129–141. doi: 10.1093/plankt/fbx071

Servais, P., Casamayor, E. O., Courties, C., Catala, P., Parthuisot, N., and Lebaron, P. (2003). Activity and diversity of bacterial cells with high and low nucleic acid content. *Aquat. Microb. Ecol.* 33, 41–51. doi: 10.3354/ame033041

Sherr, E. B., Caron, D. A., and Sherr, B. F. (1993). "Staining of heterotrophic protists for visualization via epifluorescence microscope," in *Handbook of Methods in Aquatic,* eds P. F. Kemp, B. F. Sherr, E. B. Sherr, and J. J. Cole (Boca Raton, FL: Lewis Publishers), 213–228.

Sintes, E., and del Giorgio, P. A. (2014). Feedbacks between protistan single-cell activity and bacterial physiological structure reinforce the predator/prey link in microbial foodwebs. *Front. Microbiol.* 5:453. doi: 10.3389/fmicb.2014.00453

Suttle, C. A. (2005). Viruses in the sea. *Nature* 437, 356–361. doi: 10.1038/nature04160

Suttle, C. A. (2007). Marine viruses — major players in the global ecosystem. *Nat. Rev. Microbiol.* 5, 801–812. doi: 10.1038/nrmicro1750

Thingstad, T. F., and Lignell, R. (1997). Theoretical models for the control of bacterial growth rate, abundance, diversity and carbon demand. *Aquat. Microb. Ecol.* 13, 19–27. doi: 10.3354/ame013019

Tsai, A.-Y., Gong, G.-C., and Chao, C.-F. (2016). Contribution of viral lysis and nanoflagellate grazing to bacterial mortality at surface waters and deeper depths in the coastal ecosystem of subtropical Western Pacific. *Estuaries Coasts* 39, 1357–1366. doi: 10.1007/s12237-016-0098-9

Tsai, A. Y., Gong, G.-C., and Hung, J. (2013a). Seasonal variations of virus- and nanoflagellate-mediated mortality of heterotrophic bacteria in the coastal ecosystem of subtropical western Pacific. *Biogeosciences* 10, 3055–3065. doi: 10.5194/bg-10-3055-2013

Tsai, A.-Y., Gong, G.-C., Sanders, R. W., and Huang, J. K. (2013b). Contribution of viral lysis and nanoflagellate grazing to bacterial mortality in the inner and outer regions of the Changjiang River plume during summer. *J. Plankton Res.* 35, 1283–1293. doi: 10.1093/plankt/fbt074

Våge, S., Storesund, J. E., and Thingstad, T. F. (2013). SAR11 viruses and defensive host strains. *Nature* 499, E3–E4. doi: 10.1038/nature12387

Vazquez-Dominguez, E., Gasol, J. M., Agusti, S., Duarte, C. M., and Vaqué, D. (2006). Growth and grazing losses of prokaryotes in the central Atlantic Ocean. *J. Plankton Res.* 28, 879–879. doi: 10.1093/plankt/fbl026

Wei, W., Wang, N., Cai, L., Zhang, C., Jiao, N., and Zhang, R. (2019). Impacts of freshwater and seawater mixing on the production and decay of virioplankton in a subtropical estuary. *Microbial Ecol.* 78, 843–854. doi: 10.1007/s00248-019-01362-2

Weinbauer, M., Winter, C., and Höfle, M. (2002). Reconsidering transmission electron microscopy based estimates of viral infection of bacterioplankton using conversion factors derived from natural communities. *Aquat. Microb. Ecol.* 27, 103–110. doi: 10.3354/ame027103

Weinbauer, M. G. (2004). Ecology of prokaryotic viruses. *FEMS Microbiol. Rev.* 28, 127–181. doi: 10.1016/j.femsre.2003.08.001

Wigington, C. H., Sonderegger, D., Brussaard, C. P. D., Buchan, A., Finke, J. F., Fuhrman, J. A., et al. (2016). Re-examination of the relationship between marine virus and microbial cell abundances. *Nat. Microbiol.* 1:15024. doi: 10.1038/nmicrobiol.2015.24

Yang, J. P., Huang, S. X., Fan, W. X., Warren, A., Jiao, N., and Xu, D. (2020). Spatial distribution patterns of planktonic ciliate communities in the East China Sea: potential indicators of water masses. *Mar. Pollut. Bull.* 156:111253. doi: 10.1016/j.marpolbul.2020.111253

Yin, K., Qian, P., Wu, M., Chen, J., Huang, L., Song, X., et al. (2001). Shift from P to N limitation of phytoplankton growth across the Pearl River estuarine plume during summer. *Mar. Ecol. Prog. Ser.* 221, 17–28. doi: 10.3354/meps221017

Zhao, Y., Temperton, B., Thrash, J. C., Schwalbach, M. S., Vergin, K. L., Landry, Z. C., et al. (2013). Abundant SAR11 viruses in the ocean. *Nature* 494, 357–360. doi: 10.1038/nature11921

Zubkov, M. V., Allen, J. I., and Fuchs, B. M. (2004). Coexistence of dominant groups in marine bacterioplankton community—a combination of experimental and modelling approaches. *J. Mar. Biol. Assoc.* 84, 519–529. doi: 10.1017/s002531540400952xh

Zubkov, M. V., Fuchs, B. M., Burkill, P. H., and Amann, R. (2001). Comparison of cellular and biomass specific activities of dominant bacterioplankton groups in stratified waters of the Celtic Sea. *Appl. Environ. Microb.* 67, 5210–5218. doi: 10.1128/aem.67.11.5210-5218.2001

Conflict of Interest: The authors declare that the research was conducted in the absence of any commercial or financial relationships that could be construed as a potential conflict of interest.

frontiers in Microbiology

ORIGINAL RESEARCH
published: 21 December 2020
doi: 10.3389/fmicb.2020.560102

Characteristics of Different Size Phytoplankton for Primary Production and Biochemical Compositions in the Western East/Japan Sea

*Jae Joong Kang[1], Hyo Keun Jang[1], Jae-Hyun Lim[2], Dabin Lee[1], Jae Hyung Lee[3], Hyeonji Bae[1], Chang Hwa Lee[1], Chang-Keun Kang[4] and Sang Heon Lee[1]**

[1] Department of Oceanography, Pusan National University, Busan, South Korea, [2] East Sea Fisheries Research Institute, National Institute of Fisheries Science, Gangneung, South Korea, [3] South Sea Fisheries Research Institute, National Institute of Fisheries Science, Yeosu-si, South Korea, [4] School of Earth Sciences and Environmental Engineering, Gwangju Institute of Science and Technology, Gwangju, South Korea

OPEN ACCESS

Edited by:
Martin G. Klotz,
Washington State University,
United States

Reviewed by:
Hidetoshi Urakawa,
Florida Gulf Coast University,
United States
Shovonlal Roy,
University of Reading,
United Kingdom

***Correspondence:**
Sang Heon Lee
sanglee@pusan.ac.kr

Specialty section:
This article was submitted to Aquatic Microbiology, a section of the journal Frontiers in Microbiology

Received: 08 May 2020
Accepted: 01 December 2020
Published: 21 December 2020

Citation:
Kang JJ, Jang HK, Lim J-H, Lee D, Lee JH, Bae H, Lee CH, Kang C-K and Lee SH (2020) Characteristics of Different Size Phytoplankton for Primary Production and Biochemical Compositions in the Western East/Japan Sea. Front. Microbiol. 11:560102. doi: 10.3389/fmicb.2020.560102

The current phytoplankton community structure is expected to change, with small phytoplankton becoming dominant under ongoing warming conditions. To understand and evaluate the ecological roles of small phytoplankton in terms of food quantity and quality, the carbon uptake rates and intracellular biochemical compositions (i.e., carbohydrates, CHO; proteins, PRT; and lipids, LIP) of phytoplankton of different sizes were analyzed and compared in two different regions of the western East/Japan Sea (EJS): the Ulleung Basin (UB) and northwestern East/Japan Sea (NES). The average carbon uptake rate by the whole phytoplankton community in the UB (79.0 ± 12.2 mg C m^{-2} h^{-1}) was approximately two times higher than that in the NES (40.7 ± 2.2 mg C m^{-2} h^{-1}), although the average chlorophyll *a* (chl *a*) concentration was similar between the UB (31.0 ± 8.4 mg chl *a* m^{-2}) and NES (28.4 ± 7.9 mg chl *a* m^{-2}). The main reasons for the large difference in the carbon uptake rates are believed to be water temperature, which affects metabolic activity and growth rate, and the difference in euphotic depths. The contributions of small phytoplankton to the total carbon uptake rate were not significantly different between the regions studied. However, the rate of decrease in the total carbon uptake with increasing contributions from small phytoplankton was substantially higher in the UB than in the NES. This result suggests that compared to other regions in the EJS, the primary production in the UB could decrease rapidly under ongoing climate change. The calorific contents calculated based on biochemical compositions were similar between the small (1.01 ± 0.33 Kcal m^{-3}) and large (1.14 ± 0.36 Kcal m^{-3}) phytoplankton in the UB, whereas the biochemical contents were higher in the large phytoplankton (1.88 ± 0.54 Kcal m^{-3}) than in the small phytoplankton (1.06 ± 0.18 Kcal m^{-3}) in the NES. The calorific values per unit of chl *a* were higher for the large phytoplankton than for the small phytoplankton in both regions, which suggests that large phytoplankton could provide a more energy efficient food source to organisms in higher trophic levels in the western EJS.

Keywords: primary production, biochemical compositions, small phytoplankton, large phytoplankton, calorific content, East/Japan Sea

INTRODUCTION

Phytoplankton, as primary producers, play an important role in the food web as well as the biogeochemical cycling of aquatic ecosystems. Primary production by the phytoplankton community is an important factor in controlling the quantity of food sources for higher trophic level organisms and subsequently could affect the recruitment, biomass, and production of fishery resources (Whyte, 1987; Kleppel and Burkart, 1995; Kang et al., 2017). Intracellular biochemical compositions (i.e., carbohydrates, CHO; proteins, PRT; and lipids, LIP) of phytoplankton could provide helpful information related to their physiological status and the nutritional value of food available to grazers (Lee et al., 2020). According to previous studies, the different biochemical compositions of phytoplankton are closely connected with the nutritional status and survival strategies of zooplankton communities (Scott, 1980; Sterner et al., 1993; Hessen et al., 1997; Lindqvist and Lignell, 1997; Yun et al., 2015; Jo et al., 2017). The quantity and quality of food provided by phytoplankton can be largely affected by various environmental conditions, such as light conditions, major nutrient availability, and phytoplankton species composition (Morris et al., 1974; Mortensen et al., 1988; Kilham et al., 1997; Lee et al., 2017a). In particular, phytoplankton size structure is one of the major factors controlling the efficiency of the transfer of energy fixed by photosynthesis toward upper trophic levels or into the ocean's interior (Legendre and Rassoulzadegan, 1996; Falkowski and Oliver, 2007; Finkel et al., 2010; Marañón et al., 2012). Marine ecosystems dominated by small phytoplankton have low carbon export rates due to slow sinking rates and intense microbial decomposition of organic matter, whereas high downward export fluxes and efficient transfer of food material (FM) through short food chains appear in systems dominated by large phytoplankton (Marañón et al., 2012). Several studies have reported that recent climate change could lead to an increase in the contribution of small phytoplankton to the total phytoplankton biomass; thus, determining the ecological role of small phytoplankton as primary producers providing basic food sources in marine ecosystems is important under ongoing warming conditions (Agawin et al., 2000; Morán et al., 2010; Hilligsøe et al., 2011; Mousing et al., 2014).

The East/Japan Sea (EJS), located in the northwestern Pacific Ocean, is one of the highly productive oceanic regions and is regarded as a "miniature ocean" due to its dynamic environmental conditions (i.e., upwelling, eddies, and fronts) (Kwak et al., 2014; Lee et al., 2017b). The EJS includes three deep (>2000 m) basins: the Ulleung Basin, Yamato Basin, and Japan Basin. Among these basins, the most productive region is the Ulleung Basin (UB), which is located in the southwestern part of the EJS (Kwak et al., 2014; Lee et al., 2017b). Recently, the EJS, including the UB, has experienced notable changes in its physicochemical properties, such as drastic increases in sea surface temperature and rapid ocean acidification (Kim et al., 2001; Kang et al., 2003). These changes could accompany variations in biological characteristics, especially in phytoplankton communities and, subsequently, upper trophic levels (Chiba et al., 2012; Kang et al., 2017; Lee et al., 2017b). Indeed, remarkable changes in the duration and intensity of the phytoplankton spring bloom in the EJS (Lee et al., 2014) and a significant decline in the annual primary production in the UB (Joo et al., 2014) were reported by previous studies. In addition, Lee et al. (2017b) found decreasing trends in primary productivity with increasing contributions from small phytoplankton to the total community in the northern EJS. However, few studies have focused on the role of small phytoplankton as primary producers and basic food sources in the EJS, especially in the UB, which is considered a biological hotspot in the EJS.

In this research, differences in primary production and biochemical compositions by phytoplankton size were analyzed at two regions in the western EJS (i.e., the UB and northwestern East/Japan Sea – NES) during the spring bloom season. The primary objective in this study was to evaluate the effect of contributions from small phytoplankton on the total primary production in the western EJS. The other objective was to compare the difference in the physiological status and energy efficiency of the small and large phytoplankton in the western EJS.

MATERIALS AND METHODS

Sample Collection and Environmental Data

Sampling of the carbon uptake rates of phytoplankton in the western EJS was carried out at 10 stations (UB: five stations and NES: five stations) selected from a total of 34 stations sampled during a joint Korean-Russian cruise conducted from 05 to 15 April 2016 (**Figure 1** and **Table 1**). Temperature, salinity and density data were obtained using a CTD tool (conductivity, temperature, and depth tool; SBE 911 plus, Seabird Electronics Inc., Bellevue, WA, United States). The mixed layer depth (MLD) at each station was defined as the depth with a difference of 0.125 σ_t from the surface value (Gardner et al., 1995; Kwak et al., 2014). Water samples were collected to assess nutrient levels (nitrate, NO_3; ammonium, NH_4; phosphate, PO_4; and silicate, SiO_4) from three light depths (100, 30, and 1% penetration of surface photosynthetically active radiation, PAR) using Niskin bottles (12 L) attached to a CTD/rosette sampler at all the stations at which productivity was sampled. After the seawater samples were filtered through Whatman GF/F filters, each sample was immediately transferred into high-density polyethylene bottles (50 mL) and kept frozen at –80°C until analysis. The samples were returned to the home laboratory at Pusan National University, South Korea, and then nutrient concentrations were determined using an automated nutrient analyzer (Auto analyzer, Quaatro, Germany).

Small and Large Size-Fractionated Chlorophyll *a* Measurement

Seawater samples for small (0.7–2.0 μm) and large (>2.0 μm) size-fractionated chlorophyll *a* (chl *a*) molecules were obtained from the three depths at which light was measured (i.e., 100, 30, and 1% PAR penetration). To estimate the size composition of the phytoplankton assemblages, the seawater samples were passed

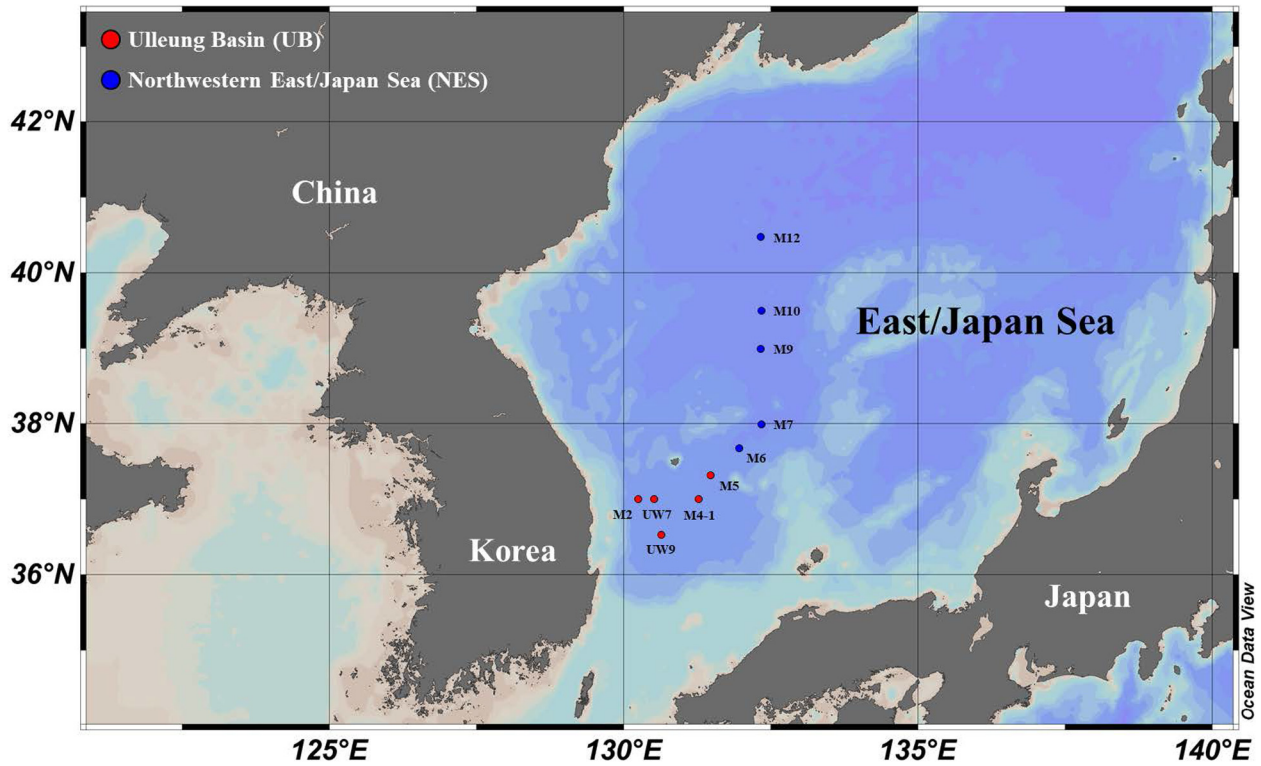

FIGURE 1 | Locations of sampling stations for primary productivity and biochemical composition measurements in the western EJS in 2016.

sequentially through a 2 μm (large chl *a*) Nuclepore membrane filter (47 mm) and then a 0.7 μm (small chl *a*) Whatman GF/F paper (47 mm). The filters were frozen immediately for further analysis in the laboratory. After extraction in 90% acetone, the concentrations of the size-fractionated chl *a* were determined with a previously calibrated fluorometer (Turner Designs model 10-AU) based on methods described by Kim et al. (2015).

Measurement of the Carbon Uptake Rate of Phytoplankton

The carbon uptake rates of small (0.7–2.0 μm) and large (>2.0 μm) phytoplankton in the western EJS were measured with a ^{13}C stable isotope technique. Seawater samples for carbon uptake rate measurement were obtained from six light depths (100, 50, 30, 12, 5, and 1%) at the selected productivity stations where incubation was available on deck under natural light conditions. A water sample from each of the different light depths was transferred into a polycarbonate incubation bottle (1 L) with a screen filter that created conditions corresponding to each light depth. A labeled carbon ($NaH^{13}CO_3$) solution, which corresponded to approximately 10% of the ambient concentration, was injected into all the incubation bottles to determine the carbon uptake rates of the phytoplankton (Dugdale and Goering, 1967; Hama et al., 1983; Lee et al., 2007, 2017b). The bottles were cultured in an acrylic incubator cooled by circulating surface seawater on deck for 4–5 h. To estimate the carbon uptake rate of the large phytoplankton, which was calculated as the difference in the carbon uptake rates of the total and small phytoplankton, the seawater samples used to assess the total phytoplankton carbon uptake rate from each incubation bottle were filtered through 25 mm GF/F filters after incubation. To assess the carbon uptake rate of the small phytoplankton, the seawater samples were first passed through a 2 μm Nuclepore filter (47 mm) to remove the large cells, and then the filtrate was passed through a 25 mm GF/F filter. The filters were immediately stored in a deep freezer for later mass spectrometer analysis. At the laboratory, acid fuming was applied overnight to all the samples for carbonate removal. The carbon stable isotope (^{13}C) of the treated samples was measured using a Finnigan Delta + XL mass spectrometer at the stable isotope laboratory of the University of Alaska Fairbanks, United States. The carbon uptake rate was calculated following methods described by Hama et al. (1983).

Biochemical Composition Measurements

To determine the biochemical compositions (carbohydrates, CHO; proteins, PRT; and lipids, LIP) of the phytoplankton, seawater samples were collected from three light depths (100, 30, and 1%) at seven stations selected from the 10 productivity stations (UB: three stations and NES: four stations). Each sample for the analysis of the total phytoplankton biochemical composition was filtered through 0.7 μm Whatman GF/F filters (47 mm). To evaluate the biochemical compositions of the small phytoplankton, additional water samples were

TABLE 1 | Environmental variables, euphotic depth-integral chl *a* concentration and carbon uptake rates in the western EJS during the 2016 cruise.

Region	Station	Date (2016)	T_{eu} (°C)	S_{eu} (psu)	Z_{eu} (m)	Z_m (m)	NO_3 (μM)	NH_4 (μM)	SiO_2 (μM)	PO_4 (μM)	Integrated Chl *a* (mg Chl *a* m^{-2})		Integrated carbon uptake rate (mg C m^{-2} h^{-1})	
											Small	Large	Small	Large
Ulleung Basin (UB)	M2	07-April	12.9	34.4	51	49	1.47	0.62	1.55	0.22	26.7	18.4	34.9	36.1
	M4-1	08-April	13.8	34.5	33	28	1.10	0.60	2.01	0.24	16.3	10.7	36.4	43.9
	M5	09-April	14.5	34.5	35	56	0.74	0.45	1.26	0.12	10.5	12.7	39.3	59.3
	UW7	13-April	12.3	34.2	27	75	2.10	0.48	3.57	0.28	14.6	17.0	34.2	43.9
	UW9	14-April	13.4	34.4	27	88	1.34	0.53	3.18	0.15	19.0	9.4	32.2	34.8
North western EJS (NES)	M6	12-April	10.6	34.2	22	27	0.86	0.55	3.26	0.07	12.6	7.7	15.0	26.5
	M7	12-April	10.2	34.1	22	21	0.63	0.63	3.20	0.02	12.6	10.2	15.1	28.4
	M9	11-April	7.4	34.0	19	32	0.84	0.63	4.81	0.09	13.4	14.7	15.2	26.1
	M10	11-April	6.3	34.0	22	33	1.58	0.53	5.70	0.18	14.0	16.2	20.2	17.6
	M12	10-April	4.9	33.9	24	37	2.05	0.56	5.07	0.20	12.9	27.7	14.2	25.0

T_{eu}, water temperature averaged over the depth of the euphotic zone (Z_{eu}); S_{eu}, salinity averaged over Z_{eu}; Z_m, mixed layer depth.

passed sequentially through 2 μm Nucleopore membrane filters (47 mm) and 0.7 μm Whatman GF/F filters (47 mm). The biochemical compositions of the large phytoplankton were estimated as the difference in the compositions between the total and small phytoplankton. The filters were frozen immediately and preserved for further analysis at the laboratory. Each biochemical compound (CHO, PRT, and LIP) was analyzed at the laboratory based on the methods of Lowry et al. (1951); Dubois et al. (1956), and Bligh and Dyer (1959), respectively. The detailed methods used for analyzing each biochemical compound are described in Bhavya et al. (2019). FM represented the sum of the three biochemical components (CHO, PRT, and LIP), and calorific contents were calculated following Winberg (1971).

RESULTS

Environmental Conditions

The hydrographic conditions were different between the UB and NES during the spring season in 2016. The MLD (derived from the density difference) at the UB stations had a relatively wide range, from 28 to 88 m (mean ± *SD* = 59.2 m ± 23.3 m), whereas the MLD at the NES stations ranged from 21 to 37 m, with a mean of 30.0 m (*SD* = ±6.2 m) (**Figure 2** and **Table 1**). The MLDs at all the stations in the UB [except for station M4-1 (28 m)] were deeper (*t*-test, $p < 0.05$) than the those in the NES (**Figure 2** and **Table 1**). The euphotic depths (i.e., the depth receiving 1% of the surface PAR) were also relatively deeper (*t*-test, $p < 0.05$) in the UB stations (range = 27–51 m; mean ± *SD* = 34.6 ± 9.8 m) than in the NES stations (range = 19–24 m; mean ± *SD* = 21.8 ± 1.8 m) (**Table 1**). Overall, the MLD was similar to the euphotic depth or deeper than the euphotic depth in both regions (**Table 1**), which indicates that the euphotic water columns were well mixed during our observation period (**Figure 2**). The water temperatures averaged over the depths of the euphotic zone in the UB ranged from 12.3 to 14.5°C (13.6 ± 0.9°C), whereas the average temperature within the euphotic zone in the NES ranged from 4.9 to 10.6°C (7.9 ± 2.5°C) (**Table 1**). The salinity ranged from 34.2 to 34.5 psu in the UB (34.4 ± 0.1 psu) and 33.9 to 34.2 psu in the NES (34.0 ± 0.1 psu) (**Table 1**). Temperature and salinity were higher (*t*-test, $p < 0.01$) in the UB than in the NES during the study period (**Table 1**).

No noticeable differences in any of the major nutrient (NH_4, NO_3, PO_4, and SiO_2) concentrations were found at the different light depths (100, 30, and 1%) (one-way ANOVA, $p > 0.05$) in either region (**Figure 3**) since the water column within the euphotic zone was well mixed. The mean concentrations of all the major nutrients (NH_4, NO_3, and PO_4) except for SiO_2 averaged over the euphotic zone were not significantly different (*t*-test, $p > 0.05$) between the UB (NH_4 = 0.54 ± 0.08 μM; NO_3 = 1.35 ± 0.50 μM; PO_4 = 0.20 ± 0.07 μM) and the NES (NH_4 = 0.58 ± 0.05 μM; NO_3 = 1.19 ± 0.60 μM; PO_4 = 0.11 ± 0.07 μM) (**Table 1**). In contrast, the averaged SiO_2 concentration was lower (*t*-test, $p < 0.05$) in the UB (mean ± *SD* = 2.31 ± 1.01 μM) than in the NES (mean ± *SD* = 4.41 ± 1.37 μM) (**Table 1**).

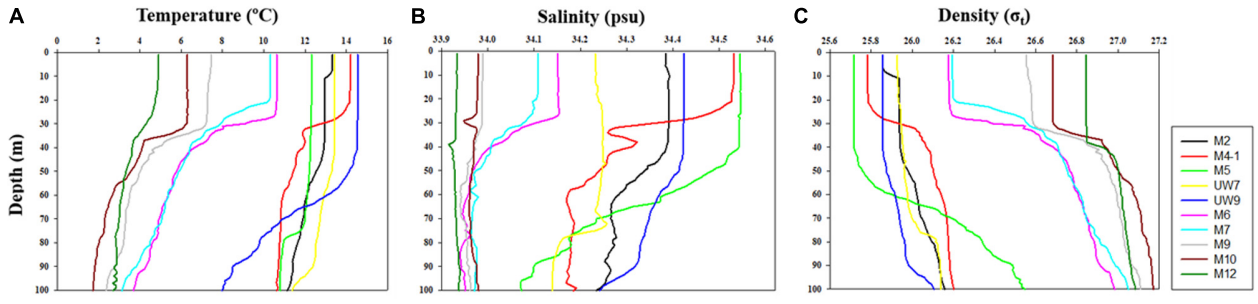

FIGURE 2 | Vertical structures of **(A)** temperature, **(B)** salinity, and **(C)** density at all the experimental stations in the western EJS in 2016.

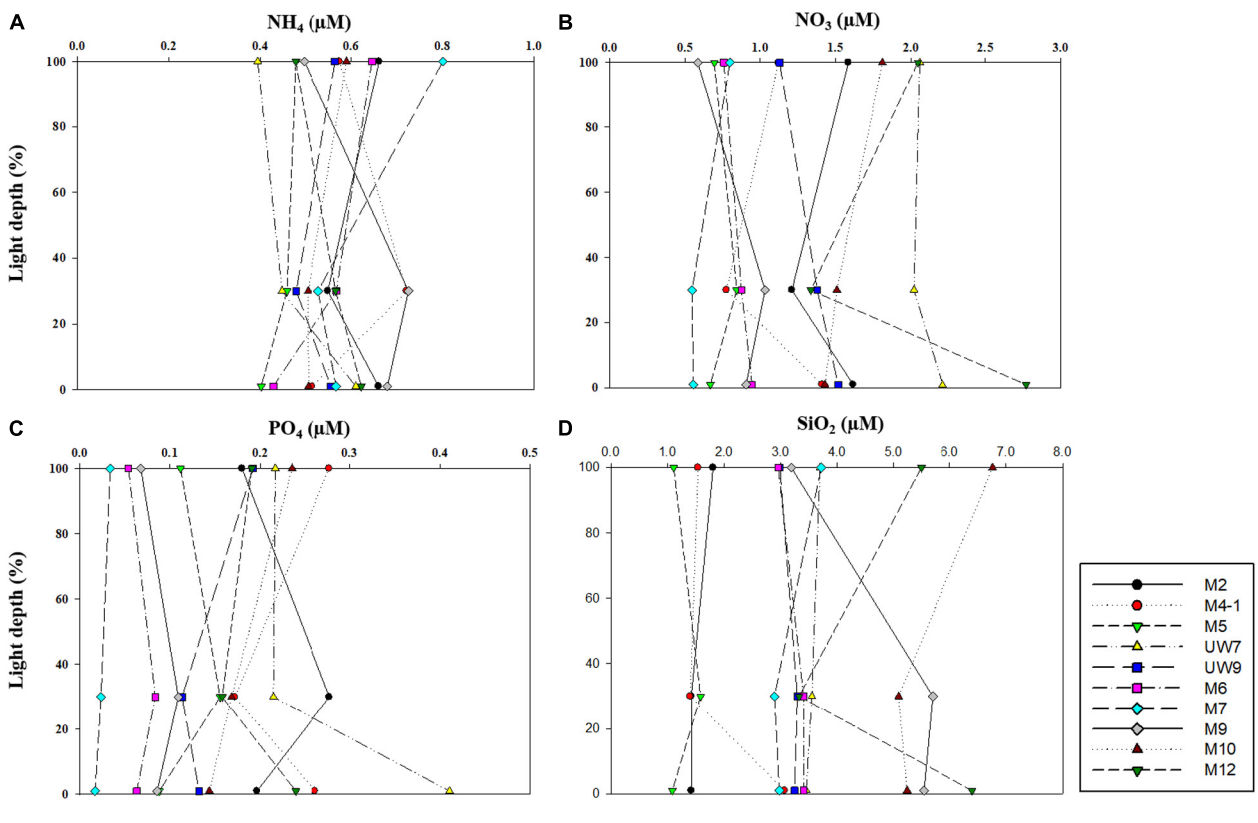

FIGURE 3 | Concentrations of **(A)** ammonium (NH_4), **(B)** nitrate (NO_3), **(C)** phosphate (PO_4), and **(D)** silicate (SiO_4) within euphotic depth (100, 30, and 1% light depth) in 2016.

Spatial Distribution of Phytoplankton Chl *a* Concentration in the UB and NES

No distinct vertical differences in the concentrations of the total (sum of the small and large chl *a* concentrations), small or large chl *a* molecules were found within the euphotic depth at each station (one-way ANOVA, $p > 0.05$; **Figures 4A,B**) in this study. The total chl *a* concentration integrated from the surface to a depth with 1% light penetration in the UB ranged from 23.2 to 45.1 mg chl *a* m^{-2}, with an average of 31.0 mg chl *a* m^{-2} (*SD* = ± 8.4 mg chl *a* m^{-2}), and that in the NES ranged from 20.3 to 40.7 mg chl *a* m^{-2}, with an average of 28.4 mg chl *a* m^{-2} (*SD* = ± 7.9 mg chl *a* m^{-2}) (**Figure 5A** and **Table 1**). In the UB region, the average values of the concentrations of chl *a* from small and large phytoplankton integrated over depths with light penetration ranging from 100 to 1% were 17.4 ± 6.0 mg chl *a* m^{-2} (range: 10.5–26.7 mg chl *a* m^{-2}) and 13.6 ± 3.9 mg chl *a* m^{-2} (range: 9.4–18.4 mg chl *a* m^{-2}), which contributed 55.6 ± 9.5% and 44.4 ± 9.5% to the total chl *a* concentration, respectively (**Figure 5A** and **Table 1**). In contrast, the average chl *a* concentrations of the small and large phytoplankton over the same depth in the NES were 13.1 ± 0.6 mg chl *a* m^{-2} (range: 12.6–14.0 mg chl *a* m^{-2}) and 15.3 ± 7.7 mg chl *a* m^{-2} (range: 7.7–27.7 mg chl *a* m^{-2}), which contributed 48.6 ± 11.3% and 51.4 ± 11.3%

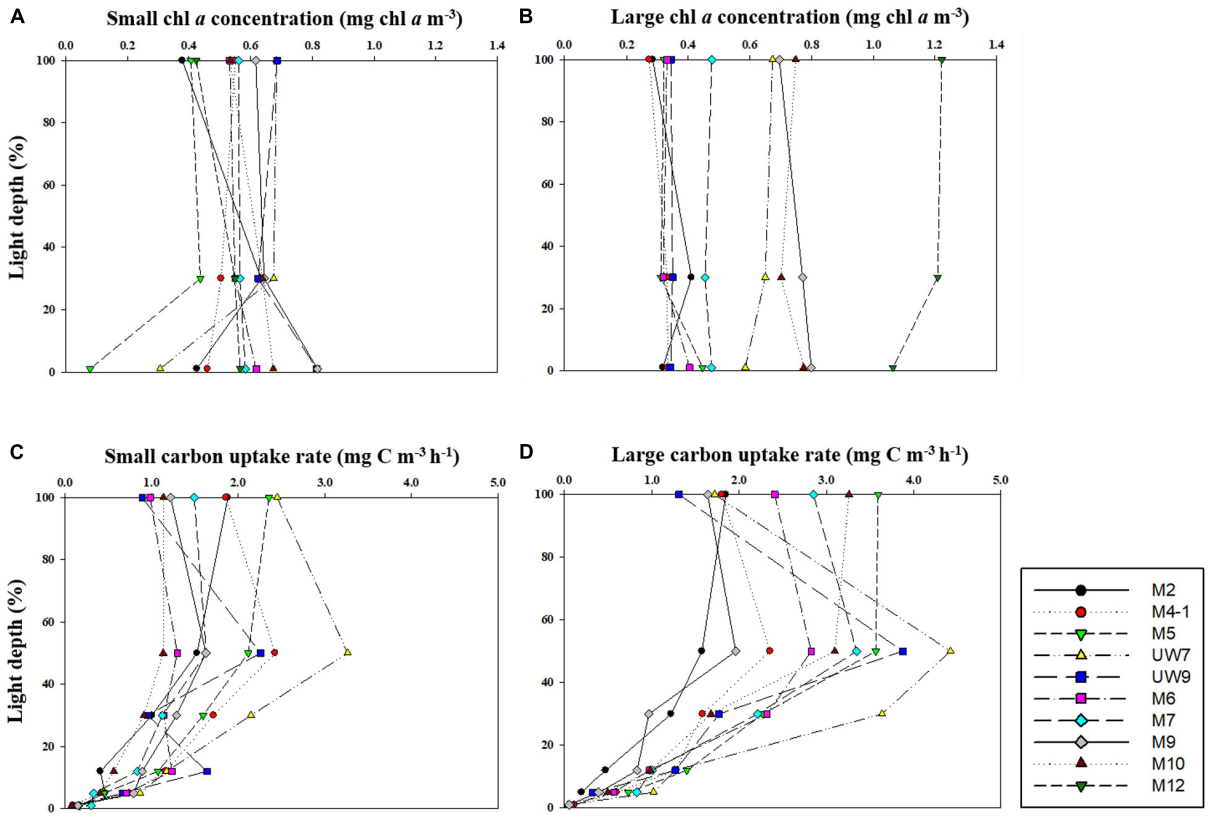

FIGURE 4 | Vertical distributions of chl *a* concentration for **(A)** small and **(B)** large size phytoplankton and carbon uptake rates for **(C)** small and **(D)** large size phytoplankton at different light depths in 2016.

to the total chl *a* concentration, respectively (**Figure 5A** and **Table 1**).

Carbon Uptake Rates of Phytoplankton in the UB and NES

The hourly carbon uptake rates of the total, small and large phytoplankton communities within the euphotic water column differed at each light depth in the UB and the NES (**Figures 4C,D**). In general, the maximum hourly carbon uptake rates of the phytoplankton were observed in the surface layer (within a water depth of 10 m), which corresponded to a light depth of 50% (**Figures 4C,D**). The hourly carbon uptake rates of the total phytoplankton community integrated from the surface to the 1% light depth were approximately two times higher in the UB than in the NES during the observation period (**Table 1**). The range of the total carbon uptake rates from the surface to the 1% light depth was from 67.0 to 98.7 mg C m^{-2} h^{-1}, with a mean of 79.0 mg C m^{-2} h^{-1} (*SD* = ± 12.2 mg C m^{-2} h^{-1}) in the UB, whereas the range of the total hourly carbon uptake rates over the same depth in the NES was from 37.7 to 43.6 mg C m^{-2} h^{-1}, with a mean of 40.7 mg C m^{-2} h^{-1} (*SD* = ± 2.2 mg C m^{-2} h^{-1}) during the study period (**Figure 5B** and **Table 1**). The hourly carbon uptake rates of the small and large phytoplankton communities integrated from the surface to the 1% light depth in the UB ranged from 32.2 to 39.3 mg C m^{-2} h^{-1} (35.4 ± 2.7 mg C m^{-2} h^{-1}) and from 34.8 to 59.3 mg C m^{-2} h^{-1} (43.6 ± 9.8 mg C m^{-2} h^{-1}), respectively (**Figure 6** and **Table 1**). In contrast, the integrated carbon uptake rates by the small and large phytoplankton communities in the NES ranged from 14.2 to 20.2 (15.9 ± 2.4 mg C m^{-2} h^{-1}) and from 17.6 to 28.4 (24.7 ± 4.2 mg C m^{-2} h^{-1}), respectively (**Figure 6** and **Table 1**). The average carbon uptake rates (*t*-test, $p < 0.05$) of the small and large phytoplankton communities were higher in the UB than in the NES during our observation period (**Figure 6** and **Table 1**). The contributions of small phytoplankton in the UB to the total carbon uptake rate ranged from 39.9 to 49.2%, with an average of 45.2% (*SD* = ± 3.7%), whereas those of large phytoplankton in the UB ranged from 50.8 to 60.1%, with an average of 54.8% (*SD* = ± 3.7%). In the NES, the small phytoplankton contributed 39.5 ± 7.8% (range: 34.8–53.4%) to the total phytoplankton carbon uptake rate, while the large phytoplankton contributed 60.5 ± 7.8% (range: 46.6–65.2%) (**Figure 5B** and **Table 1**).

Principal component analysis (PCA; SPSS 12.0) was conducted to evaluate the relationship between the environmental conditions and carbon uptake rates of the phytoplankton. The first two ordination axes of the PCA explained 79.8% of the carbon uptake rates of the total, small and large phytoplankton communities relative to the environmental conditions during our research period (**Figure 7**). Water

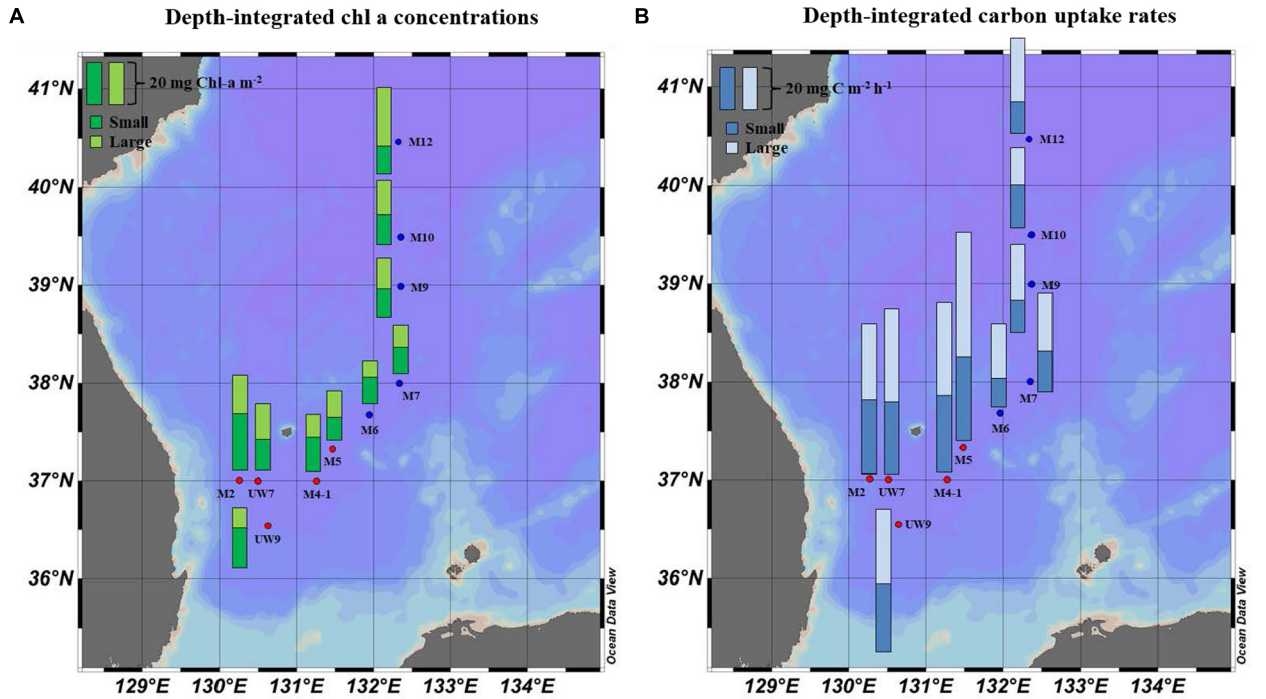

FIGURE 5 | Spatial distributions of **(A)** chl *a* concentration and **(B)** hourly carbon uptake rates for small and large size phytoplankton integrated within the euphotic depths from 100 to 1% light depth at the productivity stations in 2016.

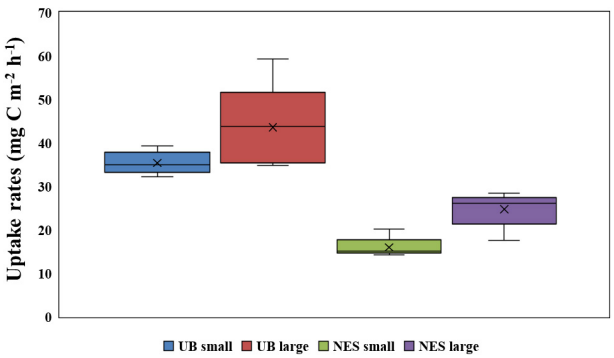

FIGURE 6 | Comparison of depth-integral carbon uptake rates for small and large size phytoplankton in the UB and NES.

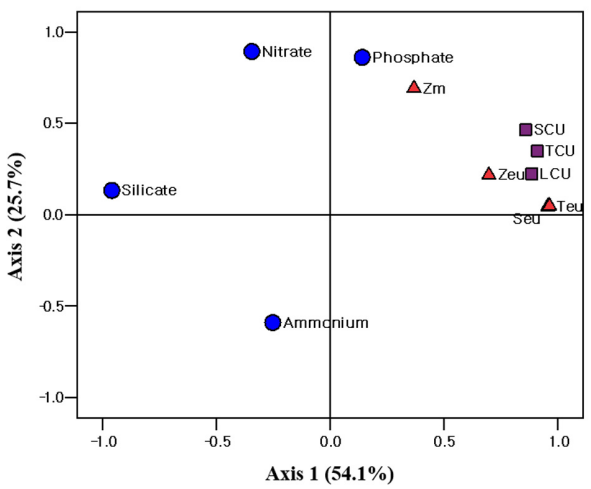

FIGURE 7 | Principle component analysis (PCA) ordination plots of axes 1 and 2 showing carbon uptake rate of different size phytoplankton in relation to environmental variables in the western EJS during the 2016 cruise. T_{eu}, water temperature averaged over the depth of the euphotic zone (Z_{eu}); S_{eu}, salinity averaged over Z_{eu}; Z_m, mixed layer depth; TCU, total carbon uptake rate; SCU, small carbon uptake rate; LCU, large carbon uptake rate.

temperature, salinity, and euphotic depth were positively correlated with the carbon uptake rates of the total, small, and large phytoplankton communities (**Figure 7**). The effect of nutrients on the carbon uptake rates of the entire phytoplankton group was not significant during the study period (**Figure 7**).

Biochemical Compositions of the Phytoplankton in the UB and NES

The concentrations of the biochemical components (CHO, PRT, and LIP) in both regions are summarized in **Table 2**. The relative abundances of the biochemical components in the small and large phytoplankton communities in the UB and NES were averaged from the surface to 1% light depth to detect their spatial variation (**Figure 8**). In the UB, the average compositions of CHO, PRT, and LIP in the small phytoplankton were

TABLE 2 | Concentrations of biochemical compositions, food materials, and calorific contents in the western EJS during the 2016 cruise.

			Small size phytoplankton					Large size phytoplankton				
Region	**Station**	**light depth**	**CHO (mg m^{-3})**	**PRT (mg m^{-3})**	**LIP (mg m^{-3})**	**FM (mg m^{-3})**	**Cal (Kcal m^{-3})**	**CHO (mg m^{-3})**	**PRT (mg m^{-3})**	**LIP (mg m^{-3})**	**FM (mg m^{-3})**	**Cal (Kcal m^{-3})**
Ulleung Basin (UB)	M5	100	56.1	10.2	47.5	113.8	0.74	32.8	30.5	54.8	118.1	0.82
	M5	30			N/A					N/A		
	M5	1	55.7	12.1	53.9	121.7	0.81	16.4	36.4	134.6	187.5	1.55
	UW7	100	176.8	14.5	94.1	285.4	1.70	37.8	57.1	20.6	115.6	0.67
	UW7	30	50.9	20.8	50.2	121.9	0.80	149.3	71.2	53.3	273.9	1.51
	UW7	1			N/A					N/A		
	UW9	100	115.9	4.3	63.7	183.9	1.10	29.2	69.7	73.9	172.7	1.20
	UW9	30	78.0	17.9	51.2	147.2	0.91	103.3	56.1	71.6	230.9	1.41
	UW9	1	86.0	13.9	59.8	159.7	1.00	71.4	45.0	31.4	147.9	0.84
North western EJS (NES)	M6	100	81.3	19.6	45.6	146.5	0.87	19.4	32.1	148.8	200.4	1.67
	M6	30	85.1	18.1	54.1	157.4	0.96	42.0	27.3	191.2	260.5	2.14
	M6	1	71.6	32.2	54.6	158.4	0.99	53.4	10.1	172.8	236.3	1.92
	M7	100	71.1	27.9	49.3	148.3	0.91	35.7	64.8	234.3	334.8	2.73
	M7	30	71.9	19.0	86.3	177.1	1.22	76.3	65.9	126.9	269.0	1.88
	M7	1	38.8	30.7	67.7	137.2	0.97	86.8	63.6	151.4	301.8	2.14
	M9	100	74.4	41.8	101.4	217.5	1.50	116.9	101.4	158.2	376.5	2.54
	M9	30	79.2	32.0	75.5	186.7	1.22	100.3	79.6	138.5	318.3	2.16
	M9	1	74.6	38.5	55.6	168.8	1.05	14.0	62.1	152.3	228.4	1.85
	M12	100	68.5	27.1	64.2	159.8	1.04	120.3	45.2	92.0	257.5	1.62
	M12	30	63.8	33.4	63.9	161.1	1.05	78.7	41.3	27.7	147.7	0.81
	M12	1	52.9	22.0	61.9	136.8	0.93	95.8	27.5	57.0	180.3	1.09

CHO, carbohydrates; PRT, proteins; LIP, lipids; FM, food material; Cal, calorific content; N/A, not available.

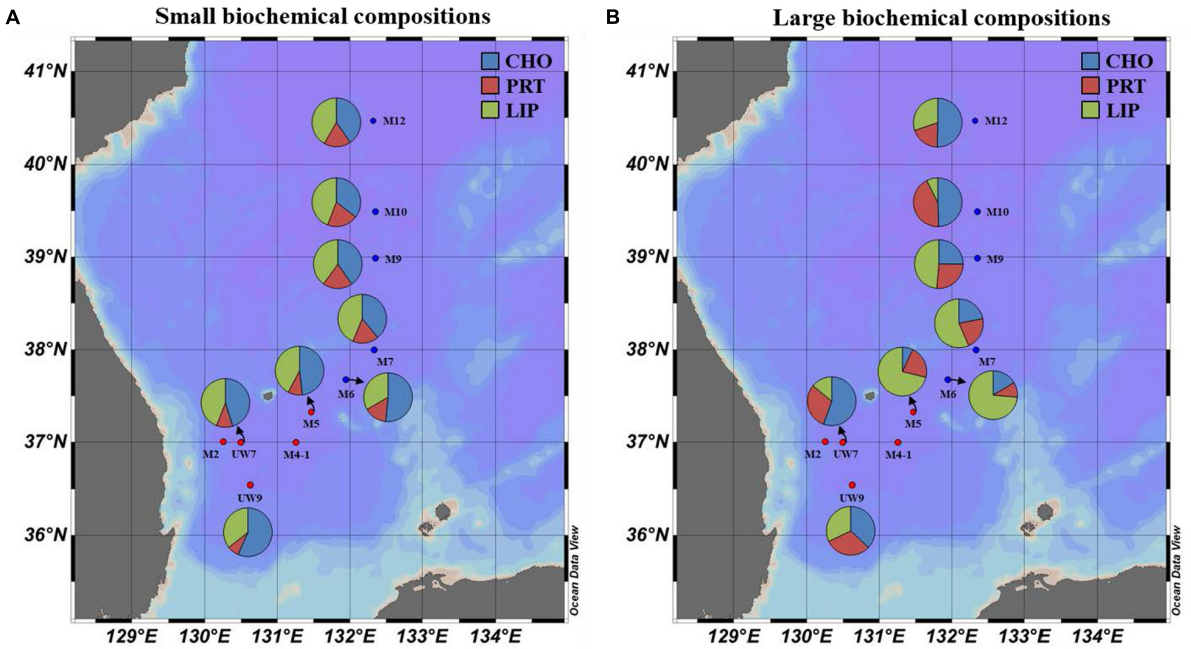

FIGURE 8 | Spatial distributions of biochemical compositions (carbohydrates, proteins, and lipids) for **(A)** small and **(B)** large size phytoplankton in the western EJS in 2016. CHO, carbohydrates; PRT, proteins; LIP, lipids.

52.7 ± 7.9% (range: 41.8–63.0%), 9.2 ± 4.8% (range: 2.3–17.1%), and 38.1 ± 4.3% (range: 33.0–44.2%), respectively, whereas those of the large phytoplankton were 33.4 ± 16.9% (range: 8.8–54.5%), 30.8 ± 10.5% (range: 19.4–49.4%), and 35.8 ± 19.5% (range: 17.8–71.8%) (**Figure 8** and **Table 2**), respectively. In the NES, the CHO, PRT, and LIP contents in the small phytoplankton comprised 42.8 ± 7.6% (range: 28.3–55.5%), 17.5 ± 4.0% (range: 10.7–22.8%), and 39.7 ± 6.5% (range: 31.1–49.4%), respectively, while the average proportions of three biochemical components (CHO, PRT, and LIP) within the large phytoplankton were 28.2 ± 16.3% (range: 6.1–53.3%), 19.6 ± 7.3% (range: 4.3–28.0%), and 52.2 ± 18.9% (range: 18.7–74.3%), respectively (**Figure 8** and **Table 2**).

The calorific contents averaged from the euphotic depths in the UB ranged from 0.74 to 1.70 Kcal m^{-3}, with a mean of 1.01 ± 0.33 Kcal m^{-3}, for the small phytoplankton and from 0.67 to 1.55 Kcal m^{-3}, with a mean of 1.14 ± 0.36 Kcal m^{-3}, for the large phytoplankton (**Table 2**). The average calorific contents in the NES ranged from 0.87 to 1.50 Kcal m^{-3} (1.06 ± 0.18 Kcal m^{-3}) for the small phytoplankton and from 0.81 to 2.73 Kcal m^{-3} (1.88 ± 0.54 Kcal m^{-3}) for the large phytoplankton (**Table 2**).

DISCUSSION

Spatial Distributions of Size-Fractionated Chl *a* Concentration in the Two Different Regions of the Western EJS

The average total chl *a* concentrations in both regions were similar; the phytoplankton community compositions differed slightly by size between the UB and the NES (**Figure 5A** and **Table 1**), although no significant difference was found. Based on the size-fractionated chl *a* concentration, small phytoplankton (55.6 ± 9.6%) had a relatively higher contribution to the total biomass in the UB, whereas the contribution of large phytoplankton (51.4 ± 11.3%) was slightly higher than that of small phytoplankton in the NES (**Table 1**).

Noticeable patterns in the spatial distributions of the chl *a* concentrations of small and large phytoplankton integrated over the depths sampled were not found in the UB, whereas the integrated chl *a* concentration of the large phytoplankton in the NES increased with latitude, with the lowest value at M6 (7.7 mg chl *a* m^{-2}) and the highest value at M12 (27.7 mg chl *a* m^{-2}) (**Figure 5A** and **Table 1**). The spatial variations in the concentration of chl *a* from the large phytoplankton integrated from the surface to a light depth of 1% in the NES were mostly related to temperature (Pearson's $r = -0.93$, $p < 0.05$) and nitrate concentration (Pearson's $r = 0.90$, $p < 0.05$) during the study period. Phytoplankton community size structure is sensitive to environmental conditions. According to previous studies, the size compositions of phytoplankton assemblages in the ocean can be affected by water temperature (Morán et al., 2010; Mousing et al., 2014) and nutrient availability (Agawin et al., 2000; Finkel et al., 2005, 2007; Marañón et al., 2012). Increasing water temperature increases the metabolic rate of phytoplankton (Gillooly et al., 2001), which increases resource requirements and, therefore, competition for nutrients (Mousing et al., 2014). In addition, warming temperatures increase the development of water stratification, resulting in nutrient depletion in the euphotic layer (Calvo-Díaz and Morán,

2006; Marañón et al., 2012). In other words, both the increasing cellular nutrient demands due to high metabolic rates as a function of temperature and a reduction in upward nutrient concentration in the euphotic layer due to water stratification can be expected to cause increasing resource competition and a smaller community mean cell size (Mousing et al., 2014). Among the major inorganic nutrients in the ocean, source of nitrogen (e.g., nitrate and ammonium) are the main factors controlling phytoplankton cell size (Stolte et al., 1994; Stolte and Riegman, 1995). In general, large phytoplankton tend to prefer nitrate, which is abundant in upwelling areas, in coastal areas in early spring, and on continental shelves, whereas ammonium is favored by small phytoplankton (Dauchez et al., 1996; Stolte and Riegman, 1995). Indeed, relatively low temperatures and high nitrate concentrations were generally observed in the higher latitudes of the NES during our research period (**Table 1**).

Overall, the average total chl *a* concentrations in the UB (31.0 mg chl *a* m^{-2}) and NES (28.4 mg chl *a* m^{-2}) during the spring season of 2016 were lower than those reported previously in the EJS (Kang et al., 2004; Lee et al., 2017b). During the spring bloom in the UB during April 2001, a high chl *a* concentration (43.8 mg chl *a* m^{-2}) was observed (Kang et al., 2004). During this period, autotrophic nanoflagellates and picoeukaryotes were the main components of the total chl *a* (Kang et al., 2004). This finding was similar to our results, which showed that the contribution of small phytoplankton to the total chl *a* was high (55.6%) in the UB. In the northern EJS, including the NES region in spring 2015, Lee et al. (2017b) reported significantly higher chl *a* concentrations (84.6 mg chl *a* m^{-2}), which were predominantly (47.7–72.5%) due to large phytoplankton. In contrast, the chl *a* concentration (28.8 mg chl *a* m^{-2}) in the shelf region of the southern East China Sea (Chen, 2000) is similar to those in the UB and NES during our research period, and the size compositions (small: 57.4% and large: 42.6%) in the shelf region are close to those in the UB in this study. Currently experiencing rapid environmental changes, the northern Chukchi Sea in the Arctic Ocean also had similar chl *a* concentrations (30.5 mg chl *a* m^{-2}) and size compositions (small: 55.1% and large: 44.9%) (Yun et al., 2015) as those found in this study. The relatively high contributions of small phytoplankton to the total community in the shelf regions of the southern East China Sea and the northern Chukchi Sea are known to result from depleted nitrogen sources, especially nitrate (Chen, 2000; Yun et al., 2015).

Difference in the Carbon Uptake Rate Between the UB and NES

Based on the chl *a* concentration, the total phytoplankton biomass was not significantly different between the UB (31.0 ± 8.4 mg chl *a* m^{-2}) and NES (28.4 ± 7.9 mg chl *a* m^{-2}) during our research period. However, the hourly carbon uptake rate of the total phytoplankton community in the UB (79.0 ± 12.2 mg C m^{-2} h^{-1}) was approximately two times higher (*t*-test, $p < 0.01$) than that in the NES (40.7 ± 2.2 mg C m^{-2} h^{-1}) (**Figure 6** and **Table 1**). Primary production can be affected by various physicochemical and biological factors, such as temperature, light availability, ambient nutrient concentrations, phytoplankton community structure, and grazing pressure (Kwak et al., 2014; Lee et al., 2020). Based on the PCA, temperature and euphotic depth were major controlling factors for the total and size-fractionated carbon uptake rates in both regions during the observation period (**Figure 7**). Lewandowska et al. (2012) found strong relationships between primary production by phytoplankton and temperature. Primary production had positive correlations with water temperature when nutrient concentrations and light availability were not limiting, whereas increased water temperature under unsaturated light conditions, which limits the carbon incorporation process, led to decreased primary production due to the enhancement of grazing activity and community respiration (Lewandowska et al., 2012). Other studies have also reported similar results on the positive effects of temperature on the photosynthesis (Andersson et al., 1994) and growth rate (Rhee and Gotham, 1981) of phytoplankton. In general, phytoplankton spring blooms start when light intensity increases in the upper water column through the development of stratification after well-mixed conditions during the winter (Huisman et al., 1999; Jo et al., 2007). This means that the main controlling factor for phytoplankton blooms in the spring season is not nutrients but light, since the major nutrients required for photosynthesis are made available by the mixing of the water column by wind in the winter season. Light availability might also not be a main limiting factor for photosynthesis during the peak timing of spring blooms. Indeed, the maximum carbon uptake rates during the study period were observed at the surface layer (100%–50% light depth: 0–8 m; **Table 1**). Therefore, the colder water temperature in the NES (7.9 ± 2.5°C) compared to that in the UB (13.4 ± 0.8°C) could have a negative effect on the phytoplankton community in terms of photosynthesis (i.e., carbon uptake rate). During the study period, the deeper euphotic depth in the UB than in the NES could have enabled the light to penetrate deeper, allowing more phytoplankton within the euphotic water column to photosynthesize. This can be another reason for the higher integrated carbon uptake rate of phytoplankton in the UB than in the NES.

Based on the average daily carbon uptake rate in this study, the estimated annual primary production in the UB and NES was 284 g C m^{-2} y^{-1} and 147 g C m^{-2} y^{-1}, respectively. The annual production in both regions during our research period is consistent with previous studies in the UB (273 g C m^{-2} y^{-1} and 280 g C m^{-2} y^{-1}) (Kwak et al., 2013; Joo et al., 2014) and in the northern EJS (159 g C m^{-2} y^{-1}), including the NES regions (Lee et al., 2017b). The annual primary production in the UB (a deep basin with a water depth > 2,000 m) was markedly higher than that in oceanic regions and other basins deeper than 200 m, whereas the annual primary production in the NES was similar to that in these regions. The annual primary production in oceanic regions was generally low, with a range from 55 to 102 g C m^{-2} y^{-1}, whereas upwelling regions had considerably higher primary production rates (300–398 g C m^{-2} y^{-1}) (Joo et al., 2014; references therein).

In the eastern and western basins of the Mediterranean Sea, which have environmental conditions similar to those in the EJS, the annual carbon uptake rates were 109 g C m^{-2} y^{-1} and 158 g C m^{-2} y^{-1}, respectively (Estrada, 1996). Because of its high productivity compared to those in other oceanic regions, the UB is considered a prominent biologically productive region and is referred to as a "hotspot" in the EJS (Kwak et al., 2013; Joo et al., 2014). This hot-spot is sustained by several potential mechanisms, such as different types of subpolar fronts (Chiba et al., 2008), frequent eddies (Hyun et al., 2009; Kim et al., 2012; Lim et al., 2012), and coastal upwellings (Yoo and Park, 2009).

Contributions of Small and Large Phytoplankton to the Total Carbon Uptake Rate

The contributions of small and large phytoplankton to the total carbon uptake rate were different from their contributions to the chl *a* in both regions. The large phytoplankton (mean ± *SD* = 54.8 ± 3.7%) had a higher contribution than the small phytoplankton (45.2 ± 3.7%) to the total carbon uptake rate of the total phytoplankton in the UB. In the NES, the contribution of large phytoplankton (60.5 ± 7.8%) to the total carbon uptake rate was significantly higher (*t*-test, $p < 0.01$) than that of small phytoplankton (39.5 ± 7.8%) (**Figure 5** and **Table 1**). The different contributions of small and large phytoplankton to the total chl *a* and carbon uptake rate during spring 2016 could have been caused by several environmental conditions (i.e., temperature and euphotic depth), as mentioned above. In the UB, the contribution of small phytoplankton to the total primary production for our cruise period (45.2%; spring season) was higher than that in July (35%; summer season) (Kwak et al., 2014). In general, small phytoplankton are predominant under warming conditions (Morán et al., 2010; Mousing et al., 2014). The low contribution of small phytoplankton observed in the UB, even in the summer season (Kwak et al., 2014), could be the result of dynamic environmental conditions (i.e., upwelling, eddies, and fronts), which allow the UB to have higher primary productivity than other oceanic regions and relatively constant primary production among different months and years (Lee et al., 2017b). Indeed, Kwak et al. (2014) measured a relatively high primary production rate (716 mg C m^{-2} d^{-1}) even in the summer season (June–August), when phytoplankton are not normally actively growing at other temperate locations (Lee et al., 2017b). The value observed in summer by Kwak et al. (2014) is comparable to the primary production rate observed during the spring bloom in this study (790 mg C m^{-2} d^{-1}).

According to previous studies (Agawin et al., 2000; Morán et al., 2010; Hilligsøe et al., 2011; Mousing et al., 2014), recent climate changes, especially warming temperatures, are expected to increase the contribution of small phytoplankton to the total phytoplankton community, which enhances the importance of small phytoplankton as a basic food source in marine ecosystems. Indeed, negative correlations between total primary production and small phytoplankton contributions were consistently observed in the Chukchi Sea (unpublished data) and the Amundsen Sea (Lee et al., 2017c), which have experienced rapid climate change. Lee et al. (2017b) reported a negative relationship between the small phytoplankton contribution and the total primary production in the northern EJS, which has been experiencing a drastic increase in sea surface temperature for several decades (Kim et al., 2001). We also found a marked decreasing trend in the total carbon uptake rates with increasing contributions of small phytoplankton in the UB (**Figure 9**). In addition, our data points observed in the NES are consistent with the regression line reported in Lee et al. (2017b). An interesting feature is that the rate of decrease in the total carbon uptake rate with increasing contributions of small phytoplankton is considerably faster (by approximately three times) in the UB than in the northern EJS (**Figure 9**). This is very meaningful, as it could indicate that the primary production in the UB, a biological hotspot in the EJS, might respond more sensitively to ongoing warming conditions.

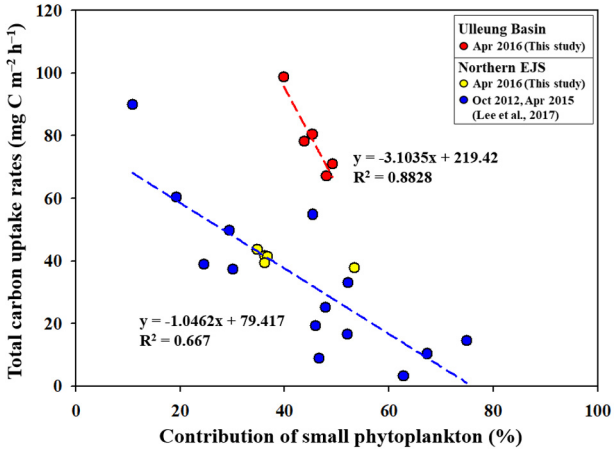

FIGURE 9 | Relationships between productivity contributions of small phytoplankton and the total primary productions in the UB and northern EJS.

Physiological Status and Food Quality of Phytoplankton in the Two Different Regions

The biochemical compositions of phytoplankton provide important information about their physiological status (Kang et al., 2017; Lee et al., 2020). According to previous studies, biochemical compositions are affected by environmental factors, such as nutrient concentrations (Morris et al., 1974; Kilham et al., 1997) and growth stages (Smith et al., 1987; Kang et al., 2017). The relative proportions of LIP and CHO, known as storage compounds, tend to be high under nutrient deficient conditions (especially when nitrogen sources are limiting) (Yun et al., 2015; Kim et al., 2016; Kang et al., 2017) and during stationary growth phases (Morris, 1981; Ríos et al., 1998; Kang et al., 2017), whereas the allocation of PRT increases when there are abundant nutrient resources (DiTullio and Laws, 1983; Palmisano et al., 1988). Overall, the biochemical composition of

the small phytoplankton during the study period as dominated by CHO (UB: 52.7 ± 7.9%; CE: 42.8 ± 7.6%), followed by LIP (UB: 38.1 ± 4.3%; CE: 39.7 ± 6.5%) in both regions (**Figure 8A** and **Table 2**). The small phytoplankton in the UB may have experienced a limitation in nutrient uptake due to competition with large phytoplankton during the study period. Large phytoplankton, such as diatoms, have a competitive advantage over small cells in nutrient-sufficient conditions due to their higher nutrient uptake rate (Litchman et al., 2007; Marañón et al., 2012) and accumulation ability (Thingstad et al., 2005; Marañón et al., 2012). In a parallel study on the species compositions of phytoplankton (unpublished data), the major classes for large phytoplankton in the UB were diatoms (28.5%) and cryptophytes (25.6%) which are known to assimilate significantly higher biochemical components during the active growth period with sufficient nutrients (Moal et al., 1987); small phytoplankton in the UB consisted of the prasinophytes (19.5%), prymnesiophytes (13.6%), and cyanophytes (7.2%) during our study period. Roy (2018) also reported that the contribution of large phytoplankton to the biochemical components is higher in coastal regions, which generally have sufficient nutrient conditions due to river input and coastal upwelling. In the NES, the small phytoplankton which mostly consisted of prasinophytes (11.7%), prymnesiophytes (11.5%), and cyanophytes (13.3%) (unpublished data) may have had low metabolic rates (Gillooly et al., 2001) and been in a stationary growth phase (Rhee and Gotham, 1981) due to the cold water temperature, resulting in the high CHO and LIP contents observed during the study period. The physiological status of the large phytoplankton in the UB, except M5, appears to be better than that in NES (diatoms: 34.4% and cryptophytes: 16.5%), since the contributions of PRT contents to the total biochemical compositions were relatively high in UW7 (37.7 ± 10.0%) and UW9 (31.7 ± 12.3%) (**Figure 8B** and **Table 2**). A potential reason for the relatively large contribution of PRT by the large phytoplankton in the UB is that they were in an active growth phase with an increased nutrient uptake rate because of the warmer water temperature, contrary to large phytoplankton in the NES (Rhee and Gotham, 1981; Lee et al., 2009). On the other hand, the large phytoplankton in M5 had significantly higher LIP contents than those at other sites (**Figure 8B** and **Table 2**), although the highest carbon uptake rate was observed during our cruise period (**Figure 5B** and **Table 1**). This unexpected observation might have resulted from a deficiency in nitrogen and phosphate sources, as they had already been exhausted by phytoplankton photosynthesis. de Madariaga and Joint (1992) reported that phytoplankton under nitrogen- (nitrate and ammonium) and phosphate-limited conditions had high LIP concentrations. At station M5, nitrogen, especially nitrate, and phosphate concentrations were lower than those at the other stations in the UB (**Table 1**). However, we are uncertain whether consumption or other mechanisms drove this nutrient deficiency; therefore, more research and data are needed to understand the exact mechanism for the mismatch between the productivity and physiological status of the phytoplankton in M5 during our research period. In the NES, the large phytoplankton had relatively high lipid compositions, except at site M12, where the dominant component was CHO (**Figure 8B** and **Table 2**). The physiological status of these large phytoplankton seemed to suggest that they were in a stationary growth phase caused by cold water temperatures, as mentioned above (Rhee and Gotham, 1981; Lee et al., 2009; Kwak et al., 2014).

The average calorific contents in the UB were similar between the small (1.01 ± 0.33 Kcal m^{-3}) and large (1.14 ± 0.36 Kcal m^{-3}) phytoplankton, whereas those in the NES were higher (*t*-test, $p < 0.01$) for the large phytoplankton (1.88 ± 0.54 Kcal m^{-3}) than the small phytoplankton (1.06 ± 0.18 Kcal m^{-3}) (**Table 2**). There was no spatial difference in the calorific value for the small phytoplankton between the UB and the NES (**Table 2**). In contrast, the calorific values of the large phytoplankton in the UB were significantly lower (*t*-test, $p < 0.01$) than those in the NES, although the total primary production was

TABLE 3 | Comparison of Cal/chl ratios between small and large phytoplankton.

Region	Season	Contents	Phytoplankton size			Ratio		References
			Small	Large	Total	Small: Total	Large: Total	
Northern East/Japan Sea	Spring and fall	Cal. (Kcal m^{-3})	0.60	0.80	1.40	0.43	0.57	Kang et al., 2017
		Chl *a* (mg m^{-3})	0.60	1.70	2.30	0.26	0.74	
		Cal/Chl *a* (Kcal mg^{-1})	1.00	0.47	0.61	1.64	0.77	
Southern coastal areas in Korea: Gwangyang Bay	Four seasons	Cal. (Kcal m–3)	1.70	2.10	3.80	0.45	0.55	Kim et al., 2019
		Chl *a* (mg m–3)	0.80	2.50	3.30	0.24	0.76	
		Cal/Chl *a* (Kcal mg^{-1})	2.13	0.84	1.15	1.85	0.73	
South western East/Japan Sea: Ulleung Basin (UB)	Spring	Cal. (Kcal m^{-3})	1.01	1.14	2.15	0.47	0.53	This study
		Chl *a* (mg m^{-3})	0.52	0.45	0.97	0.54	0.46	
		Cal/Chl *a* (Kcal mg^{-1})	1.92	2.56	2.21	0.87	1.15	
Northwestern East/Japan Sea (NES)	Spring	Cal. (Kcal m^{-3})	1.06	1.88	2.94	0.36	0.64	
		Chl *a* (mg m^{-3})	0.59	0.69	1.27	0.46	0.54	
		Cal/Chl *a* (Kcal mg^{-1})	1.81	2.74	2.31	0.78	1.19	

Cal/chl, calorific content per unit of chl a.

approximately two times lower in the NES than in the UB (**Table 2**). This pattern was caused mainly by the difference in the amount of FM, especially LIP, in the large phytoplankton between the UB and the NES (**Table 2**). There was no significant difference in the average CHO (UB: 62.9 ± 48.3 mg m^{-3}; NES: 70.0 ± 36.5 mg m^{-3}) or PRT (UB: 52.3 ± 15.7 mg m^{-3}; NES: 51.7 ± 25.8 mg m^{-3}) concentrations in the large phytoplankton between the two regions (**Table 2**). In contrast, the average LIP concentration of the large phytoplankton was significantly higher (*t*-test, $p < 0.01$) in the NES (137.6 ± 56.6 mg m^{-3}) than in the UB (62.9 ± 37.1 mg m^{-3}) (**Table 2**). Moreover, the higher energy content of LIP compared to other components led to the significant difference in the calorific value between the UB and the NES. Therefore, the relatively low primary production rate in the NES can be compensated by high calorie LIP-dominant FM.

Considering the importance of small phytoplankton, which will contribute increasing amounts to the total biomass under warming conditions (Morán et al., 2010), we assessed the calorific value per small and large phytoplankton cell by dividing the calorific content by the chl *a* concentration (**Table 3**). Overall, the calorific content per unit of chl *a* (hereafter Cal/chl) was higher for the large phytoplankton than the small phytoplankton in both regions (**Table 3**). Furthermore, the contribution of the large phytoplankton to the Cal/chl of the total phytoplankton was higher than that of the small phytoplankton in both regions (**Table 3**). This means that large phytoplankton could be more efficient as a food source, providing a higher energy value per unit to organisms in higher trophic levels. This finding is in contrast to the previous results from Kang et al. (2017) and Kim et al. (2019), who observed that small phytoplankton assimilated more FMs and energy per unit of chl *a* concentration. These inconsistent results might be caused by different research regions and periods. Kang et al. (2017) conducted their research in the northern EJS during the post-spring bloom period in 2015, when the phytoplankton had entered a stationary growth phase, whereas our study was conducted during the peak of the spring bloom based on satellite ocean color data provided in a parallel study (unpublished data). Kim et al. (2019) carried out their study in Gwangyang Bay, South Korea, which is largely affected by river inputs.

SUMMARY AND CONCLUSION

Under current climate changes, an increase in the contribution of small phytoplankton to the total phytoplankton community has been observed in various oceans (Agawin et al., 2000; Li et al., 2009; Morán et al., 2010; Hilligsøe et al., 2011; Mousing et al., 2014; Joo et al., 2017), which indicates a growing importance of small size phytoplankton as a basic food source for higher trophic level organisms in the marine ecosystems. This study in the two different regions (i.e., UB and NES) of the western EJS reported the influence of small phytoplankton contribution to the primary production and different energy efficiencies between small and large phytoplankton based on their biochemical components. According to previous studies (Lee et al., 2017b,c), the total primary production could be decreased by the increase of small phytoplankton contribution. Indeed, this study also proved a negative correlation between the total carbon uptake rates and the contribution of small phytoplankton in the UB and NES (**Figure 9**). In particular, the decreasing trend of the total carbon uptake rates in the UB under increasing small phytoplankton contributions is more faster in this study (**Figure 9**) compared to previous studies in the polar regions (the Chukchi Sea–unpublished data; the Amundsen Sea–Lee et al., 2017c.) and the northern EJS (Lee et al., 2017b) which have been experiencing drastic environmental changes. It means that the primary production in the UB as a biological hot spot of the EJS could be responded sensitively to ongoing climate changes, especially warming water temperature. However, there are some uncertainties for that since only a few data points were available in the UB in this study. Further evaluation for the rapid decreasing trend in the total primary production with increasing small phytoplankton contribution should be conducted in the UB. Therefore, long term observations for the seasonal and annual primary productions and contributions of small phytoplankton in the EJS, including the UB, are needed for a better understanding of potential ecosystem change under ongoing climate change.

In terms of energy efficiency in differential size phytoplankton, large phytoplankton could provide higher energy value per unit cell than small phytoplankton based on the Cal/chl of the two different cell-sized of phytoplankton in the UB and NES during this study (**Table 3**). In contrast, previous studies found opposite results that small phytoplankton had relatively higher Cal/chl than large phytoplankton (Kang et al., 2017; Kim et al., 2019). This inconsistency between this and other studies might be resulted from different research regions and periods. Further studies for the contrasting patterns are necessary to understand the subsequent nutritional effects of small phytoplankton as a potential food source on higher trophic levels in a projected warmer oceanic condition.

DATA AVAILABILITY STATEMENT

The original contributions presented in the study are included in the article/supplementary material, further inquiries can be directed to the corresponding author/s.

AUTHOR CONTRIBUTIONS

SL conceived the ideas and designed the methodology. JK performed the field experiments, data analysis, and wrote the manuscript. HJ and JLe performed the field experiments and conducted the lab experiment. J-HLi and CL conducted the lab experiment. DL and HB analyzed the satellite data. C-KK critically reviewed the manuscript. All authors contributed to the article and approved the submitted version.

FUNDING

This research was supported by the project entitled "Long-term change of structure and function in marine ecosystems of Korea" and partly by the grant (R2020028) from the National Institute of Fisheries Science (NIFS), which were funded by the Ministry of Oceans and Fisheries, South Korea.

ACKNOWLEDGMENTS

We thank the research project entitled "East Asian Seas Time series-I (EAST-I)" for providing a research opportunity in the EJS. We are grateful to the captain, all of the crews, and researchers for their outstanding assistance during the cruise.

REFERENCES

Agawin, N. S., Duarte, C. M., and Agustí, S. (2000). Nutrient and temperature control of the contribution of picoplankton to phytoplankton biomass and production. *Limnol. Oceanogr.* 45, 591–600. doi: 10.4319/lo.2000.45.3.0591

Andersson, A., Haecky, P., and Hagström, Å. (1994). Effect of temperature and light on the growth of micro-nano-and pico-plankton: impact on algal succession. *Mar. Biol.* 120, 511–520. doi: 10.1007/BF00350071

Bhavya, P. S., Kim, B. K., Jo, N., Kim, K., Kang, J. J., Lee, J. H., et al. (2019). A review on the macromolecular compositions of phytoplankton and the implications for aquatic biogeochemistry. *Ocean Sci. J.* 54, 1–14. doi: 10.1007/s12601-018-0061-8

Bligh, E. G., and Dyer, W. J. (1959). A rapid method of total lipid extraction and purification. *Can. J. Biochem. Phys.* 37, 911–917. doi: 10.1139/y59-099

Calvo-Díaz, A., and Morán, X. A. G. (2006). Seasonal dynamics of picoplankton in shelf waters of the southern Bay of Biscay. *Aquat. Microb. Ecol.* 42, 159–174. doi: 10.3354/ame042159

Chen, Y. L. L. (2000). Comparisons of primary productivity and phytoplankton size structure in the marginal regions of southern East China Sea. *Cont. Shelf Res.* 20, 437–458. doi: 10.1016/S0278-4343(99)00080-1

Chiba, S., Aita, M. N., Tadokoro, K., Saino, T., Sugisaki, H., and Nakata, K. (2008). From climate regime shifts to lower-trophic level phenology: synthesis of recent progress in retrospective studies of the western North Pacific. *Prog. Oceanogr.* 77, 112–126. doi: 10.1016/j.pocean.2008.03.004

Chiba, S., Batten, S., Sasaoka, K., Sasai, Y., and Sugisaki, H. (2012). Influence of the Pacific Decadal Oscillation on phytoplankton phenology and community structure in the western North Pacific. *Geophys. Res. Lett.* 39:L15603. doi: 10.1029/2012GL052912

Dauchez, S., Legendre, L., Fortier, L., and Levasseur, M. (1996). Nitrate uptake by size-fractionated phytoplankton on the Scotian Shelf (Northwest Atlantic): spatial and temporal variability. *J. Plankton Res.* 18, 577–595. doi: 10.1093/plankt/18.4.577

de Madariaga, I., and Joint, I. (1992). A comparative study of phytoplankton physiological indicators. *J. Exp. Mar. Biol. Ecol.* 158, 149–165. doi: 10.1016/0022-0981(92)90223-W

DiTullio, G. R., and Laws, E. A. (1983). Estimates of phytoplankton N uptake based on 14CO2 incorporation into protein. *Limnol. Oceanogr.* 28, 177–185. doi: 10.4319/lo.1983.28.1.0177

Dubois, M., Gilles, K. A., Hamilton, J. K., Rebers, P. A., and Smith, F. (1956). Colorimetric method for determination of sugars and related substances. *Anal. Chem.* 28, 350–356. doi: 10.1021/ac60111a017

Dugdale, R. C., and Goering, J. J. (1967). Uptake of new and regenerated forms of nitrogen in primary productivity. *Limnol. Oceanogr.* 12, 196–206. doi: 10.4319/lo.1967.12.2.0196

Estrada, M. (1996). Primary production in the northwestern Mediterranean. *Sci. Mar.* 60, 55–64.

Falkowski, P. G., and Oliver, M. J. (2007). Mix and match: how climate selects phytoplankton. *Nat. Rev. Microbiol.* 5, 813–819. doi: 10.1038/nrmicro1751

Finkel, Z. V., Beardall, J., Flynn, K. J., Quigg, A., Rees, T. A. V., and Raven, J. A. (2010). Phytoplankton in a changing world: cell size and elemental stoichiometry. *J. Plankton Res.* 32, 119–137. doi: 10.1093/plankt/fbp098

Finkel, Z. V., Katz, M. E., Wright, J. D., Schofield, O. M. E., and Falkowski, P. G. (2005). Climatically driven macroevolutionary patterns in the size of marine diatoms over the Cenozoic. *Proc. Natl. Acad. Sci. U.S.A.* 102, 8927–8932. doi: 10.1073/pnas.0409907102

Finkel, Z. V., Sebbo, J., Feist-Burkhardt, S., Irwin, A. J., Katz, M. E., Schofield, O. M. E., et al. (2007). A universal driver of macroevolutionary change in the size of marine phytoplankton over the Cenozoic. *Proc. Natl. Acad. Sci. U.S.A.* 104, 20416–20420. doi: 10.1073/pnas.0709381104

Gardner, W. D., Chung, S. P., Richardson, M. J., and Walsh, I. D. (1995). The oceanic mixed-layer pump. *Deep Sea Res. II Top. Stud. Oceanogr.* 42, 757–775. doi: 10.1016/0967-0645(95)00037-Q

Gillooly, J. F., Brown, J. H., West, G. B., Savage, V. M., and Charnov, E. L. (2001). Effects of size and temperature on metabolic rate. *Science* 293, 2248–2251. doi: 10.1126/science.1061967

Hama, T., Miyazaki, T., Ogawa, Y., Iwakuma, T., Takahashi, M., Otsuki, A., et al. (1983). Measurement of photosynthetic production of a marine phytoplankton population using a stable 13C isotope. *Mar. Biol.* 73, 31–36. doi: 10.1007/BF00396282

Hessen, D. A. G., De Lange, H., and Van Donk, E. (1997). UV-induced changes in phytoplankton cells and its effects on grazers. *Freshw. Biol.* 38, 513–524. doi: 10.1046/j.1365-2427.1997.00223.x

Hilligsøe, K. M., Richardson, K., Bendtsen, J., Sørensen, L. L., Nielsen, T. G., and Lyngsgaard, M. M. (2011). Linking phytoplankton community size composition with temperature, plankton food web structure and sea–air CO2 flux. *Deep Sea Res. Part I Oceanogr. Res. Pap.* 58, 826–838. doi: 10.1016/j.dsr.2011.06.004

Huisman, J. E. F., van Oostveen, P., and Weissing, F. J. (1999). Critical depth and critical turbulence: two different mechanisms for the development of phytoplankton blooms. *Limnol. Oceanogr.* 44, 1781–1787. doi: 10.4319/lo.1999.44.7.1781

Hyun, J. H., Kim, D., Shin, C. W., Noh, J. H., Yang, E. J., Mok, J. S., et al. (2009). Enhanced phytoplankton and bacterioplankton production coupled to coastal upwelling and an anticyclonic eddy in the Ulleung Basin, East Sea. *Aquat. Microb. Ecol.* 54, 45–54. doi: 10.3354/ame01280

Jo, C. O., Lee, J. Y., Park, K. A., Kim, Y. H., and Kim, K. R. (2007). Asian dust initiated early spring bloom in the northern East/Japan Sea. *Geophys. Res. Lett.* 34:L05602. doi: 10.1029/2006GL027395

Jo, N., Kang, J. J., Park, W. G., Lee, B. R., Yun, M. S., Lee, J. H., et al. (2017). Seasonal variation in the biochemical compositions of phytoplankton and zooplankton communities in the southwestern East/Japan Sea. *Deep Sea Res. II Top. Stud. Oceanogr.* 143, 82–90. doi: 10.1016/j.dsr2.2016.12.001

Joo, H., Park, J. W., Son, S., Noh, J. H., Jeong, J. Y., Kwak, J. H., et al. (2014). Long-term annual primary production in the Ulleung Basin as a biological hot spot in the East/Japan Sea. *J. Geophys. Res. Oceans* 119, 3002–3011. doi: 10.1002/2014JC009862

Joo, H., Son, S., Park, J. W., Kang, J. J., Jeong, J. Y., Kwon, J. I., et al. (2017). Small phytoplankton contribution to the total primary production in the highly productive Ulleung Basin in the East/Japan Sea. *Deep Sea Res. II Top. Stud. Oceanogr.* 143, 54–61. doi: 10.1016/j.dsr2.2017.06.007

Kang, D. J., Park, S., Kim, Y. G., Kim, K., and Kim, K.-R. (2003). A moving-boundary box model (MBBM) for oceans in change: an application to the East/Japan Sea. *Geophys. Res. Lett.* 30:1299. doi: 10.1029/2002GL016486

Kang, J. H., Kim, W. S., Chang, K. I., and Noh, J. H. (2004). Distribution of plankton related to the mesoscale physical structure within the surface mixed layer in the southwestern East Sea, Korea. *J. Plankton Res.* 26, 1515–1528. doi: 10.1093/plankt/fbh140

Kang, J. J., Joo, H., Lee, J. H., Lee, H. W., Lee, D., et al. (2017). Comparison of biochemical compositions of phytoplankton during spring and fall seasons in the northern East/Japan Sea. *Deep Sea Res. II Top. Stud. Oceanogr.* 143, 73–81. doi: 10.1016/j.dsr2.2017.06.006

Kilham, S. S., Kreeger, D. A., Goulden, C. E., and Lynn, S. G. (1997). Effects of nutrient limitation on biochemical constituents of *Ankistrodesmus falcatus*. *Freshw. Biol.* 38, 591–596. doi: 10.1046/j.1365-2427.1997.00231.x

Kim, B. K., Joo, H., Song, H. J., Yang, E. J., Lee, S. H., Hahm, D., et al. (2015). Large seasonal variation in phytoplankton production in the Amundsen Sea. *Polar Biol.* 38, 319–331. doi: 10.1007/s00300-014-1588-5

Kim, B. K., Lee, J. H., Joo, H., Song, H. J., Yang, E. J., Lee, S. H., et al. (2016). Macromolecular compositions of phytoplankton in the Amundsen Sea, Antarctica. *Deep Sea Res. II Top. Stud. Oceanogr.* 123, 42–49. doi: 10.1016/j.dsr2.2015.04.024

Kim, D., Yang, E. J., Kim, K. H., Shin, C. W., Park, J., Yoo, S., et al. (2012). Impact of an anticyclonic eddy on the summer nutrient and chlorophyll a distributions in the Ulleung Basin, East Sea (Japan Sea). *ICES J. Mar. Sci.* 69, 23–29. doi: 10.1093/icesjms/fsr178

Kim, K., Kim, K. R., Min, D. H., Volkov, Y., Yoon, J. H., and Takematsu, M. (2001). Warming and structural changes in the East (Japan) Sea: a clue to future changes in global oceans? *Geophys. Res. Lett.* 28, 3293–3296. doi: 10.1029/2001GL013078

Kim, Y., Lee, J. H., Kang, J. J., Lee, J. H., Lee, H. W., Kang, C. K., et al. (2019). River discharge effects on the contribution of small-sized phytoplankton to the total biochemical composition of POM in the Gwangyang Bay, Korea. *Estuar. Coast. Shelf Sci.* 226:106293. doi: 10.1016/j.ecss.2019.106293

Kleppel, G. S., and Burkart, C. A. (1995). Egg production and the nutritional environment of Acartia tonsa: the role of food quality in copepod nutrition. *ICES J. Mar. Sci.* 52, 297–304. doi: 10.1016/1054-3139(95)80045-X

Kwak, J. H., Lee, S. H., Hwang, J., Suh, Y. S., Park, H., Chang, K. I., et al. (2014). Summer primary productivity and phytoplankton community composition driven by different hydrographic structures in the East/Japan Sea and the Western Subarctic Pacific. *J. Geophys. Res. Oceans* 119, 4505–4519. doi: 10.1002/2014JC009874

Kwak, J. H., Lee, S. H., Park, H. J., Choy, E. J., Jeong, H. D., Kim, K. R., et al. (2013). Monthly measured primary and new productivities in the Ulleung Basin as a biological" hot spot" in the East/Japan Sea. *Biogeosciences* 10, 4405–4417. doi: 10.5194/bg-10-4405-2013

Lee, J. H., Kang, J. J., Jang, H. K., Jo, N., Lee, D., Yun, M., et al. (2020). Major controlling factors for spatio-temporal variations in the macromolecular composition and primary production by phytoplankton in Garolim and Asan bays in the Yellow Sea. *Reg. Stud. Mar. Sci.* 36:101269. doi: 10.1016/j.rsma.2020.101269

Lee, J. H., Lee, D., Kang, J. J., Joo, H. T., Lee, J. H., Lee, H. W., et al. (2017a). The effects of different environmental factors on the biochemical composition of particulate organic matter in Gwangyang Bay, South Korea. *Biogeosciences* 14, 1903–1917. doi: 10.5194/bg-14-1903-2017

Lee, S. H., Joo, H., Lee, J. H., Lee, J. H., Kang, J. J., Lee, H. W., et al. (2017b). Seasonal carbon uptake rates of phytoplankton in the northern East/Japan Sea. *Deep Sea Res. II Top. Stud. Oceanogr.* 143, 45–53. doi: 10.1016/j.dsr2.2017.04.009

Lee, S. H., Kim, B. K., Lim, Y. J., Joo, H., Kang, J. J., Lee, D., et al. (2017c). Small phytoplankton contribution to the standing stocks and the total primary production in the Amundsen Sea. *Biogeosciences* 14, 3705–3713. doi: 10.5194/bg-14-3705-2017

Lee, S. H., Kim, H. J., and Whitledge, T. E. (2009). High incorporation of carbon into proteins by the phytoplankton of the Bering Strait and Chukchi Sea. *Cont. Shelf Res.* 29, 1689–1696. doi: 10.1016/j.csr.2009.05.012

Lee, S. H., Son, S., Dahms, H.-U., Park, J. W., Lim, J.-H., Noh, J.-H., et al. (2014). Decadal changes of phytoplankton Chl-a-a in the East Sea/Sea of Japan. *Oceanology* 6, 771–779. doi: 10.1134/s0001437014060058

Lee, S. H., Whitledge, T. E., and Kang, S. H. (2007). Recent carbon and nitrogen uptake rates of phytoplankton in Bering Strait and the Chukchi Sea. *Cont. Shelf Res.* 27, 2231–2249. doi: 10.1016/j.csr.2007.05.009

Legendre, L., and Rassoulzadegan, F. (1996). Food-web mediated export of biogenic carbon in oceans: hydrodynamic control. *Mar. Ecol. Prog. Ser.* 145, 179–193. doi: 10.3354/meps145179

Lewandowska, A. M., Breithaupt, P., Hillebrand, H., Hoppe, H. G., Jürgens, K., and Sommer, U. (2012). Responses of primary productivity to increased temperature and phytoplankton diversity. *J. Sea Res.* 72, 87–93. doi: 10.1016/j.seares.2011.10.003

Li, W. K., McLaughlin, F. A., Lovejoy, C., and Carmack, E. C. (2009). Smallest algae thrive as the Arctic Ocean freshens. *Science* 326, 539–539. doi: 10.1126/science.1179798

Lim, J. H., Son, S., Park, J. W., Kwak, J. H., Kang, C. K., Son, Y. B., et al. (2012). Enhanced biological activity by an anticyclonic warm eddy during early spring in the East Sea (Japan Sea) detected by the geostationary ocean color satellite. *Ocean Sci. J.* 47, 377–385. doi: 10.1007/s12601-012-0035-1

Lindqvist, K., and Lignell, R. (1997). Intracellular partitioning of 14CO2 in phytoplankton during a growth season in the northern Baltic. *Mar. Ecol. Prog. Ser.* 152, 41–50. doi: 10.3354/meps152041

Litchman, E., Klausmeier, C. A., Schofield, O. M., and Falkowski, P. G. (2007). The role of functional traits and trade-offs in structuring phytoplankton communities: scaling from cellular to ecosystem level. *Ecol. Lett.* 10, 1170–1181. doi: 10.1111/j.1461-0248.2007.01117.x

Lowry, O. H., Rosebrough, N. J., Farr, A. L., and Randall, R. J. (1951). Protein measurement with the folin phenol reagent. *J. Biol. Chem.* 193, 265–275.

Marañón, E., Cermeño, P., Latasa, M., and Tadonléké, R. D. (2012). Temperature, resources, and phytoplankton community size structure in the ocean. *Limnol. Oceanogr.* 57, 1266–1278. doi: 10.4319/lo.2012.57.5.1266

Moal, J., Martin-Jezequel, V., Harris, R. P., Samain, J. F., and Poulet, S. A. (1987). Interspecific and intraspecific variability of the chemical composition of marine phytoplankton. *Oceanol. Acta* 10, 339–346.

Morán, X. A. G., López-urrutia, Á., Calvo-díaz, A., and Li, W. K. (2010). Increasing importance of small phytoplankton in a warmer ocean. *Glob. Change Biol.* 16, 1137–1144. doi: 10.1111/j.1365-2486.2009.01960.x

Morris, I. (1981). Photosynthetic products, physiological state, and phytoplankton growth. *Can. Bull. Fish. Aquat. Sci.* 210, 83–102.

Morris, I., Glover, H. E., and Yentsch, C. S. (1974). Products of photosynthesis by marine phytoplankton: the effect of environmental factors on the relative rates of protein synthesis. *Mar. Biol.* 21, 1–9. doi: 10.1007/BF00394754

Mortensen, S. H., Børsheim, K. Y., Rainuzzo, J., and Knutsen, G. (1988). Fatty acid and elemental composition of the marine diatom *Chaetoceros gracilis* Schütt. Effects of silicate deprivation, temperature and light intensity. *J. Exp. Mar. Biol. Ecol.* 122, 173–185. doi: 10.1016/0022-0981(88)90183-9

Mousing, E. A., Ellegaard, M., and Richardson, K. (2014). Global patterns in phytoplankton community size structure—evidence for a direct temperature effect. *Mar. Ecol. Prog. Ser.* 497, 25–38. doi: 10.3354/meps10583

Palmisano, A. C., Lizotte, M. P., Smith, G. A., Nichols, P. D., White, D. C., and Sullivan, C. W. (1988). Changes in photosynthetic carbon assimilation in Antarctic sea-ice diatoms during spring bloom: variation in synthesis of lipid classes. *J. Exp. Mar. Biol. Ecol.* 116, 1–13. doi: 10.1016/0022-0981(88)90241-9

Rhee, G. Y., and Gotham, I. J. (1981). The effect of environmental factors on phytoplankton growth: temperature and the interactions of temperature with nutrient limitation 1. *Limnol. Oceanogr.* 26, 635–648. doi: 10.4319/lo.1981.26.4.0635

Ríos, A. F., Fraga, F., Pérez, F. F., and Figueiras, F. G. (1998). Chemical composition of phytoplankton and particulate organic matter in the Ría de Vigo (NW Spain). *Sci. Mar.* 62, 257–271. doi: 10.3989/scimar.1998.62n3257

Roy, S. (2018). Distributions of phytoplankton carbohydrate, protein and lipid in the world oceans from satellite ocean colour. *ISME J.* 12, 1457–1472. doi: 10.1038/s41396-018-0054-8

Scott, J. M. (1980). Effect of growth rate of the food alga on the growth/ingestion efficiency of a marine herbivore. *J. Mar. Biol. Assoc. U.K.* 60, 681–702. doi: 10.1017/S0025315400040376

Smith, R. E. H., Clement, P., Cota, G. F., and Li, W. K. W. (1987). Intracellular photosynthate allocation and the control of Arctic marine ice algal production. *J. Phycol.* 23, 251–263. doi: 10.1111/j.1529-8817.1987.tb04434.x

Sterner, R. W., Hagemeier, D. D., Smith, W. L., and Smith, R. F. (1993). Phytoplankton nutrient limitation and food quality for Daphnia. *Limnol. Oceanogr.* 38, 857–871. doi: 10.4319/lo.1993.38.4.0857

Stolte, W., McCollin, T., Noordeloos, A. A., and Riegman, R. (1994). Effect of nitrogen source on the size distribution within marine phytoplankton populations. *J. Exp. Mar. Biol. Ecol.* 184, 83–97. doi: 10.1016/0022-0981(94)90167-8

Stolte, W., and Riegman, R. (1995). Effect of phytoplankton cell size on transient-state nitrate and ammonium uptake kinetics. *Microbiology* 141, 1221–1229. doi: 10.1099/13500872-141-5-1221

Thingstad, T. F., Øvreås, L., Egge, J. K., Løvdal, T., and Heldal, M. (2005). Use of non-limiting substrates to increase size; a generic strategy to simultaneously optimize uptake and minimize predation in pelagic osmotrophs? *Ecol. Lett.* 8, 675–682. doi: 10.1111/j.1461-0248.2005.00768.x

Whyte, J. N. (1987). Biochemical composition and energy content of six species of phytoplankton used in mariculture of bivalves. *Aquaculture* 60, 231–241. doi: 10.1016/0044-8486(87)90290-0

Winberg, G. G. (1971). Symbols, units and conversion factors in study of fresh waters productivity. *Int. Biol.* 23.

Yoo, S., and Park, J. (2009). Why is the southwest the most productive region of the East Sea/Sea of Japan? *J. Mar. Syst.* 78, 301–315. doi: 10.1016/j.jmarsys.2009.02.014

Yun, M. S., Lee, D. B., Kim, B. K., Kang, J. J., Lee, J. H., Yang, E. J., et al. (2015). Comparison of phytoplankton macromolecular compositions and zooplankton proximate compositions in the northern Chukchi Sea. *Deep Sea Res. II Top. Stud. Oceanogr.* 120, 82–90. doi: 10.1016/j.dsr2.2014.05.018

Conflict of Interest: The authors declare that the research was conducted in the absence of any commercial or financial relationships that could be construed as a potential conflict of interest.

frontiers in Microbiology

ORIGINAL RESEARCH
published: 14 January 2021
doi: 10.3389/fmicb.2020.554832

Quantitative Proteomic Profiling of Marine Diatom *Skeletonema dohrnii* in Response to Temperature and Silicate Induced Environmental Stress

*Satheeswaran Thangaraj[1], Satheesh Kumar Palanisamy[2], Guicheng Zhang[3,4] and Jun Sun[1]**

[1] College of Marine Science and Technology, China University of Geosciences, Wuhan, China, [2] Department of Zoology, School of Natural Science, Ryan Institute, National University of Ireland, Galway, Ireland, [3] Research Center for Indian Ocean Ecosystem, Tianjin University of Science and Technology, Tianjin, China, [4] Tianjin Key Laboratory of Marine Resources and Chemistry, Tianjin University of Science and Technology, Tianjin, China

OPEN ACCESS

Edited by:
Debora Iglesias-Rodriguez, University of California, Santa Barbara, United States

Reviewed by:
Jin Zhou, Tsinghua University, China
Wanderson Marques da Silva, Consejo Nacional de Investigaciones Científicas y Técnicas (CONICET), Argentina

***Correspondence:**
Jun Sun
phytoplankton@163.com

Specialty section:
This article was submitted to Aquatic Microbiology, a section of the journal Frontiers in Microbiology

Received: *23 April 2020*
Accepted: *23 December 2020*
Published: *14 January 2021*

Citation:
Thangaraj S, Palanisamy SK, Zhang G and Sun J (2021) Quantitative Proteomic Profiling of Marine Diatom Skeletonema dohrnii in Response to Temperature and Silicate Induced Environmental Stress. Front. Microbiol. 11:554832. doi: 10.3389/fmicb.2020.554832

Global warming is expected to reduce the nutrient concentration in the upper ocean and affect the physiology of marine diatoms, but the underlying molecular mechanisms controlling these physiological changes are currently unknown. To understand these mechanisms, here we investigated iTRAQ based proteomic profiling of diatom *Skeletonema dohrnii* in a multifactorial experimental with a combining change of temperature and silicate concentrations. In total, 3369 differently abundant proteins were detected in four different environmental conditions, and the function of all proteins was identified using Gene Ontology and KEGG pathway analysis. For discriminating the proteome variation among samples, multivariate statistical analysis (PCA, PLS-DA) was performed by comparing the protein ratio differences. Further, performing pathway analysis on diatom proteomes, we here demonstrated downregulation of photosynthesis, carbon metabolism, and ribosome biogenesis in the cellular process that leads to decrease the oxidoreductase activity and affects the cell cycle of the diatom. Using PLS-DA VIP score plot analysis, we identified 15 protein biomarkers for discriminating studied samples. Of these, five proteins or gene (rbcL, PRK, atpB, DNA-binding, and signal transduction) identified as key biomarkers, induced by temperature and silicate stress in diatom metabolism. Our results show that proteomic finger-printing of *S. dohrnii* with different environmental conditions adds biological information that strengthens marine phytoplankton proteome analysis.

Keywords: global warming, photosynthesis, carbon metabolism, nutrient stratifications, iTRAQ-proteomics, climate change, biomarkers, ribosome biogenesis

INTRODUCTION

The increasing amount of anthropogenic greenhouse gas emission has resulted significant changes in the physical and chemical properties of the global ocean that have intense implications to the marine ecosystem (Pörtner et al., 2014). It is assumed that the warming ocean will enhance the nutrient stratification and modulates the ecophysiology of marine organisms

(Reinfelder et al., 2000). A recent report described increasing sea surface temperature (SST), and depletion of nutrients affects the phytoplankton community resulting in 6% global biomass decrease by the end of this century (Chust et al., 2014). Further, it is reported that warming ocean will cause phytoplankton cell shifting (Lewandowska et al., 2014), cell size reduction, and grazing effects (Lindh et al., 2013; Peter and Sommer, 2013). However, the metabolic response of phytoplankton with combining environmental stress (i.e., temperature and nutrient limitation) remains unknown (Philippart et al., 2011).

The unicellular microalgae (i.e., diatoms) are the dominant phytoplankton group covering 20% of global net primary productivity and fixing 30%–50% of the inorganic carbon in the ocean; it's equivalent to all rainforest accounts (Field et al., 1998). The macronutrients: nitrate, phosphate, and silicate are essential for the primary productivity, growth, and distribution of diatoms in the ocean (Katayama et al., 2012). Diatoms are the largest group of silicifying organisms (Otzen, 2012; Shrestha et al., 2012), and, changes in silicate concentration in the environment regulate their cell physiology and metabolism (Thangaraj et al., 2019). Earlier investigations noted during temperature fluctuation an autotroph physiological photoprotective mechanism was strongly regulated (Ruban and Johnson, 2009). As diatoms are autotroph, temperature plays a vital role in their photosynthetic mechanisms (PSII, PSI, and LHCs), and transition in temperature could alter their photosynthetic mechanisms and regulate their carbon fixation process (Dong et al., 2016).

The genus *Skeletonema* (Bacillariophyta, family: *Skeletonemaceae*) are commonly found in marine and coastal environment (Sarno et al., 2005); this genus (*Skeletonema*) has been considered a key group in diatom research due to its tropic importance to grazers, global abundance, and similar physiology of other species (Thangaraj and Sun, 2020). Among them, *Skeletonema dohrnii* is a cosmopolitan species with chain-forming cylindrical type, first identified by Sarno et al. (2005), and reported as widely distributed in temperate regions of the southern and northern hemispheres with an optimal temperature of 15–25°C (Kaeriyama et al., 2011). The occurrence and distribution of this species likely to variant as functions of environmental conditions such as temperature, nutrients, and other symbiotic organisms (Gu et al., 2012). It forms an algal blooms in Chinese coastal waters during spring season with a diameter size 3–10 microns (Gu et al., 2012) and makes a considerable impact in a coastal ecosystem.

It is predicted that temperature changes in the future will decrease diatom distribution by 10% globally and by 60% of North Atlantic and sub-Antarctic regions alone (Bopp et al., 2005). Besides, diatom provides an energy-efficient food web to support coastal fisheries (Mann, 1993). Hence, changes in diatom populations have an intense impact on the marine ecosystem and human food sources. Therefore, the continued changes in marine ecosystem by human activities could impact the future projections of mechanistic diatom response to climate change (Halpern et al., 2012).

Metabolomic profiling, transcriptomic, and proteomic approaches are powerful tools to understand the organism strategies to thrive in different environments (Darby et al., 2014; Qing et al., 2016). In the case of diatoms, their individual proteomic responses to different environments, i.e., silica limitation (Thangaraj et al., 2019) phosphorus limitation (Feng et al., 2015), nitrogen starvation (Hockin et al., 2012), iron restriction (Nunn et al., 2013), temperature stress (Dong et al., 2016), and salinity changes (Lyon et al., 2011; Kettles et al., 2014). Especially, in our recent proteomic investigation of *S. dohrnii,* between Si-deplete and replete conditions, we revealed that Si-deprivation alone led to regulate the cellular metabolism (Thangaraj et al., 2019). However, in another proteomic study on the diatom *Thalassiosira pseudonana* revealed the influence of higher temperature on the photosystem electron transport and pigment variation (Dong et al., 2016). Despite these investigations reporting significant metabolic responses to individual temperature and silicate conditions, to date, the effects of combined stressors remains unknown to predict the impact of a concomitant warming ocean and nutrient stratification.

The new method using isobaric peptide tags for relative and absolute quantification (iTRAQ) of proteins in different samples was a significant breakthrough in the qualitative and quantitative analysis of proteomics using mass spectrometry. These chemical tags attached to all peptides in a protein digest via free amines at the peptide N-terminus and on the side chain of lysine residues (Van Domselaar et al., 2005). Shotgun proteomic profiling enables us to identify proteins that are up-regulated or down-regulated under specific conditions, and this can be studied in different cell and tissue lysates. In this study, we applied mass spectrometry and iTRAQ combined proteomic profiling of the diatom *S. dohrnii* to identify and quantify the proteins to elucidate their molecular function and interactions with other proteins. Further, the multivariate statistical tool, principal component analysis (PCA), partial least squares discriminant analysis (PLS-DA) can be applied to discriminate the sample group and to identify the protein biomarkers within a given sample group.'

The primary objective of this study is to apply mass spectrometry-based proteomic profiling to identify and quantify the response of proteins to combined multiple stressors; specifically, variations in temperature and silicate, in the marine diatom *S. dohrnii.* The results are discussed in the context of diatom response mechanisms to the concomitant warming and nutrient stratification in the marine environment, and subsequent implications on the marine ecosystem, photosynthetic efficiency, and carbon fixation.

MATERIALS AND METHODS

Chemicals and Reagents

The chemical composition of the Artificial Sea Water (ASW) is given in the supplementary section (General methods; **Supplementary Table S4**). Further experimental setup and bioinformatics and proteomic data analysis are shown in **Supplementary Table S4** and **Figure S1**.

Experimental Design: Algal Culture and Multiple Climate-Related Variables

A diatom *S. dohrnii* used in this study was isolated from the Yellow Sea coastal waters and cultured in the f/2 medium (Guillard and Ryther, 1962) in the laboratory by applying 12 h:12 h light:dark cycle using cool white fluorescent light, with a light irradiance of 170 μmol photons m^2 s^{-1}. To ensure axenic condition, 0.05 mg ml^{-1} of the antibiotic gentamicin, 0.8 mg ml^{-1} of streptomycin, and 1.6 mg ml^{-1} of penicillin was used according to published protocols (Kobayashi et al., 2003; Bahulikar and Kroth, 2008). We applied a semi-continuous culturing approach to study the impact of temperature (T) and silicate (Si) conditions on the proteome using iTRAQ based proteomic analysis.

The experiment, *S. dohrnii* was maintained in two different temperature conditions [low temperature (15°C) and high temperature (25°C)] in the Aquil, synthetic ocean water/Artificial Sea Water (SOW/ASW), medium with different concentrations of silicate [low silicate (0.2 ml/L) and high silicate (2ml/L)]. In order to prevent silicate contamination from the bottles, and therefore extra silicate utilization of *S. dohrnii* during the experiment, cells were grown in Nalgene, Reusable Baffled Erlenmeyer Culture flasks made of polycarbonate. The four different sample conditions (with replication) were as follows: HTHS (T: 25°C and Si: 2 ml/L), HTLS (25°C and 0.2 ml/L), LTHS (15°C and 2 ml/L), and LTLS (15°C and 0.2 ml/L). Cultures were maintained for up to five generations to ensure cell acclimation. Cultures were harvested 21 days after the start of the experiment for quantitative proteomic analysis. At each generation, less than 15% of cells were obtained during mid-exponential stage (day 4) and transferred to inoculate fresh 1 L cultures.

The reproducibility of each condition was tested using three independent triplicate experiments. Cell growth and density were analyzed using a Qiujing hemocytometer and inverted microscope AE 2000 (Motic Group Co., Ltd., China). The cell density was calculated as follows: CD = (N/80) Å∼400 Å∼104, where CD is the cell density, N is the cell abundance counted in 80 grids on the slide. After five generations, the acclimated cells were harvested by centrifugation at 4000 Å∼10 min at 4°C for proteomics analysis.

Pigment Analysis

For pigment analysis, 100 ml per each sample were collected and filtered using GF/F filters, and the membrane was flash-frozen with liquid nitrogen and stored at −80°C until further analysis. Pigments were extracted using 3 ml methanol, then ultrasound was applied in an ice bath for 30 s, and kept at −20°C for 1 h. Initially, the extracted samples were filtered through a 0.22 μM membrane filter to remove the detritus and mixed with 28 mmol/L of tetrabutylammonium acetate (TBAA). Subsequent grinding, centrifugation, and filtration steps were performed following Zapata et al. (2000). All the procedures were done under subdued light.

Pigment quantification was performed using HPLC (Agilent 1260 Series Infinity, United States) following Zapata et al. (2000). The HPLC system was equipped with an Eclipse XDB C8 column (150 mm × 4.6 mm, 3.5 μm particle size), an Agilent diode array detector with wavelength range 350–750 nm (absorbance at 440 nm) and the ChemStation software (Agilent Tech). Mobile phase A comprised 28 mM TBAA (pH = 6.5): methyl alcohol = 3/7 (v/v) and reagent B: 100% methyl alcohol. Solvents were mixed using linear gradients along the following time program: (0 min: 80%A, 20%B), (32 min: 25%A, 75%B), (48 min: 5% A, 95%B), (56 min: 80%A, 20%B), (60 min: 80%A, 20%B). The flow rate was set 1.0 ml/min, and the temperature of the column oven was at 45°C.

In the present study, all the pigments were identified and quantified using the pigment standard, which was purchased from DHI Water & Environment, Hørsholm, Denmark. The following pigments were detected and quantified: Chlorophyll *c*3 (Chl *c*3), Chlorophyll *c*2 (Chl *c*2), Peridinin (Perid), Fucoxanthin (Fuco), Diadinoxanthin (Diadino), Diatoxanthin (Diato), Chlorophyll *a* (Chl *a*), and β-carotene (β-car). Generated peaks were integrated by using Agilent software, but all peak integrations were checked manually and corrected when necessary and quantified, using the standard external method. Diatom pigment were identified using the comparison of chromatographic and recorded spectral data with standard pigments. For all the physiological parameters, multiple analysis of variance (MANOVA) was performed using the R basic package to determine any significant changes among four different samples (HTHS, HTLS, LTHS, and LTLS).

Protein Preparation and Digestion

One liter of culture from each sample was collected through a 2 μM filter and subsequently suspended in 10 ml medium using 15 ml centrifuge tubes for protein preparation (Du et al., 2014). The resulting cell pellets were then suspended in a lysis buffer (8 M urea, 40 mM Tris–HCl or TEAB with 1 mM PMSF, 2 mM EDTA, and 10 mM DTT, pH 8.5). The mixture of samples was placed into a tissue lyser for 2 min at 50 Hz to achieve cell lysis, and then centrifuged at 25,000 × *g* for 20 min at 4°C. The supernatant was then transferred into a new tube; samples were reduced with 10 mM dithiothreitol (DTT) at 56°C for 1 h and alkylated by 55 mM iodoacetamide (IAM) in the dark at room temperature for 45 min to block the cysteine residues of the proteins. Following centrifugation (25,000 × *g*, for 20 min at 4°C), the supernatant containing proteins was quantified by the Bradford assay method (Kruger, 2009). The protein solution (100 μg) with 8 M urea was diluted four times with 100 mM TEAB and then incubated for at least 1 h at −20°C, followed by centrifugation of the precipitate. The pellet washed with 90% ice-cold ethanol, and the supernatant was removed, and the pellet resuspend in a buffer (8 M urea, 2 M thiourea, 2% SDS, and 40 mM Tris). Trypsin Gold (Promega, Madison, WI, United States) was used for the protein digestion with a ratio of: trypsin = 40:1 at 37°C overnight. After trypsin digestion, peptides were desalted with a Strata X C18 column (Phenomenex) and vacuum-dried according to the manufacturer's protocol for 8-plex iTRAQ (Applied Biosystems, Foster City, CA, United States).

Analytical Procedure and Peptide Labeling

Eight samples consisting of two biological replicates for four-time points were labeled with different iTRAQ tags. Briefly, peptides were labeled with iTRAQ reagents 113 and 114 for HTHS samples; 115 and 116 for HTLS samples; 117 and 118 for LTHS samples; and 119 and 121 for LTLS samples. The labeled peptide blends were pooled and dried through vacuum centrifugation and fractionated. All solvents used for high-performance liquid chromatography (HPLC) was HPLC grade (Sigma-Aldrich), and the H_2O was Millipore Milli-Q PF filtered. The peptides, were separated on a Shimadzu LC-20AB HPLC Pump system coupled with a high pH reverse phase column (Gemini C_{18} 5 μM, 4.6 mm × 250 mm), The peptides were reconstituted to HPLC separation with following mobile phase (A) 5% ACN, (B) 95% H_2O (adjusted pH to 9.8 with 2 ml of NH_3), sample input and acquisition; 2 ml/min flow rate and 1 ml/min injection volume. Crude peptide compound elution was monitored by measuring UV absorbance at 214 nm, and the 40 fractions were collected every 1 min. All the eluted peptides were combined as 20 fractions and vacuum-dried for further process. Furthermore, each fraction was resuspended in buffer A (2% ACN and 0.1% Formic Acid in H_2O) and then centrifuged at 20,000 × *g* for 10 min and independently subjected to HPLC separation (LC-20AD nano-HPLC instrument, Shimadzu, Kyoto, Japan) using C_{18} column (inner diameter 75 μm). Sample input and acquisition; 300 nl/min flow rate and 1 μl injection volume for 8 min, the 35 min gradient was run at 300 nl/min starting from 8% to 35% of buffer B (2% H_2O and 0.1% FA in ACN), followed by a 5 min linear gradient to 80% solution B, maintenance at 80% solution B for 4 min, and return to 5% in 0.1 min and equilibrated for 10 min.

LC-MS/MS Proteomic Analysis

Liquid Chromatography and Mass Spectrometry (LC-MS) analysis of diatom peptide were performed on LC-20AD (Shimadzu, Kyoto, Japan) using C_{18} column (size 75 μm). The LC-MS data were acquired in positive ion mode of data independent acquisition (DIA) within a selected mass range of 350–1500 *m/z*. Based on the intensity in MS1 survey, as many as 30 production scans were collected if beyond a threshold of 120 counts per second (counts/s) and with charge-state 2+ to 5+ dynamic exclusion was set for 1/2 of peak width (12 s). For MS data acquisition, the collision energy was adjusted to all precursor ions for collision-induced dissociation and the Q2 transmission window for 100 Da was 100%.

Bioinformatics and Proteomic Data Analysis

All the mass spectral data were processed using the ProteoWizard software-msConvert with default parameters for generating peak list. The data alignment was performed with Analyst QS 2.0 software (Applied Biosystems/MDS SCIEX). Further, protein identification and quantification were achieved using Mascot 2.3.02 (Matrix Science, London, United Kingdom) (Charbonneau et al., 2007). The greatest extents of the iTRAQ reporter ions mimic the relative abundance of the proteins in the samples. TripleTOF 5600 mass spectrometer with high mass accuracy resolution (less than 2 ppm) was used in this study for peptide identification. Other identification parameters used included: fragment mass tolerance: ±0.1 Da; mass values: monoisotopic; variable modifications: Gln->pyro-Glu (N-term Q), oxidation (M), iTRAQ8plex (Y); peptide mass tolerance: 0.05 Da; max missed cleavages: 1; fixed modifications: carbamidomethyl (C), iTRAQ8plex (N-term), iTRAQ8plex (K); other parameters: default. For iTRAQ quantification, the peptide for quantification was automatically selected by the algorithm to calculate the reporter peak area (using default parameters in the Mascot Software package). The acquiring data was auto bias-corrected to get rid of any differences imparted due to the unequal mixing during combining differently labeled samples. Proteins with the 1.2-fold change between each different sample and a *p*-value of statistical evaluation less than 0.05 were determined as differentially expressed proteins (DEPs). All proteins were identified by MS/MS ion search using Mascot version 2.3.02, mass tolerance 0.05 Da. The students' *t*-test was performed using the mascot 2.3.02 software. Briefly, a protein ratio is reported in the boldface if it is significantly different from unity. The comparison test is:

$$|X - \mu| \leq t^* \frac{S}{\sqrt{N}}$$

If this dissimilarity is real, then there is no important difference at the stated sureness level. Further, N is the number of peptide ratios, S is the standard deviation, and x the mean of the peptide ratios, both numbers calculated in log space. The metabolic pathway analysis of the identified proteins was conducted according to the KEGG Pathway Database (Kanehisa and Goto, 2000; Kanehisa et al., 2016). The Gene Ontology (GO) and Cluster of Orthologous Groups of proteins (COG) analyses (http://www.geneontology.org) were performed according to the method reported in the early literature (Unwin, 2010). The enhancement of differentially regulated proteins in GO terms was carried out using the following formula:

$$P = 1 - \sum_{i=0}^{m-1} \frac{\binom{M}{i}\binom{N-M}{n-i}}{\binom{N}{n}}$$

where N is the number of all proteins with GO annotation information, n is the number of the differentially regulated proteins with GO annotation information, M is the number of proteins with a given GO term annotation, m is the number of the differentially regulated proteins with a given GO term annotation. The GO terms with a *p*-value of less than 0.05 were considered as enriched GO terms by the stress-responsive proteins which may be involved in temperature and silicate induces stress. The multivariate analysis model PCA and PLS-DA analysis was performed with R package (version 1.78).

RESULTS

Physiological Changes

Cells were cultured in four different environmental conditions as described in the Materials and Methods. The results of cell density in each condition are shown in **Figure 1A**. Different cell responses to each environment were evident from day 2. Notably, during the exponential phase (day 5) the cell density in HTHS increased drastically, whereas it decreased in HTLS and LTHS. Both silicate stressed HTLS and temperature stressed LTHS treatments showing a similar physiological regulation (**Figure 1A**). The cell density of LTLS in the exponential phase (1.03×10^6) was three times lower than the HTHS sample (4.47×10^6), and two times lower than HTLS (3.2×10^6). Further, once cells reach the peak density (day 6), cells in the HTHS and HTLS treatments-maintained growth rates whereas, in the LTHS and LTLS conditions, growth declining rapidly.

Quantification of Pigments

The pigment analysis has been carried out using HPLC to understand the impact of abiotic stress on the pigment composition of the *S. dohrnii* (**Figure 1B**). Overall, eight pigments were identified from each sample including chlorophyll-a (Chl-a), fucoxanthin, diadinoxanthin, and β-carotene. Among all the pigments in HTHS, Chl-a was the highest (37.32 μg/L) followed by the diadinoxanthin (24.21 μg/L). In the remaining samples, the diadinoxanthin was the highest followed by Chl-a, whereas, the other accessory pigments such as peridinin, fucoxanthin, and β-carotene were lower in the composition.

Protein Identification

Using i-TRAQ-labeled LC-MS/MS analysis from *S. dohrnii*, a total of 3,70,713 spectra were identified from all samples; a total of 3359 peptides and 1803 proteins were identified with 1% FDR. Several studies reported similar results using the iTRAQ method on *T. pseudonana* 1831 (Du et al., 2014), and 1850 (Nunn et al., 2013) from silicate and iron-deplete and replete conditions respectively. However, this result varies with other proteomic studies on diatoms between higher and lower light 4183 proteins (Dong et al., 2016) multiple nutrient stress (Si, N, P) 3798 (Chen et al., 2018) Fe deprivation, 1204 (Cohen et al., 2018) nitrogen depletion, 1043 (Longworth et al., 2016), phosphorus stress 1264 (Dyhrman et al., 2012), and phosphate limitation, 1151 (Lin et al., 2017) and in our previous study *S. dohrnii* 1768 proteins (Thangaraj et al., 2019), respectively. The differential protein expression identified in this study between groups showed that the repeatability between the replicates was acceptable with 1.2-fold change, mean CV of 0.16, and statistically significant in between the group comparisons ($p < 0.05$). The distribution of protein mass, peptide length distribution, unique peptide number distribution, spectral number, and coverage distribution is shown in **Supplementary Table S4** and **Figure S2**.

Quantification of Identified Proteins

In our study, a total of 1803 proteins were identified (See **Supplementary Table S1**) in response to changes in temperature and silicate concentrations in diatom *S. dohrnii*. Further, among the overall quantified proteins, 536 differently expressed proteins were identified between a higher temperature (HT) and lower temperature (LT), of which 263 were downregulated (**Supplementary Table S2**) and 273 up-regulated (**Supplementary Table S3**). Interestingly, 577 differentially expressed proteins were distinguished between higher silicate (HS) and lower silicate (LS), of which diatom 331 proteins down-regulated (**Supplementary Table S2**) and 246 proteins up-regulated (**Supplementary Table S3**). The comparison of differently expressed proteins between each sample groups is given in **Figure 2A**. The differently expressed proteins also have been identified using the volcano plot analysis method (**Supplementary Table S4** and **Figure S3**). In this study, the maximum number of down-regulated proteins was observed in group HTHS versus HTLS and up-regulated proteins in group HTHS versus LTHS. The differentially changed proteins identified in our experiments were grouped into different sample groups based on cluster analysis using Euclidean distance method and hierarchical algorithm (**Figure 2B** and

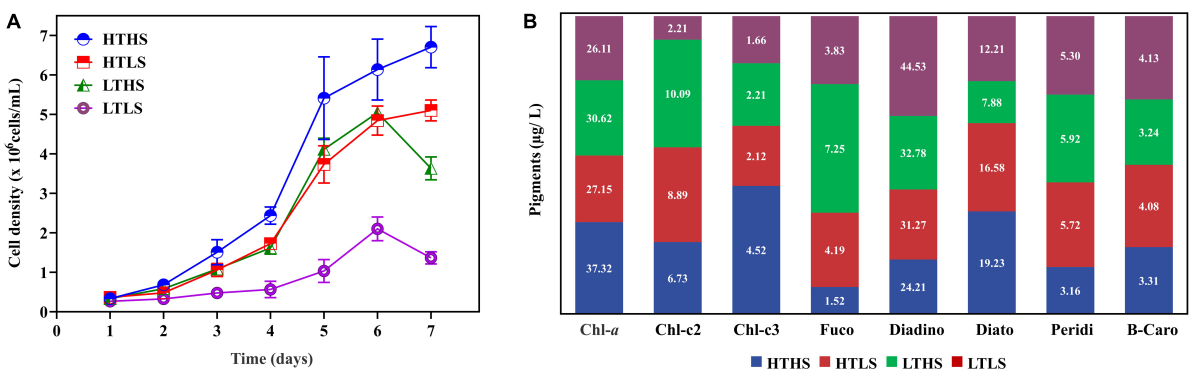

FIGURE 1 | (A) Cell density in four different conditions. HTHS, high silicate high temperature; HTLS, high silicate low temperature; LTHS. low-temperature high silicate; LTLS, low-temperature low silicate. The error bars represent the standard errors from triplicate measurements and **(B)**, the observed pigment composition in *Skeletonema dohrnii* under different stress conditions.

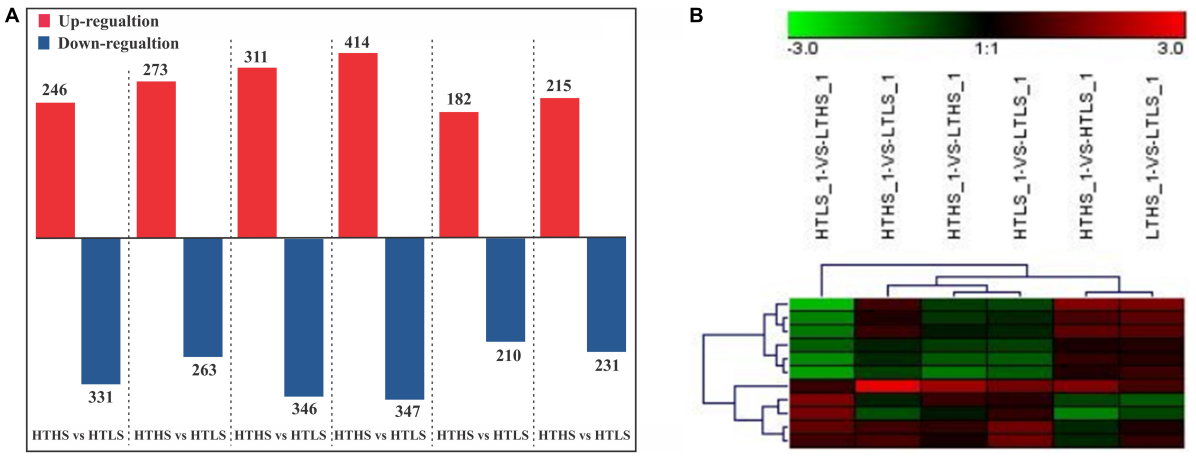

FIGURE 2 | (A) Bar plot of differentially expressed protein in each pairwise comparison and **(B)** the differently expressed proteins (down- and up-regulation). *X*-axis, names of the comparison groups; *Y*-axis, the number of the differentially expressed protein. Red column, up-regulation protein; Green column, down-regulation protein.

Supplementary Table S4 and **Figure S4**). To understand how unique or similar of proteins identified from diatom *S. dohrnii*, those were compared with other diatoms (See **Supplementary Table S4A**). Among all the maximum number proteins (1030) and (627) in *S. dohrnii* was similar with *T. pseudonana*, *T. oceanica* respectively. Additionally, only fewer proteins (12) and (5) of *S. dohrnii* was similar with *S. costatum* and *S. marinoi* despite the same genus.

Functional Annotation of Temperature and Silicate Responsive Proteins

Gene Ontology (GO) was analyzed to identify significant biological changes of the differently abundant protein of diatom *S. dohrnii* to changes of temperature (15 and 25°C), and silicate (0.2 and 2 ml) in the cultures. A total of 43 functional groups were identified (**Supplementary Table S4** and **Figure S5**), of which molecular function accounted for 11 GO terms, cellular component accounted for 13 GO terms, and biological process accounted for 19 GO terms. The four-primary molecular function of the GO terms was a catalytic activity, binding, structural molecular activity, and transporter activity. In cellular component GO annotation, cell, cell part, organelle, macromolecular complex, and membrane part was the top cellular components GO categories. In the biological process GO annotation, more than 85% of the proteins were annotated with the metabolic process, i.e., cellular process, single-organism process, and response to a stimulus. Further, the Gene Ontology enrichment analysis indicated that many processes were associated with responses to changes of temperature and silicates in diatoms, including photosynthesis ($p < 0.01$), carbon metabolism and carbon fixation in photosynthetic organisms ($p < 0.02$), glycolysis or gluconeogenesis ($p < 0.02$), oxidative phosphorylation ($p < 0.04$), biosynthesis of amino acids ($p < 0.01$), and biosynthesis of secondary metabolites ($p < 0.01$).

COG Annotation for All Identified Proteins

The Clusters of Orthologous Groups of proteins (COGs) annotation was applied to classify proteins from the sequenced genomes using orthologs concept (**Figure 3**). The COGs were classified into 25 functional categories according to Riley (1993), showing that the maximum of 216 proteins involved in translation and ribosomal process, followed by 179 proteins in posttranslational modification, 142 proteins in energy production and conversion, 137 proteins in amino acid transport, 95 proteins in signal mechanisms, 89 proteins in carbohydrate transport, and 82 proteins in coenzyme transport and metabolisms.

Multivariate Statistical Analysis

An unsupervised Principal Component Analysis (PCA) was applied to discriminate the samples of different environmental conditions using the proteins ratio and mass spectral variables of each culture. In PCA analysis, the samples were clearly discriminated four different cultures or environmental conditions based on the up- or down-regulation of proteins (**Figure 4A**). The supervised Partial Least Square Analysis model (PLS-DA) was also applied to emphasize the variation in dataset and used to predict Variable Importance Projection (VIP) score to identify the discriminating the samples based on the environmental conditions. The PLS-DA analysis showed similar discrimination among samples HTHS, HTLS, LTHS, and LTLS (**Figure 4B**). Even with the two biological replicates ($n = 2$) per group that is employed in our study, the VIP score of the top 15 proteins is higher than 3 (**Figure 4C**). The first 15 proteins (protein biomarkers) that explain the differences between the four samples groups (HTHS, HTLS, LTHS, LTLS) are given in **Table 1**.

Protein Involvement in Metabolic Pathways

To further investigate the biological function of differentially expressed proteins from diatom *S. dohrnii,* these DEPs were

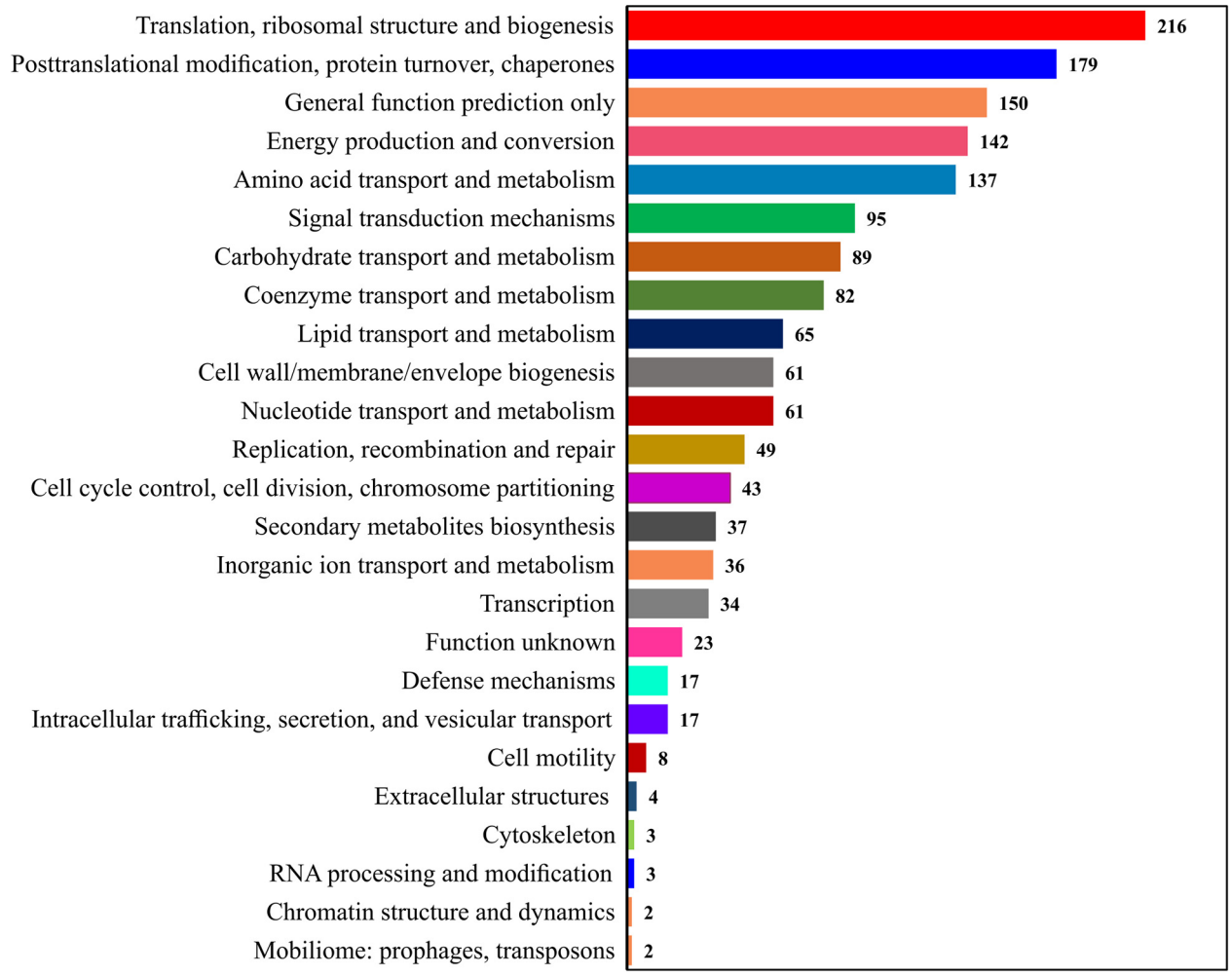

FIGURE 3 | Representation of the protein sets from complete genomes in the COGs.

annotated to the KEGG pathways. In these six groups, the maximum 127–241 proteins involved metabolic pathways was the most significant term among biological processes, following that biosynthesis of amino acids (31–73 proteins), carbon metabolism (41–68 proteins), glycolysis or gluconeogenesis (13–27 proteins), and photosynthesis (9–25 proteins) were the most enriched KEGG pathways (**Supplementary Tables S4B–G**).

We proposed the top most influential or significant pathways ($p < 0.05$) of temperature and silicate response to *S. dohrnii* using pathway enrichment analysis of each condition (**Figure 5**). The results indicated that in HTHS versus HTLS conditions the differentially expressed proteins were predominately enriched in ribosome metabolism, 68 proteins, ($p < 0.0000053$), followed by 68 proteins in carbon metabolism ($p < 0.03$), and 24 proteins in photosynthesis metabolism ($p < 0.05$). In HTHS versus LTHS, 180 proteins were enriched in 90 pathways in the KEGG database, represents, 41 DEPs in ribosome pathways ($p < 0.001$), 20 DEPs in photosynthesis metabolism ($p < 0.001$), and 22 DEPs in carbon fixation metabolism ($p < 0.04$). In group HTHS versus LTLS, 204 DEPs were enriched in 96 metabolic pathways in the KEGG database. Further, pathway enrichment analysis shows, with 32 proteins alteration in carbon fixation metabolism, ($p < 0.001$), 68 proteins in carbon utilization metabolism ($p < 0.03$), and 64 proteins in ribosome pathway ($p < 0.0001$), were the significant metabolism response to this condition. Similarly, the comparison between HTLS versus LTHS sample, shows, 61 DEPs in ribosome pathways, ($p < 0.006$) followed by 19 DEPs in pigment metabolism ($p < 0.00002$), and 73 proteins amino acid biosynthesis were the most influenced biological pathways in *S. dohrnii*. In group HTLS versus LTLS, 127 DEPs were enriched in 93 pathways in the KEGG database. Among all, carbon metabolism was the most represented pathway ($p < 0.06$), followed by thiamine metabolism ($p < 0.01$), and vitamin B6 metabolism ($p < 0.04$). Whereas, DEPs involved in the amino acid biosynthesis ($p < 0.001$), and carbon metabolism ($p < 0.06$) were the most altered pathways of *S. dohrnii* in LTHS versus LTLS group.

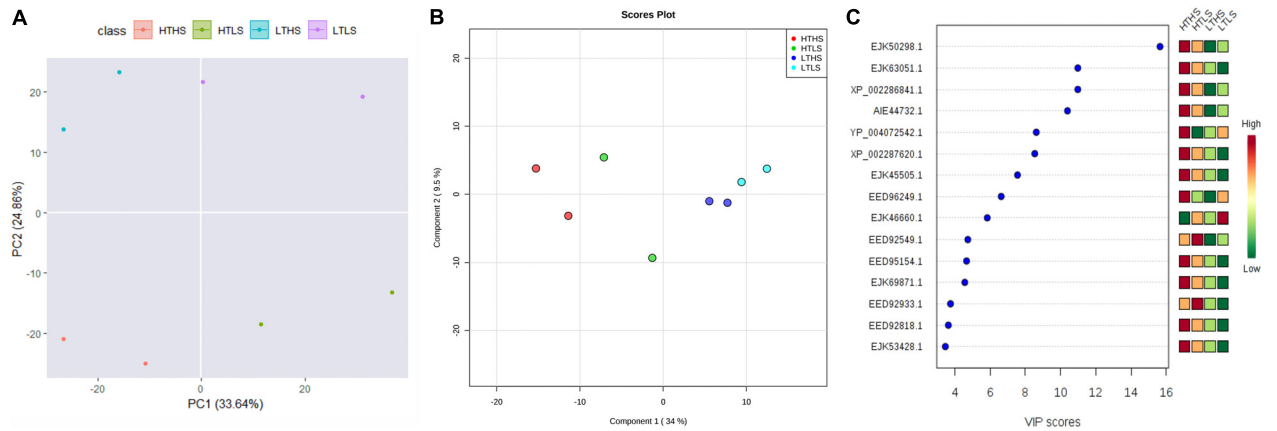

FIGURE 4 | The multivariate statistical analysis score plots on *S. dohrnii* proteins quantified across all eight samples. **(A)** Scatter plot of the first two principal component analysis (PCA) of diatom *S. dohrnii* iTRAQ data. **(B)** PLS-DA score plot analysis obtained from diatom *S. dohrnii.* **(C)** Variable Important in Projection (VIP Score plot) the estimation of important variables in the projection used in PLS-DA model.

TABLE 1 | The protein chemo markers responsible for the discrimination of four sample groups.

Gene name	Protein ID	Name	GO function	Mass	Protein coverage
THAOC_30748	EJK50298.1	ERCC4 domain-containing protein	DNA binding/nuclease activity	73,282.17	0.018
THAOC_16311	EJK63051.1	hypothetical protein	Protein phosphorylation	71,182.03	0.083
THAPSDRAFT_31562	XP_002286841.1	Predicted protein	Plasma membrane	9040.44	0.163
THAPSDRAFT_233	XP_002287620.1	Predicted protein	—	29,947.35	0.088
rbcL	AIE44732.1	Ribulose-1,5-bisphosphate carboxylase (chloroplast)	Reductive pentose-phosphate cycle	24,004.25	0.363
THAOC_35879	EJK45505.1	Protein YIF1B	Endoplasmic reticulum to Golgi vesicle-mediated transport	37,548.29	0.038
atpB	YP_004072542.1	ATP synthase CF1 subunit beta (chloroplast)	ATP synthesis coupled proton transport	51,155.44	0.319
THAOC_08831	EJK69871.1	PRK domain-containing protein	Carbohydrate metabolic process	20,838.29	0.267
THAPSDRAFT_2247	EED95154.1	Predicted protein	—	14,816.54	0.108
THAPSDRAFT_31510	EED96249.1	Fe-S_biosyn domain-containing protein	Iron–sulfur cluster assembly/protein maturation	18,689.72	0.07
PRK1	EED92818.1	Phosphoribulokinase (PRK)	Phosphorylation	42,515.47	0.072
THAOC_34663	EJK46660.1	PAS domain-containing protein	Signal transduction/protein kinase	24,629.05	0.057
THAPS_10777	XP_002295511.1	Hypothetical protein	Integral component of membrane	43,249.56	0.029
THAOC_27143	EJK53428.1	Hypothetical protein	—	33,381.81	0.026
ANS1	EED92933.1	Asparagine synthase	Asparagine biosynthetic process	66,174.51	0.073

All proteins were identified by MS/MS ion search using Mascot version 2.3.02, mass tolerance 0.05 Da.

DISCUSSION

In this study, we demonstrated the application iTRAQ, bioinformatics analysis (GO, COG, VIP score plot), and prediction of protein-enriched pathway (KEGG pathway) in quantitative proteome profiling of the ecologically important marine diatom *S. dohrnii*. The results of this study demonstrated that phenotypic plasticity of diatom proteome could be widely regulated of tolerance limits in response to global warming. The changes of proteome profile and associated cellular functions in different environmental conditions of the diatom *S. dohrnii* in response to climate change and impacts on marine ecosystem are discussed here.

Physiological Changes

Elevated temperature under conditions of nutrient availability led to higher intrinsic growth rates, promoting enhancement in energetic, metabolic, and gene expression that induces smooth cell cycle and cell division in diatoms. In addition to warming, to cope with nutrient limitation diatoms could modify several metabolic pathways. For instance, diatoms responded to phosphate limitation expressed modification in the glycolysis pathway and induce a higher level of lipids and primary triacylglycerols (Longworth et al., 2016). During the phosphate limitation diatom replaces phospholipids with non-phosphorous membrane lipids to reduce the demand of phosphate (Van Mooy et al., 2009) and cope up with nutrient limitation. *S. dohrnii*

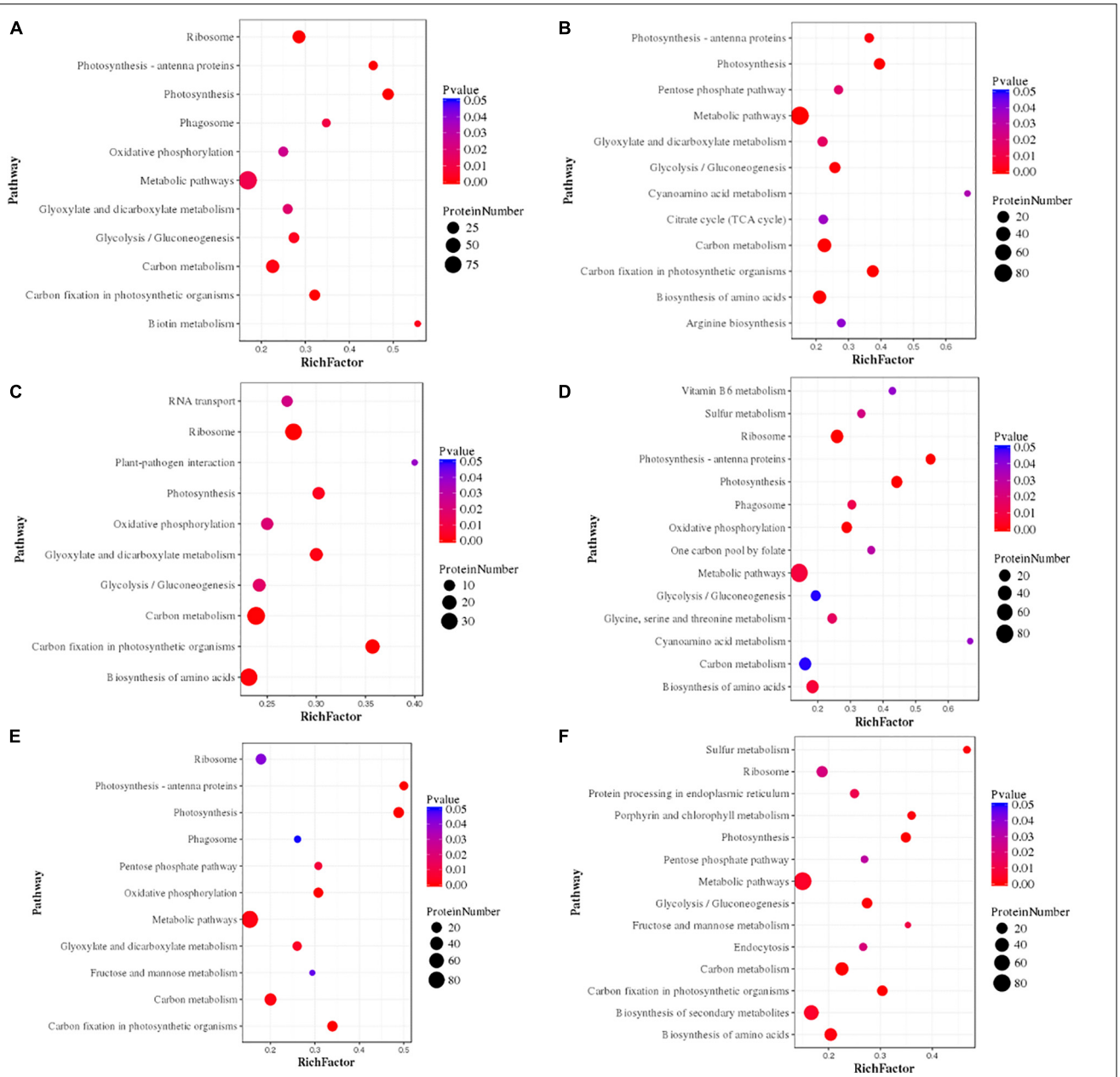

FIGURE 5 | Pathway enrichment analysis of differentially expressed proteins in each pairwise. In the figure greater rich factor means greater intensiveness and *p*-value ranges from 0 to 1, and less *p*-value means greater intensiveness. **(A)** (HTHS-HTLS), **(B)** (HTHS-LTHS), **(C)** (HTHS-LTLS), **(D)** (HTLS-LTHS), **(E)** (HTLS-LTLS), **(F)** (LTHS-LTLS).

may have a similar strategy in HTLS condition to cope with the warming ocean with under silicate limitation.

It was proposed that acetyl-CoA metabolism in diatom played a key role when diatom grew in lower temperature. A supply of acetyl-CoA to fatty acid and Branched-Chain Amino Acid (BCAA) metabolism will reduce the cell division rates (Cai et al., 2011; Pietrocola et al., 2015; Lin et al., 2017) while excessive cytosolic acetyl-CoA resulting in the over acetylation of cytosolic proteins and consequent inhibition of enzymatic activity (Weinert et al., 2014). Therefore, it is proposed that invested pathways in fatty acid and BCAA play a key during the LTHS adaptation. Moreover, in diatoms cell division and cell cycle consist of light-dependent and light-independent segments (Ashworth et al., 2013) which regulates diatom cell cycle G1 and G2/M phases (Huysman et al., 2014). However, in some instances cell division determined by light phasing in diatom can be regulated and by nutrient addition, suggesting nutrient control of the cell cycle is increased during the temperature variation (Olson and Chisholm, 1983). Besides, diatom treated lower temperature, and lower silicate expressed lower protein

ratio, which could decrease membrane fluidity and can affect the compensatory investment of photosynthesis proteins and biosynthesis of fatty acids. This eventually induces cell cycle arrest at the G1 phase, which has been linked with silica requirement for DNA replication (Huysman et al., 2010) could be the reason for lower cell growth and replication in LTLS condition.

Mechanisms Underlying Tolerance to Temperature and Silicate – Proteomics Perspective

Marine organisms responses to various environmental stresses, i.e., warming, ocean acidification, low salinity, lower silicate, doxycycline at proteomics level have been studied and reviewed (Allen et al., 2008; Clement et al., 2017; Jian et al., 2017; Tomanek, 2011). The iTRAQ based proteomic profiling revealed a systematic temperature tolerance mechanism of marine diatom. This study reveled the down-regulation of various proteins involved in the metabolic process in response to the changes in temperature and silicate level. Similarly, molecular catalytic activity process also appears to be speeded up in response to a change of temperature and silicate. The rearrangement of cellular process in energy production and conversion, biogenesis, and amino acid transport and metabolism were known to be the vital physiological adjustments in marine organisms undergo due to the effect of climate change and ocean acidification (Dupont et al., 2012; Stumpp et al., 2012; Jian et al., 2017). The effect noticed in these metabolic process pathways appears to be necessary for marine diatom because it could allow them to allocate more bioenergy for stress acclimation during higher temperature with less silicate for cell wall formation and cellular process.

Similarly, differential expression of 293 proteins involved in diatom *S. dohrnii* tissue metabolism, cell division and cycle control (43 proteins), translation and ribosomal structure (216 proteins), transcription (34 proteins) signal transduction mechanisms (95 proteins), appears to have significant role during the changes of temperature and silicate concentration at cellular level. Marine organisms including larvae and adults, tend to elevate lipid and carbohydrate metabolism to meet the higher bioenergetics demands of temperature stress, but with a physiological cost, reduced the expression of proteins involved in growth and repair (three proteins) and immune system process (eight proteins). These results indicate the presence of systematic temperature tolerance mechanisms in diatom *S. dohrnii.* The response of marine diatom *S. dohrnii* to changes of temperature and silicate at proteomics level in our study is consistent with earlier investigations (Jian et al., 2017; Thangaraj et al., 2019). The functional role of some of these differentially expressed proteins and associated pathways are discussed here.

Down-Regulation of Photosynthesis

Earlier investigation noted depletion of nitrogen on *T. pseudonana* (Jian et al., 2017) and low iron supply to *Phaeodactylum tricornutum* (Allen et al., 2008) causing significant changes in the photosynthesis process. Similarly, in our study, the higher temperature and silicate limitation lead to down-regulation of photosynthesis in diatom *S. dohrnii* (**Figure 6**). Based on the KEGG pathway analysis 20 photosynthesis-related proteins associated with changes of temperature and silicate (HTHS vs. HTLS), from which 16 proteins were downregulated including photosystem II protein (PsbA, PsbD, PsbC, PsbB, PsbE, PsbH), photosystem I proteins (PsaA, PsaB, PsaF, and PsaL) cytochrome (PetA, PetC, PetD), and including proton-transporting ATP synthase activity and regulate rotational mechanism proteins (F-type ATPase α, γ, and β). Four proteins were upregulated (red color) photosystem I and II proteins (PsbO, PsbV, PsaD) and F-type ATPase (β). PsaB and PsaC were two photosystem II protein binds chlorophyll and supports catalyze the primary light-induced photochemical processes of PSII (Zhang et al., 2015). PsbA, PsbB, and PsbC are three subunits assembled in photosystem II with PsbA acting as the reaction center protein, and PsbB and PsbC responsible for light-harvesting (Barber, 2002). The upregulated protein PsbO responsible for the oxidation–reduction process and PsaD protein involves in ferredoxin-binding and form complexes with ferredoxin and ferredoxin-oxidoreductase in photosystem I (PSI) reaction center of chromoplast cells. The higher abundance of downregulated proteins indicated decreased photosynthetic carbon fixation and energy production, which may contribute to reducing growth rate similar results was observed on macroalgae (Fan et al., 2018). In our experimental analysis (HTLS vs. LTHS), a total of 14 proteins were upregulated such as photosystem proteins I and II (PsbA, PsbB, PsbF, PsbV, PsaJ) and F-type ATPase (i.e., α, β, γ, and δ). It binds chlorophyll and helps catalyze the primary light-induced photochemical processes of PSII. In diatoms, protein PsbF is stimulating electron transfer, heme-binding or iron-binding process. Four proteins were downregulated (HTLS vs. LTHS), like PsbU, PetA, PetF, PetH, and α. In diatom *S. dohrnii* protein PetH involved in molecular function, particularly oxidoreductase activity. In a low-temperature experiment (LTHS vs. LTLS), KEGG analysis reveals that a total of 16 downregulated proteins were involved in the photosynthetic pathway and one upregulated protein PsbO serve as oxygen-evolving enhancer protein and regulate the oxidation–reduction process. Results indicated that both photosynthesis and other metabolic pathways were significantly associated with proteomic alteration of higher temperature and deprivation of silicate. Our findings revealed that different molecular metabolism of diatom *S. dohrnii* could be temperature and silicate dependent, specifically during with higher temperature and silicate can induce expression of upregulated proteins like photosystem I and II and could increase the growth of diatoms through photosynthesis and metabolic pathways. By contrast in high temperature and low silicate level, the photosynthetic proteins are down-regulated and reducing the planktonic metabolism, photosynthesis process, and ATP formation in diatoms, resulting the subsequent impact of zooplankton biomass and fishery production. In associated with photosynthesis metabolic regulation, the proteins regulate the light-harvesting process (pigment metabolism) are given in **Supplementary Table S4H**. In *S. dohrnii,* the photosynthetic pigments fucoxanthin is bound along with chlorophyll, it

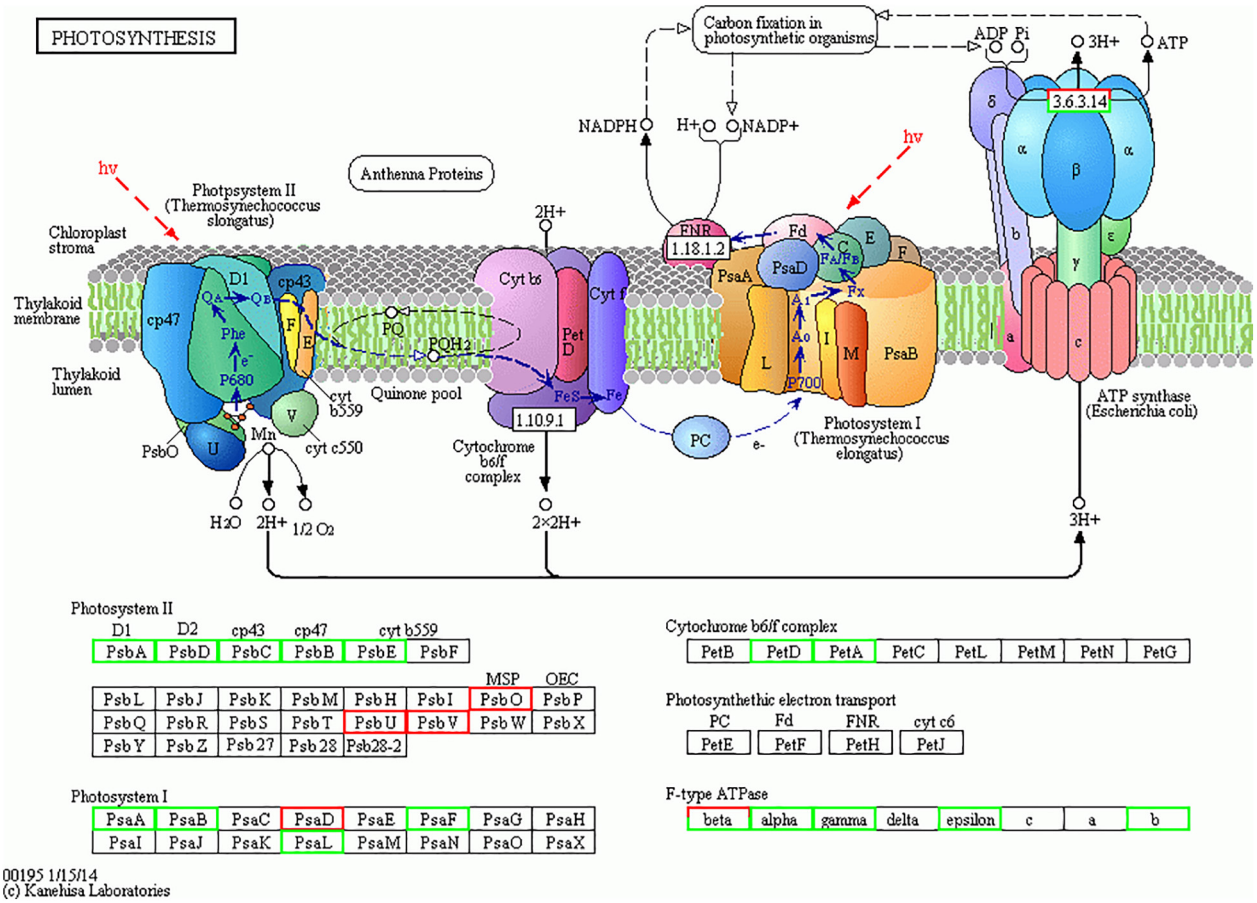

FIGURE 6 | The photosynthesis pathway map for *Skeletonema dohrnii* during the changes of temperature and silicate (HTHS vs. HTLS). The down-regulated proteins were shown in light green color boxes and up-regulated proteins are given in red color. The comprehensive information of all the regulated proteins associated with photosynthesis metabolism are given in **Supplementary Tables S2, S3**. This image is obtained from KEGG website (http://www.kegg.jp/kegg/kegg1.html) with copy right permission.

encompasses the light-harvesting from solar energy and its involvement in the early stages of the photosynthesis process (Thangaraj et al., 2020). In this study, fucoxanthin and chlorophyll relevant proteins were mostly downregulated with higher temperature and lower silicate concentration (HTHS vs. HTLS) and upregulated in lower temperature with higher silicate concentration (HTLS vs. LTHS), the above results suggest that the lower silicate concentration reduced the photosynthetic efficiency compared to another environmental parameter like temperature.

Photosynthesis and Carbon-Fixation-Related Genes Decreased

The combining elevation of temperature and silicate limitation affect the photosynthetic efficiency of *S. dohrnii*, as shown in **Figure 6**. As marine diatom fixes 20% of global CO_2, their photosynthetic efficiency enhanced by RuBisCO as it involves in the first carbon step of carbon fixation. In this study, RuBisCO was downregulated by both temperature and silicate limitation (**Supplementary Table S2**). Further, many proteins involved in the Calvin cycle were down-regulated in HTHS versus LTLS (**Figure 7**) shows combining temperature or silicate stress suppressed C3 photosynthesis and carbon fixation, and influence in the carbon that inside the cell toward RuBisCO are adjusted to the match reductant supply (Allen et al., 2008).

Diatom has major enzymes of phosphoenolpyruvate carboxylase (PEPC), phosphoenolpyruvate carboxykinase, and pyruvate phosphate dikinase (PPDK) to perform C4 photosynthesis (Armbrust et al., 2004; Poulson-Ellestad et al., 2014). In this study PEPC was differentially expressed in HTHS versus HTLS and HTHS versus LTHS condition, whereas, the PPDK was only differentially expressed in HTHS versus LTLS (**Figure 7**), indicating suppression of C4 photosynthesis by both temperature and silicate stress. The regulated PPDK and carbonic anhydrase in our study show the proteomic modification of *S. dohrnii* central carbon metabolism (CCM). Similarly, many downregulating genes related to CCM were observed in the nutrient-limited condition of the diatom

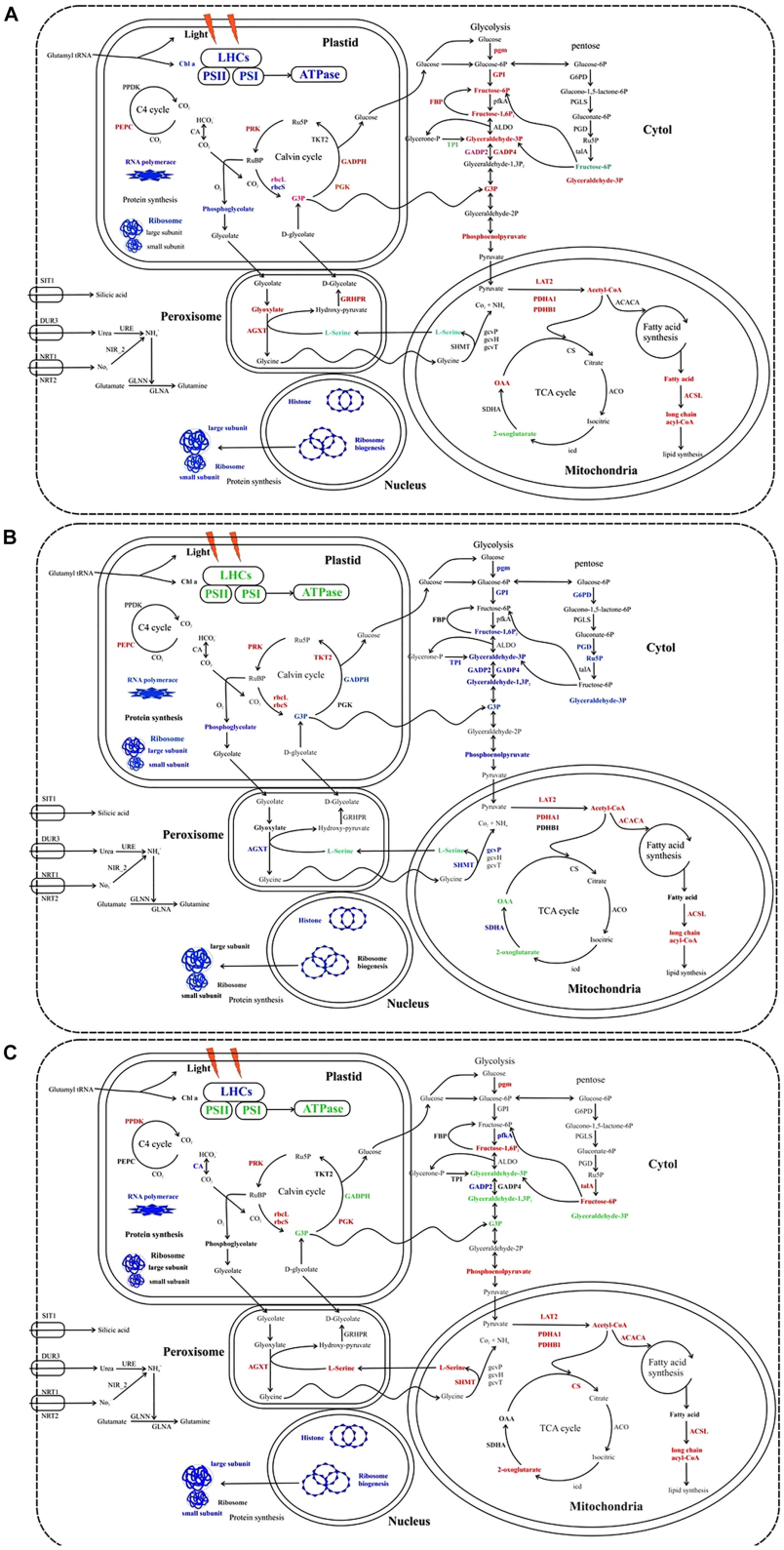

FIGURE 7 | Cellular metabolic pathways and processes influenced by the different stress condition in *S. dohrnii.* **(A)** HTHS versus HTLS; **(B)** HTHS versus LTHS; **(C)** HTHS versus LTLS condition. Red, blue, green, and black text indicates upregulation, downregulation, both up and downregulation, and no changes of pathways or

(Continued)

FIGURE 7 | Continued
proteins. LHCs, light harvesting complexes; PSII, photosystem II; PSI, photosystem I; PPDK, pyruvate phosphate kinase; PEPC, phosphoenolpyruvate; CA, carbonic anhydrase; PRK, phosphoribulokinase; rbcL, Rubisco large subunit; rbcS, Rubisco small subunit; PGK, phosphoglycerate kinase; TKT2, fructose-bisphosphate aldolase; GAPDH, glyceraldehyde-3-phosphate dehydrogenase; pgm, phosphoglucomutase; GPI, glucose-6-phosphate isomerase; FEP, fructose-1,6-bisphosphatase; pfka, 6-phosphofructokinase; ALDO, fructose-bisphosphate aldolase; GAPD, glyceraldehyde-3-phosphate dehydrogenase; TPI, triose-phosphate isomerase; ENO, α-enolase; PYK, pyruvate kinase; G6PD, glugose-6-phospahate 1-dehydrogenase; PGLS, 6-phosphogluconolactonase; PGD, 6-phosphogluconate dehrdrogenase; talA, transaldolase; LAT2, pyruvate dehydrogenase E2 (dihydrolipoamide *s*-acetyltransferase); PDHA1, pyruvate dehydrogenase E1 component subunit alpha-1, PDHB1, pyruvate dehydrogenase E1 component subunit beta-1; ACACA, acetyl-CoA carboxylase; ACSL, long chan acyl-COA synthetases, CS, citrate synthase; ACO, aconitate hydratase 2; icd, isocitrate dehydrogenase; SDHA, succinate dehydrogenase; gcvT, glycine decarboxylase T protein; gcvH, glycine decarboxylase H protein; gcvP, glycine decarboxylase P protein; SHMT, glycine/serine hydroxymethyltransferase; AGXT, alanine-glyoxylate transaminase; GLN, glutamine synthetase; NIR_2, Ferredoxin0nitrite reductase; URE, urease; NRT, nitrate/nitrite transporters; SIT, silicic acid transporter. The comprehensive information of all the identified regulated proteins associated with carbon metabolism are given in **Supplementary Tables S2, S3**. These images were created using Corel Draw Graphics suite.

(Alipanah et al., 2015). In this study, most of the glycolysis and TCA proteins were upregulated under HTHS versus HTLS cells, while most of the proteins were decreased in HTHS versus LTHS cells (**Figure 7**), indicating that these metabolisms were sensitive to the temperature changes. Among them, increased abundance of pyruvate dehydrogenase (PDHA) in HTHS versus HTLS, HTHS versus LTHS, and HTHS versus LTLS shows direct carbon away from intracellular carbohydrate store to the TCA cycle (**Figure 7**). The TCA cycle in diatom generally upregulated in response to high levels of amino acids, and protein degradation, which creates intermediates and provides for nutrient assimilation bender (Lyon et al., 2011). Further, under combining temperature and silicate stress of HTHS versus LTLS, citrate synthase, and succinate dehydrogenase (SDH) were also regulated (**Figure 7**), which catalyzes succinate–fumarate coupling and then direct to the oxidation of TCA cycle, that intermediate with the photosynthetic electron chain. The up-regulation of (G3P) protein in HTHS versus HTLS shows *S. dohrnii* would enhance the Calvin cycle by catalyzing the dephosphorylation of 1,3-bisphosphoglycerateacid (BPGA) to produce glyceraldehyde-3-phosphate (GAP) (Trost et al., 2006). Down-regulation of phosphoglycerate kinase (PDHA1) in HTLS versus LTHS (See **Supplementary Table S2**) indicating reduced efficiency step 7 process of glycolysis. However, it shows the opposite trend as upregulation proteins in HTHS versus HTLS, and HTHS versus LTLS, (**Figure 7**) resulting an increasing process. Collectively, these gene expressions indicating that combine temperature and silicate stress reduced these processes in diatom *S. dohrnii*.

Metabolic regulation of glycolytic proteins shows that nutrient deficiency has a different bypass mechanism in diatom (Dyhrman et al., 2012). Similarly, the glycolysis, and the pentose phosphate pathway generates NAD(P)H and pentoses (5-carbon sugars) as well as ribose 5-phosphate. Collectively, both stress condition (temperature and silicate) activated the phosphate-reaction participation (**Figure 7**) and enhance the capacity of NAD(P)H production, aiming to promote silicate utilization under lower silicate condition and supply under reduction of ATP. It is clear that when combining temperature and silicate changes occur in the environment, there are positive and negative impacts on diatom carbon metabolism; regulation of RuBisCO would alter the efficiency of diatom carbon fixation. Our findings are in line with previous studies experimental demonstrations in response to the limitation of CO_2, silicate, and ocean acidification of plankton and oysters (Allen et al., 2008; Clement et al., 2017; Jian et al., 2017).

Downregulation of Ribosome Biogenesis

Ribosome biogenesis is vital to a cellular process for all the living organisms, but remarkably insufficient information is known about the underlying pathway. Compared to prokaryotes (i.e., yeasts) much is poorly known about the ribosome biogenesis pathway in plants, animals and particularly of marine planktons (Henras et al., 2008). Thomson et al. (2013) reported that the core of higher eukaryotic ribosome biogenesis pathway was different from the yeast counterpart. Based on the KEGG pathway analysis, eight ribosome biogenesis proteins were observed during the changes of temperature and silicate (HTLS) from these six proteins were downregulated (green color) (**Supplementary Table S4** and **Figure S6**) including three 90S-pre-ribosome components (CK2A, CK2B, UTP6), these proteins play an essential coenzyme and enzyme regulator in ribosome biogenesis pathway.

Furthermore, it is interacting selectively and non-covalently with small nucleolar RNA and non-covalently with ATP, adenosine 5′-triphosphate. The other three rRNA modification proteins NKP6, DKC1, and KRE33, which involved in catalysis of the reactions (RNA uridine = RNA pseudouridine). It converts the uridine in RNA molecule to pseudouridine by rotation of the C1′-N-1 glycosidic bond of uridine in RNA to a C1′-C5 (Foster et al., 2000). The protein KRE33 also involved in catalysis of the reaction: acetyl-CoA + cytidine = CoA + N4-acetylcytidine. The precise role of these downregulated proteins is yet to be defined. Two proteins were upregulated (red color) in ribosome biogenesis SNU13 and Ran which involved in nucleocytoplasmic transport and chromatin condensation and control of cell cycle. However, there is also evidence for differences in the ribosome biogenesis pathway between higher temperature and lower temperature, and lower silicate level during the culture of diatoms *S. dohrnii*. In our proteomic profiling, based on the temperature (HTLS vs. LTHS) four proteins were upregulating (i.e., CK2A, CK2B, NOP56, KRE33), which intricate in the metabolic functions and support the RNA involving in the processing of ribosomes and reduce the oxidoreductase activity (Smith et al., 2013). Three proteins were downregulating

(SNU13, EMG1, Ran), which modulates the activity of protein kinase and involved in chromatin condensation in the cell cycle. SNU13 protein is involving in the maturation of a precursor Large SubUnit (LSU) ribosomal RNA (rRNA) molecule into a mature LSU-rRNA molecule (Ebersberger et al., 2014). Besides, in our diatom, proteomic profiling of LTHS versus LTLS, five genes (Imp3, NOP58, NOP56, Nog1, CRM1) were downregulating with lower temperature and silicate (**Supplementary Table S2**). The Imp3 gene involved in the conversion of an important ribosomal RNA (rRNA) transcript into one or more mature rRNA molecules and protein NOP58, NOP56 involves the DNA binding and snoRNA binding in cells. Besides, one gene NAN1 was upregulating in this study, NAN1 serves as a metal-binding cofactor and bound tightly inactive sites or loosely with the substrate. In our study, the downregulated proteins Imp3, NOP58, NOP56, Nog1, CRM1 be a specific response to combining changes of temperature and limitation of silicate could affect the cell growth and cell cycle of marine diatom *S. dohrnii.*

Protein Biomarkers

The PCA and PLS-DA model applied to discriminate the results of diatom *S. dohrnii* iTRAQ data. PCA and PLS-DA score plots demonstrated the good separation between higher temperature, lower temperature versus higher silicate and lower silicate level of culture conditions. The higher value of VIP score indicates the great contribution of the proteins to the discrimination of diatom samples in this study. Fifteen protein biomarkers were identified based on the VIP scores given in **Table 1**. Two proteins (EJK63051.1) and (EJK50298.1) play a vital role in the regulation of metabolic process including cell cycle, growth, DNA binding, and transmitting the signals throughout the cell. Gene, atpB encodes a subunit of mitochondrial ATP synthase, it catalyses ATP synthesis utilizing an electrochemical gradient of protons across the inner membrane during oxidative phosphorylation (Weber, 2006). The other protein, (AIE44732.1) or gene rbcL plays a critical role in carbon dioxide fixation, as well as the oxidative fragmentation of the pentose substrate in the photorespiration process (Chen et al., 2018). Furthermore, two proteins (EJK69871.1) and (EED92818.1) involved in the regulation of actin cytoskeleton organization and endocytosis (Cope et al., 1999).

Gene Redundancy

The different biochemical pathways were identified from different diatoms including photosynthesis (Grouneva et al., 2011), and carbon cycle in *S. costatum* (Zhang et al., 2015), urea cycle in *T. pseudonana* (Armbrust et al., 2004), and mitochondrial in *P. tricornutum* (Kroth et al., 2008). Additionally, the phylogenetic affinities to other organisms such as the genes of bacterial (Bowler et al., 2008), and green algal origins identified in *T. pseudonana* and *P. tricornutum* (Moustafa et al., 2009). The cellular metabolic pathways and processes influenced by the different stress condition in *S. dohrnii* are given in **Figure 7**. In KEGG pathways, Genes, PDHA1, PDHB1 catalyzes the overall conversion of pyruvate to acetyl-CoA and CO(2) and provides the primary link between glycolysis and the tricarboxylic acid (TCA) cycle. Similar to this study, Carvalho and Lettieri (2011) were reported that redundant gene (THAPSDRAFT_25042) in *T. pseudonana* responsible for the upregulation of metabolic process (long-chain acyl-CoA synthetase), upon exposure to benzo(a)pyrene. The following photosystem PSI and II two encoded proteins or genes were identified as part of the photosynthetic electron transport of diatom *T. pseudonana* (Grouneva et al., 2011) in *P. tricornutum* (Alipanah et al., 2015) in *S. costatum* (Zhang et al., 2015). PS1 subunits consists of PsaA, PsaB, PsaL, PsaE, PsaJ, PsaM, and PSII units consists of PsbO (O), PsbU, PsbV, Psb31, PsbQ. In our study, we demonstrated the response of these genes on photosynthesis in different stress condition and these results were confirmed in diatom *S. dohrnii*. Additionally, Carvalho and Lettieri (2011) were reported the upregulated proteins or gene, cfxX (RuBisCO expression protein) and Lhcr4, Lhcr10 (fucoxanthin chl a/c light-harvesting protein) responsible for the regulation of photosynthesis in *T. pseudonana* upon exposure to benzo(a)pyrene. The genes (PPdk, PGK, pfkA, PYK1, PDHA1, and PDHB1) responsible for the regulation of carbon metabolism of model diatom *P. tricornutum* during N deprivation (Alipanah et al., 2015), were also reported in field-collected and laboratory-cultured *S. costatum* (Zhang et al., 2015). In our study, the regulation of carbon metabolism was assessed in *S. dohrnii* and confirmed the involvement of above-mentioned genes in carbon fixation process.

CONCLUSION

Our investigation of the responses of diatom *S. dohrnii* to the concomitant warming ocean and limiting nutrients (Si) with multivariate statistics and pathway analysis gave new insights into intracellular metabolic processes. We observed downregulation of the photosynthesis process, carbon assimilation and utilization mechanisms and biological processes related to cell cycle regulation during elevated temperature and Si limitation in the diatom. Further protein biomarkers revealed signal transduction, ATP production, and carbon fixation pathways associated to thermal and nutrient stress. Our findings contribute to our understanding of the impact of climate change on the physiological adjustment to molecular mechanism of diatoms.

DATA AVAILABILITY STATEMENT

The raw proteomics data and analysis files for the manuscript have been submitted to ProteomeXchange via Pride database (www.ebi.ac.uk/pride/archive/) with identifier PXD022918.

AUTHOR CONTRIBUTIONS

ST and JS designed this study. ST performed the laboratory experiment, carried out data analysis, and defined the manuscript contents in discussion with SP and JS. GZ performed pigment analysis and drafted pigment part. JS coordinated this investigation and provided guidance and facilities to perform this

experiment. All authors contributed to the article and approved the submitted version.

FUNDING

This research was financially supported by the National Key Research and Development project of China (2019YFC1407805), the National Natural Science Foundation of China (41876134, 41676112, and 41276124), the Tianjin 131 Innovation Team Program (20180314), and Changjiang Scholar Program of Chinese Ministry of Education (T2014253) to JS.

SUPPLEMENTARY MATERIAL

The Supplementary Material for this article can be found online at: https://www.frontiersin.org/articles/10.3389/fmicb.2020.554832/full#supplementary-material

REFERENCES

Alipanah, L., Rohloff, J., Winge, P., Bones, A. M., and Brembu, T. (2015). Whole-cell response to nitrogen deprivation in the diatom *Phaeodactylum tricornutum*. *J. Exp. Botany*. 66, 6281–6296.

Allen, A. E., Laroche, J., Maheswari, U., Lommer, M., Schauer, N., Lopez, P. J., et al. (2008). Whole-cell response of the pennate diatom *Phaeodactylum tricornutum* to iron starvation. *Proc. Natl. Acad. Sci. U.S.A.* 105, 10438–10443. doi: 10.1073/pnas.0711370105

Armbrust, E. V., Berges, J. A., Bowler, C., Green, B. R., Martinez, D., Putnam, N. H., et al. (2004). The genome of the diatom *Thalassiosira pseudonana*: ecology, evolution, and metabolism. *Science* 306, 79–86. doi: 10.1126/science.1101156

Ashworth, J., Coesel, S., Lee, A., Armbrust, E. V., Orellana, M. V., and Baliga, N. S. (2013). Genome-wide diel growth state transitions in the diatom *Thalassiosira pseudonana*. *Proc. Natl. Acad. Sci. U.S.A.* 110, 7518–7523. doi: 10.1073/pnas.1300962110

Bahulikar, R. A., and Kroth, P. G. (2008). The complex extracellular polysaccharides of mainly chain-forming freshwater diatom species from Epilithic Biofilms(1). *J. Phycol.* 44, 1465–1475. doi: 10.1111/j.1529-8817.2008.00609.x

Barber, J. (2002). Photosystem II: a multisubunit membrane protein that oxidises water. *Curr. Opit. Struct. Biol.* 12, 523–530. doi: 10.1016/s0959-440x(02)00357-3

Bopp, L., Aumont, O., Cadule, P., Alvain, S., and Gehlen, M. (2005). Response of diatoms distribution to global warming and potential implications: a global model study. *Geogr. Res. Let.* 32:L19606.

Bowler, C., Allen, A. E., Badger, J. H., Grimwood, J., Jabbari, K., Kuo, A., et al. (2008). The *Phaeodactylum* genome reveals the evolutionary history of diatom genomes. *Nature* 456, 239–244.

Cai, L., Sutter, B. M., Li, B., and Tu, B. P. (2011). Acetyl-CoA induces cell growth and proliferation by promoting the acetylation of histones at growth genes. *Mol. Cell* 42, 426–437. doi: 10.1016/j.molcel.2011.05.004

Carvalho, R. N., and Lettieri, T. (2011). Proteomic analysis of the marine diatom *Thalassiosira pseudonana* upon exposure to benzo (a) pyrene. *BMC Genom.* 12:159. doi: 10.1186/1471-2164-12-159

Charbonneau, M. E., Girard, V., Nikolakakis, A., Campos, M., Berthiaume, F., Dumas, F., et al. (2007). O-linked glycosylation ensures the normal conformation of the autotransporter adhesin involved in diffuse adherence. *J. Bacteriol.* 189, 8880–8889. doi: 10.1128/jb.00969-07

Chen, X. H., Li, Y. Y., Zhang, H., Liu, J. L., Xie, Z. X., Lin, L., et al. (2018). Quantitative proteomics reveals common and specific responses of a marine diatom *Thalassiosira pseudonana* to different macronutrient deficiencies. *Front. Microbiol.* 9:2761. doi: 10.3389/fmicb.2018.02761

Chust, G., Allen, J. I., Bopp, L., Schrum, C., Holt, J., Tsiaras, K., et al. (2014). Biomass changes and trophic amplification of plankton in a warmer ocean. *Glob. Chang. Biol.* 20, 2124–2139. doi: 10.1111/gcb.12562

Clement, R., Lignon, S., Mansuelle, P., Jensen, E., Pophillat, M., Lebrun, R., et al. (2017). Responses of the marine diatom *Thalassiosira pseudonana* to changes in CO_2 concentration: a proteomic approach. *Sci. Rep.* 7:42333.

Cohen, N. R., Gong, W., Moran, D. M., Mcilvin, M. R., Saito, M. A., and Marchetti, A. (2018). Transcriptomic and proteomic responses of the oceanic diatom *Pseudo-nitzschia granii* to iron limitation. *Environ. Microbiol.* 20, 3109–3126. doi: 10.1111/1462-2920.14386

Cope, M. J. T., Yang, S., Shang, C., and Drubin, D. G. (1999). Novel protein kinases Ark1p and Prk1p associate with and regulate the cortical actin cytoskeleton in budding yeast. *J. Cell Biol.* 144, 1203–1218. doi: 10.1083/jcb.144.6.1203

Darby, A. C., Gill, A. C., Armstrong, S. D., Hartley, C. S., Xia, D., Wastling, J. M., et al. (2014). Integrated transcriptomic and proteomic analysis of the global response of Wolbachia to doxycycline-induced stress. *ISME J.* 8, 925–937. doi: 10.1038/ismej.2013.192

Dong, H. P., Dong, Y. L., Cui, L., Balamurugan, S., Gao, J., Lu, S. H., et al. (2016). High light stress triggers distinct proteomic responses in the marine diatom *Thalassiosira pseudonana*. *BMC Genom.* 17:994. doi: 10.1186/s12864-016-3335-5

Du, C., Liang, J.-R., Chen, D.-D., Xu, B., Zhuo, W.-H., Gao, Y.-H., et al. (2014). iTRAQ-based proteomic analysis of the metabolism mechanism associated with silicon response in the marine diatom *Thalassiosira pseudonana*. *J. Proteome Res.* 13, 720–734. doi: 10.1021/pr400803w

Dupont, S., Dorey, N., Stumpp, M., Melzner, F., and Thorndyke, M. (2012). Long-term and trans-life-cycle effects of exposure to ocean acidification in the green sea urchin *Strongylocentrotus droebachiensis*. *Mar. Biol.* 160, 1835–1843. doi: 10.1007/s00227-012-1921-x

Dyhrman, S. T., Jenkins, B. D., Rynearson, T. A., Saito, M. A., Mercier, M. L., Alexander, H., et al. (2012). The transcriptome and proteome of the diatom *Thalassiosira pseudonana* reveal a diverse phosphorus stress response. *PLoS One* 7:e33768. doi: 10.1371/journal.pone.0033768

Ebersberger, I., Simm, S., Leisegang, M. S., Schmitzberger, P., Mirus, O., Von Haeseler, A., et al. (2014). The evolution of the ribosome biogenesis pathway from a yeast perspective. *Nucleic Acids Res.* 42, 1509–1523. doi: 10.1093/nar/gkt1137

Fan, M., Sun, X., Liao, Z., Wang, J., Li, Y., and Xu, N. (2018). Comparative proteomic analysis of *Ulva prolifera* response to high temperature stress. *Proteome Sci.* 16:17.

Feng, T.-Y., Yang, Z.-K., Zheng, J.-W., Xie, Y., Li, D.-W., Murugan, S. B., et al. (2015). Examination of metabolic responses to phosphorus limitation via proteomic analyses in the marine diatom *Phaeodactylum tricornutum*. *Sci. Rep.* 5:10373.

Field, C. B., Behrenfeld, M. J., Randerson, J. T., and Falkowski, P. (1998). Primary production of the biosphere: integrating terrestrial and oceanic components. *Science* 281, 237–240. doi: 10.1126/science.281.5374.237

Foster, P. G., Huang, L., Santi, D. V., and Stroud, R. M. (2000). The structural basis for tRNA recognition and pseudouridine formation by pseudouridine synthase I. *Nat. Struct. Mol. Biol.* 7:23.

Grouneva, I., Rokka, A., and Aro, E.-M. (2011). The thylakoid membrane proteome of two marine diatoms outlines both diatom-specific and species-specific features of the photosynthetic machinery. *J. Proteome Res.* 10, 5338–5353. doi: 10.1021/pr200600f

Gu, H., Zhang, X., Sun, J., and Luo, Z. (2012). Diversity and seasonal occurrence of *Skeletonema* (*Bacillariophyta*) species in Xiamen Harbour and surrounding seas, China. *Cryptogam. Algol.* 33, 245–263. doi: 10.7872/crya.v33.iss3.2012.245

Guillard, R. R., and Ryther, J. H. (1962). Studies of marine planktonic diatoms: I. *Cyclotella* nana Hustedt, and *Detonula confervacea* (Cleve) Gran. *Can. J. Mic.* 8, 229–239. doi: 10.1139/m62-029

Halpern, B. S., Longo, C., Hardy, D., Mcleod, K. L., Samhouri, J. F., Katona, S. K., et al. (2012). An index to assess the health and benefits of the global ocean. *Nature* 488, 615–620.

Henras, A. K., Soudet, J., Gerus, M., Lebaron, S., Caizergues-Ferrer, M., Mougin, A., et al. (2008). The post-transcriptional steps of eukaryotic ribosome biogenesis. *Cell Mol. Life Sci.* 65, 2334–2359. doi: 10.1007/s00018-008-8027-0

Hockin, N. L., Mock, T., Mulholland, F., Kopriva, S., and Malin, G. (2012). The response of diatom central carbon metabolism to nitrogen starvation is different from that of green algae and higher plants. *Plant Physiol.* 158, 299–312. doi: 10.1104/pp.111.184333

Huysman, M. J., Martens, C., Vandepoele, K., Gillard, J., Rayko, E., Heijde, M., et al. (2010). Genome-wide analysis of the diatom cell cycle unveils a novel type of cyclins involved in environmental signaling. *Gen. Biol.* 11:R17.

Huysman, M. J., Vyverman, W., and De Veylder, L. (2014). Molecular regulation of the diatom cell cycle. *J. Exp. Bot.* 65, 2573–2584. doi: 10.1093/jxb/ert387

Jian, J., Zeng, D., Wei, W., Lin, H., Li, P., and Liu, W. (2017). The combination of RNA and protein profiling reveals the response to nitrogen depletion in *Thalassiosira pseudonana*. *Sci. Rep.* 7:8989.

Kaeriyama, H., Katsuki, E., Otsubo, M., Yamada, M., Ichimi, K., Tada, K., et al. (2011). Effects of temperature and irradiance on growth of strains belonging to seven *Skeletonema* species isolated from Dokai Bay, southern Japan. *E. J. Phy.* 46, 113–124. doi: 10.1080/09670262.2011.565128

Kanehisa, M., and Goto, S. (2000). KEGG: kyoto encyclopedia of genes and genomes. *Nucleic Acids Res.* 28, 27–30.

Kanehisa, M., Sato, Y., Kawashima, M., Furumichi, M., and Tanabe, M. (2016). KEGG as a reference resource for gene and protein annotation. *Nucleic Acids Res.* 44, D457–D462.

Katayama, T., Murata, A., and Taguchi, S. (2012). Responses of pigment composition of the marine diatom *Thalassiosira weissflogii* to silicate availability during dark survival and recovery. *Plan. Ben. Res.* 7, 158–158. doi: 10.3800/pbr.7.158

Kettles, N. L., Kopriva, S., and Malin, G. (2014). Insights into the regulation of DMSP synthesis in the diatom *Thalassiosira pseudonana* through APR activity, proteomics and gene expression analyses on cells acclimating to changes in salinity, light and nitrogen. *PLoS One* 9:e94795. doi: 10.1371/journal.pone.094795

Kobayashi, K., Kobiyama, A., Kotaki, Y., and Kodama, M. (2003). Possible occurrence of intracellular bacteria in *Pseudonitzschia multiseries*, a causative diatom of amnesic shellfish poisoning. *Fish. Sci.* 69, 974–978. doi: 10.1046/j.1444-2906.2003.00715.x

Kroth, P. G., Chiovitti, A., Gruber, A., Martin-Jezequel, V., Mock, T., Parker, M. S., et al. (2008). A model for carbohydrate metabolism in the diatom *Phaeodactylum tricornutum* deduced from comparative whole genome analysis. *PloS One*, 3:e1426. doi: 10.1371/journal.pone.0001426

Kruger, N. J. (2009). "The Bradford method for protein quantitation," in *The Protein Protocols Handbook*, ed. J. M. Walker (Totowa, NJ: Humana Press), 17–24. doi: 10.1007/978-1-59745-198-7_4

Lewandowska, A. M., Hillebrand, H., Lengfellner, K., and Sommer, U. (2014). Temperature effects on phytoplankton diversity — The zooplankton link. *J. Sea Res.* 85, 359–364. doi: 10.1016/j.seares.2013.07.003

Lin, Q., Liang, J.-R., Huang, Q.-Q., Luo, C.-S., Anderson, D. M., Bowler, C., et al. (2017). Differential cellular responses associated with oxidative stress and cell fate decision under nitrate and phosphate limitations in *Thalassiosira pseudonana:* comparative proteomics. *PLoS One* 12:e0184849. doi: 10.1371/journal.pone.0184849

Lindh, M. V., Riemann, L., Baltar, F., Romero-Oliva, C., Salomon, P. S., Graneli, E., et al. (2013). Consequences of increased temperature and acidification on bacterioplankton community composition during a mesocosm spring bloom in the Baltic Sea. *Environ. Microbiol. Rep.* 5, 252–262. doi: 10.1111/1758-2229.12009

Longworth, J., Wu, D., Huete-Ortega, M., Wright, P. C., and Vaidyanathan, S. (2016). Proteome response of *Phaeodactylum tricornutum*, during lipid accumulation induced by nitrogen depletion. *Algal. Res.* 18, 213–224. doi: 10.1016/j.algal.2016.06.015

Lyon, B. R., Lee, P. A., Bennett, J. M., Ditullio, G. R., and Janech, M. G. (2011). Proteomic analysis of a sea-ice diatom: salinity acclimation provides new insight into the dimethylsulfoniopropionate production pathway. *Plant Physiol.* 157, 1926–1941. doi: 10.1104/pp.111.185025

Mann, K. (1993). Physical oceanography, food chains, and fish stocks: a review. *ICES J. Mar. Sci.* 50, 105–119. doi: 10.1006/jmsc.1993.1013

Moustafa, A., Beszteri, B., Maier, U. G., Bowler, C., Valentin, K., and Bhattacharya, D. (2009). Genomic footprints of a cryptic plastid endosymbiosis in diatoms. *Science* 324, 1724–1726. doi: 10.1126/science.1172983

Nunn, B. L., Faux, J. F., Hippmann, A. A., Maldonado, M. T., Harvey, H. R., Goodlett, D. R., et al. (2013). Diatom proteomics reveals unique acclimation strategies to mitigate Fe limitation. *PLoS One* 8:e75653. doi: 10.1371/journal.pone.075653

Olson, R., and Chisholm, S. (1983). Effects of photocycles and periodic ammonium supply on three marine phytoplankton species. I. Cell division patterns [*Thalassiosira weissflogii, Hymenomonas carteri, Amphidinium carteri*, Algae]. *J. Phy.* 19, 522–528. doi: 10.1111/j.0022-3646.1983.00522.x

Otzen, D. (2012). The role of proteins in biosilicification. *Scientifica* 2012:867562.

Peter, K. H., and Sommer, U. (2013). Phytoplankton cell size reduction in response to warming mediated by nutrient limitation. *PLoS One* 8:e71528. doi: 10.1371/journal.pone.0071528

Philippart, C. J. M., Anadón, R., Danovaro, R., Dippner, J. W., Drinkwater, K. F., Hawkins, S. J., et al. (2011). Impacts of climate change on European marine ecosystems: observations, expectations and indicators. *J. Exp. Mar. Biol. Ecol.* 400, 52–69. doi: 10.1016/j.jembe.2011.02.023

Pietrocola, F., Galluzzi, L., Bravo-San Pedro, J. M., Madeo, F., and Kroemer, G. (2015). Acetyl coenzyme a: a central metabolite and second messenger. *Cell Metab.* 21, 805–821. doi: 10.1016/j.cmet.2015.05.014

Pörtner, H., Karl, D., Boyd, P., Cheung, W., Lluch-Cota, S., and Nojiri, Y. (2014). "Ocean systems," in *Climate Change 2014: Impacts, Adaptation, and Vulnerability Part A: Global and Sectoral Aspects Contribution of Working Group II to the Fifth Assessment Report of the Intergovernmental Panel on Climate Change*, eds C. B. Field, V. R. Barros, D. J. Dokken, K. J. Mach, M. D. Mastrandrea, T. E. Bilir, et al. (New York, NY: Cambridge University Press).

Poulson-Ellestad, K. L., Jones, C. M., Roy, J., Viant, M. R., Fernandez, F. M., Kubanek, J., et al. (2014). Metabolomics and proteomics reveal impacts of chemically mediated competition on marine plankton. *Proc. Natl. Acad. Sci. U.S.A.* 111, 9009–9014. doi: 10.1073/pnas.1402130111

Qing, D., Yang, Z., Li, M., Wong, W. S., Guo, G., Liu, S., et al. (2016). Quantitative and functional phosphoproteomic analysis reveals that ethylene regulates water transport via the C-terminal phosphorylation of aquaporin PIP2;1 in *Arabidopsis*. *Mol. Plant* 9, 158–174. doi: 10.1016/j.molp.2015.10.001

Reinfelder, J. R., Kraepiel, A. M., and Morel, F. M. (2000). Unicellular C 4 photosynthesis in a marine diatom. *Nature* 407:996. doi: 10.1038/35039612

Riley, M. (1993). Functions of the gene products of *Escherichia coli*. *Microbiol. Mol. Biol. Rev.* 57, 862–952. doi: 10.1128/mmbr.57.4.862-952.1993

Ruban, A. V., and Johnson, M. P. (2009). Dynamics of higher plant photosystem cross-section associated with state transitions. *Photosynth. Res.* 99, 173–183. doi: 10.1007/s11120-008-9387-x

Sarno, D., Kooistra, W. H. C. F., Medlin, L. K., Percopo, I., and Zingone, A. (2005). Diversity in the genus *Skeletonema*(*Bacillariophyceae*). Ii. an assessment of the taxonomy ofs. costatum-like species with the description of four new species. *J. Phys.* 41, 151–176. doi: 10.1111/j.1529-8817.2005.04067.x

Shrestha, R. P., Tesson, B., Norden-Krichmar, T., Federowicz, S., Hildebrand, M., and Allen, A. E. (2012). Whole transcriptome analysis of the silicon response of the diatom *Thalassiosira pseudonana*. *BMC Genom.* 13:499. doi: 10.1186/1471-2164-13-499

Smith, S., Bernatchez, L., and Beheregaray, L. B. (2013). RNA-seq analysis reveals extensive transcriptional plasticity to temperature stress in a freshwater fish species. *BMC Genom.* 14:375. doi: 10.1186/1471-2164-14-375

Stumpp, M., Hu, M. Y., Melzner, F., Gutowska, M. A., Dorey, N., Himmerkus, N., et al. (2012). Acidified seawater impacts sea urchin larvae pH regulatory systems relevant for calcification. *Proc. Natl. Acad. Sci. U.S.A.* 109, 18192–18197. doi: 10.1073/pnas.1209174109

Thangaraj, S., Giordano, M., and Sun, J. (2020). Comparative proteomic analysis reveals new insights into the common and specific metabolic regulation of the diatom *Skeletonema dohrnii* to the silicate and temperature availability. *Fron. Plant Sci.* 11:578915. doi: 10.3389/fpls.2020.578915

Thangaraj, S., Shang, X., Sun, J., and Liu, H. (2019). Quantitative proteomic analysis reveals novel insights into intracellular silicate stress-responsive mechanisms in the diatom *Skeletonema dohrnii*. *Int. J. Mol. Sci.* 20:2540. doi: 10.3390/ijms20102540

Thangaraj, S., and Sun, J. (2020). The biotechnological potential of the marine diatom *Skeletonema dohrnii* to the elevated temperature and pCO2. *Mar. Drugs* 18:259. doi: 10.3390/md18050259

Thomson, E., Ferreira-Cerca, S., and Hurt, E. (2013). Eukaryotic ribosome biogenesis at a glance. *J. Cell Sci.* 126, 4815–4821. doi: 10.1242/jcs.111948

Tomanek, L. (2011). Environmental proteomics: changes in the proteome of marine organisms in response to environmental stress, pollutants, infection, symbiosis, and development. *Ann. Rev. Mar. Sci.* 3, 373–399. doi: 10.1146/annurev-marine-120709-142729

Trost, P., Fermani, S., Marri, L., Zaffagnini, M., Falini, G., Scagliarini, S., et al. (2006). Thioredoxin-dependent regulation of photosynthetic glyceraldehyde-3-phosphate dehydrogenase: autonomous vs. *CP*12-dependent mechanisms. *Photosynth. Res.* 89, 263–275. doi: 10.1007/s11120-006-9099-z

Unwin, R. D. (2010). Quantification of proteins by iTRAQ. *Methods Mol. Biol.* 658, 205–215. doi: 10.1007/978-1-60761-780-8_12

Van Domselaar, G. H., Stothard, P., Shrivastava, S., Cruz, J. A., Guo, A., Dong, X., et al. (2005). BASys: a web server for automated bacterial genome annotation. *Nucleic Acids Res.* 33, W455–W459.

Van Mooy, B. A., Fredricks, H. F., Pedler, B. E., Dyhrman, S. T., Karl, D. M., Koblizek, M., et al. (2009). Phytoplankton in the ocean use non-phosphorus lipids in response to phosphorus scarcity. *Nature* 458, 69–72. doi: 10.1038/nature07659

Weber, J. (2006). ATP synthase: subunit-subunit interactions in the stator stalk. *Biochim. Biophys. Acta* 1757, 1162–1170. doi: 10.1016/j.bbabio.2006.04.007

Weinert, B. T., Iesmantavicius, V., Moustafa, T., Scholz, C., Wagner, S. A., Magnes, C., et al. (2014). Acetylation dynamics and stoichiometry in *Saccharomyces cerevisiae*. *Mol. Syst. Biol.* 10:716.

Zapata, M., Rodríguez, F., and Garrido, J. L. (2000). Separation of chlorophylls and carotenoids from marine phytoplankton: a new HPLC method using a reversed phase C8 column and pyridine-containing mobile phases. *Mar. Ecol. Proc. Ser.* 195, 29–45. doi: 10.3354/meps195029

Zhang, H., Wang, D. Z., Xie, Z. X., Zhang, S. F., Wang, M. H., and Lin, L. (2015). Comparative proteomics reveals highly and differentially expressed proteins in field-collected and laboratory-cultured blooming cells of the diatom *Skeletonema costatum*. *Environ. Microbiol.* 17, 3976–3991. doi: 10.1111/1462-2920.12914

Conflict of Interest: The authors declare that the research was conducted in the absence of any commercial or financial relationships that could be construed as a potential conflict of interest.

frontiers in Microbiology

ORIGINAL RESEARCH
published: 21 January 2021
doi: 10.3389/fmicb.2021.623600

Different Biochemical Compositions of Particulate Organic Matter Driven by Major Phytoplankton Communities in the Northwestern Ross Sea

*Naeun Jo[1], Hyoung Sul La[2], Jeong-Hoon Kim[3], Kwanwoo Kim[1], Bo Kyung Kim[2], Myung Joon Kim[1], Wuju Son[2,4] and Sang Heon Lee[1]**

[1] Department of Oceanography, Pusan National University, Busan, South Korea, [2] Division of Ocean Sciences, Korea Polar Research Institute, Incheon, South Korea, [3] Division of Life Sciences, Korea Polar Research Institute, Incheon, South Korea, [4] Department of Polar Science, University of Science and Technology, Daejeon, South Korea

OPEN ACCESS

Edited by:
Eva Ortega-Retuerta, UMR 7621 Laboratoire d'océanographie microbienne (LOMIC), France

Reviewed by:
Frédéric André Corentin Le Moigne, UMR 7294 Institut Méditerranéen d'océanographie (MIO), France
Tiantian Tang, Xiamen University, China

***Correspondence:**
Sang Heon Lee
sanglee@pusan.ac.kr

Specialty section:
This article was submitted to Aquatic Microbiology, a section of the journal Frontiers in Microbiology

Received: *30 October 2020*
Accepted: *04 January 2021*
Published: *21 January 2021*

Citation:
Jo N, La HS, Kim J-H, Kim K, Kim BK, Kim MJ, Son W and Lee SH (2021) Different Biochemical Compositions of Particulate Organic Matter Driven by Major Phytoplankton Communities in the Northwestern Ross Sea. Front. Microbiol. 12:623600. doi: 10.3389/fmicb.2021.623600

Marine particulate organic matter (POM) largely derived from phytoplankton is a primary food source for upper trophic consumers. Their biochemical compositions are important for heterotrophs. Especially, essential amino acids (EAAs) in phytoplankton are well known to have impacts on the survival and egg productions of herbivorous zooplankton. To estimate the nutritional quality of POM, the biochemical compositions [biomolecular and amino acid (AA) compositions] of POM were investigated in the northwestern Ross Sea during the late austral summer in 2018. Carbohydrates (CHO) accounted for the highest portion among different biomolecules [CHO, proteins (PRT), and lipids (LIP)] of POM. However, the higher contribution of PRT and lower contribution of CHO were observed in the southern section of our study area compared to those in the northern section. The spatial distribution of total hydrolyzable AAs in POM was considerably influenced by phytoplankton biomass, which indicates that the main source of particulate AA was generated by phytoplankton. Our results showed that the relative contribution of EAA to the total AAs was strongly associated with EAA index (EAAI) for determining protein quality. This result indicates that higher EAA contribution in POM suggests a better protein quality in consistency with high EAAI values. In this study, variations in the biochemical compositions in POM were principally determined by two different bloom-forming taxa (diatoms and *Phaeocystis antarctica*). The southern region dominated majorly by diatoms was positively correlated with PRT, EAA, and EAAI indicating a good protein quality, while *P. antarctica*-abundant northern region with higher CHO contribution was negatively correlated with good protein quality factors. Climate-driven environmental changes could alter not only the phytoplankton community but also the physiological conditions of phytoplankton. Our findings could provide a better understanding for future climate-induced changes in the biochemical compositions of phytoplankton and consequently their potential impacts on higher trophic levels.

Keywords: phytoplankton, biomolecular composition, amino acid composition, food quality, Ross Sea

INTRODUCTION

Marine particulate organic matter (POM) is derived from a variety of living and non-living sources, including detritus matter, bacterial cells, and phytoplankton (Volkman and Tanoue, 2002). Although the relative importance of these diverse sources cannot be clarified, phytoplankton is definitely the most important part of marine POM in surface waters (Riley, 1971; Kharbush et al., 2020). POM largely derived from phytoplankton plays a significant role in linking the primary producers to herbivores as a crucial food source (Dzierzbicka-Głowacka et al., 2010; Lowe et al., 2014; Andersson et al., 2017) and potential carbon export to the deep ocean (Ducklow et al., 2001; Basu and Mackey, 2018). Biochemical properties of POM, especially biomolecular and amino acid (AA) compositions, are useful indicators of nutritional quality for higher trophic consumers (Dell'Anno et al., 2000; Lee et al., 2004; Bhavya et al., 2019). The various biomolecular components, including carbohydrates (CHO), proteins (PRT), and lipids (LIP), are generated through photosynthetic assimilation of dissolved inorganic carbon into organic compounds within phytoplankton (Fernández-Reiriz et al., 1989; Fichez, 1991). The relative contribution of the biomolecular compounds produced by phytoplankton is tightly linked to the prevailing environmental conditions (e.g., availability of nutrients and light), major phytoplankton groups, and the growth phase of phytoplankton (Ahn et al., 2019; Bhavya et al., 2019 and the references therein). Thus, the biomolecular composition of phytoplankton has also been considered a suitable indicator of the physiological responses of phytoplankton to the limitation of macro and micronutrients (i.e., bioavailable N, P, Si, and Fe) (Morris et al., 1974; Sterner and Elser, 2002; Saito et al., 2008; Moore et al., 2013) and light stress (Morris et al., 1974; Smith and Morris, 1980; Sunda and Huntaman, 1997; Klausmeier et al., 2008) which is consequently connected with their nutritional quality for higher trophic consumers (Bhavya et al., 2019).

On the one hand, it is well known that AAs are the building blocks of different biomolecules which are mainly peptides and PRT (Kolmakova and Kolmakov, 2019; Shields et al., 2019). Previous studies have shown that compositional changes in AAs are related to the degradation state of POM, phytoplankton community structure, and growth phase of phytoplankton (Hecky et al., 1973; Kolmakova and Kolmakov, 2019; Shields et al., 2019). Therefore, these compositional changes of AAs have widely been used to indicate the organic matter degradation (Cowie and Hedges, 1992; Mente et al., 2002; Becker and Richmond, 2004) and protein quality (Oser, 1959; Mente et al., 2002; Becker and Richmond, 2004). The degradation index (DI) based on the changes in the relative abundance of each AA to total AAs during organic matter diagenesis can be applied to estimate the degradation degree of POM in sediment as well as sinking particles (Dauwe and Middelburg, 1998; Dauwe et al., 1999; Le Moigne et al., 2017). Among different AAs, essential AAs (EAAs) cannot be synthesized *de novo* by most heterotrophic organisms and must therefore be fulfilled by prey to meet consumer's nutritional needs for their growth and reproduction (Muller-Navarra, 1995; Kleppel et al., 1998; Kolmakova and Kolmakov, 2019). However, nutritional quality for higher trophic levels comprises not only the quantity of EAA but also balance in individual EAAs (Müller-Navarra, 2008). Hence, the EAA index (EAAI) allows us to evaluate the protein quality in terms of the AA composition of POM as consumers' diets.

The Ross Sea is one of the most productive regions in the Southern Ocean and thus supporting considerable standing stocks of apex predators such as penguins, seals, and whales (Nelson et al., 1996; Pinkerton et al., 2010). In 2016, this region was established as a massive Marine Protected Area (MPA) safeguarding 1.55 million km^2 of ocean bordering Antarctica from ice edge to deep ocean by the Commission for the Conservation of Antarctic Marine Living Resources (CCAMLR). Of that, cape Hallett located at the northern Victoria Land is one of the specially protected areas and large populations of breeding penguins relevant to large aggregations of krill as their primary food source (Lyver et al., 2011). The marine top predators (e.g., penguins, seals, and whales) depend directly or indirectly on organic matter by photosynthetic microalgae since the quantity and quality of POM produced by phytoplankton have consequences for the entire marine ecosystem of the Ross Sea through bottom-up processes (Oksanen and Oksanen, 2000; Gruner et al., 2008). Indeed, the Ross Sea food webs are supported at their foundation by phytoplankton comprising of two key algal groups: diatoms and haptophytes, particularly *Phaeocystis antatarctica* (DiTullio and Smith, 1996; Alderkamp et al., 2012; Smith et al., 2014; Mangoni et al., 2017). The relative abundance of major two phytoplankton communities varies with spatial and temporal patterns in the Ross Sea and subsequently can have significant influences on the spatial and temporal diet variability of higher trophic levels (trophodynamics) (Young et al., 2015b; Mangoni et al., 2019). According to current climate trends, the Ross Sea is expected to experience extreme warming, decreased sea ice concentrations, and shallower mixed layers throughout the next century (Bracegirdle et al., 2008; Ainley et al., 2010; Bracegirdle and Stephenson, 2012). The changes in the predominant phytoplankton community and physiological status of phytoplankton caused by this predicted climate change (e.g., increase in sea surface temperatures, decreases in the mixed layer depths, sea ice concentrations, and macronutrient concentrations; Rickard and Behrens, 2016) can have profound implications on diet variability of higher trophic levels (Smith et al., 2003; Smetacek et al., 2004; Tang et al., 2008). Therefore, the aims of the paper were to (1) investigate biochemical compositions (biomolecular and AA compositions) of POM derived mainly phytoplankton and main factors in controlling the relative dominance of these biochemical compositions and (2) evaluate physiological conditions of phytoplankton and potential food quality as prey for consumers.

MATERIALS AND METHODS

Study Sites and Sampling

The field survey was performed closely to Cape Adare and Cape Hallett during the Ross Sea Marine Projected Area Expedition

(ANA08C; from 25 February to 1 March 2018) in Antarctica on the IBR/V Araon (**Figure 1**). The vertical temperature and salinity profiles were collected using a conductivity-temperature-depth (CTD) recorder (SeaBird Electronics Inc., SBE 911 plus). At all sampling stations, discrete water samples for biological and chemical analyses were obtained from three different light levels (100, 30, and 1% light penetration depths which were estimated from the Secchi depth) employing CTD/rosette sampler attached to 24-10 L Niskin bottles. The depth of the euphotic zone (Z_{eu}) was defined as the depth at which 99% of the surface irradiance is attenuated (Kirk, 1985) and estimated using a Secchi disk. The mixed layer depth (Z_m) was defined as the depth where a change of 0.01 kg m^{-3} in potential density (σ_t) from the stable surface layer value (Smith et al., 2000; Asper and Smith, 2019).

Particulate Organic Carbon (POC), Nitrogen (PON), and Stable Carbon Isotopes ($\delta^{13}C$) Analyses of POM

For the analyses of POC, PON, and $\delta^{13}C$, 0.3 L of sampled sample was filtered through Whatman GF/F filter (25 mm, 0.7 μm pore) and immediately stored at −80°C. The filtered samples were acidified over fuming HCl to eliminate inorganic carbon before further analysis. Then, the filters were analyzed for carbon and nitrogen contents and isotope ratios using a Finnigan Delta + XL mass spectrometer at the stable isotope laboratory of the University of Alaska Fairbanks, United States.

Major Inorganic Nutrients, Chlorophyll a, and Other Phytoplankton Pigments Analyses

Samples for the determination of dissolved inorganic nutrients (phosphate, nitrate + nitrite, ammonium, and silicate) were collected directly from the Niskin rosette into 50 mL conical tubes and immediately stored at 4°C until analysis within 24 h. Nutrient concentrations were measured on board with a QuAAtro Continuous Segmented Flow Analyzer (Seal Analytical, Norderstedt, Germany) using standard colorimetric methods according to the "QuAAtro Applications."

Water samples (0.3 L) were filtered through 25 mm GF/F filter papers (Whatman, 0.7 μm pore) to measure the total chlorophyll a (chl-*a*) concentration. Sequential filtrations were performed to determine each size-fractionated chl-*a* concentration (>20, 5–20, and <5 μm). First, 0.5 L of seawater was filtered through the Polycarbonate Track Etched (PCTE) membrane 20 μm filter (GVS, 47 mm). Then, the filtrate was passed through the PCTE membrane 5 μm filter (Whatman, 47 mm) and 47 mm GF/F filters (Whatman, 0.7 μm pore) in sequence. The chl-*a* pigment was extracted by submerging filtered samples in 90% acetone for 24 h in dark and cold conditions (Parsons et al., 1984). The chl-*a* fluorescence was measured onboard using the pre-calibrated Trilogy fluorometer (Turner Designs, United States).

Phytoplankton pigment analysis using a high-performance liquid chromatography (HPLC) system can be used to quantify concentrations of each pigment that were determined by measuring the integrated peak area based on the method of Zapata et al. (2000). The pigments on the filtered samples (1 or 2 L of seawater) were extracted in 5 mL of 100% acetone with canthaxanthin (internal standard) for 24 h in dark at 4°C. The extract was filtered through a 0.2 μm Advantec syringe filter. HPLC measurements were performed on an Agilent 1200 HPLC system (Agilent infinite 1260, Agilent, United States) and the separating column was used Zobrax Eclipse XDB C8 column (250 × 4.6 mm, 5 μm, Agilent Technologies). The same analysis procedures of Kang et al. (2018) were performed for quantifying of pigment concentrations. As suggested by Mackey et al. (1996), the contribution of various phytoplankton classes could be estimated by the ratio of each diagnostic pigment to total chl-*a* using the CHEMTAX program. The initial pigment ratio to chl-*a* for each mark pigment used in the CHEMTAX

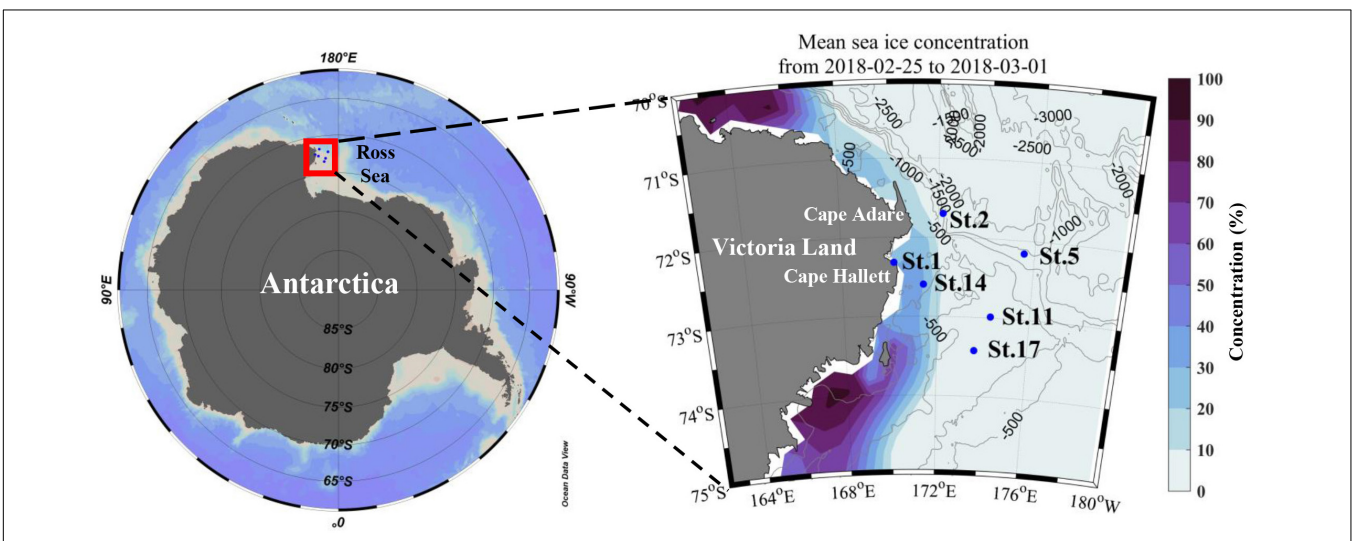

FIGURE 1 | Map of the study area and sampling stations (with depth contours in meters). Mean sea ice concentration (%) data during the sampling period from Nimbus-7 SMMR and DMSP SSM/I-SSMIS Passive Microwave data provided by National Snow and Ice Data Center.

program was modified by Mackey et al. (1996); Wright et al. (1996), and DiTullio et al. (2011).

Biomolecular Composition of Phytoplankton

Water samples were obtained from three light depths (100, 30, and 1%) for biomolecular compositions (CHO, PRT, and LIP) of phytoplankton and filtered through a 47 mm GF/F filter. The filters were stored at −80°C for spectrometric analysis using a UV–visible spectrometer (Hitachi UH-5300, Japan) to measure each biomolecular concentration. CHO concentration was determined using the phenol-sulfuric method according to Dubois et al. (1956). After 1 mL of deionized water was added to the polypropylene tube containing the filtered sample, samples were ultrasonicated for 20 min for CHO extraction. 1 mL of 5% phenol reagent was additionally added, and the extracted samples were kept at room temperature for 40 min. The CHO after reaction with concentrated sulfuric acid were quantified by measuring the absorbance at 490 mm and then calculated from the calibration glucose standard (1 mg mL^{-1}, SIGMA) curve. To measure PRT concentration based on Lowry et al. (1951), 1 mL of deionized water and 5 mL of alkaline copper solution (a mixture of 2% Na_2CO_3 in 0.1 N NaOH with 0.5% $CuSO_4 \cdot 5H_2O$ in 1% sodium or potassium tartrate; 50:1, v:v) were added into vials with the filtered samples for PRT extraction. After 20 min of ultrasonication, 0.5 mL of diluted Folin-Ciocalteu phenol reagent (1:1, v:v) was added into sample vials for the colorimetric reaction. The absolute concentration of PRT was calculated from the absorbance at 750 nm comparing with a protein standard solution (2 mg mL^{-1}, SIGMA). The total LIP was extracted by chloroform and methanol (1:2, v:v) according to the modified method of Bligh and Dyer (1959) and Marsh and Weinstein (1966). The absorbance at 360 nm was expressed as tripalmitin equivalents. More detailed methods are explained in Bhavya et al. (2019).

Amino Acid Composition Analysis

Samples for the analysis of total particulate hydrolyzable AAs (PAAs) were collected from three light depths (100, 30, and 1%) at six stations. Water samples (1 L) from each station were passed through 47 mm GF/F filters (Whatman, 0.7 μm pore) and then frozen at −80°C for later analysis. Acid hydrolysis was performed using the modified methods of Lobbes et al. (1999) and Bartolomeo and Maisano (2006). A filtered paper is transferred into the 5 mL reaction vial containing 2 mL HCl (6 M) and 10 μL ascorbic acid (11 mM). The vials were capped tightly after flushing with N_2 gas and then moved into a pre-heated heating block at 110°C for 24 h. After acidic hydrolysis, hydrolysates were cooled at room temperature and filtered through 0.2 μm PTFE syringe filters (Advantec, Tokyo, Japan). Each remaining liquid was evaporated to dryness using a nitrogen evaporator at 60°C. The dried residues were reconstituted with 200 μL of 0.1 N HCl and transferred into glass vials for analysis. Samples were analyzed using HPLC (Agilent 1260 Infinity, Germany) equipped with an autosampler, a Zorbax-Eclipse AAA column (4.6 × 250 mm, 5 μm), and UV/VIS detector (338 and 262 nm). In the pre-column method, the samples and AA standard solutions were automatically derivatized with ortho-phthalaldehyde (OPA) and 9-fluorenylmethyl chloroformate (FMOC) by programming autosampler according to Agilent Application note (Henderson et al., 2000). The column temperature was maintained at 40°C with a flow rate of 1.5 mL/min. The mobile phase A contained 40 mM sodium phosphate (di-basic) with 0.1% phosphoric acid and mobile phase B was acetonitrile/methanol/deionized water (45:45:10, v:v:v). AA standard mixture with 21 L-AAs and L-norvaline (surrogate standard) was prepared for AA identification and quantification. AA standard solutions contained 22 L-AAs: Aspartic acid (ASP), Glutamic acid (GLU), Asparagine (ASN), Serine (SER), Glutamine (GLN), Histidine (HIS), Glycine (GLY), Threonine (THR), Arginine (ARG), Alanine (ALA), Tyrosine (TYR), Cystine (CY2), Valine (VAL), Methionine (MET), Tryptophan (TRP), Phenylalanine (PHE), Isoleucine (ILE), Leucine (LEU), Lysine (LYS), Hydroxyproline (HYP), Proline (PRO) and Norvaline (NVA). Hydroxyproline (HYP), and proline (PRO) could not be quantified because of their low responses and high detection limits in our HPLC. A representative chromatogram for the mixed standard is shown in **Supplementary Figure S1**. Each linear relationship for the four-point calibration curve of individual AAs was obtained with a correlation coefficient being above 0.999. The relative standard deviations of peak areas for each AA in each point ranged from 1.6 to 9.5% ($n = 3$) for measurement precisions. Before injecting, 20 μL of norvaline as a surrogate standard has added a sample of each vial and each sample was injected twice for HPLC analysis. Peak areas of AA measured that the average value of three blanks was subtracted from each sample analyzed. Then, individual AA concentrations in injected samples were calculated using the slope of the calibration curve of each AA and the known concentration of Norvaline. Glutamine (GLN) and asparagine (ASN) were quantified as glutamic acid (GLU) and aspartic acid (ASP) because glutamine (GLN) and asparagine (ASN) react into glutamic acid (GLU) and aspartic acid (ASP) during hydrolysis, respectively. Moreover, tryptophan (TRP) and cystine (CY2) are omitted from our AA results since they are fully or partially destroyed during acid hydrolysis. Therefore, the concentration of each remaining AA was expressed as a mole percentage (mol%) of the total AA.

Amino Acid Index Calculations

The quantitative DI for POM was calculated using mol% AA composition and the factor coefficient of Dauwe et al. (1999). According to Dauwe et al. (1999), this index could reflect the reactivity of POM as degradation proceeds. DI was estimated using this equation derived by Dauwe et al. (1999).

$$DI = \sum_i \left[\frac{var_i - AVGvar_i}{STDvar_i}\right] \times fac \cdot coef_i$$

In this equation, var_i is the mol% of the individual AA, $AVGvar_i$ and $STDvar_i$ are the mean and standard deviation of the AA mol% in a given dataset, and $fac{\cdot}coef_i$ is the factor coefficient in Dauwe et al. (1999).

Individual AA of each sample is divided into EAA and non-EAA (NEAA): nine essential (histidine, threonine, arginine, valine, methionine, phenylalanine, isoleucine, leucine, and lysine) and six non-essential (aspartic acid, glutamic acid, serine, glycine, alanine, and proline). The EAAI is a common index for estimating the quality of phytoplankton as a diet for higher trophic levels such as zooplankton (Oser, 1959; Mente et al., 2002; Becker and Richmond, 2004). The EAAI is defined as a ratio of EAA in prey to corresponding EAA in reference egg protein (Oser, 1959). However, the mean fraction of EAA in the zooplankton community in this study (unpublished data) was used as the reference AA since efficient food has a similar AA profile to that of the consumer (Guisande et al., 2002). The modified EAAI of POM was determined from this formula:

$$EAAI = \sqrt[n]{\frac{aa_1}{AA_1} \times \frac{aa_2}{AA_2} \times \frac{aa_3}{AA_3} \times \frac{aa_4}{AA_4} \times \cdots \times \frac{aa_n}{AA_n}}$$

where aa_1, . . ., aa_n are the ratio of each EAA to total EAA in POM and AA_1, . . ., AA_n are the average ratio of each EAA to total EAA in zooplankton communities in this study (unpublished data). To calculate EAAI, the values of aa_1/AA_1, . . ., aa_n/AA_n were constrained between 0.01 minimally and 1 maximally (Hayashi et al., 1986).

Statistical Analysis

Significant differences of biochemical properties (concentrations of biomolecules and biomolecular composition) between northern and southern stations were tested using the Student's *t*-test. The results of statistical analyses were assumed to be significant at *p*-values < 0.05. All correlation analyses were performed in this study using Pearson's correlation coefficients. Statistical analyses were performed using Statistical Package for the Social Sciences (SPSS ver.12.0). For the multivariate analysis of the analyzed and investigated parameters, we carried out the principal component analysis (PCA) with the rotation method of Varimax with Kaiser normalization using the XLSTAT software (Addinsoft, Boston, MA, United States). Further, to calculate the dissimilarity between samples, agglomerative hierarchical clustering (AHC) analysis with Euclidean distance dissimilarity and Ward's method was conducted using the XLSTAT software (Addinsoft, Boston, MA, United States).

RESULTS

Hydrographical and Chemical Properties

The vertical profiles of potential temperature and salinity within the upper 100 m ranged from −1.82 to −0.52°C and from 33.96 to 34.58, respectively (**Figure 2**). The lowest potential temperature and salinity were measured at station (St.) 1, whereas other stations never reached freezing temperature and had relatively higher salinities. The higher salinity values over 34.40 with depth showed at Sts. 14 and 17 which also had higher temperature values. The Z_{eu} and Z_m were 30–43 and 20–117 m, respectively (**Table 1**). The Z_{eu} at most stations was shallower than Z_m except for Sts. 1 and 11.

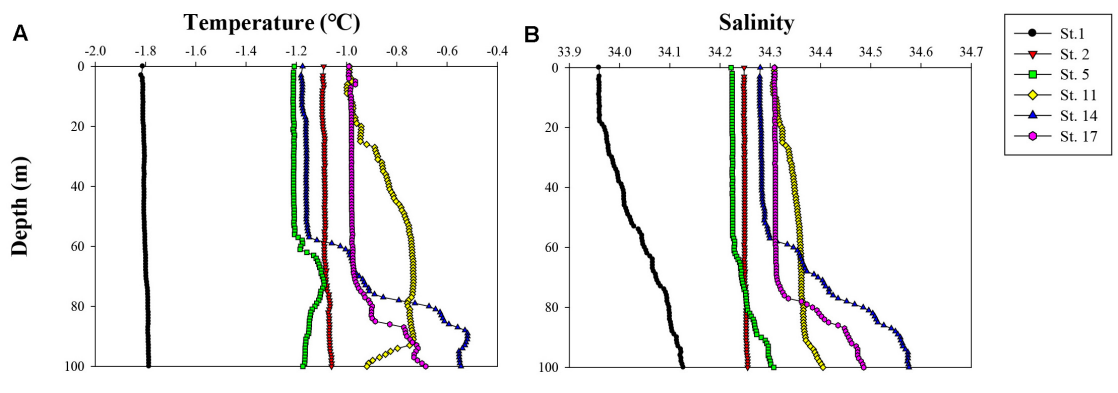

FIGURE 2 | Vertical profiles of **(A)** temperature (°C) and **(B)** salinity in the upper 100 m of the water column during this cruise ANA08C.

TABLE 1 | Description of sampling stations and associated environmental variables during ANA08C cruise.

Station	Latitude (°N)	Logitude (°E)	Date (mm/dd/yy)	T_{eu}	S_{eu}	Bottom depth (m)	Z_{eu} (m)	Z_m (m)
1	−72.318	170.177	25/02/18	−1.8	34.0	165	43	21
2	−71.698	172.186	26/02/18	−1.1	34.2	1043	35	117
5	−72.163	175.566	27/02/18	−1.2	34.2	1342	38	65
11	−72.987	174.315	28/02/18	−1.0	34.3	345	30	20
14	−72.596	171.413	28/02/18	−1.2	34.3	387	41	53
17	−73.421	173.662	01/03/18	−1.0	34.3	287	30	75

T_{eu} and S_{eu}: water temperature and salinity averaged from surface to the euphotic zone depth (Z_{eu}).
Z_m: mixed layer depth.

Figure 3 shows vertical distributions of dissolved inorganic nutrients (phosphate, nitrate + nitrite, ammonium, and silicate) from the surface to 100 m depth. The concentrations of dissolved inorganic nutrients except for ammonium mostly increased with depth from the surface to 100 m. At Sts. 14 and 17, the concentrations of phosphate, nitrate + nitrite, and silicate increased sharply below the euphotic layers compared with those at other stations. In the upper 100 m, the concentrations of phosphate, nitrate + nitrite, and silicate were 1.89–2.38, 19.11–22.66, and 60.74–81.53 μM, respectively. Dissolved inorganic ammonium had low concentrations, ranging from 0 to 1.49 μM, and did not show a clear spatial pattern.

Particulate Organic Carbon (POC), Nitrogen (PON), and Stable Carbon Isotopes ($\delta^{13}C$) of POM

The averaged concentrations of POC, PON, and C/N ratio within the euphotic zone and $\delta^{13}C$ values of surface POM are summarized in **Table 2**. The POC and PON concentrations were 108.0–194.5 and 11.1–27.5 μg L^{-1}, respectively. The lowest mean values of the euphotic depth-averaged POC and PON were observed at St. 2 while the highest values were found at St. 17 (**Table 2**). The C/N ratios were in a range of 7.7–11.4 and the average C/N ratio value was highest at St. 1 (10.8 ± 0.6) and lowest at St. 17 (8.0 ± 0.3) (**Table 2**). The $\delta^{13}C$ values of surface POM ranged from −25.1 (St. 1) to −29.2‰ (St. 17) (**Table 2**).

Phytoplankton Biomass and Community Structure

The vertical patterns of the total chl-*a* concentrations between the surface and 1% light depth are shown in **Table 3** and were almost uniform throughout the euphotic zone at each station (**Table 3**). Depth-integrated total chl-*a* concentrations throughout the euphotic zone (from the surface to depth of Z_{eu}) ranged between 13.1 and 42.6 mg chl-*a* m^{-2}, with a mean value of 24.7 mg chl-*a* m^{-2} (SD = ±11.1 mg chl-*a* m^{-2}). The lowest integrated chl-*a* values were observed at the northernmost Sts. 2 and 5, while the highest value was found at the southernmost and near the offshore station (St. 17). We found a distinct difference in chl-a contributions of different size classes (>20, 5–20, and 0.7–5 μm) to the total chl-*a* concentration among the stations (**Table 3**). The large-sized phytoplankton (>20 μm) contributed most to the total phytoplankton biomass in the southern part of the study area (Sts. 11, 14, and 17), whereas relatively smaller cells (0.7–5 and 5–20 μm) were dominating in the northern part (Sts. 1, 2, and 5). The overall contributions of large (>20 μm), middle (5–20 μm), and small-sized (0.7–5 μm) phytoplankton to the total chl-*a* concentrations were 14.7–82.8, 11.1–47.4, and 5.6–47.1%, respectively. Moreover, the contribution of large-sized fraction (>20 μm) showed a statistically significant positive correlation with integrated total chl-*a* concentration ($r = 0.888$, $p < 0.05$), whereas a significant negative correlation was found between small size-class (0.7–5 μm) and integrated total chl-*a* value ($r = -0.910$, $p < 0.05$) in our study area.

Concerning the relative contributions of individual phytoplankton groups based on CHEMTAX analysis

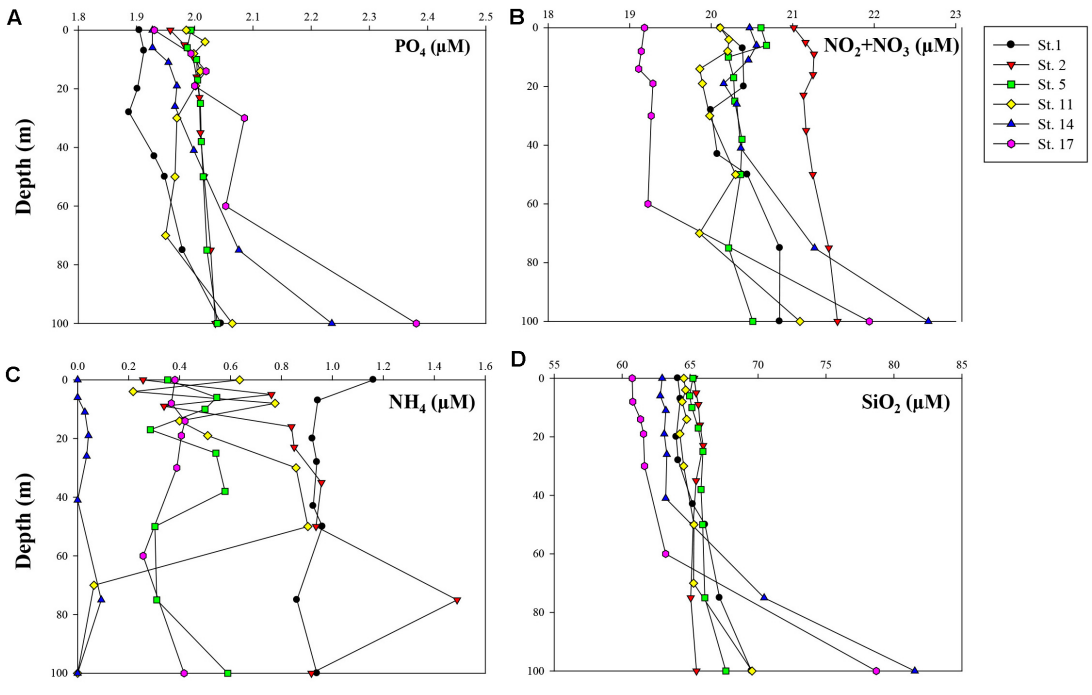

FIGURE 3 | Vertical profiles of measured concentrations (μM) of major inorganic nutrients within 100 m depth: **(A)** phosphate (PO_4), **(B)** nitrate + nitrite (NO_2 + NO_3), **(C)** ammonium (NH_4), and **(D)** silicate (SiO_2).

TABLE 2 | The concentrations of POC and PON, and δ13C (‰) of particulate organic matter (POM) in the northwestern Ross Sea.

Station	Light depth (%)	Sampling depth (m)	POC (μg L^{-1})	PON (μg L^{-1})	C/N ratio (molar:molar)	POC/Chl-*a*	δ13C (‰)
1	100	0	166.4	19.0	10.2	299.7	−25.1
	30	11	147.4	15.1	11.4	262.9	
	1	43	128.3	13.8	10.9	225.4	
2	100	0	108.2	11.1	11.4	282.3	−26.3
	30	9	116.0	13.6	10.0	297.3	
	1	35	133.0	15.3	10.2	381.3	
5	100	0	125.0	15.7	9.3	343.2	−27.1
	30	10	127.4	15.2	9.8	354.0	
	1	38	108.0	14.3	8.9	295.4	
11	100	0	153.1	18.7	9.6	226.7	−26.9
	30	8	140.4	17.6	9.3	206.6	
	1	30	142.7	16.3	10.2	142.9	
14	100	0	141.7	17.6	9.4	192.1	−26.8
	30	11	133.5	16.6	9.4	188.6	
	1	41	144.4	17.5	9.6	173.7	
17	100	0	175.4	25.7	8.0	128.1	−29.2
	30	8	194.5	27.5	8.3	139.2	
	1	30	174.9	26.6	7.7	118.9	

TABLE 3 | Total and euphotic-depth integrated chl-*a* concentrations (from the surface to 1% light depth) and compositions of different size-fractionated chl-*a* and phytoplankton communities.

Station	Light depth (%)	Total		Size-fractionated (%)			Phytoplankton community composition (%)			
		Chl-*a* (μg L^{-1})	Integrated (mg chl-*a* m^{-2})	>20 μm	5–20 μm	0.7–5 μm	Diatoms	Haptophytes	Dinoflagellates	Others
1	100	0.6	24.2	16.6	40.0	43.4	74.3	25.2	0.3	0.2
	30	0.6		29.0	43.1	27.9	76.4	23.1	0.3	0.2
	1	0.6		25.4	47.4	27.2	77.5	22.0	0.4	0.0
2	100	0.4	13.1	17.1	39.2	43.7	37.1	62.4	0.3	0.2
	30	0.4		16.2	36.7	47.1	25.3	74.4	0.4	0.0
	1	0.3		14.7	42.8	42.5	33.9	65.7	0.4	0.0
5	100	0.4	13.8	15.3	43.5	41.2	48.7	48.1	0.0	3.2
	30	0.4		16.5	43.2	40.3	54.6	42.0	0.0	3.4
	1	0.4		18.8	42.4	38.8	55.2	41.0	0.0	3.8
11	100	0.7	23.9	59.4	22.0	18.7	72.2	20.8	0.6	6.4
	30	0.7		60.7	22.3	17.0	79.6	16.1	0.5	3.8
	1	1.0		71.5	18.6	9.9	91.4	5.6	0.6	2.5
14	100	0.7	30.7	59.2	25.9	14.9	93.1	0.2	0.6	6.1
	30	0.7		64.4	21.4	14.3	79.1	18.9	0.6	1.4
	1	0.8		50.4	35.0	14.6	74.6	22.3	0.9	2.2
17	100	1.4	42.6	82.5	11.9	5.6	95.5	0.1	0.3	4.1
	30	1.4		82.5	11.1	6.3	95.1	0.0	0.6	4.3
	1	1.5		82.8	11.3	5.9	95.8	0.1	0.3	3.7

(Mackey et al., 1996; Wright et al., 1996; DiTullio et al., 2011), the combined contributions of diatoms and haptophytes (hereinafter *Phaeocystis antarctica*) contributed up to 99.6% of the total phytoplankton biomass during this study (**Table 3**). The phytoplankton community composition exhibited varying vertical distribution patterns and did not show clear differences between the three light depths (**Table 3**). Although most of the stations were diatoms-dominated with relatively low contributions of *P. antarctica*, *P. antarctica* presented markedly higher contributions at Sts. 2 and 5 (mean ± SD = 67.5 ± 6.2 and 43.7 ± 3.8%, respectively) (**Table 3**). Since two major groups, diatoms and *P. antarctica*, were distinctly observed during our study period, they could be related with different cell sizes based on our size-fractionated chl-*a* results. The size-fractionated chl-*a* and pigment analyses revealed that the larger phytoplankton assemblage (>5 μm) was dominated by diatoms (r = 0.917, $p < 0.05$). In comparison, the greater fraction of chl-*a* contained in small cells (<5 μm) accounted for mainly *P. antarctica*

(r = 0.929, $p < 0.01$), presumably indicative for solitary cells of *P. antarctica* (∼4 μm in size; Schoemann et al., 2005).

Biomolecular Composition of POM

The concentrations and relative composition of CHO, PRT, LIP, and food material (FM; the sum of CHO, PRT, and LIP; Danovaro et al., 2000) concentrations are presented in **Table 4**. The differences in concentrations of each biochemical pool (CHO, PRT, and LIP) and FM at these different three-light depths did not show a clear pattern. The absolute concentrations of each biomolecule (CHO, PRT, and LIP) and FM were 67.4–161.6, 7.9–75.6, 43.8–118.0, and 163.4–278.4 μg L^{-1}, respectively (**Table 4**). There was no clear difference in the CHO concentrations among the stations. In contrast, the PRT, LIP, and FM contents exhibited higher values in the southern part compared to those in the northern part (t-test, $p < 0.05$), in particular for PRT and FM contents (t-test, $p < 0.001$). Based on Pearson's correlation analysis, the PRT, LIP, and FM contents were found to have a positive relationship with chl-*a* concentration as an indicator of phytoplankton biomass (PRT vs. Chl-*a*: r = 0.915, $p < 0.01$; LIP vs. Chl-*a:* r = 0.787, $p < 0.01$; FM vs. Chl-*a*: r = 0.806, $p < 0.01$). Regarding the relative percentages of biomolecular components at each station, CHO made up the largest portion with a mean percentage of 54.0 ± 10.2%, increasing to ∼66.7% at the 1% light depth, followed by LIP (mean ± SD = 29.9 ± 5.4%) and PRT (mean ± SD = 16.1 ± 6.8%) (**Table 4**). Although the biomolecular compositions of phytoplankton varied without vertical trends, the CHO and PRT compositions exhibited spatial variability between the northern and southern parts (**Table 4**). More specifically, CHO compositions in the northern part (Sts. 1, 2, and 5) were higher than those in the southern part (Sts. 11, 14, and 17) (t-test, $p < 0.01$). In comparison, PRT composition in the euphotic layer of the southern part has much higher values compared to those measured in the northern part (t-test, $p < 0.001$). Meanwhile, we found that the proportion of CHO positively correlated with *P. antactica* composition (r = 0.609, $p < 0.01$) while the proportion of PRT positively correlated with diatom composition (r = 0.592, $p < 0.01$).

TABLE 4 | Concentrations of each biomolecular component (CHO, PRT, and LIP) and food materials (FMs) and percentages of the biomolecular composition of POM at each station in the northwestern Ross Sea.

Station	Light depth (%)	Concentration (μg L^{-1})				Composition (%)		
		CHO	PRT	LIP	FM	CHO	PRT	LIP
1	100	122.8	23.1	53.3	199.2	61.6	11.6	26.8
	30	118.4	7.9	58.4	184.7	64.1	4.3	31.6
	1	121.3	11.4	49.3	182.0	66.7	6.2	27.1
2	100	122.8	22.4	50.7	195.9	62.7	11.4	25.9
	30	97.8	23.1	43.8	164.7	59.4	14.0	26.6
	1	114.8	16.9	47.4	179.1	64.1	9.4	26.5
5	100	96.8	21.7	44.9	163.4	59.2	13.3	27.5
	30	102.4	22.4	70.5	195.3	52.4	11.5	36.1
	1	84.4	23.1	58.4	166.0	50.9	13.9	35.2
11	100	125.7	42.5	54.4	222.5	56.5	19.1	24.4
	30	161.6	36.9	62.1	260.6	62.0	14.2	23.8
	1	97.1	42.5	64.3	203.8	47.6	20.8	31.5
14	100	86.9	37.6	62.8	187.3	46.4	20.1	33.5
	30	109.4	43.1	56.9	209.5	52.2	20.6	27.2
	1	121.3	41.8	61.0	224.1	54.1	18.6	27.2
17	100	100.5	61.1	73.8	235.3	42.7	26.0	31.3
	30	67.4	69.4	118.0	254.9	26.5	27.2	46.3
	1	118.4	75.6	84.4	278.4	42.5	27.2	30.3

Amino Acid Composition of POM and Amino Acid Indices

Particulate hydrolyzable AA concentrations were quantified from the sum of each measured concentration of 14 detected AA since tyrosine, cystine, and tryptophan were not detected in our POM samples (**Table 5**). The PAA concentrations within the euphotic zone ranged from 0.18 μM at the 30% light depth of St. 2 to 1.04 μM at the 30% light depth of St. 17, with an average value of 0.40 ± 0.21 μM (**Table 5**). However, the significant spatial distinction of PAA concentrations was not observed although the concentrations of biomolecular components had a clear spatial pattern as mentioned above. We calculated the carbon and nitrogen normalized yields of AAs (AA-POC% and AA-PON%) for our PAA samples (**Table 5**). The PAA accounted for 7.8–26.6% of total POC (mean ± SD = 14.2 ± 5.9%) and 21.3–81.8% of total PON (mean ± SD = 41.7 ± 19.7%), respectively (**Table 5**).

The contributions of each AA in the PAA are presented in **Table 5**. The AA composition in the PAA was variable among the stations, and especially lysine and histidine have substantial variability. The major constituents of the PAA were glycine, glutamic acid, and alanine whereas lysine, histidine, methionine, and phenylalanine were minor components (**Table 5**). Among individual AA, glycine was the most dominant constituent (mean ± SD = 20.99 ± 3.74%), followed by glutamic acid, alanine, leucine, and serine. Lysine had the lowest molar percentage (mean ± SD = 2.78 ± 2.93%) and particularly was below the detection limit in most samples obtained from Sts. 2 and 5. The percentage compositions of NEAA and EAA to total PAA were in the ranges of 46.5–65.3 and 34.7–53.5%, respectively (**Table 5**). The proportion of NEAA was higher than those of the EAA fraction except for the sample at the 30% light depth of St. 11.

The calculated DI and EAAI values ranged from −0.87 to 1.00 and from 0.34 to 0.95, respectively (**Table 5**). In this study, strong positive correlation was found between the relative contribution of EAA (%) and EAAI (**Figure 4**; r = 0.629, $p < 0.01$).

Multivariate Analysis (AHC Analysis and PCA) Between Biochemical (Biomolecular and Amino Acid) Compositions of POM and Other Chemical and Biological Features

The dendrogram according to AHC analysis based on the same 28 variables used with PCA revealed three distinct groups (**Figure 5**). Cluster 1 (C1) had the southern part samples and one sample collected from 100% light depth at St. 1 whereas Cluster 2 (C2) contained almost all the samples obtained from the northern

TABLE 5 | PAA concentrations, carbon and nitrogen normalized yields of PAA (AA-POC% and AA-PON%), mol fractions of individual amino acids, NEAA, and EAA, and values of AA-based indices (DI and EAAI).

Station	light depth (%)	PAA (μM)	AA-POC%	AA-PON%	Amino acid composition (mol%)														NEAA (mol%)	EAA (mol%)	DI	EAAI
					ASP	GLU	SER	GLY	ALA	HIS	THR	ARG	VAL	MET	PHE	ILE	LEU	LYS				
1	100	0.30	9.6	28.9	6.40	14.48	7.67	17.98	8.83	3.59	7.69	6.14	5.94	1.51	3.92	4.31	7.62	3.94	55.4	44.6	−0.10	0.87
	30	0.61	21.3	76.9	6.61	18.01	7.64	22.86	8.98	4.03	3.00	8.18	3.77	2.48	2.54	3.50	7.24	5.52	64.1	40.3	−0.72	0.83
	1	0.61	24.0	81.8	4.65	10.33	9.45	25.39	6.87	4.04	7.23	7.67	4.13	4.33	3.59	3.62	8.68	N.D.	56.7	43.3	−0.03	0.56
2	100	0.22	10.2	36.6	6.64	10.75	7.69	22.88	11.26	4.96	6.02	7.35	1.55	6.30	4.01	3.36	7.90	N.D.	59.2	41.5	−0.11	0.51
	30	0.18	7.8	23.6	6.31	10.06	7.84	20.74	13.30	6.04	4.30	5.82	1.72	7.16	4.32	4.28	8.11	N.D.	58.2	41.8	0.84	0.51
	1	0.37	13.8	44.2	5.42	13.28	7.82	24.80	9.75	4.67	4.68	7.49	1.39	6.02	3.36	3.42	7.28	N.D.	61.1	38.3	−0.02	0.51
5	100	0.21	8.2	21.3	9.65	11.71	8.68	24.90	10.38	N.D.	5.27	4.71	6.93	1.88	4.31	4.25	7.33	N.D.	65.3	34.7	−0.54	0.34
	30	0.46	18.8	59.1	7.57	15.38	6.71	23.69	7.65	5.49	4.11	7.04	1.26	4.90	4.00	3.04	3.33	9.68	61.0	42.8	−0.04	0.71
	1	0.43	20.7	56.3	7.63	20.28	6.05	22.23	7.62	6.59	3.44	7.06	2.31	1.50	3.87	3.23	8.18	N.D.	63.8	36.2	0.00	0.49
11	100	0.29	9.9	28.4	5.35	10.84	7.53	21.56	11.20	3.71	7.25	7.11	3.92	3.87	4.25	4.26	9.16	N.D.	56.5	43.5	0.29	0.57
	30	0.26	10.4	27.1	10.01	13.38	8.14	14.97	N.D.	3.60	8.60	6.10	4.28	4.71	4.76	5.99	9.33	6.11	46.5	53.5	1.00	0.94
	1	0.51	18.5	56.7	6.16	10.58	7.56	19.91	11.05	2.67	7.48	6.62	3.63	3.85	4.05	4.57	8.21	3.65	55.3	44.7	0.03	0.92
14	100	0.25	9.5	23.8	9.83	12.79	7.26	11.96	11.75	N.D.	7.51	4.64	4.46	5.00	4.27	6.18	8.39	6.44	53.6	46.9	0.45	0.57
	30	0.25	10.0	27.9	6.67	11.27	7.53	18.04	10.71	4.23	6.75	5.72	4.75	3.39	3.92	4.85	7.91	4.26	54.2	45.8	0.24	0.95
	1	0.29	10.5	28.3	7.17	12.84	7.96	16.48	11.05	N.D.	7.72	6.06	6.68	2.37	3.91	4.93	8.18	4.64	55.5	44.5	−0.18	0.57
17	100	0.41	12.0	29.0	6.19	9.82	7.44	22.44	10.31	3.55	7.35	6.34	4.36	3.23	3.80	4.50	7.92	2.73	56.2	43.8	−0.16	0.90
	30	1.04	26.6	68.6	6.39	12.83	6.71	23.91	9.80	4.42	7.12	6.37	5.57	1.75	2.38	3.14	7.88	0.64	59.6	39.3	−0.87	0.71
	1	0.47	13.7	32.9	5.98	8.91	6.88	23.09	9.85	5.78	7.20	6.22	5.48	1.99	3.40	4.04	8.71	2.48	54.7	45.3	−0.07	0.84
Mean ± SD		0.40 ± 0.21	14.2 ± 5.9	41.7 ± 19.7	6.92 ± 1.52	12.64 ± 2.94	7.59 ± 0.76	20.99 ± 3.74	9.46 ± 2.85	3.74 ± 1.99	6.26 ± 1.68	6.48 ± 0.95	4.01 ± 1.78	3.68 ± 1.75	3.85 ± 0.60	4.19 ± 0.91	7.85 ± 1.27	2.78 ± 2.93	57.6 ± 4.5	42.8 ± 4.3	0.00 ± 0.47	0.68 ± 0.19

The list of AA abbreviations is as follows: aspartic acid (ASP), glutamic acid (GLU), serine (SER), glycine (GLY), alanine (ALA), histidine (HIS), threonine (THR), arginine (ARG), valine (VAL), methionine (MET), phenylalanine (PHE), isoleucine (ILE), leucine (LEU), and lysine (LYS).

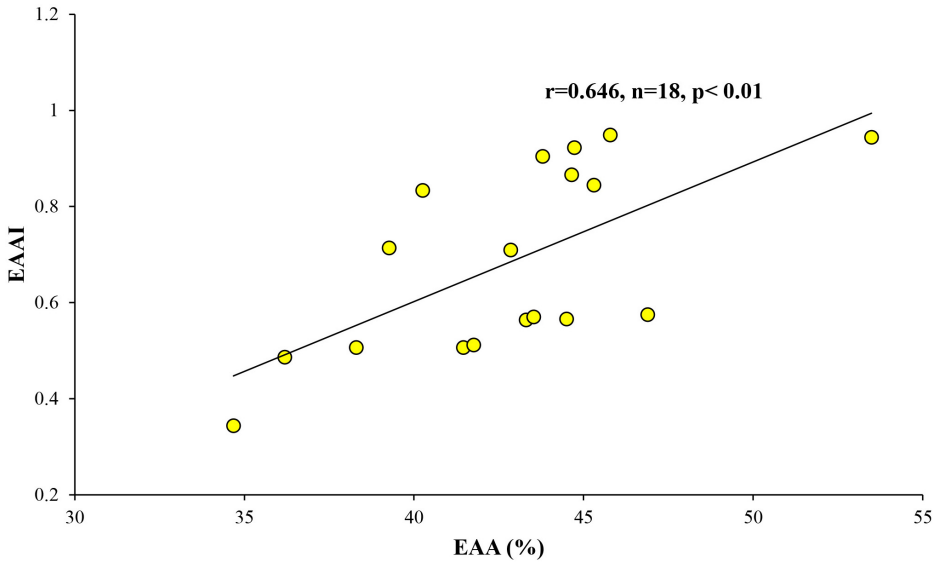

FIGURE 4 | Relationship between the relative contribution of EAA (%) and EAAI.

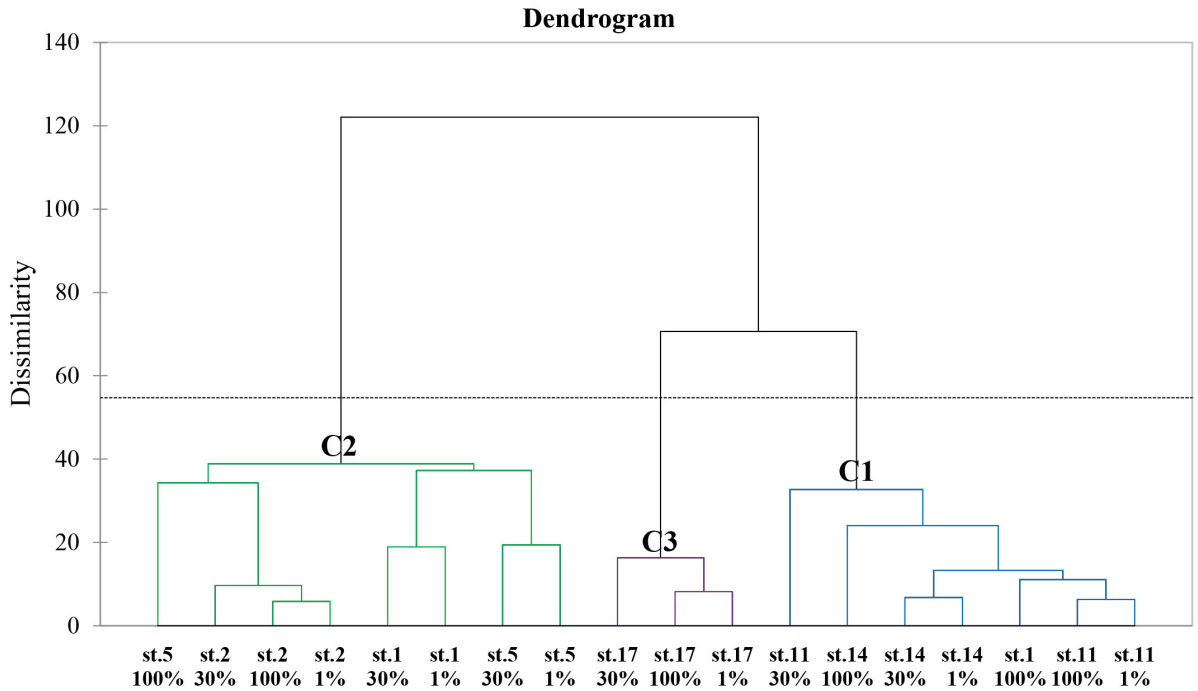

FIGURE 5 | Dendrogram representing the agglomerative hierarchical clustering (AHC) based on dissimilarities using Ward's method between the biochemical (biomolecular and amino acid) compositions of POM and other 11 chemical and biological features.

section. Cluster 3 (C3) included the samples collected from only St. 17 in the southern part. The maximum value of distances between the class centroids was observed between C2 and C3 (29.743), and C1 and C3 had a small difference in dissimilarity.

As a result of the PCA, the principal components (PC) 1 and 2 explained 29.30 and 21.41% of the data variance in the biochemical compositions and other parameters among the stations (**Figure 6**). The PC1 was positively correlated with $NO_2 + NO_3$, SiO_2, C/N ratio, CHO composition (%), *P. antarctica*, methionine, and serine whereas negatively loaded with Chl-a, PRT and LIP composition (%), Diatoms, EAAI, and valine. The PC2 was found to be positively loaded with EAA composition (%), isoleucine, threonine, phenylalanine, leucine, aspartic acid, and DI score while had negative loadings

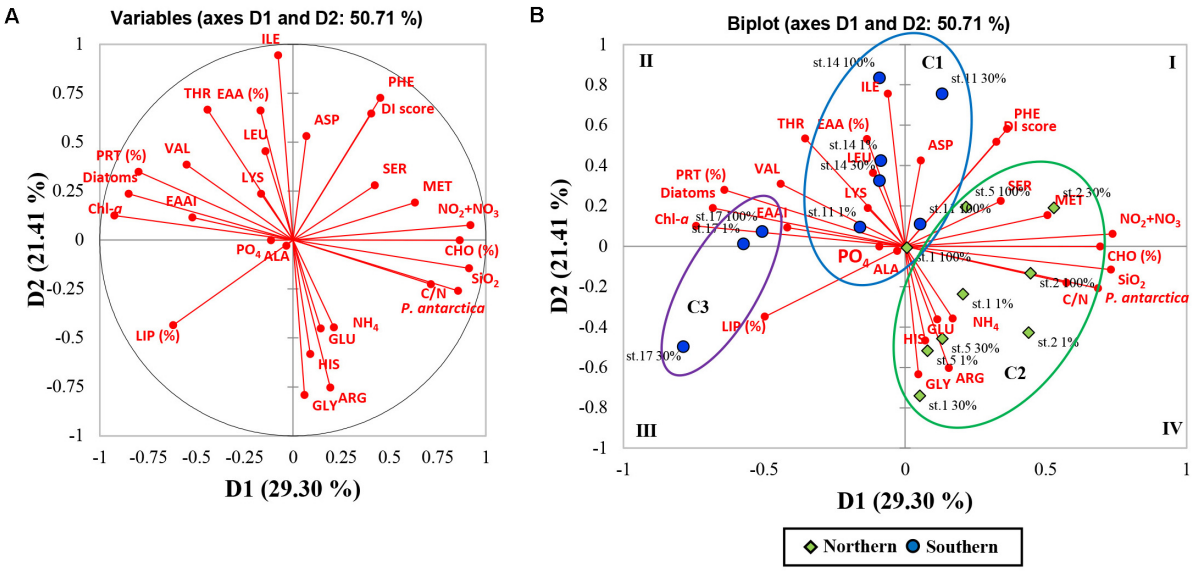

FIGURE 6 | Principal component analysis (PCA; after normalized varimax rotation) based on the biochemical (biomolecular and amino acid) compositions of POM and other chemical and biological features. **(A)** Correlation circle and projection obtained by PCA of the 28 variables; each red arrow represents the squared cosine corresponding to an individual variable. **(B)** Biplot of PCA on the 28 variables and observations for the first and second axis (variability explained: 50.71%). Observations are grouped according to the classes obtained from agglomerative hierarchical clustering (AHC). Each abbreviation represents as aspartic acid (ASP), glutamic acid (GLU), serine (SER), glycine (GLY), alanine (ALA), histidine (HIS), threonine (THR), arginine (ARG), valine (VAL), methionine (MET), phenylalanine (PHE), isoleucine (ILE), leucine (LEU), lysine (LYS), compositions of essential amino acids (EAAs), essential amino acid index (EAAI), degradation index (DI), relative contributions of diatoms (Diatoms) and haptophytes (*P. antarctica*), biomolecular composition (CHO, PRT, and LIP), carbon to nitrogen ratio (C:N), phosphate (PO_4), nitrate + nitrite (NO_2 + NO_3), ammonium (NH_4), silicate (SiO_2), and chlorophyll a (Chl-*a*).

for glycine, arginine, and histidine. To determine whether correlations were worthy of interpretation, we examined the squared cosines of the variables and then excluded low values of squared cosines between the variables and PCs (**Figure 6**; i.e., glutamic acid, alanine, lysine, PO_4, and NH_4). A distinct spatial separation between the northern and southern parts of our study area was founded along the PC1 axis. In other words, most of the samples collected from the southern part were on the left side of the biplot (quadrants II and III) whereas most of the northern part samples were placed on the lower right-hand side (quadrant IV). Moreover, the observations in the PCA space showed a similar pattern of clustering as the AHC analysis (**Figures 5**, **6**).

DISCUSSION

Source of the Bulk POM

The marine POM filtered on filter paper includes diverse organic matter derived from phytoplankton, bacterial plankton, detritus, and terrestrial organic matter (Harmelin-Vivien et al., 2008). Both of C/N molar ratio and $\delta^{13}C$ value in bulk POM have long been used as indicators of the nature of the organic matter in various marine ecosystems (Wada et al., 1975; Zweifel et al., 1993; Montagnes et al., 1994; Lee and Whitledge, 2005). Generally, phytoplankton have higher C/N ratios in a range of 6–10 than bacteria (3–5), whereas terrestrial organic matters have 2–20 times higher than the C/N values of phytoplankton (Brzezinski, 1985; Montagnes et al., 1994; Tyson, 1995; Goñi et al., 2003; Lamb et al., 2006). The range of C/N molar ratios of 7.7–11.4 (mean ± S.D = 9.6 ± 1.0) for POM in this study is within the previously reported range of C/N ratio for phytoplankton (**Table 2**). However, Fabiano et al. (1993) reported lower C/N molar ratios within the euphotic zone than our observation, ranging from 5.4 and 9.1 at the stations near Cape Adare and 5.4–6.6 at the stations located in Terra Nova Bay, Ross Sea. Moreover, Coale et al. (2003) obtained slightly lower ratios ranging from 6.5 to 7.9 in the southern Ross Sea. Generally, lower C/N ratios within the euphotic layer were reported during the bloom period in Antarctic water according to previous studies (Bodungen et al., 1986; Nelson et al., 1989; Fabiano et al., 1993). The relatively higher values of the C/N ratio in this study could be due to our sampling period conducted at the end of February 2018 in a post-bloom period which will be discussed later.

In general, $\delta^{13}C$ values derived from marine phytoplankton range from −23 to −19‰ (Fry and Sherr, 1989; Harmelin-Vivien et al., 2008). In comparison, $\delta^{13}C$ values in phytoplankton communities of Antarctic surface waters are lower than those observed in lower-latitude oceans (Wada et al., 1987; Rau et al., 1989, 1991; Dehairs et al., 1997). In this study, the $\delta^{13}C$ values in the surface bulk POM were in a range of −29.2 to −25.1‰ (mean ± SD = −26.9 ± 1.3‰) (**Table 2**). Although our study has $\delta^{13}C$ values closer to terrestrial organic matters (−30 to −26‰; Fry and Sherr, 1989), previous studies have reported that input of terrestrial organic matter from the ice-covered continent is

negligible in the Ross Sea (Rogers and Dunbar, 1993; Villinski et al., 2000). Based on the results of both C/N ration and $\delta^{13}C$ values of POM, the main source of POM in this study could be phytoplankton-derived organic matter.

Biomolecular Composition of POM

In general, the temporal dynamics of the two major types of phytoplankton blooms have been well documented in the Ross Sea (Arrigo et al., 1999; Smith et al., 2000, 2011). The initial bloom dominated by the haptophyte *P. antarctica* is commonly found in the south-central Ross Sea during austral spring (Peloquin and Smith, 2007). The following second bloom dominated by diatoms commonly is observed in the western and eastern portions of the Ross Sea in summer (DiTullio and Smith, 1996; Peloquin and Smith, 2007). Considering temporal and spatial phytoplankton bloom patterns in the northwestern Ross Sea, we infer that our sampling period (end of February–the beginning of March) was in the post-bloom. In the present study, haptophytes dominated by solitary *P. antarctica* cells and nano-sized diatom assemblages with low chl-*a* concentrations (<0.6 $\mu g\ L^{-1}$) and high POC/Chl-*a* values potentially indicate mostly inactive cells (Mangoni et al., 2017) prevailed in the northern part of the study area (**Tables 2**, **3**). Smith et al. (2003) reported that the abundance of solitary *P. antarctica* cells increases in the Ross Sea during late summer under inorganic nutrient and/or iron limitation. Furthermore, Mathot et al. (2000) and Shields and Smith (2009) suggested that colonial *P. antarctica* cells can be associated with their maximum biomass under nutrient-replete conditions and exponential phase whereas solitary *P. antarctica* cells numerically dominate when their growth rate declined and the senescence phase began after bloom. In this study, the micro-sized diatoms with their elevated chl-*a* concentrations (up to 1.5 $\mu g\ L^{-1}$) and low POC/Chl-*a* values indicate relatively active cells (Mangoni et al., 2017) predominated in the southern part (**Tables 2**, **3**) in comparison to the northern part. Therefore, taking into account the bloom phase and biological features (phytoplankton community, cell size, chl-*a* concentration, and POC/Chl-*a* value), it seems reasonable to suggest that solitary *P. antarctica* cells and nano-sized diatoms observed in the northern section were in a senescent status, while micro-sized diatoms dominated in the southern section were in a relatively active condition.

There have been numerous studies published in the literature that the synthesis of biomolecular classes could be influenced by different growth phases of phytoplankton (Moal et al., 1987; Fernández-Reiriz et al., 1989; de Madariaga, 1992; Ríos et al., 1998; Ahn et al., 2019). Considerable changes in the biomolecular composition of the phytoplankton occurred throughout different growth phases (i.e., exponential, stationary, and senescent phases) (Ahn et al., 2019 and the references therein). The amounts of PRT as biomolecular products of photosynthesis increased during the exponential growth phase, indicating a higher PRT demand for exponential cell division and growth (Mayzaud et al., 1990; Berdalet et al., 1994). When phytoplankton become stationary and senescent conditions concurrent with the nutrient deficiency thereafter, CHO and LIP levels increase for energy reserves (Myklestad, 1974; Mague et al., 1980; Barlow, 1982; Tonon et al., 2002). Generally, phytoplankton growth in the Ross Sea is limited by irradiance during austral spring (Smith et al., 2000; Peloquin and Smith, 2007), but by nutrient bioavailability (particularly iron) in austral summer (Sedwick and Ditullio, 1997; Sedwick et al., 2000; Peloquin and Smith, 2007). In this study, major inorganic nutrient concentrations (phosphate, nitrate + nitrite, ammonium, and silicate) in seawater were not depleted (**Figure 3**). Furthermore, Si* (defined as [Si]- [NO_3^-] in μM) for the identification of potential iron limitation had positive values from all stations, suggesting that there was no evidence for iron limitation during this study (Sarmiento et al., 2004; Le Moigne et al., 2013). However, scarcity of iron is a very common feature in the Ross Sea during the summer season (Olson et al., 2000; Smith and Asper, 2001), and Si* could be restricted as a community-wide iron limitation index because Si* represents the silicic acid uptake and growth related to only diatom communities under iron limitation (Hogle et al., 2018; Louropoulou et al., 2019). On the other hand, the specific carbon uptake rates of phytoplankton in parallel with our study were highest at surface water from all stations, which suggests potential light limited conditions in late austral summer period (Lee et al., 2008). Hence, phytoplankton during this study could have been a physiologically inactive condition under unfavorable environmental conditions.

In our study, CHO accounted for the highest portion (mean $\pm$ SD = 54.0 $\pm$ 10.2%) among different biomolecules (CHO, PRT, and LIP) of POM (**Table 4**). However, the higher contribution of PRT (up to 27.2%) and lower contribution of CHO were observed in the southern section of our study area compared to those in the northern section (**Table 4**). Furthermore, we found significant differences in CHO and PRT compositions between the northern and southern stations (*t*-test, $p < 0.05$). These discrepancies could explain that CHO-rich solitary *P. antarctica* cells and nano-sized diatoms were in a senescent phase in the northern part whereas micro-sized diatoms having relatively higher PRT had more active conditions in the southern part. On the other hand, marked spatial variations in biomolecular compositions among the stations were probably due to taxonomic differences. The composition of CHO-rich POM may be linked with structural and/or storage CHO synthesis of *P. antarctica* (Lancelot and Mathot, 1985; Alderkamp et al., 2007; Mangoni et al., 2017; Kim et al., 2018). *P. antarctica* produces a mucous colony matrix which is mostly composed of polysaccharides as a kind of structural CHO (Alderkamp et al., 2007; Mangoni et al., 2017). Hong et al. (1997) suggested that when *P. antarctica* colony matrix begins to break up during the senescent phase, transparent exopolymer particle (TEP) production by *P. antarctica* is closely related with increased particulate CHO. Moreover, CHO accumulation has been observed when both single-cell and colonial *P. antarctica* reach the end of the bloom phase since they store the surplus energy as storage CHO (Lancelot and Mathot, 1985; Alderkamp et al., 2007 and the references therein). In contrast, Young et al. (2015a) found that Antarctic diatoms adapted to cold temperatures tend to increase PRT concentrations to compensate for slow enzyme rates. In conclusion, spatial variability of the biomolecular composition in the bulk POM during this study was

not only influenced by phytoplankton growth phases but also by those taxonomic compositions.

Influence of Origin and Degradation Status on the Amino Acid Composition of POM

The measured concentrations of the PAA during this study (**Table 5**; 0.18–1.04 μM) varied significantly but were in agreement well with the range of values previously reported from polar regions (Hubberten et al., 1995; Dittmar et al., 2001; Tsukasaki and Tanoue, 2010; Tremblay et al., 2015). Based on the Antarctic data (Weddell Sea), Hubberten et al. (1995) found relatively higher PAA concentrations (0.75 ± 0.60 μM) averaged in the upper 100 m depth than those reported in the Arctic water (mean ± SD = 0.57 ± 0.61 μM). Tremblay et al. (2015) observed higher concentrations of PAA at the most productive stations (up to 0.82 μM) while lower concentrations of PAA (0.16–0.22 μM) at the stations with low phytoplankton biomass in the Southern Ocean. Our results are also consistent with that the positive relationship between PAA and total chl-*a* concentrations ($r = 0.510$, $p < 0.05$). Therefore, the source of PAA in this study is probably mostly phytoplankton-produced PRT (Kalachova et al., 2004 and the references therein).

It is well known that AAs in hydrolyzed POM accounted for approximately 30% of POC and 50% of PON in various oceans (Handa, 1970; Siezen and Mague, 1978; Liebezeit and Bölter, 1986; Misic et al., 2017). All of the AA contributions to POC (**Table 5**; 7.8–26.6% of total POC) in the present study are lower than those in previous studies (Handa, 1970; Siezen and Mague, 1978; Liebezeit and Bölter, 1986). In contrast, the averaged proportions of AA to PON (mean ± SD = 41.7 ± 19.7% of total PON) are comparable to those in previous studies (Handa, 1970; Siezen and Mague, 1978; Liebezeit and Bölter, 1986), although they varied greatly (21.3–81.8% of total PON) (**Table 5**). According to Shields et al. (2019), the carbon normalized yield of AAs (AA-POC%) had higher values in less degraded organic matter and decreased with degradation. In other words, values of AA-POC% were highest during the mid-exponential bloom phase, while they decreased in the stationary and degradation phases of phytoplankton growth (Shields et al., 2019). Furthermore, AA-PON% could also be indicated for diagenesis in phytoplankton (Duan and Bianchi, 2007). Therefore, the relatively low AA contributions to the total POC and PON in this study imply that the majority of PAA might have undergone degradation to some degree (Duan and Bianchi, 2007; Shields et al., 2019).

The major constituents of PAA during this cruise were glycine, glutamic acid, and alanine, occupying 43.1% (±5.1%) of total PAA in the bulk POM (**Table 5**). Generally, previous studies reported that the predominant AAs of phytoplankton are glutamic acid, aspartic acid, alanine, and leucine regardless of marine or freshwater species although there are little differences in the AA composition of phytoplankton depending on the species (Hayashi et al., 1986 and the references therein). However, Hecky et al. (1973) suggested that serine + threonine and glycine could be enriched in the cell wall PRT of diatoms. We found that mol% serine + threonine only positively correlated with diatom composition ($r = 0.473$, $p < 0.05$) while mol% glycine had no correlation with diatoms. Although the correlation directly with diatoms was poor as diatom frustules can be preferentially preserved after cell death, glycine and serine were found to be bounded on the diatom frustules and this may be a reason why glycine was enriched in the POM (Ingalls et al., 2006). On the other hand, Liebezeit and Bölter (1986) found that glutamic acid, aspartic acid, glycine, and serine are the most dominant compounds of phytoplankton-derived PAA whereas glycine becomes dominant in the PAA of deeper waters with an appreciable quantity of detrital materials. Thus, the composition of PAA was caused by the combined effects of diatom-dominated phytoplankton communities and phytodetritus in this study after the bloom. Further evidence for supporting the degraded POM in our study was relatively low DI values of PAA (**Table 5**). Over half of calculated DI scores for our PAA samples showed negative values indicating that PAA appeared to be highly degraded phytodetritus (Dauwe et al., 1999; Wu et al., 2007; Shields et al., 2019). In general, the DI scores can provide information on the degree of degradation in bulk POM (Dauwe et al., 1999; Wu et al., 2007; Shields et al., 2019). The more negative DI value indicates the more degraded condition, while a positive DI value is indicative of fresh phytoplankton (Dauwe et al., 1999; Wu et al., 2007; Shields et al., 2019).

The Potential Impacts of the AA Composition on Food Quality for Zooplankton Nutrition

The nutritional quality of PRT can be estimated by the proportion of total EAA and EAAI (Mente et al., 2002; Ju et al., 2008). As shown in **Table 5**, total EAA contributed 42.8 ± 4.3% during this study, which is within the range (41–55%) of compositional data on the EAA of microalgae and cyanobacteria conducted both in laboratory cultures and natural conditions (Kolmakova and Kolmakov, 2019 and the references therein). The general profile for individual EAA of phytoplankton composed high contributions of leucine and arginine whereas methionine and histidine were significantly lower than other EAA (Kolmakova and Kolmakov, 2019 and the references therein). In this study, however, lysine and histidine were limited in our POM samples collected from some stations with concurrent lower values of the EAAI (**Table 5**). EAAI scores can be evaluated for protein quality by comparing the geometric mean value of EAA in an FM relative to a reference protein derived from consumers (Peñaflorida, 1989). Based on the classification of Oser (1959), scores of the calculated EAAI over 0.9 are defined as good protein material, EAAI of approximately 0.8 is indicated as a useful protein, and EAAI below 0.7 can be classified as inadequate PRT. Thus, efficient protein food can be considered by the most similar AA profile between prey and their consumer and EAAI scores approaching 1.0 (Ju et al., 2008). The mean EAAI (0.68 ± 0.19) was classified as inadequate protein FMs during this study although the scores of the total EAAI (0.34–0.95) varied significantly (**Table 5**). Based on the results of EAA in this study, we found that significant positive relationship between

the proportion of EAA and AA EAAI (**Figure 4**). This result may be surmised that a greater proportion of EAA in POM was composed with EAA composition with balanced in an optimal proportion.

Anderson et al. (2004) suggested that individual EAA-deficient diets had a greater impact on the limitation of the growth of higher trophic levels rather than bulk amounts of protein and nitrogen. The previously published studies found that imbalances in dietary EAA could cause a bad influence on the growth of marine zooplankton (Kleppel et al., 1998; Guisande et al., 2000). Furthermore, the total AA composition of the copepod diets, as well as EAA composition, can be important for the higher reproductive success of copepods (Guisande et al., 2002). According to Guisande et al. (2000), AA from ingested food could not be converted into consumer's biomass for egg production with an optimal proportion of AA if AA composition in prey is highly dissimilar to that of female copepods. Thus, the higher reproductive success of female copepods is observed when the AA composition of the ingested food is similar to that of the consumers (Guisande et al., 1999, 2000). In this study, we compared the averaged each AA profile of two phytoplankton communities that were divided into diatoms-dominant (Sts. 1, 11, 14, and 17) and relatively higher *P. antarctica*-abundant communities (Sts. 2 and 5) with those of bulk zooplankton communities (unpublished data) (**Figure 7**). The reason why we separated into two groups is that variable grazing by herbivores appears to discriminate based on the food quality, preference of ingesting cells, and distributions of the phytoplankton community (Haberman et al., 2003 and the references therein). In addition, lysine was nearly absent throughout the euphotic zone at *P. antarctica*-abundant stations 2 and 5 (**Table 5**). Assuming that the same assimilation rates of total AA between the two groups, we observed that the relationship for the diatoms-dominant group was closer to the 1:1 line considered as the ideal line in comparison to *P. antarctica*-abundant group with greater deviations of glycine, lysine, valine, methionine, and histidine from the line (**Figure 7**). Therefore, it seems reasonable to suggest that diatoms-dominant diets were better protein sources because they had an AA composition similar to their consumers and higher EAAI value. Our findings are also consistent with the conclusions of Boyd (1989) and Burford (1997).

The Application of Multivariate Statistical Analysis for Evaluating Food Quality for Consumers

In this work, the multivariate statistical analysis was conducted for finding relationships between biochemical compositions (biomolecular and AA compositions) and other chemical and biological data. The PC1 of PCA results separated two different groups of biochemical parameters and phytoplankton communities. These two groups formed high proportions of CHO and high C/N values with a haptophytes-abundant group dominated by solitary *P. antarctica* cells while relatively higher

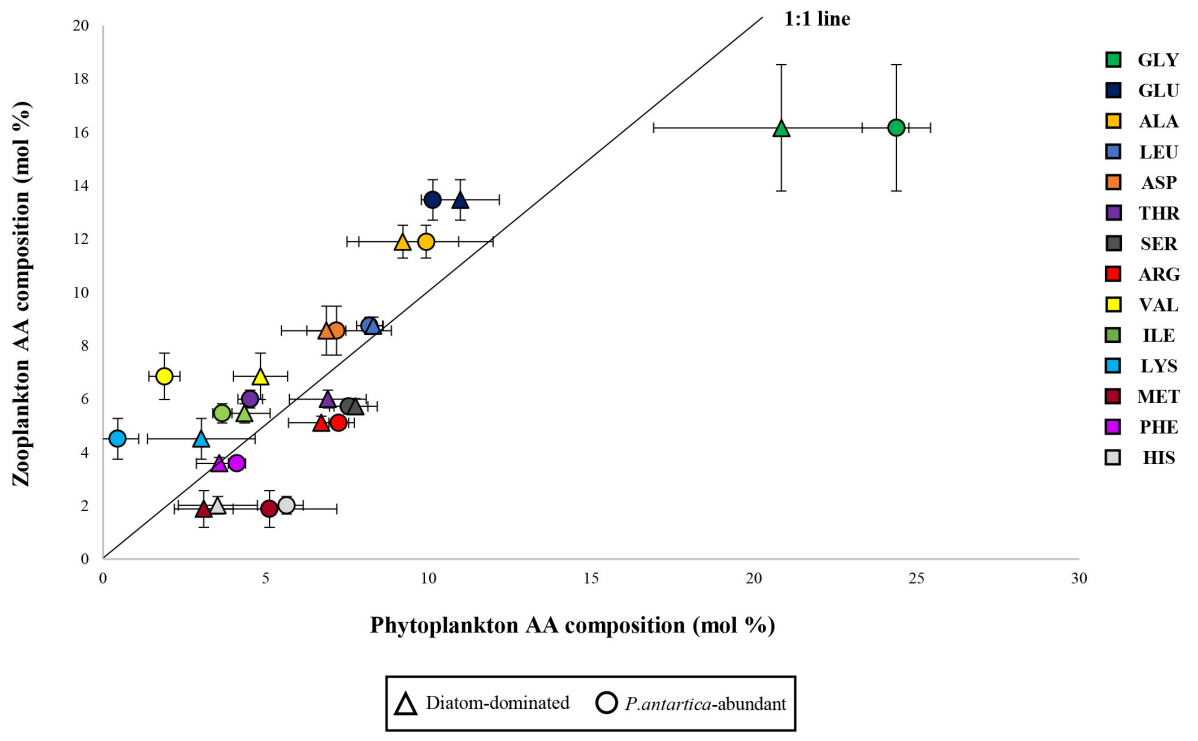

FIGURE 7 | Relationship between amino acid profiles of diatom-dominant and *P. antartica*-abundant communities and those in zooplankton communities as potential consumers. Each abbreviation represents aspartic acid (ASP), glutamic acid (GLU), serine (SER), glycine (GLY), alanine (ALA), histidine (HIS), threonine (THR), arginine (ARG), valine (VAL), methionine (MET), phenylalanine (PHE), isoleucine (ILE), leucine (LEU), and lysine (LYS).

proportions of PRT and high EAAI scores with diatom-dominant communities (**Figure 6**). In the PC2, EAA composition and DI score were negatively related to glycine which is considered as an indicator of organic matter degradation as discussed above (**Figure 6**) (Liebezeit and Bölter, 1986; Petersson and Floderus, 2001). Overall, our results revealed that the southern region dominated majorly by micro-sized diatoms was positively correlated with PRT, EAA, and EAAI indicating a good protein quality, while the relatively solitary *P. antarctica*-abundant northern region with higher CHO contribution was negatively correlated with good protein quality factors.

CONCLUSION

Our study found remarkable differences in biochemical compositions (biomolecular and AA compositions) of the phytoplankton communities (i.e., CHO-rich vs. relatively higher PRT and good vs. bad protein quality) depending upon the growth phase and community structure of phytoplankton. These changes in the biochemical compositions (biomolecular and AA compositions) and protein quality of phytoplankton as a valuable nutrition source could be important for the growth, reproduction, and naupliar survival of herbivorous zooplankton as well as their biochemical composition (Gulati and Demott, 1997; Guisande et al., 2000; Vargas et al., 2006; Yun et al., 2015; Jo et al., 2017). Furthermore, differences in biochemical compositions of POM could also influence the degree of subsequent bacterial degradation and recycling since the lability of individual biochemical compounds varies widely (Harvey et al., 1995; Ingalls et al., 2006; Sabadel et al., 2019; Lehmann et al., 2020). The more refractory compounds could be preserved highly selective with the loss of labile compounds through the microbial process, thereby changing the biochemical compositions of sinking particles and consequently in sediments (Harvey et al., 1995; Alkhatib et al., 2012; Lehmann et al., 2020). Recently, significant changes in physical conditions such as increasing summer temperatures in the atmosphere and surrounding waters were observed in the southwestern Ross Sea continental shelf and lengthening of the free ice season was found in Ross Sea polynya induced by climate change (Stammerjohn et al., 2008; Comiso et al., 2011; Schine et al., 2016; Kaufman et al., 2017). These climate-induced stressors can lead to changes in the size structure and assemblage composition of phytoplankton and physiological shifts in the phytoplankton communities (Yun et al., 2019; Antoni et al., 2020; Hernando et al., 2020). Moreover, herbivores encounter rapidly changing food quality in company with changes in the diverse species, quantity, and biochemical characteristics of their prey (Scott, 1980; Finkel et al., 2010). In addition, differential preservation of biochemical compounds in accordance with reactive changes of the altered biochemical composition of POM under ongoing climate changes could have effects on remineralization rates and sinking particles in the deep sea (Ingalls et al., 2006; Kharbush et al., 2020; Lehmann et al., 2020). Therefore, additional research with multidiscipline approaches is required to evaluate the important food quality as a food source for higher trophic level organisms and understand complicated biochemical parameters associated with climate changes.

DATA AVAILABILITY STATEMENT

The original contributions presented in the study are included in the article/**Supplementary Material.** Further inquiries can be directed to the corresponding author/s.

AUTHOR CONTRIBUTIONS

SL, NJ, and J-HK contributed to conceptualization. NJ, HL, KK, BK, and MK contributed to data curation. NJ, KK, BK, MK, and WS contributed to sample analysis. NJ, HL, J-HK, BK, and WS contributed to investigation. SL, NJ, and KK contributed to methodology and data validation. HL and J-HK gave scientific advice. NJ and SL contributed to writing—original draft. NJ, HL, and SL contributed to writing—review and editing. All authors agreed with the submission of the manuscript, and read and agreed to the published version of the manuscript.

FUNDING

This research was supported by the "Ecosystem Structure and Function of Marine Protected Area (MPA) in Antarctica" project (PM20060), funded by the Ministry of Oceans and Fisheries (20170336), South Korea.

SUPPLEMENTARY MATERIAL

The Supplementary Material for this article can be found online at: https://www.frontiersin.org/articles/10.3389/fmicb.2021.623600/full#supplementary-material

Supplementary Figure 1 | Representative chromatogram for L-amino acids mixed standard; 1: ASP, 2: GLU, 3: ASN, 4: SER, 5: GLN, 6: HIS, 7: GLY, 8: THR, 9: ARG, 10.ALA, 11: TYR, 12: CY2, 13: VAL, 14: MET, 15: NVA, 16: TRP, 17: PHE, 18: ILE, 19: LEU, and 20: LYS.

REFERENCES

Ahn, S. H., Whitledge, T. E., Stockwell, D. A., Lee, J. H., Lee, H., and Lee, S. H. (2019). The biochemical composition of phytoplankton in the Laptev and East Siberian seas during the summer of 2013. *Polar Biol.* 42, 133–148. doi: 10.1007/s00300-018-2408-0

Ainley, D., Russell, J., Jenouvrier, S., Woehler, E., Lyver, P. O. B., Fraser, W. R., et al. (2010). Antarctic penguin response to habitat change as earth's troposphere reaches 2° C above preindustrial levels. *Ecol. Monogr.* 80, 49–66. doi: 10.1890/08-2289.1

Alderkamp, A. C., Buma, A. G. J., and Van Rijssel, M. (2007). The carbohydrates of phaeocystis and their degradation in the microbial food web. *Biogeochemistry* 83, 99–118. doi: 10.1007/978-1-4020-6214-8_9

Alderkamp, A. C., Kulk, G., Buma, A. G. J., Visser, R. J. W., Van Dijken, G. L., Mills, M. M., et al. (2012). The effect of iron limitation on the photophysiology of phaeocystis antarctica (prymnesiophyceae) and fragilariopsis cylindrus

(bacillariophyceae) under dynamic irradiance. *J. Phycol.* 48, 45–59. doi: 10.1111/j.1529-8817.2011.01098.x

Alkhatib, M., Schubert, C. J., Del Giorgio, P. A., Gelinas, Y., and Lehmann, M. F. (2012). Organic matter reactivity indicators in sediments of the St. Lawrence Estuary. *Estuar. Coast. Shelf Sci.* 10, 36–47. doi: 10.1016/j.ecss.2012.03.002

Anderson, T. R., Boersma, M., and Raubenheimer, D. (2004). Stoichiometry: linking elements to biochemicals. *Ecology* 85, 1193–1202. doi: 10.1890/02-0252

Andersson, A., Tamminen, T., Lehtinen, S., Jürgens, K., Labrenz, M., and Viitasalo, M. (2017). "The pelagic food web," in *Radziejewska. Biological Oceanography of the Baltic Sea*, eds P. Snoeijs-Leijonmalm and H. Schubert (Berlin: Springer), 281–332.

Antoni, J. S., Almandoz, G. O., Ferrario, M. E., Hernando, M. P., Varela, D. E., Rozema, P. D., et al. (2020). Response of a natural Antarctic phytoplankton assemblage to changes in temperature and salinity. *J. Exp. Mar. Bio. Ecol.* 532:151444. doi: 10.1016/j.jembe.2020.151444

Arrigo, K. R., Robinson, D. H., Worthen, D. L., Dunbar, R. B., DiTullio, G. R., VanWoert, M., et al. (1999). Phytoplankton community structure and the drawdown of nutrients and CO2 in the Southern ocean. *Science* 283, 365–367. doi: 10.1126/science.283.5400.365

Asper, V. L., and Smith, W. O. (2019). Variations in the abundance and distribution of aggregates in the Ross sea. Antarctica. *Elementa* 7:23. doi: 10.1525/elementa.355

Barlow, R. G. (1982). Phytoplankton ecology in the Southern Benguela current. III. dynamics of a bloom. *J. Exp. Mar. Bio. Ecol.* 165, 171–189.

Bartolomeo, M. P., and Maisano, F. (2006). Validation of a reversed-phase HPLC method for quantitative amino acid analysis. *J. Biomol. Tech.* 17, 131–137.

Basu, S., and Mackey, K. R. M. (2018). Phytoplankton as key mediators of the biological carbon pump: their responses to a changing climate. *Sustain* 10:1. doi: 10.3390/su10030869

Becker, W., and Richmond, A. (2004). "Microalgae in human and animal nutrition," in *Handbook of Microalgal Culture Biotechnology Applied Phycology* (London: Blackwell Science).

Berdalet, E., Latasa, M., and Estrada, M. (1994). Effects of nitrogen and phosphorus starvation on nucleic acid and protein content of *Heterocapsa* sp. *J. Plankton Res.* 16, 303–316. doi: 10.1093/plankt/16.4.303

Bhavya, P. S., Kim, B. K., Jo, N., Kim, K., Kang, J. J., Lee, J. H., et al. (2019). A review on the macromolecular compositions of phytoplankton and the implications for aquatic biogeochemistry. *Ocean Sci. J.* 54, 1–14. doi: 10.1007/s12601-018-0061-8

Bligh, E. G., and Dyer, W. J. (1959). A rapid method of total lipid extraction and purification. *Can. J. Biochem. Physiol.* 37, 911–917. doi: 10.1139/o59-099

Bodungen, B. V., Smetacek, V. S., Tilzer, M. M., and Zeitzschel, B. (1986). Primary production and sedimentation during spring in the Antarctic Peninsula region. *Deep Sea Res. Part A Oceanogr. Res. Pap.* 33, 177–194. doi: 10.1016/0198-0149(86)90117-2

Boyd, C. E. (1989). *Water Quality Management and Aeration in Shrimp Farming. Fisheries and Allied Aquaculture Departmental. Series No. 2.* Auburn, AL: Auburn University, Alabama Agricultural Experiment Station, 83.

Bracegirdle, T. J., and Stephenson, D. B. (2012). Higher precision estimates of regional polar warming by ensemble regression of climate model projections. *Clim. Dyn.* 39, 2805–2821. doi: 10.1007/s00382-012-1330-3

Bracegirdle, T. J., Connolley, W. M., and Turner, J. (2008). Antarctic climate change over the twenty first century. *J. Geophys. Res. Atmos.* 8:D03103. doi: 10.1029/2007JD008933

Brzezinski, M. A. (1985). The Si: C: N ratio of marine diatoms: interspecific variability and the effect of some environmental variables 1. *J. Phycol.* 21, 347–357. doi: 10.1111/j.0022-3646.1985.00347.x

Burford, M. (1997). Phytoplankton dynamics in shrimp ponds. *Aquac. Res.* 28, 351–360. doi: 10.1111/j.1365-2109.1997.tb01052.x

Coale, K. H., Wang, X., Tanner, S. J., and Johnson, K. S. (2003). Phytoplankton growth and biological response to iron and zinc addition in the Ross Sea and Antarctic circumpolar current along 170°W. *Deep. Res. Part II Top. Stud. Oceanogr.* 50, 635–653. doi: 10.1016/S0967-0645(02)00588-X

Comiso, J. C., Kwok, R., Martin, S., and Gordon, A. L. (2011). Variability and trends in sea ice extent and ice production in the Ross sea. *J. Geophys. Res. Oceans* 116:C04021. doi: 10.1029/2010JC006391

Cowie, G. L., and Hedges, J. I. (1992). Improved amino acid quantification in environmental samples: charge-matched recovery standards and reduced analysis time. *Mar. Chem.* 37, 223–238. doi: 10.1016/0304-4203(92)90079-p

Danovaro, R., Dell'Anno, A., Pusceddu, A., Marrale, D., Della Croce, N., Fabiano, M., et al. (2000). Biochemical composition of pico-, nano- and micro-particulate organic matter and bacterioplankton biomass in the oligotrophic Cretan sea (NE Mediterranean). *Prog. Oceanogr.* 46, 279–310. doi: 10.1016/s0079-6611(00)00023-9

Dauwe, B., and Middelburg, J. J. (1998). Amino acids and hexosamines as indicators of organic matter degradation state in North sea sediments. *Limnol. Oceanogr.* 43, 782–798. doi: 10.4319/lo.1998.43.5.0782

Dauwe, B., Middelburg, J. J., Herman, P. M. J., and Heip, C. H. R. (1999). Linking diagenetic alteration of amino acids and bulk organic matter reactivity. *Limnol. Oceanogr.* 44, 1809–1814. doi: 10.4319/lo.1999.44.7.1809

de Madariaga, I. (1992). Interspecific differences in the photosynthetic carbon metabolism of marine phytoplankton. *Mar. Biol.* 114, 509–515. doi: 10.1007/BF00350043

Dehairs, F., Kopczynska, E., Nielsen, P., Lancelot, C., Bakker, D. C. E., Koeve, W., et al. (1997). δ13C of Southern Ocean suspended organic matter during spring and early summer: regional and temporal variability. *Deep. Res. Part II Top. Stud. Oceanogr.* 144, 129–142. doi: 10.1016/s0967-0645(96)00073-2

Dell'Anno, A., Fabiano, M., Mei, M. L., and Danovaro, R. (2000). Enzymatically hydrolysed protein and carbohydrate pools in deep-sea sediments: estimates of the potentially bioavailable fraction and methodological considerations. *Mar. Ecol. Prog. Ser.* 196, 15–23. doi: 10.3354/meps196015

Dittmar, T., Fitznar, H. P., and Kattner, G. (2001). Origin and biogeochemical cycling of organic nitrogen in the Eastern Arctic ocean as evident from D- and L-amino acids. *Geochim. Cosmochim. Acta* 65, 4103–4114. doi: 10.1016/s0016-7037(01)00688-3

DiTullio, G. R., and Smith, W. O. (1996). Spatial patterns in phytoplankton biomass and pigment distributions in the Ross sea. *J. Geophys. Res. C Ocean* 101, 18467–18477. doi: 10.1029/96JC00034

DiTullio, G. R., Geesey, M. E., Leventer, A., and Lizotte, M. P. (2011). Algal pigment ratios in the Ross Sea: implications for chemtax analysis of Southern Ocean data. *Adv. Earth Spaces Sci.* 78, 35–51. doi: 10.1029/078ars03

Duan, S., and Bianchi, T. S. (2007). Particulate and dissolved amino acids in the lower mississippi and Pearl rivers (USA). *Mar. Chem.* 107, 214–229. doi: 10.1016/j.marchem.2007.07.003

Dubois, M., Gilles, K. A., Hamilton, J. K., Rebers, P. A., and Smith, F. (1956). Colorimetric method for determination of sugars and related substances. *Anal. Chem.* 28, 350–356. doi: 10.1021/ac60111a017

Ducklow, H. W., Steinberg, D. K., and Buesseler, K. O. (2001). Upper ocean carbon export and the biological pump. *Oceanography* 14, 50–58. doi: 10.5670/oceanog.2001.06

Dzierzbicka-Głowacka, L., Kuliński, K., Maciejewska, A., Jakacki, J., and Pempkowiak, J. (2010). Particulate organic carbon in the southern baltic sea: numerical simulations and ttyexperimental data. *Oceanologia* 52, 621–648. doi: 10.5697/oc.52-4.621

Fabiano, M., Povero, P., and Danovaro, R. (1993). Distribution and composition of particulate organic matter in the Ross sea (Antarctica). *Polar Biol.* 13, 525–533. doi: 10.1007/BF00236394

Fernández-Reiriz, M. J., Perez-Camacho, A., Ferreiro, M. J., Blanco, J., Planas, M., Campos, M. J., et al. (1989). Biomass production and variation in the biochemical profile (total protein, carbohydrates, RNA, lipids and fatty acids) of seven species of marine microalgae. *Aquaculture* 83, 17–37. doi: 10.1016/0044-8486(89)90057-4

Fichez, R. (1991). Composition and fate of organic matter in submarine cave sediments; implications for the biogeochemical cycle of organic carbon. *Oceanol. Acta.* 14, 369–377.

Finkel, Z. V., Beardall, J., Flynn, K. J., Quigg, A., Rees, T. A. V., and Raven, J. A. (2010). Phytoplankton in a changing world: cell size and elemental stoichiometry. *J. Plankton Res.* 32, 119–137. doi: 10.1093/plankt/fbp098

Fry, B., and Sherr, E. B. (1989). δ13C measurements as indicators of carbon flow in marine and freshwater ecosystems. *Ecol. Stud.* 68, 196–229. doi: 10.1007/978-1-4612-3498-2_12

Goñi, M. A., Teixeira, M. J., and Perkeya, D. W. (2003). Sources and distribution of organic matter in a river-dominated estuary (Winyah Bay, SC, USA). *Estuar. Coast. Shelf Sci.* 57, 1023–1048. doi: 10.1016/s0272-7714(03)00008-8

Gruner, D. S., Smith, J. E., Seabloom, E. W., Sandin, S. A., Ngai, J. T., Hillebrand, H., et al. (2008). A cross-system synthesis of consumer and nutrient resource control on producer biomass. *Ecol. Lett.* 11, 740–755. doi: 10.1111/j.1461-0248.2008.01192.x

Guisande, C., Maneiro, I., and Riveiro, I. (1999). Homeostasis in the essential amino acid composition of the marine copepod *Euterpina acutifrons*. *Limnol. Oceanogr.* 44, 691–696. doi: 10.4319/lo.1999.44.3.0691

Guisande, C., Maneiro, I., Riveiro, I., Barreiro, A., and Pazos, Y. (2002). Estimation of copepod trophic niche in the field using amino acids and marker pigments. *Mar. Ecol. Prog. Ser.* 239, 147–156. doi: 10.3354/meps239147

Guisande, C., Riveiro, I., and Maneiro, I. (2000). Comparisons among the amino acid composition of females, eggs and food to determine the relative importance of food quantity and food quality to copepod reproduction. *Mar. Ecol. Prog. Ser.* 202, 135–142. doi: 10.3354/meps202135

Gulati, R. D., and Demott, W. R. (1997). The role of food quality for zooplankton: remarks on the state -of-the-art, perspectives and priorities. *Freshw. Biol.* 38, 753–768. doi: 10.1046/j.1365-2427.1997.00275.x

Haberman, K. L., Ross, R. M., and Quetin, L. B. (2003). Diet of the Antarctic krill (*Euphausia superba* Dana): II. selective grazing in mixed phytoplankton assemblages. *J. Exp. Mar. Bio. Ecol.* 283, 97–113. doi: 10.1016/s0022-0981(02)00467-7

Handa, N. (1970). "Dissolved and particulate carbohydrates,". in *Organic Matter in Natural Waters*. ed. D. W. Hood. Alaska: Instutional Marine Science, 129–152

Harmelin-Vivien, M., Loizeau, V., Mellon, C., Beker, B., Arlhac, D., Bodiguel, X., et al. (2008). Comparison of C and N stable isotope ratios between surface particulate organic matter and microphytoplankton in the Gulf of lions (NW Mediterranean). *Cont. Shelf Res.* 28, 1911–1919. doi: 10.1016/j.csr.2008.03.002

Harvey, H. R., Tuttle, J. H., and Bell, J. T. (1995). Kinetics of phytoplankton decay during simulated sedimentation: changes in biochemical composition and microbial activity under oxic and anoxic conditions. *Geochim. Cosmochim. Acta* 59, 3367–3377. doi: 10.1016/0016-7037(95)00217-n

Hayashi, T., Suitani, Y., Murakami, M., Yamaguchi, K., Konosu, S., and Noda, H. (1986). Chemistry and utilization of plankton. VII. protein and amino acid compositions of five species of marine phytoplankton. *Nippon Suisan Gakkaishi.* 52, 337–343. doi: 10.2331/suisan.52.337

Hecky, R. E., Mopper, K., Kilham, P., and Degens, E. T. (1973). The amino acid and sugar composition of diatom cell-walls. *Mar. Biol.* 19, 323–331. doi: 10.1007/BF00348902

Henderson, J. W., Ricker, R. D., Bidlingmeyer, B. A., and Woodward, C. (2000). *Rapid, Accurate, Sensitive, and Reproducible HPLC Analysis of Amino Acids*. Santa Clara: Agilent Technologies

Hernando, M., Varela, D. E., Malanga, G., Almandoz, G. O., and Schloss, I. R. (2020). Effects of climate-induced changes in temperature and salinity on phytoplankton physiology and stress responses in coastal Antarctica. *J. Exp. Mar. Bio. Ecol.* 53:151400. doi: 10.1016/j.jembe.2020.151400

Hogle, S. L., Dupont, C. L., Hopkinson, B. M., King, A. L., Buck, K. N., Roe, K. L., et al. (2018). Pervasive iron limitation at subsurface chlorophyll maxima of the California current. *Proc. Natl. Acad. Sci. U. S. A.* 115, 13300–13305. doi: 10.1073/pnas.1813192115

Hong, Y., Smith, W. O., and White, A. M. (1997). Studies on transparent exopolymer particles (TEP) produced in the ross sea (Antarctica) and by *Phaeocystis antarctica* (*Prymnesiophyceae*). *J. Phycol.* 33, 368–376. doi: 10.1111/j.0022-3646.1997.00368.x

Hubberten, U., Lara, R. J., and Kattner, G. (1995). Refractory organic compounds in polar waters: relationship between humic substances and amino acids in the Arctic and Antarctic. *J. Mar. Res.* 53, 137–149. doi: 10.1357/002224095321332322

Ingalls, A. E., Liu, Z., and Lee, C. (2006). Seasonal trends in the pigment and amino acid compositions of sinking particles in biogenic CaCO3 and SiO2 dominated regions of the Pacific sector of the Southern Ocean along 170°W. *Deep. Res. Part I Oceanogr. Res. Pap.* 53, 836–859. doi: 10.1016/j.dsr.2006.01.004

Jo, N., Kang, J. J., Park, W. G., Lee, B. R., Yun, M. S., Lee, J. H., et al. (2017). Seasonal variation in the biochemical compositions of phytoplankton and zooplankton communities in the southwestern East/Japan Sea. *Deep. Res. Part II Top. Stud. Oceanogr.* 143, 82–90. doi: 10.1016/j.dsr2.2016.12.001

Ju, Z. Y., Forster, I., Conquest, L., Dominy, W., Kuo, W. C., and David Horgen, F. (2008). Determination of microbial community structures of shrimp floc cultures by biomarkers and analysis of floc amino acid profiles. *Aquac. Res.* 39, 118–133. doi: 10.1111/j.1365-2109.2007.01856.x

Kalachova, G. S., Kolmakova, A. A., Gladyshev, M. I., Kravchuk, E. S., and Ivanova, E. A. (2004). Seasonal dynamics of amino acids in two small Siberian reservoirs dominated by prokaryotic and eukaryotic phytoplankton. *Aquat. Ecol.* 38, 3–15. doi: 10.1023/b:aeco.0000021044.55658.71

Kang, J. J., Lee, J. H., Kim, H. C., Lee, W. C., Lee, D., Jo, N., et al. (2018). Monthly variations of phytoplankton community in geoje-hansan bay of the southern part of Korea based on HPLC pigment analysis. *J. Coast. Res.* 85, 356–360. doi: 10.2112/SI85-072.1

Kaufman, D. E., Friedrichs, M. A. M., Smith, W. O., Hofmann, E. E., Dinniman, M. S., and Hemmings, J. C. P. (2017). Climate change impacts on southern Ross Sea phytoplankton composition, productivity, and export. *J. Geophys. Res. Ocean.* 122, 2339–2359. doi: 10.1002/2016JC012514

Kharbush, J. J., Close, H. G., Van Mooy, B. A. S., Arnosti, C., Smittenberg, R. H., Le Moigne, F. A. C., et al. (2020). Particulate organic carbon deconstructed: molecular and chemical composition of particulate organic carbon in the ocean. *Front. Mar. Sci.* 7:518. doi: 10.3389/fmars.2020.00518

Kim, B. K., Lee, S. H., Ha, S. Y., Jung, J., Kim, T. W., Yang, E. J., et al. (2018). Vertical Distributions of macromolecular composition of particulate organic matter in the water column of the amundsen sea polynya during the summer in 2014. *J. Geophys. Res. Ocean.* 123, 1393–1405. doi: 10.1002/2017JC013457

Kirk, J. T. O. (1985). "Effects of suspensoids (turbidity) on penetration of solar radiation in aquatic ecosystems," in *Perspectives in Southern Hemisphere Limnology. Developments in Hydrobiology*, eds B. R. Davies and R. D. Walmsley (Dordrecht: Springer).

Klausmeier, C. A., Litchman, E., Daufresne, T., and Levin, S. A. (2008). Phytoplankton stoichiometry. *Ecol. Res.* 23, 479–485.

Kleppel, G. S., Burkart, C. A., and Houchin, L. (1998). Nutrition and the regulation of egg production in the calanoid copepod *Acartia tonsa*. *Limnol. Oceanogr.* 43, 1000–1007. doi: 10.4319/lo.1998.43.5.1000

Kolmakova, A. A., and Kolmakov, V. I. (2019). Amino acid composition of green microalgae and diatoms, cyanobacteria, and zooplankton (Review). *Inl. Water Biol.* 12, 452–461. doi: 10.1134/s1995082919040060

Lamb, A. L., Wilson, G. P., and Leng, M. J. (2006). A review of coastal palaeoclimate and relative sea-level reconstructions using δ13C and C/N ratios in organic material. *Earth Sci. Rev.* 75, 29–57. doi: 10.1016/j.earscirev.2005.10.003

Lancelot, C., and Mathot, S. (1985). Biochemical fractionation of primary production by phytoplankton in Belgian coastal waters during short- and long-term incubations with 14C-bicarbonate - I. mixed diatom population. *Mar. Biol.* 86, 219–226. doi: 10.1007/BF00397507

Le Moigne, F. A. C., Boye, M., Masson, A., Corvaisier, R., Grossteffan, E., Guéneugues, A., et al. (2013). Description of the biogeochemical features of the subtropical southeastern Atlantic and the Southern Ocean south of South Africa during the austral summer of the international polar year. *Biogeosciences* 10, 281–295. doi: 10.5194/bg-10-281-2013

Le Moigne, F. A. C., Cisternas-Novoa, C., Piontek, J., Maßmig, M., and Engel, A. (2017). On the effect of low oxygen concentrations on bacterial degradation of sinking particles. *Sci. Rep.* 7:16722.

Lee, C., Wakeham, S., and Arnosti, C. (2004). Particulate organic matter in the sea: the composition conundrum. *Ambio J. Hum. Environ.* 33, 565–575. doi: 10.1579/0044-7447-33.8.565

Lee, S. H., and Whitledge, T. E. (2005). Primary and new production in the deep Canada basin during summer 2002. *Polar Biol.* 28, 190–197. doi: 10.1007/s00300-004-0676-3

Lee, S. H., Whitledge, T. E., and Kang, S. H. (2008). Carbon uptake rates of sea ice algae and phytoplankton under different light intensities in a landfast sea ice zone, barrow, Alaska. *Arctic* 61, 233–346.

Lehmann, M. F., Carstens, D., Deek, A., McCarthy, M., Schubert, C. J., and Zopfi, J. (2020). Amino acid and amino sugar compositional changes during in vitro degradation of algal organic matter indicate rapid bacterial re-synthesis. *Geochim. Cosmochim. Acta* 283, 67–84. doi: 10.1016/j.gca.2020.05.025

Liebezeit, G., and Bölter, M. (1986). Distribution of particulate amino acids in the Bransfield Strait. *Polar Biol.* 5, 199–206. doi: 10.1007/BF00446087

Lobbes, M., Kattner, G., and Fitznar, H. P. (1999). Determination of enantiomeric amino acids with high-performance liquid chromatography and pre-column derivatisation with o -phthaldialdehyde and N -isobutyrylcysteine in seawater

and fossil samples (mollusks). *J. Chromatogr. A* 832, 123–132. doi: 10.1016/s0021-9673(98)01000-0

Louropoulou, E., Gledhill, M., Browning, T. J., Desai, D. K., Barraqueta, J. L. M., Tonnard, M., et al. (2019). Regulation of the phytoplankton heme B iron pool during the North Atlantic spring bloom. *Front. Microbiol.* 10:1566. doi: 10.3389/fmicb.2019.01566

Lowe, A. T., Galloway, A. W. E., Yeung, J. S., Dethier, M. N., and Duggins, D. O. (2014). Broad sampling and diverse biomarkers allow characterization of nearshore particulate organic matter. *Oikos* 123, 1341–1354. doi: 10.1111/oik.01392

Lowry, O. H., Rosebrough, N. J., Farr, A. L., and Randall, R. J. (1951). Protein measurement with the Folin phenol reagent. *J. Biol. Chem.* 193, 265–275. doi: 10.1016/s0021-9258(19)52451-6

Lyver, P. O. B., MacLeod, C. J., Ballard, G., Karl, B. J., Barton, K. J., Adams, J., et al. (2011). Intra-seasonal variation in foraging behavior among Adélie penguins (*Pygocelis adeliae*) breeding at Cape Hallett, Ross sea, Antarctica. *Polar Biol.* 34, 49–67. doi: 10.1007/s00300-010-0858-0

Mackey, M. D., Mackey, D. J., Higgins, H. W., and Wright, S. W. (1996). CHEMTAX - A program for estimating class abundances from chemical markers: application to HPLC measurements of phytoplankton. *Mar. Ecol. Prog. Ser.* 144, 265–283. doi: 10.3354/meps144265

Mague, T. H., Friberg, E., Hughes, D. J., and Morris, I. (1980). Extracellular release of carbon by marine phytoplankton; a physiological approach. *Limnol. Oceanogr.* 25, 262–279. doi: 10.4319/lo.1980.25.2.0262

Mangoni, O., Saggiomo, M., Bolinesi, F., Castellano, M., Povero, P., Saggiomo, V., et al. (2019). Phaeocystis antarctica unusual summer bloom in stratified antarctic coastal waters (Terra Nova Bay, Ross sea). *Mar. Environ. Res.* 151:104733. doi: 10.1016/j.marenvres.2019.05.012

Mangoni, O., Saggiomo, V., Bolinesi, F., Margiotta, F., Budillon, G., Cotroneo, Y., et al. (2017). Phytoplankton blooms during austral summer in the Ross sea, Antarctica: driving factors and trophic implications. *PLoS One* 12:0176033. doi: PMIDNOPMID10.1371/journal.phone.0176033.g005

Marsh, J. B., and Weinstein, D. B. (1966). Simple charring method for determination of lipids. *J. Lipid Res.* 7, 574–576.

Mathot, S., Smith, W. O., Carlson, C. A., Garrison, D. L., Gowing, M. M., and Vickers, C. L. (2000). Carbon partitioning within phaeocystis antarctica (*Prymnesiophyceae*) colonies in the ross sea, antarctica. *J. Phycol.* 36, 1049–1056. doi: 10.1046/j.1529-8817.2000.99078.x

Mayzaud, P., Claustre, H., and Augier, P. (1990). Effect of variable nutrient supply on fatty acid composition of phytoplankton grown in an enclosed experimental ecosystem. *Mar. Ecol. Prog. Ser.* 60, 123–140. doi: 10.3354/meps060123

Mente, E., Coutteau, P., Houlihan, D., Davidson, I., and Sorgeloos, P. (2002). Protein turnover, amino acid profile and amino acid flux in juvenile shrimp *Litopenaeus vannamei*: effects of dietary protein source. *J. Exp. Biol.* 205, 3107–3122.

Misic, C., Covazzi Harriague, A., Mangoni, O., Aulicino, G., Castagno, P., and Cotroneo, Y. (2017). Effects of physical constraints on the lability of POM during summer in the Ross sea. *J. Mar. Syst.* 166, 132–143. doi: 10.1016/j.jmarsys.2016.06.012

Moal, J., Martin-Jezequel, V., Harris, R., Samain, J., and Poulet, S. (1987). Interspecific and intraspecific variability of the chemical composition of marine phytoplankton. *Oceanol. Acta* 10, 339–346.

Montagnes, D. J. S., Berges, J. A., Harrison, P. J., and Taylor, F. J. R. (1994). Estimating carbon, nitrogen, protein, and chlorophyll a from volume in marine phytoplankton. *Limnol. Oceanogr.* 39, 1044–1060. doi: 10.4319/lo.1994.39.5.1044

Moore, C. M., Mills, M. M., Arrigo, K. R., Berman-Frank, I., Bopp, L., Boyd, P. W., et al. (2013). Processes and patterns of oceanic nutrient limitation. *Nat. Geosci.* 6, 701–710. doi: 10.1038/ngeo1765

Morris, I., Glover, H. E., and Yentsch, C. S. (1974). Products of photosynthesis by marine phytoplankton: the effect of environmental factors on the relative rates of protein synthesis. *Mar. Biol.* 27, 1–9. doi: 10.1007/BF00394754

Muller-Navarra, D. (1995). Evidence that a highly unsaturated fatty acid limits Daphnia growth in nature. *Arch. Fur. Hydrobiol.* 132, 297–307.

Müller-Navarra, D. C. (2008). Food web paradigms: the biochemical view on trophic interactions. *Int. Rev. Hydrobiol.* 93, 489–505. doi: 10.1002/iroh.200711046

Myklestad, S. (1974). Production of carbohydrates by marine planktonic diatoms. I. comparison of nine different species in culture. *J. Exp. Mar. Bio. Ecol.* 15, 261–274. doi: 10.1016/0022-0981(74)90049-5

Nelson, D. M., DeMaster, D. J., Dunbar, R. B., and Smith, W. O. (1996). Cycling of organic carbon and biogenic silica in the Southern ocean: estimates of water-column and sedimentary fluxes on the Ross sea continental shelf. *J. Geophys. Res. C Ocean* 5, 146–153. doi: 10.1029/96JC01573

Nelson, D. M., Smith, W. O., Muench, R. D., Gordon, L. I., Sullivan, C. W., and Husby, D. M. (1989). Particulate matter and nutrient distributions in the ice-edge zone of the Weddell sea: relationship to hydrography during late summer. *Deep Sea Res. Part A, Oceanogr. Res. Pap.* 36, 191–209. doi: 10.1016/0198-0149(89)90133-7

Oksanen, L., and Oksanen, T. (2000). The logic and realism of the hypothesis of exploitation ecosystems. *Am. Nat.* 153, 703–723. doi: 10.1086/303354

Olson, R. J., Sosik, H. M., Chekalyuk, A. M., and Shalapyonok, A. (2000). Effects of iron enrichment on phytoplankton in the Southern Ocean during late summer: active fluorescence and flow cystometric analyses. *Deep. Res. Part II Top. Stud. Oceanogr.* 47, 3181–3200. doi: 10.1016/s0967-0645(00)00064-3

Oser, B. L. (1959). "An integrated essential amino acid index for predicting the biological value of proteins," in *Protein and Amino Acid Nutrition*, ed. A. A. Albanese (Amsterdam: Elsevier).

Parsons, T. R., Maita, Y., and Lalli, C. M. (1984). A manual of chemical & biological methods for seawater analysis. *Mar. Pollut. Bull.* 15, 419–420.

Peloquin, J. A., and Smith, W. O. (2007). Phytoplankton blooms in the Ross Sea, Antarctica: interannual variability in magnitude, temporal patterns, and composition. *J. Geophys. Res. Ocean.* 112:C08013. doi: 10.1029/2006JC003816

Peñaflorida, V. D. (1989). An evaluation of indigenous protein sources as potential component in the diet formulation for tiger prawn, *Penaeus monodon*, using essential amino acid index (EAAI). *Aquaculture* 83, 319–330. doi: 10.1016/0044-8486(89)90043-4

Petersson, M., and Floderus, S. (2001). Use of amino acid composition to investigate settling and resuspension of a spring bloom in the southern Skagerrak. *Limnol. Oceanogr.* 46, 1111–1120. doi: 10.4319/lo.2001.46.5.1111

Pinkerton, M. H., Bradford-Grieve, J. M., and Hanchet, S. M. (2010). A balanced model of the food web of the Ross sea, Antarctica. *CCAMLR Sci.* 17, 1–31.

Rau, G. H., Sullivan, C. W., and Gordon, L. I. (1991). δ 13C and δ15N variations in Weddell sea particulate organic matter. *Mar. Chem.* 35, 355–369. doi: 10.1016/s0304-4203(09)90028-7

Rau, G. H., Takahashi, T., and Des Marais, D. J. (1989). Latitudinal variations in plankton δ13C: implications for CO2 and productivity in past oceans. *Nature* 341, 516–518. doi: 10.1038/341516a0

Rickard, G., and Behrens, E. (2016). CMIP5 earth system models with biogeochemistry: a Ross sea assessment. *Antarct. Sci.* 5, 1–20. doi: 10.1029/078ars01

Riley, G. A. (1971). Particulate organic matter in sea water. *Adv. Mar. Biol.* 8, 1–118. doi: 10.1016/s0065-2881(08)60491-5

Ríos, A. F., Fraga, F., Pérez, F. F., and Figueiras, F. G. (1998). Chemical composition of phytoplankton and particulate organic matter in the Ría de Vigo (NW Spain). *Sci. Mar.* 62, 257–271.

Rogers, J., and Dunbar, R. (1993). Carbon isotopic composition of particulate organic carbon in Ross sea surface waters during austral summer. *Antarct. J. U. S.* 28, 81–83.

Sabadel, A. J. M., Van Oostende, N., Ward, B. B. S., Woodward, E. M., Van Hale, R., and Frew, R. D. (2019). Characterization of particulate organic matter cycling during a summer North Atlantic phytoplankton bloom using amino acid C and N stable isotopes. *Mar. Chem.* 214:103670. doi: 10.1016/j.marchem.2019.103670

Saito, M. A., Goepfert, T. J., and Ritt, J. T. (2008). Some thoughts on the concept of colimitation: three definitions and the importance of bioavailability. *Limnol. Oceanogr.* 53, 276–290. doi: 10.4319/lo.2008.53.1.0276

Sarmiento, J. L., Gruber, N., Brzezinski, M. A., and Dunne, J. P. (2004). High-latitude controls of thermocline nutrients and low latitude biological productivity. *Nature* 427, 56–60. doi: 10.1038/nature02127

Schine, C. M. S., Van Dijken, G., and Arrigo, K. R. (2016). Spatial analysis of trends in primary production and relationship with large-scale climate variability in the Ross sea, Antarctica (1997-2013). *J. Geophys. Res. Ocean* 121, n/a–n/a. doi: 10.1002/2015JC011014

Schoemann, V., Becquevort, S., Stefels, J., Rousseau, V., and Lancelot, C. (2005). Phaeocystis blooms in the global ocean and their controlling mechanisms: a review. *J. Sea Res.* 53, 43–66. doi: 10.1016/j.seares.2004.01.008

Scott, J. M. (1980). Effect of growth rate of the food alga on the growth/ingestion efficiency of a marine herbivore. *J. Mar. Biol. Assoc. U. K.* 60, 681–702. doi: 10.1017/s0025315400040376

Sedwick, P. N., and Ditullio, G. R. (1997). Regulation of algal blooms in Antarctic shelf waters by the release of iron from melting sea ice. *Geophys. Res. Lett.* 24, 2515–2518. doi: 10.1029/97GL02596

Sedwick, P. N., Di Tullio, G. R., and Mackey, D. J. (2000). Iron and manganese in the Ross sea, seasonal iron limitation in Antarctic. *J. Geophys. Res. Ocean* 102, 11321–11336. doi: 10.1029/2000jc000256

Shields, A. R., and Smith, W. O. (2009). Size-fractionated photosynthesis/irradiance relationships during Phaeocystis antarctica-dominated blooms in the Ross sea, Antarctica. *J. Plankton Res.* 31, 701–712. doi: 10.1093/plankt/fbp022

Shields, M. R., Bianchi, T. S., Osburn, C. L., Kinsey, J. D., Ziervogel, K., Schnetzer, A., et al. (2019). Linking chromophoric organic matter transformation with biomarker indices in a marine phytoplankton growth and degradation experiment. *Mar. Chem.* 214:103665. doi: 10.1016/j.marchem.2019.103665

Siezen, R. J., and Mague, T. H. (1978). Amino acids in suspended particulate matter from oceanic and coastal waters of the Pacific. *Mar. Chem.* 6, 215–231. doi: 10.1016/0304-4203(78)90031-2

Smetacek, V., Assmy, P., and Henjes, J. (2004). The role of grazing in structuring Southern Ocean pelagic ecosystems and biogeochemical cycles. *Antarct. Sci.* 16, 541–558. doi: 10.1017/s0954102004002317

Smith, A. E., and Morris, I. (1980). Pathways of carbon assimilation in phytoplankton from the Antarctic ocean. *Limnol. Oceanogr.* 85, 865–872. doi: 10.4319/lo.1980.25.5.0865

Smith, W. O., Ainley, D. G., Arrigo, K. R., and Dinniman, M. S. (2014). The oceanography and ecology of the ross sea. *Ann. Rev. Mar. Sci.* 6, 469–487.

Smith, W. O., and Asper, V. L. (2001). The influence of phytoplankton assemblage composition on biogeochemical characteristics and cycles in the southern Ross sea, Antarctica. *Deep. Res. Part I Oceanogr. Res. Pap.* 48, 137–161. doi: 10.1016/s0967-0637(00)00045-5

Smith, W. O., Asper, V., Tozzi, S., Liu, X., and Stammerjohn, S. E. (2011). Surface layer variability in the Ross sea, Antarctica as assessed by in situ fluorescence measurements. *Prog. Oceanogr.* 88, 28–45. doi: 10.1016/j.pocean.2010.08.002

Smith, W. O., Dennett, M. R., Mathot, S., and Caron, D. A. (2003). The temporal dynamics of the flagellated and colonial stages of Phaeocystis antarctica in the Ross sea. *Deep. Res. Part II Top. Stud. Oceanogr.* 50, 605–617. doi: 10.1016/s0967-0645(02)00586-6

Smith, W. O., Marra, J., Hiscock, M. R., and Barber, R. T. (2000). The seasonal cycle of phytoplankton biomass and primary productivity in the Ross sea, Antarctica. *Deep. Res. Part II Top. Stud. Oceanogr.* 47, 3119–3140. doi: 10.1016/s0967-0645(00)00061-8

Stammerjohn, S. E., Martinson, D. G., Smith, R. C., Yuan, X., and Rind, D. (2008). Trends in Antarctic annual sea ice retreat and advance and their relation to El Niño–Southern Oscillation and Southern Annular Mode variability. *J. Geophys. Res.* 113:C03S90. doi: 10.1029/2007jc004269.a

Sterner, R., and Elser, J. (2002). "Ecological stoichiometry," in *The Biology of Elements from Molecules to the Biosphere*, eds R. W. Sterner, J. J. Elser, and P. M. Vitousek (Princeton, NJ: Princeton University Press).

Sunda, W. G., and Huntaman, S. A. (1997). Interrelated influence of iron, light and cell size on marine phytoplankton growth. *Nature* 390, 389–392. doi: 10.1038/37093

Tang, K. W., Smith, W. O., Elliott, D. T., and Shields, A. R. (2008). Colony size of Phaeocystis antarctica (Prymnesiophyceae) as influenced by zooplankton grazers. *J. Phycol.* 44, 1372–1378. doi: 10.1111/j.1529-8817.2008.00595.x

Tonon, T., Harvey, D., Larson, T. R., and Graham, I. A. (2002). Long chain polyunsaturated fatty acid production and partitioning to triacylglycerols in four microalgae. *Phytochemistry* 61, 15–24. doi: 10.1016/s0031-9422(02)00201-7

Tremblay, L., Caparros, J., Leblanc, K., and Obernosterer, I. (2015). Origin and fate of particulate and dissolved organic matter in a naturally iron-fertilized region of the Southern ocean. *Biogeosciences* 12, 607–621. doi: 10.5194/bg-12-607-2015

Tsukasaki, A., and Tanoue, E. (2010). Chemical characterization and dynamics of particulate combined amino acids in Pacific surface waters. *J. Mar. Syst.* 79, 173–184. doi: 10.1016/j.jmarsys.2009.08.003

Tyson, R. V. (1995). "The nature of organic matter in sediments," in *Sedimentary Organic Matter: Organic Facies and Palynofacies*, ed. R. V. Tyson (London: Chaman & Hall), 7–28.

Vargas, C. A., Escribano, R., and Poulet, S. (2006). Phytoplankton food quality determines time windows for successful zooplankton reproductive pulses. *Ecology* 87, 2992–2999. doi: 10.1890/0012-9658(2006)87[2992:pfqdtw]2.0.co;2

Villinski, J. C., Dunbar, R. B., and Mucciarone, D. A. (2000). Carbon 13 / Carbon 12 ratios of sedimentary organic matter from the Ross sea, Antarctica?: a record of phytoplankton bloom dynamics the carbon isotopic composition of phytoplankton input from sea ice communities enriched increased heterotrophic these fac. *J. Geophys. Res.* 105, 14163–14172. doi: 10.1029/1999jc000309

Volkman, J. K., and Tanoue, E. (2002). Chemical and biological studies of particulate organic matter in the ocean. *J. Oceanogr.* 58, 265–279.

Wada, E., Kadonaga, T., and Matsuo, S. (1975). 15N abundance in nitrogen of naturally occurring substances and global assessment of denitrification from isotopic viewpoint. *Geochem. J.* 9, 139–148. doi: 10.2343/geochemj.9.139

Wada, E., Terazaki, M., Kabaya, Y., and Nemoto, T. (1987). 15N and 13C abundances in the Antartic ocean with emphasis on the biogeochemical structure of the food web. *Deep Sea Res. Part A, Oceanogr. Res. Pap.* 34, 829–841. doi: 10.1016/0198-0149(87)90039-2

Wright, S. W., Thomas, D. P., Marchant, H. J., Higgins, H. W., Mackey, M. D., and Mackey, D. J. (1996). Analysis of phytoplankton of the Australian sector of the Southern ocean: comparisons of microscopy and size frequency data with interpretations of pigment HPLC data using the "CHEMTAX" matrix factorisation program. *Mar. Ecol. Prog. Ser.* 144, 285–298. doi: 10.3354/meps144285

Wu, Y., Dittmar, T., Ludwichowski, K. U., Kattner, G., Zhang, J., Zhu, Z. Y., et al. (2007). Tracing suspended organic nitrogen from the Yangtze river catchment into the East China Sea. *Mar. Chem.* 107, 367–377. doi: 10.1016/j.marchem.2007.01.022

Young, J. N., Goldman, J. A. L., Kranz, S. A., Tortell, P. D., and Morel, F. M. M. (2015a). Slow carboxylation of Rubisco constrains the rate of carbon fixation during *Antarctic phytoplankton* blooms. *New Phytol.* 205, 172–181. doi: 10.1111/nph.13021

Young, J. W., Hunt, B. P. V., Cook, T. R., Llopiz, J. K., Hazen, E. L., Pethybridge, H. R., et al. (2015b). The trophodynamics of marine top predators: current knowledge, recent advances and challenges. *Deep. Res. Part II Top. Stud. Oceanogr.* 113, 170–187. doi: 10.1016/j.dsr2.2014.05.015

Yun, M. S., Joo, H. M., Kang, J. J., Park, J. W., Lee, J. H., Kang, S. H., et al. (2019). Potential implications of changing photosynthetic end-products of phytoplankton caused by sea ice conditions in the Northern Chukchi sea. *Front. Microbiol.* 10:2274. doi: 10.3389/fmicb.2019.02274

Yun, M. S., Lee, D. B., Kim, B. K., Kang, J. J., Lee, J. H., Yang, E. J., et al. (2015). Comparison of phytoplankton macromolecular compositions and zooplankton proximate compositions in the northern Chukchi sea. *Deep. Res. Part II Top. Stud. Oceanogr.* 120, 82–90. doi: 10.1016/j.dsr2.2014.05.018

Zapata, M., Rodríguez, F., and Garrido, J. L. (2000). Separation of chlorophylls and carotenoids from marine phytoplankton: a new HPLC method using a reversed phase C8 column and pyridine-containing mobile phases. *Mar. Ecol. Prog. Ser.* 195, 29–45. doi: 10.3354/meps195029

Zweifel, U. L., Norrman, B., and Hagstrom, A. (1993). Consumption of dissolved organic carbon by marine bacteria and demand for inorganic nutrients. *Mar. Ecol. Prog. Ser.* 101, 23–32. doi: 10.3354/meps101023

Conflict of Interest: The authors declare that the research was conducted in the absence of any commercial or financial relationships that could be construed as a potential conflict of interest.

frontiers in Microbiology

ORIGINAL RESEARCH
published: 11 February 2021
doi: 10.3389/fmicb.2021.618999

Monthly Variation in the Macromolecular Composition of Phytoplankton Communities at Jang Bogo Station, Terra Nova Bay, Ross Sea

*Kwanwoo Kim[1], Jisoo Park[2], Naeun Jo[1], Sanghoon Park[1], Hyeju Yoo[1], Jaehong Kim[1] and Sang Heon Lee[1]**

[1] Department of Oceanography, Pusan National University, Busan, South Korea, [2] Division of Ocean Sciences, Korea Polar Research Institute, Incheon, South Korea

Organic carbon fixed by photosynthesis of phytoplankton during the polar growing period could be important for their survival and consumers during the long polar night. Differences in biochemical traits of phytoplankton between ice-free and polar night periods were investigated in biweekly water samples obtained at the Korean "Jang Bogo Station" located in Terra Nova Bay, Antarctica. The average concentration of total Chl-*a* from phytoplankton dominated by micro-sized species from the entire sampling period was 0.32 $\mu g\ L^{-1}$ (SD = ± 0.88 $\mu g\ L^{-1}$), with the highest concentration of 4.29 $\mu g\ L^{-1}$ in February and the lowest concentration of 0.01 $\mu g\ L^{-1}$ during the ice-covered polar night (April–October) in 2015. The highest protein concentration coincided with the peak Chl-*a* concentration in February and decreased rapidly relative to the carbohydrate and lipid concentrations in the early part of polar night. Among the different biochemical components, carbohydrates were the predominant constituent, accounting for 69% (SD = ± 14%) of the total particulate organic matter (POM) during the entire study period. The carbohydrate contributions to the total POM markedly increased from 39 ± 8% during the ice-free period to 73 ± 9% during the polar night period. In comparison, while we found a significant negative correlation (r^2 = 0.92, $p < 0.01$) between protein contributions and carbohydrate contributions, lipid contributions did not show any particular trend with relatively small temporal variations during the entire observation period. The substantial decrease in the average weight ratio of proteins to carbohydrates from the ice-free period (mean ± SD = 1.0 ± 0.3) to the ice-covered period (mean ± SD = 0.1 ± 0.1) indicates a preferential loss of nitrogen-based proteins compared to carbohydrates during the polar night period. Overall, the average food material (FM) concentration and calorific contents of FM in this study were within the range reported previously from the Southern Ocean. The results from this study may serve as important background data for long-term monitoring of the regional and interannual variations in the physiological state and biochemical compositions of phytoplankton resulting from future climate change in Antarctica.

Keywords: Ross Sea (Antarctica), phytoplankton biomass, macromolecular composition, food material, polar night

OPEN ACCESS

Edited by:
Ilka Peeken, Alfred Wegener Institute Helmholtz Centre for Polar and Marine Research (AWI), Germany

Reviewed by:
Sebastien Moreau, Norwegian Polar Institute, Norway
Katherina Petrou, University of Technology Sydney, Australia

****Correspondence:***
Sang Heon Lee
sanglee@pusan.ac.kr

Specialty section:
This article was submitted to Aquatic Microbiology, a section of the journal Frontiers in Microbiology

Received: *19 October 2020*
Accepted: *21 January 2021*
Published: *11 February 2021*

Citation:
Kim K, Park J, Jo N, Park S, Yoo H, Kim J and Lee SH (2021) Monthly Variation in the Macromolecular Composition of Phytoplankton Communities at Jang Bogo Station, Terra Nova Bay, Ross Sea. Front. Microbiol. 12:618999. doi: 10.3389/fmicb.2021.618999

INTRODUCTION

In high latitude polar waters, the light availability of phytoplankton is limited to a short ice-free period during summer (Arrigo and Van Dijken, 2004; Borrione and Schlitzer, 2013). During this period, phytoplankton can synthesize particulate organic matter (POM) through photosynthesis and provide an important food source supporting almost the entire marine ecosystem from the ice-free period to the end of the ice-covered polar night (Falkowski, 1994; Fabiano et al., 1996). Ongoing climate change has caused a remarkable reduction in the Arctic sea ice extent and a small increase in sea ice in the Southern Ocean for several decades (Arrigo et al., 2008; Markus et al., 2009; Liu and Curry, 2010; Comiso, 2012; Hobbs et al., 2016). In addition to the changes in sea ice coverage, the timing and duration of sea ice cover are also changing (Hobbs et al., 2016; Eayrs et al., 2019). In the Southern Ocean, the annual ice-free period has shortened by 2.6 months in the Western Ross Sea but increased by 3.3 months in the Bellingshausen Sea (Parkinson, 1994, 2002; Stammerjohn et al., 2008, 2012; Hobbs et al., 2016; Eayrs et al., 2019). These variations in the ice-free period can affect the duration of the growing season of phytoplankton as well as the nutritional conditions of upper trophic grazers (Quetin et al., 2007; Arrigo et al., 2008; Ross et al., 2008; Markus et al., 2009; Quetin and Ross, 2009; Massom et al., 2013).

Previous studies on the biochemical composition of phytoplankton in the Southern Ocean have been mainly conducted during the Austral summer (Fabiano et al., 1995; Fabiano and Pusceddu, 1998; Kim et al., 2016, 2018; Song et al., 2016), which provides essential information on the physiological state of phytoplankton during the ice-free period. However, these studies do not cover how the biochemical composition changes after the ocean is covered with sea ice again. As mentioned earlier, the ice-free and ice-covered periods and timing of each period vary locally in the Southern Ocean under the potential influence of climate change (Stammerjohn et al., 2008, 2012; Hobbs et al., 2016; Eayrs et al., 2019). These variations could affect the biomass and physiological state of phytoplankton.

The Jang Bogo Station (JBS) is the second overwintering research station of South Korea, located in Terra Nova Bay (TNB) in the Ross Sea (74° 37.4′ S, 164° 12.0′ E). The presence of thick seasonal sea ice and the absence of light during the polar night period limit access of researchers to the coastal region of the Southern Ocean, but the JBS provides the research opportunity during the polar night period. Previous studies have focused on the ice-free period in the TNB (Gambi et al., 2000; Majewska et al., 2013; Illuminati et al., 2017). Our study period covers almost an entire year from the ice-free period in February to the ice-covered polar night period in October 2015. Our objectives in this study were to investigate the biochemical characteristics of phytoplankton and to evaluate the calorific content of phytoplankton as the primary food source during the ice-free and ice-covered periods at the JBS in the TNB, Ross Sea. This study is important as a basis for future studies to understand the impact of current climate change on phytoplankton in the Antarctic Ocean.

MATERIALS AND METHODS

Study Area and Water Sampling

Sample collection was performed at one fixed station (74°37′39.59″S, 164°14′25.75″E) near the Jang Bogo Station (JBS) located in Terra Nova Bay (TNB), Antarctica, from 2 February to 20 October 2015 (**Figure 1**). The polar night period was from 7 May to 7 August, and we divided the whole study period between the ice-free period (February) and the ice-covered period (April–October), including the polar night.

Surface water samples were collected with a 5 L Niskin water sampler when the coastal area was opened in February. During the ice-covered period, sampling was performed from a tank where the under-ice seawater (4–7 m below the sea ice) was continuously pumped. The tank had an inflow of surface seawater, and fresh surface seawater was always supplied in it by an overflowing system. Water samples were placed in dark containers and moved to the laboratory for filtration and further analysis.

Chlorophyll *a* Analysis

Seawater samples for total chlorophyll *a* (Chl-*a*) concentration were filtered onto 25 mm GF/F filters (Whatman, nominal 0.7 μm pore size). For size-fractionated Chl-*a*, the samples were passed sequentially through 20 μm and 2 μm membrane filters and then 47 μm GF/F filters (Whatman, nominal 0.7 μm) with gentle pressure. Chl-*a* was extracted in 90% acetone for 24 h at 4°C following Parsons et al. (1984) and quantified using a Trilogy fluorometer (Turner Designs, United States), which had been calibrated with commercially purified Chl-*a* preparations.

Analysis of Particulate Organic Carbon, Nitrogen, and $\delta^{13}C$

Water samples for particulate organic carbon (POC), nitrogen (PON), and $\delta^{13}C$ of the total microbial community (>0.7 μm) were collected and filtered onto pre-combusted GF/F filters (25 mm) from April to October 2015. In the case of pico-sized POC and PON (0.7–2 μm), samples were filtered through a 2 μm pore-sized membrane filter, and then the filtrates were filtered onto pre-combusted GF/F filters (25 mm). The filters were immediately frozen and preserved at −80°C until analysis. We obtained the POC, PON, and isotopic values of filtered samples from a Finnigan Delta^{plus} XL mass spectrometer at the Stable Isotope Laboratory of the University of Alaska Fairbanks. The final concentrations of POC and PON were derived by dividing the volume of the filtered water sample.

Analysis of Macromolecular Compositions of Phytoplankton

In order to determine macromolecular compositions of total POM, water samples were filtered onto 47 mm GF/F filters (nominal pore size = 0.7 μm) and stored at −80°C until analysis. In the case of pico-sized POM, water samples were passed sequentially through 2 μm membrane filters and 47 mm GF/F filters (nominal pore size = 0.7 μm) before being stored at −80°C. Extractions and quantifications of macromolecular components

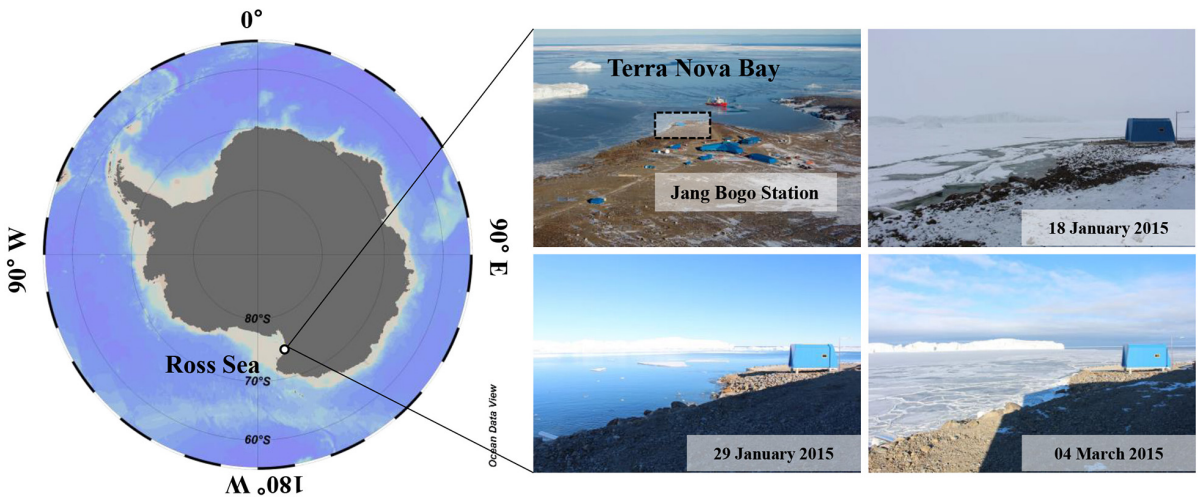

FIGURE 1 | Study area and photos for the sampling station at JBS, 2015. A dashed box is a sampling location in our study.

were executed in the laboratory located at Pusan National University of South Korea following Bhavya et al. (2019). In brief, for the quantitative analysis of total carbohydrates, we used the phenol-sulfuric acid method described by Dubois et al. (1956) and used a glucose solution (1 mg mL^{-1}, Sigma) as a standard. To measure other macromolecular components, we performed an experiment according to a method described by Lowry et al. (1951) for total proteins and Bligh and Dyer (1959) and Marsh and Weinstein (1966) for total lipids. We used a protein standard (2 mg mL^{-1}, Sigma) and a tripalmitin solution (Sigma) to calculate the final concentrations of proteins and lipids, respectively. Each extracted biochemical component was quantified with a HITACHI UH5300 spectrophotometer. The carbon contents of each biochemical component were calculated using 0.40, 0.49, and 0.75 g C g^{-1} conversion factors (carbohydrates, proteins, and lipids, respectively) (Fichez, 1991a,b; Danovaro et al., 2000). The biopolymeric carbon (BPC) was defined as the sum of the carbon concentration of each parameter (Fichez, 1991a,b; Danovaro et al., 2000).

Calculation of Food Material (FM) Concentration, Calorific Value of FM, and Calorific Content of FM

Food materials (FM) were defined as the sum of carbohydrate, protein, and lipid concentrations (Danovaro et al., 2000). We calculated the calorific value (Kcal g FM^{-1}) and calorific content of FM (Kcal m^{-3}) (Fabiano et al., 1993, 1996) according to the Winberg (1971) equation (Kcal g^{-1} = 0.041*CHO% + 0.055*PRT% + 0.095*LIP%).

Statistical Analysis

Statistical analyses were carried out with the software SPSS (version 22) for *t*-tests and Pearson's correlation coefficient. We set the level of significance at $p < 0.05$.

RESULTS

Particulate Organic Matter at JBS in 2015

During the ice-covered period, the total POC concentration (>0.7 μm) ranged from 58.2 to 158.1 μg L^{-1} (mean ± SD = 78.8 ± 20.6 μg L^{-1}), whereas the pico-sized POC concentration ranged from 49.0 to 88.8 μg L^{-1} (mean ± SD = 64.8 ± 11.6 μg L^{-1}) (**Figure 2** and **Supplementary Tables 1**, **2**). The ranges for the total and pico-sized PON were between 13.6 and 42.0 μg L^{-1} (mean ± SD = 18.1 ± 5.9 μg L^{-1}) and 11.5–23.3 μg L^{-1} (mean ± SD = 15.2 ± 3.0 μg L^{-1}), respectively (**Figure 2** and **Supplementary Tables 1**, **2**). A strong linear relationship was found between total POC and PON concentrations in our study (POC = 3.44*PON + 16.66, $r^2 = 0.95$, $p < 0.01$) (**Figure 3**). Based on the POC and PON concentrations, the average C/N ratio during the entire study period was 5.15 with a small temporal variation (SD = ± 0.36) (**Supplementary Table 1**). The $\delta^{13}C$ value of POC ranged from −30.83 to −27.17 ‰, with an average of −29.31% (SD = ± 1.11%) over the sampling period.

The BPC concentration of total POM ranged from 99.4 to 310.4 μg C L^{-1} with an average of 202.8 μg C L^{-1} (SD = ± 105.6 μg C L^{-1}) during the ice-free period (**Supplementary Table 1**). In comparison, relatively lower concentrations were observed in the ice-covered period, with an average of 57.7 μg C L^{-1} (SD = ± 10.9 μg C L^{-1}) (**Supplementary Table 1**). A strong linear relationship was found between total POC and total BPC concentrations in our study (POC = 1.48*BPC −6.46, $r^2 = 0.61$, $p < 0.01$) (**Figure 4A**). Compared to the total POM, the estimated BPC concentrations for pico-sized POM were relatively low, with a small variation during the ice-free period (mean ± SD = 68.6 ± 11.9 μg C L^{-1}) (**Supplementary Table 2**). The average BPC concentration for pico-sized POM was 42.0 μg C L^{-1} (SD = ± 7.6 μg C L^{-1}), and no significant relationship was found in concentrations between pico-sized POC and pico-sized BPC concentrations during the ice-covered period (**Figure 4B**).

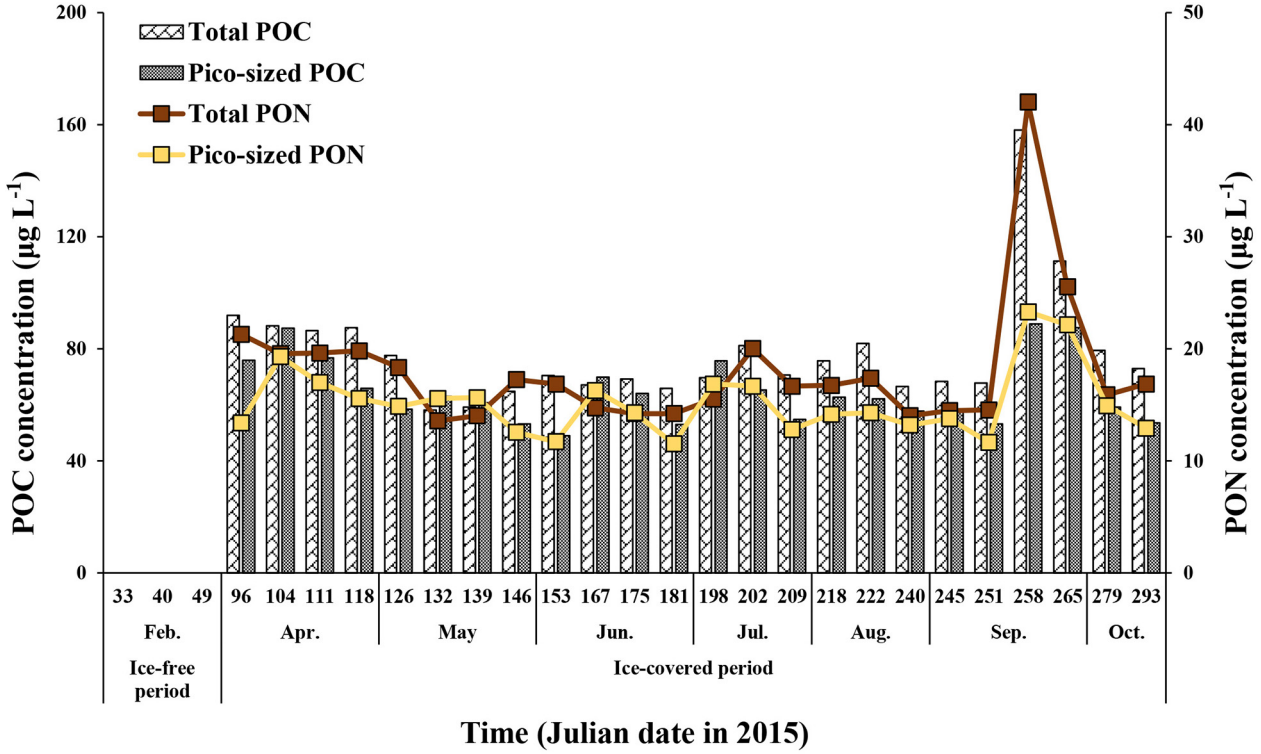

FIGURE 2 | The total (>0.7 μm) and pico-sized (0.7–2 μm) POC and PON concentrations at JBS during the ice-covered period, 2015.

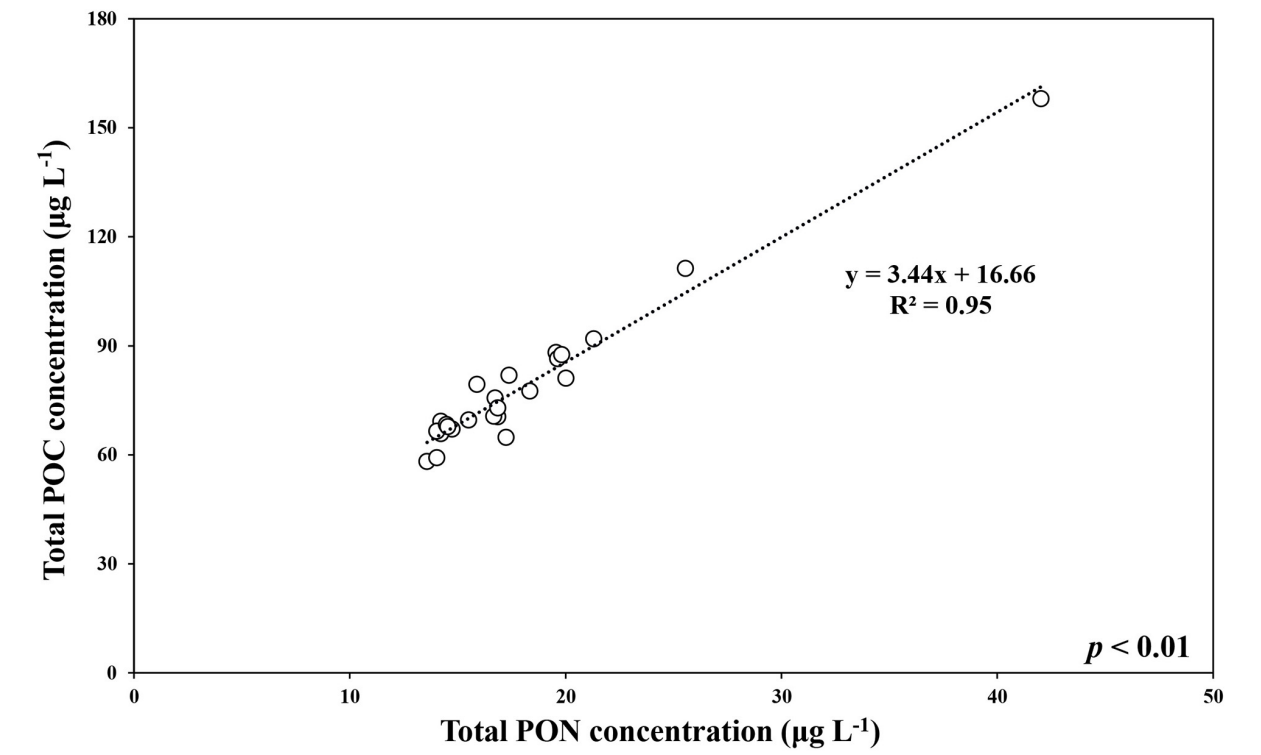

FIGURE 3 | The relationship between total POC and total PON concentrations at JBS during the ice-covered period, 2015.

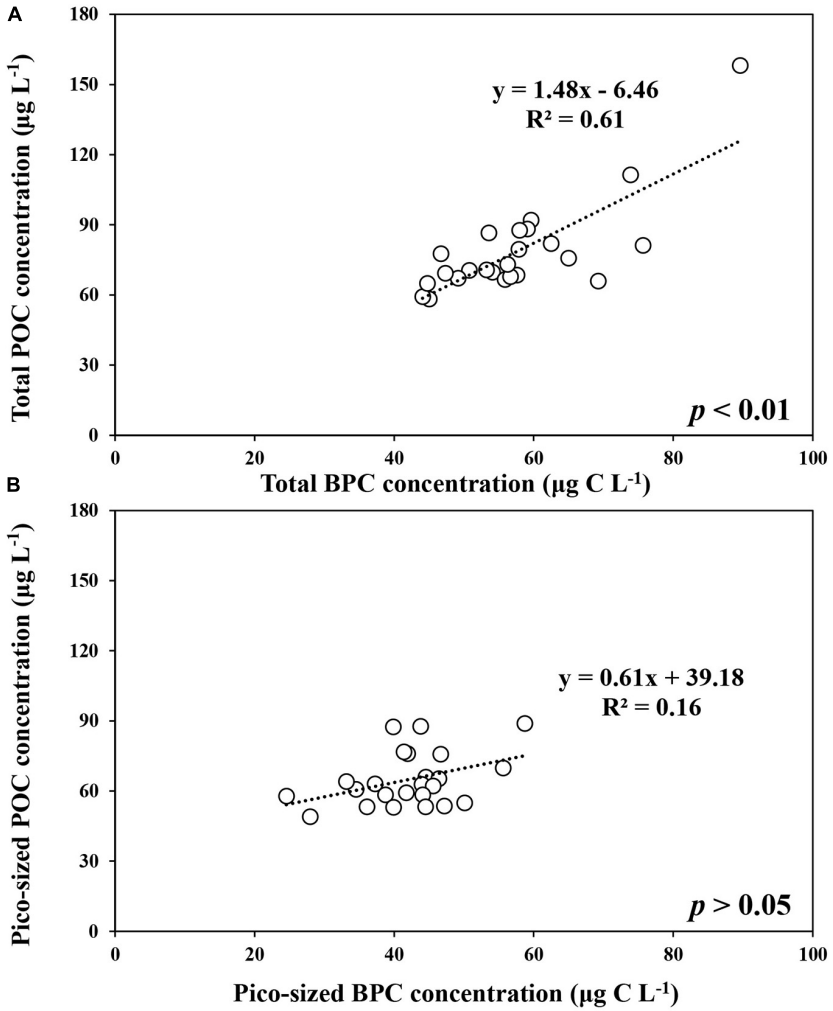

FIGURE 4 | The relationship between POC and BPC concentrations of total (>0.7 μm) **(A)** and pico-sized (0.7–2 μm) **(B)** POM at JBS during the ice-covered period, 2015.

Chlorophyll *a* Concentration of Phytoplankton at JBS in 2015

The total chlorophyll *a* (Chl-*a*) concentrations of phytoplankton ranged from 0.01 to 4.29 μg L^{-1} (mean ± SD = 0.32 ± 0.88 μg L^{-1}) during the whole study period (**Figure 5**). The maximum concentration was 4.29 μg L^{-1}, which was observed in February when the entire sea ice retreated and the coastal area was opened. The average total Chl-*a* concentrations during the ice-free and ice-covered periods were 2.25 ± 1.93 and 0.08 ± 0.09 μg L^{-1}, respectively. Although the average total Chl-*a* concentrations varied considerably between the ice-free period and ice-covered period, there was no statistically significant difference between the two periods (*t*-test, $p > 0.05$) because of a large variation in the Chl-*a* concentration during the ice-free period in this study (**Figure 5**).

Micro-sized (>20 μm) phytoplankton accounted for up to 91% of the total Chl-*a* during the ice-free period (**Figure 6**). The average contributions of micro-sized cells to the total Chl-*a* concentration during the ice-free and ice-covered periods were 66 ± 37 and 58 ± 16%, respectively. The contributions of nano- (2–20 μm) and pico-sized (0.7–2 μm) cells were 21 ± 22 and 13 ± 15% during the ice-free period and 28 ± 9 and 14 ± 9% during the ice-covered period, respectively. In other words, micro-sized cells accounted for the largest fraction of Chl-*a* in both periods. Pico-sized cells contributed the least in February (4%) when the micro-sized cells were predominant.

Macromolecular Composition of the Phytoplankton Community During the Ice-Free and Ice-Covered Periods at JBS in 2015

The average carbohydrate, protein, and lipid concentrations in the total POM during the ice-free period were 142.9 ± 55.9, 143.6 ± 80.5, and 100.3 ± 59.1 μg L^{-1}, respectively (**Figure 7A** and **Supplementary Table 1**). In comparison, the average

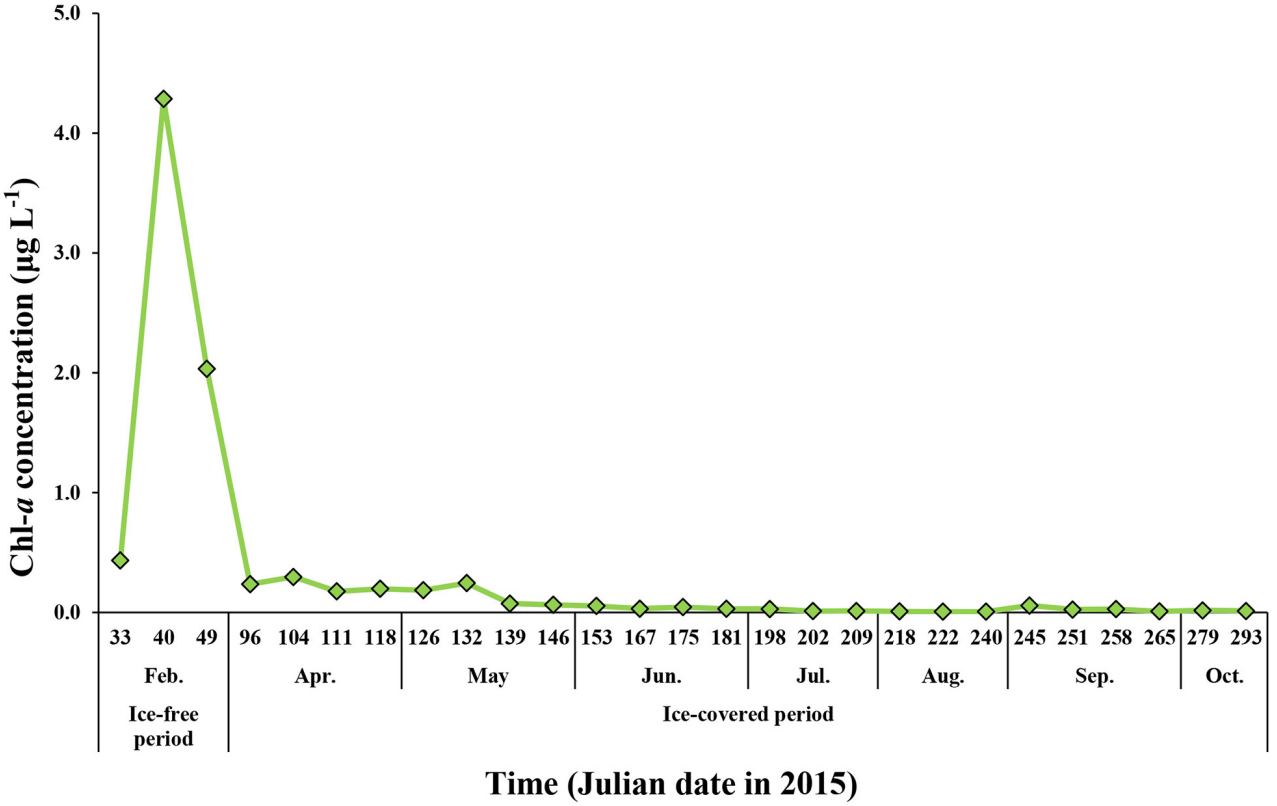

FIGURE 5 | The Chl-*a* concentration for total (>0.7 μm) phytoplankton at JBS during the entire study period, 2015.

carbohydrate, protein, and lipid concentrations in the total POM during the ice-covered period were 89.0 ± 23.0, 7.4 ± 7.8, and 24.7 ± 4.6 μg L^{-1}, respectively. Each biochemical component was present at higher concentrations during the ice-free period. Among different biochemical components, carbohydrates contributed the most to the total POM (mean ± SD = 69 ± 14%) throughout the entire sampling period, except for on 9 and 18 February, when protein contributed the most (38 and 40% for proteins on each date, respectively) (**Figure 7B**). The average contribution of carbohydrates to total POM was significantly higher during the ice-covered period, whereas protein contribution was significantly higher during the ice-free period (*t*-test, $p < 0.05$). As the protein concentration decreased more sharply than other macromolecules after the ice-free period, whereas the protein contribution was rapidly decreased over time as well. Similarly, higher lipid concentrations were observed in February, and the concentrations decreased rapidly toward the ice-covered period. In contrast to proteins, lipids were not consumed entirely during the dark winter period, and the average concentration and contribution to the total POM were 24.7 μg L^{-1} (SD = ± 4.6 μg L^{-1}) and 21% (SD = ± 4%), respectively. During the ice-covered period, lipid concentrations showed a strong linear relationship with POC (**Figure 8A**). Overall, the contributions of protein and carbohydrates to the total POM showed a strong negative relationship ($r^2 = 0.92$, $p < 0.01$) during the entire study period (**Figure 8B**).

The carbohydrate, protein, and lipid concentrations in pico-sized (0.7–2 μm) POM during the ice-free period were 54.4 ± 4.4, 37.1 ± 16.6, and 38.1 ± 5.5 μg L^{-1}, respectively (**Figure 9A** and **Supplementary Table 2**). In comparison, the average concentrations of carbohydrates, proteins, and lipids during the ice-covered period were 63.1 ± 16.3, 3.2 ± 4.0, and 20.3 ± 4.9 μg L^{-1}, respectively. Similar to the total POM, the dominant biochemical component of pico-sized POM was carbohydrates (mean ± SD = 69 ± 12%) throughout the entire study period (**Figure 9B**). Protein concentrations of pico-sized POM were higher in February and decreased sharply over time. However, lipid concentrations and contributions (22.2 ± 7.5 μg L^{-1} and 25 ± 6%, respectively) showed relatively small seasonal variations in pico-sized POM compared to other components during the entire study period.

Food Materials and Energy Content of Phytoplankton

The average FM (carbohydrates + lipids + proteins) concentration, the calorific value of FM, and calorific content of FM in total POM during the ice-free period were 386.9 μg L^{-1} (SD = ± 194.2 μg L^{-1}), 6.0 Kcal g^{-1} (SD = ± 0.2 Kcal g^{-1}), and 2.3 Kcal m^{-3} (SD = ± 1.2 Kcal m^{-3}), respectively (**Supplementary Table 1**). During the ice-covered period, the average values for each parameter were 121.1 μg L^{-1}

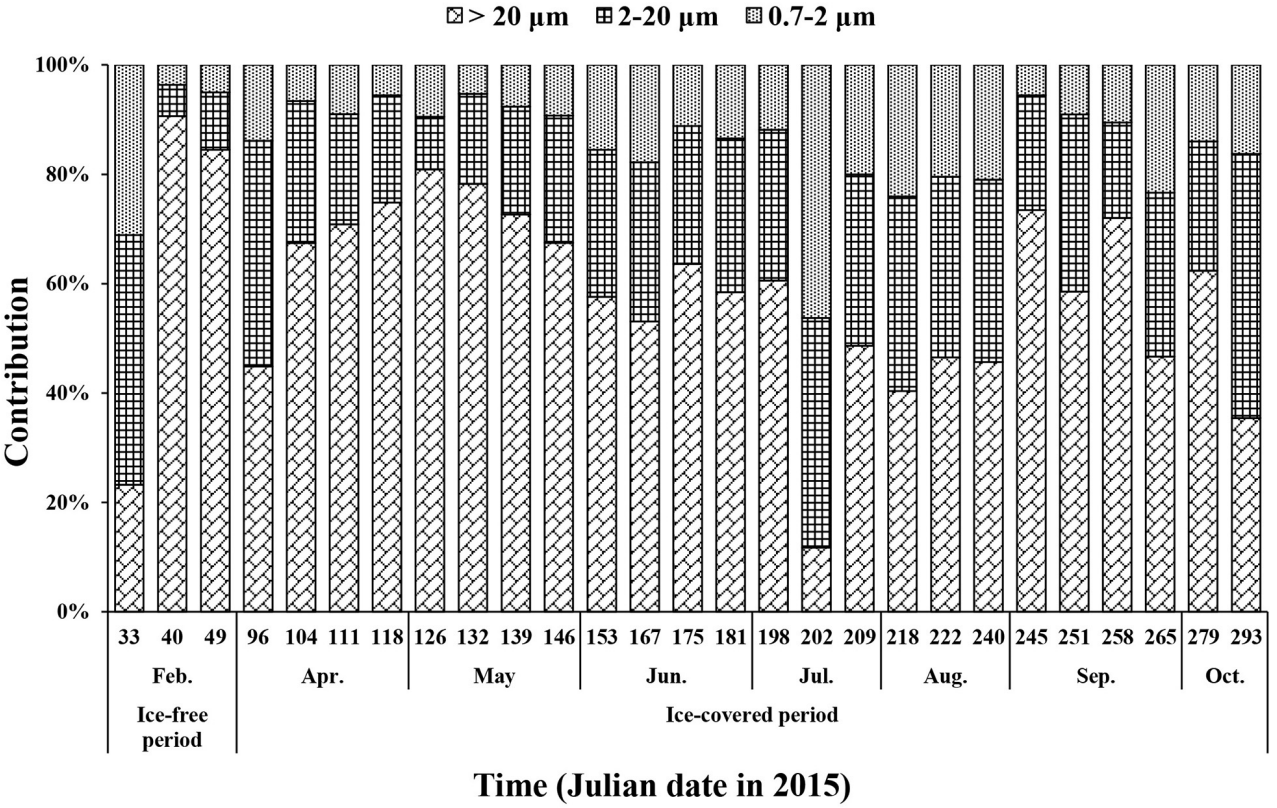

FIGURE 6 | The contributions of size-fractionated Chl-*a* concentration to the total Chl-*a* concentration of phytoplankton at JBS during the entire study period, 2015.

(SD = ± 24.6 µg L^{-1}), 5.3 Kcal g^{-1} (SD = ± 0.3 Kcal g^{-1}), and 0.6 Kcal m^{-3} (SD = ± 0.1 Kcal m^{-3}), respectively (**Supplementary Table 1**).

The average FM concentration, the calorific value of FM, and the calorific content of FM in pico-sized POM during the ice-free period were 129.7 µg L^{-1} (SD = ± 21.3 µg L^{-1}), 6.9 Kcal g^{-1} (SD = ± 0.1 Kcal g^{-1}), and 0.8 Kcal m^{-3} (SD = ± 0.1 Kcal m^{-3}), respectively (**Supplementary Table 2**). During the ice-covered period, the average values for each parameter were 86.6 µg L^{-1} (SD = ± 17.0 µg L^{-1}), 5.5 Kcal g^{-1} (SD = ± 0.3 Kcal g^{-1}), and 0.5 Kcal m^{-3} (SD = ± 0.1 Kcal m^{-3}), respectively (**Supplementary Table 2**).

DISCUSSION

Origin of Particulate Organic Matter and Chl-*a* Concentration at JBS in 2015

Seawater is a mixture of various particulate matters, including phytoplankton as well as terrestrial materials. In general, it is well known that the $\delta^{13}C$ value and C/N ratio provide important information on the origin of organic matter in the oceans (Lobbes et al., 2000; Lee and Whitledge, 2005; Kim et al., 2016). Based on previous results from various oceans (Wada et al., 1987; Zweifel et al., 1993; Fagerbakke et al., 1996; Lobbes et al., 2000; Lee and Whitledge, 2005; Lee et al., 2012; Martiny et al., 2014; Kim et al., 2016), the mean $\delta^{13}C$ value and C/N ratio obtained during this study indicate that POM was mainly from pelagic phytoplankton. In addition, the BPC contribution to the total POC can vary from 40 to 80% depending on the origin of POM and decrease with increasing terrestrial input (Pusceddu et al., 1996; Fabiano et al., 1997; Danovaro et al., 2000). In this study, the average contribution of BPC to POC (mean ± SD = 74 ± 10%) and the strong positive relationship between BPC and POC during the overall observation period (**Figure 4A**) suggest that the major source of POM in our study was arguably of oceanic origin. This is not a surprising result given the little terrigenous inputs from Antarctica to the Southern Ocean.

We observed a wide range of total Chl-*a* concentrations (0.01–4.29 µg L^{-1}) from February to October in the TNB in 2015. The total Chl-*a* range during the ice-free period in this study is consistent with previous results from the Italian Antarctic Base (Zucchelli Station), which is located at a distance of 10 km from the JBS (Fabiano et al., 1997; Lazzara et al., 1997; Misic et al., 2006) and TNB (Rivaro et al., 2012; Mangoni et al., 2017). During the polar night period, the total Chl-*a* concentrations decreased to 0.01 µg L^{-1} in our current study, which is consistent with the results from McMinn et al. (2010), which ranged from 0.01 to 0.02 µg L^{-1} at McMurdo Sound. These low Chl-*a* concentrations observed in our study site and McMurdo Sound in the Antarctic Ocean are comparable with the results from the Arctic polar night season (Iversen and Seuthe, 2011; Berge et al., 2015).

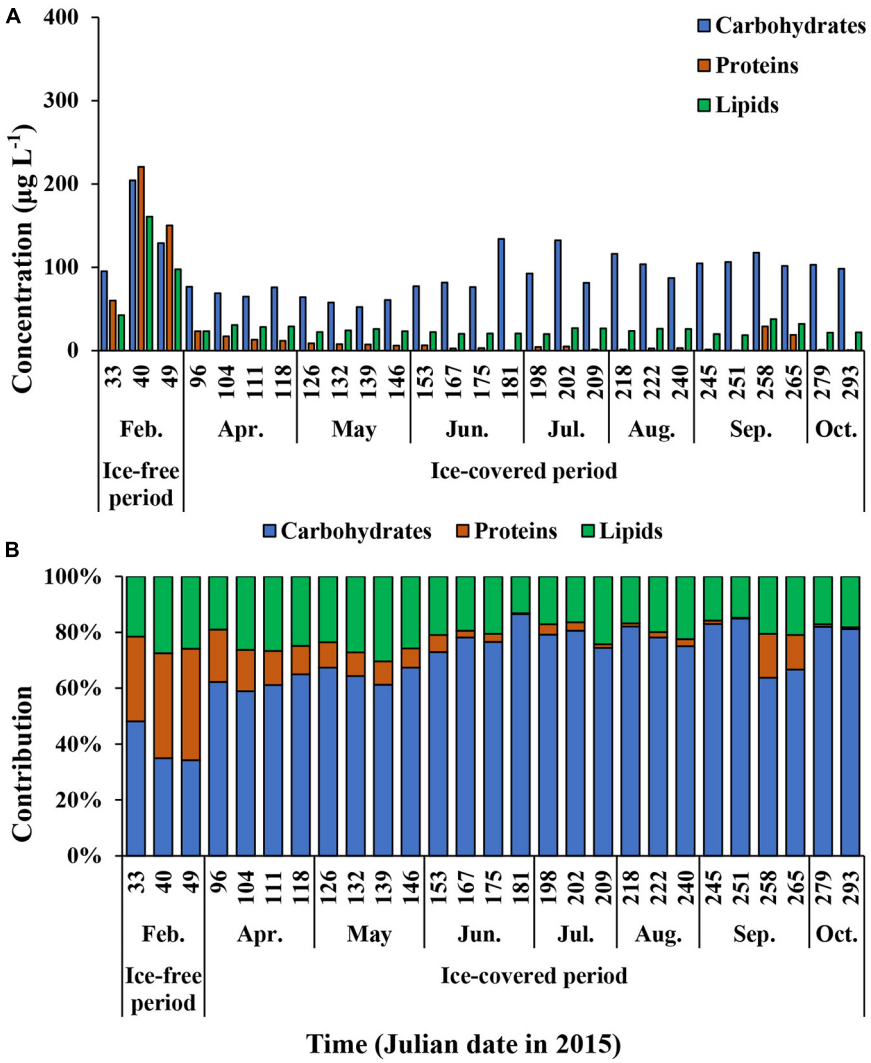

FIGURE 7 | The carbohydrates, proteins, and lipids concentrations **(A)** and the contribution of each biochemical component of total (>0.7 μm) POM **(B)** at JBS during the entire study period, 2015.

Macromolecular Composition During the Ice-Free and Ice-Covered Periods at JBS

The biochemical composition of each constituent in total and pico-sized POM showed a marked difference between the ice-free and ice-covered periods. All components were present at the highest concentrations in February, while they were at the lowest during the ice-covered period. Carbohydrates and lipids were not completely consumed and remained relatively constant, whereas proteins were rarely detected during the ice-covered period. The reason for the maximum concentrations of different macromolecular components during the ice-free period can be explained by the increased light exposure of the phytoplankton community in the surface water layer. Factors controlling the biochemical compositions of phytoplankton in the ocean are light (Fiala and Oriol, 1990; Suárez and Marañón, 2003; Lee et al., 2009), water temperature (Pirt, 1975; Fiala and Oriol, 1990; Kakinuma et al., 2006; Doney et al., 2012), macro-nutrients (Fabiano et al., 1993; Biddanda and Benner, 1997; Lee et al., 2009; Kim et al., 2015), and micro-nutrients availability (Sedwick et al., 2000, 2011; Zhu et al., 2016). Favorable light conditions can increase the growth rate of phytoplankton (Fiala and Oriol, 1990). Excessive light intensity, however, can decrease the protein content of phytoplankton (Suárez and Marañón, 2003; Lee et al., 2008, 2009), whereas insufficient light can increase the carbohydrate and lipid composition in phytoplankton (Friedman et al., 1991; Suárez and Marañón, 2003). Low water temperatures can reduce the metabolic rate and growth rate of phytoplankton (Fiala and Oriol, 1990). In a nitrogen-rich environment, phytoplankton can actively accumulate proteins in the cell body during photosynthesis (Fabiano et al., 1993; Lee et al., 2009), whereas in the opposite environments, lipid

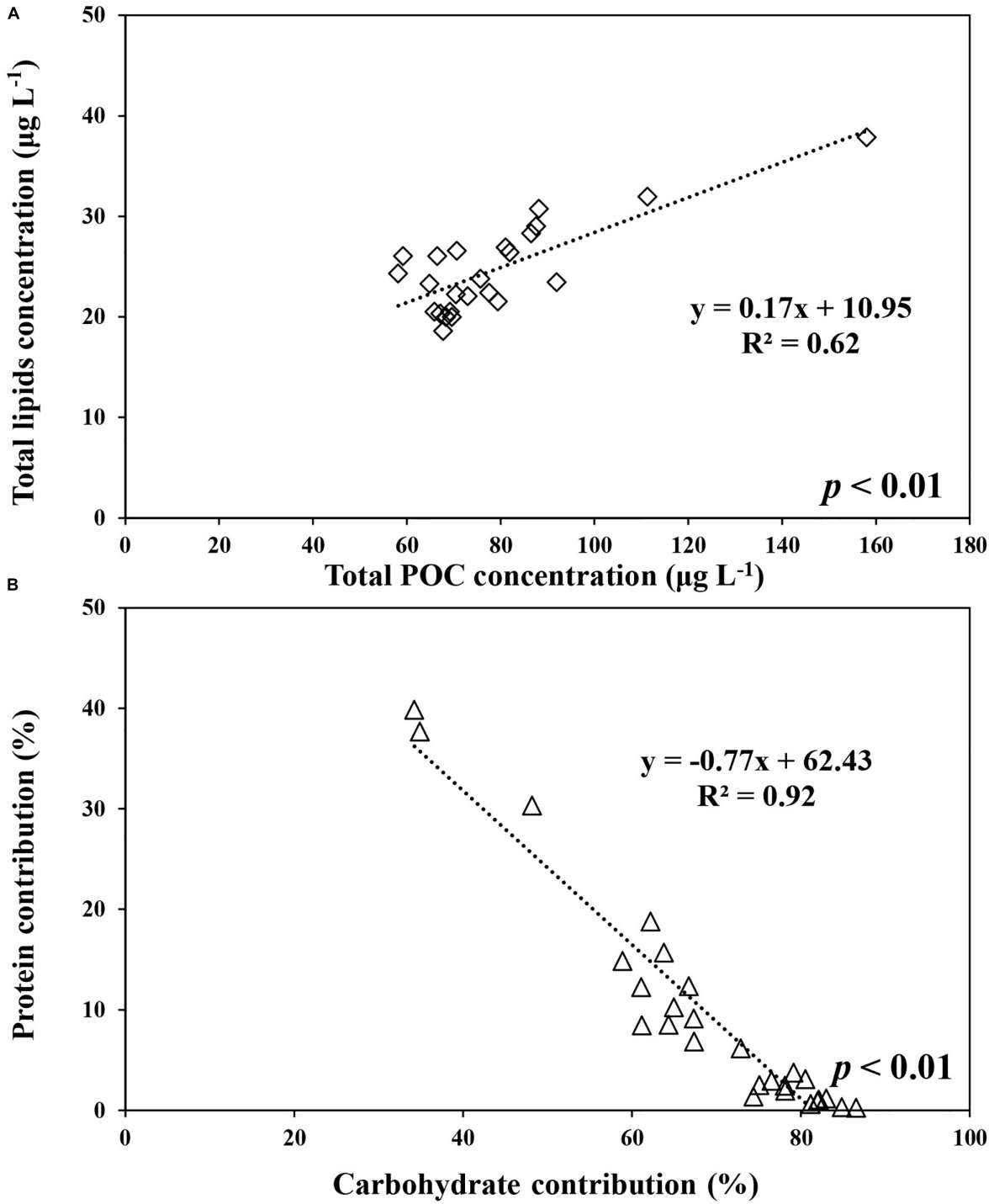

FIGURE 8 | The relationship between lipids and POC concentrations in total (>0.7 μm) POM during the ice-covered period **(A)** and between proteins and carbohydrates contributions to total POM at JBS during the entire study period **(B)**, 2015.

and carbohydrate synthesis predominates (Shifrin and Chisholm, 1981; Harrison et al., 1990).

Among the environmental conditions affecting the primary productivity and biochemical composition of phytoplankton, light undergoes the most dramatic seasonal changes depending on sea ice conditions. Our study area was covered with land-fast sea ice before February and opened during February. As mentioned above, extreme light intensity could limit the protein synthesis of phytoplankton (Suárez and Marañón, 2003; Lee et al., 2008, 2009). However, the increased protein content

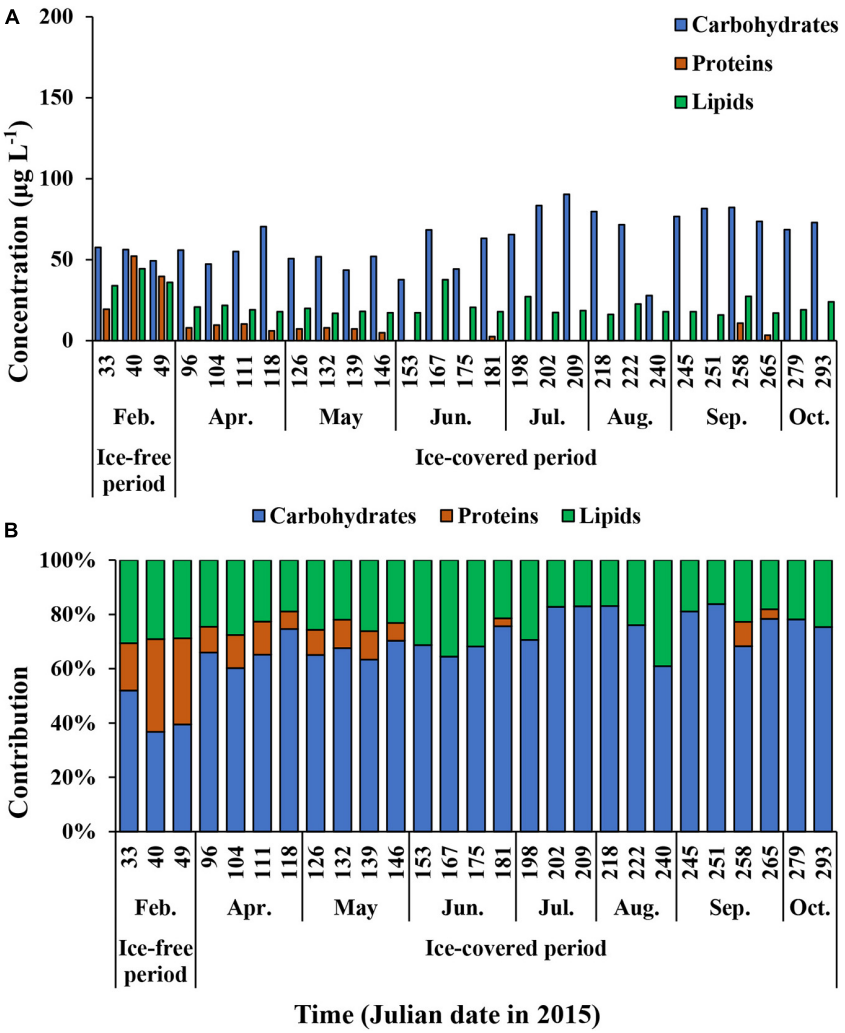

FIGURE 9 | The carbohydrates, proteins, and lipids concentrations **(A)** and the contribution of each biochemical component of pico-sized (0.7–2 μm) POM **(B)** at JBS during the entire study period, 2015.

observed in February indicates that phytoplankton did not experience strong light inhibition during the growing period. The protein:carbohydrate ratios could reflect the nutrient availability and productivity for phytoplankton (Fabiano et al., 1984, 1992, 1993; Mayzaud et al., 1989; Lizotte and Sullivan, 1992; Danovaro et al., 2000). A ratio less than 1 indicates nitrogen deficiency for phytoplankton growth (Mayzaud et al., 1989; Lizotte and Sullivan, 1992; Danovaro et al., 2000; Lee et al., 2009; Yun et al., 2015), whereas a ratio higher than 1 could be observed in productive areas or phytoplankton bloom periods (Fabiano et al., 1984, 1992, 1993; Lee et al., 2009). The average protein:carbohydrate ratio was 1.0 ± 0.3 during the ice-free period, which suggests that no nitrogen limitation occurred during this period in February. Previous studies demonstrate that nitrogen limitation is typically not observed in the Southern Ocean (de Baar et al., 1995; Boyd et al., 2000; Franck et al., 2000; Henley et al., 2020). Unfortunately, we did not measure macronutrient concentrations to confirm this.

In the ice-covered period, the phytoplankton community undergoes extremely low light conditions because of sea ice cover as well as polar night. Handa (1969) reported a change in the biochemical composition of the marine diatom *Skeletonema costatum* after 18 days of incubation under dark conditions. At the beginning of the dark condition, *Skeletonema costatum* used readily available non-structural carbohydrates, glucose, and β-1,3-glucan, while cell-structural carbohydrates such as mannan and pentosan were not used for respiration (Handa, 1969). After consuming non-structural carbohydrates, they consume proteins for survival. In contrast to carbohydrates and proteins, no significant fluctuations in lipids were observed. Smayda and Mitchell-Innes (1974) reported how long *Skeletonema costatum* could survive in dark conditions. Interestingly, they survived only 1–4 weeks at 20°C under dark conditions, but they survived 24 weeks at 2°C without light. In addition, Bunt and Lee (1972) reported that two diatoms isolated from Antarctic sea ice also survived for 90 days (duration of the experiment) of

darkness at −1.8°C. This suggests that low temperatures under dark conditions can play an important role in the survival of diatoms. In our study, the average water temperature during the ice-covered periods was −1.78°C (SD = ± 0.04℃) in 2015. In addition, the coastal area of the TNB is well known to be dominated with diatoms (Arrigo et al., 2003; Fonda Umani et al., 2005; Mangoni et al., 2019).

Many types of phytoplankton are known to experience a resting stage in their life cycle (Ellegaard and Ribeiro, 2018). Some resting stages are related to sexual reproduction, while other resting stages are asexual and form solely following changes in environmental conditions toward the end of the growing season, such as akinetes in some cyanobacteria and resting spores in some diatoms (Ellegaard and Ribeiro, 2018). Diatom resting spores have morphological characteristics distinct from those of fresh living cells, and they are more heavily silicified (Oku and Kamatani, 1995; McQuoid and Hobson, 1996). In addition, they are known to accumulate carbohydrates and lipids as energy storage materials in resting spores, and they accumulate large amounts of organic carbon in the form of neutral lipids (Oku and Kamatani, 1999). In this study, a strong positive relationship between lipid concentrations and total POC during the ice-covered period (**Figure 9A**) suggests that phytoplankton survived with lipids as their energy source during the long cold darkness in our observation period.

The average protein:carbohydrate ratio decreased markedly during the ice-covered period (mean ± SD = 0.1 ± 0.1) compared to the ice-free period (mean ± SD = 1.0 ± 0.3). This observation may be explained by the difference in the physiological state of phytoplankton during the two periods. In the ice-free period, phytoplankton could utilize sufficient photosynthetically available radiation and nutrients, and as a result, the overall macromolecules in the cell body were increased, with a particularly marked increase in proteins. During the ice-covered period, however, the active growing season was over due to the formation of sea ice. Phytoplankton might consume immediately available forms of carbohydrates such as glucose as a strategy for survival followed by most of the proteins. Therefore, the physiological conditions of phytoplankton in the two different periods could cause a negative relationship between the protein and carbohydrate contributions to the total POM in our study. Another possibility for different macromolecular compositions between the ice-free and ice-covered periods could be a change in dominant phytoplankton groups that affects the biochemical composition of POM (Moal et al., 1987; Rivkin and Voytek, 1987; Harrison et al., 1990; Kim et al., 2018). Kim et al. (2018) found that high carbohydrate compositions were caused by the enhanced contribution of *P. Antarctica* in the Amundsen Sea. However, we did not verify the potential effects of the shift in the species makeup on the macromolecular compositions because we did not investigate species breakdown of phytoplankton in this study. Generally speaking, diatoms are reported to be dominant in the phytoplankton community in the TNB (Arrigo et al., 2003; Fonda Umani et al., 2005; Mangoni et al., 2019). In particular, at JBS in the TNB, the phytoplankton community was predominated by diatoms during summer (85.3%) and during fall and winter periods (>95%) in 2018 (unpublished data). Therefore, the change in major species compositions of phytoplankton is less likely to account for the difference in macromolecular compositions between the ice-free and ice-covered periods.

Among the three biochemical components, proteins decreased most rapidly with time and were low from April to October 2015. The substantial decrease in protein concentrations observed in this study is similar to the composition change in sinking particles from the euphotic layer to the aphotic layer in the Amundsen Sea reported by Kim et al. (2018). Previous studies reported that proteins consisted of various amino acids that could be consumed more easily than other compounds (Handa and Tominaga, 1969; Dawson and Liebezeit, 1982; Fabiano et al., 1995; Hedges et al., 2001; Danovaro et al., 2000). In addition, several previous studies reported that the carbohydrates in sinking particles underwent limited decomposition compared to the other components (Ittekkot et al., 1982; Liebezeit, 1984; Fabiano et al., 1993; Danovaro et al., 2000; Kim et al., 2018). Approximately 5% of proteins and 60% of carbohydrates produced during the ice-free period remained during the ice-covered period. Compared to carbohydrates and proteins, relatively higher fraction of lipids (25%) remained during the ice-covered period. Lipids might play an important role in the survival of phytoplankton, lowering the metabolic rate during the long ice-covered period. Bunt et al. (1966) reported that lower water temperatures reduced the metabolism of *Fragilaria sublinearis* and that at 3°C dark respiration decreased to less than 50% of that at 10°C. Palmisano and Sullivan, 1982 reported that diatoms could use stored energy products to survive under lowered metabolic activity at low temperatures. The use of carbohydrates and lipids in the cell body might be a critical survival strategy for phytoplankton during the long ice-covered polar night.

Food Materials and Energy Content of Phytoplankton

Previous studies reported high FM concentrations in the euphotic zone in the Southern Ocean with a large proportion of proteins (Fabiano et al., 1993, 1996; Kim et al., 2016) although Kim et al. (2018) observed carbohydrate-dominant POM in the *P. antarctica*-prevalent community of the Amundsen Sea. While the POM in the euphotic layer sinks to the aphotic layer upon decomposition, the relative contribution of carbohydrates could increase due to the selective degradation of proteins by heterotrophs such as bacteria (Fabiano et al., 1993, 1996; Kim et al., 2016, 2018). The average calorific contents of FM were 2.3 ± 1.2 and 0.6 ± 0.1 Kcal m^{-3} for the ice-free and ice-covered periods, respectively. These values fall in the range reported from the Southern Ocean (**Supplementary Table 3**). Generally, the calorific content of FM has a very low value in the aphotic layer compared to that in the photic layer due to a decrease in the overall FM concentration as well as an increasing contribution of carbohydrates, which has the smallest energy content per unit weight among the three different types of macromolecules (Fabiano et al., 1993, 1996; Kim et al., 2016, 2018). Similar to previous studies reporting the high biochemical components in the euphotic zone (Fabiano et al., 1993, 1996; Kim et al., 2016,

2018), we found the highest FM concentrations (585.8 μg L^{-1}) as well as the calorific content of FM (3.6 Kcal m^{-3}) in the surface layer at JBS during the active growth phase in the ice-free period. In this period, the protein concentration was the highest among the different biochemical components. After that, the protein concentrations decreased rapidly over time, and the FM concentration and calorific content of FM had minimum values (85.8 μg L^{-1} and 0.5 Kcal m^{-3} for the minimum FM concentration and calorific content of FM, respectively) during the ice-covered period.

Previous studies reported that the dominant phytoplankton size might change to pico-sized cells due to the warming ocean (Li et al., 2009; Morán et al., 2010). To assess the relative contribution of the pico-sized cell to the total POM in the current study, we calculated the ratios (pico-size:total) of Chl-*a*, FM, and calorific content of FM based on the cell size of POM. During the ice-free period, the ratio of Chl-*a* was 0.13 ± 0.16, and the ratios of FM and calorific content were 0.38 ± 0.16 and 0.40 ± 0.17, respectively. In addition, the ratio of Chl-*a* was 0.15 ± 0.10, and the ratios of FM and calorific content were 0.73 ± 0.14 and 0.74 ± 0.14 during the ice-covered period, respectively. The contribution of pico-sized Chl-*a* to the total Chl-*a* was lower than those of FM and calorific content during the entire study period (*t*-test, $p < 0.05$). Moreover, the FM and the calorific content per unit of Chl-*a* of pico-sized POM were higher than those of the total POM (*t*-test, $p < 0.05$). This suggests that the pico-sized cells could accumulate FM and energy per unit Chl-*a* into the cell body more efficiently than larger cells. Consistent with our findings, Kang et al. (2017) observed higher FM and calorific content per unit Chl-*a* of small phytoplankton (0.7–2 μm) compared to the total phytoplankton in the East Sea.

SUMMARY AND CONCLUSION

This study reported on the biweekly variations in biomass and physiological state of phytoplankton from the JBS located in the coastal region of the TNB in the Ross Sea from the ice-free growing period to the ice-covered polar night. During the ice-free period, we observed a high Chl-*a* concentration with a high proportion of micro-sized cells for the whole phytoplankton community. Each macromolecular component in phytoplankton showed maximum values during the ice-free period. Interestingly, a relatively higher protein contribution was found compared to carbohydrates and lipids in this period. After the study area was covered with sea ice in early March, the Chl-*a* concentration decreased sharply, and the concentration of macromolecules in phytoplankton also decreased, but each component showed different patterns. Carbohydrates showed only a small decrease compared to the other two constituents and consequently became a major component of POM during the dark winter period. Similar to the pattern of Chl-*a*, the protein concentration decreased rapidly over time and was close to detection levels during the ice-covered period, while the lipids were not consumed completely. The proteins appear to be consumed favorably, and lipids might be an important energy source for living during the long ice-covered period for phytoplankton.

Earlier studies reported different trends in the sea ice extent in the different regions of the Southern Ocean. Changes in the timing of sea ice melt onset and duration of the ice-free period could influence the growing conditions and consequently biochemical compositions of phytoplankton. Because of the limitation of geographical accessibility, very little information is available on how the biochemical compositions of phytoplankton vary from the ice-free period and ice-covered period. This study could provide valuable basic data for understanding the effect of future climate change on phytoplankton in the Southern Ocean. Continuous monitoring is needed on the macromolecular compositions of phytoplankton as an indicator of climate change in the Southern Ocean, which is facing dramatic environmental changes.

DATA AVAILABILITY STATEMENT

The original contributions presented in the study are included in the article/**Supplementary Material**, further inquiries can be directed to the corresponding author/s.

AUTHOR CONTRIBUTIONS

SL conceived the ideas and designed the methodology. KK performed the field experiments and data analysis. KK, NJ, SP, HY, and JK conducted the lab experiment. KK and SL contributed to writing–original draft. KK, JP, and SL contributed to writing–review and editing. All authors agreed with the submission of the published version of the manuscript.

FUNDING

This research was supported by the National Research Foundation of Korea (NRF) grant funded by the Korean government (MSIT; NRF-2019R1A2C1003515) and supported by the Korea Polar Research Institute (KOPRI; PE21110).

ACKNOWLEDGMENTS

We especially thank members of the second overwintering team in JBS for collecting water samples for our project safely.

SUPPLEMENTARY MATERIAL

The Supplementary Material for this article can be found online at: https://www.frontiersin.org/articles/10.3389/fmicb.2021.618999/full#supplementary-material

Supplementary Table 1 | The macromolecules (carbohydrates, proteins, and lipids), POC, PON, BPC concentrations, and associated calorific value of FM for total (> 0.7 μm) POM at the JBS, 2015.

Supplementary Table 2 | The macromolecules (carbohydrates, proteins, and lipids), POC, PON, BPC concentrations, and associated calorific value of FM for pico-sized (0.7-2 μm) POM at the JBS, 2015.

Supplementary Table 3 | Comparison of FM concentration and calorific content of FM in the Southern Ocean (Ross Sea and Amundsen Sea).

REFERENCES

Arrigo, K. R., Van Dijken, G., and Pabi, S. (2008). Impact of a shrinking ARCTic ice cover on marine primary production. *Geophys. Res. Lett.* 35:L19603. doi: 10.1029/2008GL035028

Arrigo, K. R., and Van Dijken, G. L. (2004). Annual changes in sea-ice, chlorophyll a, and primary production in the Ross Sea, Antarctica. *Deep. Res. II Top. Stud. Oceanogr.* 51, 117–138. doi: 10.1016/j.dsr2.2003.04.003

Arrigo, K. R., Worthen, D. L., and Robinson, D. H. (2003). A coupled ocean-ecosystem model of the Ross Sea: 2. iron regulation of phytoplankton taxonomic variability and primary production. *J. Geophys. Res. Oceans* 108:3231. doi: 10.1029/2001jc000856

Berge, J., Renaud, P. E., Darnis, G., Cottier, F., Last, K., Gabrielsen, T. M., et al. (2015). In the dark: a review of ecosystem processes during the Arctic polar night. *Prog. Oceanogr.* 139, 258–271. doi: 10.1016/j.pocean.2015.08.005

Bhavya, P. S., Kim, B. K., Jo, N., Kim, K., Kang, J. J., Lee, J. H., et al. (2019). A review on the macromolecular compositions of phytoplankton and the implications for aquatic biogeochemistry. *Ocean Sci. J.* 54, 1–14. doi: 10.1007/s12601-018-0061-8

Biddanda, B., and Benner, R. (1997). Carbon, nitrogen, and carbohydrate fluxes during the production of particulate and dissolved organic matter by marine phytoplankton. *Limnol. Oceanogr.* 42, 506–518. doi: 10.4319/lo.1997.42.3.0506

Bligh, E. G., and Dyer, W. J. (1959). A rapid method of total lipid extraction and purification. *Can. J. Biochem. Physiol.* 37, 911–917. doi: 10.1139/o59-099

Borrione, I., and Schlitzer, R. (2013). Distribution and recurrence of phytoplankton blooms around South Georgia, Southern Ocean. *Biogeosciences* 10, 217–231. doi: 10.5194/bg-10-217-2013

Boyd, P. W., Watson, A. J., Law, C. S., Abraham, E. R., Trull, T., Murdoch, R., et al. (2000). A mesoscale phytoplankton bloom in the polar Southern Ocean stimulated by iron fertilization. *Nature* 407, 695–702. doi: 10.1038/35037500

Bunt, J. S., and Lee, C. C. (1972). Data on the composition an dark survival of four sea-ice microalgae. *Limnol. Oceanogr.* 17, 458–461. doi: 10.4319/lo.1972.17.3.0458

Bunt, J. S., van, H., Owens, O., and Hoch, G. (1966). Exploratory studies on the physiologyand ecology of a psychrophilic marine diatom. *J. Phycol.* 2, 96–100. doi: 10.1111/j.1529-8817.1966.tb04601.x

Comiso, J. C. (2012). Large decadal decline of the arctic multiyear ice cover. *J. Clim.* 25, 1176–1193. doi: 10.1175/JCLI-D-11-00113.1

Danovaro, R., Dell'Anno, A., Pusceddu, A., Marrale, D., Della Croce, N., Fabiano, M., et al. (2000). Biochemical composition of pico-, nano- and micro-particulate organic matter and bacterioplankton biomass in the oligotrophic Cretan Sea (NE Mediterranean). *Prog. Oceanogr.* 46, 279–310. doi: 10.1016/S0079-6611(00)00023-9

Dawson, R., and Liebezeit, G. (1982). Biochemical compounds in the pelagic and sedimentary environment of Antarctic waters. *Centre National Pour l'Exploitation des Oceans (France)* 14, 67–86.

de Baar, H. J. W., Bathmannt, U., Smetacek, V., Löscher, B. M., and Veth, C. (1995). Importance of iron for plankton blooms and carbon dioxide drawdown in the Southern Ocean. *Nature* 373, 412–415. doi: 10.1038/373412a0

Doney, S. C., Ruckelshaus, M., Emmett Duffy, J., Barry, J. P., Chan, F., English, C. A., et al. (2012). Climate change impacts on marine ecosystems. *Ann. Rev. Mar. Sci.* 4, 11–37. doi: 10.1146/annurev-marine-041911-111611

Dubois, M., Gilles, K. A., Hamilton, J. K., Rebers, P. A., and Smith, F. (1956). Colorimetric method for determination of sugars and related substances. *Anal. Chem.* 28, 350–356. doi: 10.1021/ac60111a017

Eayrs, C., Holland, D., Francis, D., Wagner, T., Kumar, R., and Li, X. (2019). Understanding the seasonal cycle of Antarctic sea ice extent in the context of longer-term variability. *Rev. Geophys.* 57, 1037–1064. doi: 10.1029/2018RG000631

Ellegaard, M., and Ribeiro, S. (2018). The long-term persistence of phytoplankton resting stages in aquatic 'seed banks.'. *Biol. Rev. Camb. Philos. Soc.* 93, 166–183. doi: 10.1111/brv.12338

Fabiano, M., Chiantore, M., Povero, P., Cattaneo-Vietti, R., Pusceddu, A., Misic, C., et al. (1997). Short-term variations in particulate matter flux in terra Nova Bay, Ross Sea. *Antarct. Sci.* 9, 143–149. doi: 10.1017/s0954102097000187

Fabiano, M., Danovaro, R., Crisafi, E., La Ferla, R., Povero, P., and Acosta-Pomar, L. (1995). Particulate matter composition and bacterial distribution in Terra Nova Bay (Antarctica) during summer 1989-1990. *Polar Biol.* 15, 393–400. doi: 10.1007/BF00239715

Fabiano, M., Povero, P., and Danovaro, R. (1993). Distribution and composition of particulate organic matter in the Ross Sea (Antarctica). *Polar Biol.* 3, 525–533. doi: 10.1007/BF00236394

Fabiano, M., Povero, P., and Danovaro, R. (1996). Participate organic matter composition in Terra Nova Bay (Ross Sea, Antarctica) during summer 1990. *Antarct. Sci.* 8, 7–13. doi: 10.1017/s095410209600003x

Fabiano, M., Povero, P., and Medica, D. (1992). Carbohydrates, proteins and chlorophylls in the particulate organic matter of surface coastal waters of Ligurian Sea. *Boll. Oceanol. Teor. Appl.* 10, 41–51.

Fabiano, M., and Pusceddu, A. (1998). Total and hydrolizable particulate organic matter (carbohydrates, proteins and lipids) at a coastal station in Terra Nova Bay (Ross Sea, Antarctica). *Polar Biol.* 19, 125–132. doi: 10.1007/s003000050223

Fabiano, M., Zavatarelli, M., and Palmero, S. (1984). Observations sur la matière organique particulaire en Mer Ligure. *Thetis.* 11, 133–140.

Fagerbakke, K. M., Heldal, M., and Norland, S. (1996). Content of carbon, nitrogen, oxygen, sulfur and phosphorus in native aquatic and cultured bacteria. *Aquat. Microb. Ecol.* 10, 15–27. doi: 10.3354/ame010015

Falkowski, P. G. (1994). The role of phytoplankton photosynthesis in global biogeochemical cycles. *Photosynth. Res.* 39, 235–258. doi: 10.1007/BF00014586

Fiala, M., and Oriol, L. (1990). Light-temperature interactions on the growth of Antarctic diatoms. *Polar Biol.* 10, 629–636. doi: 10.1007/BF00239374

Fichez, R. (1991a). Composition and fate of organic matter in submarine cave sediments; implications for the biogeochemical cycle of organic carbon. *Oceanol. Acta* 14, 369–377.

Fichez, R. (1991b). Suspended particulate organic matter in a Mediterranean submarine cave. *Mar. Biol.* 108, 167–174. doi: 10.1007/BF01313485

Fonda Umani, S., Monti, M., Bergamasco, A., Cabrini, M., De Vittor, C., Burba, N., et al. (2005). Plankton community structure and dynamics versus physical structure from Terra Nova Bay to Ross ice shelf (Antarctica). *J. Mar. Syst.* 55, 31–46. doi: 10.1016/j.jmarsys.2004.05.030

Franck, V. M., Brzezinski, M. A., Coale, K. H., and Nelson, D. M. (2000). Iron and silicic acid concentrations regulate Si uptake north and south of the polar frontal zone in the Pacific sector of the Southern Ocean. *Deep. Res. II Top. Stud. Oceanogr.* 47, 3315–3338. doi: 10.1016/S0967-0645(00)00070-9

Friedman, O., Dubinsky, Z., and Arad, S. (1991). Effect of light intensity on growth and polysaccharide production in red and blue-green rhodophyta unicells. *Bioresour. Technol.* 38, 105–110. doi: 10.1016/0960-8524(91)90139-B

Gambi, M. C., Buia, M. C., Mazzella, L., Lorenti, M., and Scipione, M. B. (2000). "Spatio-Temporal Variability in the Structure of Benthic Populations in a Physically Controlled System off Terra Nova Bay: The Shallow Hard Bottoms," in *Ross Sea Ecology*, eds F. M. Faranda, L. Guglielmo, and A. Ianora (Berlin: Springer), doi: 10.1007/978-3-642-59607-0_38

Handa, N. (1969). Carbohydrate metabolism in the marine diatom *Skeletonema costatum*. *Mar. Biol.* 4, 208–214. doi: 10.1007/BF00393894

Handa, N., and Tominaga, H. (1969). A detailed analysis of carbohydrates in marine particulate matter. *Mar. Biol.* 2, 228–235. doi: 10.1007/BF00351145

Harrison, P. J., Thompson, P. A., and Calderwood, G. S. (1990). Effects of nutrient and light limitation on the biochemical composition of phytoplankton. *J. Appl. Phycol.* 2, 45–56. doi: 10.1007/BF02179768

Hedges, J. I., Baldock, J. A., Gélinas, Y., Lee, C., Peterson, M., and Wakeham, S. G. (2001). Evidence for non-selective preservation of organic matter in sinking marine particles. *Nature* 409, 801–804. doi: 10.1038/35057247

Henley, S. F., Cavan, E. L., Fawcett, S. E., Kerr, R., Monteiro, T., Sherrell, R. M., et al. (2020). Changing biogeochemistry of the southern ocean and its ecosystem implications. *Front. Mar. Sci.* 7:581. doi: 10.3389/fmars.2020.00581

Hobbs, W. R., Massom, R., Stammerjohn, S., Reid, P., Williams, G., and Meier, W. (2016). A review of recent changes in Southern Ocean sea ice, their drivers and forcings. *Glob. Planet. Change* 143, 228–250. doi: 10.1016/j.gloplacha.2016.06.008

Illuminati, S., Annibaldi, A., Romagnoli, T., Libani, G., Antonucci, M., Scarponi, G., et al. (2017). Distribution of Cd, Pb and Cu between dissolved fraction, inorganic particulate and phytoplankton in seawater of Terra Nova Bay (Ross Sea, Antarctica) during austral summer 2011–12. *Chemosphere* 185, 1122–1135. doi: 10.1016/j.chemosphere.2017.07.087

Ittekkot, V., Degens, E. T., and Brockmann, U. (1982). Monosaccharide composition of acid−hydrolyzable carbohydrates in particulate matter during a plankton bloom. *Limnol. Oceanogr.* 24, 770–776. doi: 10.4319/lo.1982.27.4.0770

Iversen, K. R., and Seuthe, L. (2011). Seasonal microbial processes in a high-latitude fjord (Kongsfjorden, Svalbard): I. Heterotrophic bacteria, picoplankton and nanoflagellates. *Polar Biol.* 34, 731–749. doi: 10.1007/s00300-010-0929-2

Kakinuma, M., Coury, D. A., Kuno, Y., Itoh, S., Kozawa, Y., Inagaki, E., et al. (2006). Physiological and biochemical responses to thermal and salinity stresses in a sterile mutant of Ulva pertusa (Ulvales, Chlorophyta). *Mar. Biol.* 149, 97–106. doi: 10.1007/s00227-005-0215-y

Kang, J. J., Joo, H. T., Lee, J. H., Lee, J. H., Lee, H. W., Lee, D., et al. (2017). Comparison of biochemical compositions of phytoplankton during spring and fall seasons in the northern East/Japan Sea. *Deep.Res. Part II Top. Stud. Oceanogr.* 143, 73–81. doi: 10.1016/j.dsr2.2017.06.006

Kim, B. K., Lee, J. H., Joo, H. T., Song, H. J., Yang, E. J., Lee, S. H., et al. (2016). Macromolecular compositions of phytoplankton in the Amundsen Sea, Antarctica. *Deep. Res. II Top. Stud. Oceanogr.* 123, 42–49. doi: 10.1016/j.dsr2.2015.04.024

Kim, B. K., Lee, J. H., Yun, M. S., Joo, H. T., Song, H. J., Yang, E. J., et al. (2015). High lipid composition of particulate organic matter in the northern Chukchi Sea, 2011. *Deep. Res. II Top. Stud. Oceanogr.* 120, 72–81. doi: 10.1016/j.dsr2.2014.03.022

Kim, B. K., Lee, S. H., Ha, S. Y., Jung, J., Kim, T. W., Yang, E. J., et al. (2018). Vertical distributions of macromolecular composition of particulate organic matter in the water column of the Amundsen Sea polynya during the summer in 2014. *J. Geophys. Res. Ocean* 123, 1393–1405. doi: 10.1002/2017JC013457

Lazzara, L., Massi, L., Nuccio, C., and Biondi, N. (1997). "Phytoplankton ecology: irradiance, particles, gilvin, pigments, absorption, fluorescence, production and species density in Terra Nova Bay, Ross Sea," in *ROSSMIZE 93–95*, eds F. M. Faranda, L. Guglielmo, and P. Povero (Alexandria: National Program of Antarctic), 229–279.

Lee, S. H., Kim, B. K., Yun, M. S., Joo, H. T., Yang, E. J., Kim, Y. N., et al. (2012). Spatial distribution of phytoplankton productivity in the Amundsen Sea, Antarctica. *Polar Biol.* 35, 1721–1733. doi: 10.1007/s00300-012-1220-5

Lee, S. H., Kim, H. J., and Whitledge, T. E. (2009). High incorporation of carbon into proteins by the phytoplankton of the Bering Strait and Chukchi Sea. *Cont. Shelf Res.* 29, 1689–1696. doi: 10.1016/j.csr.2009.05.012

Lee, S. H., and Whitledge, T. E. (2005). Primary and new production in the deep Canada Basin during summer 2002. *Polar Biol.* 28, 190–197. doi: 10.1007/s00300-004-0676-3

Lee, S. H., Whitledge, T. E., and Kang, S. H. (2008). Spring time production of bottom ice algae in the landfast sea ice zone at Barrow, Alaska. *J. Exp. Mar. Bio. Ecol.* 367, 204–212. doi: 10.1016/j.jembe.2008.09.018

Li, W. K. W., McLaughlin, F. A., Lovejoy, C., and Carmack, E. C. (2009). Supporting online material for: smallest algae thrive as the Arctic Ocean freshens. *Science* 326:539. doi: 10.1126/science.1179798

Liebezeit, G. (1984). Particulate carbohydrates in relation to phytoplankton in the euphotic zone of the Bransfield Strait. *Polar Biol.* 2, 225–228. doi: 10.1007/BF00263628

Liu, J., and Curry, J. A. (2010). Accelerated warming of the Southern Ocean and its impacts on the hydrological cycle and sea ice. *Proc. Natl. Acad. Sci. U.S.A.* 107, 14987–14992. doi: 10.1073/pnas.1003336107

Lizotte, M. P., and Sullivan, C. W. (1992). Biochemical composition and photosynthate distribution in sea ice microalgae of McMurdo Sound, Antarctica: evidence for nutrient stress during the spring bloom. *Antarct. Sci.* 4, 23–30. doi: 10.1017/S0954102092000063

Lobbes, J. M., Fitznar, H. P., and Kattner, G. (2000). Biogeochemical characteristics of dissolved and particulate organic matter in Russian rivers entering the Arctic Ocean. *Geochim. Cosmochim. Acta* 64, 2973–2983. doi: 10.1016/S0016-7037(00)00409-9

Lowry, O. H., Rosebrough, N. J., Farr, A. L., and Randall, R. J. (1951). Protein measurement with the Folin phenol reagent. *J. Biol. Chem.* 193, 265–275. doi: 10.1016/0922-338X(96)89160-4

Majewska, R., Gambi, M. C., Totti, C. M., Pennesi, C., and De Stefano, M. (2013). Growth form analysis of epiphytic diatom communities of Terra Nova Bay (Ross Sea, Antarctica). *Polar Biol.* 36, 73–86. doi: 10.1007/s00300-012-1240-1

Mangoni, O., Saggiomo, M., Bolinesi, F., Castellano, M., Povero, P., Saggiomo, V., et al. (2019). Phaeocystis antarctica unusual summer bloom in stratified antarctic coastal waters (Terra Nova Bay, Ross Sea). *Mar. Environ. Res.* 151:104733. doi: 10.1016/j.marenvres.2019.05.012

Mangoni, O., Saggiomo, V., Bolinesi, F., Margiotta, F., Budillon, G., Cotroneo, Y., et al. (2017). Phytoplankton blooms during austral summer in the Ross Sea, Antarctica: driving factors and trophic implications. *PLoS One* 12:e0176033. doi: 10.1371/journal.pone.0176033

Markus, T., Stroeve, J. C., and Miller, J. (2009). Recent changes in Arctic sea ice melt onset, freezeup, and melt season length. *J. Geophys. Res.* 114:C12024. doi: 10.1029/2009JC005436

Marsh, J. B., and Weinstein, D. B. (1966). Simple charring method for determination of lipids. *J. Lipid Res.* 7, 574–576. doi: 10.1016/s0022-2275(20)39274-9

Martiny, A. C., Vrugt, J. A., and Lomas, M. W. (2014). Concentrations and ratios of particulate organic carbon, nitrogen, and phosphorus in the global ocean. *Sci. Data*. 1:140048. doi: 10.1038/sdata.2014.48

Massom, R., Reid, P., Stammerjohn, S., Raymond, B., Fraser, A., and Ushio, S. (2013). Change and variability in East Antarctic Sea ice seasonality, 1979/80-2009/10. *PLoS One* 8:e64756. doi: 10.1371/journal.pone.0064756

Mayzaud, P., Chanut, J., and Ackman, R. (1989). Seasonal changes of the biochemical composition of marine particulate matter with special reference to fatty acids and sterols. *Mar. Ecol. Prog. Ser.* 56, 189–204. doi: 10.3354/meps056189

McMinn, A., Martin, A., and Ryan, K. (2010). Phytoplankton and sea ice algal biomass and physiology during the transition between winter and spring (McMurdo Sound, Antarctica). *Polar Biol.* 33, 1547–1556. doi: 10.1007/s00300-010-0844-6

McQuoid, M. R., and Hobson, L. A. (1996). Diatom resting stages. *J. Phycol.* 32, 889–902. doi: 10.1111/j.0022-3646.1996.00889.x

Misic, C., Castellano, M., Ruggieri, N., and Povero, P. (2006). Dissolved organic matter characterisation and temporal trends in Terra Nova Bay (Ross Sea, Antarctica). *Estuar. Coast. Shelf Sci.* 70, 405–414. doi: 10.1016/j.ecss.2006.06.024

Moal, J., Martin-Jezequel, V., Harris, R. P., Samain, J. F., and Poulet, S. A. (1987). Interspecific and intraspecific variability of the chemical composition of marine phytoplankton. *Oceanol. Acta* 10, 339–346.

Morán, X. A. G., López-Urrutia, Á, Calvo-Díaz, A., and Li, W. K. W. (2010). Increasing importance of small phytoplankton in a warmer ocean. *Glob. Chang. Biol.* 16, 1137–1144. doi: 10.1111/j.1365-2486.2009.01960.x

Oku, O., and Kamatani, A. (1995). Resting spore formation and phosphorus composition of the marine diatom *Chaetoceros pseudocurvisetus* under various nutrient conditions. *Mar. Biol.* 123, 393–399. doi: 10.1007/BF00353630

Oku, O., and Kamatani, A. (1999). Resting spore formation and biochemical composition of the marine planktonic diatom *Chaetoceros pseudocurvisetus* in culture: ecological significance of decreased nucleotide content and activation of the xanthophyll cycle by resting spore formation. *Mar. Biol.* 135, 425–436. doi: 10.1007/s002270050643

Palmisano, A. C., and Sullivan, C. W. (1982). Physiology of sea ice diatoms. I. response of three polar diatoms to a simulated summerwinter transition. *J. Phycol.* 18, 489–498. doi: 10.1111/j.1529-8817.1982.tb03215.x

Parkinson, C. L. (1994). Spatial patterns in the length of the sea ice season in the Southern Ocean, 1979–1986. *J. Geophys. Res.* 99, 16327–16339. doi: 10.1029/94jc01146

Parkinson, C. L. (2002). Trends in the length of the Southern Ocean sea-ice season, 1979–99. *Ann. Glaciol.* 34, 435–440. doi: 10.3189/172756402781817482

Parsons, T. R., Maita, Y., and Lalli, C. M. (1984). *A Manual of Chemical and Biological Methods for Seawater Analysis*. New York, NY: Pergamon Press.

Pirt, S. J. (1975). *Principles of Microbe and Cell Cultivation*. Oxford: Blackwell Scientific Publications, 274.

Pusceddu, A., Serra, E., Sanna, O., and Fabiano, M. (1996). Seasonal fluctuations in the nutritional value of particulate organic matter in a lagoon. *Chem. Ecol.* 13, 21–37. doi: 10.1080/02757549608039099

Quetin, L. B., and Ross, R. M. (2009). "Life Under Antarctic Pack Ice: A Krill Perspective," in *Smithsonian at the Poles: Contributions to International Polar Year Science*, eds I. Krupnik, M. A. Lang, and S. E. Miller (Washington, DC: Smithsonian Institution), doi: 10.5479/si.097884601x.21

Quetin, L. B., Ross, R. M., Fritsen, C. H., and Vernet, M. (2007). Ecological responses of Antarctic krill to environmental variability: can we predict the future? *Antarct. Sci.* 19, 253–266. doi: 10.1017/S0954102007000363

Rivaro, P., Luisa Abelmoschi, M., Grotti, M., Ianni, C., Magi, E., Margiotta, F., et al. (2012). Combined effects of hydrographic structure and iron and copper availability on the phytoplankton growth in Terra Nova Bay Polynya (Ross Sea, Antarctica). *Deep. Res. I Oceanogr. Res. Pap.* 62, 97–110. doi: 10.1016/j.dsr.2011.12.008

Rivkin, R. B., and Voytek, M. A. (1987). Photoadaptations of photosynthesis and carbon metabolism by phytoplankton from McMurdo sound, Antarctica. 1. species−specific and community responses to reduced irradiances. *Limnol. Oceanogr.* 32, 249–259. doi: 10.4319/lo.1987.32.1.0249

Ross, R. M., Quetin, L. B., Martinson, D. G., Iannuzzi, R. A., Stammerjohn, S. E., and Smith, R. C. (2008). Palmer LTER: patterns of distribution of five dominant zooplankton species in the epipelagic zone west of the Antarctic Peninsula, 1993–2004. *Deep. Res. II Top. Stud. Oceanogr.* 55, 2086–2105. doi: 10.1016/j.dsr2.2008.04.037

Sedwick, P. N., Di Tullio, G. R., and Mackey, D. J. (2000). Iron and manganese in the Ross Sea, seasonal iron limitation in Antarctic. *J. Geophys. Res. Ocean* 105, 11321–11336. doi: 10.1029/2000JC000256

Sedwick, P. N., Marsay, C. M., Sohst, B. M., Aguilar-Islas, A. M., Lohan, M. C., Long, M. C., et al. (2011). Early season depletion of dissolved iron in the Ross Sea polynya: implications for iron dynamics on the Antarctic continental shelf. *J. Geophys. Res. Ocean* 116:C12019. doi: 10.1029/2010JC006553

Shifrin, N. S., and Chisholm, S. W. (1981). Phytoplankton lipids: interspecific differences and effects of nitrate, silicate and light–dark cycles. *J. Phycol.* 17, 374–384. doi: 10.1111/j.0022-3646.1981.00374.x

Smayda, T. J., and Mitchell-Innes, B. (1974). Dark survival of autotrophic, planktonic marine diatoms. *Mar. Biol.* 25, 195–202. doi: 10.1007/BF00394965

Song, H. J., Kang, J. J., Kim, B. K., Joo, H. T., Yang, E. J., Park, J., et al. (2016). High protein production of phytoplankton in the Amundsen Sea. *Deep Sea Res.* 123, 50–57. doi: 10.1016/j.dsr2.2015.07.015

Stammerjohn, S., Massom, R., Rind, D., and Martinson, D. (2012). Regions of rapid sea ice change: an inter-hemispheric seasonal comparison. *Geophys. Res. Lett.* 39:L06501. doi: 10.1029/2012GL050874

Stammerjohn, S. E., Martinson, D. G., Smith, R. C., Yuan, X., and Rind, D. (2008). Trends in Antarctic annual sea ice retreat and advance and their relation to El Niño–Southern oscillation and southern annular mode variability. *J. Geophys. Res.* 113:C03S90. doi: 10.1029/2007jc004269

Suárez, I., and Marañón, E. (2003). Photosynthate allocation in a temperate sea over an annual cycle: the relationship between protein synthesis and phytoplankton physiological state. *J. Sea Res.* 50, 285–299. doi: 10.1016/j.seares.2003.04.002

Wada, E., Terazaki, M., Kabaya, Y., and Nemoto, T. (1987). 15N and 13C abundances in the Antartic Ocean with emphasis on the biogeochemical structure of the food web. *Deep Sea Res. A Oceanogr. Res. Pap.* 34, 829–841. doi: 10.1016/0198-0149(87)90039-2

Winberg, G. G. (1971). *Symbols, Units and Conversion Factors in Study of Fresh Waters Productivity*. London: International Biological Programme, 23.

Yun, M. S., Lee, D. B., Kim, B. K., Kang, J. J., Lee, J. H., Yang, E. J., et al. (2015). Comparison of phytoplankton macromolecular compositions and zooplankton proximate compositions in the northern Chukchi Sea. *Deep. Res. II Top. Stud. Oceanogr.* 120, 82–90. doi: 10.1016/j.dsr2.2014.05.018

Zhu, Z., Xu, K., Fu, F., Spackeen, J. L., Bronk, D. A., and Hutchins, D. A. (2016). A comparative study of iron and temperature interactive effects on diatoms and *Phaeocystis* Antarctica from the Ross Sea, Antarctica. *Mar. Ecol. Prog. Ser.* 550, 39–51. doi: 10.3354/meps11732

Zweifel, U. L., Norrman, B., and Hagstrom, A. (1993). Consumption of dissolved organic carbon by marine bacteria and demand for inorganic nutrients. *Mar. Ecol. Prog. Ser.* 10, 23–32. doi: 10.3354/meps101023

Conflict of Interest: The authors declare that the research was conducted in the absence of any commercial or financial relationships that could be construed as a potential conflict of interest.

frontiers in Microbiology

ORIGINAL RESEARCH
published: 11 February 2021
doi: 10.3389/fmicb.2021.607601

Temperature Stress Induces Shift From Co-Existence to Competition for Organic Carbon in Microalgae-Bacterial Photobioreactor Community – Enabling Continuous Production of Microalgal Biomass

*Eva Sörenson[1], Eric Capo[2], Hanna Farnelid[1], Elin Lindehoff[1] and Catherine Legrand[1]**

[1]*Department of Biology and Environmental Science, Centre of Ecology and Evolution and Microbial Model Systems, Linnaeus University, Kalmar, Sweden,* [2]*Department of Chemistry, Umeå University, Umeå, Sweden*

OPEN ACCESS

Edited by:
Jun Sun, Tianjin University of Science and Technology, China

Reviewed by:
Claudia Coleine, University of Tuscia, Italy
Sarahi L. Garcia, Stockholm University, Sweden

***Correspondence:**
Catherine Legrand
catherine.legrand@lnu.se

Specialty section:
This article was submitted to Aquatic Microbiology, a section of the journal Frontiers in Microbiology

Received: *17 September 2020*
Accepted: *12 January 2021*
Published: *11 February 2021*

Citation:
Sörenson E, Capo E, Farnelid H, Lindehoff E and Legrand C (2021) Temperature Stress Induces Shift From Co-Existence to Competition for Organic Carbon in Microalgae-Bacterial Photobioreactor Community – Enabling Continuous Production of Microalgal Biomass. Front. Microbiol. 12:607601. doi: 10.3389/fmicb.2021.607601

To better predict the consequences of environmental change on aquatic microbial ecosystems it is important to understand what enables community resilience. The mechanisms by which a microbial community maintain its overall function, for example, the cycling of carbon, when exposed to a stressor, can be explored by considering three concepts: biotic interactions, functional adaptations, and community structure. Interactions between species are traditionally considered as, e.g., mutualistic, parasitic, or neutral but are here broadly defined as either coexistence or competition, while functions relate to their metabolism (e.g., autotrophy or heterotrophy) and roles in ecosystem functioning (e.g., oxygen production, organic matter degradation). The term structure here align with species richness and diversity, where a more diverse community is though to exhibit a broader functional capacity than a less diverse community. These concepts have here been combined with ecological theories commonly used in resilience studies, i.e., adaptive cycles, panarchy, and cross-scale resilience, that describe how the status and behavior at one trophic level impact that of surrounding levels. This allows us to explore the resilience of a marine microbial community, cultivated in an outdoor photobioreactor, when exposed to a naturally occurring seasonal stress. The culture was monitored for 6 weeks during which it was exposed to two different temperature regimes (21 ± 2 and 11 ± 1°C). Samples were taken for metatranscriptomic analysis, in order to assess the regulation of carbon uptake and utilization, and for amplicon (18S and 16S rRNA gene) sequencing, to characterize the community structure of both autotrophs (dominated by the green microalgae *Mychonastes*) and heterotrophs (associated bacterioplankton). Differential gene expression analyses suggested that community function at warm temperatures was based on concomitant utilization of inorganic and organic carbon assigned to autotrophs and heterotrophs, while at colder temperatures, the uptake of organic carbon was performed primarily by autotrophs. Upon the shift from high to low temperature, community interactions shifted from coexistence to competition for organic carbon. Network analysis

indicated that the community structure showed opposite trends for autotrophs and heterotrophs in having either high or low diversity. Despite an abrupt change of temperature, the microbial community as a whole responded in a way that maintained the overall level of diversity and function within and across autotrophic and heterotrophic levels. This is in line with cross-scale resilience theory describing how ecosystems may balance functional overlaps within and functional redundancy between levels in order to be resilient to environmental change (such as temperature).

Keywords: microalgae, bacteria, community, resilience, coexistence, competition, adaptive cycles, interactions

INTRODUCTION

Microorganisms make up ≈70% of the aquatic biomass and their interactions in the microbial loop are vital for the recycling of energy and nutrients that ensure the ecosystem services provided by aquatic food webs (Azam et al., 1983; Bar-On et al., 2018). In addition, aquatic microorganisms contribute ≈50% of the O_2 in the atmosphere today (Field et al., 1998; Behrenfeld et al., 2001). The impact of current and predicted environmental changes on aquatic microorganisms, including the increasing sea surface temperatures (Collins and Knutti, 2013), is difficult to assess due to the lack of studies using high-resolution molecular methods of microbial community interactions. The ability of aquatic microbial ecosystems to be resilient to disturbances, on shorter or longer scales, depends on the interplay of multiple factors (Allison and Martiny, 2008; Shade et al., 2012a). Identifying the behavior of key resilience mechanisms in response to changed environmental conditions may lead to more accurate predictions of the effects of environmental changes on biogeochemical cycles. Such knowledge could for instance enable the implementation of more locally adapted monitoring and management programs of aquatic microbial ecosystems (Bernhardt and Leslie, 2013; Andersson et al., 2015). Several studies have suggested that the functional capabilities of experimental microbial ecosystems, and thus their resilience, were not found to be related to the composition of the communities (Fernandez et al., 2000; Wang et al., 2011; Vanwonterghem et al., 2014; Louca and Doebeli, 2016), which might be explained by the large functional redundancy and diversity that exists among microbial species (Louca et al., 2017, 2018, 2020). Microbial ecosystems are complex and consist of several interacting levels, such as trophic levels, that enable the transfer of energy and nutrients within the microbial loop and further up in the food web. Adaptations to changed conditions seen at one level likely have an influence on the levels above or below (Gunderson and Holling, 2002). Thus, in order to gain a deeper understanding of the underlying mechanisms of the resilience of microbial communities, it is important to link experimental results with theories. In this study, we focused on three interlinked mechanisms that together have the potential to influence microbial ecosystem resilience in response to changed environmental conditions: biotic interactions, functional adaptations, and community structure. Interactions between organisms in microbial ecosystems are commonly described through the presence or absence of the exchange of signals or metabolites, including mutualistic, parasitic, or neutral relationships (Tipton et al., 2019). Here, the focus is on broad-scale community interactions, disregarding any potential microalgal-bacterial cooperation apart from that that involves carbon. Broadly, the considered interactions may primarily be characterized by either coexistence, governed by resource partitioning (Sörenson et al., 2020), or by competition for energy and nutrients, which may lead to competitive exclusion (Schoener, 1974; Chesson, 2000). Both types of interactions influence biogeochemical cycles, e.g., that of carbon, through potential functional changes and variations in microbial community structure (Lindh and Pinhassi, 2018; Sörenson et al., 2020). Functions relevant for studies of aquatic microbial ecosystems commonly relate to whether organisms are autotrophs, heterotrophs, or mixotrophs, which is defined by the type of carbon (inorganic, organic, or both) they have the capacity to acquire as a food source and to use for energy production. Temporal dynamics in the structure of a community relate to its species richness or diversity, in which a more diverse community is characterized by a more efficient use of resources compared to a less diverse community that likely have a more narrow functional range (Cardinale et al., 2006; Ptacnik et al., 2008).

In resilience theory, the term panarchy has been used together with adaptive cycles and cross-scale resilience theories to describe the sustainability of both social and ecological systems (Holling, 1973; Peterson et al., 1998; Gunderson and Holling, 2002). Adaptive cycles postulate four phases that a system continuously pass through: birth – growth and accumulation of resources (r), maturation – conservation of established processes (K), death – the release upon changed conditions (Ω), and renewal – the creative phase of reorganization and adaptation to new conditions (α; Holling, 1973). Panarchy describes how separate levels within an ecosystem, each with their own adaptive cycle, interact in order to accommodate and adapt to changed conditions. Where lower levels, primarily when entering the Ω-phase, influence the level above (termed revolt) while the upper levels, primarily during the K-phase, are able to buffer the impact (termed remember), and thereby the levels together affect the community resilience (Gunderson and Holling, 2002). Cross-scale resilience describes how ecosystems may become resilient by balancing overlapping functional diversity within and functional redundancy across levels (Peterson et al., 1998). In this study, levels are interpreted as trophic levels.

Ecosystem resilience may be explained as the capacity to harbor, through internal fluctuations of function and structure, smaller or larger environmental changes (Holling, 1973), while maintaining over-all function, structure, and identity (Walker, 2004). The capacity of aquatic microbial ecosystems to respond in a resilient manner to the regime shifts in, e.g., temperature that might be the result of present and future climate change is difficult, by important, to assess (O'Gorman et al., 2012). Currently, few studies have empirically investigated resilience within aquatic microbial ecosystems (e.g., Shade et al., 2012b; Lindh and Pinhassi, 2018). For the coastal regions of Scandinavia projected environmental changes are increasing temperature, precipitation, land run-off, and ocean acidification (Collins and Knutti, 2013). Coupling analyses of the responses in controlled and simplified ecosystems to environmental change, in terms of structural and functional dynamics together with analyses of the impact on community interactions, with established ecological theories, models of aquatic ecosystem responses to climate change may be improved (Prosser and Martiny, 2020).

Using model systems with only a few species and controlled conditions in a laboratory help to gain a regulatory mechanistic insight of microbial interactions at the detailed level (Segev et al., 2016; Bolch et al., 2017). It is, however, important to study more complex, yet simplified systems, with several interacting levels, as ecosystem responses to environmental change, depend on the response at each contained level (Gunderson and Holling, 2002). Thus, systems of medium complexity, with several interacting functional groups (auto-, hetero-, and mixotrophs), kept under controlled nutrient conditions and influenced by a few environmental parameters, will help in predicting the consequences of environmental change on microbial communities and the impact of this on larger scale biogeochemical cycles (Otwell et al., 2018). In the present study, an algal polyculture kept in an outdoor photobioreactor (PBR), with a capacity to produce up to 0.88 gl^{-1} biomass per day (**Supplementary Figure S1**), was investigated. The PBR community, composed of a few naturally selected microalgae species, dominated by a mixotrophic green microalgae (with the ability to utilize both inorganic and organic carbon), and a mixed, naturally established, bacterial community, was provided with inorganic carbon, and studied under two different temperature conditions (warm/cold). As the availability of light influence the efficiency of photosynthesis and uptake of carbon, this was also studied in addition to temperature as a potential structuring factor. The aim of the study was to elucidate the effect that changes in temperature regimes have on microalgae-bacteria interactions, by focusing on the functional regulation in the acquisition of carbon (organic and/or inorganic) and on the impact of this regulation on the dynamics of community structure. Further, we wanted to investigate the influence of interlevel interactions on the resilience of the community, in terms of maintained production of microalgal biomass. Analyses of community structural dynamics were made by generating amplicon sequencing data and using co-occurrence network analysis. Analyses of the functional regulation in the acquisition of carbon by the PBR community were made using a metatranscriptomic approach. The capacity of the microbial community for resilience was investigated using adaptive cycles, panarchy, and cross-scale resilience theories.

MATERIALS AND METHODS

Photobioreactor Setup

A large-scale outdoor PBR, PBR, remediating cement factory flue gas emissions between April and November since 2014 (Olofsson, 2015; Mattsson et al., in prep), located at the southern part of Öland (56°21.2'N 16°24.6'E, Sweden), in the Kalmar Strait/Baltic Proper, was sampled bi-weekly (Wednesdays and Fridays), around 10 a.m., during September and October of 2018. The closed non-heated system containing 3,200 L brackish (salinity 6.9 ± 0.3) Baltic Sea water, was circulated between eight vertical flat panels and designed to take up CO_2 from the emitted flue gas through algal photosynthesis. Stable pH (7.8 ± 0.3) and O_2 levels were monitored and maintained within a constant range. After each bi-weekly sampling (1 L) and subsequent harvest of biomass (30–50% of total volume), the reactor was supplied with nutrients in the form of Cell-Hi f/2 powder (Varicon Aqua), according to Guillard's f/2 medium (Guillard, 1975), amended with 19 mM of NaH_2PO_4, along with a refill of filtered seawater (0.2 µm cylinder polypropylene filters cartridge), to the full volume. The 6 weeks covered in the study included two periods, with four sampling events each: S1–S4 and S5–S8 respectively, with distinct seasonally induced temperature conditions (**Figure 1**). The light reaching the panels was reduced by thin nets with a 40–60% reduction efficiency, with negligible influence on reactor panel temperature, between first and second sampling occasion each week (corresponding to sampling events S4, S6, and S8, **Figure 1**).

Measurements of Biomass and Environmental Parameters

Algal biomass was measured as dry weight (DW) of 10 ml algal culture for each date. The culture was filtered onto rinsed, pre-dried and weighed, 47 mm GF/F filters (0.5 µm, Whatman), and dried again at 100°C overnight. The weight of the dry algal biomass was measured the following day. Daily sunlight hours were measured using a CSD three sunshine duration sensor (Kipp & Zonen), counting direct solar radiation >120 Wm^{2-1}. The sensor was located at Ottenby (ca 10 km south of the location of algal PBR). Daytime length was retrieved from Soltimmar.se (location Kalmar). Temperature in the PBR panels was measured by the monitoring system of the reactor. Ambient temperature of the region was retrieved from the Swedish Meteorological and Hydrological Institute (SMHI).

16S and 18S Amplicon Sequencing Analysis

For DNA sampling, 5–7 ml of culture was filtered, with a vacuum hand-pump, through 0.2 µm pore-sized filters (Supor-200, 47 mm, PALL), with three replicates per sampling event. All filters were immediately immersed in RNAlater (Sigma Scientific) and snap-frozen in dry ice, and upon return to the laboratory (~1–2 h later) stored at −80°C, until further processing.

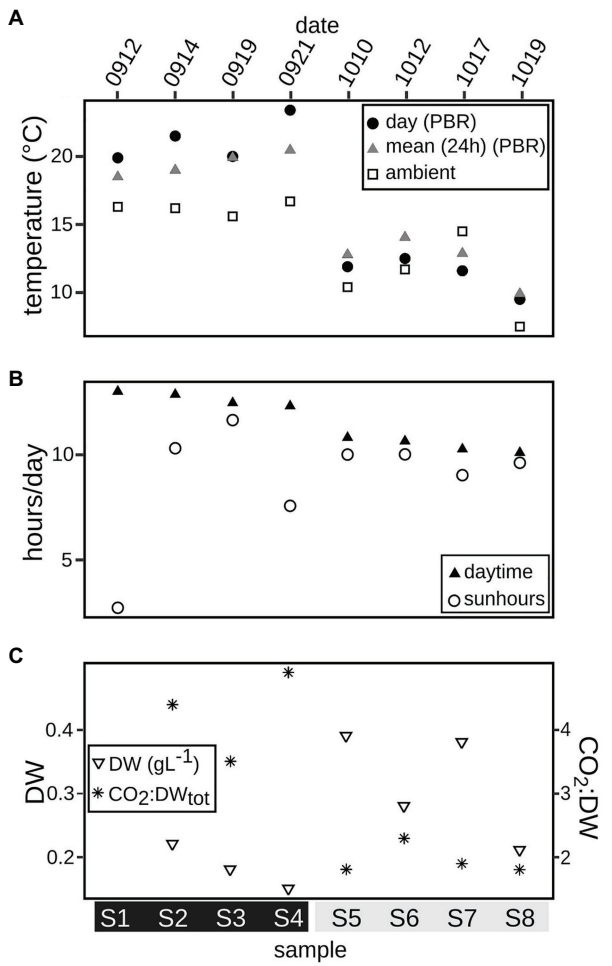

FIGURE 1 | Parameters associated with the photobioreactor (PBR) during the sampling period, dates of sampling specified on top, sample names S1–S8 at the bottom. **(A)** Daytime temperature (°C) in PBR (closed circles), mean temperature per 24 h in PBR (gray triangles), regional ambient daytime temperature (measured by SMHI; open squares). **(B)** Number of hours day^{-1} with sunshine (direct solar radiation > 120 Wm^{-2}, 10 km south of PBR location; open circles), daytime hours/day (black triangles). **(C)** For S2–S8 sampling events (S1 omitted due to lack of data), left *y*-axis: Dry weight (DW) of biomass (gl^{-1}; open triangles) and right *y*-axis: ratio of flow in added mass (g) of CO_2:total dry weight (in 3200 L; asterisks).

DNA was extracted using the FastDNA Spin Kit for soil (MPBio, Irvine, CA, United States) according to protocol, with the modification that a 1 h incubation step at 55°C with proteinaseK (20 mg/ml final concentration) was included after the homogenization step, to increase DNA precipitation. The 48 DNA extracts were quantified using a Qubit fluorometer (Invitrogen, Carlsbad, CA, United States) and checked for purity with Nanodrop 2000 spectrophotometer (Thermo Fisher Scientific, Waltham, MA, United States). The V3–V4 region of the 16S rRNA gene was amplified using primers 341F (CCTACGGGNGGCWGCAG) and 805R (GACTACHVGGG TATCTAATCC), and the V4–V5-region of the 18S rRNA gene was amplified using primers 574*F (CGGTAAYTCCAGCTCYV) and 1132R (CCGTCAATTHCTTYAART), connected to Nextera DNA Dual-index adaptors in accordance with Herlemann et al. (2011) and Hugerth et al. (2014), respectively. The PCRs were performed using Phusion Mastermix (Thermo Scientific), and the following settings: (i) 16S [1 x (98°C, 30 s), 20 x (98°C, 10 s, 58°C, 30 s, 72°C, 15 s), 1 x (72°C, 2 min)], modified from Bunse et al. (2016), (ii) 18S [1 x (98°C, 30 s), 28 x (98°C, 20 s, 50.4°C, 20 s, 72°C, 15 s), 1 x (72°C, 2 min)]. In a second PCR assay, Nextera indices (i7 and i5) were attached to both the 16S and 18S products with settings: [1 x (98°C, 30 s), 12 x (98°C, 20 s, 62°C, 30 s, 72°C, 30 s), 1 x (72°C, 2 min)], modified from Hugerth et al. (2014). The PCR products were purified both after the first and the second amplification steps, using the Agencourt AMPure XP kit (Beckman-Coulter) according to the manufacturer's instructions. Products were quantified using a Qubit fluorometer and quality checked using a NanoDrop 2000 spectrophotometer. Fragment sizes were validated to ca 600 base pairs (bp) for both 16S and 18S samples using gel electrophoresis. Samples were pooled at equimolar concentrations, and the pool was purified using E.Z.N.A Gel extraction Kit (Omega Bio-tek) and sequenced using Illumina MiSeq v3, PE (Illumina Inc., United States), 2 × 300 bp, at SciLifeLab (Stockholm, Sweden).

Raw reads of 16S and 18S rRNA gene amplicon data were processed separately with dada2 (version 1.6.0; Callahan et al., 2016), implemented in R (version 3.4.3; Core, 2018). Of the 6,434,529 18S raw reads, 76% remained after error model filtration, and of the 12,981,918 16S reads, 87% remained after error model filtration (**Supplementary Tables S1, S2**). Only forward reads were used to construct the sequence table of amplicon sequence variants (ASV's), due to uninformative overlaps of reverse reads. This resulted in 1,110 18S ASVs and 6,467 16S ASVs, which were used for further analyses. For both 16S and 18S ASVs the taxonomy was assigned using SILVA database (v132; Quast et al., 2013). Of the 16S ASVs 299 were assigned as chloroplasts (**Supplementary Figure S2**), which were filtered from the 16S dataset before further analyses. Relative abundances of both 16S and 18S ASVs were plotted in R with ggplot2 (Wickham, 2016), and an assessment of independent environmental parameters was made using function *varclus* from R package Hmisc (Harrell and Dupont, 2019) with Spearman's rank correlations. Canonical correspondence analysis (CCA) was made with independent environmental parameters in the model, with function *cca* (999 permutations) from R package vegan (Oksanen et al., 2008) and plotted with ggplot2. PERMANOVA analyses of both 16S and 18S ASVs were made using *adonis2*, richness (Chao1) and diversity (Shannon and Simpson) were estimated using functions *estimateR* and *diversity*, respectively, from the vegan package (Oksanen et al., 2008). For the 16S data, functions *rarefy* and *rarecurve*, with step = 20, from the vegan package were used to make rarefaction curves, and R package RAD analysis (Saeedghalati et al., 2017) was used to make normalized, by minimum richness = 136, rank abundance curves. As most environmental parameters were missing from the initial date (0912, S1) this date was excluded from the CCA's.

Amplicon data was analyzed for patterns of co-occurrences between relative abundances of 18S and 16S ASVs with

environmental parameters including temperature, light/shade, sun hours, and biomass (DW), using the R package Weighted Correlation Network Analysis (WGCNA, v1.68) (Langfelder and Horvath, 2008) in R (v3.6.1). The 18S and 16S datasets were first rarefied to the smallest library size (39,469 and 10,824 sequences, respectively) and to reduce the complexity of the data, ASVs with <0.1% counts per library were excluded, resulting in 55 18S ASVs and 309 16S ASVs that were used for further analysis. Functions from WGCNA R package was performed according to Capo et al. (2017). Briefly, relative abundance data was standardized with Hellinger transformation (function *decostand*; Oksanen et al., 2019). A signed network of clustered ASVs was created using function *adjacency* and a minimum of eight nodes (ASVs) per module, and power four was used as the threshold value. The relationships between the values of environmental factors, and modules eigenvalues were displayed using a heatmap. Only edges with pair-wise correlations values >0.3 and positive Pearson coefficient correlation's values >0.34, were included for network visualization, made using the software Gephi (Bastian et al., 2009).

Metatranscriptomic Analysis

For RNA sampling, 7.5–10 ml of culture was filtered sequentially, using a vacuum hand-pump, through 3 µm pore-sized filters (Versapor-3000, 47 mm, PALL) followed by 0.2 µm pore-sized filters (Supor-200, 47 mm, PALL), with six replicates per sampling event. All filters were immediately immersed in RNAlater (Sigma Scientific) and snap-frozen in dry ice, until −80°C conditions were available (~1–2 h later).

Within 4 months after sampling, filters were thawed on ice. 12 filters (6 × 0.2 and 6 × 3 µm) were retrieved per sampling occasion, of which one filter each of 0.2 and 3 µm were combined, resulting in six replicates. Filters were combined for RNA-extraction to maximize yield. On ice, filters were cut with scissors, and placed in MatrixE tubes (MPBio) prepared with, in total 1 ml, of RLT-buffer (Qiagen, Venlo, Netherlands), TE-buffer, B-mercaptoethanol [1:100], and Lysozyme (0.04 mg/ml). A FastPrep-24 instrument with a QuickPrep adaptor (MPBio) was used for lysing the cells, three rounds each at 6 ms^{-1} for 40 s, with 1 min on ice in between runs. After lysing, RNA was extracted using Qiagen RNeasy mini kit, according to protocol. The extracted RNA was treated with DNase to remove DNA (AMBIONTurbo DNA free). At this stage 24 samples were sent for poly-A selection followed by mRNA fragmentation and synthesis of cDNA at SciLifeLab (Stockholm, Sweden), to be used for eukaryotic gene expression analyses. Remaining 24 samples, to be used for prokaryotic gene expression analyses, were depleted of rRNA using RiboMinus Transcription isolation kit (Invitrogen), with a RiboMinus Concentration module. This was followed by a cDNA to aRNA protocol (MessageAmp II-Bacteria RNA amplification kit, Invitrogen). All 48 samples were sequenced on one lane of Illumina NovaSeq 6000 S1, PE 2 × 150 bp, at SciLife lab in Stockholm, Sweden.

Metatranscriptomes obtained from the poly-A selected (eukaryotic) and the amplified aRNA (prokaryotic) fractions were computationally processed using the same procedure. Quality was initially checked with FastQC (v0.11.8; Andrews, 2009) and MultiQC (v1.7; Ewels et al., 2016). Adaptors were removed using Cutadapt (v2.3; Martin, 2011). An additional check with FastQC/MultiQC showed that the remaining adaptors were below 0.1% for all samples. Reads were quality trimmed using Sickle (v1.33; Joshi and Fass, 2011). For the eukaryote data, there were in total 1,019,068,864 raw reads of which 94 ± 1% remained after quality filtration. For the prokaryote data, there were in total 966,439,508 raw reads of which 99 ± 0.4% remained after quality filtration (**Supplementary Tables S3, S2**). rRNA was filtered out by aligning reads to a local rRNA database using Bowtie2 (v2.3.5.1; Langmead and Salzberg, 2012). Samtools (v 1.9; Li et al., 2009) was then used to retrieve reads that did not match to the rRNA-db. Reads were assembled using Megahit (v.1.1.2; Li et al., 2016), and annotated against NCBI-RefSeq protein db, using Diamond (v0.9.24; Buchfink et al., 2015). These resulted in 571,442 eukaryote open reading frames (ORFs) and 58,151 prokaryote ORFs, of which 149,303 (26%) and 38,113 (66%) ORFs, respectively, were functionally annotated with SEED db (July 2019) using MEGAN (community edition, v6.12.8; Huson et al., 2016). MEGAN was also used for taxonomic annotations to NCBI-nr db (July 2019). Reads were then mapped against the assembly with Bowtie2 (v2.3.5.1) and Samtools (v 1.9).

Data Deposition

Sequence data have been submitted to European Nucleotide Archive, ENA, understudy ERP116148; amplicon raw reads: ERR3419055-ERR3419102; metatranscriptome raw reads: ERR3421213-ERR3421260.

RESULTS

Temporal Changes in Temperature and Light Conditions During the Experiment

The PBR was located outside throughout the study at northern hemisphere fall conditions (**Figure 1**). During the initial sampling period (S1–S4), the average daytime temperature in the PBR was significantly higher, at an average temperature of 21 ± 2°C (average ambient temperature 16 ± 0.5°C), compared to the second period (*t*-test, p = 3.1e-14), starting 2 weeks later (S5–S8), at an average temperature of 11 ± 1°C (average ambient temperature 11 ± 3°C). Between the first sampling (S1) and the last (S8), the length of daytime decreased by 2 h and 55 min. Daily sunshine hours varied between 2 and 11 h during the warmer period, while it was more stable, 9–10 h, during the colder period (**Figure 1**).

Nutrient Conditions and Production of Biomass

Inorganic nutrients (NH_4 and PO_4) were added to the PBR to assure non-limiting concentrations during the study period (**Supporting Information Table 1**). Significantly less biomass was produced during the initial (warmer) period (0.18 ± 0.04 gl^{-1})

compared to the second (colder) period (0.32 ± 0.09 gl^{-1}; *t*-test, p = 7.8e-05; **Figure 1**). The increased production pushed the capacity of the system towards carbon limitation, shown by the ratio between the flow of CO_2 to total biomass (gl^{-1}) produced, that shifted from 3.5 to 4.9 during the warmer period to 1.8–2.3 during the colder period (**Figure 1**).

Environmental Parameters Structuring the PBR Microbial Community

Analyses of the amplicon sequencing data with CCA (**Figure 2A**) and PERMANOVA showed that the structure of the microbial eukaryotes was significantly affected by the temperature in the PBR (PERMANOVA; temp, *df* = 2; *F* = 11.8, *R2* = 0.34, p = 0.004**) but not by the availability of light (reduced by shading; PERMANOVA; light, *df* = 2; *F* = 2.2, *R2* = 0.17, p = 0.069), while the structure of the microbial prokaryotes was significantly affected by both temperature and light (PERMANOVA; temp, *df* = 2; *F* = 27, *R2* = 0.55, $p < 0.001$***; light, *df* = 2; *F* = 8.0, *R2* = 0.43, $p < 0.001$***; **Figure 2B**). Further, the CCA plots suggested that the algal biomass, measured in DW (gl^{-1}), was clearly linked to the structure of both the microbial eukaryotes and prokaryotes, and was highly dependent on the temperature regime (warm or cold; **Figure 2**).

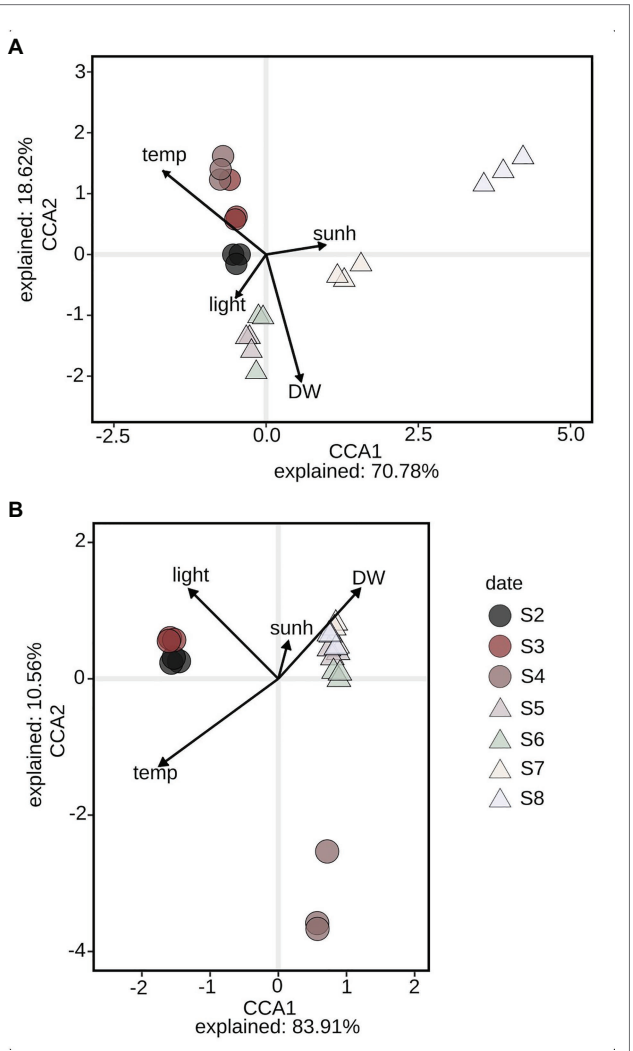

FIGURE 2 | Canonical correspondence analysis (CCA) biplot of the eukaryote **(A)** and prokaryote **(B)** community, plotting samples with independent environmental parameters at each date of sampling (S2–S8) in the reactor: Temp – temperature in PBR (°C), DW – biomass dry weight (gl^{-1}), sunh – number of sunshine hours at day of sampling (h), light – unshaded/shaded (reduced light input by 40–60%). Dates are denoted by color, warm period by (○), and cold period by (△). Date S1 is excluded due to missing nutrient data.

Composition of Microbial Eukaryotes

The 18S ASVs with a relative abundance >0.1% were taxonomically annotated at the genus level, corresponding to 98–99% relative abundance per sample (**Figure 3A**). The majority of sequences (ranging between 90 and 98% in samples) were annotated as green microalgae *Mychonastes*, of which one ASV (ASV_1) dominated all samples with relative abundances of 85–95% per sample (**Supplementary Figure S3**). The ASV had 100% sequence similarity to *Mychonastes* sp. with GenBank accession number MF595077 (**Supplementary Figure S4**). The average relative abundance of ASV_1 increased from the warm to the cold period. This coincided with a significant drop in both average species richness from 65 ± 11 to 38 ± 11 (std; Chao1; *t*-test, p = 4e-06) and average diversity from 0.65 ± 0.22 to 0.43 ± 0.09 (std; Shannon Index; *t*-test, p = 0.007; **Supplementary Figure S5A**). During the warm period, the relative abundance of ASVs assigned to green microalgae *Oocystis* (**Supplementary Figures S3, S4**) fluctuated between 1 and 6%, while they were almost absent during the colder period, as did the ASVs assigned to green microalgae *Chlorochytrium*, with relative abundances 0.1–0.4% during the warm period while they were not present during the cold period (**Supplementary Figures S3, S4**). Instead, ASVs assigned to the green microalgae *Monoraphidium* (**Supplementary Figures S3, S4**), increased from 0.3 to 0.8% during the warm period to a relative abundance of 1% during the cold period (**Figure 3A**).

Composition of Microbial Prokaryotes

The 16S ASVs with a relative abundance >0.1%, excluding ASVs annotated as chloroplasts, were annotated at the order level (**Figure 3B**). Rarefaction curves indicate that the sample depth, including both warm and cold periods, were sufficient to capture the species richness within the community (**Figure 4**). There was a significant drop in species richness from an average of 492 ± 133 to 300 ± 113 (std) going from warm to cold temperature (*t*-test, p = 0.001; **Supplementary Figure S5B**) and normalized rank abundance curves suggest that rank abundances were lower for the colder period, compared to the warmer period (**Figure 4**). There was however a significant increase in average Shannon index diversity from 4.8 ± 0.1 to 5.1 ± 0.3 (std; *t*-test, p = 0.03), that take both abundance and evenness into account (**Supplementary Figure S5B**), indicating an increased diversity among the bacteria during the cold period. During the warm period, the bacterial community was dominated by alphaproteobacterial Rhizobiales (45 ± 9%

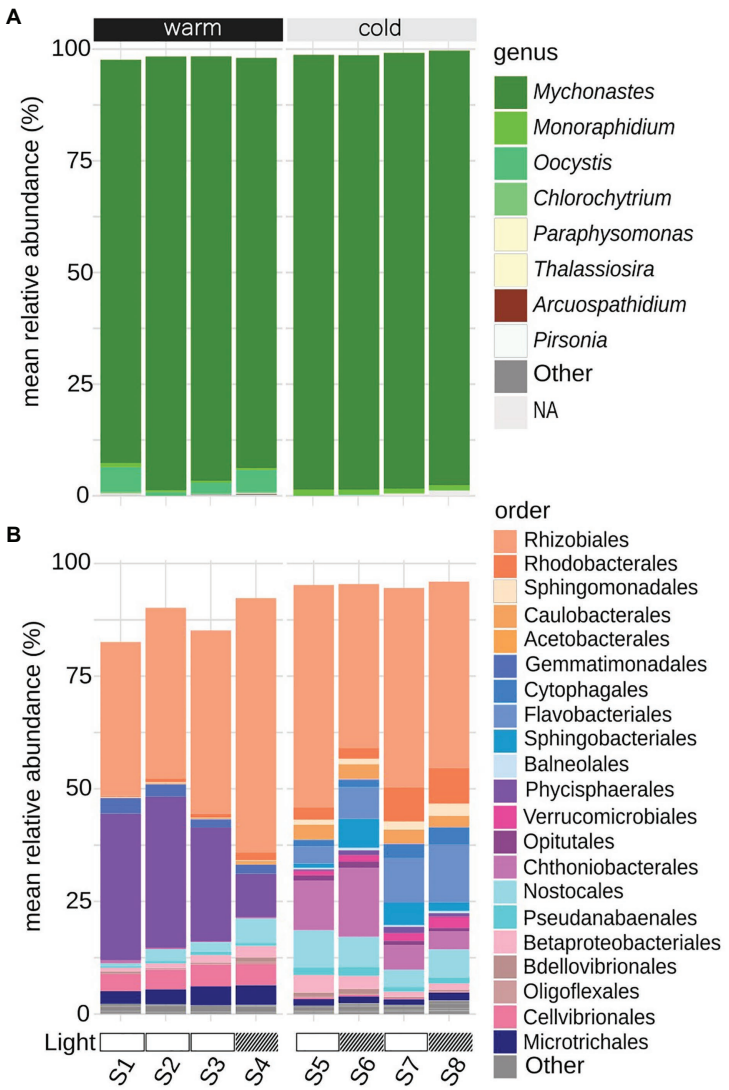

FIGURE 3 | Taxonomic affiliation of ASVs, mean of triplicates per sampling date (S1–S8), with a relative abundance > 0.1%. **(A)** 18S ASVs with assigned taxonomy at the genus level. **(B)** 16S ASVs with assigned taxonomy at the order level. Warm: 19.5 ± 0.89°C, cold: 12.4 ± 1.76°C (mean temperature per 24 h in PBR); Light: light reduction, open bar → natural light, striped bar → light reduced by 40–60% by shading.

relative abundance) and planctomycetal Phycisphaerales (26 ± 11% relative abundance), together making up >66% of the community (**Figure 3B**). Gammaproteobacterial Cellvibrionales, actinobacterial Microtrichales, and gemmatimonadetal Gemmatimonadales occurred during this period at low relative abundances 3–5%, and they were reduced to <1% of relative abundance during the colder period (**Figure 3B**). Several bacterial orders increased as the temperature dropped, verrucomicrobial Chthoniobacterales (9 ± 5% relative abundance), bacteriodetal Flavobacteriales (9 ± 4% relative abundance), and alphaproteobacterial Caulobacterales (at 3% relative abundance), while the occurrence of previously dominating order Phycisphaera was reduced to <1% relative abundance, as was less frequent planctomycetal Pirellulales (from 1% relative abundance to 0.8%). Rhizobiales remained at similar levels during the whole study (44 ± 7% relative abundance). Three orders increased, Rhodobacterales (from 2% relative abundance to 5 ± 3%), cyanobacterial Nostocales (from 4 ± 2% relative abundance to 7 ± 2%) and Betaproteobacteriales (from 2 ± 1% relative abundance to 3 ± 1%; **Figure 3B**).

Differential Functional Gene Expression Analysis in the PBR Microbial Community

As the study covered two periods, capturing a temperature shift from warmer to colder temperature, raw unfiltered counts, normalized by contig length, of the metatranscriptome data were by differential expression analysis contrasted either for temperature regime or for the availability of light (affected by shading). This was done in order to establish which of the two factors influenced the functional repertoire the most.

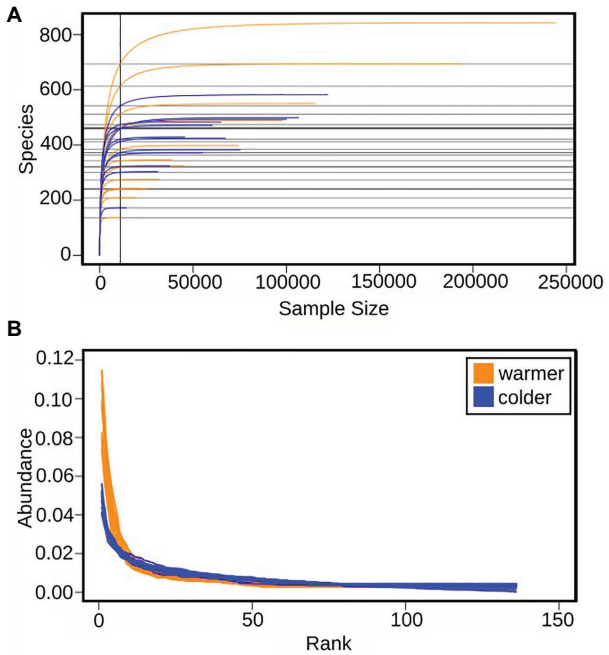

FIGURE 4 | Diversity measures of 16S ASVs, excluding ASVs annotated as chloroplasts. **(A)** Rarefaction curves, plotting sample size vs. number of ASVs. **(B)** Normalized rank abundance curves, plotting ASVs, ranked by abundance vs. abundance (counts). Orange – warmer period, blue – colder period.

For the eukaryote data, the availability of light (shaded vs. not shaded) gave 53 (0.01%) significant (log2 fold changes, *p*adj < 0.01) differentially expressed ORFs, while temperature in the PBR (warm vs. cold) gave 114,783 (21%) significant (log2 fold changes, *p*adj < 0.01) differentially expressed ORFs. For the prokaryote data, 358 (0.6%) ORFs were significantly (log2 fold changes, *p*adj < 0.01) differentially expressed, when contrasted for the availability of light, while temperature resulted in 7438 (13%) significant (log2 fold changes, *p*adj < 0.01) differentially expressed ORFs. Temperature was thus identified as the most influential factor compared to light, for both eukaryotes and prokaryotes. The analysis of the gene expression data was focused on ORFs annotated to processes related to the acquisition and utilization of carbon and the log2 fold changes and adjusted *p*-values of included ORFs are given in **Supplementary Tables S5** (eukaryotes) and **S6** (prokaryotes).

Eukaryotic Gene Expression Associated With Acquisition of Carbon

Eukaryote metatranscriptomic data indicated expression of enzymes associated with photosynthesis (Ribulose bisphosphate carboxylase, Rubisco, EC 4.1.1.39) and the carbon concentrating enzyme carbonic anhydrase (EC 4.2.1.1), primarily during the period with warmer temperature (S1–S4), along with representatives from photosystem I (PsaD, PsaK, PsaK1; **Figure 5**). Other components of photosystem I (PsaF, PsaL, PsaO) and II (PsbO, PsbP, PsbW) were expressed at high levels during both the warmer period (S2) and during the colder period (S5–S7; **Figure 5**). During the second, colder, period the expression of hydrolases [sucrose-6-phosphate, EC 3.2.1.B3, gamma-glutamyl hydrolase, EC 3.4.19.9, S-formyl glutathione hydrolase, EC 3.1.2.12, inosine-uridine preferring nucleoside hydrolase, EC 3.2.2.1, possible alpha/beta hydrolase superfamily (lr1917 homolog), and uridine diphosphate glucose pyrophosphatase, EC 3.6.1.45], breaking larger molecules into smaller ones, were more frequent than during the initial, warmer, period (**Figure 5**). The expression of carbon transporters (2-oxoglutarate/malate translocator, branched-chain amino acid ABC transporter, TC 3.A.1.4.1, L-proline/glycine betaine transporter ProP) and glycerol-3-phosphate transporter, which is associated with glycolysis, occurred primarily during the colder period, and at S1 (**Figure 5**). The expression of hydroxymethylglutaryl-CoA lyase, EC 4.1.3.4, that is involved in the formation of ketone bodies, indicates that other carbon sources than carbohydrates were also used for metabolism, especially during the colder period (**Figure 5**).

Prokaryotic Gene Expression Associated With Acquisition of Carbon

Prokaryote transcription patterns suggest a lower carbon uptake during the colder period, compared to the warmer (**Figure 6**). During the initial, warmer, period the prokaryotes primarily expressed a range of ABC-transporters for sugars: fructose (FrcC/B), L-rhamnose, ribose (RbsA, TC 3.A.1.2.1), xylose (XylF), maltose (MalE), inositol, and allose; along with other carbohydrates, such as nucleosides, polyols, and pyrimidines (**Figure 6**). Transporters of alternative carbon sources were also expressed initially: lipids (lipopolysaccharide ABC transporter, LptB), and amino acids (branched-chain amino acids, LivM, TC 3.A.1.4.1, and leucine, LivK, TC 3.A.1.4.1). So was alkaline phosphatase, EC 3.1.3.1 (**Figure 6**), an enzyme that cleaves off inorganic phosphorus from larger organic molecules. A process which may result in the release of readily available organic carbon sources (Benitez-Nelson and Buesseler, 1999). In addition to uptake of organic carbon sources, there were indications of inorganic carbon-fixation through the expression of Rubisco small and large chain, EC 4.1.1.39, during the warmer period (**Figure 6**). During the colder period, especially at S7–S8, the prokaryotes expressed enzymes associated with the formation of extracellular polysaccharides (UDP-glucose 4-epimerase, EC 5.1.3.2), and for survival during stationary phase and cellular stress (survival protein SurA, EC 5.2.1.8; Degeest and De Vuyst, 2000). Enzymes involved in bacterial respiration [glycolysis, pyruvate metabolism, tricarboxylic acid-cycle (TCA), and oxidative phosphorylation] were in general expressed at higher levels during the colder period, with a clear dip in numbers at S6, compared to the warmer period (**Figure 6**).

Temporal Co-Occurrences Within PBR Microbial Community

The network analysis, investigating the possible effects of temperature, light/shade, sunshine hours, and biomass on the PBR microbial community, resulted in the description of 11 modules (i.e., groups of co-occurring ASVs), of which some

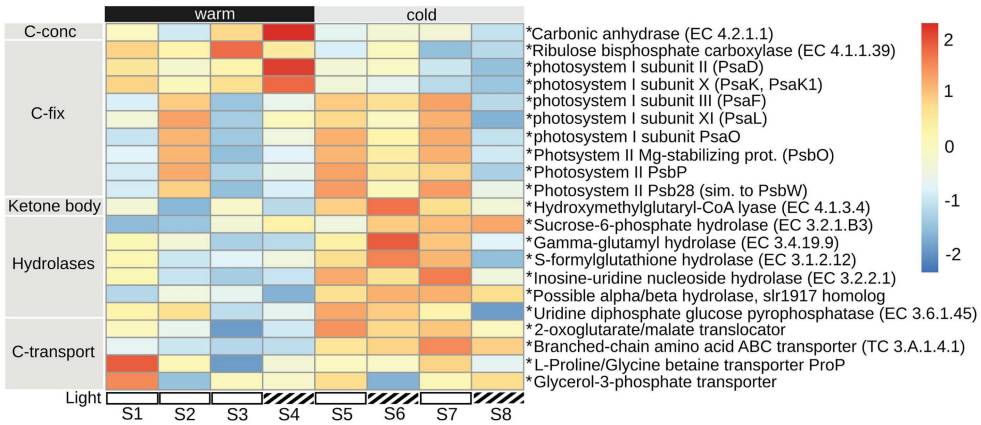

FIGURE 5 | Eukaryote gene expression (metatranscriptome) of mechanisms associated with carbon acquisition. Included are key enzymes representative of: carbon concentration (C-conc) and carbon fixation (C-fix), ketone body formation, hydrolases, and carbon transport. Heatmap shows the mean of triplicates per sampling date (S1–S8), of counts normalized to TPM and then square root transformed. Heatmap was made using R package pheatmap, with setting scale by "row." Warm: 19.5 ± 0.89°C, cold: 12.4 ± 1.76°C (mean temperature per 24 h in PBR); Light: light reduction, open bar → natural light, striped bar → light reduced by 40–60% by shading. * indicate *p*adj < 0.01 for log2 fold change of differential expression, contrasted for warm vs. cold time period.

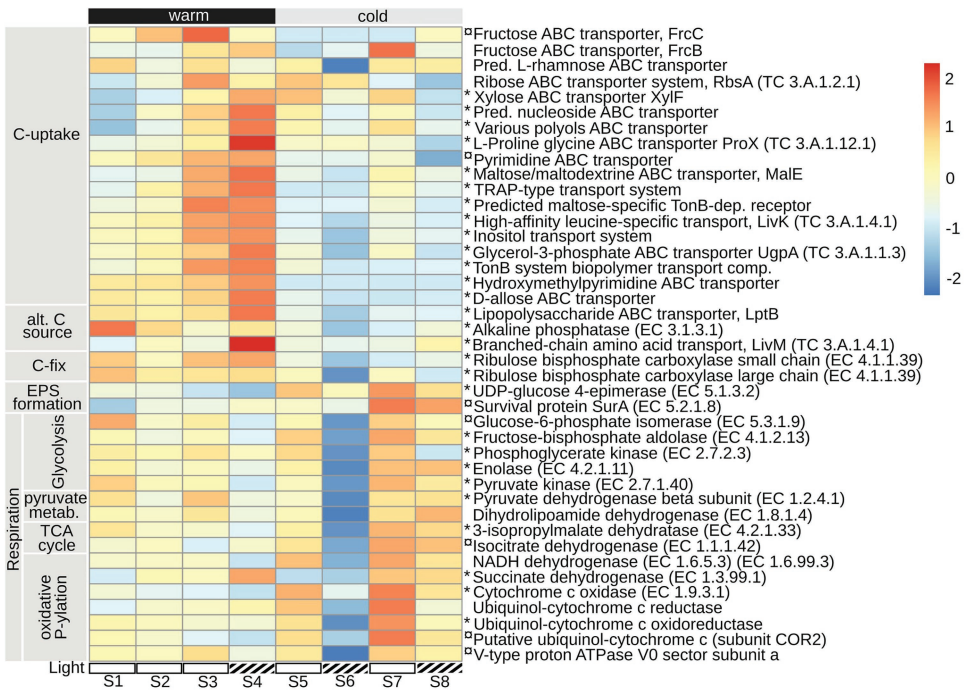

FIGURE 6 | Prokaryote gene expression (excluding transcripts annotated as eukaryotes in the prokaryotic dataset) of mechanisms associated with carbon acquisition, putative extracellular polysaccharide (EPS) formation, and respiration. Included are key enzymes representative of: carbon uptake (C-uptake), alternative carbon sources, carbon fixation, EPS-formation, glycolysis, pyruvate metabolism, tricarboxylic acid (TCA) cycle, and oxidative phosphorylation. Heatmap shows the mean of triplicates per sampling date (S1–S8), normalized to TPM and square-root transformed, made using R package pheatmap, with setting scale by "row." Warm: 19.5 ± 0.89°C, cold: 12.4 ± 1.76°C (mean temperature per 24 h in PBR); Light: light reduction, open bar → natural light, striped bar → light reduced by 40–60% by shading. * indicate *p*adj < 0.01, and ¤ *p*adj < 0.05, for log2 fold change, differential expression, contrasted for warm vs. cold time period.

were interconnected with other modules by shared edges (weighted > 0.3; **Figure 7A**). The heatmap of Pearson correlations indicated that the temporal changes of certain ASV modules were correlated to temperature and biomass changes over time (**Figure 8**). Modules were grouped based on similarity in Pearson correlations together with the sharing of edges into

MI – 1, 9, and 2, MII – 3 and 5, and MIII – 4, 6, and 7, for further analyses. Due to the use of cut-off values for edge weight, modules appear to spread out in the network displayed in **Figure 7A**, especially those in group MII. The ASVs in MI were mainly assigned to prokaryote ASVs representing the community during the initial, warmer, period (**Figures 7B**,**C**). During the colder period, the community was primarily represented by the ASVs in MII (**Figures 7D**,**E**), containing both eukaryotes and prokaryotes, and MIII, dominated by prokaryotes (**Figure 7F**). MI–MIII are described in more detail below.

MI – ASVs Positively Correlated to Temperature

The interconnected modules in MI (**Figure 7A**) together contained 130 nodes, of which 35 were assigned to eukaryote (18S) taxa and 95 to prokaryotes (16S) taxa. Of the 18S ASVs, most were assigned to green algae of either *Mychonastes* or *Oocystis*, together representing 3–11% (relative abundance) of the microalgal community (**Figure 7B**) during the warmer period. The 16S ASVs were primarily assigned to Rhizobiales and Phycisphaerales, with lower levels of Gemmatimonadales, Microtrichales, Cellvibrionales, and Oligoflexales, together representing 55–65% (relative abundance) of the prokaryote community during the warmer period (**Figure 7C**). Signifying for all of these modules was a significant (p = 0.03) positive Pearson correlation (0.62 ± 0.17) with PBR temperature, and significant (p = 0.03) negative correlations with biomass (−0.53 ± 0.16 DW gl^{-1}) and negative correlations with hours of sunshine (h; −0.40 ± 0.2), of which only those for module 9 were significant (p = 0.001; **Figure 8**).

MII – ASVs Negatively Correlated With Temperature

The modules in MII together contained 62 nodes, of which 17 were assigned to 18S ASVs and 45 to 16S ASVs and (**Figure 7A**), primarily representing the community during the colder period. The 18S nodes were to large extent assigned

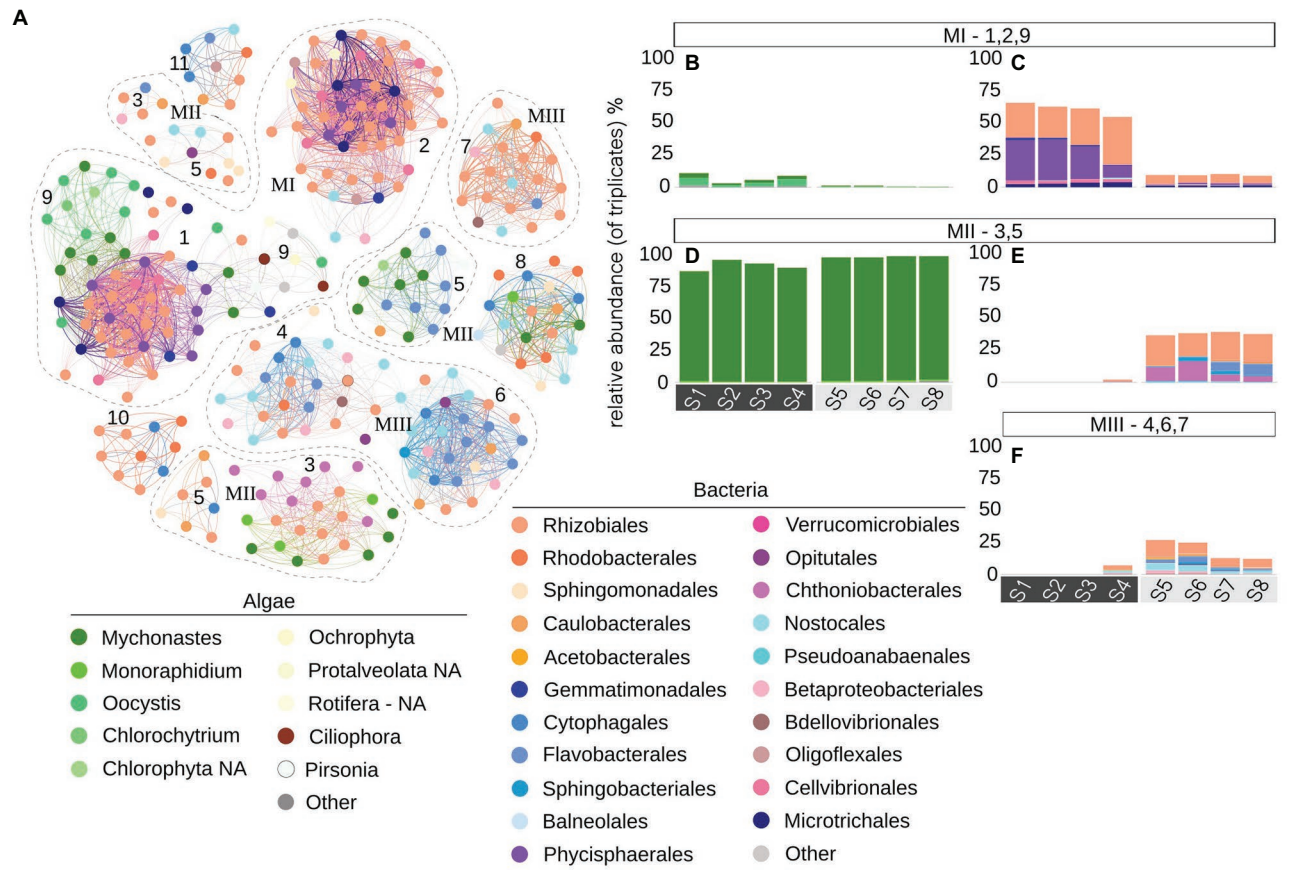

FIGURE 7 | (A) Co-occurrence network (Pearson) of eukaryote (genus level) and prokaryote (order level) ASVs (network nodes). Only edges with weight > 0.3 were included in the plot for ease in visualization, and nodes with zero edges were excluded. Modules represent node clusters grouped based on their shared positive correlations (edges). We clustered modules into three major clusters (based on their correlation values with temperature, see **Figure 8**). MI (modules 1, 2, 9), MII (modules 3, 5 – spread out due to the exclusion of edges with weight < 0.3), and MIII (modules 4, 6, 7). Relative abundances of ASVs of grouped modules are displayed in **(B)** (MI – 18S), **(C)** (MI – 16S), **(D)** (MII – 18S), **(E)** (MII – 16S), and **(F)** (MIII – 16S). Bar plot facets indicate temperature regime in PBR, warm: S1–S4, cold: S5–S8.

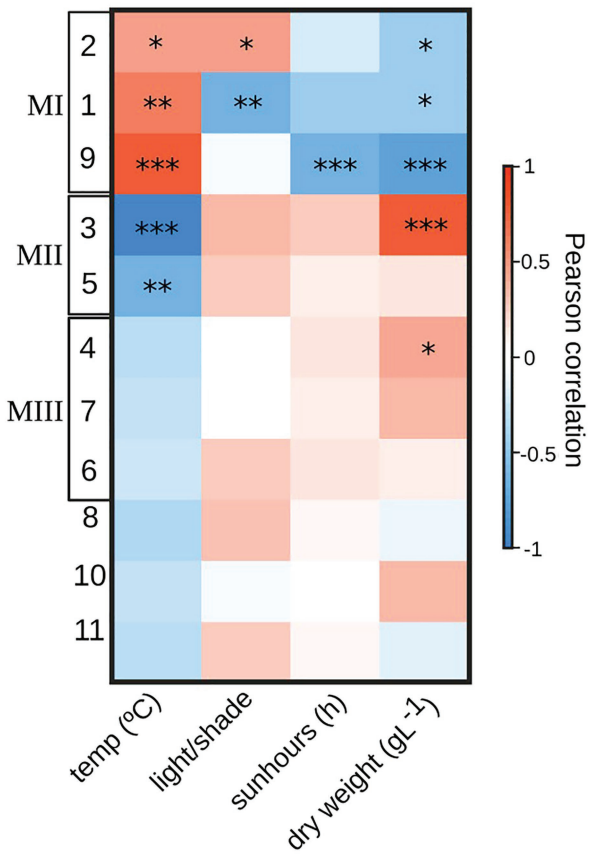

FIGURE 8 | Pearson coefficient correlation values (red – positive; blue – negative) of network analysis modules with parameters: temp – temperature (°C); light/shade – induced shade (40–60% reduction of light); sunhours (h) – number of hours day^{-1} with sunshine; Dry weight – of biomass (gl^{-1}). Significances indicated by $^{*}p < 0.05$, $^{**}p < 0.01$, and $^{***}p \leq 0.001$. Module groups (MI, MII, and MIII) were based on shared edges (**Figure 7**) and similarity in correlation to temperature.

to *Mychonastes* (including ASV_1, highly dominant during both warm and cold conditions; **Figure 7D**). The 16S nodes were primarily affiliated to: Rhizobiales, Bacteroidetes (Flavobacterales and Sphingobacteriales), and Chthoniobacterales, together representing 37–39% (relative abundance) of the prokaryote community during the colder period (**Figure 7E**) while largely absent in the warm period. Modules in MII showed significant ($p = 0.002$) negative correlation (−0.92, −0.61) with temperature in the PBR, and a significant positive correlation with biomass (0.77, $p = 1e\text{-}05$), and positive, though non-significant ($p = 0.09$) correlations with light/shade and sunshine hours (**Figure 8**).

MIII – Diverse Prokaryote ASVs Associated With Cold Temperature

The modules in MIII together contained 101 nodes (**Figure 7A**) primarily representing the community during the colder period. This includes a single 18S node, of 0.5% relative abundance, assigned to Mychonastes while the remaining 100 nodes were assigned to a diverse set of 16S ASVs. These were annotated to orders Rhizobiales, Rhodobacterales, Sphingomonadales, Caulobacterales, Flavobacterales, Cytophagales, Nostocales, Betaproteobacteria, Opitutales, and Bdellovibrionales, together representing 12–27% (relative abundance) of the prokaryote community during the colder period (**Figure 7F**). MIII was significantly ($p = 0.03$) correlated to biomass, but had non-significant negative correlations (Pearson; −0.27 ± 0.04) with PBR temperature and positive correlations to light/shade and sunshine hours (**Figure 8**).

DISCUSSION

It is of importance to increase our understanding of how microbial communities respond to environmental change. This can be achieved by revealing the mechanisms these communities use either to maintain their function, structure, and identity through internal adaptations or use to reform into a new type of system with new functions, structure, and identity. For aquatic microbes, this is relevant both with regard to the ecosystem services that they provide and to the impact that these changes might have on the biogeochemical cycling of nutrients in aquatic ecosystems (Daufresne and Loreau, 2001; Zell and Hubbart, 2013). The results from the present study illustrate how a PBR microbial community regain its ability to produce biomass at high capacity after having been exposed to temperature stress (during the exceptionally hot summer of 2018, 3.5°C above normal; Swedish Meteorological and Hydrological Institute), i.e., is able to respond in a resilient manner (**Figure 9**; Levin and Lubchenco, 2008; Feng et al., 2017). The underlying mechanisms behind this behavior are suggested to be regulated by dynamic interlevel shifts in both community structure and function, ultimately leading to interactions between eukaryotes (microalgae) and prokaryotes (bacteria) going from coexistence to competition, as seen in the regulation of uptake and utilization of organic carbon. Despite being exposed to shifts both in temperature and light, the shift in temperature was found to be the most influential structuring factor of both community structure and function (**Figures 2, 8**).

During the initial, warmer period, the microalgal growth was repressed, likely by heat stress, resulting in less introduced inorganic carbon through photosynthesis to the system and a significantly ($p < 7.9e\text{-}05$) lower production of biomass, and excretion of organic carbon by the microalgae (**Figure 9A**). Microalgal responses to abiotic stress, such as heat, include reduction in photosynthesis, as a mechanism to balance cellular energy levels necessary for metabolism (Biswal et al., 2011). Other modifications involve alterations of the cellular membrane, changes in protein and carbohydrate production, increase of cellular antioxidant and scavenge mechanisms, increased DNA-repair, as well as the induction of cell death (reviewed by Barati et al., 2019). Microalgae exposed to heat stress for a limited time have been shown to be retarded in growth, both in direct connection to the stress and up to 6 h afterwards (Béchet et al., 2017). Thus, the heat stress likely induced

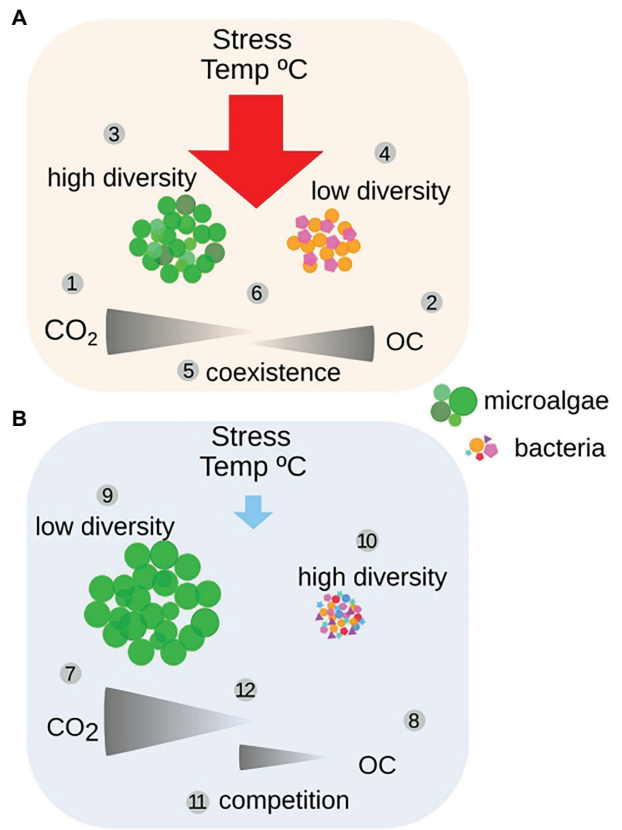

FIGURE 9 | Conceptual model of the impact in microalgae-bacteria interactions induced by temperature stress **(A)**. Less CO_2 got incorporated (1) while microalgal excretion of organic C (OC) was utilized by bacteria (2), leading to a higher diversity of the microalgae (3) and a lower diversity of the bacterial community (4). Resulting in coexistence (5), due to the partitioning of carbon resources (6). The release from temperature stress **(B)** introduced more CO_2 to the system resulting in a higher accumulation of microalgal biomass (7), while less OC got excreted (8), leading to a lower diversity of the microalgae, being dominated by one species (9), while the bacterial diversity became higher (10). This resulted in competition between microalgae and bacteria for organic carbon (11), due to mixotrophic microalgal uptake of both CO_2 and OC (12). The partitioning of carbon resources is indicated by CO_2 (flue gas) and OC (autochthonously produced carbon; see Discussion for details).

both a lower level of photosynthesis and repressed the microalgal growth rate. The heat stress is here suspected to have opened up niches for more microalgal species, thus leading to a significantly higher diversity, p = 0.007, and richness, p = 4.4e-06, of the microalgae population (**Supplementary Figure S5A**). A higher diversity and richness, both in community structure and function, have been suggested to act as stabilizing factors and increase the ability of communities to be resilient to temporary disturbances (Steiner et al., 2006; Downing and Leibold, 2010; Loreau and de Mazancourt, 2013). Having a broad response diversity, a community could respond rapidly upon an environmental challenge, which could lead to the domination of one or a few species (Steiner et al., 2006). This can be exemplified by the bacterial population in the PBR where a few taxa significantly (p = 0.001) dominate the community during the warmer period (**Figure 4** and **Supplementary Figure S5B**). Thus, the high availability of organic carbon appeared to have led to a lower diversity of the bacterial population structure. During the warm period, there was a partitioning of the carbon resources between microalgae and bacteria, where the microalgae primarily utilized inorganic carbon and the bacteria a range of organic carbon sources, benefitting a few groups such as Phycisphaerales and Cellvibrionales (**Figure 3**). Representatives from these bacterial groups have previously been found to be associated with algae. Planctomycetal Phycisphaerales was first isolated from the surface of a macroalgae (Fukunaga et al., 2009), and planctomycetal organisms have been found associated with phytoplankton biomass in the Baltic Sea (Bunse et al., 2016). Gammaproteobacterial Cellvibrionales has been shown to assimilate specific organic carbon sources, such as amino acids, glucose, and starch in coastal surface waters (Bryson et al., 2017). Indicating that a close association with an organic carbon-producing microalgae such as *Mychonastes* could be beneficial to these bacterial groups. During the colder period, the ratio of CO_2 flow to total DW was below two, indicative of carbon limitation (Herzog and Golomb, 2004; **Figure 1, Supplementary Table S7**), suggesting high uptake of inorganic carbon together with a significantly higher production of microalgal biomass (p = 7.8e-05), which seemed to reduce the availability of organic carbon for the bacteria (**Figures 6, 9B**). This is indicated by a lower diversity of the microalgal population structure, favoring *Mychonastes* (**Figure 7D**), while there was a significant increase in bacterial diversity (p = 0.03; **Supplementary Figure S5B**). The suggested carbon limitation, leading to competition between the two levels could have been influenced by the ability of the dominant microalgal species *Mychonastes* for both C-fixation and uptake of organic carbon (**Figure 5**). This dual carbon utilization provides the microalgae with a competitive advantage over the bacteria, which are left to rely on respiration in order to maintain cellular processes (**Figure 6**). During bacterial respiration, O_2 will be utilized and CO_2 produced, thereby facilitating microalgal photosynthesis. This phenomenon has previously been demonstrated in laboratory co-cultures of microalgae and bacteria (Mouget et al., 1995; Danger et al., 2007). Thus, the response of the PBR microbial community upon the two different temperature conditions may have been regulated at two interconnected levels, through function (auto-, hetero-, or mixotrophy) and population structure (increased or reduced diversity), which together affect microalgae-bacteria interactions, going from coexistence to competition (**Figure 9**). These results suggest that the PBR microbial community, with lower complexity than natural systems, but more complex than 2-3 species model systems, has the ability to respond in a manner to temperature stress, by structural and functional modulations that span across levels, which could be considered as resilient (**Supplementary Figure S1**). To be resilient a community must not lose its over-all function (production of biomass), deviate from its original level of diversity, or become too different in taxonomic identity (Walker, 2004).

As the interactions shift from coexistence to competition the functional guild (Vanwonterghem et al., 2014; Bryson et al., 2017) with an organic carbon preference, initially represented by bacteria become represented by both microalgae and bacteria during the colder period. This suggests that the function of organic carbon acquisition is not limited to one level, or taxonomic entity (bacteria), but may cross the inter-level boundary. Thus, the decoupling previously seen in strictly bacterial experimental systems between function and taxonomy (Fernandez et al., 2000; Wang et al., 2011; Vanwonterghem et al., 2014; Louca and Doebeli, 2016; Louca et al., 2020) is seen also in our system consisting of two levels. This underlines the importance of interlevel interactions for the ability of a community to maintain its over-all functional capacity, structure, and identity, in order to be able to respond in a resilient manner when faced with the environmental challenge (Holling, 1973).

Theoretical Models to Describe Resilience Mechanisms

In order to study how interlevel interactions influence community resilience, the adaptive cycle model might be used (Gunderson and Holling, 2002; Walker, 2004). This cycle describes four stages that a community are thought to pass at shorter or longer intervals: birth (r), maturation (K), death (Ω), and renewal (α; **Figure 10**). Adaptive cycles have been used to describe the seasonal successions of algal blooms in the Baltic Sea (Angeler et al., 2015), but are more commonly applied for describing resilience in socio-ecological systems consisting of nested levels (Berkes and Ross, 2016) within the panarchy theory (Gunderson and Holling, 2002). The rationale behind the panarchy theory is that as ecosystems are made up of multiple and interconnected levels (e.g., autotrophs and heterotrophs), and each level have their own adaptive cycle, adaptations occurring at one level will influence the cycling of surrounding levels. This primarily occurs as a lower level is passing through its death/release phase, Ω, the "window of opportunity" during which it may collapse or start to adjust to changed conditions. If this collapse occurs when an upper level is in its least resilient phase, between birth or maturation, r or K, or in the maturation phase, it will be affected by the impact from below. When this occurs, the upper level may harbor or absorb the impact posed from below. In turn, this absorption affects the renewal/adaptation phase, α, of the lower level impacting the readjustments that are made to face the new conditions (**Figure 10**; Gunderson and Holling, 2002; Walker, 2004; Allen et al., 2014). When combining these theories with that of cross-scale resilience, that describes ecosystem resilience by functional overlaps and redundancy within and across levels (Peterson et al., 1998; Sundstrom et al., 2018), the mechanisms behind the ability of the PBR microbial community to increase its production of biomass after having been exposed to temperature stress may be explained. The cross-scale resilience model has previously been tested to describe resilience for natural ecosystems consisting of avian and mammalian populations (Wardwell et al., 2008) and of lake algae exposed to chemical waste and vertical mixing (Baho et al., 2019). Our study is the first to apply these three theories to explain the resilience of a PBR community. Here, the microalgae, representing the upper level, would – while adapting to the temperature stress during the warmer period – be somewhere in between the death/release, Ω, and renewal/reorganization, α, phases, as indicated by the more diverse microalgal population. While the bacteria – during the warmer period – would be in the steadily growing maturation/conservation, K, phase, as indicated by a lower population diversity (**Figure 10**). This suggests that the levels during this period are not posing an immediate influence on each other and are coexisting through acquiring different types of carbon (**Figures 5, 6**). While, during the colder period, the microalgae would have entered into r phase, becoming more structurally homogenous and starting to express new functions, and the bacteria into Ω phase, becoming less structurally homogenous and functionally less diverse. Leading to that the levels thus are able to have more influence on each other, according to panarchy theory. This is here ultimately represented by the evidence of competition for organic carbon manifested by microalgal expression of hydrolases for acquiring organic carbon and by a higher level of expression of bacterial transcripts associated with respiration than during the warmer period (**Figures 5, 6**). These expression patterns are connected to similar but opposing structural and functional adjustments among the two levels (**Figure 9**), where a significantly more diverse microalgal population is matched by a significantly less diverse bacterial population during the warmer period, and vice versa for the colder period (**Figures 4, 9**). Beyter et al. (2016) present a similar pattern in a reactor

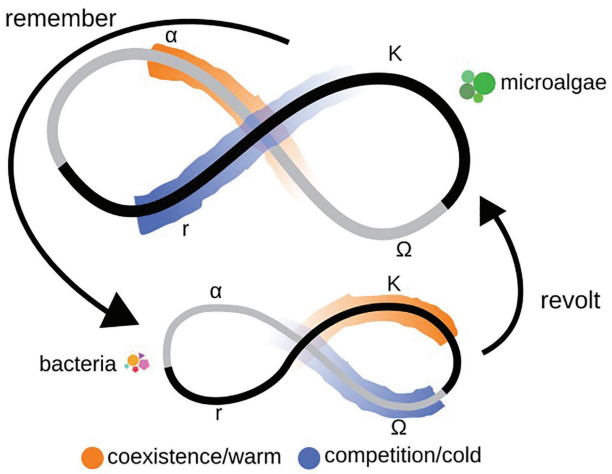

FIGURE 10 | An illustration of adaptive cycles and the concept of panarchy, used to describe the interactions between the microalgae (upper level) and bacteria (lower level), going from coexistence during the warmer (orange) temperature regime to competition during the colder (blue) temperature regime. r – growth phase, K – conservation phase, Ω – release phase, and α – adaptation phase. Remember – impact on lower level by upper level, revolt – influence from lower level on upper level.

community of primarily green algae (ITS2) and bacteria (16S), where higher diversity of one coincides with lower diversity of the other during a 1 year study. The combined panarchy and cross-scale resilience theories could help explain these opposing responses, saying that the response at one level help balance the response at the other level through functional overlap and redundancy (Peterson et al., 1998; Sundstrom et al., 2018). This mechanism would thus enable the maintenance of both the total structural diversity, by balancing the population diversity across the levels, and of the functional overlap in the ability for the acquisition of organic carbon found both among the bacteria and the microalgae (**Figure 10**; Gunderson and Holling, 2002). Thus, by applying these theoretical models, not previously used for this type of system, the regulatory mechanism by which the community responds to temperature stress may be explained (**Figure 9**).

Biotic Interactions of Importance for Microbial Community Resilience

An important aspect of the concept of panarchy is the influence of interactions between levels on the resilience of a community (Gunderson and Holling, 2002). In this study, either of the two modes of interaction, coexistence or competition, dominate during a specific temperature regime linking the dynamics of interactions with the resilience of the system. When microalgae were stressed by warmer temperature, bacterial growth was promoted, leading to microalgal-bacteria coexistence, while when relieved from temperature stress the microalgal growth was promoted, and the community was governed by the competition between the levels (**Figure 10**). The shift in community interactions follows dynamics as proposed by Chesson (2000) in the modern coexistence theory. In which stabilizing effects of increasing niche differentiation (the use of different resources), in combination with the equalizing effects of decreasing fitness (more evenly distributed abundances) describe a situation favoring coexistence, while the opposite conditions favor competition and competitive exclusion. Examples of niche differentiation, of either light or nutrient preferences, and coexistence of different microalgal groups have been suggested by previous studies both in laboratory experiments and nature (Alexander et al., 2015; Burson et al., 2019). Studies of interactions among microbial communities often focus on niche overlaps/differentiations between similar organisms. For instance, Hunt et al. (2008) describe how members of a bacterial family in a coastal environment may coexist through resource partitioning. Previous works performed in large scale reactors with microalgae and bacteria commonly explored community stability (Stockenreiter et al., 2012; Beyter et al., 2016; Fulbright et al., 2018) rather than interlevel interactions. Interlevel interaction analysis have mostly been performed in well-designed co-cultures (Durham et al., 2014; Seyedsayamdost et al., 2014; Amin et al., 2015; Segev et al., 2016; Landa et al., 2017) or in association with natural algal blooms (Mayali et al., 2011; Teeling et al., 2012, 2016; Zhou et al., 2018), but rarely with regards to competition or coexistence (Sörenson et al., 2020). However, Le Chevanton et al. (2016) suggest that nitrogen limitation may have caused competition between algae and bacteria in a laboratory co-culture. The results from the present study suggest that interlevel interactions, in relation to functional and structural dynamics, are of importance for microbial community resilience.

Considerations Related to our PBR Experimental Setup

This study was performed under replete nutrient conditions, enabling the focus of the study on carbon and the transfer of energy between the microalgal and bacterial populations in the PBR community. The availability of inorganic carbon was likely pushing the PBR community towards carbon limitation during the colder, more productive period, with a ratio of supplied CO_2 to biomass at just below two (**Figure 1**). This is suggested by our data to have lead to the upregulation of organic carbon uptake pathways expressed by the mixotrophic microalgae (**Figure 4**), thus forcing the community into competition for organic carbon. In the PBR, the shift from coexistence to competition did not impact the carbon cycle flux *per se*, as the resilience of the system maintained the over-all system function, but the magnitude of cycled carbon increased as more inorganic carbon was introduced through photosynthesis during the colder period, as significantly more biomass was produced. The limited complexity in terms of community structure and influential environmental parameters of the system facilitated the analysis and allowed for the application of established ecological theories. The relatively short time scale in which the study was conducted (6 weeks in total), was enough time to capture the shifts seen in response to significantly changed temperature conditions, nonetheless, more extensive sampling before and after the perturbation would have been beneficial but are not considered to limit the conclusions of this study. Models of climate change and projected environmental disturbances are based on changes seen over long periods of time (Collins and Knutti, 2013). Short-scale studies, with controlled conditions, are however important in order to reveal short-term mechanisms in microbial ecosystems, such as those seen in this study.

CONCLUSIONS

Responses within a PBR with a mixed community of both microalgae and bacteria, when faced with changed environmental conditions, suggest that interlevel interactions, decoupling function and taxonomy, have a strong impact on the resilience of the system. The two-level system shifted from coexistence, with separate resource niches (inorganic carbon for microalgae and organic carbon for bacteria), to competition for organic carbon, with overlapping resource niches (where both microalgae and bacteria utilized organic carbon), when relieved from temperature stress. By analyzing these results with resilience theory *sensu* Holling (1973), cross-scale resilience and modern coexistence theory we may describe the mechanisms by which this system of medium complexity adapted to temperature

stress through overlapping functional diversity within and functional redundancy across levels. Knowledge about these mechanisms may help improve studies related to environmental change through improved models of aquatic microbial ecosystems, and their behavior when faced with environmental perturbations.

DATA AVAILABILITY STATEMENT

The datasets presented in this study can be found in online repositories. The names of the repository/repositories and accession number(s) can be found below: https://www.ebi.ac.uk/ena, ERR3419055-ERR3419102 https://www.ebi.ac.uk/ena, ERR3421213-ERR3421260.

AUTHOR CONTRIBUTIONS

ES designed the study and performed sampling, laboratory, and bioinformatic work. EC contributed to methods for analysis. HF, EL, and CL contributed with interpretations and methods for analysis. ES led the writing of the manuscript together with all co-authors. All authors contributed to the article and approved the submitted version.

FUNDING

The authors acknowledge support from the National Genomics Infrastructure in Stockholm funded by Science for Life Laboratory, the Knut and Alice Wallenberg Foundation and the Swedish Research Council, and SNIC/Uppsala Multidisciplinary Center for Advanced Computational Science for assistance with massively parallel sequencing and access to the UPPMAX computational infrastructure. This work was funded by the Knowledge Foundation (KK- Stiftelsen, 20150219 to CL), Stiftelsen Lantbruksforskning (SLF O-15-20-559 to CL), Familjen Kamprads stiftelse (20160169 to CL), Carl Tryggers Foundation (CTS 16:270 to CL), Energimyndigheten (44677-1 to CL), the Swedish Research Council FORMAS (SFO Ecochange to CL, 2018-00692 to EL), Linnaeus University – Faculty of Health and Life Science, CementaHeidelberg AB, SMA Mineral, KalmarEnergi, and Kalmarsundsregionens renhållare (KSRR).

ACKNOWLEDGMENTS

We would like to thank Diego Brambilla and Daniel Lundin for assistance with the metatranscriptomics pipeline and Maurice Hirwa, Soran Mahmoudi and Fredrik Svensson for assistance at the sampling site and Quyen Nham for assistance with nutrient analyses.

SUPPLEMENTARY MATERIAL

The Supplementary Material for this article can be found online at: https://www.frontiersin.org/articles/10.3389/fmicb.2021.607601/full#supplementary-material

REFERENCES

Alexander, H., Jenkins, B. D., Rynearson, T. A., and Dyhrman, S. T. (2015). Metatranscriptome analyses indicate resource partitioning between diatoms in the field. *Proc. Natl. Acad. Sci.* 112, E2182–E2190. doi: 10.1073/pnas.1421993112

Allen, C. R., Angeler, D. G., Garmestani, A. S., Gunderson, L. H., and Holling, C. S. (2014). Panarchy: theory and application. *Ecosystems* 17, 578–589. doi: 10.1007/s10021-013-9744-2

Allison, S. D., and Martiny, J. B. H. (2008). Resistance, resilience, and redundancy in microbial communities. *PNAS* 105, 11512–11519. doi: 10.1073/pnas.0801925105

Amin, S. A., Hmelo, L. R., van Tol, H. M., Durham, B. P., Carlson, L. T., Heal, K. R., et al. (2015). Interaction and signalling between a cosmopolitan phytoplankton and associated bacteria. *Nature* 522, 98–101. doi: 10.1038/nature14488

Andersson, A., Meier, H. E. M., Ripszam, M., Rowe, O., Wikner, J., Haglund, P., et al. (2015). Projected future climate change and Baltic Sea ecosystem management. *Ambio* 44, 345–356. doi: 10.1007/s13280-015-0654-8

Andrews, S. (2009). FastQC. A quality control tool for high throughput sequence data. Available at: http://www.bioinformatics.babraham.ac.uk/projects/fastqc/ (Accessed January 21, 2021).

Angeler, D. G., Allen, C. R., Garmestani, A. S., Gunderson, L. H., Hjerne, O., and Winder, M. (2015). Quantifying the adaptive cycle. *PLoS One* 10:e0146053. doi: 10.1371/journal.pone.0146053

Azam, F., Fenchel, T., Field, J. G., Gray, L. A., Meyer-Reil, L. A., and Thingstad, F. (1983). The ecological role of water-column microbes in the sea. *Mar. Ecol. Prog. Ser.* 10, 257–264. doi: 10.3354/meps010257

Baho, D. L., Leu, E., Pomati, F., Hessen, D. O., Norberg, J., Moe, S. J., et al. (2019). Resilience of natural phytoplankton communities to pulse disturbances from micropollutant exposure and vertical mixing. *Environ. Toxicol. Chem.* 38, 2197–2208. doi: 10.1002/etc.4536

Barati, B., Gan, S. -Y., Lim, P. -E., Beardall, J., and Phang, S. -M. (2019). Green algal molecular responses to temperature stress. *Acta Physiol. Plant.* 41:26. doi: 10.1007/s11738-019-2813-1

Bar-On, Y. M., Phillips, R., and Milo, R. (2018). The biomass distribution on earth. *Proc. Natl. Acad. Sci. U. S. A.* 115, 6506–6511. doi: 10.1073/pnas.1711842115

Bastian, M., Heymann, S., and Jacomy, M. (2009). Gephi: An open source software for exploring and manipulating networks. in *International AAAI Conference on Weblogs and Social Media*; May 17-20, 2010; 361–362.

Béchet, Q., Laviale, M., Arsapin, N., Bonnefond, H., and Bernard, O. (2017). Modeling the impact of high temperatures on microalgal viability and photosynthetic activity. *Biotechnol. Biofuels* 10:136. doi: 10.1186/s13068-017-0823-z

Behrenfeld, M. J., Randerson, J. T., McClain, C. R., Feldman, G. C., Los, S. O., Tucker, C. J., et al. (2001). Biospheric primary production during an ENSO transition. *Science* 291, 2594–2597. doi: 10.1126/science.1055071

Benitez-Nelson, C. R., and Buesseler, K. O. (1999). Variability of inorganic and organic phosphorus turnover rates in the coastal ocean. *Nature* 398, 502–505. doi: 10.1038/19061

Berkes, F., and Ross, H. (2016). Panarchy and community resilience: sustainability science and policy implications. *Environ. Sci. Pol.* 61, 185–193. doi: 10.1016/j.envsci.2016.04.004

Bernhardt, J. R., and Leslie, H. M. (2013). Resilience to climate change in coastal marine ecosystems. *Annu. Rev. Mar. Sci.* 5, 371–392. doi: 10.1146/annurev-marine-121211-172411

Beyter, D., Tang, P. -Z., Becker, S., Hoang, T., Bilgin, D., Lim, Y. W., et al. (2016). Diversity, productivity, and stability of an industrial microbial ecosystem. *Appl. Environ. Microbiol.* 82, 2494–2505. doi: 10.1128/AEM.03965-15

Biswal, B., Joshi, P. N., Raval, M. K., and Biswal, U. C. (2011). Photosynthesis, a global sensor of environmental stress in green plants: stress signalling and adaptation. *Curr. Sci.* 101, 47–56.

Bolch, C. J. S., Bejoy, T. A., and Green, D. H. (2017). Bacterial associates modify growth dynamics of the dinoflagellate *Gymnodinium catenatum*. *Front. Microbiol.* 8:670. doi: 10.3389/fmicb.2017.00670

Bryson, S., Li, Z., Chavez, F., Weber, P. K., Pett-Ridge, J., Hettich, R. L., et al. (2017). Phylogenetically conserved resource partitioning in the coastal microbial loop. *ISME J.* 11, 2781–2792. doi: 10.1038/ismej.2017.128

Buchfink, B., Xie, C., and Huson, D. H. (2015). Fast and sensitive protein alignment using DIAMOND. *Nat. Methods* 12, 59–60. doi: 10.1038/nmeth.3176

Bunse, C., Bertos-Fortis, M., Sassenhagen, I., Sildever, S., Sjöqvist, C., Godhe, A., et al. (2016). Spatio-temporal interdependence of bacteria and phytoplankton during a Baltic Sea spring bloom. *Front. Microbiol.* 7:517. doi: 10.3389/fmicb.2016.00517

Burson, A., Stomp, M., Mekkes, L., and Huisman, J. (2019). Stable coexistence of equivalent nutrient competitors through niche differentiation in the light spectrum. *Ecology* 100:e02873. doi: 10.1002/ecy.2873

Callahan, B. J., McMurdie, P. J., Rosen, M. J., Han, A. W., Johnson, A. J. A., and Holmes, S. P. (2016). DADA2: high-resolution sample inference from Illumina amplicon data. *Nat. Methods* 13, 581–583. doi: 10.1038/nmeth.3869

Capo, E., Debroas, D., Arnaud, F., Perga, M. -E., Chardon, C., and Domaizon, I. (2017). Tracking a century of changes in microbial eukaryotic diversity in lakes driven by nutrient enrichment and climate warming. *Environ. Microbiol.* 19, 2873–2892. doi: 10.1111/1462-2920.13815

Cardinale, B. J., Srivastava, D. S., Emmett Duffy, J., Wright, J. P., Downing, A. L., Sankaran, M., et al. (2006). Effects of biodiversity on the functioning of trophic groups and ecosystems. *Nature* 443, 989–992. doi: 10.1038/nature05202

Chesson, P. (2000). Mechanisms of maintenance of species diversity. *Annu. Rev. Ecol. Syst.* 31, 343–366. doi: 10.1146/annurev.ecolsys.31.1.343

Collins, M., and Knutti, R. (2013). "Long-term climate change: projections, commitments and irreversibility" in *Climate Change 2013 - The Physical Science Basis*. ed. Intergovernmental Panel on Climate Change (Cambridge: Cambridge University Press), 1029–1136.

Core, T. R. (2018). R: A language and environment for statistical computing. Available at: https://www.r-project.org/ (Accessed January 21, 2021).

Danger, M., Leflaive, J., Oumarou, C., Ten-Hage, L., and Lacroix, G. (2007). Control of phytoplankton - bacteria interactions by stoichiometric constraints. *Oikos* 116, 1079–1086. doi: 10.1111/j.2007.0030-1299.15424.x

Daufresne, T., and Loreau, M. (2001). Ecological stoichiometry, primary producer-decomposer interactions, and ecosystem persistence. *Ecology* 82, 3069–3082. doi: 10.1890/0012-9658(2001)082[3069:ESPPDI]2.0.CO;2

Degeest, B., and De Vuyst, L. (2000). Correlation of activities of the enzymes alpha -Phosphoglucomutase, UDP-Galactose 4-Epimerase, and UDP-glucose Pyrophosphorylase with exopolysaccharide biosynthesis by Streptococcus thermophilus LY03. *Appl. Environ. Microbiol.* 66, 3519–3527. doi: 10.1128/AEM.66.8.3519-3527.2000

Downing, A. L., and Leibold, M. A. (2010). Species richness facilitates ecosystem resilience in aquatic food webs. *Freshw. Biol.* 55, 2123–2137. doi: 10.1111/j.1365-2427.2010.02472.x

Durham, B. P., Grote, J., Whittaker, K. A., Bender, S. J., Luo, H., Grim, S. L., et al. (2014). Draft genome sequence of marine alphaproteobacterial strain HIMB11, the first cultivated representative of a unique lineage within the *Roseobacter* clade possessing an unusually small genome. *Stand. Genomic Sci.* 9, 632–645. doi: 10.4056/sigs.4998989

Ewels, P., Magnusson, M., Lundin, S., and Käller, M. (2016). MultiQC: summarize analysis results for multiple tools and samples in a single report. *Bioinformatics* 32, 3047–3048. doi: 10.1093/bioinformatics/btw354

Feng, K., Zhang, Z., Cai, W., Liu, W., Xu, M., Yin, H., et al. (2017). Biodiversity and species competition regulate the resilience of microbial biofilm community. *Mol. Ecol.* 26, 6170–6182. doi: 10.1111/mec.14356

Fernandez, A. S., Dollhopf, S. L., Dazzo, F. B., Hickey, R. F., Tiedje, J. M., and Criddle, C. S. (2000). Flexible community structure correlates with stable community function in methanogenic bioreactor communities perturbed by glucose. *Appl. Environ. Microbiol.* 66, 4058–4067. doi: 10.1128/AEM.66.9.4058-4067.2000

Field, C. B., Behrenfeld, M. J., Randerson, J. T., and Falkowski, P. (1998). Primary production of the biosphere: integrating terrestrial and oceanic components. *Science* 281, 237–241. doi: 10.1126/science.281.5374.237

Fukunaga, Y., Kurahashi, M., Sakiyama, Y., Ohuchi, M., Yokota, A., and Harayama, S.. (2009). *Phycisphaera mikurensis* gen. nov., sp. nov., isolated from a marine alga, and proposal of *Phycisphaeraceae* fam. nov., *Phycisphaerales* ord. nov. and *Phycisphaerae* classis nov. in the phylum *Planctomycetes*. *J. Gen. Appl. Microbiol.* 55, 267–257. doi: 10.2323/jgam.55.267

Fulbright, S. P., Robbins-pianka, A., Berg-lyons, D., Knight, R., Reardon, K. F., and Chisholm, S. T. (2018). Bacterial community changes in an industrial algae production system. *Algal Res.* 31, 147–156. doi: 10.1016/j.algal.2017.09.010

Guillard, R. R. L. (1975). "Culture of phytoplankton for feeding marine invertebrates" in *Culture of marine invertebrate animals*. eds. W. L. Smith and M. H. Chanley (PlenumPress, New York: Springer), 29–60.

Gunderson, L. H., and Holling, C. S. (2002). *Panarchy: Understanding transformations in human and natural systems*. Washington: Island Press.

Harrell, F. E., and Dupont, C. (2019). Hmisc: Harrell Miscellaneous. Available at: https://cran.r-project.org/package=Hmisc (Accessed January 21, 2021).

Herlemann, D. P., Labrenz, M., Jürgens, K., Bertilsson, S., Waniek, J. J., and Andersson, A. F. (2011). Transitions in bacterial communities along the 2000 km salinity gradient of the Baltic Sea. *ISME J.* 5, 1571–1579. doi: 10.1038/ismej.2011.41

Herzog, H., and Golomb, D. (2004). "Carbon capture and storage from fossil fuel use" in *Encyclopedia of energy*. ed. C. J. Cleveland (New York: Elsevier), 277–287.

Holling, C. S. (1973). Resilience and stability of ecological systems. *Annu. Rev. Ecol. Syst.* 4, 1–23.

Hugerth, L. W., Muller, E. E. L., Hu, Y. O. O., Lebrun, L. A. M., Roume, H., Lundin, D., et al. (2014). Systematic design of 18S rRNA gene primers for determining eukaryotic diversity in microbial consortia. *PLoS One* 9:e95567. doi: 10.1371/journal.pone.0095567

Hunt, D. E., David, L. A., Gevers, D., Preheim, S. P., Alm, E. J., and Polz, M. F. (2008). Resource partitioning and sympatric differentiation among closely related bacterioplankton. *Science* 320, 1081–1085. doi: 10.1126/science.1157890

Huson, D. H., Beier, S., Flade, I., Górska, A., El-Hadidi, M., Mitra, S., et al. (2016). MEGAN community edition - interactive exploration and analysis of large-scale microbiome sequencing data. *PLoS Comput. Biol.* 12:e1004957. doi: 10.1371/journal.pcbi.1004957

Joshi, N., and Fass, N. (2011). Sickle: A sliding-window, adaptive, quality-based trimming tool for FastQ files. Available at: https://github.com/najoshi/sickle (Accessed January 21, 2021).

Landa, M., Burns, A. S., Roth, S. J., and Moran, M. A. (2017). Bacterial transcriptome remodeling during sequential co-culture with a marine dinoflagellate and diatom. *ISME J.* 11, 2677–2690. doi: 10.1038/ismej.2017.117

Langfelder, P., and Horvath, S. (2008). WGCNA: an R package for weighted correlation network analysis. *BMC Bioinformatics* 9:559. doi: 10.1186/1471-2105-9-559

Langmead, B., and Salzberg, S. L. (2012). Fast gapped-read alignment with bowtie 2. *Nat. Methods* 9, 357–359. doi: 10.1038/nmeth.1923

Le Chevanton, M., Garnier, M., Lukomska, E., Schreiber, N., Cadoret, J. -P., Saint-Jean, B., et al. (2016). Effects of nitrogen limitation on *Dunaliella sp.–Alteromonas* sp. interactions: from mutualistic to competitive relationships. *Front. Mar. Sci.* 3, 1–11. doi: 10.3389/fmars.2016.00123

Levin, S. A., and Lubchenco, J. (2008). Resilience, robustness, and marine ecosystem-based management. *Bioscience* 58, 27–32. doi: 10.1641/B580107

Li, H., Handsaker, B., Wysoker, A., Fennell, T., Ruan, J., Homer, N., et al. (2009). The sequence alignment/map format and SAMtools. *Bioinformatics* 25, 2078–2079. doi: 10.1093/bioinformatics/btp352

Li, D., Luo, R., Liu, C. -M., Leung, C. -M., Ting, H. -F., Sadakane, K., et al. (2016). MEGAHIT v1.0: a fast and scalable metagenome assembler driven by advanced methodologies and community practices. *Methods* 102, 3–11. doi: 10.1016/j.ymeth.2016.02.020

Lindh, M. V., and Pinhassi, J. (2018). Sensitivity of Bacterioplankton to environmental disturbance: a review of Baltic Sea field studies and experiments. *Front. Mar. Sci.* 5, 1–17. doi: 10.3389/fmars.2018.00361

Loreau, M., and de Mazancourt, C. (2013). Biodiversity and ecosystem stability: a synthesis of underlying mechanisms. *Ecol. Lett.* 16, 106–115. doi: 10.1111/ele.12073

Louca, S., and Doebeli, M. (2016). Transient dynamics of competitive exclusion in microbial communities. *Environ. Microbiol.* 18, 1863–1874. doi: 10.1111/1462-2920.13058

Louca, S., Jacques, S. M. S., Pires, A. P. F., Leal, J. S., Srivastava, D. S., Parfrey, L. W., et al. (2017). High taxonomic variability despite stable

functional structure across microbial communities. *Nat. Ecol. Evol.* 1:15. doi: 10.1038/s41559-016-0015

Louca, S., Polz, M. F., Mazel, F., Albright, M. B. N., Huber, J. A., O'Connor, M. I., et al. (2018). Function and functional redundancy in microbial systems. *Nat. Ecol. Evol.* 2, 936–943. doi: 10.1038/s41559-018-0519-1

Louca, S., Rubin, I. N., Madilao, L. L., Bohlmann, J., Doebeli, M., and Wegener Parfrey, L. (2020). Effects of forced taxonomic transitions on metabolic composition and function in microbial microcosms. *Environ. Microbiol. Rep.* 12, 514–524.12866. doi: 10.1111/1758-2229.12866

Martin, M. (2011). Cutadapt removes adapter sequences from high-throughput sequencing reads. *EMBnet J.* 17, 10–12. doi: 10.14806/ej.17.1.200

Mattsson, L., Handsaker, B., Sörenson, E., Capo, E., Farnelid, H., Hirwa, M., et al. (in press). Functional diversity facilitates stability under environmental changes in an outdoor microalgal cultivation system.

Mayali, X., Franks, P. J. S., and Burton, R. S. (2011). Temporal attachment dynamics by distinct bacterial taxa during a dinoflagellate bloom. *Aquat. Microb. Ecol.* 63, 111–122. doi: 10.3354/ame01483

Mouget, J. L., Dakhama, A., Lavoie, M. C., and Delanoue, J. (1995). Algal growth enhancement by bacteria: is consumption of photosynthetic oxygen involved. *FEMS Microbiol. Ecol.* 18, 35–43. doi: 10.1016/0168-6496(95)00038-C

O'Gorman, E. J., Pichler, D. E., Adams, G., Benstead, J. P., Cohen, H., Craig, N., et al. (2012). "Impacts of warming on the structure and functioning of aquatic communities" in *Advances in ecological research*. eds. G. Woodward, U. Jacob and E. J. O'Gorman (Academic Press), 81–176.

Oksanen, J., Blanchet, F. G., Friendly, M., Kindt, R., Legendre, P., McGlinn, D., et al. (2019). vegan: Community Ecology Package. Available at: https://cran.r-project.org/package=vegan (Accessed January 21, 2021).

Oksanen, J., Kindt, R., Legendre, P., O'Hara, B., Simpson, G. L., Solymos, P. M., et al. (2008). The vegan package. *Community Ecol. Packag.*, 190. Available at: http://vegan.r-forge.r-project.org/ (Accessed January 21, 2021).

Olofsson, M. (2015). Microalgae - future bioresource of the sea? PhD dissertation. Växjö. Available at: http://urn.kb.se/resolve?urn=urn:nbn:se:lnu:diva-46512

Otwell, A. E., López García de Lomana, A., Gibbons, S. M., Orellana, M. V., and Baliga, N. S. (2018). Systems biology approaches towards predictive microbial ecology. *Environ. Microbiol.* 20, 4197–4209. doi: 10.1111/1462-2920.14378

Peterson, G., Allen, C. R., and Holling, C. S. (1998). Ecological resilience, biodiversity, and scale. *Ecosystems* 1, 6–18. doi: 10.1007/s100219900002

Prosser, J. I., and Martiny, J. B. H. (2020). Conceptual challenges in microbial community ecology. *Philos. Trans. R. Soc. B Biol. Sci.* 375:20190241. doi: 10.1098/rstb.2019.0241

Ptacnik, R., Solimini, A. G., Andersen, T., Tamminen, T., Brettum, P., Lepistö, L., et al. (2008). Diversity predicts stability and resource use efficiency in natural phytoplankton communities. *Proc. Natl. Acad. Sci.* 105, 5134–5138. doi: 10.1073/pnas.0708328105

Quast, C., Pruesse, E., Yilmaz, P., Gerken, J., Schweer, T., Yarza, P., et al. (2013). The SILVA ribosomal RNA gene database project: improved data processing and web-based tools. *Nucleic Acids Res.* 41, 590–596. doi: 10.1093/nar/gks1219

Saeedghalati, M., Farahpour, F., Budeus, B., Lange, A., Westendorf, A. M., Seifert, M., et al. (2017). Quantitative comparison of abundance structures of generalized communities: from B-cell receptor repertoires to microbiomes. *PLoS Comput. Biol.* 13:e1005362. doi: 10.1371/journal.pcbi.1005362

Schoener, T. W. (1974). Resource partitioning in ecological communities. *Science* 185, 27–39. doi: 10.1126/science.185.4145.27

Segev, E., Wyche, T. P., Kim, K. H., Petersen, J., Ellebrandt, C., Vlamakis, H., et al. (2016). Dynamic metabolic exchange governs a marine algal-bacterial interaction. *elife* 5:e17473. doi: 10.7554/eLife.17473

Seyedsayamdost, M. R., Wang, R., Kolter, R., and Clardy, J. (2014). Hybrid biosynthesis of roseobacticides from algal and bacterial precursor molecules. *J. Am. Chem. Soc.* 136, 15150–15153. doi: 10.1021/ja508782y

Shade, A., Peter, H., Allison, S. D., Baho, D. L., Berga, M., Bürgmann, H., et al. (2012a). Fundamentals of microbial community resistance and resilience. *Front. Microbiol.* 3:417. doi: 10.3389/fmicb.2012.00417

Shade, A., Read, J. S., Youngblut, N. D., Fierer, N., Knight, R., Kratz, T. K., et al. (2012b). Lake microbial communities are resilient after a whole-ecosystem disturbance. *ISME J.* 6, 2153–2167. doi: 10.1038/ismej.2012.56

Sörenson, E., Farnelid, H., Lindehoff, E., and Legrand, C. (2020). Resource partitioning between phytoplankton and bacteria in the coastal Baltic Sea. *Front. Mar. Sci.* 7, 1–19. doi: 10.3389/fmars.2020.608244

Steiner, C. F., Long, Z. T., Krumins, J. A., and Morin, P. J. (2006). Population and community resilience in multitrophic communities. *Ecology* 87, 996–1007. doi: 10.1890/0012-9658(2006)87

Stockenreiter, M., Graber, A. -K., Haupt, F., and Stibor, H. (2012). The effect of species diversity on lipid production by micro-algal communities. *J. Appl. Phycol.* 24, 45–54. doi: 10.1007/s10811-010-9644-1

Sundstrom, S. M., Angeler, D. G., Barichievy, C., Eason, T., Garmestani, A., Gunderson, L., et al. (2018). The distribution and role of functional abundance in cross-scale resilience. *Ecology* 99, 2421–2432. doi: 10.1002/ecy.2508

Teeling, H., Fuchs, B. M., Becher, D., Klockow, C., Gardebrecht, A., Bennke, C. M., et al. (2012). Substrate-controlled succession of marine bacterioplankton populations induced by a phytoplankton bloom. *Science* 336, 608–611. doi: 10.1126/science.1218344

Teeling, H., Fuchs, B. M., Bennke, C. M., Krüger, K., Chafee, M., Kappelmann, L., et al. (2016). Recurring patterns in bacterioplankton dynamics during coastal spring algae blooms. *elife* 5, 1–31. doi: 10.7554/eLife.11888

Tipton, L., Darcy, J. L., and Hynson, N. A. (2019). A developing symbiosis: enabling cross-talk between ecologists and microbiome scientists. *Front. Microbiol.* 10, 1–10. doi: 10.3389/fmicb.2019.00292

Vanwonterghem, I., Jensen, P. D., Dennis, P. G., Hugenholtz, P., Rabaey, K., and Tyson, G. W. (2014). Deterministic processes guide long-term synchronised population dynamics in replicate anaerobic digesters. *ISME J.* 8, 2015–2028. doi: 10.1038/ismej.2014.50

Walker, B., Holling, C. S., Carpenter, S. R., and Kinzig, R. (2004). Resilience, adaptability and transformability in social-scological systems. *Ecol. Soc.* 9:5.

Wang, X., Wen, X., Yan, H., Ding, K., Zhao, F., and Hu, M. (2011). Bacterial community dynamics in a functionally stable pilot-scale wastewater treatment plant. *Bioresour. Technol.* 102, 2352–2357. doi: 10.1016/j.biortech.2010.10.095

Wardwell, D. A., Allen, C. R., Peterson, G. D., and Tyre, A. J. (2008). A test of the cross-scale resilience model: functional richness in Mediterranean-climate ecosystems. *Ecol. Complex.* 5, 165–182. doi: 10.1016/j.ecocom.2007.11.001

Wickham, H. (2016). *ggplot2: Elegant graphics for data analysis*. New York: Springer International Publishing.

Zell, C., and Hubbart, J. A. (2013). Interdisciplinary linkages of biophysical processes and resilience theory: pursuing predictability. *Ecol. Model.* 248, 1–10. doi: 10.1016/j.ecolmodel.2012.09.021

Zhou, J., Richlen, M. L., Sehein, T. R., Kulis, D. M., Anderson, D. M., and Cai, Z. (2018). Microbial community structure and associations during a marine dinoflagellate bloom. *Front. Microbiol.* 9:1201. doi: 10.3389/fmicb.2018.01201

Conflict of Interest: The authors declare that the research was conducted in the absence of any commercial or financial relationships that could be construed as a potential conflict of interest.

frontiers in Microbiology

ORIGINAL RESEARCH
published: 02 March 2021
doi: 10.3389/fmicb.2021.596015

Distribution of Chromophytic Phytoplankton in the Eddy-Induced Upwelling Region of the West Pacific Ocean Revealed Using *rbc*L Genes

*Laxman Pujari[1], Dhiraj Narale[1], Jinjun Kan[2], Chao Wu[1], Guicheng Zhang[1], Changling Ding[1], Liuyang Li[1,3] and Jun Sun[4]**

[1]Research Center for Indian Ocean Ecosystem, Tianjin University of Science and Technology, Tianjin, China, [2]Stroud Water Research Center, Avondale, PA, United States, [3]School of Life Sciences and Biotechnology, Shanghai Jiao Tong University, Shanghai, China, [4]College of Marine Science and Technology, China University of Geosciences, Wuhan, China

Marine chromophytic phytoplankton are a diverse group of algae and contribute significantly to the total oceanic primary production. However, the spatial distribution of chromophytic phytoplankton is understudied in the West Pacific Ocean (WPO). In this study, we have investigated the community structure and spatial distribution of chromophytic phytoplankton using RuBisCO genes (Form ID *rbc*L). Our results showed that Haptophyceae, Pelagophyceae, Cyanophyceae, Xanthophyceae, and Bacillariophyceae were the dominant groups. Further, chromophytic phytoplankton can be distinguished between upwelling and non-upwelling zones of the WPO. Surface and 75 m depths of a non-upwelling area were dominated by *Prochlorococcus* strains, whereas chromophytic phytoplankton were homogenously distributed at the surface layer in the upwelling zone. Meanwhile, *Pelagomonas*-like sequences were dominant at DCM (75 m) and 150 m depths of the upwelling zone. Non-metric multidimensional scaling (NMDS) analysis did not differentiate between chromophytic phytoplankton in the upwelling and non-upwelling areas, however, it showed clear trends of them at different depths. Further, redundancy analysis (RDA) showed the influence of physicochemical parameters on the distribution of chromophytic phytoplankton. Along with phosphate ($p < 0.01$), temperature and other dissolved nutrients were important in driving community structure. The upwelling zone was impacted by a decrease in temperature, salinity, and re-supplement of nutrients, where *Pelagomonas*-like sequences outnumbered other chromophytic groups presented.

Keywords: West Pacific Ocean, Western boundary currents, upwelling, *rbc*L gene, chromophytic phytoplankton, high throughput sequencing

OPEN ACCESS

Edited by:
Debora Iglesias-Rodriguez, University of California, Santa Barbara, United States

Reviewed by:
Francois Ribalet, University of Washington, United States
Yonghong Bi, Chinese Academy of Sciences, China

***Correspondence:**
Jun Sun
phytoplankton@163.com

Specialty section:
This article was submitted to Aquatic Microbiology, a section of the journal Frontiers in Microbiology

Received: *18 August 2020*
Accepted: *19 January 2021*
Published: *02 March 2021*

Citation:
Pujari L, Narale D, Kan J, Wu C, Zhang G, Ding C, Li L and Sun J (2021) Distribution of Chromophytic Phytoplankton in the Eddy-Induced Upwelling Region of the West Pacific Ocean Revealed Using rbcL Genes. Front. Microbiol. 12:596015. doi: 10.3389/fmicb.2021.596015

INTRODUCTION

Marine phytoplankton are accountable for half of the world's primary production. They are the key players of the global carbon cycle (Falkowski, 1994; Smetacek, 1999). In recent years, research on phytoplankton diversity has evolved at a rapid pace in which molecular tools have increasingly been used in place of more conventional approaches. Consequently, the high-resolution phytoplankton molecular diversity being recovered across different ecosystems

has been achieved through characterizing functional genes involved in metabolisms (such as carbon and nitrogen; Samanta and Bhadury, 2014; Wu et al., 2019). Ribulose-1, 5-bisphosphate carboxylase/oxygenase (RuBisCO) enzyme-encoding *rbc*L gene, is an important gene marker for assessing phylogenetic relationships among photosynthetic organisms, as it is mostly found in chloroplasts where photosynthesis occurs (Gielly and Taberlet, 1994). RuBisCO is a rate-limiting enzyme for photosynthetic CO_2 fixation in phytoplankton. Until now, four different forms of RuBisCO (I, II, III, and IV) have been discovered. Form I is the most abundant (Tabita, 1999), and it is subdivided into four subclasses, i.e., IA, IB, IC, and ID. Generally, these genes are also divided into the terms 'green' and 'red' lineages. From ID, RuBisCO contains non-green (red lineage) phytoplankton groups such as Bacillariophyceae, Haptophyceae, Pelagophyceae, Cryptophyceae, Chrysophyceae, and Eustigmatophyceae, and these are termed chromophytic phytoplankton (Tabita, 1999). Earlier studies on functional gene *rbc*L form ID have emphasized its importance through gene abundance, expression and have also provided high-resolution community composition of chromophytic phytoplankton in different marine ecosystems (Pichard et al., 1993; Samanta and Bhadury, 2014). As the *rbc*L gene is chloroplast encoded, the chloroplast gene copy number swithin chromophytic phytoplankton differ, particularly in diatoms. Diatoms may comprise of up to 2000 chloroplast-encoding *rbc*L genes in addition to two copies of *rbc*L gene in their genome (Douglas, 1988).

The understanding of fundamental factors regulating the distribution of microorganisms including phytoplankton in diverse marine ecosystems is important for the interpretation of global biogeochemistry and climate systems as well as ecological and evolutionary changes (Hanson et al., 2012). The West Pacific Ocean (WPO) is one of the most dynamic and intensive mass water transportation systems in the world (Loder et al., 1998). The WPO possesses various Western Boundary Current (WBC) systems (**Figure 1**), and these are swift and narrow oceanic currents found in all major oceanic gyre. The North Equatorial Current (NEC) impinges upon the Philippine coast and gives rise to the northward Kuroshio Current (KC) and southward Mindanao Current (MC; Zhang et al., 2017). The KC plays a vital role in the northern Pacific circulation system, which carries warm, saline, and oligotrophic waters. The MC flows southwards along the Philippine coast and further divides to form the North Equatorial Countercurrent (NECC) and Indonesia Throughflow (ITF). The groups of currents known as the Low-Latitude western boundary currents (LLWBCs) and New Guinea Coastal Current/undercurrent (NGCC/NGCCU) flow along New Guinea and meet near Halmahera Island (Kashino et al., 2013). This complex feature of retroflection gives rise to two semipersistent eddies, i.e., the Mindanao Eddy (ME) and Halmahera Eddy (HE). The formation of the Mindanao upwelling system at the retroflection area is a critical physical phenomenon. Such eddy-induced upwelling systems are considered to be the most productive zones of the world ocean (Cushing, 1971). Generally, upwelling zones are recognized by their horizontal anomaly in temperature, salinity, density, oxygen, nutrients, and chlorophyll. The Mindanao eddy upwelling zone is recognized by its cold anomaly at 100 m depth east of Mindanao (Udarbe-Walker and Villanoy, 2001). Although it reaches its maximum size in winter and decreases towards summer, it presents throughout the year with varying sizes (Udarbe-Walker and Villanoy, 2001). Earlier studies elucidated the diversity of chromophytic phytoplankton and their significant contribution in other upwelling zones, including the California coast upwelling zone (Bhadury and Ward, 2009) and Monterey Bay upwelling zone (Paerl et al., 2012). Different currents and upwelling zones in the WPO comprehensively provide a unique environment for the proliferation of the primary producers, including the chromophytic phytoplankton. However, to date, there has been no study carried out to assess the molecular characterization and phylogenetic diversity of chromophytic phytoplankton community structure in the upwelling zone of WPO.

The purpose of the present study was to investigate the community composition of chromophytic phytoplankton in the WPO. Furthermore, this study also assessed the influence of environmental variability on chromophytic phytoplankton community structure in the eddy-induced upwelling region of the WPO using high throughput sequencing of form ID *rbc*L genes.

MATERIALS AND METHODS

Study Area, Sample Collection, and Physicochemical Analysis

The cruise was carried out in the WPO onboard research vessel *KeXue* from October 25th to November 12th 2017 (**Figure 1**). Samples were collected from 10 different stations, including several vertical depths. Among them, six stations (WPO 1, WPO 2, WPO 3, WPO 4, WPO 5, and WPO 6) were sampled for three depths (0, 75, and 150 m). Due to technical complications, we could not obtain sequences from station "WPO 7" 150 m depth and Station "WPO 8" 0 m and 150 m depths. The other two stations, "WPO A" and "WPO B", were in the upwelling zone. Therefore, to obtain a comprehensive community structure of chromophytic phytoplankton at the upwelling zone, we collected samples from five different depths (0, 50, 75, 100, and 150 m). Details of the geographical location of stations are drawn in **Figure 1A** [Ocean Data View (v4.7.7),[1] 2001; Schlitzer, 2007]. **Figure 1B** indicates the mean sea level anomaly (m) variations at sampling stations. Samples were collected using a rosette multi-sampler mounted with probes and sensors for conductivity, temperature, and depth (Sea-Bird SBE 911Plus, Sea-Bird Electronics, United States). Subsamples (100 ml) were collected in HCL-rinsed bottles and stored at 4°C for nutrient analysis. Nutrient analysis was performed (in duplicate) on Technicon AA3 Auto-Analyzer (Bran+ Luebbe, Norderstedt, Germany) for phosphate (PO_4^{3-}),

[1]https://odv.awi.de/

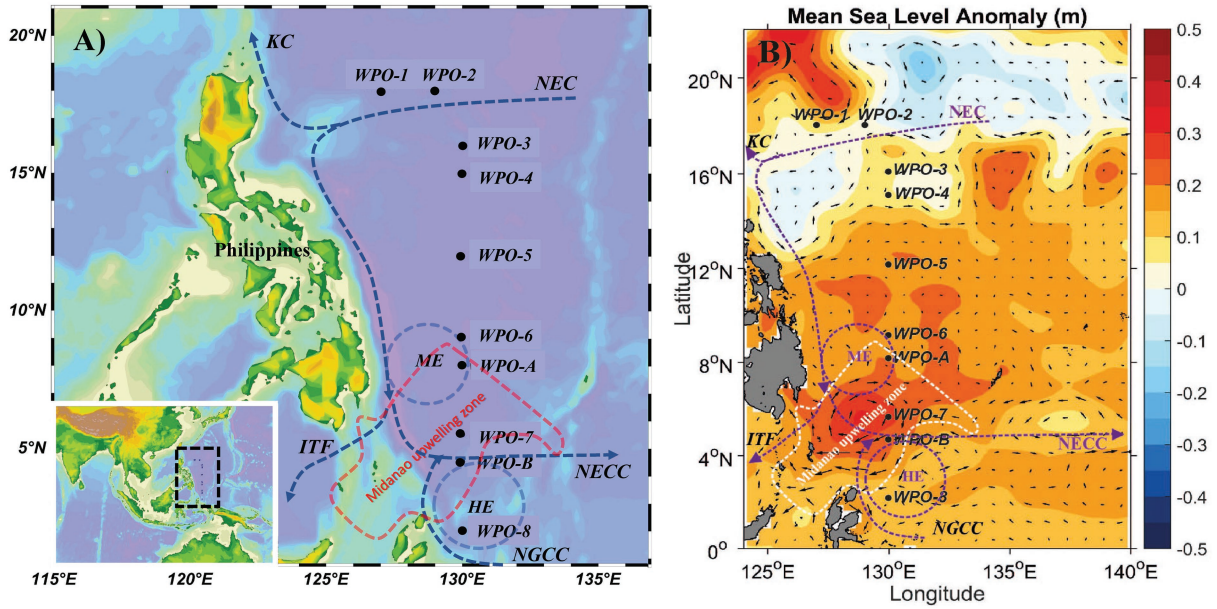

FIGURE 1 | A map showing **(A)** geographic location, and **(B)** mean sea level anomaly (in m) at the sampling sites in the WPO. The mean sea level anomaly is color-coded with scale bar shown on the right side. The major Western Boundary Currents (WBCs) are coded as, the Kuroshio Current (KC), the North Equatorial Current (NEC), the North Equatorial Countercurrent (NECC), the New Guinea Coastal Current (NGCC), the Indonesian Throughflow (ITF) and the Mindanao Eddy (ME), the Halmahera Eddy (HE), and Mindanao upwelling zone are shown on the map (Udarbe-Walker and Villanoy, 2001; Hu et al., 2015; Chen et al., 2018).

ammonium (NH_4^+), nitrite (NO_2^-), nitrate (NO_3^-), and silicic acid [$Si(OH)_4$]. The detection limits of the Auto-Analyzer for each inorganic nutrient were; 0.024–39 μM (for phosphate), 0.04–27 μM (ammonium), 0.003–6 μM (nitrite), 0.015–50 μM (nitrate), and 0.03–100 μM (silicic acid). For analysis of Chlorophyll (Chl-*a*), 500 ml of seawater was vacuum filtered (<10 mm Hg) through Whatman GF/F filter membranes (25 mm), packed carefully in aluminum foil, and stored at −20°C in the dark until further analysis. Chl-*a* was extracted with the 90% acetone method and analyzed using a fluorometer (CHL NA, Model # 046, Turner designs, San Jose, CA, United States). For molecular analysis, 2 L seawater was filtered on a 0.22 μm GTTP filter (Millipore, Eschborn, Germany). The filters were flash-frozen in liquid nitrogen, transferred to the laboratory, and stored at −80°C until DNA extraction.

DNA Extraction and Amplification of Form ID *rbc*L Gene

The genomic DNA was extracted using the DNeasy PowerWater DNA extraction kit (QIAGEN, Hilden, Germany) according to the manufacturer's instruction. Further quality and quantity of DNA were checked on 1% agarose gel electrophoresis (Thermo Fisher Scientific, Wilmington, Delaware, United States). Form ID *rbc*L gene (554 bp), fragments were amplified using the previously published *rbc*L primer (Wawrik et al., 2002). Each PCR reaction was performed using the following reaction ingredients: 2 μl template DNA, 10 μl Premix Taq (Takara, Tokyo, Japan), 1 mM each primer, and 6 μl of double-distilled water to make a final volume of 20 μl. Further, while performing PCR, conditions were set as follows: initial denaturation at 95°C for 5 min, 30 cycles of 95°C for 1 min, 56°C for 1 min, 72°C for 1 min, and a final extension at 72°C for 1.2 min. PCR reactions of environmental samples were performed in triplicate, pooled together, and purified using Universal DNA purification kits (Tiangen Biotech, Beijing, China) following the manufacturer's instruction. All libraries were constructed and sequenced *via* a paired-end approach (PE300) on an Illumina MiSeq PE300 platform (Illumina, San Diego, CA, United States) at Allwegene Technology Co. Ltd. Beijing, China.

Data Processing and Statistical Analysis

Raw sequences were obtained from the Illumina Miseq PE300 platform, which then transformed into sequence reads by base calling using the Illumina Analysis Pipeline (v2.6). These sequences were stored in FASTQ files with respective sequencing quality. Based on samples and their barcodes, raw sequence data were separated, permitting up to one mismatch. Further, open-source software QIIME (v1.8; Caporaso et al., 2010) was used to quality filter the raw sequence. According to the relation between paired-end reads, the paired-end was merged into full-length sequences by FLASH software (v1.2.7), and a minimum overlap of 10 bp length was kept. The maximum mismatch ratio allowed by the overlap was kept at 0.1. Every sample raw tag was quality filtered to obtain clean tags by Trimmomatic software (v0.33; Bolger et al., 2014), and sequences meeting the following three criteria were included in downstream analyses: (1) sequences with precise primers and bar-codes;

(2) quality score >30; (3) sequences >200 bp in length. The sequencing quality score is based on the probability that the base is called incorrectly. The Q30 quality score can be inferred with 1 in 1000 probability of an incorrect base call, which corresponds to 99.99% base call accuracy. A sequence length >200 was kept as *rbc*L gene length is 554 bp. The sequencing platform that we used was Illumina MiSeq PE300. Illumina reads are relatively shorter (150–300 bp) compared to the *rbc*L gene of 554 bp. This shortcoming was addressed by the paired-end sequencing that covered the 554 bp *rbc*L gene. Further, To eliminate erroneous and chimeric sequences, USEARCH (v10.0.240; Edgar, 2010) was used. After removing non-*rbc*L sequence reads, sequences were clustered into operational taxonomic units (OTUs) at a 97% similarity level using UCLUST (v1.2.22). Different methods use a defined yet arbitrary clustering threshold, called the sequence similarity threshold, as a cutoff value to ensure that the sequence within OUTs is identical. We used a 97% cutoff value, which can effectively maximize genetic diversity. Low-abundance OTUs (fewer than two reads, including singletons), which might influence richness and diversity estimates, were excluded from the subsequent analyses (Dickie, 2010). The remaining high-quality sequences were queried against the GenBank database at NCBI using local BLASTn. The MEGAN program (Huson et al., 2007) was used to assign BLAST hits to taxa in the NCBI database. A phylogenetic tree was constructed based on top genera recovered from this study. Prior to construction of the phylogenetic tree, top genus sequences were first translated to amino acid sequences. These amino acid sequences were then blasted in the protein database at National Center for Biotechnology Information (NCBI) using BLASTX (v2.8.1+) to identify the most closely related sequences (Altschul et al., 1997). These sequences were then further aligned with ClustalW, and a phylogenetic neighbor-joining tree was constructed using MEGA (v7.0; Huson et al., 2007; Kumar et al., 2016). Later, the cluster stability was verified by bootstrap resampling for 1,000 times. Further, this phylogenetic tree was edited with online webpage iTOL (Letunic and Bork, 2011). The sequences obtained from this study have been deposited in the NCBI Sequence Read Archive with accession number SUB6119769.

Chao1 (richness estimator) and Shannon diversity indices were calculated using QIIME (v1.8). The coverage of sequencing and abundance was calculated by a random sampling method (mothur), and the rarefaction curve was drawn using R (v3.3.1). In the present study, nonmetric multidimensional scaling (NMDS) was used to show vertical and horizontal distribution outline of the chromophytic community using Primer (v6; Clarke and Gorley, 2006). Before NMDS analysis, data were log-transformed in primer software, and clusters were overlaid using a resemblance matrix of Bray-Curtis similarity. To understand the spatial distribution of chromophytic phytoplankton and their relationship within environmental parameters, we performed redundancy analysis (RDA). Before RDA analysis, detrended correspondence analysis (DCA) was carried out to know whether RDA or canonical correspondence analysis is suitable for the current study. Since the length of the first axis was less than 2.0, RDA was selected. The differences of various environmental parameters with different depths were evaluated by *t*-test using Excel (Command TTEST, two-tailed).

RESULTS

Environmental Variability

The oceanographic setup had a strong bearing on the environmental characteristics in the WPO (**Figure 2**). Regional differentiation in the surface environmental variables was observed (two-tailed *t*-test) within the northern stations (WPO-1–WPO-5) and equatorward (southern) stations (WPO-6–WPO-8, WPO-A, and WPO-B). During the study period, Sea Surface Temperature (SST) and Sea Surface Salinity (SSS) values ranged from 27.9 to 29.9°C and 33.4 to 34.6, respectively. The lowest SST was recorded in the northern study area, especially at 15°N (station WPO-4; 27.9°C), whereas towards the equator, SST increased up to 29.9°C (at 4.5°N; station WPO-B). Contrastingly, high SSS was observed in the northern region, at 18°N (station WPO-2; 34.6), which eventually decreased (33.4) towards the south (5.4°N, at station WPO-7). Surface Chl-*a* concentration was higher (0.65 μg L^{-1}) in the upwelling zone (station WPO-7), which substantially decreased (up to 0.14 μg L^{-1}) towards the northern non-upwelling region. The surface dissolved nutrients, except phosphate showed an unequal distribution pattern ($p > 0.05$) along the study area. Surface phosphate concentration was below the detection limit at station WPO-1 (18°N), WPO-4 (15°N), WPO-5 (11.9°N), and WPO-8 (2°N), whereas the highest concentration was recorded at WPO-6 (8.9°N; 0.11 μmol L^{-1}). The low surface nitrite concentration (0.05 μmol L^{-1}) was observed at stations WPO-3 (15.9°N), WPO-4 (15°N; 0.06 μmol L^{-1}) and WPO-7 (5.4°N; 0.05 μmol L^{-1}), whereas highest values were recovered from station WPO-B (4.5°N; 0.19 μmol L^{-1}), WPO-8 (2°N; 0.17 μmol L^{-1}), and WPO-A (8°N; 0.10 μmol L^{-1}). Similarly, surface nitrate concentration was high (2.01 μmol L^{-1}) at southern area 8°N (station WPO-A) and WPO-B (4.5°N; 1.19 μmol L^{-1}), and the lowest (0.01 μmol L^{-1}) concentration reported at WPO-4 (15°N), WPO-5 (11.9°N; 0.46 μmol L^{-1}), and WPO-6 (8.9°N; 0.46 μmol L^{-1}). Surface ammonia concentration was below the detection limit at stations WPO-5 (11.9°N) and WPO-7 (2°N), whereas the highest concentration was recorded at WPO-2 (18°N; 1.09 μmol L^{-1}). The highest silicic acid concentration was recorded at stations WPO-7 (5.49°N; 1.17 μmol L^{-1}) and WPO-8 (2°N; 1.02 μmol L^{-1}), whereas the lowest was recorded at WPO-6 (8.9°N; 0.46 μmol L^{-1}).

The vertical profile of the temperature and salinity evinced the presence of two distinct water masses in the region (**Figure 2**). The equatorial surface water (ESW) was characterized by high temperature and low salinity, whereas equatorial subsurface water (ESSW) was characterized by lower temperature and higher salinity. Towards the northern stations (18°N–11.9°N), strong stratification was evidenced in the upper layers till ~75 m depth. The ESW above the thermocline was nutrient depleted as a consequence of stratification, whereas below the thermocline (in the ESSW), the nutrient concentration was moderate. This restricted the Depth Chlorophyll Maximum (DCM) in between the 75 m and 100 m depth in the non-upwelling stations.

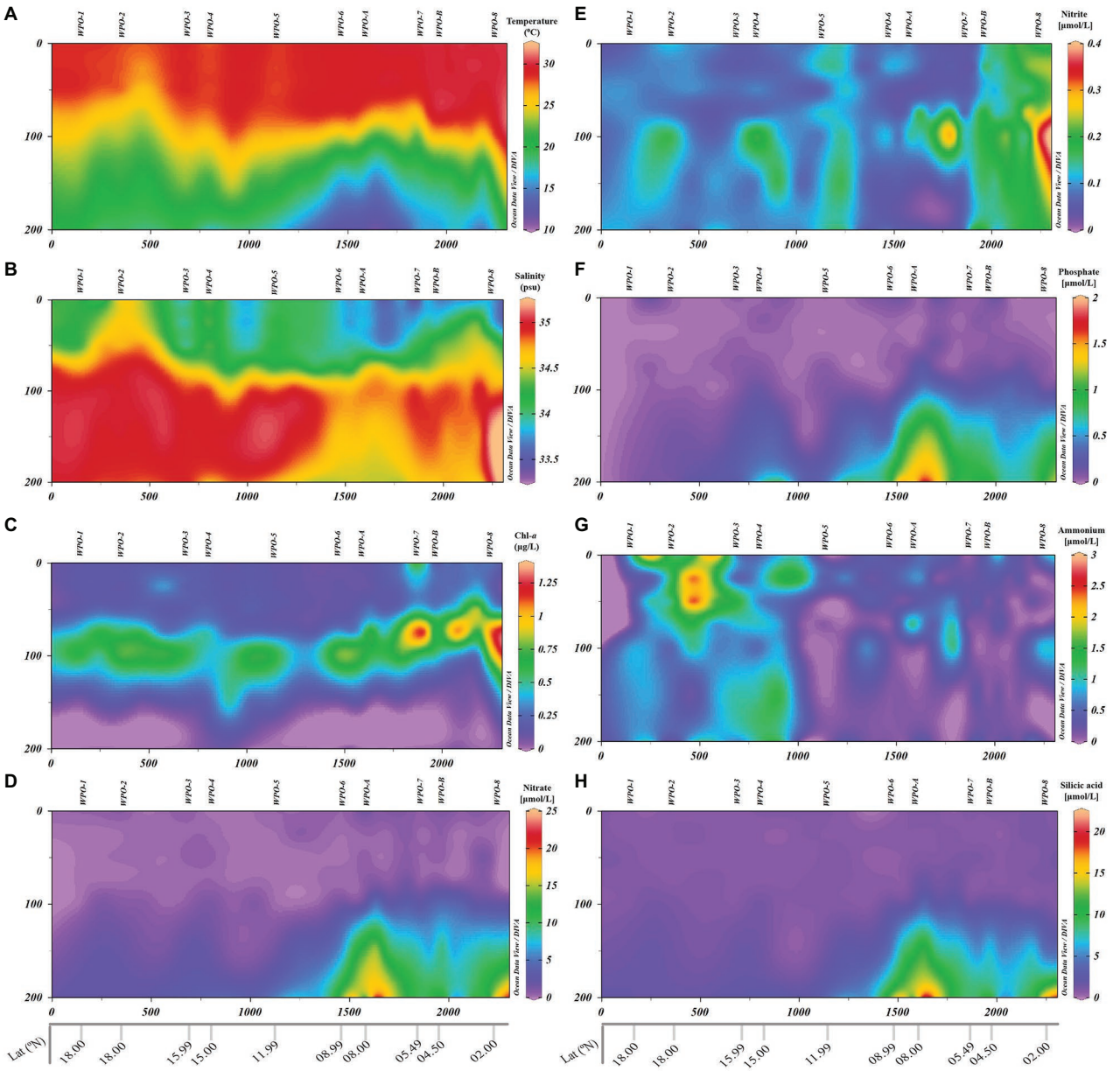

FIGURE 2 | Vertical depth profiles of environmental parameters measured in the WPO. **(A)**: Temperature (°C), **(B)**: Salinity-*a*, **(C)**: Chl-*a*, **(D)**: Nitrate (NO_3^-), **(E)**: Nitrite (NO_2^-), **(F)**: Phosphate (PO_4^{3-}), **(G)**: Ammonia (NH_4^+), and **(H)**: Silicic acid [$Si(OH)_4$].

The influence of upwelling signatures was clear on vertical profiles of physicochemical features in the southern upwelling zone (8.9°N–4.5°N) stations, i.e., WPO-6–WPO-8, WPO-A, and WPO-B (**Figure 2**). Eddy-driven upwelling transported cold, high-saline, and nutrient-enriched water towards the surface layer. This upward intrusion eventually decreased temperature and increased salinity upward from 200 m to ~100 m depth in the upwelling zone ($p < 0.01$; **Figures 2A,B**). Similarly, the dissolved inorganic nutrients (except nitrite and ammonia) concentration increased due to vertical transport of enriched water from 200 m to ~100 m depth ($p < 0.01$; **Figures 2D,F,H**). However, nitrite and ammonia concentration were unevenly dispersed in the upwelling zone (**Figures 2E,G**). The nutrient pumping from the deeper depths eventually supported the phytoplankton growth as revealed by Chl-*a* signatures. This significantly resulted ($p < 0.05$) in shallowing of DCM (~75 m) in the upwelling and neighboring stations (**Figure 2C**).

Sequencing Statistics and Estimates of Diversity Indices

A total of 1,476,652 raw sequences were generated from different vertical depth samples. Among 1,476,652 raw sequences, 312,108

clean sequences were included in the downstream analysis, and the details are given in **Tables 1** and **2**. **Table 1** represents the sequencing data of stations (WPO-1 to WPO-8), which were sampled for three depths (0 m, 75 m, and 150 m). **Table 2** represents two stations (WPO-A and WPO-B), which were sampled for five depths (0 m, 50 m, 75 m, 100 m, and 150 m). As we recovered a large number of OTUs, here, only OTUs with an abundance of more than 10 were considered for further analysis. Therefore, based on 97% similarity, we included a total of 755 OTUs. Further, the Shannon-Weiner diversity (H′) index was calculated for all samples. The highest diversity (6.67) was observed at 2°N, station WPO-8 (75 m), whereas the lowest value (3.67) was recorded at 4.5°N, station WPO-B (100 m; **Tables 1** and **2**). Chao 1 (OTU richness) was observed highest at station WPO 8 (75 m), and the lowest Chao 1 value was recorded at WPO-A (0 m; **Tables 1** and **2**). The observed species and Goods coverage were also listed in **Tables 1** and **2**.

Community Composition and Phylogenetic Analysis of Chromophytic Phytoplankton

All major chromophytic phytoplankton groups containing form ID *rbc*L gene, such as Bacillariophyceae, Haptophyceae, Pelagophyceae, Pinguiophyceae, Xanthophyceae, Eustigamtophyceae, Cyanophyceae, Syrunophyceae, Chrysophyceae, and Dictyochophyceae, were detected. The most abundant genera and classes are shown in **Figures 3, 4**, respectively. In general, the relative abundance at the class level revealed the dominance of the Haptophyceae rather than the Bacillariophyceae (**Figure 4**). At the genera level, *Pelagomonas* and *Prochlorococcus* outnumbered other chromophytic phytoplankton (**Figure 3**).

A neighbor-joining phylogenetic tree was constructed based on the *rbc*L gene amino acid sequences (**Figure 5**). Bacillariophyceae was retrieved as the most diverse group (with a total of 18 OTUs), than the dominant Haptophyceae group. Among Bacillariophyceae, *Nitzschia* was the dominant genus recovered at 4.5°N (station WPO-B) 50 m depth (**Figure 3B**). Within Bacillariophyceae, genus *Bolidomonas* (Class-Bolidiophyceeae) was clustered with *Rhizosolenia*, which is a genus of class Bacillariophyceae (**Figure 5**). *Bolidomonas* are picoplanktonic flagellated algae, which have a symbiotic relationship with diatoms (Kuwata et al., 2018). Further, Haptophyceae recovered as a second most diverse group, represented by a total of 12 OTUs, among which *Chrysochromulina* was dominant at 15°N (station WPO-4) 150 m depth followed by *Calyptrosphaera* at 5.4°N (station WPO-7) 75 m depth (**Figures 3B,C**). Class Pelagophyceae was represented by four genera, including *Pelagococcus*, *Pelagomonas*, *Sarcinochrysis*, and *Aureococcus*. The dominance of *Pelagomonas* has been recorded at 8°N (station WPO-A) 150 m depth, whereas the lowest value was recorded at the same location in surface waters (**Figures 3A,C**). Class Cyanophyceae represented by *Prochlorococcus* and *Synechococcus*, wherein *Prochlorococcus* was recorded as the most dominant genus at 15.9°N (stations WPO-3) at 75 m (**Figure 3B**). Other classes, including Dictyochophyceae (6 OTUs), Xanthophyceae (3 OTUs), Piguiophyceae (2 OTUs), Bolidiophyceae (1 OTU), Synurophyceae (1 OTU), and Eustigmatophyceae (1 OTU) were also recovered in the study region (**Figure 5**).

Effect of Environmental Variables on Chromophytic Phytoplankton

The nonmetric multidimensional scaling (NMDS) separated clusters of surfaces, DCM, and 150 m depths on the basis of 50% similarity (**Figure 6**). At the surface layers (0 m), the chromophytic

TABLE 1 | Summary of OTU numbers and diversity indices for *rbc*L sequences recovered from the various depths of the WPO stations WPO-1 to WPO-8.

Sites		WPO-1	WPO-2	WPO-3	WPO-4	WPO-5	WPO-6	WPO-7	WPO-8
Surface (0 m)	No. of OTUs	399	477	508	499	486	497	484	-
	Raw tags	46136	57290	81868	74410	19980	79214	39952	-
	Final tags	10068	10068	10068	10068	10068	10068	10068	-
	Observed species	385.5	459.2	490.7	480.8	469.6	478.8	466.4	-
	Chao1	534.68	661.14	648.48	667.65	652.87	678.02	657.17	-
	Good's coverage	0.98	0.98	0.98	0.98	0.98	0.98	0.98	-
	Shannon-weiner	5.08	5.28	5.36	5.71	5.46	5.3	5.64	-
DCM (75 m)	No. of OTUs	482	436	435	588	513	526	462	917
	Raw tags	52514	22804	12012	19424	41414	23453	52581	44905
	Final tags	10068	10068	10068	10068	10068	10068	10068	10068
	Observed species	465	416.3	419.6	568.1	495.2	507.3	441.2	884.4
	Chao1	646.13	681.31	590.84	739.74	715.73	676.18	661.54	1139.88
	Good's coverage	0.98	0.97	0.98	0.98	0.97	0.98	0.98	0.96
	Shannon-weiner	5.65	4.39	4.58	6.66	5.39	5.48	4.53	6.67
Bottom (150 m)	No. of OTUs	520	585	656	476	515	514	-	-
	Raw tags	62191	29585	24453	84994	30019	17038	-	-
	Final tags	10068	10068	10068	10068	10068	10068	-	-
	Observed species	498.2	561.1	633	458	491.5	493.3	-	-
	Chao1	744.05	839.72	900.19	624.33	782.02	775.94	-	-
	Good's coverage	0.97	0.97	0.97	0.98	0.97	0.97	-	-
	Shannon-weiner	4.8	5.2	5.78	4.72	4.17	4.93	-	-

Archive with accession number SUB4422106.

TABLE 2 | Summary of OTU numbers and diversity indices for *rbc*L sequences recovered from the various depths of the WPO stations WPO-A to WPO-B.

Sites		WPO-A	WPO-B
Surface (0 m)	No. of OTUs	391	543
	Raw tags	68709	29508
	Final tags	10068	10068
	Observed species	376.8	518.2
	Chao1	493.42	794.42
	Good's coverage	0.98	0.97
	Shannon-weiner	4.79	5.48
50 m	No. of OTUs	546	507
	Raw tags	55416	69512
	Final tags	10068	10068
	Observed species	524.5	487.5
	Chao1	746.22	694.91
	Good's coverage	0.97	0.98
	Shannon-weiner	5.57	5.12
DCM (75 m)	No. of OTUs	533	400
	Raw tags	26617	22350
	Final tags	10068	10068
	Observed species	512.4	384.2
	Chao1	748.9	561.48
	Good's coverage	0.97	0.98
	Shannon-weiner	5.59	4.63
100 m	No. of OTUs	481	428
	Raw tags	61819	21032
	Final tags	10068	10068
	Observed species	464.3	407.6
	Chao1	641.4	666.76
	Good's coverage	0.98	0.97
	Shannon-weiner	5.11	3.67
Bottom (150 m)	No. of OTUs	359	601
	Raw tags	88026	117426
	Final tags	10068	10068
	Observed species	342.8	578.1
	Chao1	509.67	831.83
	Good's coverage	0.98	0.97
	Shannon-weiner	3.74	5.12

phytoplankton community was relatively dominated by species belonging to Haptophyceae (Chrysochromulina, Calyptroshaera), Cyanophyceae (Prochlorococcus), and Xanthophyceae (Xanthonema, Ophiocytium) in both the non-upwelling and upwelling regions (**Figures 3A**, **4A**). In the DCM depths (50 and 75 m), the relative percentage of Cyanophyceae (Prochlorococcus) was more than Haptophyceae (Chrysochromulina, Calyptroshaera) in the non-upwelling stations. However, towards the upwelling zones, the relative percentage of Cyanophyceae was suppressed by Haptophyceae (Chrysochromulina, Calyptroshaera) (**Figures 3B**, **4B**). At the deeper depths, Pelagophyceae were relatively dominated over the Haptophyceae in non-upwelling (150 m) as well as upwelling zones (100 m and 150 m) (**Figures 3C**, **4C**). Notably, Bacillariophyceae was observed in-between DCM and 150 m depth in the upwelling zone (**Figures 4B**,**C**). Contrary, Xanthophyceae, and Chrysophyceae were relatively more on surface than deeper waters in both the non-upwelling and upwelling zone (**Figures 3** and **4**).

The comprehensive relationship between the chromophytic phytoplankton and environmental variability was evaluated with Redundancy analysis (RDA; **Figure 7**). Orientation and length of environmental vectors indicated their relative importance and approximate relations to the chromophytic phytoplankton assemblage. In the RDA triplot, the first two axes explained >35.8% cumulative variation between chromophytic phytoplankton community and environmental variables. Further, the orientation of the sampling stations on an RDA triplot reflected their chromophytic phytoplankton assemblage and associated with the environmental variables. Station orientation defined two distinct clusters representing the upwelling (cluster 1) and non-upwelling (cluster 2) sampling depths. At deeper sampling depths (DCM and 150 m) in the upwelling zone (cluster 1) salinity and nutrients (nitrate, phosphate, and silicic acid) supported the relative abundance of the Pelagophyceae and Haptophyceae. Moreover, Bacillariophyceae is significantly influenced by the nitrite concentration together with the other nutrients (**Figure 7**). In cluster 2, surface and DCM depths from the non-upwelling zone were oriented opposite to salinity and nutrients, towards the temperature vector. The more relative percentage of Cyanophyceae, Xanthophyceae, and Chrysophyceae in these samples could be resultant of the low nutrient conditions. Furthermore, the orientation of surface samples from cluster 1 towards the temperature vector could be due to the dominance of low nutrient and warmer temperature preferring chromophytic phytoplankton communities, i.e., Cyanophyceae, Xanthophyceae, and Chrysophyceae. The 150 m depths of Cluster 2 were oriented towards the salinity vector due to the dominance of Pelagophyceae and Haptophyceae. The plateaued rarefaction graph is drawn and shown in **Figure 8**.

DISCUSSION

For the last two decades, *rbc*L genes have proven to be an important and reliable phylogenetic marker for deciphering the diversity of chromophytic phytoplankton. Previous studies based on a large subunit of *rbc*L gene have recognized its significance in decrypting the community structure of chromophytic phytoplankton from different geographical and ecological settings in the global oceans (summarized in **Table 3**). However, to date, the distribution and responses of the chromophytic phytoplankton community to the ecological niche in the WPO has not been evaluated. In the WPO, diverse WBC-induced eddies and upwelling zones provide a unique environment for the proliferation of the marine phytoplankton community. Earlier phytoplankton studies in this region were restricted to satellite-derived ocean color imagery, microscopy, and flow cytometer evaluation of species composition in response to physicochemical characteristics (Chen et al., 2017, 2018). The only study on the functional *nif* H gene evaluation was focused on a wide distribution of diazotrophic community and quantification in the WPO (Chen et al., 2019). Here, we present the first study based on functional gene *rbc*L of the chromophytic phytoplankton with relation to the regional environmental characteristics (eddies and upwelling) in the WPO.

The phylogenetic analysis in this study recovered *Bolidomonas*-like *rbc*L sequences belonging to class Bolidiophyceae, which were clustered with *Rhizosolenia* (Class- Bacillariophyceae).

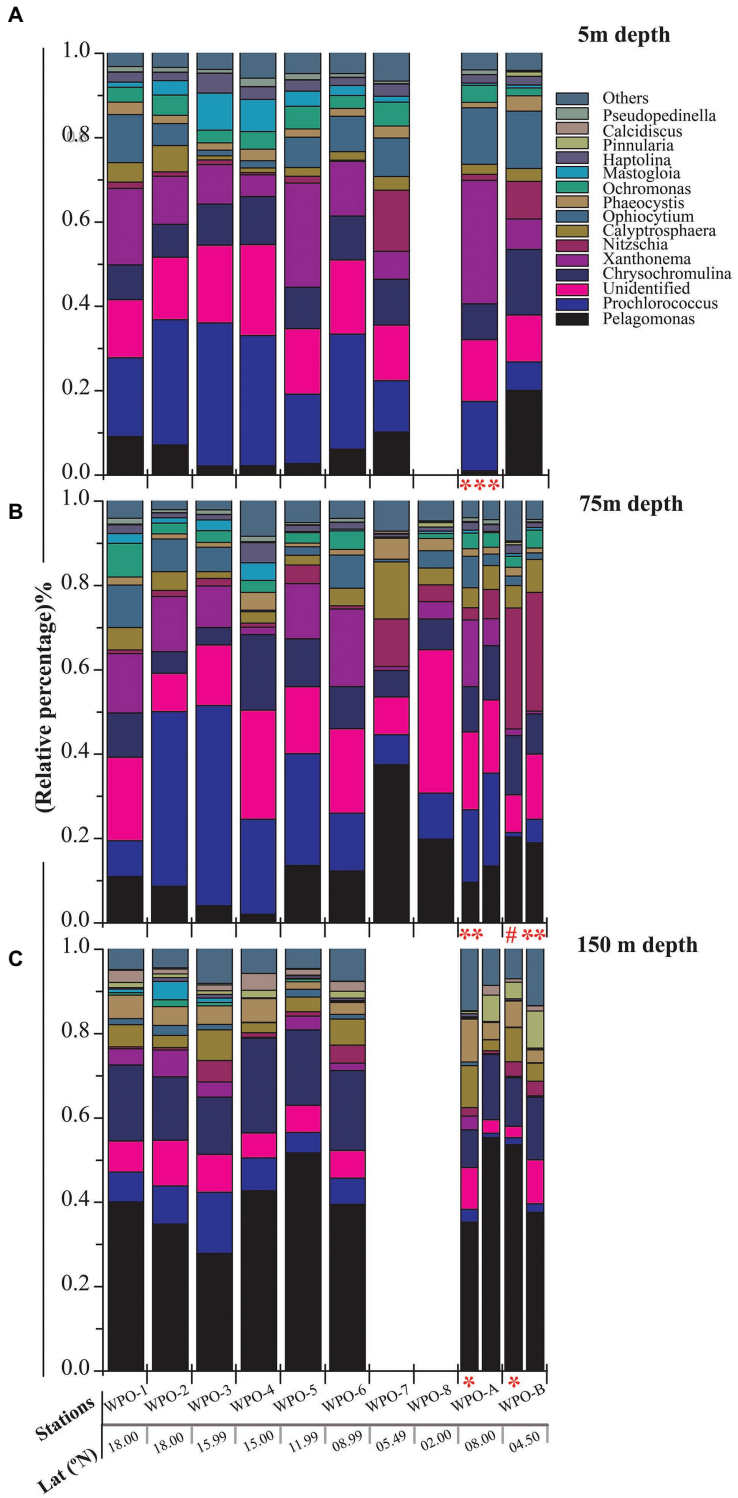

FIGURE 3 | Community structure of chromophytic phytoplankton at genus level based on *rbc*L gene sequences. **(A)** represents 5m depth, **(B)** represents 75m depth and **(C)** represents 150m depth (Note: Blank column indicate no data. Other marks indicate extra depth sampling at respected stations: ***5 m; **50 m; #25 m; *100 m).

In an earlier study, isolated strains of *Bolidomonas* using nuclear, plastidial, and mitochondrial gene markers compared *Bolidomonas* and *Triparma*, which later also included *Parmales* (Bolidiophyceae; Ichinomiya et al., 2016). Furthermore, the phylogenetic assessment revealed that *Parmales* were closely related to diatoms (Bacillariophyceae) and ubiquitously

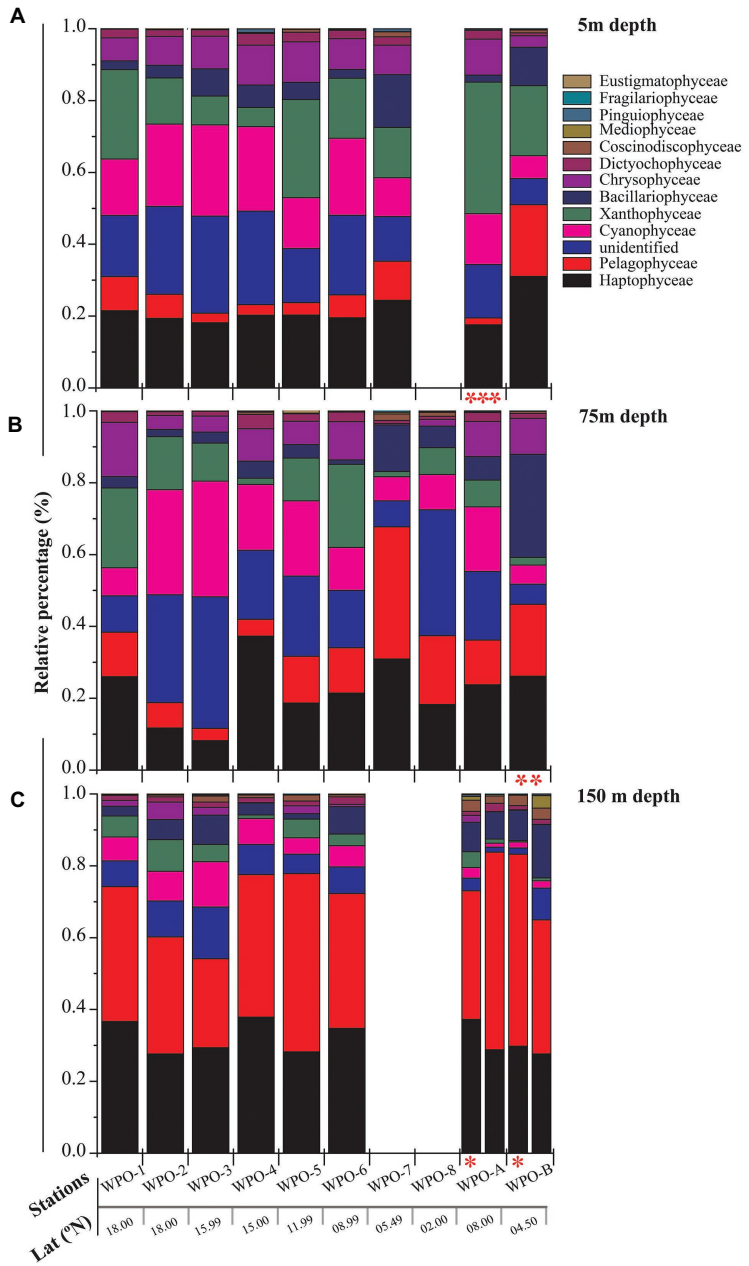

FIGURE 4 | Community structure of chromophytic phytoplankton at class level based on *rbc*L gene sequences. **(A)** represents 5m depth, **(B)** represents 75m depth and **(C)** represents 150m depth (Note: Blank column indicate no data. Other marks indicate extra depth sampling at respected stations: ***5 m; **50 m; *100 m).

distributed but constituted a minor component of the phytoplankton community (Ichinomiya et al., 2016). Similarly, another genus, *Peridinium*-like *rbc*L sequences, which represent the class Dinophyceae, was clustered in the phylogenetic tree with *Chaetoceros* (Class- Bacillariophyceae; **Figure 5**). The SSU rDNA investigation in two *Peridinium* species (*P. balticum* and *P. foliaceum*) suggested that the ancestors of these dinoflagellates engulfed pennate diatoms during tertiary endosymbiosis event (Inagaki et al., 2000), and genus *Peridinium* thus showed a close affinity to diatoms *rbc*L gene sequence in the present study.

During our study, the high-throughput sequencing analysis recovered 11 chromophytic phytoplankton groups (**Figure 5**) in 31 samples analyzed from the selected depths of 10 stations in the WPO. The recovery of these groups was consistent with previous studies carried out in different ecosystems of the world (Samanta and Bhadury, 2016). However, in contrast to previous studies, a dominance of group Haptophyceae over that of Bacillariophyceae was observed in this study. A total of 12 OTUs of group Haptophyceae were recovered during the analysis. Among them, the genus *Chrysochromulina*

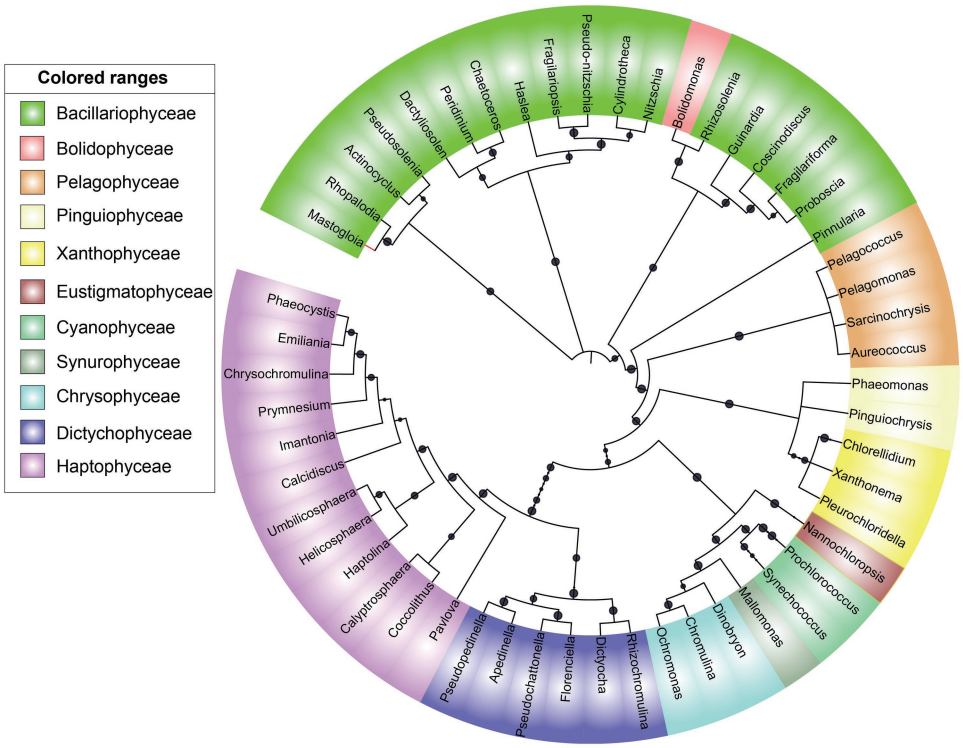

FIGURE 5 | A neighbor-joining phylogenetic tree constructed based on *rbc*L amino acid sequences. The topology of the tree was inferred from 1,000 bootstrap resampling, and bootstrap values greater than 50% were labeled with black dots at branches.

outnumbered other Haptophyceae genera recovered (**Figure 3C**). Genus *Chrysochromulina* sequences were recovered from most of the stations with varying depths of WPO. However, the highest number of *Chrysochromulina* sequences were retrieved from 150 m depth at all stations (**Figure 3C**). Haptophytes are one of the most diverse groups of picophototrophs in modern open oceans, and studies based on the analysis of SSU rDNA showed that the haptophytes were dominant in the pelagic and coastal ocean environments (Fuller et al., 2006; McDonald et al., 2007). A study carried out by McDonald (2007) concluded that, in the Gulf of Naples, >45% total and >70% eukaryotic chloroplast sequences were haptophytes in origin. Moreover, genus *Chrysochromulina* is believed to be ubiquitous in the marine environment and occupies up to 65% total number of nano-phytoplankton cells (Thomsen, 1994; Hajdu et al., 1996). The phylogenetic position of the majority of the picohaptophytes suggests that they are mixotrophic in nature, i.e., they are able to survive through the phototrophic regime with uptake and assimilation of organic nutrients (Nygaard and Tobiesen, 1993; Liu et al., 2009). Generally, it is believed that in nutrient and light-limited conditions, mixotrophy provides a competitive advantage (Pålsson and Granéli, 2004). A culture study carried out under controlled conditions suggested that *Chrysochromulina* species can feed on diverse small green flagellates. Their ingestion rate was inversely proportional to light intensity, and it changes in response to variation in light intensity and phosphate status (Jones et al., 1993). However, the occurrence of *Chrysochromuilna* species blooming with a larger chloroplast beneath the ice (off the coast of Finland) in low-light conditions suggests the complexity of mixotrophic nature within the genus *Chrysochromuilna* (Pintner, 1968; Niemi and Hallfors, 1974). Interestingly earlier studies proved that the vertical distribution of other haptophytes varies with change in temperature and light availability (Malinverno et al., 2003). Recently, Gran-Stadniczeñko (2017) observed the increased haptophyte diversity and abundance in the deep chlorophyll maximum (DCM) in Oslofjorden, Skagerrak, through 18 s rRNA and 28 s RNA evaluation. Therefore, different species of haptophytes probably respond differently to the vertically changing environmental characteristics in various regions. In the present study, the Haptophyceae oriented towards the dissolved nutrients vectors at the deeper depth upwelling stations (DCM and 150 m) in our RDA triplot (**Figure 7**). The highest abundance of Haptophyceae sequences from the depth of DCM and 150 m where nutrients were fairly high in concentration compared with the surface layer. Thus, here it can be concluded that under the light-limited conditions at deeper depths, along with the mixotrophy behavior, the availability of nutrients, high salinity, and low temperature conditions supported the growth of Haptophyceae, especially genus *Chrysochromulina*, as evinced in other studies. Few rarely occurring genera were also observed in the WPO during the present study.

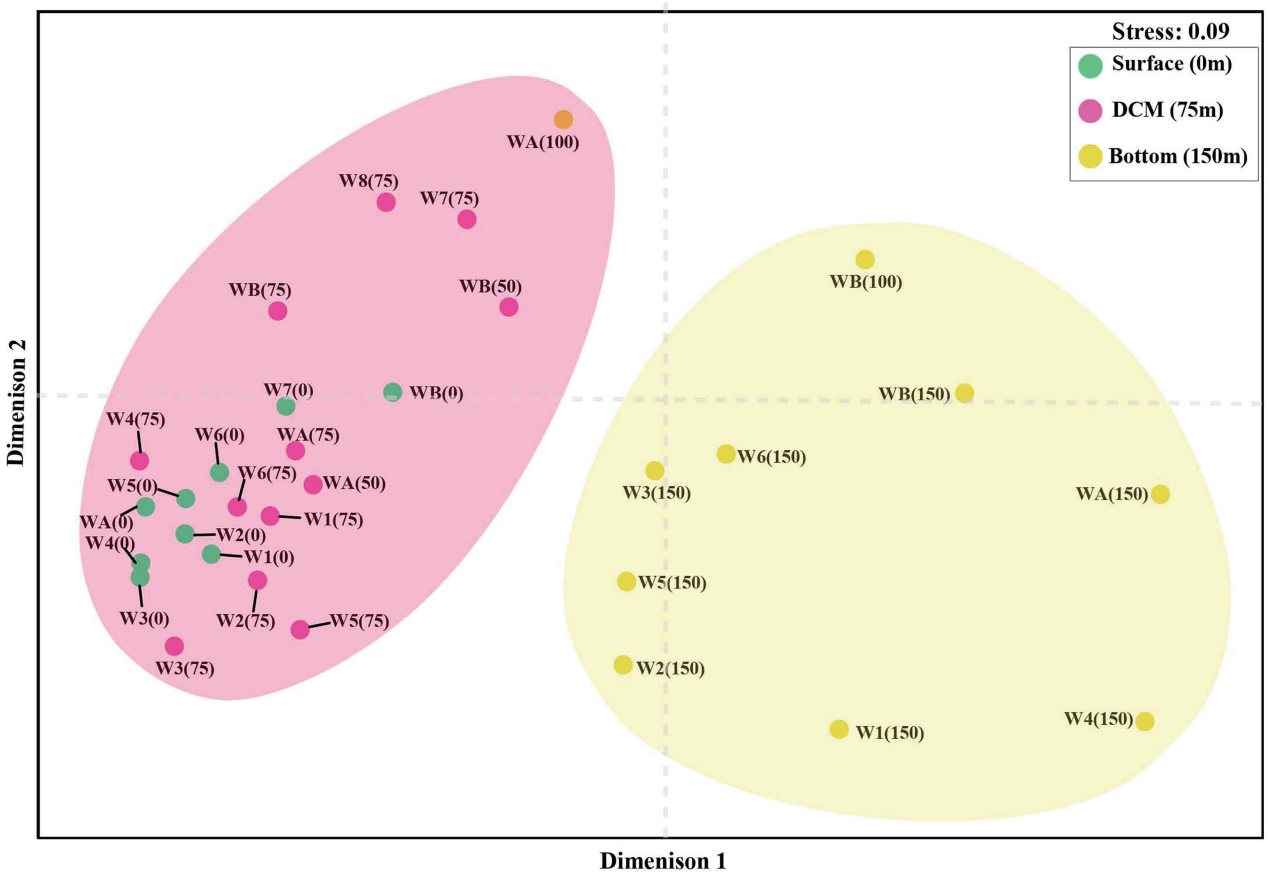

FIGURE 6 | Non-metric multidimensional scaling (NMDS) analysis of chromophytic phytoplankton community (stress = 0.09, similarity = 50%) from the WPO. [W1: WPO-1(18°N), W2: WPO-2 (18°N), W3: WPO-3 (15°N), W4: WPO-4 (15°N), W5: WPO-5 (11°N), W6: WPO-6 (8.9°N), W7: WPO-7 (5.4°N), W8: WPO-8 (2°N), WA: WPO-A (8°N), WB: WPO-B (4.5°N)].

One such rare genera *Calyptrosphaera* belonging to the class Haptophyceae was reported in the deeper depths (75 m and 150 m; **Figures 3B**,**C**). The studies related to genus *Calyptrosphaera* mainly consisted of morphological examination (Klaveness, 1973; Nöel et al., 2004), and there is very little information available on the distribution or ecology of this genus. Thus, the distribution of such rare occurring genus *Calyptrosphaera* is difficult to assess. Nöel (2004) proposed that heterococcolith-bearing cells of genus *Calyptrosphaera* had strong adhesive ability, which supports their survival under a wide range of irradiance, temperature, and nutrient concentrations. It is possibly the changing life phase under the varying stress levels that facilitate their survival. Nonetheless, our study contributes to the general distribution and ecology of genus *Calyptrosphaera*. Similarly, the sequences of other genus *Pseudopedinella* belonging to Class- Dictychophyceae were recovered in moderate numbers at surface depths during this study. Studies based on distribution of genus *Pseudopedinella* in marine niches are very scarce. The genus *Pseudopedinella* was earlier considered a member of the class Chrysophyceae, whereas it has been included within the class Dcityochophyceae since the 1980s (Hibberd, 1986).

In the present study, the genus *Ochromonas* (strain-CCMP1393) belonging to the class Chrysophyceae was recovered from most of the surface (and at a depth of 75 m) of the WPO (**Figures 3A**,**B**). The experimental studies of Lie et al. (2018) suggested that *Ochromonas* (strain-CCMP1393) is phagotrophic phytoflagellate with different nutritional strategies (phagotrophic, mixotrophic, or phototrophic nutrition). The highest growth of *Ochromonas* (strain CCMP 1393) in the presence of light was due to the upregulation of genes such as those involved in photosynthesis, light harvesting, chlorophyll synthesis, and carbon fixation (Lie et al., 2018). Thus, here it can be hypothesized that the *rbc*L gene analysis can (which is directly related to carbon assimilation) provide sufficient correlation of *Ochromonas* (strain CCMP 1393) presence mostly in the euphotic layers. Nonetheless, this is the first report of *Ochromonas* (strain CCMP 1393) from the WPO waters, and it can probably serve as the basic dataset for upcoming studies.

During this study, a high abundance of class Pelagophyceae sequences, especially genus *Pelagomonas*, was recorded from both DCM and 150 m depths in the upwelling region, whereas it was observed more in number only at 150 m depth in

non-upwelling regions of the WPO (**Figure 9**). Pelagophytes were recorded as major contributors to phytoplankton biomass and productivity in the various marine niches, including temperate, subtropical, and tropical open oceans (Suzuki et al., 2002; Ditullio et al., 2003; Cuvelier et al., 2010). Furthermore, they contribute to 10–20% of the total Chl-*a* in the equatorial Pacific Ocean. In the Northern Atlantic region, pelagophytes contributed a large fraction of phytoplankton biomass especially in the lower euphotic zone (Claustre and Marty, 1995). Previous evaluation of the form ID of the rbcL gene in coastal upwelling region of Monterey Bay by Bhadury and Ward (2009) also reported pelgophyte (such as *Pelagomonas calceolate*)-like sequences along with cosmopolitan haptophytes, including *Phaeocytis*, *chrysochromulina*, and *Emilania huxleyi*. The occurrence of this group was observed in coastal as well as open ocean upwelling regions of the WPO. Further, the cosmopolitan occurrence of these groups was also observed in the Sundarbans Mangrove Ecosystem (Samanta and Bhadury, 2014). Our previous study from the Bay of Bengal on the diversity of chromophytic phytoplankton using form ID rbcL gene showed the dominance of these groups in the southern area where wind-driven upwelling was likely the source of nutrients (Pujari et al., 2019). The orientation of Pelagophyceae in the RDA triplot at most of the deeper stations, especially in the upwelling zone, was highly correlated with most of the nutrients recorded during the study (**Figure 7**). This reveals the capability of Pelagophyceae species to utilize the nutrients at the deeper depths under light-limited conditions. The study carried out by Li et al. (2013) concluded with an *rbc*L gene study that these taxa can physiologically adapt to low light, nutrient-enriched conditions in the lower euphotic regions. However, in the upwelling regions of the WPO, the advection of nutrient-enriched deeper waters could better replenish and/or transport Pelagophyceae (especially *Pelagomonas*) population in the upper waters compared to the non-upwelling region.

A highly significant phytoplankton group for global marine biogeochemistry, Cyanophyceae, especially *Prochlorococcus*, was recorded in high abundance from most of the surface and DCM waters (**Figure 9**). However, recovery of Cyanophyceae-like sequences can be attributed to bias introduced by the primers used in this study for PCR amplification. During the evolution process, the *rbc*L gene gave rise to different forms. Form IA, IB, IC, and ID encode both green- and red-like RuBisCOs and present in different groups of phytoplankton (Watson and Tabita, 1997). Most dominant form IDs represent abundant groups such as Bacillariophyceae, Pelagophyceae, and Haptophyceae. Although, form IB encodes green lineages, including cyanobacteria (Paul et al., 1999). They mostly thrive in euphotic zones of the tropical and subtropical oligotrophic oceans, including the WPO (Chen et al., 2017) and adjacent

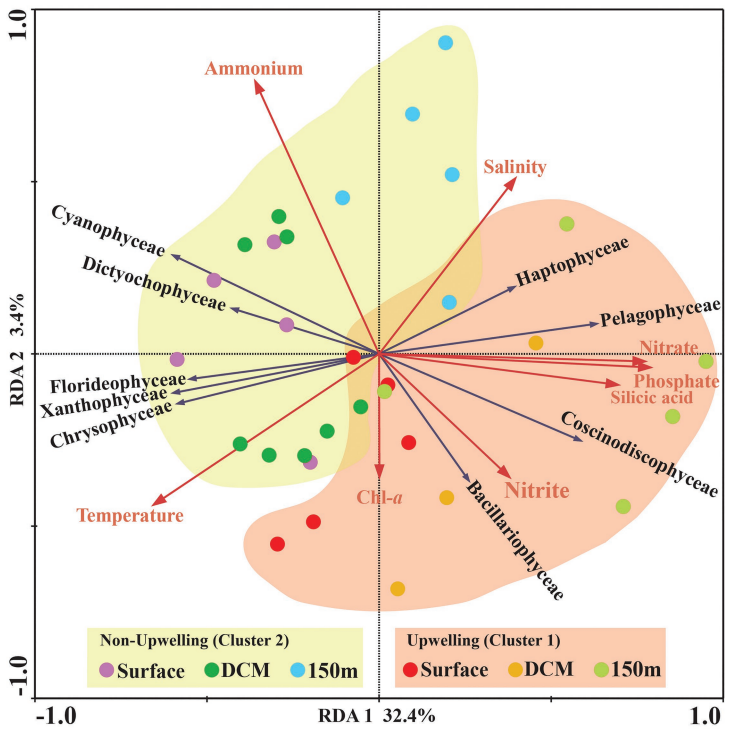

FIGURE 7 | Redundancy analysis (RDA) for *rbc*L gene-based chromophytic phytoplankton community distribution and environmental factors, the black arrow represented different classes of phytoplankton whereas environmental variables were shown with red arrows. Correlation between environmental variables [Temperature (°C), Salinity, Chl-*a*, Nitrate (NO_3^-), Nitrite (NO_2^-), Phosphate (PO_4^{3-}), Ammonia (NH_4^+) and Silicic acid [$Si(OH)_4$] and RDA] axes are shown by both length and angle of arrows. The two RDA axes explained 34.8% of the total variation.

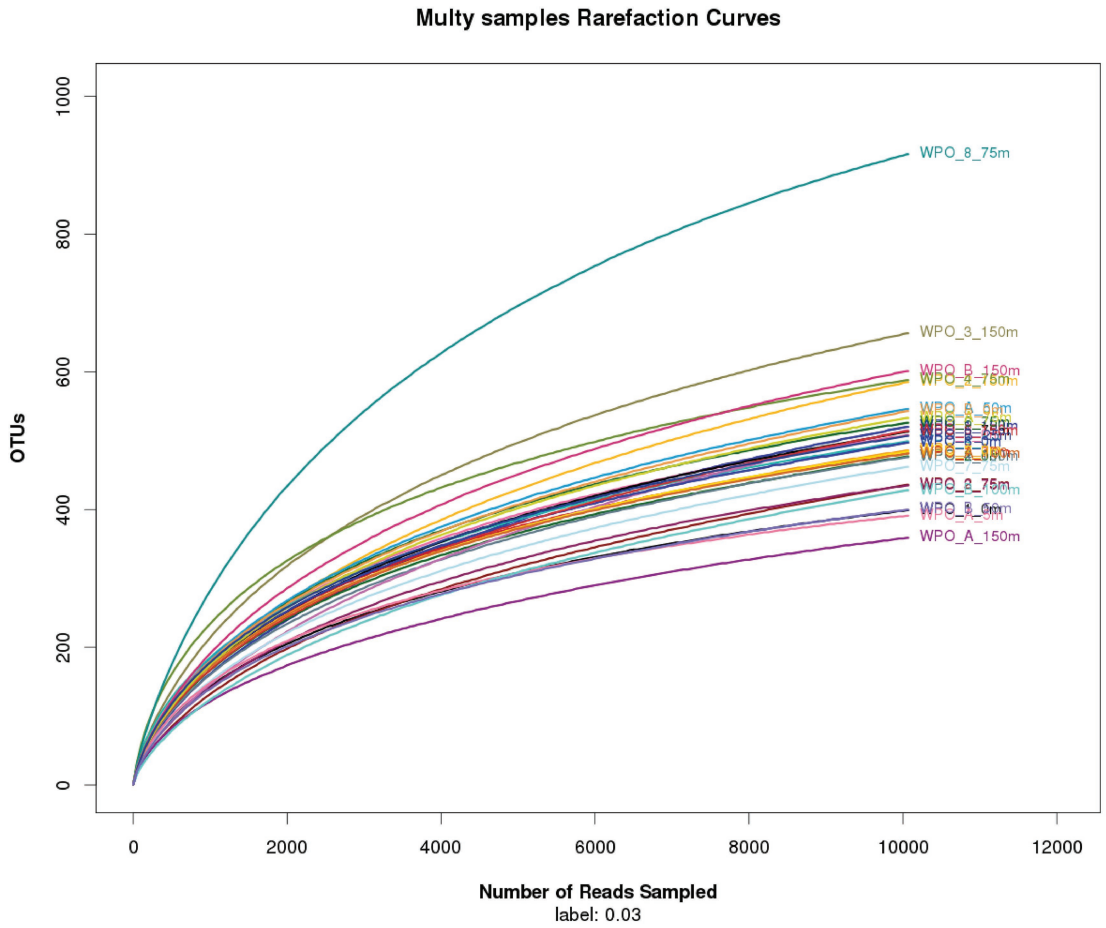

FIGURE 8 | Rarefaction curves comparing the number of reads to the number of phylotypes (OTUs) found in the WPO samples.

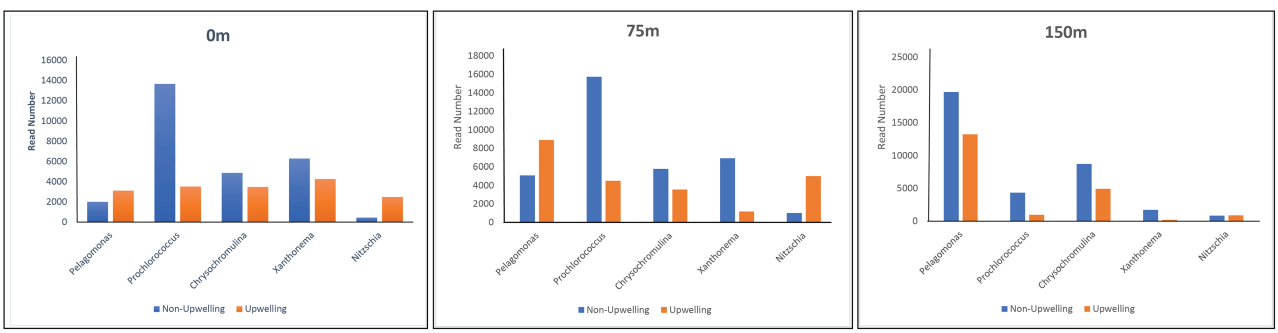

FIGURE 9 | Distribution of dominant chromophytic phytoplankton species in Non-upwelling [WPO-1 (18°N), WPO-2 (18°N), WPO-3 (15.9°N), WPO-4 (15°N) and WPO-5 (11.9°N)], and upwelling [WPO-6 (8.9°N), WPO-7 (5.4°N), WPO-8 (2°N), WPO-A (8°N) and WPO-B (4.5°N)] region of the WPO.

Philippines sea (Gajigan et al., 2018). Here, Cyanophyceae (mainly *Prochlorococcus*) was evinced to occur in the euphotic zones of the surface and a depth of 75 m. These observations were also corroborated with earlier studies on RuBisCO large subunit gene probes to examine gene expression from the offshore waters of the Gulf of Mexico (Pichard et al., 1993), where the dominance of cyano, especially *Prochlorococcus rbc*L mRNA, reported at depths

TABLE 3 | Comparison of chromophytic phytoplankton community reveled using *rbc*L gene.

Type of gene	Location	Date	Dominant genus/Class	Reference
*rbc*L Type I	Eastern Gulf of Mexico	August 1994 and Sept 1993	*Prochlorococcus* sp., *Synechococcus* sp.	Pichard et al., 1993
*rbc*L Form ID	Monterey Bay and Western English Channel	August 1998 and July 1999	Pelagophyceae, Bacillariophycea and Raphidophyceae	Bhadury and Ward, 2009
*rbc*L Form ID	North Pacific Subtropical Gyre	2007–2009	Diatoms, prymnesiophytes and pelagophytes	Li et al., 2013
*rbc*L Form ID	Northern Gulf of Mexico	July 2005	Diatoms and other heterokonts	John et al., 2007
*rbc*L Form ID	Bering Sea	September 2009	Bacillariophycea and other eukaryotes	Endo et al., 2015
*rbc*L Form ID	Sundarbans Mangroves reserve forest	2010–2011	Bacillariophyceae, Cryptophyceae, Haptophyceae, Pelagophyceae, Eustigmatophyceae, and Rhaphidophyceae	Samanta and Bhadury, 2014
*rbc*L Form ID	Northern South China Sea	August 2007	Bacillariophyceae, Haptophyceae and Cyanophyceae	Li et al., 2016
*rbc*L Form ID	Bay of Bengal	Nov-Dec 2016	Pelagophyceae, Cyanophyceae, and Haptophyceae	Pujari et al., 2019
*rbc*L Form ID	West Pacific Ocean	November 2017	Haptophyceae, Pelagophyceae, Cyanophyceae, Bacillariophyceae and Chrysophyceae	Present Study
nif H	East Indian Ocean	April 2017	Cyanobacteria (*Trichodesmium* spp.) Proteobacteria (Alpha, Beta, and Gamma)	Wu et al., 2019
nif H	South China Sea, Western Equatorial Pacific Ocean, Philippine Sea	July 2015	Cyanobacteria (*Trichodesmium*), Unicellular cyanobacterium (UCYN-B)	Chen et al., 2019
PBS gene, pcb gene, isiA gene	North American East Coast, Caribbean Sea, Eastern Tropical Pacific, Tropical South Pacific	--	*Synechococcus*, *Prochlorococcus*	Bibby et al., 2009

above 65 m. In the WPO, the occurrence of Cyanophyceae (mainly *Prochlorococcus*) in the euphotic zones were significantly correlated with the temperature and negatively correlated with most of the nutrients in RDA (**Figure 7**). Previous studies revealed that the *Prochlorococcus* population in phosphorus-limited environments contains more genes for phosphorus acquisition than the population where phosphorus is not a limiting factor (Martiny et al., 2006). Moreover, in oligotrophic oceans, the nitrogen-limited surface waters can be dominated by the High Light (HL) adapted strains, which have lower GC content and, therefore, may require less nitrogen to thrive. An amino acid encoded by low GC codons will have lower nitrogen (reduced N/C ratio) than those encoded by GC-rich codons. Therefore, we predict that the dominance of *Prochlorococcus* in surface and subsurface waters is probably attributed to the presence of HL strains, which are adapted to the high intensity of light.

SUMMARY

This study presents the first detailed investigation of a chromophytic phytoplankton community using high-throughput sequencing of *rbc*L genes in the WPO region. The variation observed in chromophytic phytoplankton suggests the strong influence of environmental variables induced by oceanographic features (eddy-induced upwelling) on the biological production in the WPO. The main chromophytic phytoplankton community signals recorded in the WPO are as follows; (1) a warmer, low-saline, and nutrient-imitated condition regulated the Cyanophyceae (mainly *Prochlorococcus* species) dominance at the surface and subsurface depths; (2) overall dominance of Haptophyceae, especially genus *Chrysochromulina*, under the light-limited conditions at deeper depths (DCM and 150 m) was probably influenced by the high salinity and fairly high dissolved nutrients. The mixotrophic mode of nutrition could also support the distribution of *Chrysochromulina* at deeper depths; (3) the capability of utilizing the nutrients under light-limited conditions supports the predominance of Pelagophyceae, especially the *Pelagomonas* species, in the deeper waters, and the advection of nutrient-enriched upwelled deeper waters could better replenish and transport the *Pelagomonas* population in the upper layers compared to the non-upwelling region of the WPO; (4) finally, compared to earlier studies, our comprehensive high-throughput sequencing analysis revealed some of the new and rare lineages, such as *Bolidomonas*, *Peridinium*, *Calyptrosphaera*, *Pseudopedinella*, and *Ochromonas* (strain-CCMP1393). Nevertheless, this is the first study to report these rare occurring genera in the WPO.

DATA AVAILABILITY STATEMENT

The datasets generated for this study can be found in NCBI SRA, https://www.ncbi.nlm.nih.gov/bioproject/PRJNA558162/.

AUTHOR CONTRIBUTIONS

LP designed the research, wrote the manuscript, and carried out the molecular and statistical analysis. DN and JK proofread

and drafted the manuscript. CW helped in the experimental analysis. GZ, CD, and LL helped in sampling and proofread the manuscript. JS designed the research and drafted the manuscript. All authors contributed to the article and approved the submitted version.

FUNDING

This research was financially supported by the National Natural Science Foundation of China (41876134, 41676112, and 41276124), the Tianjin 131 Innovation Team Program (20180314), and the Changjiang Scholar Program of Chinese Ministry of Education (T2014253) to JS. Endowment Funds from Stroud Water Research Center to JK is acknowledged.

ACKNOWLEDGMENTS

We thank Prof. Dongliang Yuan from the Institue of Oceanology of the Chinese Academy of Sciences for providing hydrographic (CTD) data. We gratefully acknowledge the crew of the R/V"*KeXue*" for their assistance and all the participants for their input and contributions during the cruise. We also thank the Open Cruise Project in the Western Pacific Ocean of the National Nature Science Foundation of China (NORC2017-09) for sharing their ship time.

REFERENCES

Altschul, S. F., Madden, T. L., Schäffer, A. A., Zhang, J., Zhang, Z., Miller, W., et al. (1997). Gapped BLAST and PSI-BLAST: a new generation of protein database search programs. *Nucleic Acids Res.* 25, 3389–3402. doi: 10.1093/nar/25.17.3389

Bhadury, P., and Ward, B. B. (2009). Molecular diversity of marine phytoplankton communities based on key functional genes 1. *J. Phycol.* 45, 1335–1347. doi: 10.1111/j.1529-8817.2009.00766.x

Bibby, T. S., Zhang, Y., and Chen, M. (2009). Biogeography of photosynthetic light-harvesting genes in marine phytoplankton. *PLoS One* 4:e4601. doi: 10.1371/journal.pone.0004601

Bolger, A. M., Lohse, M., and Usadel, B. (2014). Trimmomatic: a flexible trimmer for illumina sequence data. *Bioinformatics* 30, 2114–2120. doi: 10.1093/bioinformatics/btu170

Caporaso, J. G., Kuczynski, J., Stombaugh, J., Bittinger, K., Bushman, F. D., Costello, E. K., et al. (2010). QIIME allows analysis of high-throughput community sequencing data. *Nat. Methods* 7, 335–336. doi: 10.1038/nmeth.f.303

Chen, M., Lu, Y., Jiao, N., Tian, J., Kao, S. J., and Zhang, Y. (2019). Biogeographic drivers of diazotrophs in the western Pacific Ocean. *Limnol. Oceanogr.* 64, 1403–1421. doi: 10.1002/lno.11123

Chen, Y., Sun, X., Zhu, M., Zheng, S., Yuan, Y., and Denis, M. (2017). Spatial variability of phytoplankton in the Pacific western boundary currents during summer 2014. *Mar. Freshw. Res.* 68, 1887–1900. doi: 10.1071/MF16297

Chen, Y., Sun, X., and Zhun, M. (2018). Net-phytoplankton communities in the Western boundary currents and their environmental correlations. *J. Oceanol. Limnol.* 36, 305–316. doi: 10.1007/s00343-017-6261-8

Clarke, K., and Gorley, R. (2006). Primer. *PRIMER-e, Plymouth*.

Claustre, H., and Marty, J. C. (1995). Specific phytoplankton biomasses and their relation to primary production in the tropical North Atlantic. *Deep-Sea Res.* 42, 1475–1493. doi: 10.1016/0967-0637(95)00053-9

Cushing, D. (1971). Upwelling and the production of fish. *Adv. Mar. Biol.* 9, 255–334. doi: 10.1016/S0065-2881(08)60344

Cuvelier, M. L., Allen, A. E., Monier, A., Mccrow, J. P., Messié, M., Tringe, S. G., et al. (2010). Targeted metagenomics and ecology of globally important uncultured eukaryotic phytoplankton. *Proc. Natl. Acad. Sci. U. S. A.* 107, 14679–14684. doi: 10.1073/pnas.1001665107

Dickie, I. A. (2010). Insidious effects of sequencing errors on perceived diversity in molecular surveys. *New Phytol.* 188, 916–918. doi: 10.1111/j.1469-8137.2010.03473.x

Ditullio, G. R., Geesey, M. E., Jones, D. R., Daly, K. L., Campbell, L., and Smith, W. O. Jr. (2003). Phytoplankton assemblage structure and primary productivity along 170 W in the South Pacific Ocean. *Mar. Ecol. Prog. Ser.* 255, 55–80. doi: 10.3354/meps255055

Douglas, S. E. (1988). Physical mapping of the plastid genome from the chlorophyll c-containing alga, Cryptomonas Φ. *Curr. Genet.* 14, 591–598. doi: 10.1007/BF00434085

Edgar, R. C. (2010). Search and clustering orders of magnitude faster than BLAST. *Mar. Ecol. Prog. Ser.* 255, 55–80. doi: 10.3354/meps255055

Endo, H., Sugie, K., Yoshimura, T., and Suzuki, K. (2015). Effects of CO_2 and iron availability on *rbcL* gene expression in Bering Sea diatoms. *Biogeosciences* 12, 2247–2259. doi: 10.5194/bg-12-2247-2015

Falkowski, P. G. (1994). The role of phytoplankton photosynthesis in global biogeochemical cycles. *Photosynth. Res.* 39, 235–258. doi: 10.1007/BF00014586

Fuller, N. J., Tarran, G. A., Cummings, D. G., Woodward, E. M. S., Orcutt, K. M., Yallop, M., et al. (2006). Molecular analysis of photosynthetic picoeukaryote community structure along an Arabian sea transect. *Limnol. Oceanogr.* 51, 2502–2514. doi: 10.4319/lo.2006.51.6.2502

Gajigan, A. P., Yñiguez, A. T., Villanoy, C. L., San Diego-McGlone, M. L., Jacinto, G. S., and Conaco, C. (2018). Diversity and community structure of marine microbes around the Benham Rise underwater plateau, northeastern Philippines. *PeerJ* 6:e4781. doi: 10.7717/peerj.4781

Gielly, L., and Taberlet, P. (1994). The use of chloroplast DNA to resolve plant phylogenies: noncoding versus rbcL sequences. *Mol. Biol. Evol.* 11, 769–777. doi: 10.1093/oxfordjournals.molbev.a040157

Gran-Stadniczeñko, S., Šupraha, L., Egge, E. D., and Edvardsen, B. (2017). Haptophyte diversity and vertical distribution explored by 18S and 28S ribosomal RNA gene metabarcoding and scanning electron microscopy. *J. Eukaryot. Microbiol.* 64, 514–532. doi: 10.1111/jeu.12388

Hajdu, S., Larsson, U., and Moestrup, Ø. (1996). Seasonal dynamics of *Chrysochromulina* species (Prymnesiophyceae) in a coastal area and a nutrient-enriched inlet of the northern Baltic proper. *Bot. Mar.* 39, 281–296. doi: 10.1515/botm.1996.39.1-6.281

Hanson, C. A., Fuhrman, J. A., Horner-Devine, M. C., and Martiny, J. B. (2012). Beyond biogeographic patterns: processes shaping the microbial landscape. *Nat. Rev. Microbiol.* 10, 497–506. doi: 10.1038/nrmicro2795

Hibberd, D. J. (1986). "Ultrastructure of the Chrysophyceae: phylogenetic implications and taxonomy" in *Chrysophytes: Aspect and problems*. eds. J. Kristiansen and R. A. Andersen (Cambridge: Cambridge University Press), 23–36.

Hu, D., Wu, L., Cai, W., Gupta, A. S., Ganachaud, A., Qiu, B., et al. (2015). Pacific western boundary currents and their roles in climate. *Nature* 522, 299–308. doi: 10.1038/nature14504

Huson, D. H., Auch, A. F., Qi, J., and Schuster, S. C. (2007). MEGAN analysis of metagenomic data. *Genome Res.* 17, 377–386. doi: 10.1101/gr.5969107

Ichinomiya, M., Dos Santos, A. L., Gourvil, P., Yoshikawa, S., Kamiya, M., Ohki, K., et al. (2016). Diversity and oceanic distribution of the Parmales (Bolidophyceae), a picoplanktonic group closely related to diatoms. *ISME J.* 10, 2419–2434. doi: 10.1038/ismej.2016.38

Inagaki, Y., Dacks, J. B., Doolittle, W. F., Watanabe, K. I., and Ohama, T. (2000). Evolutionary relationship between dinoflagellates bearing obligate diatom endosymbionts: insight into tertiary endosymbiosis. *Int. J. Syst. Evol. Microbiol.* 50, 2075–2081. doi: 10.1099/00207713-50-6-2075

John, D. E., Patterson, S. S., and Paul, J. H. (2007). Phytoplankton-group specific quantitative polymerase chain reaction assays for RuBisCO mRNA transcripts in seawater. *Mar. Biotechnol.* 9, 747–759. doi: 10.1007/s10126-007-9027-z

Jones, H. L., Leadbeater, B., and Green, J. (1993). Mixotrophy in marine species of Chrysochromulina (Prymnesiophyceae): ingestion and digestion of a small

green flagellate. *J. Mar. Biol. Assoc. U. K.* 73, 283–296. doi: 10.1017/S0025315400032859

Kashino, Y., Atmadipoera, A., and Kuroda, Y. (2013). Observed features of the Halmahera and Mindanao eddies. *J. Geophys. Res. Oceans* 118, 6543–6560. doi: 10.1002/2013JC009207

Klaveness, D. (1973). The microanatomy of *Calyptrosphaera sphaeroidea*, with some supplementary observations on the motile stage of *Coccolithus pelagicus*. *Nor. J. Bot.* 20, 151–162.

Kumar, S., Stecher, G., and Tamura, K. (2016). MEGA7: molecular evolutionary genetics analysis version 7.0 for bigger datasets. *Mol. Biol. Evol.* 33, 1870–1874. doi: 10.1093/molbev/msw054

Kuwata, A., Yamada, K., Ichinomiya, M., Yoshikawa, S., Tragin, M., Vaulot, D., et al. (2018). Bolidophyceae, a sister picoplanktonic group of diatoms—a review. *Front. Mar. Sci.* 5:370. doi: 10.3389/fmars.2018.00370

Letunic, I., and Bork, P. (2011). Interactive tree of life v2: online annotation and display of phylogenetic trees made easy. *Nucleic Acids Res.* 39, W475–W478. doi: 10.1093/nar/gkr201

Li, B., Karl, D. M., Letelier, R. M., Bidigare, R. R., and Church, M. J. (2013). Variability of chromophytic phytoplankton in the North Pacific Subtropical Gyre. *Deep-Sea Res. PT II* 93, 84–95. doi: 10.1016/j.dsr2.2013.03.007

Li, N., Yu, S. X., Wang, Y. C., Li, J. L., Li, F. C., and Qin, S. (2016). Diversity of phototrophic phytoplankton in Northern South China Sea indicated by *rbcL* analysis. *J. Appl. Phycol.* 28, 773–781. doi: 10.1007/s10811-015-0624-3

Lie, A. A., Liu, Z., Terrado, R., Tatters, A. O., Heidelberg, K. B., and Caron, D. A. (2018). A tale of two mixotrophic chrysophytes: insights into the metabolisms of two Ochromonas species (Chrysophyceae) through a comparison of gene expression. *PLoS One* 13:e0192439. doi: 10.1371/journal.pone.0192439

Liu, H., Probert, I., Uitz, J., Claustre, H., Aris-Brosou, S., Frada, M., et al. (2009). Extreme diversity in noncalcifying haptophytes explains a major pigment paradox in open oceans. *Proc. Natl. Acad. Sci. U. S. A.* 106, 12803–12808. doi: 10.1073/pnas.0905841106

Loder, J. W., Boicourt, W. C., and Simpson, J. H. (1998). Western ocean boundary shelves coastal segment (W). *Sea* 11, 3–27.

Malinverno, E., Ziveri, P., and Corselli, C. (2003). Coccolithophorid distribution in the Ionian sea and its relationship to eastern Mediterranean circulation during late fall to early winter 1997. *J. Geophys. Res. Oceans* 108. doi: 10.1029/2002JC001346

Martiny, A. C., Coleman, M. L., and Chisholm, S. W. (2006). Phosphate acquisition genes in Prochlorococcus ecotypes: evidence for genome-wide adaptation. *Proc. Natl. Acad. Sci. U. S. A.* 103, 12552–12557. doi: 10.1073/pnas.0601301103

Mcdonald, S. M., Sarno, D., Scanlan, D. J., and Zingone, A. (2007). Genetic diversity of eukaryotic ultraphytoplankton in the Gulf of Naples during an annual cycle. *Aquat. Microb. Ecol.* 50, 75–89. doi: 10.3354/ame01148

Niemi, A., and Hallfors, G. (1974). Some phytoplankton species from Baltic waters. *Memoranda*.

Nöel, M. H., Kawachi, M., and Inouye, I. (2004). Induced dimorphic life cycle of a Coccolithophorid, Calyptrosphaera Sphaeroidea (Prymnesiophyceae, Haptophyta) 1. *J. Phycol.* 40, 112–129. doi: 10.1046/j.1529-8817.2004.03053.x

Nygaard, K., and Tobiesen, A. (1993). Bacterivory in algae: a survival strategy during nutrient limitation. *Limnol. Oceanogr.* 38, 273–279. doi: 10.4319/lo.1993.38.2.0273

Paerl, R. W., Turk, K. A., Beinart, R. A., Chavez, F. P., and Zehr, J. P. (2012). Seasonal change in the abundance of Synechococcus and multiple distinct phylotypes in Monterey Bay determined by rbcL and narB quantitative PCR. *Environ. Microbiol.* 14, 580–593. doi: 10.1111/j.1462-2920.2011.02594.x

Pålsson, C., and Granéli, W. (2004). Nutrient limitation of autotrophic and mixotrophic phytoplankton in a temperate and tropical humic lake gradient. *J. Plankton Res.* 26, 1005–1014. doi: 10.1093/plankt/fbh089

Paul, J. H., Pichard, S. L., Kang, J. B., Watson, G. M., and Tabita, F. R. (1999). Evidence for a clade-specific temporal and spatial separation in ribulose bisphosphate carboxylase gene expression in phytoplankton populations off Cape Hatteras and Bermuda. *Limnol. Oceanogr.* 44, 12–23. doi: 10.4319/lo.1999.44.1.0012

Pichard, S. L., Frischer, M. E., and Paul, J. H. (1993). Ribulose-bisphosphate carboxylase gene expression in subtropical marine phytoplankton populations. *Mar. Ecol. Prog. Ser.* 101:55. doi: 10.3354/meps101055

Pintner, I. (1968). Heterotrophy in subdued light of 3 Chrysochromulina species. Bull. Misaki Mar. Biol. Inst., Kyoto Univ. *Proceedings of the US-Japan seminar on Marine Microbiology*, 12 25–31.

Pujari, L., Wu, C., Kan, J., Li, N., Wang, X., Zhang, G., et al. (2019). Diversity and spatial distribution of chromophytic phytoplankton in the Bay of Bengal revealed by RuBisCO genes (*rbcL*). *Front. Microbiol.* 10:1501. doi: 10.3389/fmicb.2019.01501

Samanta, B., and Bhadury, P. (2014). Analysis of diversity of chromophytic phytoplankton in a mangrove ecosystem using rbcL gene sequencing. *J. Phycol.* 50, 328–340. doi: 10.1111/jpy.12163

Samanta, B., and Bhadury, P. (2016). A comprehensive framework for functional diversity patterns of marine chromophytic phytoplankton using rbcL phylogeny. *Sci. Rep.* 6:20783. doi: 10.1038/srep20783

Schlitzer, R. (2007). "Ocean data view. Available at: https://odv.awi.de/". ODV.

Smetacek, V. (1999). Diatoms and the ocean carbon cycle. *Protist* 150, 25–32. doi: 10.1016/S1434-4610(99)70006-4

Suzuki, K., Minami, C., Liu, H., and Saino, T. (2002). Temporal and spatial patterns of chemotaxonomic algal pigments in the subarctic Pacific and the Bering Sea during the early summer of 1999. *Deep Sea Res. Part II: Top. Stud. Oceanogr.* 49, 5685–5704. doi: 10.1016/S0967-0645(02)00218-7

Tabita, F. R. (1999). Microbial ribulose 1, 5-bisphosphate carboxylase/oxygenase: a different perspective. *Photosynth. Res.* 60, 1–28. doi: 10.1023/A:1006211417981

Thomsen, H. A. (1994). "Haptophytes as components of marine phytoplankton" in *The haptophyte algae*. eds. J. C. Green and B. S. C. Leadbeater, *Vol. 51* (Oxford: Clarendon Press), 187–208.

Udarbe-Walker, M. J. B., and Villanoy, C. L. (2001). Structure of potential upwelling areas in the Philippines. *Deep Sea Res. Part I: Oceanogr. Res. Pap.* 48, 1499–1518. doi: 10.1016/S0967-0637(00)00100-X

Watson, G. M., and Tabita, F. R. (1997). Microbial ribulose 1, 5-bisphosphate carboxylase/oxygenase: a molecule for phylogenetic and enzymological investigation. *FEMS Microbiol. Lett.* 146, 13–22. doi: 10.1111/j.1574-6968.1997.tb10165.x

Wawrik, B., Paul, J., and Tabita, F. (2002). Real-time PCR quantification of rbcL (ribulose-1, 5-bisphosphate carboxylase/oxygenase) mRNA in diatoms and pelagophytes. *Appl. Environ. Microbiol.* 68, 3771–3779. doi: 10.1128/AEM.68.8.3771-3779.2002

Wu, C., Kan, J., Liu, H., Pujari, L., Guo, C., Wang, X., et al. (2019). Heterotrophic bacteria dominate the Diazotrophic community in the Eastern Indian Ocean (EIO) during pre-southwest monsoon. *Microb. Ecol.* 78, 804–819. doi: 10.1007/s00248-019-01355-1

Zhang, L., Wang, F. J., Wang, Q., Hu, S., Wang, F., and Hu, D. (2017). Structure and variability of the north equatorial current/undercurrent from mooring measurements at 130 E in the Western Pacific. *Sci Rep. U. K.* 7:46310. doi: 10.1038/srep46310

Conflict of Interest: The authors declare that the research was conducted in the absence of any commercial or financial relationships that could be construed as a potential conflict of interest.

frontiers in Microbiology

ORIGINAL RESEARCH
published: 14 April 2021
doi: 10.3389/fmicb.2021.635821

Viral-Mediated Microbe Mortality Modulated by Ocean Acidification and Eutrophication: Consequences for the Carbon Fluxes Through the Microbial Food Web

Andrea Malits[1,2], Julia A. Boras[2], Vanessa Balagué[2], Eva Calvo[2], Josep M. Gasol[2,3], Cèlia Marrasé[2], Carles Pelejero[2,4], Jarone Pinhassi[5], Maria Montserrat Sala[2] and Dolors Vaqué[2]**

[1] Biological Oceanography Laboratory, Austral Center for Scientific Research (CONICET), Ushuaia, Argentina, [2] Department of Marine Biology and Oceanography, Institut de Ciències del Mar (CSIC), Barcelona, Spain, [3] Center for Marine Ecosystems Research, School of Sciences, Edith Cowan University, Joondalup, WA, Australia, [4] Institució Catalana de Recerca i Estudis Avançats (ICREA), Barcelona, Spain, [5] Centre for Ecology and Evolution in Microbial Model Systems, Linnaeus University, Kalmar, Sweden

OPEN ACCESS

Edited by:
Connie Lovejoy,
Laval University, Canada

Reviewed by:
Anne-Claire Baudoux,
Centre National de la Recherche Scientifique (CNRS), France
Stéphan Jacquet,
Institut National de Recherche pour l'agriculture, l'alimentation et l'environnement (INRAE), France

***Correspondence:**
Andrea Malits
amalits@cadic-conicet.gob.ar
Dolors Vaqué
dolors@icm.csic.es

Specialty section:
This article was submitted to Aquatic Microbiology, a section of the journal Frontiers in Microbiology

Received: 30 November 2020
Accepted: 22 February 2021
Published: 14 April 2021

Citation:
Malits A, Boras JA, Balagué V, Calvo E, Gasol JM, Marrasé C, Pelejero C, Pinhassi J, Sala MM and Vaqué D (2021) Viral-Mediated Microbe Mortality Modulated by Ocean Acidification and Eutrophication: Consequences for the Carbon Fluxes Through the Microbial Food Web. Front. Microbiol. 12:635821. doi: 10.3389/fmicb.2021.635821

Anthropogenic carbon emissions are causing changes in seawater carbonate chemistry including a decline in the pH of the oceans. While its aftermath for calcifying microbes has been widely studied, the effect of ocean acidification (OA) on marine viruses and their microbial hosts is controversial, and even more in combination with another anthropogenic stressor, i.e., human-induced nutrient loads. In this study, two mesocosm acidification experiments with Mediterranean waters from different seasons revealed distinct effects of OA on viruses and viral-mediated prokaryotic mortality depending on the trophic state and the successional stage of the plankton community. In the winter bloom situation, low fluorescence viruses, the most abundant virus-like particle (VLP) subpopulation comprising mostly bacteriophages, were negatively affected by lowered pH with nutrient addition, while the bacterial host abundance was stimulated. High fluorescence viruses, containing cyanophages, were stimulated by OA regardless of the nutrient conditions, while cyanobacteria of the genus *Synechococcus* were negatively affected by OA. Moreover, the abundance of very high fluorescence viruses infecting small haptophytes tended to be lower under acidification while their putative hosts' abundance was enhanced, suggesting a direct and negative effect of OA on viral–host interactions. In the oligotrophic summer situation, we found a stimulating effect of OA on total viral abundance and the viral populations, suggesting a cascading effect of the elevated pCO_2 stimulating autotrophic and heterotrophic production. In winter, viral lysis accounted for 30 ± 16% of the loss of bacterial standing stock per day (VMM_{BSS}) under increased pCO_2 compared to 53 ± 35% in the control treatments, without effects of nutrient additions while in summer, OA had no significant effects on VMM_{BSS} (35 ± 20% and 38 ± 5% per day in the OA and control treatments, respectively). We found that phage production and resulting organic carbon release rates significantly reduced under OA in the nutrient replete winter situation, but it was also observed that high nutrient loads lowered the negative effect of OA on viral lysis, suggesting an antagonistic interplay

between these two major global ocean stressors in the Anthropocene. In summer, however, viral-mediated carbon release rates were lower and not affected by lowered pH. Eutrophication consistently stimulated viral production regardless of the season or initial conditions. Given the relevant role of viruses for marine carbon cycling and the biological carbon pump, these two anthropogenic stressors may modulate carbon fluxes through their effect on viruses at the base of the pelagic food web in a future global change scenario.

Keywords: ocean acidification, eutrophication, microbial food web, viral shunt, carbon fluxes

INTRODUCTION

Current anthropogenic carbon release rates are unprecedented over the last 66 million years (Zeebe et al., 2016). Since preindustrial time until the present, the concentration of carbon dioxide (CO_2) in the atmosphere has increased from ∼277 ppm (e.g., Joos and Spahni, 2008) to 410 ppm in 2019 (Dlugokencky and Tans, 2020) due to the burning of fossil fuels, cement manufacturing, and land use changes. The ocean has absorbed about 30% of these CO_2 emissions since 1750, leading to changes in seawater carbonate chemistry and a decline in pH (Sabine et al., 2004). Preindustrial pH values in the surface ocean of about 8.2 are expected to decrease to 7.8 at the end of the twenty-first century in a high-CO_2-emission, "business-as-usual" scenario (Bopp et al., 2013), a process referred to as ocean acidification (OA, Caldeira and Wickett, 2003). During the past century, anthropogenic inputs of nitrogen (N) and phosphorus (P) to coastal ecosystems *via* river discharge have augmented mostly due to the use of fertilizers in agriculture (Galloway et al., 2004). Increased nutrient and organic matter supply to coastal environments has led to coastal eutrophication, which constitutes a major threat to ocean health (Rabalais et al., 2009). Thus, in addition to OA, eutrophication is another major global change pressure that directly affects marine ecosystems in the Anthropocene (Diaz and Rosenberg, 2008; Doney et al., 2009). Synergistic (Cai et al., 2011) or antagonistic interplays between both processes have been suggested (Borges and Gypens, 2010; Malone and Newton, 2020).

The microbial food web, composed of nano- and microalgae, autotrophic picoplankton, heterotrophic protists, heterotrophic bacteria and archaea, and virioplankton, constitutes the base of marine food webs and is a key component in the transfer of carbon and the regeneration of micro- and macronutrients (Azam, 1998). It has been estimated that ∼50% of the global primary production is generated in the oceans by phytoplankton photosynthesis (Field et al., 1998). Heterotrophic prokaryotes contribute greatly to the degradation and transformation of organic matter through their extensive metabolic activity and act as an intermediate link between the dissolved organic carbon (DOC) pool and higher trophic levels through the microbial loop (Azam et al., 1983). On the other hand, marine viruses play a pivotal role in the carbon cycle of marine planktonic food webs (Suttle, 2005). Through killing the hosts and releasing the content of the cytoplasm to the environment, viruses transfer particulate organic matter (POM) to the dissolved organic matter (DOM) pool (Wilhelm and Suttle, 1999; Sheik et al., 2014). Mathematical models have shown that this so-called viral shunt has a negative effect on zooplankton production through its link to the microbial loop, especially under oligotrophic regimes (Murray and Eldridge, 1994). However, by fueling the DOM pool, viral activity also stimulates bacterial production (Malits and Weinbauer, 2009) with synergetic effects on the microbial food web (Berdjeb et al., 2011), boosts the recycling of nutrients (Gobler et al., 1997; Poorvin et al., 2004), and stimulates autotrophic production (Weinbauer et al., 2011) and bacterial respiration (Fuhrman, 1999; Middelboe and Lyck, 2002; Bonilla-Findji et al., 2008). Overall, viral lysis shifts the food web toward a more regenerative pathway, reducing the carbon flux to higher trophic levels (Brussaard et al., 2008b). Along with the lytic viral reproduction where the phage injects its genetic material into the host in order to redirect its metabolism toward the production of new phages and cell lysis, the genome of the phage may also remain in the host in a dormant stage and replicate along with the host (lysogenic cycle), until the lytic cycle is induced by stress or other unfavorable conditions (Weinbauer, 2004). The lytic cycle is also induced when bacteria grow actively (Wilson and Mann, 1997), and lysogeny has been shown to be important at high host densities (Knowles et al., 2016). Both life styles (lysis, lysogeny) are involved in maintaining genetic diversity among the host community (Weinbauer and Rassoulzadegan, 2004; Suttle, 2007; Malits and Weinbauer, 2009) having direct implications on the bulk community enzymatic machinery and, consequently, on global biogeochemical cycles.

Ocean microbes are currently exposed to large depth, regional, seasonal, and even daily pH variations driven by biological and physical processes, e.g., CO_2 fixation during a phytoplankton bloom increases the pH in the water (Joint et al., 2011). For example, at the ocean time series station ALOHA, in the oligotrophic Central Pacific, the significant long-term decreasing trend of surface water pH by 0.04 pH units from 1988 to 2007 is superimposed to a seasonal surface pH variability of up to 0.06 pH units (Dore et al., 2009). In addition, microbes are exposed to pH values as low as those predicted in the surface oceans for the end of the twenty-first century in the thermocline, where sinking organic matter decomposition by aerobic respiration results in a reduction in pH (Joint et al., 2011). Moreover, in coastal systems, where increased nutrient loading and eutrophication stimulate microbial activity, the observed reductions in pH greatly exceed the values expected from anthropogenic CO_2 uptake alone (Provoost et al., 2010). These observations suggest that, even if

OA does not lead to dramatic changes in the biogeochemical cycles driven by microbes due to their flexibility to adjust to pH changes (Joint et al., 2011), coastal eutrophication can amplify the effects of pH change and thus affect biochemical processes.

Experimental studies have documented OA-induced changes in the phytoplankton community with shifts toward small picoplankton (Meakin and Wyman, 2011; Brussaard et al., 2013; Spilling et al., 2016; Crawfurd et al., 2017; Schulz et al., 2017), with major implications for the C fluxes in the marine planktonic food webs (Worden et al., 2015). However, mesocosm experiments in the Baltic Sea revealed that, in a picoplankton dominated food web, reduced plankton community respiration rates under high partial pressure of carbon dioxide (pCO_2) did not translate into increased carbon export (Spilling et al., 2016).

Mesocosm experiments in the Arctic (Roy et al., 2013; Sperling et al., 2013; Zhang et al., 2013) and North Sea (Newbold et al., 2012; Oliver et al., 2014) did not find evidence of a pCO_2 effect on the bulk prokaryotic community composition. However, the combined effects of acidification and nutrient additions (Baltar et al., 2015) or warming (Lindh et al., 2013) did select for specific bacterial phylotypes evidencing the synergistic effects of human-induced perturbations on marine systems. Bacterial bulk production, enzyme activity, and growth rate were indeed enhanced under future atmospheric pCO_2 levels (Grossart et al., 2006; Sala et al., 2016).

The effect of changes in pCO_2/pH on lytic viral production and viral abundance has been less studied, and the few reports available so far provide contradictory results. Classically studied *Escherichia coli* bacteriophages such as T2 and T7 are indeed sensitive to changes in pH (Danovaro et al., 2011). Elevated pCO_2 did not alter total viral abundance in mesocosm experiments in the North Sea (Rochelle-Newall et al., 2004) and the Arctic Ocean (Brussaard et al., 2013) but increased viral abundances in a Baltic Sea mesocosm study (Tsiola et al., 2017). In a mesocosm experiment, large (i.e., high fluorescence) virus abundance was higher in the control compared to elevated pCO_2, and two specific large double-stranded DNA (dsDNA) viruses infecting the haptophytes *Emiliania huxleyi* and *Crysochromulina ericina* decreased in abundance with increasing pCO_2 levels, suggesting changes in viral diversity (Larsen et al., 2008). Other studies in virus–host systems have shown a negative effect of OA on primary production of *Synecchococcus* and on the infection by its associated virus (Traving et al., 2013) but no effects on viral lysis of *Micromonas pulsilla* (Maat et al., 2014) with a potential positive feedback for carbon and nutrient cycling. No discernable effects of enhanced pCO_2 on lytic viral production could be detected in other acidification mesocosm experiments in the Baltic Sea (Crawfurd et al., 2017), Mediterranean (Tsiola et al., 2017), and Arctic Ocean (Vaqué et al., 2019), while lysogeny increased with OA in combination with warming in that Arctic Ocean study (Vaqué et al., 2019). Nonetheless, the effect of decreased pH on lysogeny remains uncertain.

Thus, no conclusive data on the effect of ocean acidification on virioplankton and the consequences for microbial food web carbon fluxes exist, even less in combination with eutrophication. In this context, we conducted two mesocosm acidification experiments with microbial communities of the Mediterranean, in which we also added excess nutrients, in two different seasons, winter and summer, to investigate the combined effect of OA and eutrophication on the microbial food web. These experiments already demonstrated a shift to medium-sized phytoplankton under acidified but oligotrophic conditions (Sala et al., 2016), eutrophication effects on dissolved organic matter quality and composition regardless of changes in pH (Aparicio et al., 2016), synergistic effects of nutrient loading and OA on prokaryotic community structure (Baltar et al., 2015), and OA effects on prokaryoplankton gene expression (Bunse et al., 2016). In the present study, we followed viral abundances along with those of their hosts and assessed phage-mediated bacterial mortality and lysogeny in these mesocosm experiments in order to evaluate the potential implications of anthropogenic perturbations of marine systems on viruses and viral-mediated processes in the microbial food web.

MATERIALS AND METHODS

Two experiments (referred to as WINTER and SUMMER hereafter) were performed with water collected from the Blanes Bay Microbial Observatory (BBMO), NW Mediterranean (Gasol et al., 2016) on February 17, 2010 and on July 6, 2011, respectively. For both experiments, surface water samples were mixed and quickly transferred to eight 200-L polyethylene mesocosms at the Institut de Ciències del Mar aquaria facilities in Barcelona (corresponding to day 0 of the experiments). Four experimental conditions were randomly assigned to duplicated containers: KB (control), KA (lowered pH), NB (nutrient amended), and NA (nutrient amended and lowered pH). Experiments were conducted in a temperature-controlled chamber, set at approximately *in situ* temperature (**Table 1**), and a combination of cool-white and grolux lamps was used to illuminate the mesocosms. Measured light intensity inside the containers was 121.3 ± 3.5 μmol m^{-2} s^{-1} in the WINTER and 140.8 ± 13.5 μmol m^{-2} s^{-1} in the SUMMER experiments. The light/dark cycle was set at 12:12 h. Further details can be found in Sala et al. (2016), Baltar et al. (2015), Aparicio et al. (2016), and Bunse et al. (2016).

Nitrogen and phosphorus were added at Redfield ratio, while silicate was added in excess to ensure diatom growth (the final molar ratio for P/N/Si was ∼1:16:30) before the lights were turned on, on February 18 and July 7, for experiments WINTER and SUMMER, respectively (corresponding to day 1). In KA and NA, pH was artificially lowered by bubbling, in a controlled way, small amounts of CO_2 (99.9% purity) directly into the mesocosms. This was done every morning in order to maintain the levels of pH in the acidified tanks at around 0.25–0.30 pH units lower than the controls (KB and NB), which were bubbled with equivalent amounts of pure air to ensure similar turbulent conditions. The lowering in pH of the acidified treatments vs. the controls is equivalent to the values projected for the end of the twenty-first century following relatively pessimistic scenarios (Bopp et al., 2013). Seawater pH in the mesocosms was continuously monitored using glass electrodes (LL Ecotrode plus—Metrohm, calibrated

TABLE 1 | *In situ* and experimental conditions in the mesocosms after adding nutrients in experiments WINTER and SUMMER.

WINTER	Temp. (°C)	Light (μmol m^{-2} s^{-1})	$NO_3^- + NO_2^-$ (μM)	PO_4^{3-} (μM)	SiO_4^{4-} (μM)	pH
In situ	13	110	2.43	0.11	2.49	8.05 ± 0.00
KB	14 ± 1	121.3 ± 3.5	2.87 ± 0.12	0.11 ± 0.01	1.73 ± 0.07	7.98 ± 0.02
KA	14 ± 1	121.3 ± 3.5	2.79	0.17 ± 0.02	2.29 ± 0.13	7.80 ± 0.02
NB	14 ± 1	121.3 ± 3.5	17.43	1.19 ± 0.04	31.40 ± 0.32	7.99 ± 0.01
NA	14 ± 1	121.3 ± 3.5	17.35 ± 0.63	1.10 ± 0.06	31.42 ± 1.33	7.82 ± 0.01
SUMMER						
In situ	22	1,001	0.05	0.03	0.52	8.07 ± 0.00
KB	22 ± 1	249.5 ± 0.7	0.94 ± 0.07	0.04 ± 0.00	0.51 ± 0.02	8.01 ± 0.00
KA	22 ± 1	232.5 ± 3.5	0.37 ± 0.06	0.03 ± 0.00	0.57 ± 0.04	7.76 ± 0.05
NB	22 ± 1	242.0 ± 1.4	4.91 ± 0.6	0.26 ± 0.02	7.22 ± 0.15	8.03 ± 0.02
NA	22 ± 1	239.0 ± 31.1	4.94 ± 0.3	0.27 ± 0.01	7.36 ± 0.01	7.76 ± 0.02

Nutrient data are the average of two replicates ± range. For NO_3^-+NO_2^- and the KA and NB conditions in WINTER, only one of the replicates was measured.

every day with a Tris buffer, following standard procedures, Dickson et al., 2007) and recorded by a D130 data logger (Consort, Belgium). In addition, prior to each controlled addition of CO_2, we performed precise measurements of the mesocosm's seawater pH using spectrophotometry (Clayton and Byrne, 1993) and alkalinity through a fast, single-point potentiometric titration (Pérez et al., 2000). Initial conditions are summarized in **Table 1**. To avoid sedimentation, we gently agitated the water during 5 min twice a day. Samples for chlorophyll, microbial abundances, and prokaryotic activity were taken daily (for details see Sala et al., 2016), while experiments for virus-mediated mortality of heterotrophic prokaryotes and the fraction of lytic and temperate viruses were performed at days 1, 5, and 8 for the WINTER and at days 0, 4, and 8 for the SUMMER experiment.

Inorganic Nutrients and Chlorophyll *a*

Samples for inorganic nutrients were kept frozen at −20°C until analysis, which were performed using a CFA Bran+Luebbe autoanalyzer following the methods described by Hansen and Koroleff (2007).

For chlorophyll *a* (chl *a*) analysis according to Yentsch and Menzel (1963), 50 ml of seawater was filtered through Whatman GF/F filters. Pigments were extracted in 90% acetone at 4°C for 24 h and determined by measuring their fluorescence using a Turner Designs fluorometer.

Microbial Abundances

For picophytoplankton, fresh, unstained samples were analyzed in a Becton Dickinson FACSCalibur flow cytometer at high speed (about 100 μl min^{-1}) following Marie et al. (2001). Phototrophic populations (*Prochlorococcus*, *Synechococcus*, small and large picoeukaryotes) were discriminated and enumerated according to their light scatter and specific autofluorescence properties.

Since the experiment took place with surface waters that do not harbor almost any Archaea (Alonso-Sáez et al., 2007), we are using the term bacteria to indicate both Bacteria and Archaea. Samples for heterotrophic bacterial abundance (BA) were fixed with paraformaldehyde (1%) and glutaraldehyde (0.05%), kept at room temperature for about 10 min and then flash frozen in liquid nitrogen. Within a few days, the samples were thawed, stained with SYBR Green I (Molecular Probes Inc.) for 10 min, and analyzed in a Becton Dickinson FACSCalibur flow cytometer as described previously (Marie et al., 1997; Gasol and Morán, 2015). Bacteria were determined in plots of 90° light scatter (SSC) vs. green DNA fluorescence (FL1). Differences in FL1 allowed to separate bacteria with low nucleic acid content (LNA) from those with high nucleic acid content (HNA) (Gasol et al., 1999).

Viral Abundances

For the abundance of virus-like particles (VLPs), samples (1 ml) were fixed with 0.2-μm-filtered glutaraldehyde (0.5% final concentration), incubated at 4°C for 15–30 min, and subsequently frozen in liquid nitrogen and stored at −80°C. Upon thawing, viruses were stained with SYBR Green I (Molecular Probes Inc.) for 10 min in the dark at 80°C and quantified after dilution with TE buffer [10 mM Tris, 1 mM ethylenediaminetetraacetic acid (EDTA), pH = 8] using flow cytometry and an optimized protocol (Marie et al., 1999; Brussaard, 2004). Four VLP populations were distinguished based on their signature in the cytometric plots of side scatter (SSC) vs. green fluorescence (FL1): low, medium, high, and very high green fluorescence VLPs (**Supplementary Figure 1**). The latter group was identified by its cytometric signature comparable to viruses infecting *Pyramimonas orientalis* and *Phaeocystis pouchetii* (Brussaard, 2004). The low and medium green fluorescence subpopulations represent mostly the numerically dominant bacteriophages (Brussaard, 2009). The sample flowrate was accurately calibrated following the protocol of Marie et al. (2001) and used to calculate the abundances of viruses.

Bacterial Activity

Bulk heterotrophic bacterial production (BP) was estimated from ^{3}H-leucine incorporation (Kirchman et al., 1985). For each sample, quadruplicate aliquots (1.2 ml) and two trichloroacetic

acid (TCA)-killed controls were incubated with 40 nM ^{3}H-leucine for about 1.5 h in the dark at *in situ* temperature. Subsequently, leucine incorporation was stopped by adding 120 µl of cold TC 50% to each replicate. Samples were stored at −20°C until processed following published methods (Smith and Azam, 1992). Leucine incorporated into bacterial biomass was converted to bacterial carbon production using the theoretical factor of 1.55 kg C mol^{-1} Leu that assumes no isotope dilution (Simon and Azam, 1989).

The numbers of actively respiring bacteria were determined using the fluorogenic tetrazolium dye 5-cyano-2,3-ditolyl tetrazolium chloride (CTC) labeling of highly active cells (Sherr et al., 1999; Sieracki et al., 1999). CTC was added to 1-ml subsamples at a final 5 mM concentration from a daily prepared 10× batch and incubated at *in situ* temperature for 3 h. After incubation, the samples were analyzed with a FACSCalibur flow cytometer as described in detail elsewhere (Gasol and Arístegui, 2007).

Lytic Viral Production, Fraction of Infected Cells and Lysogens, Viral-Mediated Mortality, and C Release Rates

Lytic viral production (VP_L), the fraction of infected cells (FIC), induced viral production from lysogens (VP_I), and the fraction of lysogenic cells (FLC) were estimated for selected samples using the virus reduction approach (VRA, Weinbauer et al., 2010). The underlying principle of the VRA is to reduce viral abundances in the water, thereby essentially preventing new viral infections. Thus, it is assumed that the viruses produced during the incubation originate from already infected cells. In order to eliminate viruses, bacteria in ∼400 ml from one replicate of each treatment were concentrated using a tangential flow system with a peristaltic pump (Watson-Marlow 323) equipped with a 0.2-µm cartridge (VIVAFLOW 200). To obtain virus-free seawater, the 0.2-µm pore-size ultrafiltrate was passed through a 30-kDa cartridge (VIVAFLOW 200). The bacterial concentrates were brought up to the original volume with virus-free seawater and incubated in triplicates in 50-ml Falcon tubes (BD Biosciences) at *in situ* temperature and in the dark (**Table 1**) for 24 h. At time 0 of these VRA experiments, three additional tubes were amended with mitomycin C (MC, Sigma) at a final concentration of 1 µg ml^{-1} in order to induce the lytic cycle of lysogens; untreated samples served as controls (Paul and Weinbauer, 2010). Subsamples (1 ml) for VA and BA from each incubation were taken every 2–4 h during the first 6–12 h and after 24 h, fixed with glutaraldehyde (0.5% final concentration), incubated at 4°C for 15–30 min, subsequently frozen in liquid nitrogen, and stored at −80°C until counted by flow cytometry as described above. VP_L was calculated as the increase in viral abundance over short time intervals (∼4 h). An increase in viral abundance in the MC treatments represents $VP_L + VP_I$ (Paul and Weinbauer, 2010; Weinbauer et al., 2010). VP_L and VP_I were corrected for the changes in the initial BA in the viral production assays with respect to *in situ* BA. The burst size (BS) was estimated following the approach of Wells and Deming (2006), i.e., dividing the number of viruses produced during the first hour of incubation by the concomitant decline of bacterial abundance. Dividing the number of produced phages by BS yields the number of lysed cells and gives an estimate of the fraction of infected cells (FIC) when divided by BA at the start of the experiments. Dividing the number of induced phages by BS and the BA at t0 gives an estimate of FLC. To obtain the rate of cell lysis, viral production corrected for *in situ* bacterial abundance was divided by the average estimated BS for WINTER and SUMMER, respectively. Lysis rates were used to calculate virus-mediated mortality of bacteria per day as a percentage of the bacterial standing stock (VMM_{BSS} day^{-1}). Carbon release rates through viral lysis were calculated based on VP by converting the number of lysed bacteria into carbon using a factor of 20 fg C cell^{-1} (Lee and Fuhrman, 1987).

Statistics

All statistical analyses were performed with JMP 7.0 (SAS). The Shapiro–Wilk *W*-test was used to check for normal distribution of data. Analysis of covariance (ANCOVA) with time as a covariate was used to discern the effects of time from those of the lowered pH and nutrient amendment for time-averaged parameters. Kruskal–Wallis tests for non-normal distributions were used to evaluate the acidification effect for K and N treatments, separately. Spearman rank correlation for non-parametric data was performed to determine the relationships between the various measured parameters.

RESULTS

Experimental Conditions

Initial temperature, light conditions, pH, and the concentrations of inorganic nutrients for the WINTER and SUMMER experiments are summarized in **Table 1**. For a detailed description of the experimental conditions and microplankton and bacterial dynamics in the experiments, see Baltar et al. (2015), Sala et al. (2016), and Aparicio et al. (2016). In WINTER, *in situ* nutrient concentrations (phosphate and silicate) were four to five times higher than in SUMMER. Initial experimental nitrogen concentrations in the N treatments were higher in the WINTER than in the SUMMER experiment, as they were added by multiplying the monthly average concentration measured in the BBMO during the last 10 years by a factor of 8 (**Table 1**). Due to the biological activity in the mesocosms, the pH in the experimental chambers of the WINTER experiment tended to increase with time and varied by up to 0.12 U (7.8 ± 0.05 in the KA, 7.9 ± 0.07 in the KB, 7.9 ± 0.12 in the NA, and 8.1 ± 0.12 in the NB treatments, **Figure 1A**). On the contrary, during SUMMER, the pH tended to decrease and was less variable (7.6 ± 0.08 in the KA, 7.9 ± 0.06 in the KB, 7.6 ± 0.07 in the NA, 7.9 ± 0.05 in the NB treatments, **Figure 1B**).

Chlorophyll a Concentration and Autotrophic Picoplankton

Average chl *a* concentration was six times higher in the WINTER (6.8 ± 8.9 µg L^{-1}) than in the SUMMER experiment (1.1 ± 0.9 µg L^{-1}, $n = 159$, $P < 0.0001$) and increased significantly in the nutrient-amended treatments with time and with respect to the

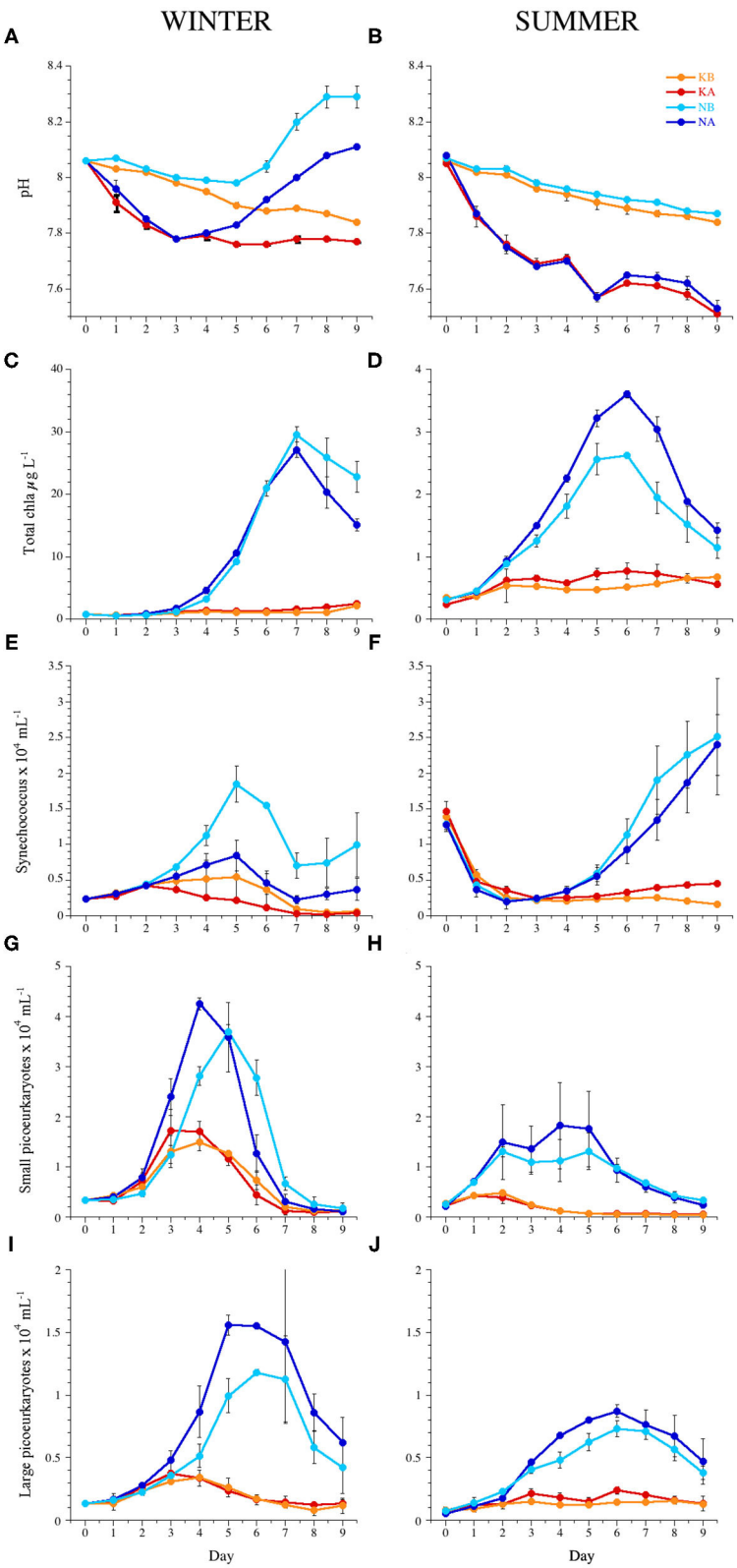

FIGURE 1 | Temporal dynamics of **(A,B)** pH, **(C,D)** total chlorophyll *a*, **(E,F)** abundance of *Synechococcus* sp., **(G,H)** small picoeukaryotes, and **(I,J)** large picoeukaryotes during the experiments WINTER (left) and SUMMER (right). Bars indicate the maximum and minimum values of experimental duplicates; when not visible, they are contained within the symbol. Note the differences in the y-axis scales of chlorophyll *a* between seasons. KB, control; KA, lowered pH; NB, nutrient amended; NA, nutrient amended and lowered pH.

controls (**Table 2**). Chl *a* peaked on days 7 and 6 in the WINTER and the SUMMER experiment, respectively, being almost 10 times higher in WINTER than in SUMMER (**Figures 1C,D**). In WINTER, chl *a* concentration increased significantly with acidification only in the K treatments (**Table 3**), while in SUMMER, chl *a* concentration was significantly stimulated in the low pH treatments, regardless the nutrient conditions (**Figure 1D** and **Table 2**).

Autotrophic picoplankton growth was stimulated by nutrient addition anticipating the chlorophyll peak at least in WINTER (**Figure 1** and **Table 2**). Cynanobacteria of the genus *Synechococcus* were negatively affected by acidification in WINTER and not affected in SUMMER (**Figures 1E,F** and **Table 2**). *Prochlorococcus* sp. was about one order of magnitude less abundant than *Synechococcus* sp. and not affected by OA (**Supplementary Figure 2** and **Table 2**). The average abundance of small picoeukaryotes in WINTER ($1.1 \pm 0.1 \times 10^4$ ml^{-1}) doubled that observed in SUMMER ($0.6 \pm 0.1 \times 10^4$ ml^{-1}, Kruskal–Wallis, $n = 143$, $P < 0.01$) and increased significantly with nutrient additions in both experiments (**Figures 1G,H** and **Table 2**). The abundance of large picoeukaryotes was not significantly different between experiments ($4.7 \pm 4.4 \times 10^3$ and $3.4 \pm 2.5 \times 10^3$ ml^{-1} in WINTER and SUMMER, respectively), increased with nutrient addition, and was stimulated by the lowered pH only in SUMMER (**Figures 1I,J** and **Tables 1**, **2**).

Heterotrophic Bacterial Abundance and Activity

Time-integrated BA was significantly higher in the WINTER ($2.3 \pm 0.1 \times 10^6$ ml^{-1}) than in the SUMMER experiment ($0.7 \pm 0.1 \times 10^6$ ml^{-1}, Kruskal–Wallis, $n = 144$, $P < 0.0001$), and BA dynamics differed between seasons: in WINTER, BA increased 7.6 times from day 0 until day 4 without differences between treatments (**Figure 2A**), while in SUMMER, BA decreased initially and increased from day 3 in all treatments but more significantly in the nutrient-amended ones. An acidification effect was found only for the treatments without nutrient addition (**Figure 2B** and **Table 2**).

Heterotrophic bacterial carbon production rates increased in WINTER from 0.26 μg C L^{-1} day^{-1} at day 0 to 24.44–29.09 μg C L^{-1} day^{-1} until day 3, while they decreased in SUMMER from initial 21.28 ± 2.91 μg C L^{-1} day^{-1} and 36.01 ± 5.18 μg C L^{-1} day^{-1} in the nutrient unamended and amended treatments, respectively, until days 2–3 (**Figures 2C,D**). BP was stimulated by nutrient addition but was not affected by lowered pH (**Table 2**) and was significantly related to the abundance of HNA bacteria except in the SUMMER treatments, where it was related to that of LNA bacteria (**Supplementary Table 1**). The percentage of CTC+ cells was significantly stimulated by acidification only in the K treatments of WINTER (ANCOVA, $n = 40$, $P < 0.05$, **Figures 2E,F**).

Abundance of the Viral Populations

Total VLP abundance increased after an initial stable phase from day 7 and 5 in experiments WINTER and SUMMER, respectively, and the same behavior was exhibited by the low subpopulation (**Figures 3A,B**); this increase was significantly higher in the N treatments than in the K treatments (**Table 2**). Total VLP abundance and the abundance of the MEDIUM subpopulation integrated over the experimental time were significantly lower in the WINTER than in the SUMMER experiment (**Figures 3C,D**, Kruskal–Wallis, $n = 144$, $P < 0.0001$).

In experiment WINTER, only the high subpopulation was stimulated by acidification (**Figures 3E,F**, **Table 2**). A cytometric group of very high fluorescence VLP (very high,

TABLE 2 | Results of an analysis of covariance (ANCOVA) with time as a covariate showing the significance of the effects of acidification and nutrient amendments during the time course (days 2–9) of the experiments WINTER and SUMMER.

	WINTER						SUMMER					
Variable	***n***	**Time**	**Lower pH**		**Nutrients**		***n***	**Time**	**Lower pH**		**Nutrients**	
VLP	64	<0.0001	ns		+	<0.0001	64	<0.0001	ns		+	<0.0001
Low VLP	64	<0.0001	ns		+	<0.0001	64	<0.0001	ns		+	<0.0001
Medium VLP	64	ns	ns		+	0.0070	64	<0.0001	ns		+	0.0085
High VLP	64	ns	+	0.0022	+	<0.0001	64	<0.0001	ns		+	0.0215
Very High VLP	58	<0.0001	ns		ns							
BA	64	<0.0001	ns		ns		64	<0.0001	ns		+	<0.0001
BP	64	<0.0001	ns		+	0.0027	64	ns	ns		+	<0.0001
% CTC+ cells	40	<0.0001	ns		ns		58	ns	ns		+	<0.0001
Chl *a*	64	<0.0001	ns		+	<0.0001	63	ns	+	0.0316	+	<0.0001
Synechococcus	64	0.0492	−	0.0002	+	<0.0001	63	<0.0001	ns		+	<0.0001
Prochlorococcus	64	<0.0001	ns		+	0.0134	62	0.0094	ns		+	0.0001
Small picoeuka	64	<0.0001	ns		+	0.0019	63	<0.0001	ns		+	<0.0001
Large picoeuka	64	ns	ns		+	<0.0001	63	ns	+	0.0217	+	<0.0001

*ns, not significant; VLP, total abundance of virus-like particles; low, medium, high, very high VLP, VLP subpopulations with low, medium, high, or very high green fluorescence in the cytometric signature, respectively (**Supplementary Figure 1**); BA, bacterial abundance; BP, bacterial heterotrophic production; % CTC+ cells, the percentage of CTC-labeled cells; chl a, chlorophyll a; picoeuka, autotrophic picoeukaryotes.*

TABLE 3 | Spearman's rank correlation coefficients (ρ) and corresponding significance (*P*) of measured pH in the experimental mesocosm with other parameters shown for the experiments WINTER ($n = 12$ for VP_L and VMM, $n = 24$ for CTC+ and $n = 36$ for the other parameters) and SUMMER ($n = 14$–15 for VP_L and VMM, $n = 26$ for LNA and HNA, and $n = 36$ for the other parameters).

	WINTER K		WINTER N		SUMMER K		SUMMER N	
Parameters	**ρ**	***P***	**ρ**	***P***	**ρ**	***P***	**ρ**	***P***
VLP	−0.258	*ns*	**0.390**	0.0187	**−0.555**	0.0004	**−0.539**	0.0007
Low VLP	**−0.371**	0.0258	**0.520**	0.0012	**−0.528**	0.0009	**−0.569**	0.0003
Medium VLP	0.124	*ns*	0.073	*ns*	**−0.414**	0.0122	**−0.519**	0.0012
High VLP	−0.050	*ns*	0.183	*ns*	**−0.562**	0.0004	**−0.579**	0.0002
Very High VLP	**−0.422**	0.0145	**0.698**	<0.0001	–	–	–	–
VP_L	**0.713**	0.0090	0.089	*ns*	−0.022	*ns*	0.577	*ns*
VMM_{BSS}	0.389	*ns*	**0.633**	0.0370	0.389	*ns*	0.866	*0.057*
C release d^{-1}	**0.713**	0.0090	0.089	*ns*	−0.022	*ns*	0.577	*ns*
BA	0.049	*ns*	**−0.426**	0.0096	**−0.481**	0.0030	**−0.399**	0.0159
LNA	−0.313	*ns*	0.301	ns	**0.394**	0.0466	0.197	*ns*
HNA	0.068	*ns*	**−0.464**	0.0044	−0.034	*ns*	**−0.392**	0.0479
BP	0.152	*ns*	−0.221	*ns*	0.087	*ns*	0.173	*ns*
% CTC+ cells	0.012	*ns*	**−0.523**	0.0087	0.240	*ns*	0.171	*ns*
chl *a*	**−0.681**	< 0.0001	**0.453**	0.0055	**−0.656**	<0.0001	**−0.428**	0.0091
Synechococcus	**0.504**	0.0017	−0.087	*ns*	**−0.341**	0.0421	**−0.394**	0.0193
Prochlorococcus	0.276	*ns*	**−0.669**	<0.0001	0.002	*ns*	**−0.429**	0.0101
Small picoeuka	0.202	*ns*	**−0.714**	<0.0001	**0.373**	0.0251	0.239	*ns*
Large picoeuka	0.110	*ns*	−0.116	*ns*	**−0.478**	0.0032	**−0.459**	0.0055

Notice that a positive ρ means a negative effect of acidification.

ns, not significant; VLP, total abundance of virus-like particles; low, medium, high, very high VLP, VLP subpopulations with low, medium, high, or very high green fluorescence in the cytometric signature, respectively; VP_L, lytic viral production; VMM_{SS} day^{-1}, viral-mediated loss of bacterial standing stock per day: BA, bacterial abundance; LNA and HNA, bacteria with low and high fluorescence in the cytometric signature, respectively; BP, bacterial heterotrophic production; % CTC+ cells, the percentage of CTC-labeled cells; chl a, chlorophyll a; picoeuka, autotrophic picoeukaryotes. Bold numbers denote significant effects of acidification; positive effects when highlighted green and negative effects when highlighted red.

Supplementary Figure 1) emerged in the second half of the WINTER experiment (**Figure 3G**). The abundance of the very high subpopulation was significantly stimulated by nutrient additions but significantly lower in the acidified treatments toward the end of the experiment (ANCOVA, $n = 24$, $P < 0.05$). Total VLP and the subpopulation of low fluorescence VLP, i.e., mostly bacteriophages, were negatively affected by lowered pH with nutrient addition (**Table 3**).

In the nutrient-deplete SUMMER experiment, in turn, total VLP abundance and the abundances of all subpopulations were correlated negatively to the measured pH in the mesocosms (**Table 3**), i.e., increased with acidification. For the growth phase of VLP (days 6–9), the lowered pH stimulated the low fluorescence subpopulation, i.e., the bacteriophages, regardless the nutrient addition (**Figure 3B**, ANCOVA, $n = 15$, $P < 0.0001$). In the nutrient treatments, the medium fluorescence subpopulation abundances, also comprising bacteriophages, were triggered in the acidified containers for the time interval 5–7 days (**Figure 3D**, ANCOVA, $P = 0.0011$).

Viral Production and Lysogeny

Initial lytic viral production rates (VP_L) did not differ significantly between seasons and averaged $0.68 \pm 0.32 \times 10^7$ VLP ml^{-1} day^{-1} but evolved differently between experiments (**Figures 4A,B**). In WINTER, VP_L increased in all treatments but were significantly lower in the KA treatments ($2.73 \pm 0.65 \times 10^7$ VLP ml^{-1} day^{-1}) with respect to KB ($4.41 \pm 0.56 \times 10^7$ VLP ml^{-1} day^{-1}, pooled data for days 5 and 8, Kruskal–Wallis, $n = 12$, $P < 0.01$). VP_L was significantly stimulated by nutrient addition (Kruskal–Wallis, $n = 23$, $P < 0.05$) with a trend of reduced VP_L due to lowered pH ($4.41 \pm 1.64 \times 10^7$ and $5.63 \pm 1.13 \times 10^7$ VLP ml^{-1} day^{-1} in NA and NB treatments, respectively, Kruskal–Wallis, $n = 11$, $P = 0.05$). Lysogenic production could only be induced at day 0 ($0.69 \pm 0.01 \times 10^7$ VLP ml^{-1} day^{-1}) and in the NA treatments at day 5 ($3.46 \pm 2.96 \times 10^7$ VLP ml^{-1} day^{-1}, **Table 4**).

In the SUMMER experiment, initial VP_L rates decreased in the K treatments on days 4 and 8 (**Figure 4B**, Kruskal–Wallis, $n = 15$, $P < 0.05$) and were not affected by lowered pH. In the NB treatments, lysogenic production rates accounted for 100% of virus production, i.e., virus production could only be detected in the treatments where lysogens were induced; VP_I were $0.30 \pm 0.11 \times 10^7$ and $0.48 \pm 0.13 \times 10^7$ VLP ml^{-1} day^{-1} at days 4 and 8, respectively, being lower or equal compared to the VP_L rates in the acidified, i.e., NA, treatments. Moreover, VP_I could only be induced at day 0 without nutrient addition ($0.33 \pm 0.11 \times 10^7$ VLP ml^{-1} day^{-1}) and at day 4 in the KA treatments ($0.19 \pm 0.14 \times 10^7$ VLP ml^{-1} day^{-1}, **Table 4**).

Calculated BS averaged 57 ± 50 in WINTER (15–226) and 16 ± 10 (4–43) in SUMMER. The fraction of infected bacteria

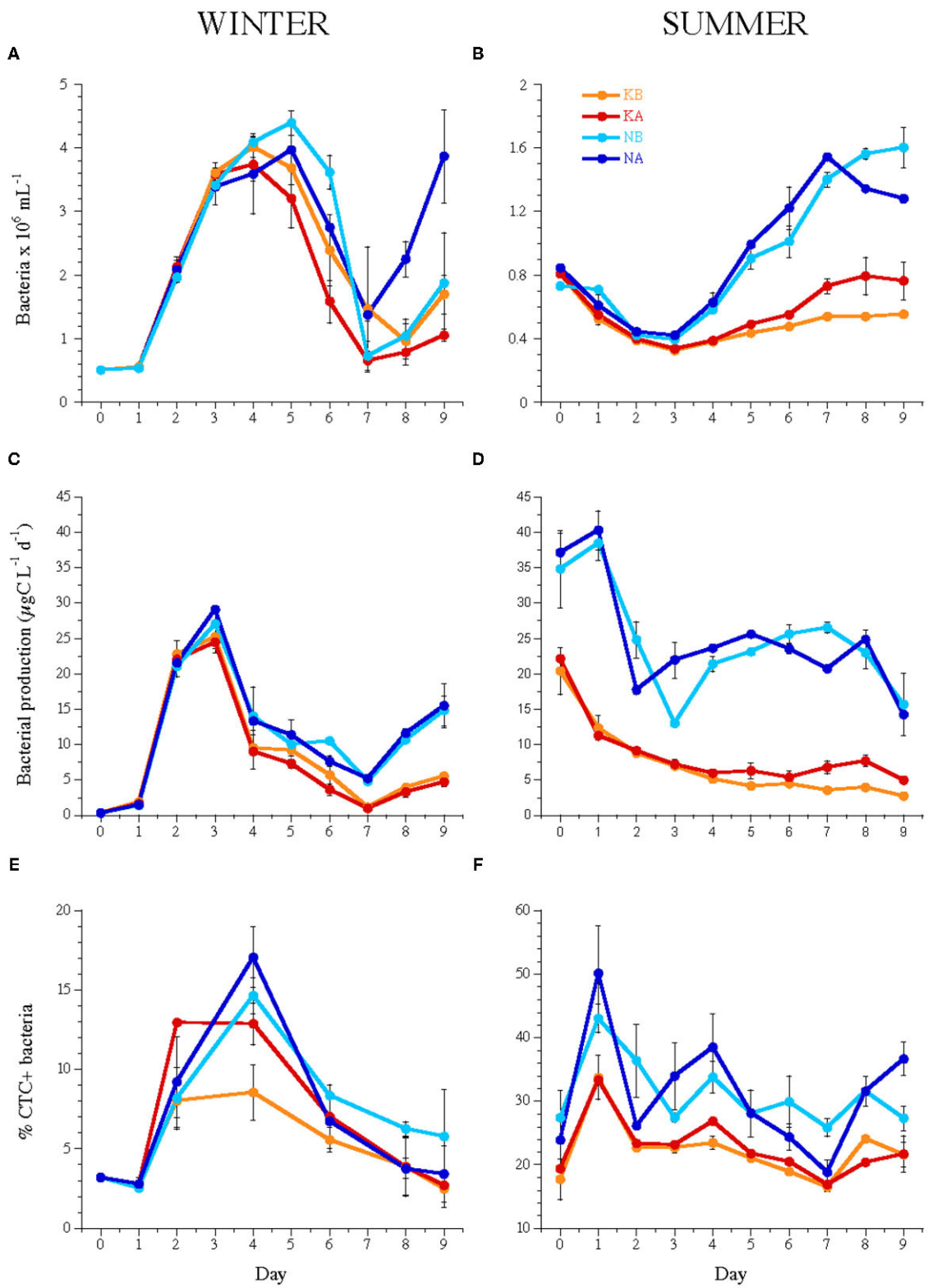

FIGURE 2 | Temporal dynamics of **(A,B)** bacterial abundance, **(C,D)** bacterial heterotrophic production, and **(E,F)** the percentage of CTC-labeled cells, i.e., actively respiring bacteria during the experiments WINTER (left) and SUMMER (right). Bars indicate the maximum and minimum values of experimental duplicates; when not visible, they are contained within the symbol. Note the differences in the y-axis scales of bacterial abundance and % CTC+ cells between seasons. For treatment codes, see **Figure 1**.

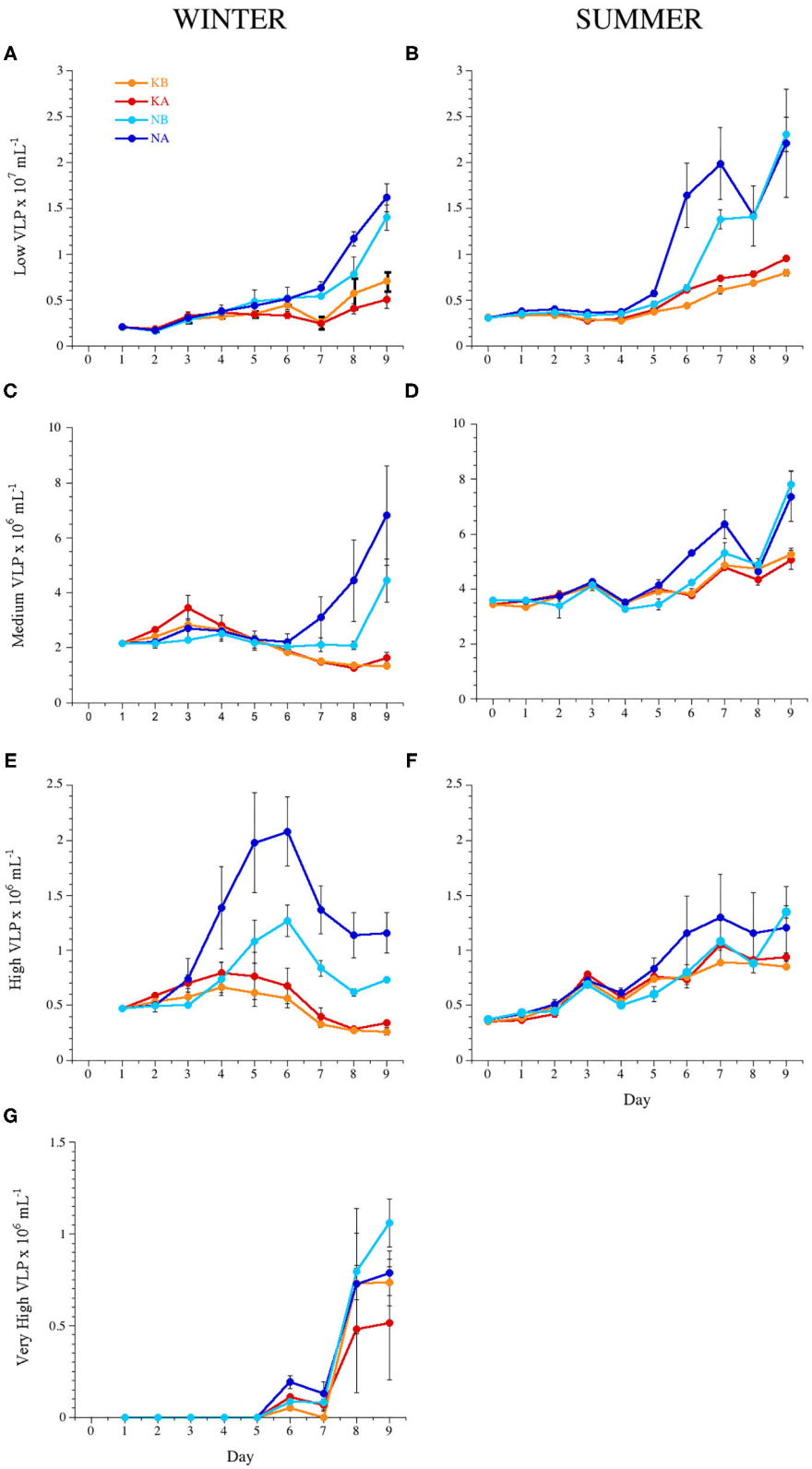

FIGURE 3 | Temporal dynamics of the abundance of the different virus-like particle (VLP) subpopulations: **(A,B)** low, **(C,D)** medium, **(E,F)** high, and **(G)** very high fluorescence VLP during experiments WINTER (left) and SUMMER (right). For treatment codes, see **Figure 1**.

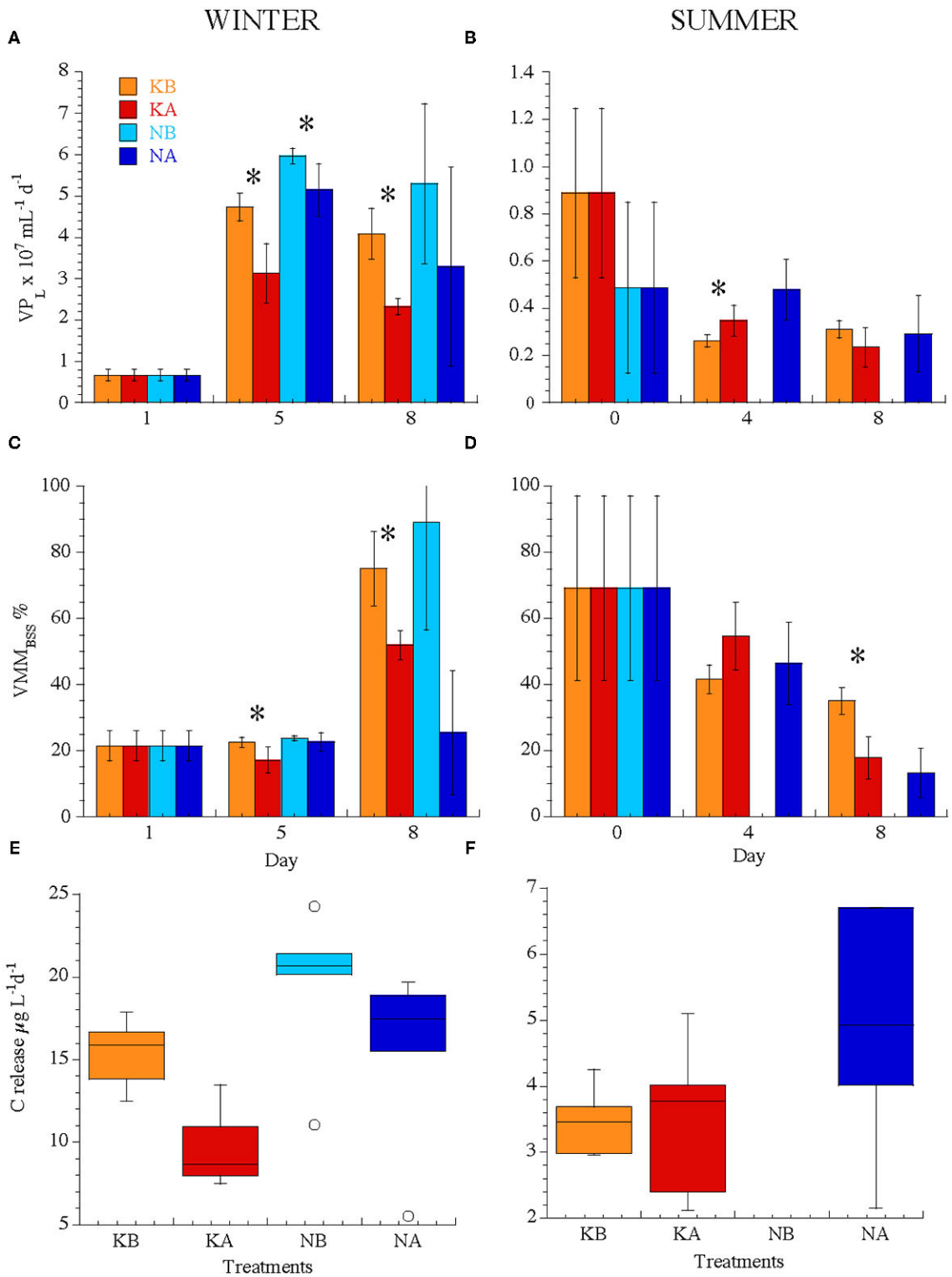

FIGURE 4 | (A,B) Lytic viral production (VP_L), **(C,D)** viral-mediated mortality expressed as a percentage of the bacterial standing stock (VMM_{BSS}), **(E,F)** carbon release rates (µg C L^{-1} day^{-1}) through viral lysis calculated from VP from all treatments in the experiments WINTER (left) and SUMMER (right). Note the difference in the y-axis scales between seasons, in particular for VP. Bars indicate standard deviations. Stars indicate significant differences between treatments ($P < 0.05$). For treatment codes, see **Figure 1**.

TABLE 4 | The fraction of lysogenic viral production (VP_I) over total viral production, the fraction of infected cells (FIC), and the fraction of lysogenic cells (FLC) in the different treatments from the WINTER and SUMMER experiments.

	VP_I (%)			FIC (%)			FLC (%)		
WINTER	**Day 1**	**Day 5**	**Day 8**	**Day 1**	**Day 5**	**Day 8**	**Day 1**	**Day 5**	**Day 8**
KB	51	*nd*	*nd*	3.4 ± 1.5	6.2 ± 0.5	53.2 ± 8.6	6.6 ± 0.3	*nd*	*nd*
KA	51	*nd*	*nd*	3.4 ± 1.5	3.6 ± 0.9	40.3 ± 4.1	6.6 ± 0.3	*nd*	*nd*
NB	51	*nd*	*nd*	3.4 ± 1.5	3.3 ± 1.9	7.4 ± 2.7	6.6 ± 0.3	*nd*	*nd*
NA	51	40	*nd*	3.4 ± 1.5	1.8 ± 0.9	2.1 ± 1.7	6.6 ± 0.3	0.9 ± 0.4	*nd*
SUMMER	**Day 0**	**Day 4**	**Day 8**	**Day 0**	**Day 4**	**Day 8**	**Day 0**	**Day 4**	**Day 8**
KB	27	*nd*	*nd*	7.5 ± 4.8	3.4 ± 1.5	6.6 ± 3.6	7.0 ± 0.8	*nd*	*nd*
KA	27	35	*nd*	7.5 ± 4.8	6.9 ± 2.7	2.6 ± 0.9	7.0 ± 0.8	6.0 ± 2.0	*nd*
NB	*nd*	100	100	2.0 ± 1.1	*nd*	*nd*	2.7 ± 0.3	4.5 ± 1.6	3.6 ± 2.2
NA	*nd*	*nd*	*nd*	2.0 ± 1.1	7.0 ± 1.8	1.5 ± 0.8	2.7 ± 0.3	*nd*	*nd*

FIC and FLC values are averages ± standard deviations from triplicates.
nd, not detected.

(FIC) was low in both experiments and all treatments and accounted for 13.9 ± 18.9% in WINTER and 4.8 ± 3.2% in SUMMER. Only in WINTER, FIC decreased with nutrient additions (Kruskal–Wallis, $n = 23$, $P < 0.05$) and was not affected by acidification. The FLC also remained low throughout the experiments and treatments without discernable treatment effects (**Table 4**).

Viral-Mediated Bacterial Mortality and Carbon Fluxes

The viral-mediated loss of bacterial standing stock (VMM_{BSS} day^{-1}) did not differ between seasons (39 ± 28% in WINTER and 41 ± 22% in SUMMER) but was initially lower in WINTER (21 ± 5%) than in SUMMER (54 ± 30%, **Figures 4C,D**). VMM_{BSS} was lowered by acidification only in WINTER (**Figures 4C,D**, Kruskal–Wallis, $n = 23$, $P < 0.05$). Carbon released from the particulate to the dissolved pool due to viral activity was four times higher in WINTER (15.0 ± 5.2 μg C L^{-1} day^{-1}) than in SUMMER (3.9 ± 1.3 μg C L^{-1} day^{-1}, Kruskal–Wallis, $n = 40$, $P < 0.0001$, **Figures 4E,F**). Only in WINTER viral-mediated carbon flux was significantly and negatively affected by acidification (**Figure 4E**, Kruskal–Wallis, $n = 23$, $P < 0.05$) and also stimulated by nutrient addition (**Figure 4**, Kruskal–Wallis, $n = 23$, $P < 0.01$).

After pooling all data from both seasons and all treatments, viral-mediated carbon flux increased with pH (Spearman $\rho = 0.56$, $P = 0.0002$, $n = 40$) and was positively correlated to chl *a* concentration and BA (Spearman $\rho = 0.67$ and 0.75, respectively, $P < 0.0001$, $n = 40$). However, when separating by seasons and nutrient treatments, the trend of increasing viral production and viral-mediated mortality with increasing pH was significant only in the K treatments of the WINTER experiment (**Table 3**). In addition, lytic viral production correlated significantly and positively with bacterial abundance and production only in WINTER without nutrient amendment (**Supplementary Tables 1, 2**).

DISCUSSION

Ex situ mesocosm experiments were performed to study the effect of acidification and eutrophication on virioplankton and viral activity under controlled laboratory conditions. Although controlled *ex situ* experimental conditions may be biased by avoiding processes that could have intervened in the natural environment, they allow to identify potential mechanisms in the response of the viral community to the studied anthropogenic stressors.

The addition of nutrients stimulated viral production regardless of the season or initial conditions. While in the nutrient-replete situation of the WINTER experiment, the abundance of viral populations and bacteriophage production tended to be negatively affected by OA; in the SUMMER experiment, we found a stimulating trend of lowered pH on viral abundance and production. Nutrient availability seems to play a major role in modulating the effect of increasing pCO_2 on viruses, but the composition and physiological state of the initial plankton communities also modified OA effects on viral-mediated mortality and on the resulting carbon fluxes.

Effect of OA and Eutrophication on Phytoplankton Viruses

In the WINTER experiment, we found a population of very high fluorescence VLP, as identified by their signature in the cytometric plot of high side scatter and fluorescence, comparable to the cytometric signature of viruses infecting small haptophytes and chlorophytes (Brussaard, 2004). The fact that this population was emerging in the decline phase of the bloom of the "large picoeukaryotes" cytometric group, mostly constituted of small mixotrophic haptophytes (2–4 μm, Massana, pers. comm.), which are the most abundant nanoflagellates at the sampling site year-round (Unrein et al., 2014), suggests that these were actually their potential viruses. Very high fluorescence VLP could not be detected in the SUMMER experiment, where large picoeukaryotes were less abundant. The abundance of these

VLP tended to be lower at lowered pH although their putative hosts' abundance was enhanced. Consistently, Larsen et al. (2008) found a decreased production of nanophytoplankton-specific viruses (e.g., infecting *Emiliania huxleyi*) coupled to increased host production under elevated pCO_2, suggesting that lower viral production was not a secondary effect of reduced host production but a direct and negative effect on viral–host interactions. Maat et al. (2014) found viral lysis of *M. pulsilla* reduced under enhanced pCO_2 and P-limited conditions. In addition, during an acidification experiment in the Arctic, very small sized picophytoplankton was stimulated by elevated levels of pCO_2, while the viral group associated to the decline in the picophytoplankton bloom and apparently responsible for that decline was not found to be affected by pCO_2 (Brussaard et al., 2013).

In WINTER, cyanobacteria of the genus *Synechococcus* were negatively affected by OA, while the subpopulation of high fluorescence VLP was stimulated regardless of the nutrient conditions (**Table 2** and **Figure 3E**). The high subpopulation is generally constituted by cyanophages and viruses of picoeukaryotes (Brussaard, 2004; Brussaard et al., 2008a; Martinez et al., 2014). The positive correlation of this subpopulation to *Synechococcus* (Spearman $\rho = 0.57$, $n = 72$, $P < 0.0001$) and to *Prochlorococcus* (Spearman $\rho = 0.41$, $n = 72$, $P = 0.0004$) lends further support that this group was mainly comprised of cyanophages. Thus, the negative response of *Synechococcus* in WINTER could be the consequence of enhanced viral lysis in this season. Indeed, freshwater cyanophages have been shown to tolerate a broad range of pH (Suttle, 2000). Moreover, in the SUMMER experiment, where the pH changed over 0.6 U, these putative cyanophages were stimulated by acidification in both nutrient treatments (**Table 3**). There, however, *Synechococcus* was stimulated in the OA treatments, at least from day 5 in the nutrient control treatments, where pH reached the lowest values due to microbial activities (**Figure 1**). Several studies suggest a stimulating effect of increased pCO_2 on cyanobacteria production due to energy savings related to the reduced use of carbon concentration mechanisms (Fu et al., 2007; Raven et al., 2012). In the case of the oligotrophic conditions of the SUMMER experiment, the enhanced production of putative cyanophages might appear as a secondary effect of enhanced host production under elevated levels of pCO_2. In fact, studies with the model system cyanophage S-PM2 and its host *Synechococcus* sp. WH7803 revealed a negative effect of OA on the growth rate of *Synecchococcus*, which compromised biogenesis and the replication cycle of S-PM2 (Traving et al., 2013).

Effect of OA and Eutrophication on Bacteriophage Production

In WINTER, bacterial production increased during the first day, when bacteriophage production was significantly reduced under OA, and this was most apparent in the nutrient control treatments. Since bacterial host abundance was stimulated or not affected by pH in the nutrient amended and control treatments, respectively (**Table 3**), phage replication rates or phage–host interactions seem to be directly affected by acidification. In fact, metatranscriptome analysis from WINTER found that phage encoding genes most similar to *Podoviridae* phages infecting SAR11-clade bacteria were negatively affected by acidification, and this was more conspicuous in the non-amended treatments (Bunse et al., 2016).

If bacterial species resistant to viral infection are promoted by ocean acidification, this could affect phage production and total bacterial mortality. High throughput sequencing of 16S ribosomal RNA (rRNA) gen amplicons from the present study showed the synergistic effects of OA and nutrient amendment selected for some specific OTUs belonging to SAR86 (Baltar et al., 2015). However, SAR86 OTUs had only a minor contribution to total bacterial community and might not have been responsible for the reduction in phage-mediated bacterial mortality in the acidification treatments of WINTER (**Figure 4C**). Moderate changes in pH were shown to cause compositional shifts in the bacterial community from the North Sea in all seasons (Krause et al., 2012). Conversely, most other OA mesocosm experiments showed a lack of clear pCO_2 effects on global bacterial community structure (Newbold et al., 2012; Roy et al., 2013; Sperling et al., 2013; Zhang et al., 2013; Oliver et al., 2014), and thus, changes in the bulk bacterial mortality are unlikely caused by the selection of lysis-resistant bacterial species through acidification.

Instead of looking at slight phylogenetic changes in the bacterial community as a response to OA, the metabolic state of the bacterial hosts, which is crucial for successful viral infection, proliferation, and bulk viral production, should be considered. Metatranscriptome analyses from the WINTER experiment showed that bacteria adjusted their gene expression patterns to acidification by enhancing the expression of genes encoding proton pumps, such as respiration complexes, proteorhodopsin, and membrane transporters in the nutrient control treatments (Bunse et al., 2016). Proton transport across membranes demands much energy at the expense of bacterial growth and growth efficiency. Since viral infection and BS rely on the bacterial growth rate and growth efficiency (Middelboe, 2000), viral production rates should decrease with lower bacterial growth efficiency. Actually, VP rates were significantly and positively correlated to bacterial heterotrophic production and abundance in the nutrient deplete controls (**Supplementary Figure 1**). There, the lowered pH stimulated the percentage of CTC-labeled cells but did not affect bacterial heterotrophic production rates (**Figure 2**), suggesting lower bacterial growth efficiency under OA as demonstrated from previous experiments (Motegi et al., 2013; Celussi et al., 2017) with implications for bacteriophage production.

Concerning lysogeny as a potential viral strategy to cope with unfavorable conditions (Weinbauer, 2004), we found a very low incidence of the lysogenic life style with no discernible effect of OA (**Table 4**) in accordance with a previous study from the Mediterranean (Tsiola et al., 2017). Excluding day 0, only 4 out of 12 measurements of viral production showed lysogenic production induced by mitomycin C (MC). Microcosm experiments to discern the effect of the viral life style on bacterial community composition have shown consistently lower viral and bacterial numbers in the MC treatments (Chen et al., 2019), suggesting harmful effects of the inducing reagent itself on bacterial growth, inhibiting certain bacterial clades (Hewson and

Fuhrman, 2007). However, in the NB treatments of SUMMER, temperate viruses accounted for the totality of viral production. It has been suggested that lysogeny dominates in oligotrophic environments with low host abundances and contact rates (Weinbauer et al., 2003a) and that prophage induction occurs in rapidly growing cells (Wilson and Mann, 1997). Moreover, protistan grazing also increases bacterial growth rates by recycling nutrients (Simek et al., 2001; Weinbauer et al., 2003b), and this might induce lysogens into the lytic cycle. Unfortunately, grazing rates were not measured in the present study, but the bacterial dynamics and total phytoplankton biomass in SUMMER were very similar to a previous experiment from the same sampling site, where grazing accounted for up to 100% of the bacterial standing stock (Baltar et al., 2016). Interestingly, and similar to the present study, VLP reached considerably high numbers at the end of that experiment (Sandaa et al., 2009).

Modulation of OA Effects on the Microbial Community by Seasonality and Nutrient Availability

The response of the microbial community and their associated viruses to lowered pH differed considerably between seasons. Higher pCO_2 did not stimulate auto- and heterotrophic production of the microbial community in a nutrient replete situation in WINTER, while it did stimulate the microbial community from an oligotrophic situation in SUMMER (**Figures 1**, **2**; Sala et al., 2016). Besides the nutrient availability, the seasonal differences were most conspicuous in the different successional stages of the plankton community with a diatom-dominated phytoplankton bloom in winter and pico- and nanoflagellates prevailing in the summer plankton community (Sala et al., 2016).

In our experiments, total VLP abundance and the abundance of VLP subpopulations were intimately linked to microbial production dynamics, in agreement with Larsen et al. (2001, 2004). They were also stimulated consistently by acidification in both nutrient treatments in SUMMER, as a consequence of the cascading effect of OA on phytoplankton and bacterial production in the oligotrophic situation (**Table 3**). This finding contrasted with the nutrient-replete WINTER situation (**Figure 4**), where phage-mediated processes were significantly reduced by OA. These differences in the pH sensitivity of viral production and host production is in accordance with results from the Pelagic Ecosystem CO_2 Enrichment studies (PeECE I–III). There, bacterial production was either not affected (Allgaier et al., 2008) or stimulated by lowered pH (Grossart et al., 2006). However, these experiments were performed under similar conditions, same site and approximately the same dates, but under different trophic conditions. This was translated into a lower total phytoplankton biomass. Riebesell et al. (2008) argued that the trophic state of the system, i.e., limitation by inorganic and organic nutrients, should influence, at least indirectly, the microbial community.

Indeed, the effects of lowered pH on viral abundance or phage-mediated bacterial mortality were more pronounced after the chlorophyll peak. Significant effects of acidification on the microbial community have been found to occur after the bloom phase (Arnosti et al., 2011; Sperling et al., 2013). During an *in situ* mesocosm experiment, elevated levels of pCO_2 triggered higher diversity of the particle-associated bacterial community only after the breakdown of the phytoplankton bloom (Sperling et al., 2013) concomitant with increased dissolved and particulate primary production (Engel et al., 2013) and bacterial production (Piontek et al., 2013), but with decreased bacterial abundance (Brussaard et al., 2013). The latter was suggested to be due to enhanced viral lysis rates in a high pCO_2 postbloom situation.

Implications for the Carbon Fluxes in the Microbial Food Web

In the experiments performed with a nano–picoplankton-dominated community, in the SUMMER oligotrophic situation, phage-mediated bacterial mortality was, in general, low without a clear effect of OA. Nonetheless, phage abundances were high. A 3-year study from the same sampling site revealed that a specific class of organic aggregates, the transparent exopolymeric particles (TEP), recurrently accumulate in the stratified, oligotrophic conditions of early summer (Ortega-Retuerta et al., 2018). Suspended organic aggregates are hotspots for bacterial growth (Azam and Long, 2001; Azam and Malfatti, 2007), and high viral abundance found on TEP (Mari et al., 2007) suggests high viral infection of TEP-attached bacteria. It must be pointed out that the virus production assays (VRAs) used in the present study exclude aggregate-attached bacteria due to prefiltration of the water and, consequently, phage production associated to TEPs. This might explain the discrepancy between the low phage production and high viral numbers observed. However, a simulation model of a *Phaeocystis globosa* bloom demonstrated that TEPs scavenge viral particles and reduce their infectivity (Ruardij et al., 2005). Moreover, infected host cells might be grazed selectively, lowering the contact rate between viruses and uninfected host cells (Ruardij et al., 2005). In fact, seasonal studies from the same sampling site show peaks of nanoflagellate abundance and relatively important grazing rates in summer (Boras et al., 2009; Unrein et al., 2014) suggesting a less efficient viral shunt in that season.

Instead, phage-mediated loss of bacterial biomass in WINTER was apparently the dominant mortality agent for bacteria there. Since bacterial abundance was higher in WINTER than in SUMMER, this may have increased the encounter probability with the host. In addition, it has been suggested that viruses are the prevailing mortality agent in eutrophic waters over protistan grazing (Steward et al., 1996), consistent with observations in nutrient-rich bloom/postbloom situations where the organic carbon in the microbial food web is mainly processed by the viral shunt (Malits et al., 2014). Viral lysis, by destroying the infected cell and releasing the content of the cytoplasm to the environment, mainly proteins and glucose (Boras et al., 2015), feeds the DOC pool and reduces the transfer of photosynthetically fixed carbon to higher trophic levels and to export; hence, retaining it in the basal levels of the planktonic food web (Sheik et al., 2014), increasing bacterial respiration (Middelboe and Lyck, 2002; Bonilla-Findji et al., 2008), and

weakening the biological carbon pump, i.e., the flux of organic carbon to the deep ocean.

We found phage production and concomitant organic carbon release rates significantly reduced in the acidified treatments of the nutrient replete WINTER experiment, especially in the non-amended treatments. When comparing the organic carbon processed by the viral shunt with the total autotrophic biomass converted to organic carbon with a C/Chl *a* ratio estimated for bloom conditions in the Northwest Mediterranean (Gutiérrez-Rodríguez et al., 2010), viral lysis transferred 41 ± 5% of the phytoplankton standing stock to the DOC pool, compared to 18 ± 8% under acidification. Although carbon release rates calculated from VP might be overestimated due to the plausible stimulation of bacterial production in the VRA experiments (Weinbauer et al., 2009), it is evident that OA reduces the DOC supply for bacterial activity mediated by viral lysis (Malits and Weinbauer, 2009).

While no significant differences in the net accumulation of DOC and the protein-like DOM compounds could be detected between the acidified and non-acidified conditions in the present study (Aparicio et al., 2016), enhanced DOC production under elevated pCO_2 concentrations has often been observed in published studies (Kim et al., 2011; Yoshimura et al., 2013; Paul et al., 2015). Mesocosm experiments in the Arctic Ocean have shown that DOC exudation by phytoplankton increased under acidification but without concomitant net DOC accumulation (Engel et al., 2013), suggesting that the increased bacterial biomass production (Piontek et al., 2013) was responsible for the DOC removal. Since bacterial heterotrophic production was not stimulated under OA in WINTER, reduced DOC release mediated by viral lysis under acidification could have been compensated by increased DOC production under lowered pH conditions (Kim et al., 2011; Engel et al., 2013; Yoshimura et al., 2013; Paul et al., 2015). This would have led to non-significant differences in net DOC accumulation between treatments, as we observed (Aparicio et al., 2016).

Seawater culture experiments with bacterioplankton communities from contrasting sites such as the coastal upwelling influenced Santa Barbara Channel, and the oligotrophic systems of the Sargasso Sea and the South Pacific Subtropical Gyre evidenced that elevated pCO_2 led to greater DOC removal by bacteria growing on a range of added DOC types, from glucose to complex phytoplankton products (James et al., 2017). The authors inferred higher bacterioplankton respiration rates under OA from changes in DOC and bacterial biomass and suggested reduced vertical DOC export. In the present study, we indeed found that actively respiring bacterial cells labeled by CTC increased with decreasing pH, at least in the nutrient amended treatments (**Table 3**), in accordance with previous studies in the Mediterranean (Celussi et al., 2017). Together with the lower calcification rates of planktonic organisms and a consequently reduced particle flux to the deep ocean in an acidified environment (Engel et al., 2005), this results in a positive feedback to atmospheric pCO_2. Reduced viral lysis under OA, however, should counterbalance these negative effects of lowered pH on the biological carbon pump, at least in bloom and postbloom situations where viral lysis plays a relevant role in carbon cycling through the microbial food web.

CONCLUSIONS

Our experimental results provide insight into how two major global change pressures, ocean acidification and eutrophication, modulate viral production and viral-mediated processes in the plankton community at different seasons. While nutrient loading consistently enhanced phage production regardless of the season, the effect of OA on viruses differed between seasons. In the nutrient-replete bloom/postbloom situation in WINTER, viral production and phage-mediated bacterial mortality were reduced under increased pCO_2. In the oligotrophic SUMMER situation, where viral-mediated carbon fluxes were less important compared to WINTER, OA stimulated viruses through the cascading effect of elevated pCO_2 on the autotrophic and heterotrophic production. Given the relevant role of viruses in marine carbon cycling and the biological carbon pump, these two anthropogenic stressors may modulate carbon fluxes through their effect on viruses at the base of the pelagic food web in future global change scenarios.

ORIGINALITY—SIGNIFICANCE STATEMENT

This is the first study that shows phage-mediated bacterial mortality leading to altered carbon fluxes in response to elevated *p*CO2 and nutrient additions simulating the combined effect of acidification and eutrophication. This work contributes to the understanding of how these two anthropogenic stressors modulate carbon fluxes at the base of the pelagic food web in future global change scenarios.

DATA AVAILABILITY STATEMENT

The original contributions presented in the study are included in the article/**Supplementary Materials**, further inquiries can be directed to the corresponding authors.

AUTHOR CONTRIBUTIONS

AM, JB, VB, EC, CP, JP, JG, CM, MS, and DV conceived, planned, and carried out the mesocosm experiments. JB and AM performed the mortality experiments. AM analyzed viruses by flow cytometry and took the lead in writing the manuscript. All authors provided critical feedback and helped to shape the manuscript.

FUNDING

The financial support was provided by the Spanish Ministry of Economy and Competitiveness in the framework of the projects STORM (CTM2009–09352), DOREMI (CTM2012-34294), MANIFEST (CTM2012-32017), and PROTOS (CTM2009-08783). We are also grateful for the funding from the Generalitat de Catalunya through the Grup de Diversitat Microbiana en Ecosistemes Acuàtics (2014SGR/1591), Grup de Biogeoquímica Marina i Canvi Global (2017SGR1011) and the Grup d'Estructura i Funció de Xarxes Tròfiques

Microbianes Planctòniques (2014SGR/1179) and a grant from the Spanish Ministry of Education (SB2010-0079) to AM. With the institutional support of the Severo Ochoa Center of Excellence accreditation (CEX2019-000928-S).

ACKNOWLEDGMENTS

The authors thank Anderson Cabral and Clara Cardelús for research assistance, the Experimental Aquarium Zone (ZAE) of the ICM-CSIC for providing the installations to deploy the containers for the experiments, and the Analytical Chemistry laboratory staff of the ICM-CSIC for performing the nutrient analyses.

SUPPLEMENTARY MATERIAL

The Supplementary Material for this article can be found online at: https://www.frontiersin.org/articles/10.3389/fmicb.2021.635821/full#supplementary-material

REFERENCES

Allgaier, M., Riebesell, U., Vogt, M., Thyrhaug, R., and Grossart, H. P. (2008). Coupling of heterotrophic bacteria to phytoplankton bloom development at different pCO_2 levels: a mesocosm study. *Biogeosciences* 5, 1007–1022. doi: 10.5194/bg-5-1007-2008

Alonso-Sáez, L., Balagué, V., Sà, E. L., Sánchez, O., González, J. M., Pinhassi, J., et al. (2007). Seasonality in bacterial diversity in north-west Mediterranean coastal waters: assessment through clone libraries, fingerprinting and FISH. *FEMS Microbiol. Ecol.* 60, 98–112. doi: 10.1111/j.1574-6941.2006.00276.x

Aparicio, F. L., Nieto-Cid, M., Borrull, E., Calvo, E., Pelejero, C., Sala, M. M., et al. (2016). Eutrophication and acidification: do they induce changes in the dissolved organic matter dynamics in the coastal Mediterranean Sea? *Sci. Total Environ.* 563–564, 179–189. doi: 10.1016/j.scitotenv.2016.04.108

Arnosti, C., Grossart, H. P., M,hling, M., Joint, I., and Passow, U. (2011). Dynamics of extracellular enzyme activities in seawater under changed atmospheric pCO_2: a mesocosm investigation. *Aquat. Microb. Ecol.* 64, 285–298. doi: 10.3354/ame01522

Azam, F. (1998). Microbial control of oceanic carbon flux: the plot thickens. *Science* 280, 694–696. doi: 10.1126/science.280.5364.694

Azam, F., Fenchel, T., Field, J. G., Gray, J. S., Meyer-Reil, L. A., and Thingstad, F. (1983). The ecological role of water-column microbes in the sea. *Mar. Ecol. Prog. Ser.* 10, 257–263. doi: 10.3354/meps010257

Azam, F., and Long, R. A. (2001). Sea snow microcosms. *Nature* 414, 495,497–498. doi: 10.1038/35107174

Azam, F., and Malfatti, F. (2007). Microbial structuring of marine ecosystems. *Nat. Rev. Micro* 5, 782–791. doi: 10.1038/nrmicro1747

Baltar, F., Palovaara, J., Unrein, F., Catala, P., Hornák, K., Šimek, K., et al. (2016). Marine bacterial community structure resilience to changes in protist predation under phytoplankton bloom conditions. *ISME J.* 10, 568–581. doi: 10.1038/ismej.2015.135

Baltar, F., Palovaara, J., Vila-Costa, M., Salazar, G., Calvo, E., Pelejero, C., et al. (2015). Response of rare, common and abundant bacterioplankton to anthropogenic perturbations in a Mediterranean coastal site. *FEMS Microbiol. Ecol.* 91:fiv058. doi: 10.1093/femsec/fiv058

Berdjeb, L., Pollet, T., Domaizon, I., and Jacquet, S. (2011). Effect of grazers and viruses on bacterial community structure and production in two contrasting trophic lakes. *BMC Microbiol.* 11:88. doi: 10.1186/1471-2180-11-88

Bonilla-Findji, O., Malits, A., Lefèvre, D., Rochelle-Newall, E., Lemée, R., Weinbauer, M. G., et al. (2008). Viral effects on bacterial respiration, production and growth efficiency: consistent trends in the Southern Ocean and the Mediterranean Sea. *Deep. Res. Part II Top. Stud. Oceanogr.* 55, 559–912. doi: 10.1016/j.dsr2.2007.12.004

Bopp, L., Resplandy, L., Orr, J. C., Doney, S. C., Dunne, J. P., Gehlen, M., et al. (2013). Multiple stressors of ocean ecosystems in the 21st century: projections with CMIP5 models. *Biogeosciences* 10, 6225–6245. doi: 10.5194/bg-10-6225-2013

Boras, J. A., Sala, M. M., Vázquez-Domínguez, E., Weinbauer, M. G., and Vaqué, D. (2009). Annual changes of bacterial mortality due to viruses and protists in an oligotrophic coastal environment (NW Mediterranean). *Env. Microbiol.* 11, 1181–1193. doi: 10.1111/j.1462-2920.2008.01849.x

Boras, J. A., Vaqué, D., Maynou, F., Sà, E. L., Weinbauer, M. G., and Sala, M. M. (2015). Factors shaping bacterial phylogenetic and functional diversity in coastal waters of the NW Mediterranean Sea. *Estuar. Coast. Shelf Sci.* 154, 102–110. doi: 10.1016/j.ecss.2014.12.039

Borges, A. V., and Gypens, N. (2010). Carbonate chemistry in the coastal zone responds more strongly to eutrophication than ocean acidification. *Limnol. Oceanogr.* 55, 346–353. doi: 10.4319/lo.2010.55.1.0346

Brussaard, C. P. D. (2004). Optimization of procedures for counting viruses by flow cytometry. *Appl. Environ. Microbiol.* 70, 1506–1513. doi: 10.1128/AEM.70.3.1506-1513.2004

Brussaard, C. P. D. (2009). "Enumeration of bacteriophages using flow cytometry," in *Bacteriophages: Methods and Protocols, Vol. 1: Isolation, Characterization, and Interactions*, eds M. R. J. Clokie and A. M. Kropinski (Totowa, NJ: Humana Press), 97–111.

Brussaard, C. P. D., Noordeloos, A. A. M., Witte, H., Collenteur, M. C. J., Schulz, K., Ludwig, A., et al. (2013). Arctic microbial community dynamics influenced by elevated CO_2 levels. *Biogeosciences* 10, 719–731. doi: 10.5194/bg-10-719-2013

Brussaard, C. P. D., Timmermans, K. R., Uitz, J., and Veldhuis, M. J. W. (2008a). Virioplankton dynamics and virally induced phytoplankton lysis versus microzooplankton grazing southeast of the Kerguelen (Southern Ocean). *Deep Sea Res. Part II Top. Stud. Oceanogr.* 55, 752–765. doi: 10.1016/j.dsr2.2007.12.034

Brussaard, C. P. D., Wilhelm, S. W., Thingstad, F., Weinbauer, M. G., Bratbak, G., Heldal, M., et al. (2008b). Global-scale processes with a nanoscale drive: the role of marine viruses. *ISME J.* 2, 575–578. doi: 10.1038/ismej.2008.31

Bunse, C., Lundin, D., Karlsson, C. M. G., Akram, N., Vila-Costa, M., Palovaara, J., et al. (2016). Response of marine bacterioplankton pH homeostasis gene expression to elevated CO_2. *Nat. Clim. Chang.* 6, 483–487. doi: 10.1038/nclimate2914

Cai, W.-J., Hu, X., Huang, W.-J., Murrell, M. C., Lehrter, J. C., Lohrenz, S. E., et al. (2011). Acidification of subsurface coastal waters enhanced by eutrophication. *Nat. Geosci.* 4:766. doi: 10.1038/ngeo1297

Caldeira, K., and Wickett, M. E. (2003). Oceanography: anthropogenic carbon and ocean pH. *Nature* 425:365. doi: 10.1038/425365a

Celussi, M., Malfatti, F., Annalisa, F., Gazeau, F., Giannakourou, A., Pitta, P., et al. (2017). Ocean acidification effect on prokaryotic metabolism tested in two diverse trophic regimes in the Mediterranean Sea. *Estuar. Coast. Shelf Sci.* 186, 125–138. doi: 10.1016/j.ecss.2015.08.015

Chen, X., Ma, R., Yang, Y., Jiao, N., and Zhang, R. (2019). Viral regulation on bacterial community impacted by lysis-lysogeny switch: a microcosm experiment in eutrophic coastal waters. *Front. Microbiol.* 10:1763. doi: 10.3389/fmicb.2019.01763

Clayton, T. D., and Byrne, R. H. (1993). Spectrophotometric seawater pH measurements: total hydrogen ion concentration scale calibration of m-cresol purple and at-sea results. *Deep Sea Res. Part I Oceanogr. Res.* 40, 2115–2129. doi: 10.1016/0967-0637(93)90048-8

Crawfurd, K. J., Alvarez-Fernandez, S., Mojica, K. D. A., Riebesell, U., and Brussaard, C. P. D. (2017). Alterations in microbial community composition with increasing f CO_2: a mesocosm study in the eastern Baltic Sea. *Biogeosciences* 14, 3831–3849. doi: 10.5194/bg-14-3831-2017

Danovaro, R., Corinaldesi, C., Dell'anno, A., Fuhrman, J. A., Middelburg, J. J., Noble, R. T., et al. (2011). Marine viruses and global climate change. *FEMS Microbiol. Rev.* 35, 993–1034. doi: 10.1111/j.1574-6976.2010.00258.x

Diaz, R. J., and Rosenberg, R. (2008). Spreading dead zones and consequences for marine ecosystems. *Science* 321, 926–929. doi: 10.1126/science.1156401

Dickson, A. G., Sabine, C. L., and Christian, J. R. (2007). *Guide to Best Practice for Ocean CO_2 Measurements*. PICES Special Publication 3 (Sidney: North Pacific Marine Science Organization).

Dlugokencky, E., and Tans, P. (2020). Trends in atmospheric carbon dioxide. National Oceanic & Atmospheric Administration, Earth System Research Laboratory (NOAA/ESRL). Available online at: http://www.esrl.noaa.gov/gmd/ccgg/trends/global.html

Doney, S. C., Fabry, V. J., Feely, R. A., and Kleypas, J. A. (2009). Ocean acidification: the other CO_2 problem. *Ann. Rev. Mar. Sci.* 1, 169–192. doi: 10.1146/annurev.marine.010908.163834

Dore, J. E., Lukas, R., Sadler, D. W., Church, M. J., and Karl, D. M. (2009). Physical and biogeochemical modulation of ocean acidification in the central North Pacific. *Proc. Natl. Acad. Sci. U.S.A.* 106, 12235–12240. doi: 10.1073/pnas.0906044106

Engel, A., Borchard, C., Piontek, J., Schulz, K. G., Riebesell, U., and Bellerby, R. (2013). CO_2 increases 14C primary production in an Arctic plankton community. *Biogeosciences* 10, 1291–1308. doi: 10.5194/bg-10-1291-2013

Engel, A., Zondervan, I., Aerts, K., Beaufort, L., Benthien, A., Chou, L., et al. (2005). Testing the direct effect of CO_2 concentration on a bloom of the coccolithophorid *Emiliania huxleyi* in mesocosm experiments. *Limnol. Oceanogr.* 50, 493–507. doi: 10.4319/lo.2005.50.2.0493

Field, C. B., Behrenfeld, M. J., Randerson, J. T., and Falkowski, P. (1998). Primary production of the biosphere: integrating terrestrial and oceanic components. *Science* 281, 237–240. doi: 10.1126/science.281.5374.237

Fu, F.-X., Warner, M. E., Zhang, Y., Feng, Y., and Hutchins, D. A. (2007). Effects of increased temperature and CO_2 on photosynthesis, growth and elemental ratios in marine in marine *Synechococcus* and *Prochlorococcus* (cyanobacteria). *J. Phycol.* 43, 485–496. doi: 10.1111/j.1529-8817.2007.00355.x

Fuhrman, J. A. (1999). Marine viruses and their biogeochemical and ecological effects. *Nature* 399, 541–548. doi: 10.1038/21119

Galloway, J. N., Dentener, F. J., Capone, D. G., Boyer, E. W., Howarth, R. W., Seitzinger, S. P., et al. (2004). Nitrogen cycles: past, present, and future. *Biogeochemistry* 70, 153–226. doi: 10.1007/s10533-004-0370-0

Gasol, J. M., and Arístegui, J. (2007). Cytometric evidence reconciling the toxicity and usefulness of CTC as a marker of bacterial activity. *Aquat. Microb. Ecol.* 46, 71–83. doi: 10.3354/ame046071

Gasol, J. M., Cardelús, C., Morán, X. A. G., Balagué, V., Forn, I., Marrasé, C., et al. (2016). Seasonal patterns in phytoplankton primary production and photosynthetic parameters in a coastal time-series station of the NW Mediterranean Sea. *Scientia Marina*, 80S1, 63–77. doi: 10.3989/scimar.04480.06E

Gasol, J. M., and Morán, X. A. G. (2015). "Flow cytometric determination of microbial abundances and its use to obtain indices of community structure and relative activity," in *Hydrocarbon and Lipid Microbiology Protocols*, eds T. J. McGenity, K. N. Timmis, and B. Nogales (Berlin; Heidelberg: Springer Protocols Handbooks). doi: 10.1007/8623_2015_139

Gasol, J. M., Zweifel, U. L., Peters, F., Fuhrman, J. A., and Hågström, A. (1999). Significance of size and nucleic acid content heterogeneity as measured by flow cytometry in natural planktonic bacteria. *Appl. Env. Microbiol.* 65, 4475–4483. doi: 10.1128/AEM.65.10.4475-4483.1999

Gobler, C. J., Hutchins, D. A., Fisher, N. S., Cosper, E. M., and Sanudo-Wilhelmy, S. A. (1997). Release and bioavailability of C, N, P, Se., and Fe following viral lysis of a marine chrysophyte. *Limnol. Ocean.* 42, 1492–1504. doi: 10.4319/lo.1997.42.7.1492

Grossart, H. P., Allgaier, M., Passow, U., and Riebesell, U. (2006). Testing the effect of CO_2 concentration on the dynamics of marine heterotrophic bacterioplankton. *Limnol. Ocean.* 51, 1–11. doi: 10.4319/lo.2006.51.1.0001

Gutiérrez-Rodríguez, A., Latasa, M., Estrada, M., Vidal, M., and Marrasé, C. (2010). Carbon fluxes through major phytoplankton groups during the spring bloom and post-bloom in the Northwestern Mediterranean Sea. *Deep Sea Res. Part I Oceanogr. Res. Pap.* 57, 486–500. doi: 10.1016/j.dsr.2009.12.013

Hansen, H. P., and Koroleff, F. (2007). "Determination of nutrients," in *Methods of Seawater Analysis*, eds K. Grasshoff, K. Kremling, and M. Ehrhardt (John Wiley & Sons), 159–228. doi: 10.1002/9783527613984.ch10

Hewson, I., and Fuhrman, J. A. (2007). Characterization of lysogens in bacterioplankton assemblages of the southern California borderland. *Microb. Ecol.* 53, 631–638. doi: 10.1007/s00248-006-9148-3

James, A. K., Passow, U., Brzezinski, M. A., Parsons, R. J., Trapani, J. N., and Carlson, C. A. (2017). Elevated pCO_2 enhances bacterioplankton removal of organic carbon. *PLoS ONE* 12:e0173145. doi: 10.1371/journal.pone.0173145

Joint, I., Doney, S. C., and Karl, D. M. (2011). Will ocean acidification affect marine microbes[quest]. *ISME J.* 5, 1–7. doi: 10.1038/ismej.2010.79

Joos, F., and Spahni, R. (2008). Rates of change in natural and anthropogenic radiative forcing over the past 20,000 years. *Proc. Natl. Acad. Sci. U.S.A.* 105, 1425 LP−1430. doi: 10.1073/pnas.0707386105

Kim, J.-M., Lee, K., Shin, K., Yang, E. J., Engel, A., Karl, D. M., et al. (2011). Shifts in biogenic carbon flow from particulate to dissolved forms under high carbon dioxide and warm ocean conditions. *Geophys. Res. Lett.* 38:L08612. doi: 10.1029/2011GL047346

Kirchman, D., K'Nees, E., and Hodson, R. (1985). Leucine incorporation and its potential as a measure of protein synthesis by bacteria in natural aquatic systems. *Appl. Env. Microbiol.* 49, 599–607. doi: 10.1128/AEM.49.3.599-607.1985

Knowles, B., Silveira, C. B., Bailey, B. A., Barott, K., Cantu, V. A., Cobián-Güemes, A. G., et al. (2016). Lytic to temperate switching of viral communities. *Nature* 531, 466–470. doi: 10.1038/nature17193

Krause, E., Wichels, A., Giménez, L., Lunau, M., Schilhabel, M. B., and Gerdts, G. (2012). Small changes in pH have direct effects on marine bacterial community composition: a microcosm approach. *PLoS ONE* 7:e47035. doi: 10.1371/journal.pone.0047035

Larsen, A., Castberg, T., Sandaa, R. A., Brussaard, C. P. D., Egge, J. K., Heldal, M., et al. (2001). Population dynamics and diversity of phytoplankton, bacteria and viruses in a seawater enclosure. *Mar. Ecol. Prog. Ser.* 221, 47–57. doi: 10.3354/meps221047

Larsen, A., Gro, A., Flaten, F., Sandaa, R. A., Castberg, T., Thyrhaug, R., et al. (2004). Spring phytoplankton bloom dynamics in Norwegian coastal waters: microbial community succession and diversity. *Limnol. Oceanogr.* 49, 180–190. doi: 10.4319/lo.2004.49.1.0180

Larsen, J. B., Larsen, A., Thyrhaug, R., Bratbak, G., and Sandaa, R. A. (2008). Response of marine viral populations to a nutrient induced phytoplankton bloom at different pCO_2 levels. *Biogeosciences* 5, 523–533. doi: 10.5194/bg-5-523-2008

Lee, S., and Fuhrman, J. E. (1987). Relationship between biovolume and biomass of naturally derived marine bacterioplankton. *Appl. Environ. Microbiol.* 53, 1298–1303. doi: 10.1128/AEM.53.6.1298-1303.1987

Lindh, M. V., Riemann, L., Baltar, F., Romero-Oliva, C., Salomon, P. S., Granéli, E., et al. (2013). Consequences of increased temperature and acidification on bacterioplankton community composition during a mesocosm spring bloom in the Baltic Sea. *Environ. Microbiol. Rep.* 5, 252–262. doi: 10.1111/1758-2229.12009

Maat, D. S., Crawfurd, K. J., Timmermans, K. R., and Brussaard, C. P. D. (2014). Elevated CO_2 and phosphate limitation favor *Micromonas pusilla* through stimulated growth and reduced viral impact. *Appl. Environ. Microbiol.* 80, 3119 LP−3127. doi: 10.1128/AEM.03639-13

Malits, A., Christaki, U., Obernosterer, I., and Weinbauer, M. G. G. (2014). Enhanced viral production and virus-mediated mortality of bacterioplankton in a natural iron-fertilized bloom event above the Kerguelen Plateau. *Biogeosciences* 11, 6841–6853. doi: 10.5194/bg-11-6841-2014

Malits, A., and Weinbauer, M. G. G. (2009). Effect of turbulence and viruses on prokaryotic cell size, production and diversity. *Aquat. Microb. Ecol.* 54, 243–254. doi: 10.3354/ame01274

Malone, T. C., and Newton, A. (2020). The globalization of cultural eutrophication in the coastal ocean: causes and consequences. *Front. Mar. Sci.* 7:670. doi: 10.3389/fmars.2020.00670

Mari, X., Kerros, M. E., and Weinbauer, M. G. (2007). Virus attachment to transparent exopolymeric particles along trophic gradients in the southwestern lagoon of New Caledonia. *Appl. Env. Microbiol.* 73, 5245–5252. doi: 10.1128/AEM.00762-07

Marie, D., Brussaard, C. P. D., Thyrhaug, R., Bratbak, G., and Vaulot, D. (1999). Enumeration of marine viruses in culture and natural samples by flow cytometry. *Appl. Env. Microbiol.* 65, 45–52. doi: 10.1128/AEM.65.1.45-52.1999

Marie, D., Partensky, F., Jacquet, S., and Vaulot, D. (1997). Enumeration and cell cycle analysis of natural populations of marine picoplankton by flow cytometry using the nucleic acid stain SYBR green I. *Appl. Env. Microbiol.* 63, 186–193. doi: 10.1128/AEM.63.1.186-193.1997

Marie, D., Partensky, F., Vaulot, D., and Brussaard, C. (2001). Enumeration of phytoplankton, bacteria, and viruses in marine samples. *Curr. Protoc. Cytom.* Chapter 11:Unit 11.11. doi: 10.1002/0471142956.cy1111s10

Martinez, J. M., Swan, B. K., and Wilson, W. H. (2014). Marine viruses, a genetic reservoir revealed by targeted viromics. *ISME J.* 8, 1079–1088. doi: 10.1038/ismej.2013.214

Meakin, N. G., and Wyman, M. (2011). Rapid shifts in picoeukaryote community structure in response to ocean acidification. *ISME J.* 5, 1397–1405. doi: 10.1038/ismej.2011.18

Middelboe, M. (2000). Bacterial growth rate and marine virus-host dynamics. *Microb. Ecol.* 40, 114–124. doi: 10.1007/s002480000050

Middelboe, M., and Lyck, P. G. (2002). Regeneration of dissolved organic matter by viral lysis in marine microbial communities. *Aquat. Microb. Ecol.* 27, 187–194. doi: 10.3354/ame027187

Motegi, C., Tanaka, T., Piontek, J., Brussaard, C. P. D., Gattuso, J. P., and Weinbauer, M. G. (2013). Effect of CO_2 enrichment on bacterial metabolism in an Arctic fjord. *Biogeosciences* 10, 3285–3296. doi: 10.5194/bg-10-3285-2013

Murray, A. G., and Eldridge, P. M. (1994). Marine viral ecology: incorporation of bacteriophage into the microbial planktonic food web paradigm. *J. Plankton Res.* 16, 627–641. doi: 10.1093/plankt/16.6.627

Newbold, L. K., Oliver, A. E., Booth, T., Tiwari, B., Desantis, T., Maguire, M., et al. (2012). The response of marine picoplankton to ocean acidification. *Env. Microbiol.* 14, 2293–2307. doi: 10.1111/j.1462-2920.2012.02762.x

Oliver, A. E., Newbold, L. K., Whiteley, A. S., and van der Gast, C. J. (2014). Marine bacterial communities are resistant to elevated carbon dioxide levels. *Environ. Microbiol. Rep.* 6, 574–582. doi: 10.1111/1758-2229.12159

Ortega-Retuerta, E., Marrasé, C., Muñoz-Fernández, A., Sala, M. M., Simó, R., and Gasol, J. M. (2018). Seasonal dynamics of transparent exopolymer particles (TEP) and their drivers in the coastal NW Mediterranean Sea. *Sci. Total Environ.* 631–632, 180–190. doi: 10.1016/j.scitotenv.2018.02.341

Paul, A. J., Bach, L. T., Schulz, K. G., Boxhammer, T., Czerny, J., Achterberg, E. P., et al. (2015). Effect of elevated CO_2 on organic matter pools and fluxes in a summer Baltic Sea plankton community. *Biogeosciences.* 12, 6181–6203. doi: 10.5194/bg-12-6181-2015

Paul, J. H., and Weinbauer, M. G. (2010). "Detection of lysogeny in marine environments," in *Manual of Aquatic Viral Ecology*, eds C. Suttle, S. W. Wilhelm, and M. G. Weinbauer (Waco: ASLO), 1–8. doi: 10.4319/mave.2010.978-0-9845591-0-7.30

Pérez, F. F., Ríos, A. F., Rellán, T., and Álvarez, M. (2000). Improvements in a fast potentiometric seawater alkalinity determination. *Ciencias Mar.* 26, 463–478. doi: 10.7773/cm.v26i3.592

Piontek, J., Borchard, C., Sperling, M., Schulz, K. G., Riebesell, U., and Engel, A. (2013). Response of bacterioplankton activity in an Arctic fjord system to elevated pCO_2: results from a mesocosm perturbation study. *Biogeosciences* 10, 297–314. doi: 10.5194/bg-10-297-2013

Poorvin, L., Rinta-Kanto, J. M., Hutchins, D. A., and Wilhelm, S. W. (2004). Viral release of iron and its bioavailability to marine plankton. *Limnol. Oceanogr.* 49, 1734–1741. doi: 10.4319/lo.2004.49.5.1734

Provoost, P., van Heuven, S., Soetaert, K., Laane, R. W. P. M., and Middelburg, J. J. (2010). Seasonal and long-term changes in pH in the Dutch coastal zone. *Biogeosciences* 7, 3869–3878. doi: 10.5194/bg-7-3869-2010

Rabalais, N. N., Turner, R. E., Díaz, R. J., and Justić, D. (2009). Global change and eutrophication of coastal waters. *ICES J. Mar. Sci.* 66, 1528–1537. doi: 10.1093/icesjms/fsp047

Raven, J. A., Giordano, M., Beardall, J., and Maberly, S. C. (2012). Algal evolution in relation to atmospheric CO_2: carboxylases, carbon-concentrating mechanisms and carbon oxidation cycles. *Philos. Trans. R. Soc. Lond. B. Biol. Sci.* 367, 493–507. doi: 10.1098/rstb.2011.0212

Riebesell, U., Bellerby, R. G. J., Grossart, H. P., and Thingstad, F. (2008). Mesocosm CO_2 perturbation studies: from organism to community level. *Biogeosciences* 5, 1157–1164. doi: 10.5194/bg-5-1157-2008

Rochelle-Newall, E., Delille, B., Frankignoulle, M., Gattuso, J. P., Jacquet, S., Riebesell, U., et al. (2004). Chromophoric dissolved organic matter in experimental mesocosms maintained under different pCO_2 levels. *Mar. Ecol. Prog. Ser.* 272, 25–31. doi: 10.3354/meps272025

Roy, A. S., Gibbons, S. M., Schunck, H., Owens, S., Caporaso, J. G., Sperling, M., et al. (2013). Ocean acidification shows negligible impacts on high-latitude bacterial community structure in coastal pelagic mesocosms. *Biogeosciences* 10, 555–566. doi: 10.5194/bg-10-555-2013

Ruardij, P., Veldhuis, M. J. W., and Brussaard, C. P. D. (2005). Modeling the bloom dynamics of the polymorphic phytoplankter *Phaeocystis globosa*: impact of grazers and viruses. *Harmful Algae* 4, 941–963. doi: 10.1016/j.hal.2004.12.011

Sabine, C. L., Feely, R. A., Gruber, N., Key, R. M., Lee, K., Bullister, J. L., et al. (2004). The oceanic sink for anthropogenic CO_2. *Science* 305, 367–371. doi: 10.1126/science.1097403

Sala, M. M., Aparicio, F. L., Balagué, V., Boras, J. A., Borrull, E., Cardelús, C., et al. (2016). Contrasting effects of ocean acidification on the microbial food web under different trophic conditions. *ICES J. Mar. Sci.* 73, 670–679. doi: 10.1093/icesjms/fsv130

Sandaa, R.-A. A., Gomez-Consarnau, L., Pinhassi, J., Riemann, L., Malits, A., Weinbauer, M. G. G., et al. (2009). Viral control of bacterial biodiversity - evidence from a nutrient-enriched marine mesocosm experiment. *Env. Microbiol.* 11, 2585–2597. doi: 10.1111/j.1462-2920.2009.01983.x

Schulz, K. G., Bach, L. T., Bellerby, R. G. J., Bermúdez, R., Büdenbender, J., Boxhammer, T., et al. (2017). Phytoplankton blooms at increasing levels of atmospheric carbon dioxide: experimental evidence for negative effects on prymnesiophytes and positive on small picoeukaryotes. *Front. Mar. Sci.* 4:64. doi: 10.3389/fmars.2017.00064

Sheik, A. R., Brussaard, C. P. D., Lavik, G., Lam, P., Musat, N., Krupke, A., et al. (2014). Responses of the coastal bacterial community to viral infection of the algae *Phaeocystis globosa*. *ISME J.* 8, 212–225. doi: 10.1038/ismej.2013.135

Sherr, B. F., del Giorgio, P. A., and Sherr, E. B. (1999). Estimating abundance and single-cell characteristics of actively respiring bacteria via the redox dye CTC. *Aquat. Microb. Ecol.* 18, 117–131. doi: 10.3354/ame018117

Sieracki, M. E., Cucci, T. L., and Nicinski, J. (1999). Flow cytometric analysis of 5-cyano-2,3-ditolyl tetrazolium chloride activity of marine bacterioplankton in dilution cultures. *Appl. Env. Microbiol.* 65, 2409–2417. doi: 10.1128/AEM.65.6.2409-2417.1999

Simek, K., Pernthaler, J., Weinbauer, M. G., Hornak, K., Dolan, J. R., Nedoma, J., et al. (2001). Changes in bacterial community composition and dynamics and viral mortality rates associated with enhanced flagellate grazing in a mesoeutrophic reservoir. *Appl. Env. Microbiol.* 67, 2723–2733. doi: 10.1128/AEM.67.6.2723-2733.2001

Simon, M., and Azam, F. (1989). Protein content and protein synthesis rates of planktonic marine bacteria. *Mar. Ecol. Prog. Ser.* 51, 201–213.

Smith, D. C., and Azam, F. (1992). A simple, economical method for measuring bacterial protein synthesis rates in seawater using 3H-leucine. *Mar. Microb. Food Webs* 6, 107–114.

Sperling, M., Piontek, J., Gerdts, G., Wichels, A., Schunck, H., Roy, A. S., et al. (2013). Effect of elevated CO_2 on the dynamics of particle-attached and free-living bacterioplankton communities in an Arctic fjord. *Biogeosciences* 10, 181–191. doi: 10.5194/bg-10-181-2013

Spilling, K., Paul, A. J., Virkkala, N., Hastings, T., Lischka, S., Stuhr, A., et al. (2016). Ocean acidification decreases plankton respiration: evidence from a mesocosm experiment. *Biogeosciences* 13, 4707–4719. doi: 10.5194/bg-13-4707-2016

Steward, G. F., Smith, D. C., and Azam, F. (1996). Abundance and production of bacteria and viruses in the Bering and Chukchi Seas. *Mar. Ecol. Prog. Ser.* 131, 287–300. doi: 10.3354/meps131287

Suttle, C. A. (2000). "Ecological, evolutionary, and geochemical consequences of viral infection of cyanobacteria and eukaryotic algae," in *Viral Ecology*, ed C. J. Hurst (Cambridge: Academic Press), 247–296. doi: 10.1016/B978-012362675-2/50007-0

Suttle, C. A. (2005). Viruses in the sea. *Nature* 437, 356–361. doi: 10.1038/nature04160

Suttle, C. A. (2007). Marine viruses–major players in the global ecosystem. *Nat. Rev. Microbiol.* 5, 801–812. doi: 10.1038/nrmicro1750

Traving, S. J., Clokie, M. R., and Middelboe, M. (2013). Increased acidification has a profound effect on the interactions between the cyanobacterium *Synechococcus* sp. WH7803 and its viruses. *FEMS Microbiol. Ecol.* 87, 133–141. doi: 10.1111/1574-6941.12199

Tsiola, A., Pitta, P., Giannakourou, A., Bourdin, G., Marro, S., Maugendre, L., et al. (2017). Ocean acidification and viral replication cycles: frequency of lytically infected and lysogenic cells during a mesocosm experiment in the NW Mediterranean Sea. *Estuar. Coast. Shelf Sci.* 186, 139–151. doi: 10.1016/j.ecss.2016.05.003

Unrein, F., Gasol, J. M., Not, F., Forn, I., and Massana, R. (2014). Mixotrophic haptophytes are key bacterial grazers in oligotrophic coastal waters. *ISME J.* 8, 164–176. doi: 10.1038/ismej.2013.132

Vaqué, D., Lara, E., Arrieta, J. M., Holding, J., Sà, E. L., Hendriks, I. E., et al. (2019). Warming and CO_2 enhance arctic heterotrophic microbial activity. *Front. Microbiol.* 10:494. doi: 10.3389/fmicb.2019.00494

Weinbauer, M. G. (2004). Ecology of prokaryotic viruses. *FEMS Microbiol. Rev.* 28, 127–181. doi: 10.1016/j.femsre.2003.08.001

Weinbauer, M. G., Arrieta, J. M., Griebler, C., and Herndl, G. J. (2009). Enhanced viral production and infection of bacterioplankton during an iron induced phytoplankton bloom in the Southern Ocean. *Limnol. Oceanogr.* 54, 774–784. doi: 10.4319/lo.2009.54.3.0774

Weinbauer, M. G., Bonilla-Findji, O., Chan, A. M., Dolan, J. R., Short, S. M., Simek, K., et al. (2011). *Synechococcus* growth in the ocean may depend on the lysis of heterotrophic bacteria. *J. Plankton Res.* 33, 1465–1476. doi: 10.1093/plankt/fbr041

Weinbauer, M. G., Brettar, I., and Höfle, M. G. (2003a). Lysogeny and virus-induced mortality of bacterioplankton in surface, deep, and anoxic marine waters. *Limnol. Oceanogr.* 48, 1457–1465. doi: 10.4319/lo.2003.48.4.1457

Weinbauer, M. G., Christaki, U., Nedoma, J., and Simek, K. (2003b). Comparing the effects of resource enrichment and grazing on viral production in a meso-eutrophic reservoir. *Aquat. Microb. Ecol.* 31, 137–144. doi: 10.3354/ame031137

Weinbauer, M. G., and Rassoulzadegan, F. (2004). Are viruses driving microbial diversification and diversity? *Environ. Microbiol.* 6, 1–11. doi: 10.1046/j.1462-2920.2003.00539.x

Weinbauer, M. G., Rowe, J. M., and Wilhelm, S. W. (2010). "Determining rates of virus production in aquatic systems by the virus reduction approach," in *Manual of Aquatic Viral Ecology*, eds C. Suttle, S. W. Wilhelm, and M. G. Weinbauer (Waco: ASLO), 1–8. doi: 10.4319/mave.2010.978-0-9845591-0-7.1

Wells, L. E., and Deming, J. W. (2006). Significance of bacterivory and viral lysis in bottom waters of Franklin Bay, Canadian Arctic, during winter. *Aquat. Microb. Ecol.* 43, 209–221. doi: 10.3354/ame043209

Wilhelm, S. W., and Suttle, C. A. (1999). Virus and nutrient cycles in the sea. *Bioscience* 49, 781–787. doi: 10.2307/1313569

Wilson, W. H., and Mann, N. H. (1997). Lysogenic and lytic viral production in marine microbial communities. *Aquat. Microb. Ecol.* 13, 95–100. doi: 10.3354/ame013095

Worden, A. Z., Follows, M. J., Giovannoni, S. J., Wilken, S., Zimmerman, A. E., and Keeling, P. J. (2015). Rethinking the marine carbon cycle: factoring in the multifarious lifestyles of microbes. *Science* 347:1257594. doi: 10.1126/science.1257594

Yentsch, C. S., and Menzel, D. W. (1963). A method for the determination of phytoplankton chlorophyll and phaeophytin by fluorescence. *Deep Sea Res.* 10, 221–231. doi: 10.1016/0011-7471(63)90358-9

Yoshimura, T., Suzuki, K., Kiyosawa, H., Ono, T., Hattori, H., Kuma, K., et al. (2013). Impacts of elevated CO_2 on particulate and dissolved organic matter production: microcosm experiments using iron-deficient plankton communities in open subarctic waters. *J. Oceanogr.* 69, 601–618. doi: 10.1007/s10872-013-0196-2

Zeebe, R. E., Ridgwell, A., and Zachos, J. C. (2016). Anthropogenic carbon release rate unprecedented during the past 66 million years. *Nat. Geosci.* 9:325. doi: 10.1038/ngeo2681

Zhang, R., Xia, X., Lau, S. C. K., Motegi, C., Weinbauer, M. G., and Jiao, N. (2013). Response of bacterioplankton community structure to an artificial gradient of pCO_2 in the Arctic Ocean. *Biogeosciences* 10, 3679–3689. doi: 10.5194/bg-10-3679-2013

Conflict of Interest: The authors declare that the research was conducted in the absence of any commercial or financial relationships that could be construed as a potential conflict of interest.

Advantages of publishing in Frontiers

OPEN ACCESS
Articles are free to read for greatest visibility and readership

FAST PUBLICATION
Around 90 days from submission to decision

HIGH QUALITY PEER-REVIEW
Rigorous, collaborative, and constructive peer-review

TRANSPARENT PEER-REVIEW
Editors and reviewers acknowledged by name on published articles

Frontiers
Avenue du Tribunal-Fédéral 34
1005 Lausanne | Switzerland

Visit us: www.frontiersin.org
Contact us: frontiersin.org/about/contact

REPRODUCIBILITY OF RESEARCH
Support open data and methods to enhance research reproducibility

DIGITAL PUBLISHING
Articles designed for optimal readership across devices

FOLLOW US
@frontiersin

IMPACT METRICS
Advanced article metrics track visibility across digital media

EXTENSIVE PROMOTION
Marketing and promotion of impactful research

LOOP RESEARCH NETWORK
Our network increases your article's readership